

Case Histories of an Electromagnetic Method for Petroleum Exploration

The results of a five-year feasibility study of the utility of electrical measurements in petroleum exploration are very encouraging. Electrical anomalies were measured over 66% of the 29 oil and gas fields involved in the study. The fact that these fields represent both stratigraphic and structural traps at a wide range of depths, with varying production characteristics, and in diverse geologic environments, provides a particularly favorable indication that this technique can be used as a reliable exploration tool, complementing existing seismic and subsurface geology programs.

Case histories of five field projects are presented in this volume in order to illustrate both the advantages and limitations of the method in the context of known geology. The field projects involve a variety of field characteristics. The results delineate the following general observations: 1) repeatable anomalies can be measured over oil and gas fields; 2) two types of anomalies are measured—an electrically conductive "deep anomaly," and a polarizable "shallow anomaly;" 3) the anomalies correlate relatively well in plan view with the limits of hydrocarbon production; 4) the anomalies are partly dependent on specific geologic characteristics of the stratigraphic sequence.

As is the case in seismic interpretations, data processing techniques are crucially important in extracting the maximum of information from electrical data. Proprietary data processing techniques have been developed for this purpose. Great care must be taken during interpretation to evaluate effects of pipelines, well casings, topography, and subsurface geology, since many of these effects may result in spurious anomalies unrelated to alteration due to hydrocarbons. The case histories demonstrate the necessity for this type of evaluation.

Table of Contents, list of PDF files:

IP-Petro_1.pdf

- PART ONE: SUMMARIES
 - Executive Summary
 - Summary and Conclusions

IP-Petro_2.pdf

- PART TWO: DATA INTERPRETATION
 - 1. Introduction to the Data
 - 1.1 Introduction
 - 1.2 Definitions and Plotting Conventions
 - 1.3 Electrical Noise
 - 1.4 Instrumentation
 - 1.5 Resistivity/Phase Data Acquisition and Field Logistics
 - 1.6 Harmonic Complex Resistivity Data Acquisition and Field Logistics
 - 1.7 Controlled Source AMT Data Acquisition and Field Logistics
 - 1.8 Data Processing Techniques, Resistivity/Phase and Complex Resistivity Data
 - 1.9 Parameters Used in Resistivity/Phase and Complex Resistivity Interpretation
 - References
 - 2. Interpreting Hydrocarbon Anomalies
 - 2.1 Introduction
 - 2.2 Statistical Analysis of Zonge Engineering Hydrocarbon Surveys, 1977 - 1982
 - 2.3 The Direct Detection of Hydrocarbons
 - 2.4 The Origin of Electrical Anomalies over Hydrocarbons
 - 2.5 Well-Casing Effects
 - 2.6 Surface Culture Effects

- 2.7 Topographic Effects
- 2.8 Subsurface Geologic Effects
- 2.9 Anomalies Due to Hydrocarbon Alteration - What to Look For
- References

IP-Petro_3.pdf

- PART THREE: CASE HISTORIES
 - 3. Ryckman Creek and Whitney Canyon Fields, Uinta County, Wyoming
 - 3.1 Introduction
 - 3.2 Geologic Background
 - 3.3 Detailed Discussion of the Data
 - 3.4 Summary and Conclusions
 - References

IP-Petro_4.pdf

- PART THREE: *(continued)*
 - 4. Desert Springs, Playa-Lewis, and Desert Springs West Fields, Sweetwater County, Wyoming
 - 4.1 Introduction
 - 4.2 Geologic Background
 - 4.3 Detailed Discussion of the Data
 - 4.4 Summary and Conclusions
 - References

IP-Petro_5.pdf

- PART THREE: *(continued)*
 - 5. Little Buck Creek Field, Niobrara County, Wyoming
 - 5.1 Introduction
 - 5.2 Geologic Background
 - 5.3 Detailed Discussion of the Data
 - 5.4 Summary and Conclusions
 - References

IP-Petro_6.pdf

- PART THREE: *(continued)*
 - 6. Lisbon Field, San Juan County, Utah
 - 6.1 Introduction
 - 6.2 Geologic Background
 - 6.3 Detailed Discussion of the Data
 - 6.4 Summary and Conclusions
 - References

IP-Petro_7.pdf

- PART THREE: *(continued)*
 - 7. Trap Spring Field, Nye County, Nevada
 - 7.1 Introduction
 - 7.2 Geologic Background
 - 7.3 Detailed Discussion of the Data
 - 7.4 Summary and Conclusions
 - References

IP-Petro_8.pdf

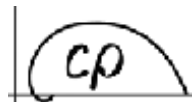
- PART FOUR: ADDITIONAL INFORMATION
 - 8. Mechanisms of Current Flow in the Earth
 - 8.1 Introduction
 - 8.2 Physical Mechanisms of Galvanic Current Flow
 - 8.3 The Origin of Inductive Coupling
 - References
 - 9. Principles of Electromagnetic Theory as Applied to Petroleum Exploration
 - 9.1 Introduction
 - 9.2 Maxwell's Equations
 - 9.3 Development of the Vector Wave Equation
 - 9.4 Boundary Conditions
 - 9.5 DC Solutions to the Vector Wave Equation
 - 9.6 AC Solutions to the Vector Wave Equation
 - 9.7 Complex Impedance of the Electric Field
 - References

IP-Petro_9.pdf

- PART FOUR: *(continued)*
 - 10. A Short History of Electrical Techniques in Petroleum Exploration
 - 10.1 Introduction
 - 10.2 The Early Years: 1900 - 1940
 - 10.3 Continued Development: 1940 - 1960
 - 10.4 Recent Electrical Work
 - 10.5 Into the Future
 - References
-

PROPRIETARY DATA SALE - 1983

Case Histories of an Electromagnetic Method for Petroleum Exploration



Zonge Engineering & Research Organization, Inc.

Note of Confidentiality

All data, interpretations, and conclusions in this volume which pertain to the case histories or data processing techniques are proprietary in nature and are covered by the non-disclosure agreement between Zonge Engineering and Research Organization, Inc., and the purchaser. No portion of this information may be disclosed to a third party until the expiration date of this agreement, which is January 1, 1988. The purchaser may copy portions of this volume for his own use within the normal course of business and under the provisions of the non-disclosure agreement, providing that proper credits are given to Zonge Engineering and Research Organization, Inc.

Copy No. _____ of _____ copies distributed to:

Issued to _____

Dr. Kenneth L. Zonge

Zonge Engineering & Research Organization, Inc.

3322 E. Fort Lowell Rd., Tucson, Arizona 85716 USA
Phone: (602) 327-5501 Telex: 165532 (CEERHO TUC)

Preface

"Case Histories of an Electromagnetic Method for Petroleum Exploration" is the culmination of five years of field measurements, theoretical studies, and research into the utility of multifrequency electrical measurements in hydrocarbon detection. This volume discusses in detail the current level of understanding by Zonge Engineering of how these types of data are interpreted, why anomalies are observed over hydrocarbon accumulations, which mechanisms cause the anomalies, and the importance of this information in drilling for oil and gas.

The work is divided into four parts for the convenience of the reader. Part One presents two summaries, the *Executive Summary*, which provides a general overview of the project, and the *Summary and Conclusions*, which offers a more detailed synopsis of the individual case histories and the results of other work over the past five years.

Part Two covers most of the topics needed to understand the case histories which follow. This includes a review of how the data are acquired, processed, and analyzed for trends indicative of alteration over hydrocarbon traps. A brief discussion of anomaly mechanisms is offered, as well as an analysis of spurious effects due to metal pipelines, well casings, topography, and subsurface geology.

Part Three presents the case histories, which are accompanied by geologic information and detailed data interpretations. The case histories involve 81 line-miles (130 line-km) of electrical data obtained over oil and gas fields in the Rocky Mountain and midwest regions of the United States.

Part Four includes supplementary information which would be of interest to those readers who require additional information on electrical methods. The material includes both a physical and a theoretical description of how electrical current flows through the earth and how **we** can make sense of all the data we obtain in the field work. The final chapter provides a historical review of electrical measurements as applied to petroleum exploration, as well as some possibilities for future research.

The general approach in this volume is to bring together many ideas and observations which may be valid in electrical exploration, to clear up several misconceptions, and to present electrical data in a way which (hopefully) will help direct further effort in productive directions. However, the real advances of the science lie beyond the presentation of more electrical data. Only through dedicated research of anomaly mechanisms and through a sustained program of geophysical discoveries can the true potential of electrical techniques be fully realized as a valuable supplement to ongoing seismic and geologic exploration programs.

Larry Hughes
March, 1983

Acknowledgments

Putting this volume together has been a fascinating exercise in trying to enlarge the science of electrical exploration, and the satisfaction of having found some preliminary answers is the chief reward of this effort. However, no scientific endeavor is without its human aspects, and it is really humanity which helps give some perspective to scientific inquiry. Many thanks are owed, first and foremost, to the employees of Zonge Engineering for their hard work and cooperation in this and in related efforts. I wish to specifically thank several persons who have been instrumental in publishing this volume: Ken Zonge, for his efforts in reprocessing all the data and for the many helpful suggestions made along the way; Norman Carlson, for much of the processing, modeling, and interpretation, as well as a fortuitously timed Chateau Margaux '78; and my wife, Laura, for her great patience.

I also wish to thank Anne Urizar, for a tremendous drafting effort; Sheryl Recker, Tammy Zonge, Julie Gabriel, and Anne Olson, for typing and finalizing a hastily scribbled manuscript without significant outbreaks of violence; Marjorie Cole, for helping with the programming and modeling; Anita Pape for modeling and editing; and the field crews, for their conscientious efforts to obtain the best possible data. A number of other people helped greatly with the research and editing: Van Reed, Angus Scott-Fleming, Victoria Foscz, Bill Clapper, Don ("Elmo") Chislow, Debbie Newkirk, and Ross Rosenwald. I wish to express my special appreciation to Richard Clark, for putting a banana in my desk. It's still there, Richard.

L.J.H.
Tucson, Arizona

Table of Contents

Note of Confidentiality	i
Preface	v
Acknowledgments	vii
Table of Contents	ix

PART ONE: SUMMARIES

Executive Summary	1
Summary and Conclusions	5

PART TWO: DATA INTERPRETATION

1. Introduction to the Data	25
1.1 Introduction	
1.2 Definitions and Plotting Conventions	
1.3 Electrical Noise	
1.4 Instrumentation	
1.5 Resistivity/Phase Data Acquisition and Field Logistics	
1.6 Harmonic Complex Resistivity Data Acquisition and Field Logistics	
1.7 Controlled Source AMT Data Acquisition and Field Logistics	
1.8 Data Processing Techniques, Resistivity/Phase and Complex Resistivity Data	
1.9 Parameters Used in Resistivity/Phase and Complex Resistivity Interpretation	
References	
2. Interpreting Hydrocarbon Anomalies	55
2.1 Introduction	
2.2 Statistical Analysis of Zonge Engineering Hydrocarbon Surveys, 1977 - 1982	
2.3 The Direct Detection of Hydrocarbons	
2.4 The Origin of Electrical Anomalies over Hydrocarbons	
2.5 Well-Casing Effects	
2.6 Surface Culture Effects	
2.7 Topographic Effects	
2.8 Subsurface Geologic Effects	
2.9 Anomalies Due to Hydrocarbon Alteration - What to Look For	
References	

PART THREE: CASE HISTORIES

3. Ryckman Creek and Whitney Canyon Fields, Uinta County, Wyoming	101
3.1 Introduction	
3.2 Geologic Background	
3.3 Detailed Discussion of the Data	
3.4 Summary and Conclusions	
References	
4. Desert Springs, Playa-Lewis, and Desert Springs West Fields, Sweetwater County, Wyoming	141
4.1 Introduction	
4.2 Geologic Background	
4.3 Detailed Discussion of the Data	
4.4 Summary and Conclusions	
References	

5. Little Buck Creek Field, Niobrara County, Wyoming 169

- 5.1 Introduction
- 5.2 Geologic Background
- 5.3 Detailed Discussion of the Data
- 5.4 Summary and Conclusions
- References

6. Lisbon Field, San Juan County, Utah

- 6.1 Introduction
- 6.2 Geologic Background
- 6.3 Detailed Discussion of the Data
- 6.4 Summary and Conclusions
- References

7. Trap Spring Field, Nye County, Nevada

- 7.1 Introduction
- 7.2 Geologic Background
- 7.3 Detailed Discussion of the Data
- 7.4 Summary and Conclusions
- References

PART FOUR: ADDITIONAL INFORMATION

8. Mechanisms of Current Flow in the Earth 283

- 8.1 Introduction
- 8.2 Physical Mechanisms of Galvanic Current Flow
- 8.3 The Origin of Inductive Coupling
- References

9. Principles of Electromagnetic Theory as Applied to Petroleum Exploration 293

- 9.1 Introduction
- 9.2 Maxwell's Equations
- 9.3 Development of the Vector Wave Equation
- 9.4 Boundary Conditions
- 9.5 DC Solutions to the Vector Wave Equation
- 9.6 AC Solutions to the Vector Wave Equation
- 9.7 Complex Impedance of the Electric Field
- References

10. A Short History of Electrical Techniques in Petroleum Exploration 315

- 10.1 Introduction
- 10.2 The Early Years: 1900 - 1940
- 10.3 Continued Development: 1940 - 1960
- 10.4 Recent Electrical Work
- 10.5 Into the Future
- References

PART ONE

SUMMARIES

Executive Summary

RESULTS OF THE STUDY

The results of a five-year feasibility study of the utility of electrical measurements in petroleum exploration are very encouraging. Electrical anomalies were measured over 66% of the 29 oil and gas fields involved in the study. The fact that these fields represent both stratigraphic and structural traps at a wide range of depths, with varying production characteristics, and in diverse geologic environments, provides a particularly favorable indication that this technique can be used as a reliable exploration tool, complementing existing seismic and subsurface geology programs.

Case histories of five field projects are presented in this volume in order to illustrate both the advantages and limitations of the method in the context of known geology. The field projects involve a variety of field characteristics, as illustrated in Table 1. The results delineate the following general observations: 1) repeatable anomalies can be measured over oil and gas fields; 2) two types of anomalies are measured—an electrically conductive "deep anomaly," and a polarizable "shallow anomaly;" 3) the anomalies correlate relatively well in plan view with the limits of hydrocarbon production; 4) the anomalies are partly dependent on specific geologic characteristics of the stratigraphic sequence.

TABLE 1
GEOLOGIC CHARACTERISTICS OF FIELDS IN CASE HISTORIES

Field and Location	Type of Trap	Original Reserves		Production Depths (feet)
		Oil (MMBO)	Gas (BCF)	
Ryckman Creek (W. Wyoming Overthrust)	Structural	50	150	7,800 - 9,800
Whitney Canyon (W. Wyoming Overthrust)	Structural	66	3,100	9,200 - 14,200
Desert Springs (Green River Basin)	Stratigraphic	3	410	5,100 - 6,000
Playa-Lewis (Green River Basin)	Stratigraphic	--	9	3,400 - 3,500
Desert Springs West (Green River Basin)	Stratigraphic	1	15	3,800 - 3,850
Little Buck Creek (Powder River Basin)	Structural	12	--	3,750 - 5,950
Lisbon (Paradox Basin)	Structural	44	250	7,500 - 8,500
Trap Spring (Basin & Range)	Structural & Stratigraphic	5	--	3,000 - 5,000
Garza (Eastern Shelf, Texas) ¹	Stratigraphic	?	--	2,900 - 3,300

¹Not included specifically as a case history, but described in the text.

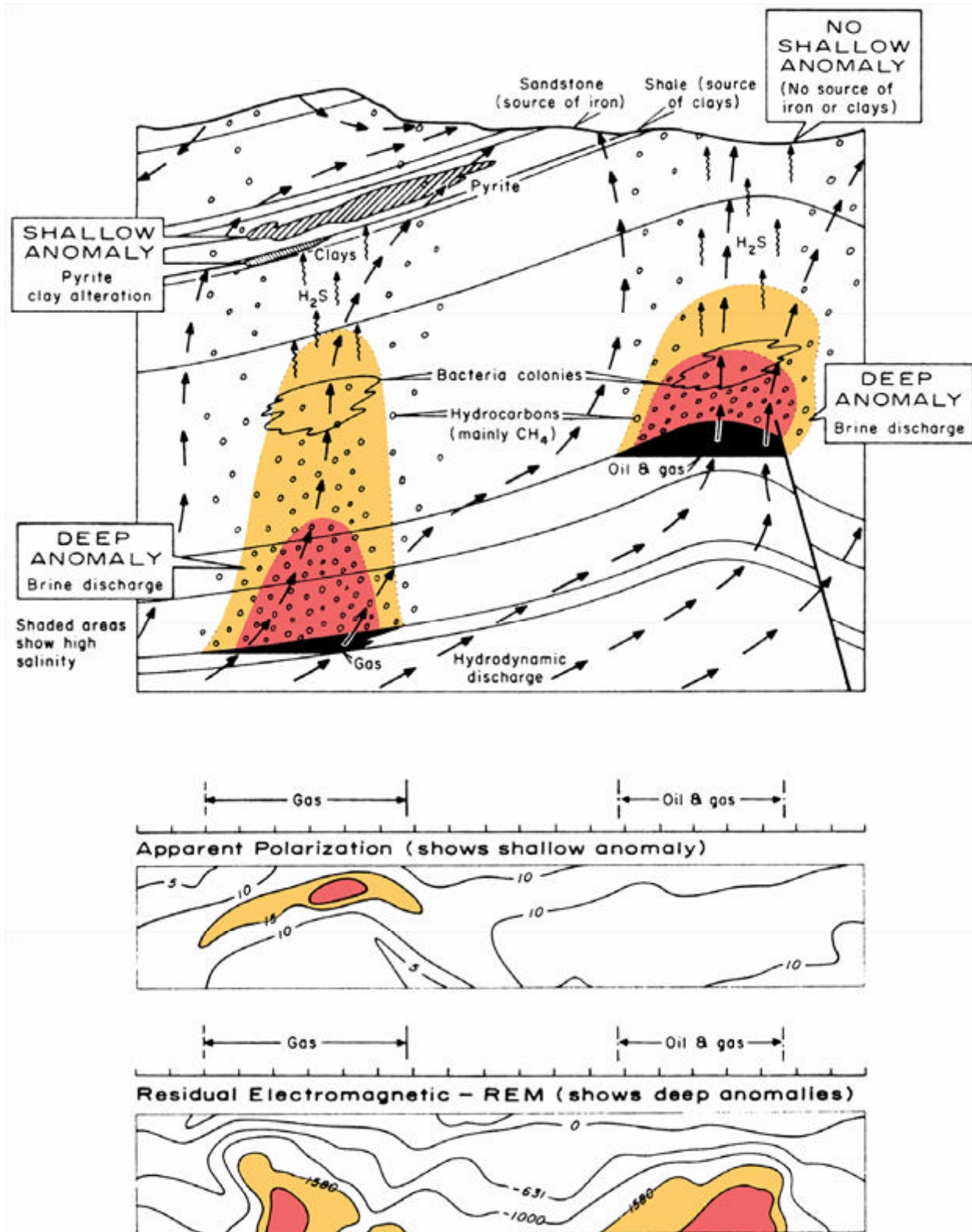


Figure 1. Schematic representation of the chief mechanisms which may be responsible for electrical anomalies over hydrocarbons, and of typical data sets used for interpretation. A third data set, apparent resistivity, is also used for interpretation but is not illustrated here.

As is the case in seismic interpretations, data processing techniques are crucially important in extracting the maximum of information from electrical data. Proprietary data processing techniques have been developed for this purpose. Great care must be taken during interpretation to evaluate effects of pipelines, well casings, topography, and subsurface geology, since many of these effects may result in spurious anomalies unrelated to alteration due to hydrocarbons. The case histories demonstrate the necessity for this type of evaluation.

ORIGIN OF THE ANOMALIES

Strong theoretical and empirical evidence is offered to demonstrate that hydrocarbons are not being detected directly. Instead, evidence shows that the technique is most sensitive to alteration of sediments overlying the oilfield. The alteration may be due to upward migration of saline waters and separate-phase light hydrocarbons from the trap at depth. The driving mechanism for the upward migration is probably related to vertical hydraulic gradients in porous traps. These ideas are in keeping with many recent hydrologic, geologic, geochemical and theoretical investigations, and are specifically compatible with modern theories of hydrodynamic control of petroleum accumulation.

Figure 1 illustrates the essential aspects of the theory of anomaly generation. The "deep anomaly" appears to be related to slow brine discharge from the traps. The "shallow anomaly" is attributed to one or both of two effects: 1) alteration of the cation-exchange characteristics of layered silicates (primarily clays); 2) the genesis of micron-sized, disseminated pyrite by the chemical combination of iron oxides in sandstones with biogenic hydrogen sulfide. The pseudosections in the lower portion of Figure 1 represent typical data from two parameters normally used for interpretation of the "deep" and "shallow" anomalies.

EXPLORATION STRATEGY

The unique sets of information offered by seismic and electrical programs suggest using both in an integrated exploration strategy. Seismic data would be essential to providing structural detail of the subsurface, since the lateral and horizontal resolution of seismics is distinctly superior to that of electrical techniques. On the other hand, electrical techniques would be used as indirect, economical methods of evaluating the presence of hydrocarbons by detection of altered sediments above the traps. They would also offer information in areas of difficulty in seismic exploration, such as exploration for subtle stratigraphic traps, and in areas involving severely weathered overburdens, surface volcanics, fractured evaporites, etc. Thus, the combined efforts of geologic, seismic, and electrical programs should prove to be an effective strategic approach to evaluating hydrocarbon potential in geologically attractive target areas.

Summary and Conclusions

INTRODUCTION

Extensive field research and theoretical studies conducted over the past five years have demonstrated that valid electrical anomalies have been measured consistently over oil and gas fields of diverse geologic characteristics, and that these anomalies are probably related in a causal way to the presence of hydrocarbons at depth. This volume presents multifrequency electrical data over nine oil and gas fields as examples of typical anomalies measured in the field. These data strongly suggest that the sediments overlying the hydrocarbons are altered by upward migrating light hydrocarbons and saline waters. Several case histories are presented to illustrate "classical" type anomalies, while other case histories serve to refine current theory as to the specific mechanisms which produce the anomalies. A significant effort is made to identify electrical anomalies which are unrelated to alteration caused by hydrocarbons, such as those due to "culture" (well casings, pipelines, powerlines, fences, etc.), topography, and subsurface geology. As is the case with seismic exploration, the use of advanced data processing techniques is essential to the proper interpretation of these data.

TYPES OF DATA OBTAINED

The present study involves multifrequency resistivity/phase and complex resistivity data, in which both magnitude and phase angle are measured and corrected for array geometry. Data in the frequency range of 0.125 - 1 Hz were obtained with the dipole-dipole array, using currents of up to 18 amperes and dipoles as large as 2,000 feet (610 m). The equipment consisted of two-channel, fully programmable, 12-bit receivers (Figure 1). The data were originally obtained in 1979 and 1980. They have been reprocessed by proprietary techniques and have been reinterpreted with the aid of computer modeling.

Three unique parameters are derived from appropriate data processing techniques: apparent resistivity, apparent polarization, and residual electromagnetic (REM). Apparent resistivity measures the bulk resistance of the ground to the flow of current. Apparent polarization measures the capacitance, or energy storage characteristics of the ground. The REM parameter is an inductive parameter which senses relatively deep lateral resistivity interfaces in the ground. These three parameters are utilized most effectively when they are used together in an integrated interpretation. Figure 2 illustrates typical pseudosection plots of these parameters.

RESULTS OVER KNOWN FIELDS

The concepts presented in this volume were developed during five years of research into the utility of electrical techniques in petroleum exploration. Some 879 line-miles (1,414 line-km) of multifrequency data have been obtained over 29 oil and gas fields and 49 prospects in the United States and Canada (Figure 3). A number of projects have been conducted during this work in order to define the conditions under which the technique works best and to establish a statistically significant data base from which conclusions can be drawn.

The results of this work indicate that two types of anomalies are normally measured in the field. The most common type of anomaly is the so-called "deep anomaly," which consists of a conductive, plume-shaped structure extending vertically from the hydrocarbon trap into the overlying sediments. It is detected by the apparent resistivity and REM parameters. The "shallow anomaly" is much less common; it consists of a polarizable, occasionally conductive feature in the near-surface sediments. The "shallow anomaly" is normally detected by the apparent polarization parameter. The two types of anomalies appear to result from alteration of the

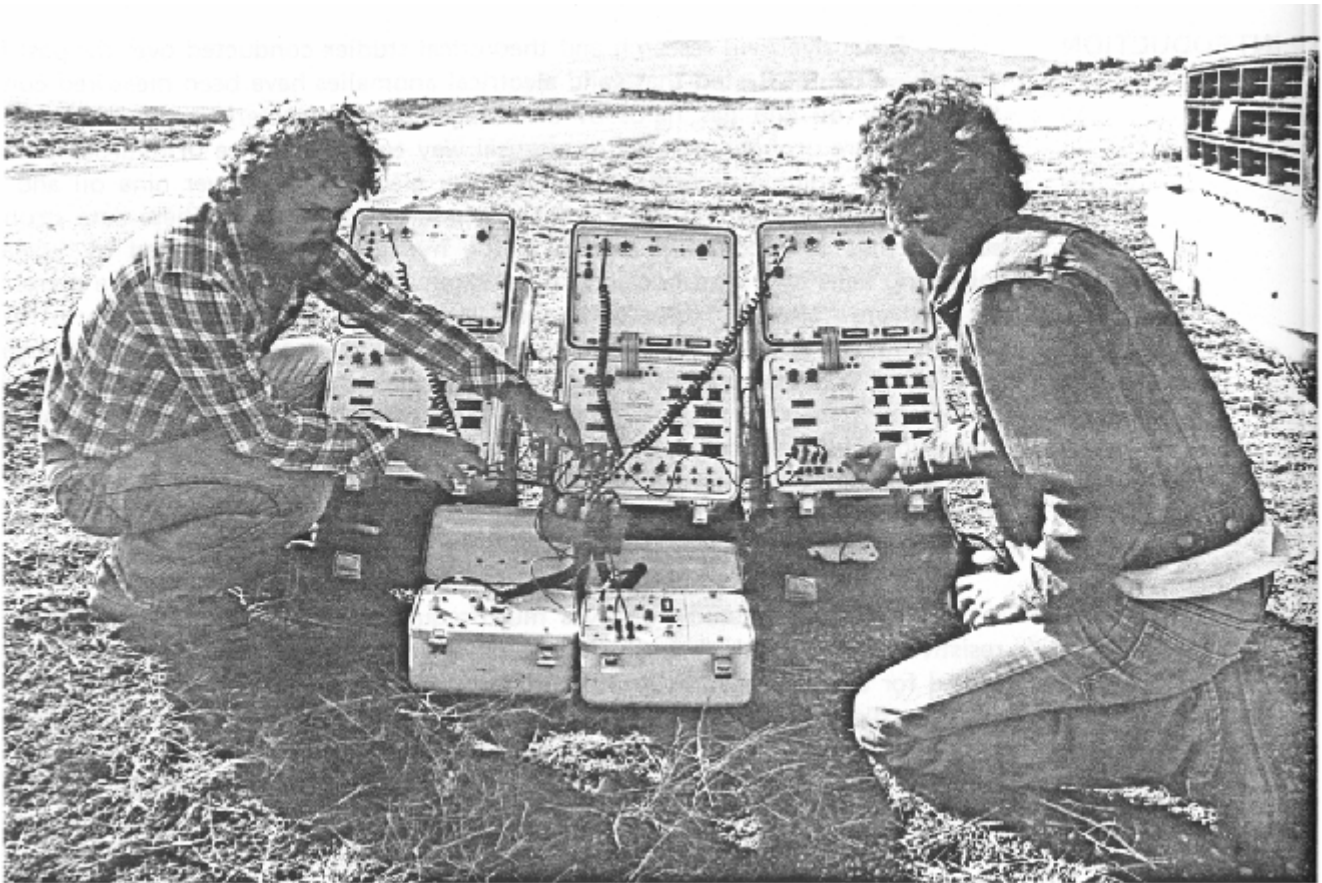


Figure 1. Equipment calibration and check prior to data acquisition at Lisbon Field. The field work involved a crew of eight, operating three backpack-mounted receivers simultaneously. Present-day surveys require smaller crews.

sediments above the hydrocarbon trap by upward-migrating hydrocarbons and saline waters. The alteration mechanisms involve brine replacement of more resistive meteoric waters, clay alteration, and sulfide mineralization (primarily pyrite).

In an effort to establish the frequency with which these anomalies are measured, a statistical analysis was performed of all projects in the Zonge Engineering data base. Apparent resistivity, apparent polarization and REM anomalies were interpreted for spurious effects due to well casings, surface culture, topography, and subsurface structure, and were then analyzed for correlation with the lateral extent of the hydrocarbons at depth. The results of this investigation show that at least one of the three parameters normally used for interpretation shows a recognizable anomaly over 66 percent of the fields. Conductive apparent resistivity and REM anomalies were seen over about two-thirds of the fields, and polarizable anomalies were observed over about one-fourth of the fields. While it is likely that some of the data are still influenced by cultural and structural effects (which are exceedingly difficult to model in some cases), it is clear that a success ratio even as low as 50 percent would be an encouragement to utilize electrical techniques in prospect evaluation. Preliminary statistics on the drilling of electrical prospects suggest that the success ratio is probably much higher than 50 percent, probably because data over prospects are often less contaminated by cultural effects than are data over heavily developed fields.

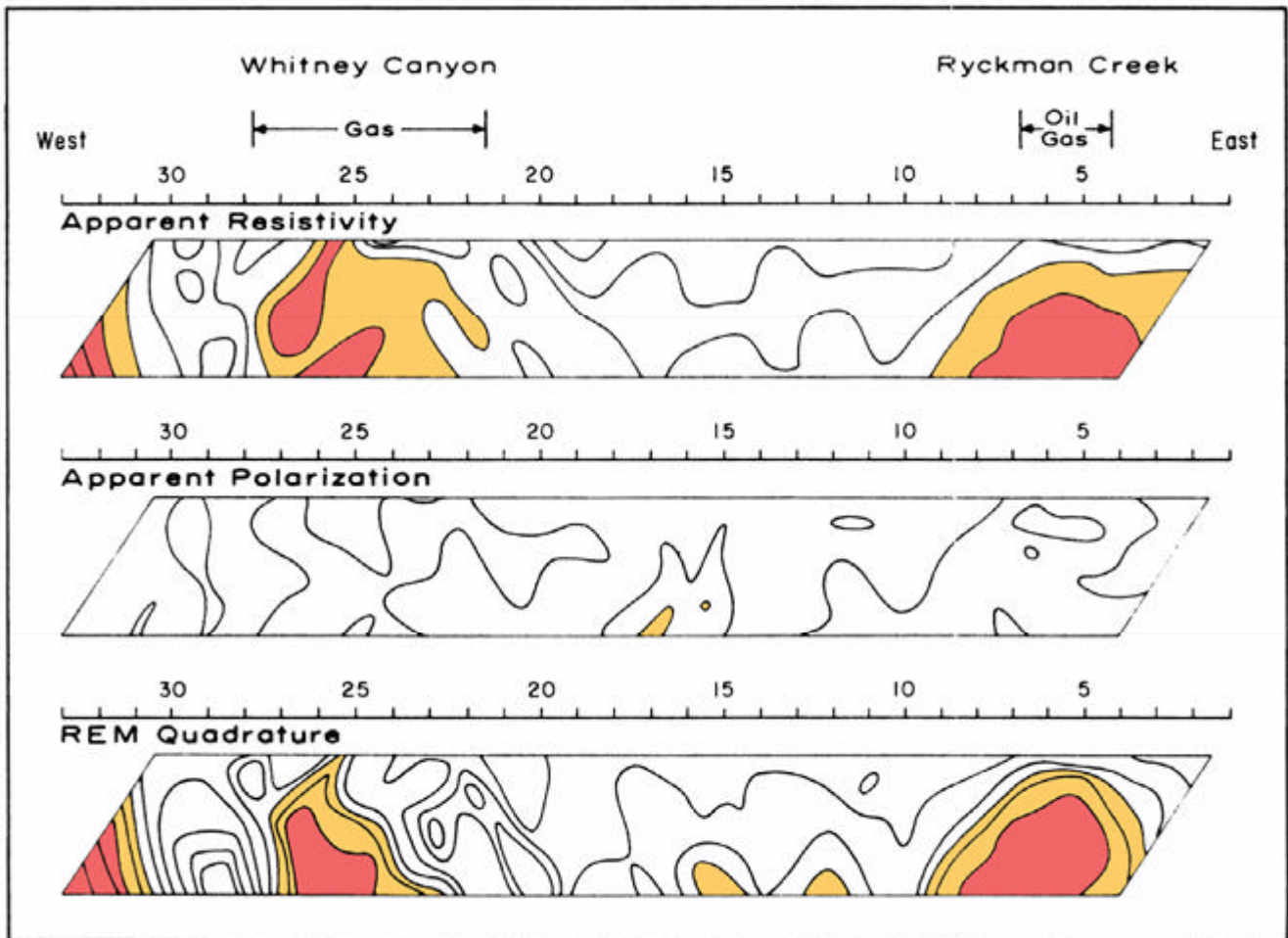


Figure 2. Typical data from a hydrocarbon survey are presented in pseudosection form, plotted here for the Ryckman Creek and Whitney Canyon survey. Shaded areas indicate electrically conductive zones (apparent resistivity and REM data) or electrically polarizable zones (apparent polarization data).

SUMMARY OF THE CASE HISTORIES

The work done over the 29 fields is represented fairly well both statistically and geologically by the nine case histories presented in this volume. The case histories show a similar "success rate" in apparent resistivity and REM parameters as compared to the larger group, and a somewhat higher "success rate" in apparent polarization. In addition, the case histories show a higher percentage of "uninterpretable" resistivity and REM data due to cultural or subsurface faulting problems. This reflects the fact that the case histories represent a somewhat more difficult group of projects than the larger group of 29 projects.

As shown in Tables 1 and 2, the case histories vary considerably in geologic Characteristics - so much so that, collected together in one volume, they present an excellent opportunity to examine some important aspects of the possible driving mechanisms for the "deep" and "shallow" anomalies. The locations of the fields are shown in Figure 4. Ryckman Creek and Whitney Canyon present classic examples of well-defined anomalies. The line in the Desert Springs area shows how the anomalies change over depressurized stratigraphic reservoirs, while the data obtained over Little Buck Creek demonstrate a similarly depressurized and even more highly depleted reservoir in a structural trap. Data over Lisbon Field provide a fascinating but enigmatic view of how the anomalies are affected by a low-permeability evaporite layer which ov-

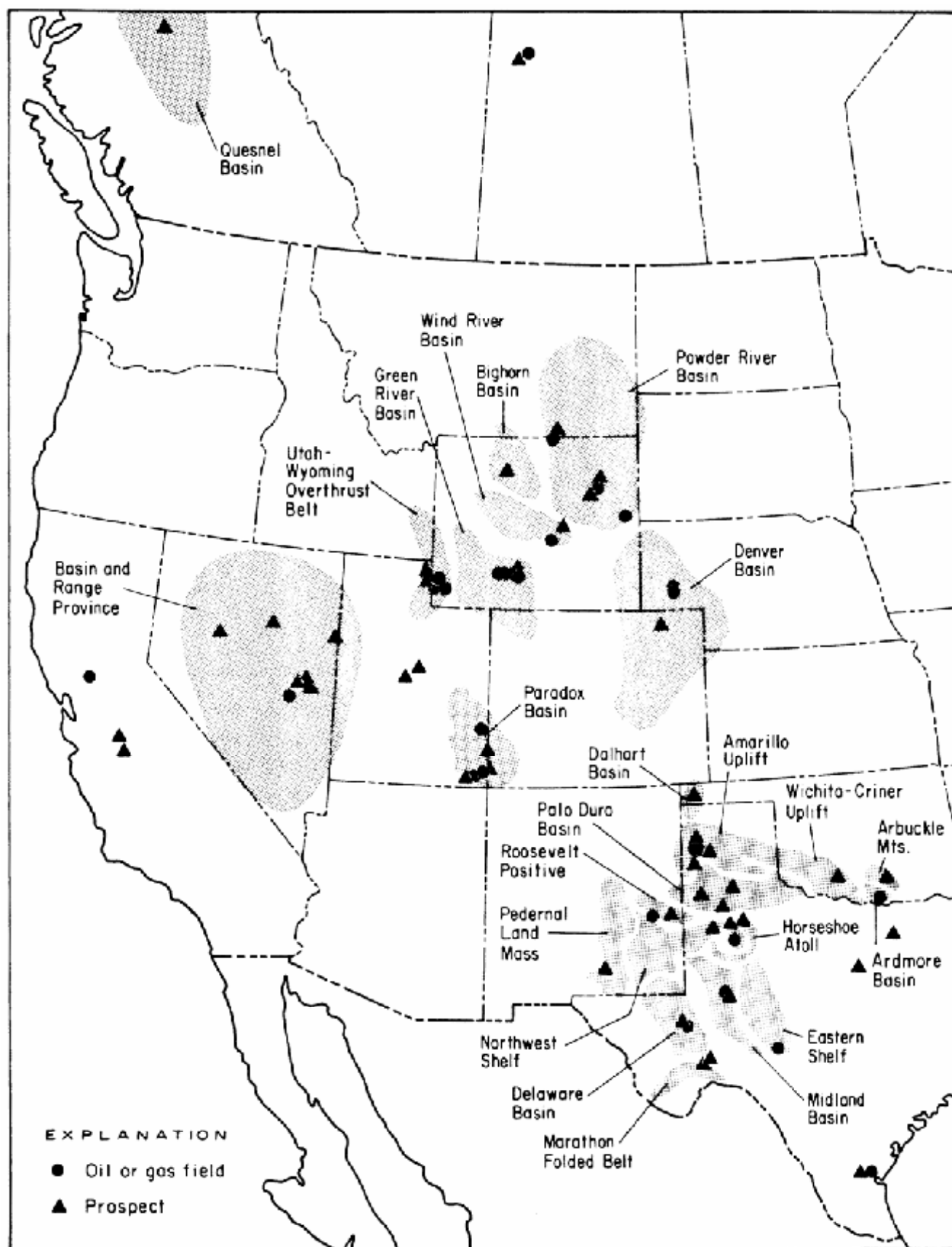


Figure 3. Locations of Zonge Engineering hydrocarbon surveys, 1977 - 1982.

TABLE 1: GEOLOGIC CHARACTERISTICS OF FIELDS IN CASE HISTORIES

Field & Location	Discovery Date	Type of Trap	Drive	Original Reserves	
				Oil (MMBO)	Gas (BCFG)
RYCKMAN CREEK W. Wyoming Overthrust Uinta Co., Wyoming	1976	Structural (thrust-faulted anticline)	Water	50	150
WHITNEY CANYON W. Wyoming Overthrust Uinta Co., Wyoming	1977	Structural (thrust-faulted anticline)	Gas expansion	66	3,100
DESERT SPRINGS Green River Basin Sweetwater Co., Wyoming	1958	Stratigraphic (updip facies pinchout)	Pressure depletion	2.5	410
PLAYA-LEWIS Green River Basin Sweetwater Co., Wyoming	1963	Stratigraphic (isolated sand lens)	Pressure depiction	- -	> 9
DESERT SPRINGS WEST Green River Basin Sweetwater Co., Wyoming	1959	Stratigraphic	Solution gas	1	15
LITTLE BUCK CREEK Powder River Basin Niobrara Co., Wyoming	1944	Structural (anticline)	Water	12	- -
LISBON Paradox Basin San Juan Co., Utah	1960	Structural (faulted anticline)	Expanding gas cap & gravity drainage (Leadville); Solution gas (McCracken)	44	250
TRAP SPRING Basin and Range Nye Co., Nevada	1976	Structural & stratigraphic	Water	> 5	- -
GARZA ¹ Eastern Shelf (Texas) Garza Co., Texas	1935	Stratigraphic	?	0.3 ²	- -

¹ Not presented as a case history, but results presented in Chapter 2.² In the vicinity of the survey line only; total field reserves are much larger.

erlies the reservoir rocks. Finally, the data over Trap Spring show the effects observed over a tight volcanic-tuff reservoir in which the oils contain no dissolved methane at all. An additional, abbreviated case history over Garza Field shows data over a well-developed but still productive stratigraphic trap before and after development drilling.

TABLE 2: RESERVOIR CHARACTERISTICS OF FIELDS IN CASE HISTORIES

Field, Producing Formation & Age	Approx. Production Depth (feet)	Field Exploitation ¹			% Methane in Trap	% H ₂ S	Connate Water Resistivity (ohm-meters)
		% Decline in Oil Reserves	% Decline in Gas Reserves	% Decline in Reservoir Pressure			
RYCKMAN CREEK		minor	minor	minor ²	normal	none	low
Nugget Ss. (TR)	7,800	3	2	4	78	0	0.2
Thaynes Ls. (TR)	9,800				79	0	
WHITNEY CANYON		minor	minor	none	normal	very high	moderate
Thaynes Ls. (TR)	9,200	minor	minor	up 1	80	0	1.05
Phosphoria Fm. (P)	11,800	0	0	0	74	6.7	
Weber Ss. (P)	11,200	0	0	0	57	21.3	
Mission Canyon Fm. (M)	12,600	0	0	0	67	15.2	
Lodgepole Ls. (M)	13,000	0	0	0		15.5	
Darby Fm. (D)	13,500	0	0	0		1.0	
Bighorn Dol. (O)	14,200	0	0	0	85	0.6	0.12
DESERT SPRINGS		major	major	major	normal	low	low
Almond Fm. (K)	5,900	90	49	54	89	< 0.1	0.5
PLAYA-LEWIS			major	major	normal		low
Lewis Sh. (K)	3,500	--	68	54			0.18
DESERT SPRINGS WEST		major	major	major	normal	low	moderate
Almond Fm. (K)	3,800	74	98		91	0.03	1.2
LITTLE BUCK CREEK		major	--			moderate	low
Fall River Ss. (K)	3,850	major	--			0.06	
Minnelusa Fm. (P)	5,500	major	--			0.63	0.2
LISBON		major	minor	minor	normal	high	very low
Leadville Fm. (M)	8,000	major	minor ³	minor ³	50	2	0.05
McCracken Ss. (D)	8,300	--					0.05
TRAP SPRING		moderate	--		low	moderate	moderate
Pritchards Stn. Fm. (T)	> 3,200	moderate	--		0	0.8	1
GARZA⁴		moderate	--		normal		very low
San Andres Fm. (P)	3,000	moderate	--				0.04

¹ Exploitation between discovery date and date of the electrical survey.

² Pressure maintained by gas injection.

³ Gas stripped and re-injected; minimal pressure depletion.

⁴ Not presented as a case history, but results presented in Chapter 2.

Ryckman Creek and Whitney Canyon

Chapter 3 presents case histories of Ryckman Creek and Whitney Canyon fields, two very important producers in the western Wyoming Overthrust Belt. Ryckman Creek production occurs from an asymmetric, overturned, north-south trending anticline on the hanging wall of the Absaroka Thrust Plate, a major feature in Overthrust geology. Low-sulfur, paraffinic, 47° API gravity oil and sweet gas are found in the Triassic Nugget Sandstone. At present, oil is recovered, and gas is stripped and re-injected back into the structure in order to maintain the reservoir pressure. The system has an active water drive. Natural gas and condensate are also produced from the Triassic Thaynes Limestone. Whitney Canyon is a gas giant, with over 3.1 TCF of gas reserves. Sour gas and condensate are produced from seven pay zones in a thrust-faulted anticlinal trap similar to that at Ryckman Creek. At the time of the electrical survey, most of the wells were shut-in awaiting completion of a gas-sweetening plant, and reservoir pressures and gas reserves were virtually unchanged from the date of discovery. Most of the gas is found in the Mission Canyon Formation of Mississippian age, but other productive zones are found in Triassic to Ordovician units. The system

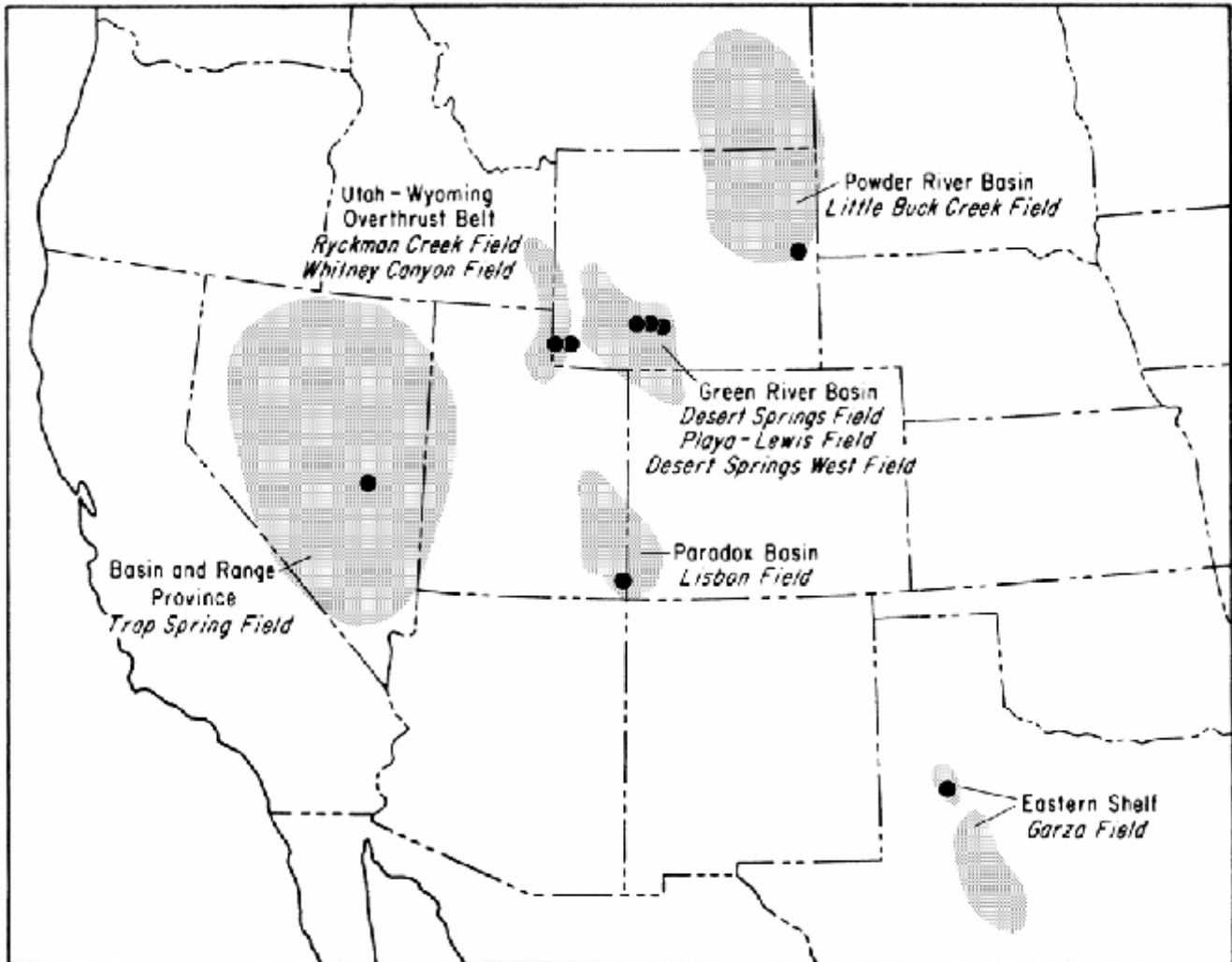


Figure 4. Locations of the case histories in this volume.

has a gas-expansion drive. Figure 5 shows the geology and inferred electrical cross-section for the project.

The case history of Whitney Canyon Field provides a classic example of a "deep" hydrocarbon-type anomaly. The apparent resistivity and REM data show strong conductive anomalies which correlate well with the lateral extent of the hydrocarbons at depth. The anomalies appear to extend from near the surface to considerable depth. Since development of the field was in suspension at the time of the survey, cultural interference was minimal. Modeling shows conclusively that the anomaly cannot be attributed to the effects of well casings, pipelines, or any other forms of culture. A study of the subsurface geology at Whitney Canyon rules out structure as an explanation of the anomaly, and modeling shows that the anomaly is not caused or significantly enhanced by the effects of topography. Hence, the very strong, conductive anomaly at Whitney Canyon appears to be the result of electrochemical alteration of some 2,500 feet (750 m) of Tertiary and Cretaceous sediments which overlie the overthrust strata. The direct correlation of the alteration zone with the lateral location of the hydrocarbons at depth suggests that the two are causally related. It is believed that the 4,500 feet (1,400 m) of closure in the Whitney Canyon anticline and the active gas-expansion

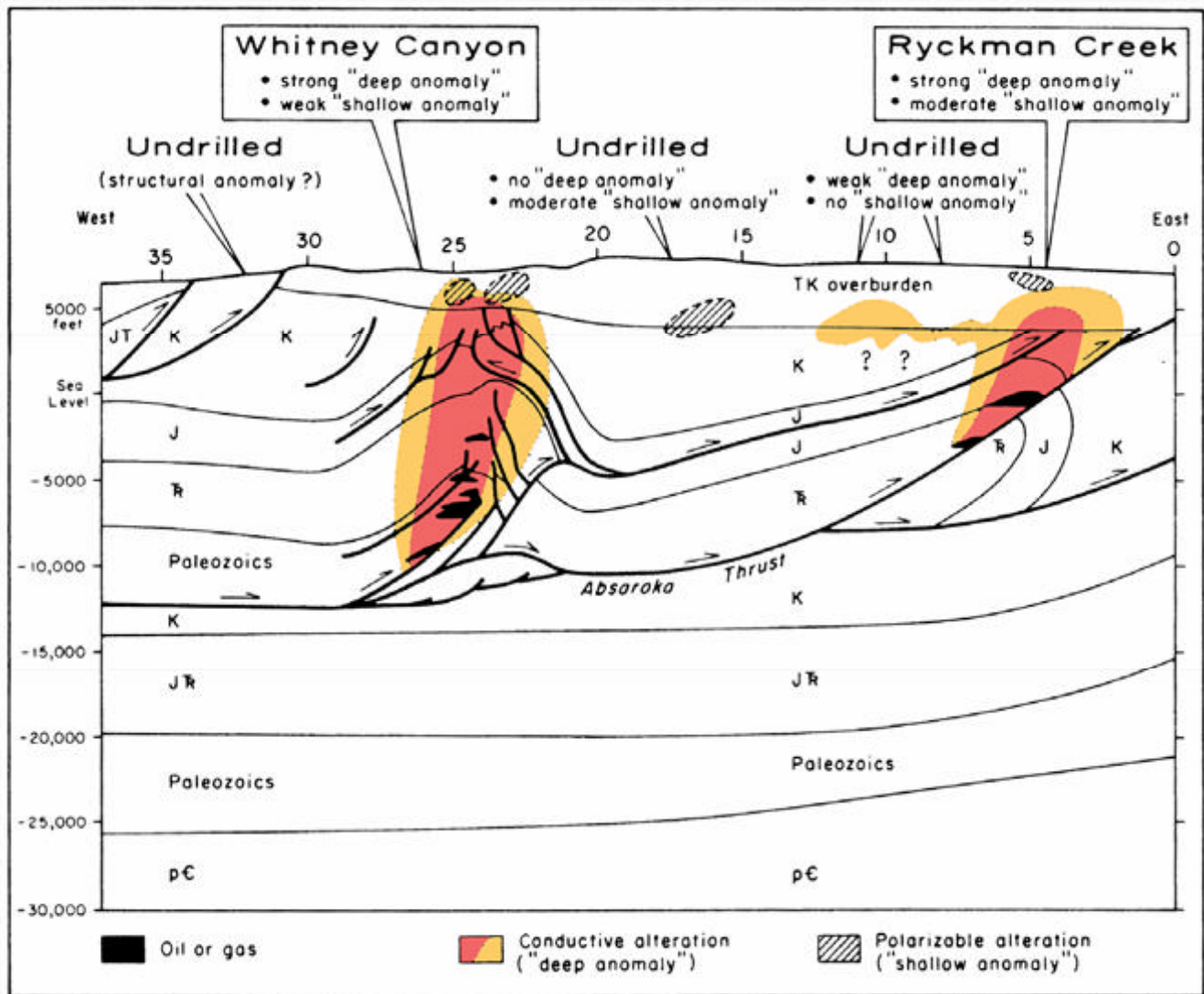


Figure 5. Combined geological and electrical cross-section of the Ryckman Creek / Whitney Canyon line, with no vertical scale exaggeration. The maximum depth of penetration of the electrical data is about 4,000 to 6,000 feet (1,200-1,800 m); the electrical interpretation below these depths is inferred.

drive there provides a strong hydraulic gradient which forces the lighter hydrocarbons and conductive brines vertically out of the trap into the overlying sediments. The brines would lower the bulk resistivities of the sediments either by displacing pore fluids of higher resistivities or by alteration of clays.

Whitney Canyon also shows a weak, polarizable, "shallow" type anomaly which correlates reasonably well with the lateral location of the hydrocarbons. This anomaly cannot be explained by effects due to well casings, surface culture, or subsurface structure. Instead, it is believed to be related to weak mineralization or clay alteration in the near-surface sediments due to upward migration of light hydrocarbons and waters from the trap below.

Ryckman Creek is located 6 miles (10 km) east of Whitney Canyon. The field shows a strong, conductive, "deep anomaly" which is somewhat broader than the extent of the hydrocarbons, partly because of influences from overthrust strata which become shallower east of the field, and partly because of the influence of subsurface thrust faulting on water and hydrocarbon migration from the trap. A well-casing model clearly "overmodels" the data (that is, calculates too strong an effect), but the qualitative results of the model suggest that the anomaly may be explained either by effects of well casings or by hydrocarbon-related alteration. The latter explanation is preferred because of the apparent lack of response of well casings at Whitney Canyon. The 1,500 feet (450 m) of structural closure and the active water drive at Ryckman Creek make it an ideal example of a strong driving mechanism for brine discharge, which is believed to cause the "deep" conductive anomaly.

A fairly polarizable "shallow anomaly" correlates well with Ryckman Creek Field. Modeling indicates that this anomaly is not caused by cultural or structural features, although effects of well casings may enhance the overall response. The anomaly is believed to be related to clay alteration or pyrite mineralization in the shallow sediments, caused by interactions with upward-migrating hydrocarbons and waters from the trap below.

Two other "deep" anomalies which are as yet undrilled are observed on the Ryckman Creek - Whitney Canyon line. A broad, conductive zone at depth just west of Ryckman Creek is a reasonably attractive electrical target. It may possibly be related to a recent Ankareh discovery just 0.5 mile (0.8 km) south of the line. A combined electric-seismic-geologic investigation of this portion of the line would provide an optimum exploration strategy. A second anomaly occurs on the west end of the line. Although insufficient coverage of this feature prevents any conclusive interpretation regarding its origin, it lies on the portion of the line where Mesozoic strata are thrust to the surface by high-angle thrust faulting; hence, the anomaly may be more related to structure than to hydrocarbon-related alteration. This illustrates the necessity of thorough geologic analysis in interpreting electrical anomalies.

**Desert Springs,
Playa-Lewis,
and Desert
Springs West**

Chapter 4 presents data from three fields which differ considerably from Ryckman Creek and Whitney Canyon. Desert Springs, Playa-Lewis, and Desert Springs West production is primarily low-sulfur gas from stratigraphic traps at intermediate depths. Desert Springs gas production in the vicinity of the line is from two sandstone units in the upper Cretaceous Almond Formation. The sands pinch out on their updip sides by a facies change to shales and siltstones; production is limited downdip by the gas-water contact and laterally by facies changes and structure. The drive is pressure depletion. Playa-Lewis gas production is from an isolated sandstone lens in the Lewis Shale of upper Cretaceous age. The field has a pressure-depletion drive. Desert Springs West produces gas along a narrow corridor which crosses the west end of the survey line. The reservoir consists of thin, discontinuous, shoreline sands within the Almond Formation. The field has a solution-gas drive. The important things to note in the reservoir data of Table 2 are the depletion of hydrocarbon reserves in the traps (50 to 90 percent), and the depressurization of the reservoirs (around 50 percent or so). If the present theory as to the anomaly mechanism is correct, the depletion of pressure and hydrocarbon reserves should considerably weaken the driving mechanisms which produce electrical anomalies. Hence, this case history provides an opportunity to test the mechanism over three nearly depleted fields. The interpreted geoelectric cross-section is shown in Figure 6.

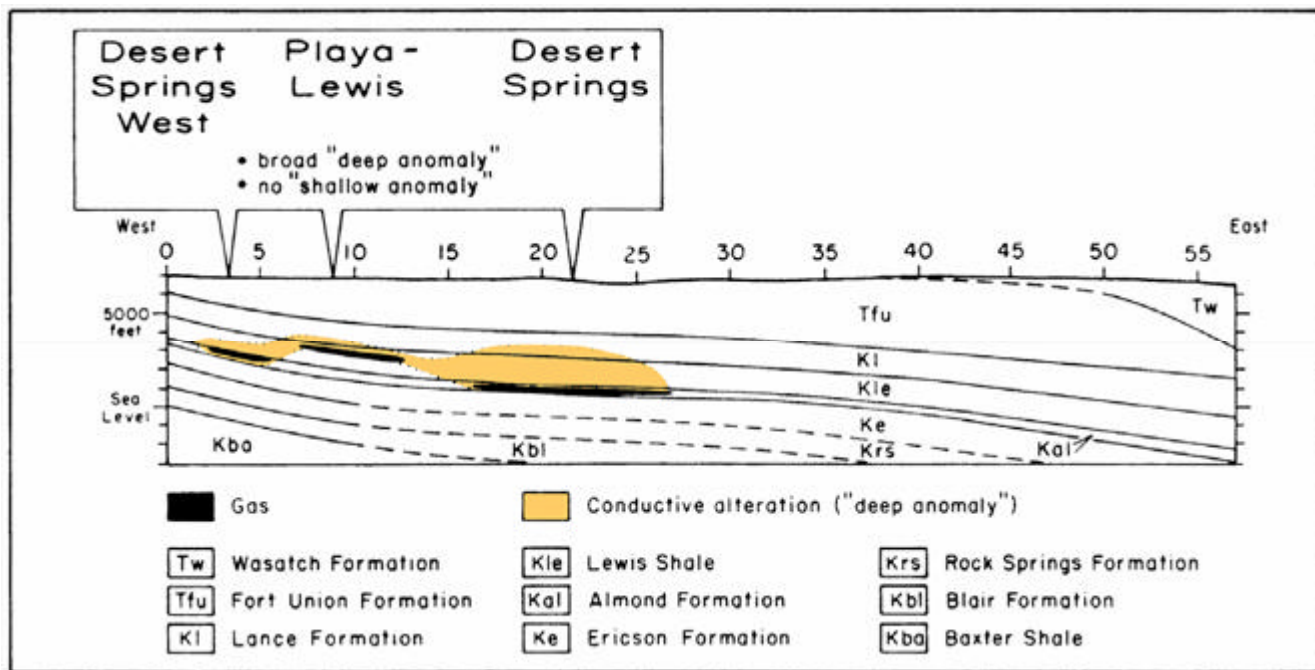


Figure 6. Combined geological and electrical cross-section of the Desert Springs | Playa-Lewis | Desert Springs West line, with no vertical scale exaggeration. The maximum depth of penetration of the electrical data is about 4,000 to 6,000 feet (1,200-1,800 m); the electrical interpretation below these depths is inferred.

The single electrical survey line traversed 10 miles (16 km) of productive area and 10 miles (16 km) of non-productive area. The productive area shows a broad, distinctive, conductive zone at depth, whereas the non-productive area does not. Apart from this broad conductive zone and a culturally-induced anomaly over Desert Springs, none of the three fields shows a strong, unique conductive anomaly which can be specifically related to alteration directly above the hydrocarbons. This is precisely what would be expected from a nearly depleted field: the pressure reduction in the trap would drastically reduce the solubility of salts, perhaps causing them to precipitate before being supplied to the overlying sediments. The broad, weak anomaly over the fields indicates that the anomaly mechanism is not yet completely neutralized.

No "shallow" anomalies are seen over any of the three fields. This suggests two possibilities: 1) "shallow" anomalies never existed in the area; 2) the anomalies existed once, but they were dependent upon resupply of hydrocarbons to maintain the anomalies, a supply which diminished as the reserves at depth were depleted. If true, this possibility could provide important information regarding migration speed.

Little Buck Creek

The discussion of depressurized reservoirs in the Desert Springs area is followed in Chapter 5 by a slightly different example over Little Buck Creek Field. This field produces oil from an anticlinal structural trap. There are three producing horizons: the lower Cretaceous Fall River Sandstone (Dakota Sandstone), the Converse sands of the Permian Minnelusa Formation, and the Leo sands of the Minnelusa. The oils are brown to green with gravities of 33° to 42° API. The field has a water drive. The Little Buck Creek reserves are almost completely exhausted; average production for the entire 34-well field is currently only 50 barrels per day. Figure 7 shows the interpreted geoelectric cross-section.

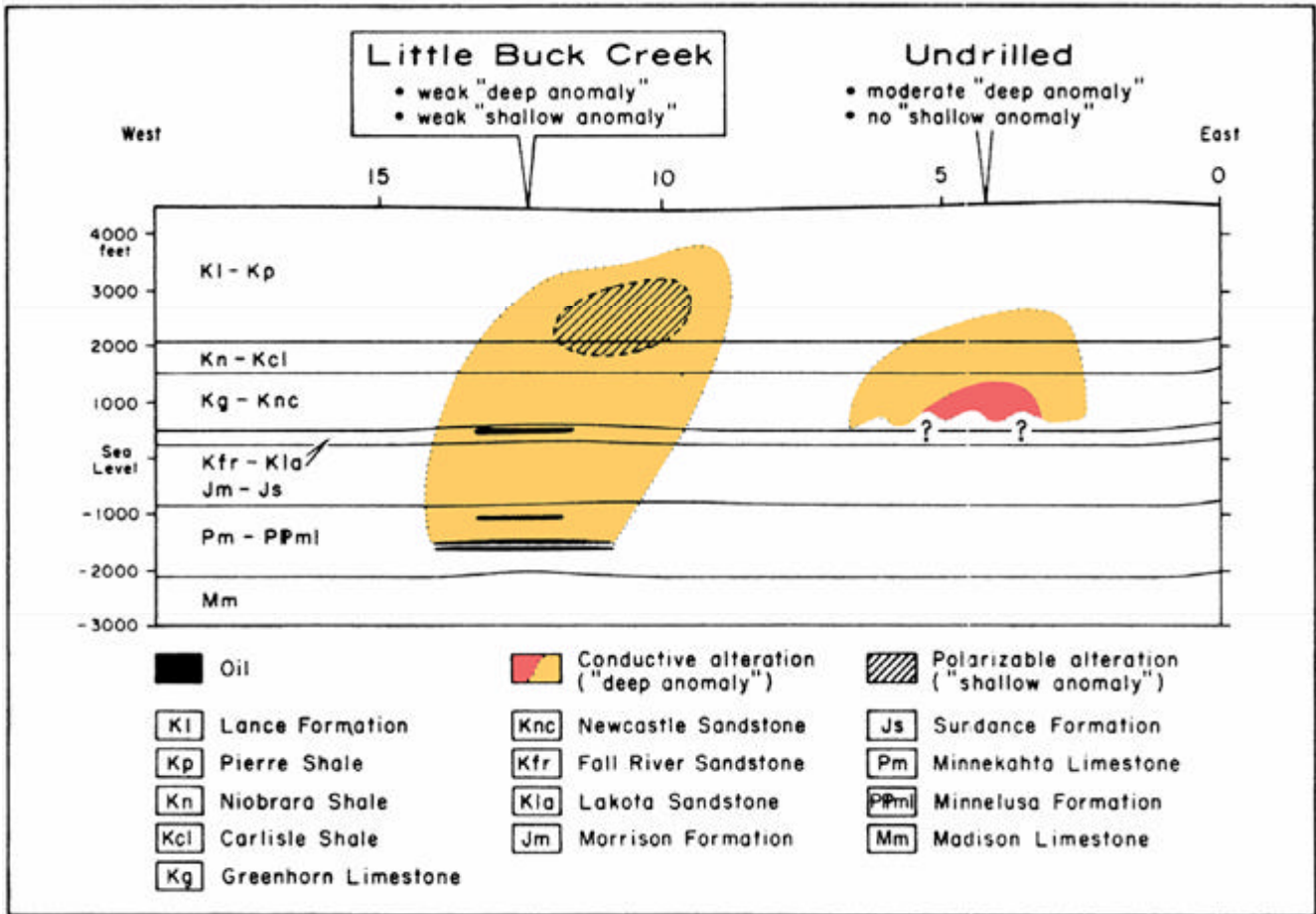


Figure 7. Combined geological, electrical, and electric-log cross-section of Little Buck Creek, line 2, with no vertical scale exaggeration. The maximum depth of penetration of the electrical data is about 2,000 to 3,000 feet (600-900 m); the electrical interpretation below these depths is inferred.

Two intersecting lines were run at Little Buck Creek. Line 1 is completely contaminated by strong conductive and polarizable effects from surface pipelines. The data from line 2 show a moderately conductive "deep" anomaly. This anomaly may be enhanced somewhat by well-casing effects, but modeling strongly suggests that a slightly conductive anomaly exists at depth on the eastern edge of the field. This anomaly cannot be explained by influences from surface culture, topography, or subsurface structure. Instead, it is believed that the anomaly results from brine discharge from the trap into the overlying sediments. The weakness of the anomaly suggests that the discharge mechanism is quite weak. The reason for this may be related to the depletion of oil and the probable loss of reservoir pressure in the trap. Pressure reduction would cause increased salt precipitation from brines rising from the trap, resulting in a weaker anomaly with less vertical extent.

A weak, polarizable, "shallow" anomaly is observed in the line 2 data. This anomaly may be the result of clay alteration by vertically-migrating hydrocarbons, or low-grade mineralization.

A very interesting conductive anomaly is observed on the east end of line 2, in an area which has not yet been drilled. The anomaly is not obvious in the apparent resistivity or apparent polarization data, but it is well defined in the REM data due to the greater penetration depth of REM on this survey. Since the anomaly has the magnitude and shape characteristic of hydrocarbon-related anomalies seen elsewhere in the basin, follow-up work is strongly recommended.

Lisbon

Lisbon Field, discussed in Chapter 6, produces oil and gas from a faulted anticlinal trap in the Paradox Basin. The primary reservoir is the Leadville Formation of Mississippian age, which has an expanding gas cap and gravity drainage system. Oil is yellow to red, sour crude of 54° API gravity; gas is sour. Although much of the oil has now been recovered, reservoir pressures are maintained at their original levels by means of gas injection. A secondary, rather limited reservoir is found in the McCracken Sandstone member of the Elbert Formation, a Devonian unit. The reservoir has a solution-gas drive. Red, waxy, 43° to 50° API gravity oil and sweet gas are produced from the McCracken. As shown in the geologic and interpreted electrical cross-section of Figure 8, the Mississippian and Devonian reservoirs at Lisbon are directly overlain by the Pennsylvanian Paradox Salt, a thick section of low-permeability evaporites. The salt is in turn overlain by permeable, water-saturated sediments. The presence of the salt makes Lisbon an interesting project, because one might expect an evaporite of this type to present a permeability barrier to the upward-migrating hydrocarbons and waters which are thought to cause the anomalies.

Two sub-parallel lines and an intersecting cross-line were run at Lisbon. Intermediate to shallow conductive anomalies are seen on all three lines over the producing field, but no classical "deep" conductive anomalies or "shallow" polarizable anomalies are observed. Worst-case well-casing models fail to explain the existing anomalies, and it is also unlikely that the combined effects of surface culture, topography, and subsurface structure can cause the anomalies. Instead, it is believed that the anomalies result from alteration of the sediments overlying the hydrocarbons, as illustrated in Figure 8.

This project represents an interesting "limiting-case" to the anomaly mechanism due to the presence of the Paradox Salt. Hydrocarbons and waters rising from the trap at depth must pass through some 3,000 feet (900 m) of salts before reaching permeable, water-saturated sediments near the surface. At this point, it is difficult to understand the dynamic processes which connect the presence of hydrocarbons at depth to the strong conductive anomaly in the shallow sediments. However, the fact that such an anomaly exists cannot be denied, and this may have important implications in the study of driving mechanisms for the anomalies.

Trap Spring

An opportunity to examine yet another "special case" of the anomaly mechanism is provided in Chapter 7 by the data over Trap Spring Field, an oil producer in the Basin and Range province of Nevada. The field is unusual because no methane is dissolved in the oils. Since methane leakage from hydrocarbon traps is believed to be important in producing "shallow" type anomalies, the data over Trap Spring are of particular interest.

Production at Trap Spring is black, 21.5° API gravity crude from the Pritchards Station Formation, a welded ash-flow tuff of Oligocene age. Intergranular permeability in the tuff is nonexistent, and oil is found exclusively in cooling joints and fractures. The trap is a combined structural and stratigraphic type; the producing zone is terminated updip by graben faulting, downdip by the oil-water contact, and laterally and vertically by loss of fracture permeability. Reserves are unknown; some 5 MMBO have been produced, and production is now declining.

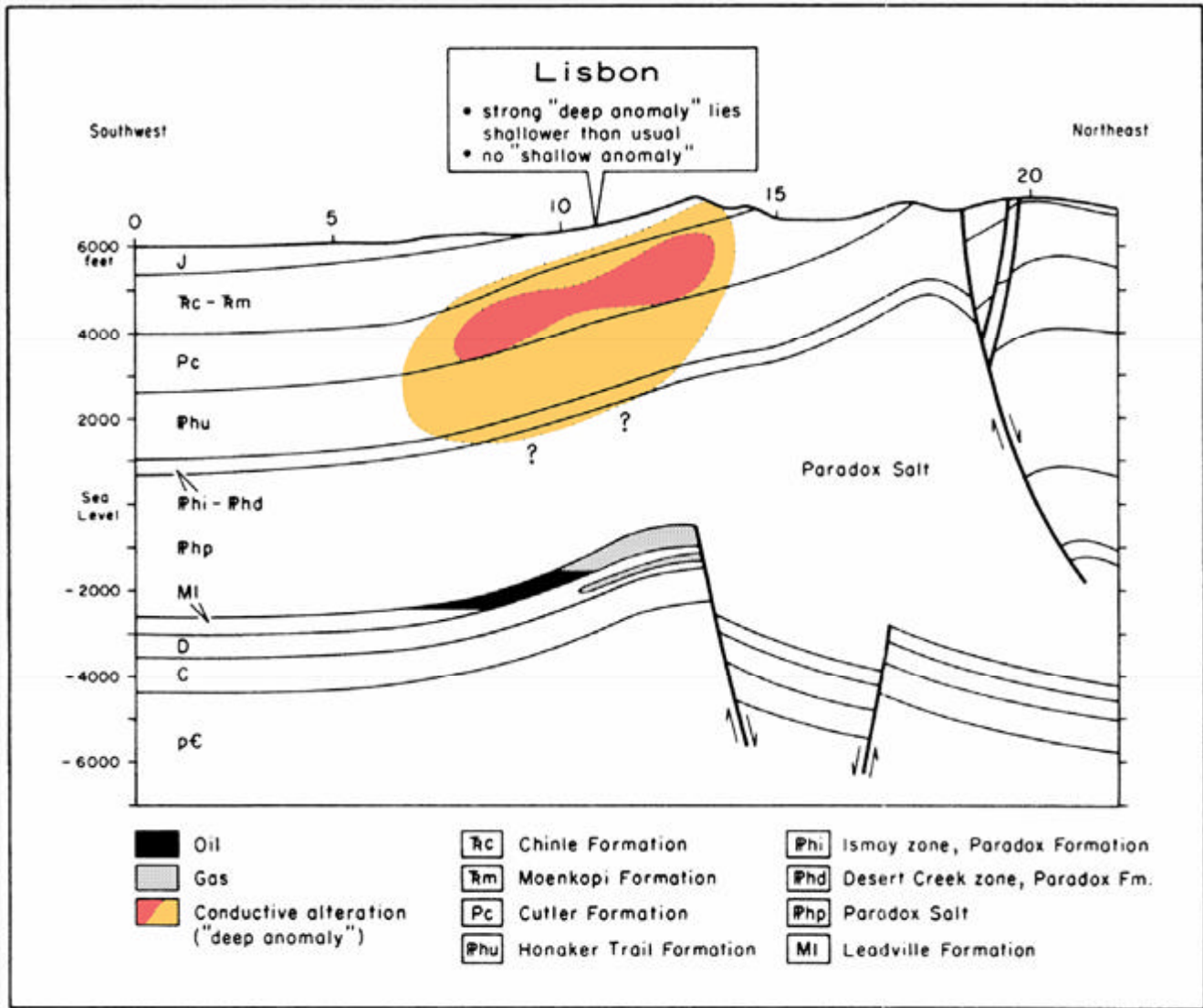


Figure 8. Combined geological, electrical, and electric-log cross-section of Lisbon, line 3, with no vertical scale exaggeration. The maximum depth of penetration of the electrical data is about 4,000 to 6,000 feet (1,200-1,800 m); the electrical interpretation below these depths is inferred.

Three lines of data were obtained over Trap Spring. Lines 1 and 2 appear to have been heavily influenced by effects due to sub-parallel graben faulting. Line 3 shows a strong "deep" anomaly, as shown in the geoelectric interpretation of Figure 9. Arguments are advanced to show that this anomaly is not easily explained by effects due to well casings, surface culture, or geologic structure. Instead, it is believed that the anomaly is the result of invasion of upward-migrating, saline waters into the overlying Horse Camp Formation, a valley fill unit. These waters could lower ground resistivities by replacing waters of higher resistivity, or by altering the abundant clays in the Horse Camp sediments.

A well-defined polarization anomaly observed on all three lines may be partly or totally due to the effects of well casings. The lack of a distinct "shallow anomaly" in the Horse Camp sediments tends to support the theory that upward migration of hydrocarbons causes polarizable mineralization and alteration. Since no light

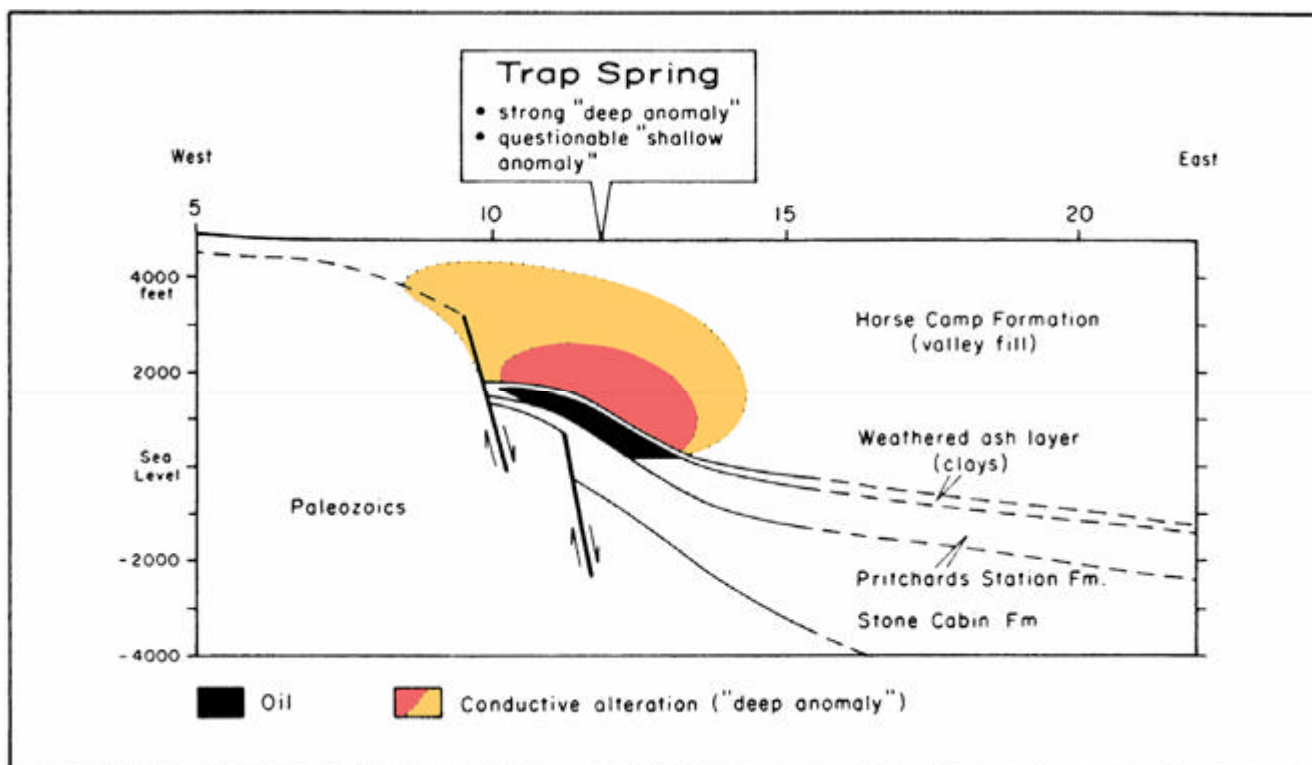


Figure 9. Combined geological and electrical cross-section of Trap Spring, line 3, with no vertical scale exaggeration. The maximum depth of penetration of the electrical data is about 2,500 to 3,500 feet (750-1,100 m); the electrical interpretation below these depths is inferred.

hydrocarbons are present in the Trap Spring oils, none are available for migration, and hence no polarization effects are observed in the sediments overlying the trap.

Garza

Presented as an illustration of ambiguities of well-casing modeling, the Garza Field data in Chapter 2 show a strong polarizable anomaly over a stratigraphic trap in north-central Texas. Data obtained before and after the drilling of four step-out wells indicate that the anomaly is influenced by, but probably not caused by, well-casing effects. Instead, the anomaly mechanism is thought to be related to pyrite mineralization in the reducing environment over the oilfield, a frequent occurrence in the Texas-Oklahoma area. Brine discharge is probably responsible for a subtle "deep anomaly".

POSSIBLE SOURCES OF THE ANOMALIES

As suggested by the case histories, the anomalies measured by multi-frequency electrical techniques appear to be related to hydraulic discharge of saline waters and light hydrocarbons from the trap at depth into the overlying sedimentary section. The upward-migration theory is in substantial agreement with recent geochemical, geothermal, and hydrological studies, and is specifically compatible with modern concepts of hydrodynamic petroleum accumulation. The theory of anomaly generation is presented in schematic form in Figure 10.

The origin of the conductive "deep anomaly" is believed to be related to the flow of saline water through the trap into the overlying sediments. Two possible anomaly mechanisms are envisioned which might lower the bulk resistivity of the sediments overlying the trap: 1) replacement of moderate resistivity interstitial pore fluids with the upward-migrating, lower resistivity, saline fluids; 2) alteration of clays by

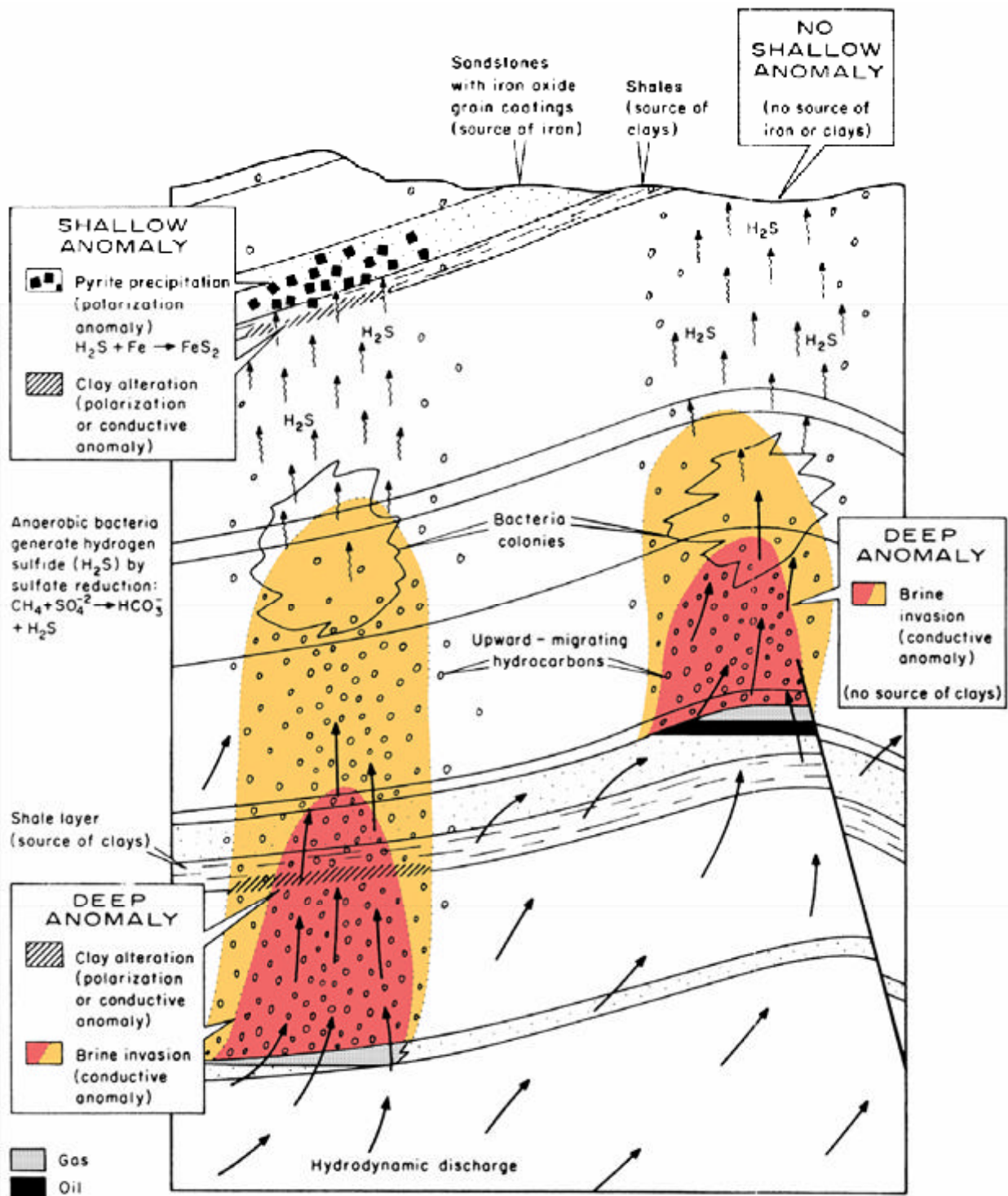


Figure 10. Proposed origin of the "deep" and "shallow" anomalies observed in electrical data. The presence and strengths of the anomalies are variable from project to project, since the anomaly mechanisms are heavily dependent upon geology of the sedimentary overburden. This illustration presents an idealized picture of some possible alteration mechanisms.

cation exchange with free calcium or sodium ions in brines, changes in pore-space geometry, or clay-hydrocarbon interactions.

The origin of the "shallow anomaly" seems to be related primarily to upward migration of light hydrocarbons. At least two theories can be advanced to explain these anomalies. The most common explanation involves the formation of pyrite in the near-surface sediments. Hydrogen sulfide, originating from the trap or created by the reduction of sulfates by anaerobic bacteria, rises through the sedimentary column and combines with iron cements and grain coatings in sandstones, precipitating pyrite. Pyrite has been found in relative abundance over many oil and gas fields, and it often shows a strong polarization response to electrical surveys of this type. The second explanation for the "shallow anomaly" involves clay alteration processes, either through interactions with the rising hydrocarbons or cation exchange interactions with the reduced waters overlying the hydrocarbons. Clays are often quite polarizable, although their responses vary considerably, depending upon clay type, pore space restrictions, lattice impurities, etc. Obviously, both the pyrite and clay theories are subject to the specific geology of the sedimentary column, and this may explain the extreme variability of the "shallow anomaly". Interpretation of the anomalies is therefore facilitated by a careful and detailed evaluation of subsurface lithology, structure, and hydrology.

CONCLUSIONS

The case histories contain a large amount of information which may ultimately prove to be of great value in understanding how electrical anomalies are influenced by geologic factors. Even today, little is known about the dynamics of hydrocarbon/fluid migration and alteration in the deep, geologically complex environments of sedimentary basins. A multidisciplinary approach involving electrical, hydrological, geochemical, geological, and theoretical studies should be undertaken in order to investigate these matters, so that the vast amount of information available in multifrequency electrical data can be utilized more fully.

However, the current problems in detailed understanding of anomaly mechanisms should not obscure the important evidence that electrical techniques such as the one illustrated in this volume seem to work well in many diverse environments, providing that great care is taken in data processing and interpretation. As an exploration tool, the chief advantage of the multifrequency electrical approach is that it can serve as an indirect indicator of the presence of hydrocarbons. This can complement existing reflection-seismic programs, which have structural mapping capabilities far superior to those of most electrical techniques, but which do not generally indicate hydrocarbon potential. In addition, electrical techniques offer valuable information in areas of difficulty in seismic exploration, such as in exploration for subtle stratigraphic traps, and in areas involving severely weathered overburdens, surface volcanics, and fractured evaporites. Hence, the combined efforts of geologic, seismic, and multifrequency electrical programs should form an effective strategy in evaluating hydrocarbon potential in geologically attractive targets.

PART TWO

DATA INTERPRETATION

Chapter 1

Introduction to the Data

1.1 INTRODUCTION

Resistivity/phase (RP) and complex resistivity (CR) are geophysical techniques in which electrical current is transmitted into a grounded dipole at specific frequencies, and the returned voltage is measured by a second dipole some distance away. The responses are measured at several frequencies, processed, and analyzed for characteristics indicative of hydrocarbon alteration, minerals, or other pertinent geologic information.

The terms "resistivity/phase" and "complex resistivity" refer to specific methods which are an extension of the more general induced polarization (IP) method. IP has been as widely used in the mining industry over the past 30 years as the seismic reflection method has been in the petroleum industry. RP and CR measure the same phenomena and the presentation of data from the two methods is identical. Throughout this volume, the use of "resistivity/phase" implies the following:

1. Measurements are made of both amplitude and phase angle.
2. Measurements are made in the frequency domain at three or more discrete frequencies.
3. The data are specially processed in order to recover electromagnetic coupling information by separating it from the induced polarization response.

The use of "complex resistivity" implies the following:

1. Measurements are made of both amplitude and phase angle.
2. Measurements are made in the frequency domain at 6 to 24 odd Fourier harmonic frequencies.
3. The data are specially processed in order to recover electromagnetic coupling information by separating it from the induced polarization response.

These distinctions will become clear upon reading the information to follow.

A third technique, controlled source audiofrequency magnetotellurics (CSAMT), is also used in petroleum applications and is discussed in section 1.7.

1.2 DEFINITIONS AND PLOTTING CONVENTIONS

Voltage and Phase Angle

In order to impress an electromagnetic field into the ground, an electric current is transmitted directly into a grounded dipole. A source current is used in which the sense of current flow alternates periodically at some specified frequency. The flow of this periodic, time-varying current in the earth produces an electromagnetic field. This field is affected by the presence of electrical inhomogeneities, such as ore deposits, alteration zones, structure, variations in pore fluids, etc. The electromagnetic field produces a voltage gradient in the ground. It is the purpose of an electrical survey to measure the amplitude and the time-dependency of this voltage gradient using a grounded "receiving" dipole.

The voltage measurement between any two points is influenced by the shape of the original source current waveform and any perturbations caused by inhomogeneities in the earth. The perturbations are the things which are interpreted for their geologic significance.

A periodic, time-varying signal may be completely measured using the following two parameters:

1. Magnitude of the response (voltage)
2. Shift in time of the received signal with respect to the transmitted signal (phase angle)

A series of measurements of magnitude and phase angle as a function of time/frequency establishes the shape of the received signal with respect to the transmitted signal.

If the grounding geometry of the dipoles and the magnitude of the original current are known, the *apparent resistivity* of the ground can be calculated using the voltage gradient measurements. This is one of the three primary interpretation parameters used in petroleum exploration with the resistivity/phase and complex resistivity techniques. Phase angle refers to how well the ground stores up electrical charge with time, a process which is commonly called induced polarization. The phase angle measurement is also influenced by electromagnetic coupling, which is an artifact of the grounding geometry of the measuring system and of the geology. When the data are processed, the induced polarization and electromagnetic effects are separated from one another by means of a proprietary Zonge Engineering decoupling algorithm, resulting in the additional two interpretational parameters of *apparent polarization* and *residual electromagnetic (REM)* data.

The unit used for apparent resistivity measurements is the ohm-meter. High apparent resistivities indicate media which resist current flow; low numbers indicate media through which current flows easily. The unit used for induced polarization data is the milliradian. High numbers indicate media with a high electrical energy storage capacity; low numbers indicate media with low energy storage capacity. REM data are normalized and hence are unitless.

Figure 1.1 illustrates how the phase angle measurement is made. At time $t=0$, a sinusoidal electric current is applied to the ground. The induced electromagnetic field results in an instantaneous voltage, V_0 . Capacitive properties of the ground cause it to charge up, and the voltage continues to rise to a peak of V at some time t . The time it takes for this voltage rise to occur, expressed as a function of the sinusoidal frequency, is the phase angle. In other words, phase angle is the amount

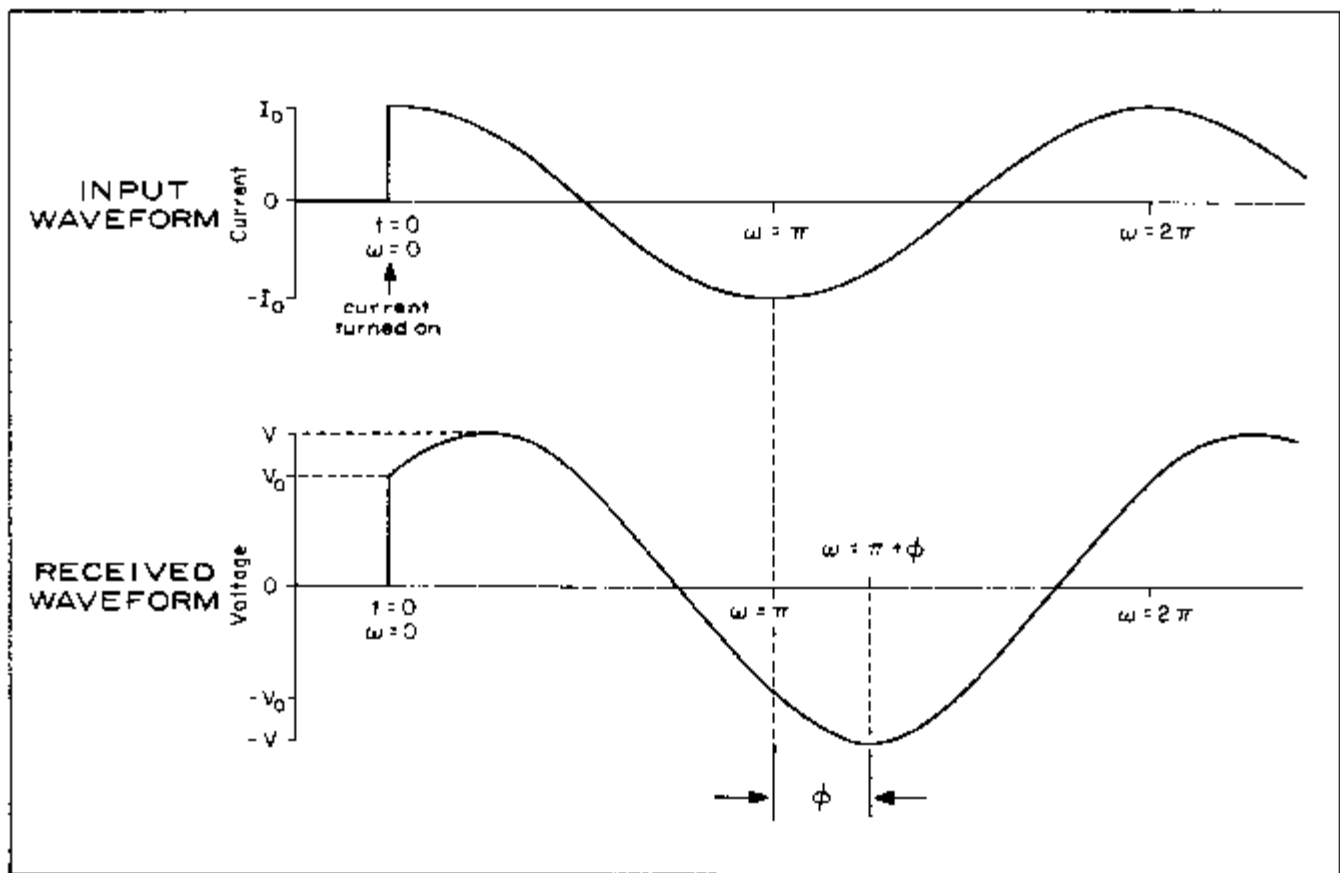


Figure 1.1. Definition of phase angle (ϕ). For the sinusoidal signals shown, phase angle is the delay in angular frequency (ω) between the peak of the input current and the peak of the received voltage.

by which the voltage lags the current. Units are in radians; a phase lag of 180 degrees (π radians) corresponds to signals which are completely out of phase (i.e., while one is at its minimum value, the other is at its maximum value). According to common convention, a negative phase angle is assigned to a measurement in which the voltage lags the current, while a positive phase angle refers to a case in which the current lags the voltage. In most ground environments, nearly all phase angles are negative. As a matter of convenience, then, the convention in electrical geophysics application is to reverse the sign of all phase angle data. Hence, all data which have positive signs correspond to voltage lagging the current; conversely, data which have negative signs correspond to voltage leading the current, a situation which occasionally results from peculiar geometric effects.

Complex Plane Plots

The two defining parameters of magnitude and phase angle permit one to plot a data point at a given frequency in polar coordinates, as illustrated in Figure 1.2(a). An equivalent plot can be constructed in terms of rectangular coordinates, as shown in Figure 1.2(b). The latter is called a "complex plane" plot, since it involves the use of complex numbers to describe the locations of the plot points. Following the standard convention used in electrical engineering, the horizontal axis is called the "real" or "in-phase" axis, since points located on it are in phase with their source, i.e., there is no phase shift between the two. The vertical axis is called the "imaginary," "quadrature," or "out-of-phase" axis, since data points which have a

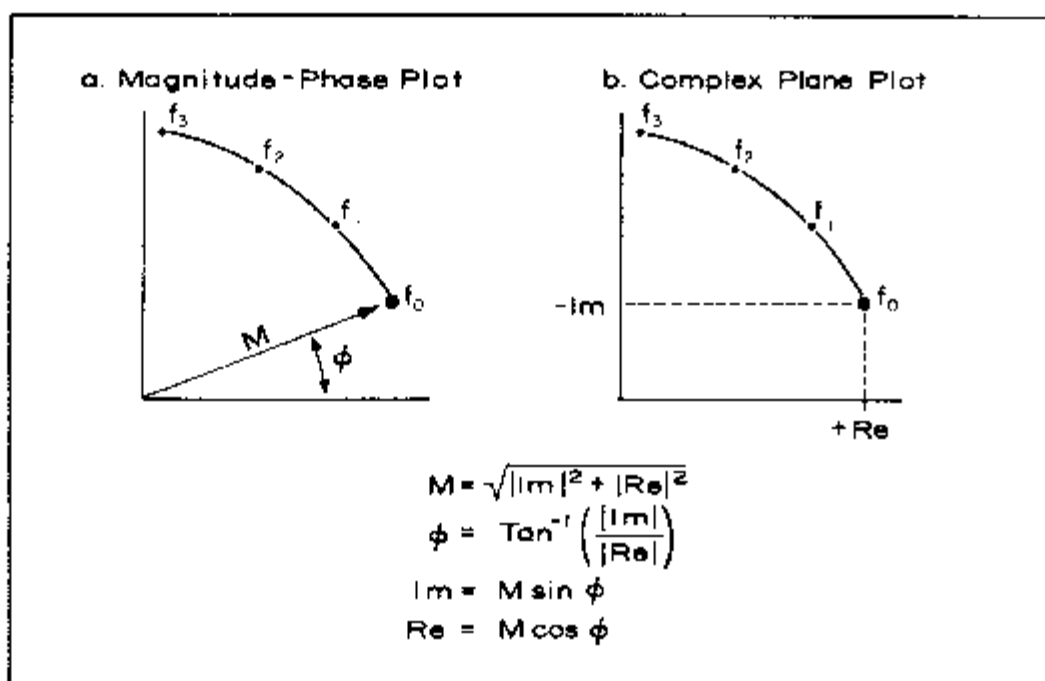


Figure 1.2. Example of a magnitude-phase plot and a complex plane plot of data at frequencies f_0 , f_1 , f_2 , and f_3 . The plots show the conversion from magnitude (M) and phase angle (ϕ) to real (Re) and imaginary (Im) coordinates.

non-zero vertical axis component are out of phase by 90 degrees ($\pi/2$ radians) with respect to their source and are described mathematically by imaginary numbers. Please note that in Figure 1.2, the negative imaginary component is up, not down, since convention dictates that negative phase angles are to be measured counter-clockwise from the positive real axis.

Pseudosection Plots

All oilfield data in this volume and nearly all resistivity/phase and complex resistivity data obtained by Zonge Engineering are acquired with the dipole-dipole array. This array employs a transmitting dipole of length " a " and a collinear receiving dipole of the same length. The separation between the two, called the " n " spacing (expressed in terms of " a "), is varied in order to control the depth of penetration.

Figure 1.3(a) shows how dipole-dipole data are normally plotted. By convention, the plot point is located midway between the transmitting and receiving dipoles at the intersection of two 45 degree lines projected from their midpoints. By plotting data at various separations and for various dipole positions on the ground, one can come up with a pseudosection plot similar to that of Figure 1.3(b). The pseudosection is not a true cross-section of the ground, for several important reasons. First, the depth of penetration is not strictly controlled by the " n " and " a " spacings, but is also dependent upon other factors, such as ground resistivity, geologic contacts, layering, etc. Secondly, the number value assigned to any given plot point does not represent the actual value of the rocks at that point, but rather the weighted averaged value of all the material affecting the measurement, with the near-surface material exerting a disproportionately high influence on all the data. The plot points, then, are strictly a matter of convention and convenience; effects observed in a pseudosection must be interpreted in order to arrive at an inferred geoelectric section. This is why the data plots are called "pseudosections."

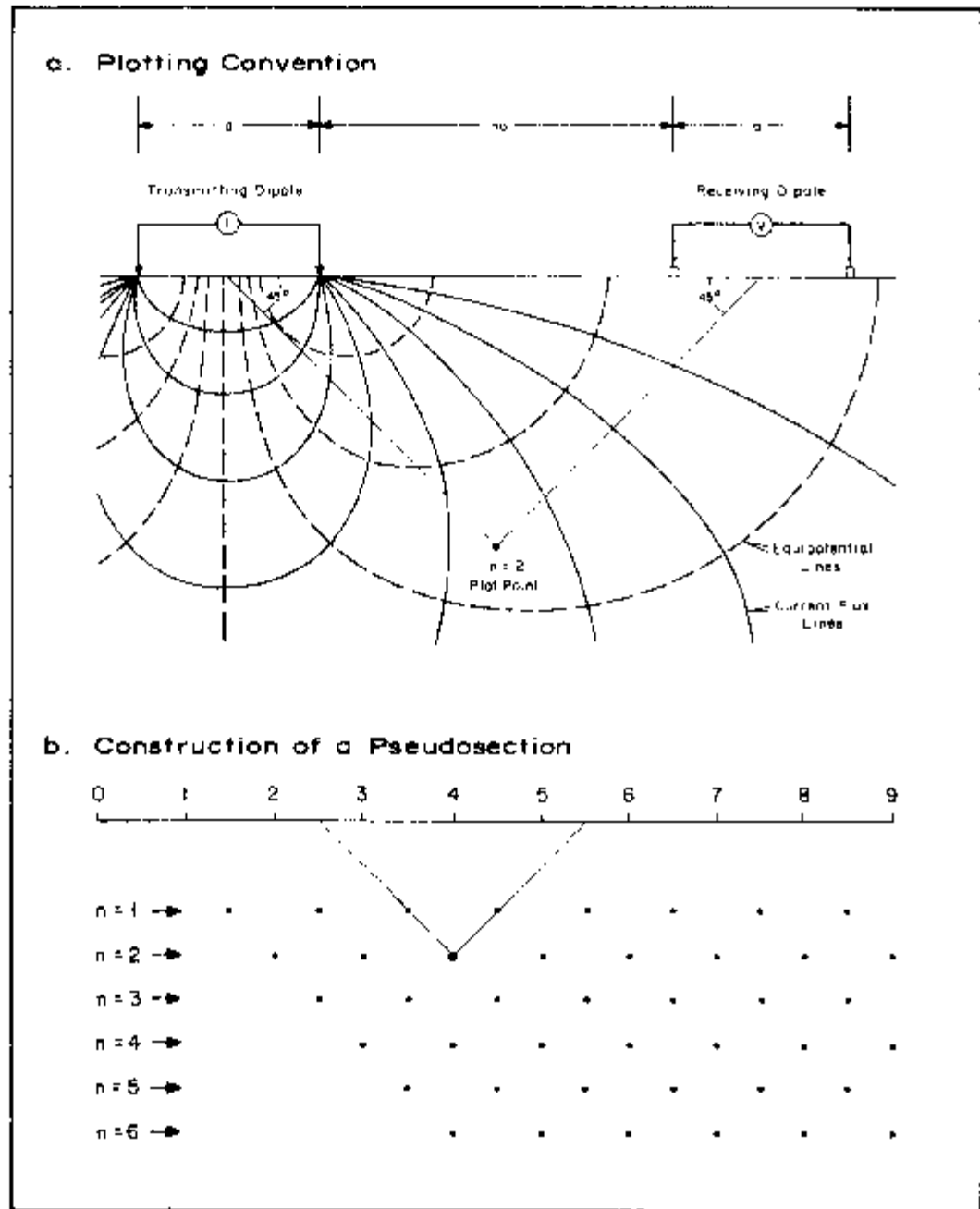


Figure 1.3. Plotting convention for dipole-dipole pseudosections.

Figure 1.4 presents an example of how the appearance of a pseudosection can differ from that of a geologic cross-section. A vertical, conductive, dike-like feature outcrops between stations 0 and 1. Since the dike essentially influences or "casts a shadow" on measurements made from dipoles on either side of it, all apparent resistivity values obtained by measuring through the dike are very low. According to our plotting convention, these low apparent resistivity values will lie along 45 degree diagonals emanating from the vicinity of dipole 0,1. This results in the triangular-shaped anomaly seen in the pseudosection of Figure 1.4. More complicated effects of this nature are also observed, necessitating the use of computer modeling to estimate the shape and magnitudes of anomalies from subsurface features.

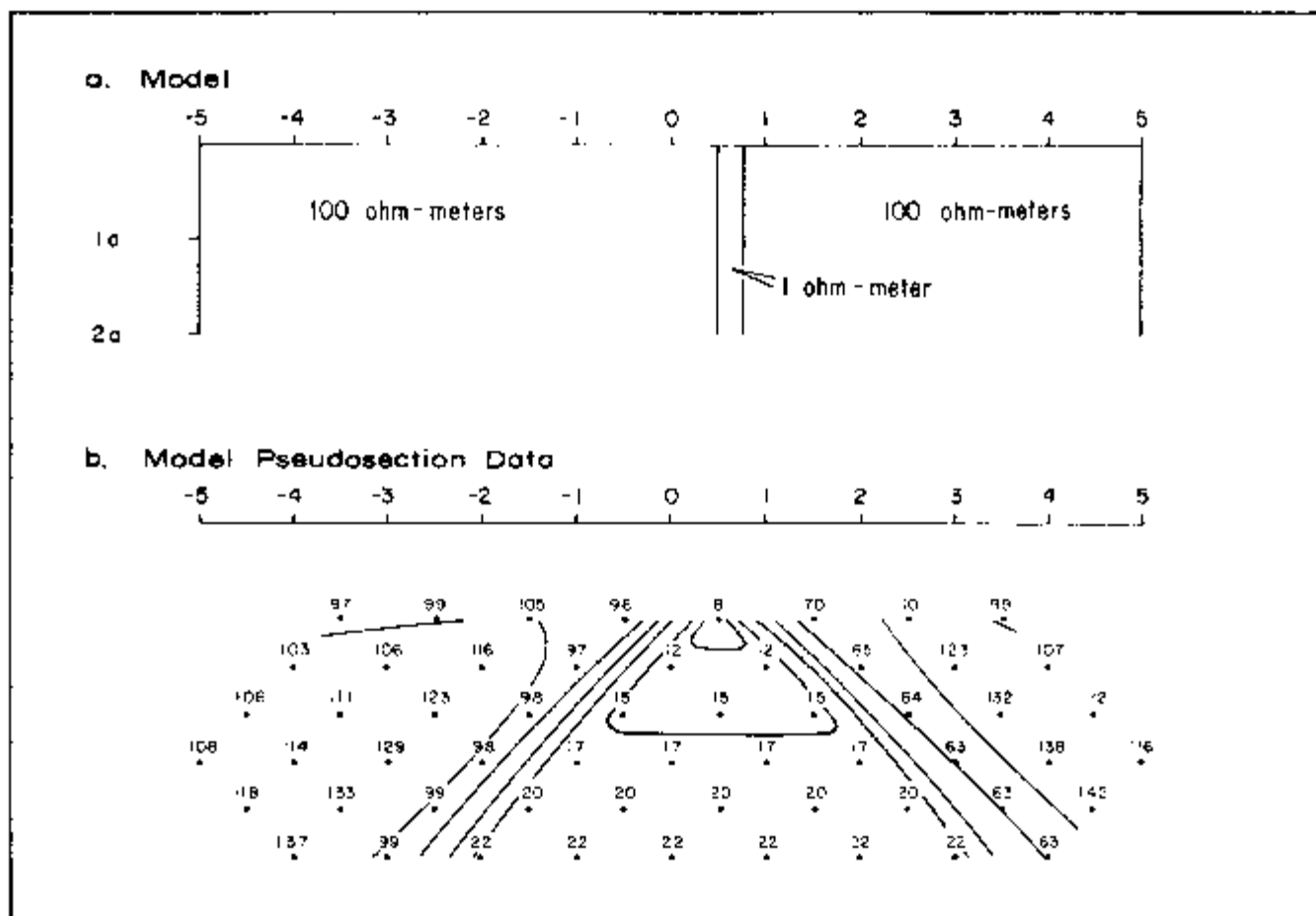


Figure 1.4. Example of a "geometric effect" from a vertical conductive dike. The data are from a two-dimensional computer model called "2DIP," which is explained in Chapter 2. Contour interval: 10.0, 15.9, 25.1, 39.8, 63.1, 100.0, ... ohm-meters.

In discussing pseudosection data, several specific terms require explanation. In order to identify which diagonals show strong effects, one refers to the dipole from which the diagonal is plotted. For example, one might refer to the "left-plunging diagonal 2,3," or "right-plunging diagonal 3,4," as illustrated in Figure 1.5. Hence, the most strongly effected diagonals of Figure 1.4 are the left-plunging 1,2 diagonal and the right plunging 1,0 diagonals. A generic term for diagonal and similar features is "geometric effects," so named because it is the specific geometric relationships of the dipole-dipole array and the geology which give the pseudosection its particular appearance.

1.3 ELECTRICAL NOISE

All electrical surveys are affected to some degree by any electrical noise present in the ground, since both the input signal and the noise contribute to the measured signal. Electrical noise measured in geophysical surveys comes from three primary sources: tellurics, atmospherics, and "culture" (man-made conductive features such as powerlines, pipelines, fences, etc.). Most of these signals are detected directly from ground contact, but at frequencies in the kilohertz range, airwave or radiation noise can also be considerable.

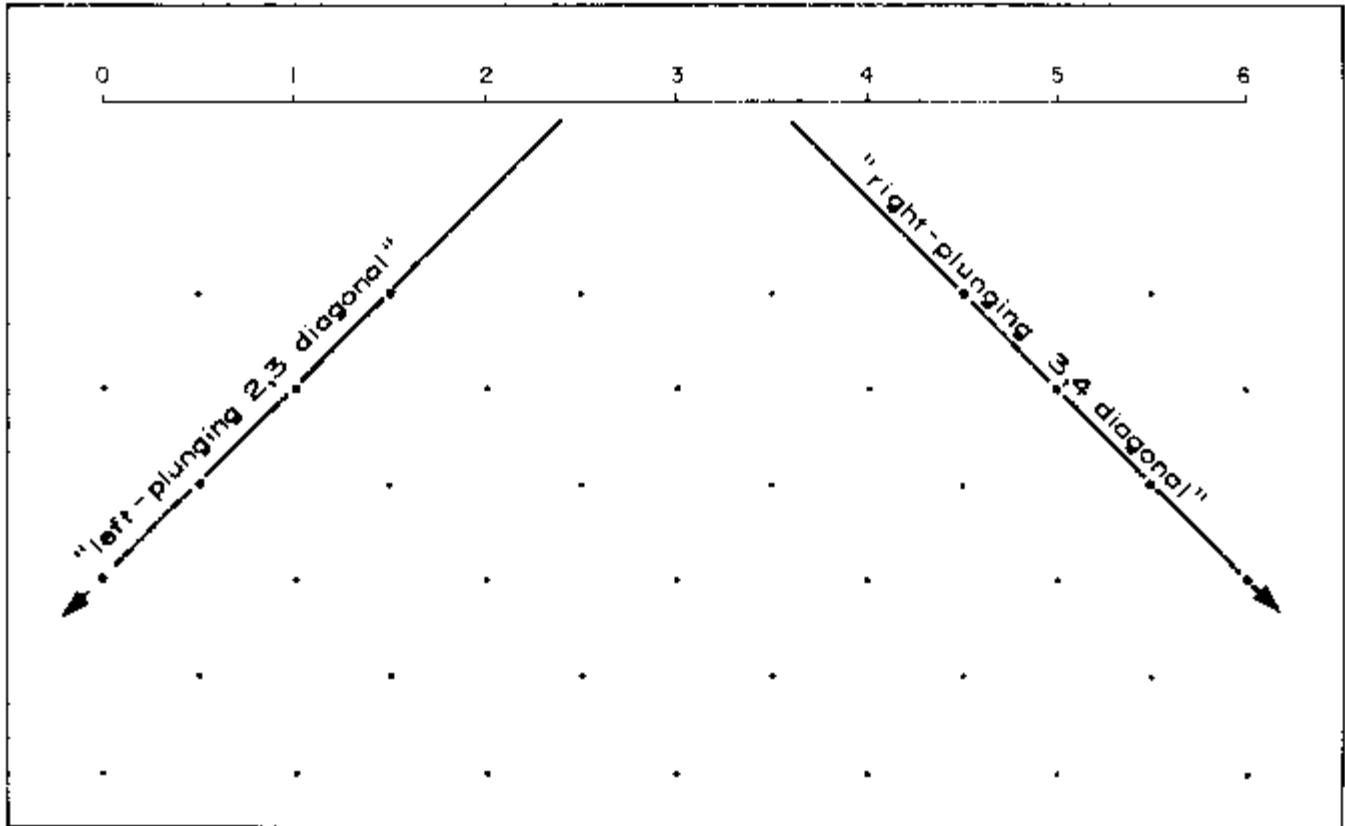


Figure 1.5. Meaning of "left-plunging" and "right-plunging" diagonals.

Tellurics

Tellurics are ground currents whose source is tied to pulsations of the earth's magnetic field and to interactions of the solar wind with it. The solar wind can be thought of as a plasma, composed of positrons and electrons, which is constantly radiated from the sun. The intensity of the solar wind is dependent upon the presence of disturbances in the sun's atmosphere which primarily fluctuate with the 11-year solar activity cycle.

The solar wind streams out from the sun and impinges upon the earth's magnetic field, forcing the field back into a plume-shaped feature. Changes in flux cause the field to pulsate, inducing an electromagnetic current which is transmitted into the earth via hydrodynamic oscillations along plasma-rich magnetic flux lines. Particles which are trapped by the field can be incorporated in the Van Allen radiation belts or can travel down the magnetic field axes near the poles. Interactions in the earth's atmosphere produce a cascade of charged particles, the EM effects of which are transmitted into the ground.

The wave motion of the solar plasma and the pulsations of the magnetic field occur at low to very low frequencies, each of which has higher frequency harmonic pulsations. Particle interactions produce their own range of wave frequencies. Telluric currents coupled into the earth therefore occur at a wide range of frequencies. Not all of these frequencies are observed, however, due to absorption by the ground. Since most telluric noise occurs in the RP/CR frequency range (DC to 100 Hz) and is noncoherent in nature, it cannot be filtered in an easy manner. Smooth, low frequency changes in ground self-potential can be partially removed from the data by digital telluric filters (referred to in this work as "moving average" filters) or

high-pass filters, and by coherent stacking and averaging of the received signal. However, due to the low frequencies used, coherent signal stacking can take an inordinate amount of time to filter out strong telluric signals. Tellurics in the 0.1 to 10 Hz range cause the most damage to data quality, and it is occasionally necessary to shut down a crew during a particularly active solar storm when the noise to-signal ratio becomes intolerable.

Atmospheric Noise

Noise caused by lightning discharges and atmospheric shear pose the most serious threat to data quality in oilfield projects. The primary energy lies in the middle to higher frequencies (above 100 Hz), but lower-range beat frequencies are observed as well. The problem is both global and local. On a global scale, tropical storms give rise to an ionosphere/troposphere resonant noise called the Schumann resonances. These occur predictably in the RP/CR range, with the larger peak occurring at 8 Hz. On a local scale, storms contribute heavily to high-frequency pulses and tend to dominate global effects. The noise results from intracloud shear, intracloud electrical discharges, and cloud to ground discharges. The higher frequency components can be partially suppressed with low-pass filtering, but a problem arises when lightning strikes are nonrandom in nature. This can occur, for example, when a thunderstorm occurs on the south end of the survey line. Ground current from a lightning strike travels radially outward from the contact point on the ground; hence, the sense of current flow with respect to the survey line is south to north. In this case, the noise is nonrandom and it cannot be properly filtered by digital stacking techniques.

High frequency atmospheric noise has a much greater effect on phase data than on resistivity data, but both sets of data can be rendered practically useless by an especially active storm. Although acceptable data have been obtained in signal to noise ratios worse than 1:100, it is often not economical to do so.

Cultural Noise

The presence of man-made conductors (known as "culture") can introduce a great deal of harmful noise into the measuring process. The worst offender is usually power transmission line noise and its odd harmonics. In the United States, a frequency of 60 Hz is used, hence 60+180+540+ . . . cycle noise is observed, with each harmonic becoming progressively smaller in amplitude. Other frequencies, primarily 50 Hz, are used in other parts of the world. Although a notch filter can be used to remove the powerline frequency and its third harmonic, DC shifts in amplitude (usually related to changes in power load) can drastically reduce data quality.

Cathodic protection of collection pipelines often causes major problems, especially if the frequency regulation is poor. Frequencies are typically 120 Hz (half-wave rectified 60 Hz) but can vary considerably. It is usually advantageous to shut off the cathodic protection circuitry during the duration of a survey, if it is possible to do so.

Carrier signals of 400 Hz, sometimes used for railroad communications, are also encountered occasionally, as are various carrier frequencies on power transmission lines used for automatic load switching. High frequency noise from aircraft navigation signals, broadcast stations, and microwave communication networks is also encountered on occasion. These can usually be filtered by low-pass filters, providing that the signals are not strong enough to cause front-end saturation of the equipment. Front-end saturation can be detected by careful field checks.

Any cultural signal which changes the ground potential in an irregular or DC fashion cannot be filtered. DC shifts due to culture can result from two signals

beating together, from a signal which changes quickly in amplitude (e.g., load switching), from DC pumping equipment, or from underground mine equipment.

Noise-avoidance procedures used on the surveys in this volume are described in section 1.5.

1.4 INSTRUMENTATION

All of the data contained in this volume were acquired with the GDP-12 Geophysical Data Processor instrumentation system. The GDP-12 system has replaced the original Zonge Engineering field system, which consisted of a PDP-8 (registered trademark of Digital Equipment Corporation) computer, a two-channel cassette drive, a teletype, and a Zonge-designed, two-channel analog receiver. This truck-mounted apparatus had been used for complex resistivity measurements since 1972, and it was used to obtain full spectral data (0.1 to 110 Hz) in oilfield work during 1977 and 1978. Once the success of the initial experiments over known oilfields had been established, the PDP-8 system was replaced with the more portable GDP-12 equipment, and the work was advanced to a production basis. The first application of the GDP-12 in oilfield work was for resistivity/phase surveys, using a limited frequency range (0.125 to 1.0 Hz) and multiple receivers in order to boost the rate of data acquisition. Most of the data in this volume came from this phase of the work. By 1980, full complex resistivity programming and instrumentation were completed for the GDP-12, and most oilfield surveys have subsequently been conducted using harmonic analysis complex resistivity.

The GDP-12 is a two-channel, microprocessor-controlled receiver which detects, filters, and amplifies two input signals simultaneously, and which processes the data according to software developed specifically for the particular type of survey desired. Figure 1.6 shows a front panel view of the receiver type used for acquisition of oilfield data during 1979 and 1980. The analog section of the GDP-12 has a 500 megohm input impedance at DC, common-mode noise rejection of better than 60 dB at 2 kHz, and channel separation of better than 80 dB at 2 kHz. The receiver is capable of detecting signals as low as 0.2 microvolts. Amplification can be selected in binary intervals from 1 to 32,768 (2^{15}), allowing full 12-bit digitization of input signals between 300 microvolts and 10 volts.

The filtering system for the receiver consists of alias and notch filters. The alias filter is a four-pole, low-pass Bessel or Butterworth filter which is engaged automatically via software when the operator selects the frequency on the front panel thumbwheel. Notch filtering for standard receivers used in the United States is set for 60 and 180 Hz powerline noise. Rejection of better than 40 dB is provided with a Q factor of 2 to 5.

The analog-to-digital converter is a 12-bit CMOS device whose speed is 16,000 conversions per second. For resistivity/phase frequencies, up to 1,024 sample points are digitized per waveform. The digital section consists of two independent Intersil or Harris 6100 microprocessors utilizing 20k words of 12-bit random access memory.

The GDP-12 can be used either as a truck mounted or portable receiver. The unit is powered by self-contained, rechargeable 12-volt batteries which provide at least 12 hours of continuous operation under field conditions. Timing is controlled by a temperature-controlled quartz crystal oscillator whose stability is one part in 10^{-9} per 24 hours (after warm-up).

The transmitter used in these surveys was a Geotronics FT-20, which transmits a constant-current squarewave signal at up to 18 amperes. Maximum practical output voltage is 800 volts. Power is supplied by a trailer-mounted, 20 kw motor/

generator set built by Zonge Engineering. For resistivity/phase work, the timing of the transmitter is controlled by a Zonge Engineering transmitter controller, which has the same crystal oscillator and timing chain as does the GDP-12.

1.5 RESISTIVITY/ PHASE DATA ACQUISITION AND FIELD LOGISTICS

Survey Planning

The dipole length for a resistivity/phase survey is selected upon the basis of two criteria: the expected or known depth to the hydrocarbons, and the expected or known plan-view extent of the field. It is alteration overlying the hydrocarbons which is being measured (not the hydrocarbons themselves). Unfortunately, the depth to the alteration zone is not always predictable, but it often extends up the sedimentary section to about half the depth of the hydrocarbons. Hence, it is desirable to achieve penetration to deeper than half the estimated depth to the hydrocarbons to insure resolution of the overlying alteration. Assuming a depth penetration of REM data to 3 dipole spacings, this consideration suggests that the dipole spacing be greater than or equal to one-sixth that of the depth to the hydrocarbons. This is not a hard-and-fast rule, but it is useful in the planning stages. The areal extent of the hydrocarbons also helps fix the dipole size. Since the lateral resolution of a dipole-dipole survey is at best one-half the a-spacing, the a-spacing should be smaller than the width of the field. If the target is a prospect, a minimum economic field size should be assumed for planning purposes.

As an example, assume that a prospect is to be run in an area in which potential reservoir rocks are expected to be Pennsylvanian to Mississippian in age, at a depth of 7,000 to 9,000 feet (2,100 to 2,700 m). The geologist for the project might suggest that an economically interesting target would probably exceed 2,000 feet (600 m) in plan dimensional width. Hence, one would need to consider both a depth and a lateral size constraint. The depth constraint would fix a minimum a-spacing at around 2,000 feet (600 m), while the lateral size constraint would require that the a-spacing not exceed 1,500 feet (450 m) or so. One would therefore be tempted in this case to make the dipole size around 1,500 feet. This would probably be acceptable, even though the depth constraint is violated, since alteration is usually found well above half the actual depth to the hydrocarbons.

Under normal field conditions, the client provides sufficient information regarding the desired location of survey lines and the geologic nature of the field site to facilitate the permitting of the field site. Actual line location and permitting should be coordinated to minimize the effects of culture on the electrical measurements and lost production time due to restricted line access.

Upon arriving at the field site, the crew normally scouts the area in order to optimize line locations. The criteria which are considered include line access, topography, the location of prime geologic target areas, the location of major faults or steeply dipping geologic contacts, and the presence of culture. Obviously, line access and topography heavily influence the cost of a survey, since these variables can affect production rates. Topography can introduce complications in the interpretation of the data, and while such complications can often be adequately reproduced by computer modeling, it is best to avoid extreme topography if the option exists.

The locations of known major faults or linear contacts in the survey area should be considered when laying out the survey lines, since running directly over and parallel to such features can make interpretation of the data difficult or impossible. A good example of such an effect is found in the case history of Trap Spring, line 2 (Chapter 7).

Culture, in the form of well casings, pipelines, powerlines, and fences, can also have a major impact on the data. Ideally, the dipoles should run perpendicular to cultural features in order to minimize their effects on the data. An electrode should never fall near a cultural feature if such a situation is avoidable. The worst cultural offenders are, in general order of effect: grounded metal pipelines, well casings, grounded metal fences, powerlines, and telephone lines. An example of severe cultural contamination is found in the discussion of Little Buck Creek, line 1 (Chapter 5).

Setting up the Survey Line

Having selected the line locations and dipole spacing, the crew locates one end of the first line via section corners or other reliable landmarks. The line is surveyed with a hand-held Brunton (or equivalent) compass, and checks are continually made against a field topographic map in order to ensure the accurate plotting of the line location, as well as to determine the relative locations of wells and other culture.

The particular type of survey which was used to collect most of the data in this volume requires a crew of eight. Three persons are responsible for acquiring data from the three GDP-12 receivers on line. Two persons lay out the wires, stake electrode positions, and scout access routes for the transmitter truck, all in advance of the receiver stations. Two persons pick up wires behind the rest of the crew, and the eighth person operates the transmitter. Crew members are usually trained for any function on the crew, so that maximum flexibility is maintained in day-to-day operation.

As shown in Figure 1.7, two transmitting dipoles are utilized for a single set-up, with each of the three receivers measuring two potential dipoles. Transmitting electrodes consisting of long steel stakes are driven into the ground. The area surrounding the stakes is doused with saltwater to reduce the ground contact impedance, and the stakes are connected to each other with a medium-grade wire. An insulated, 14-gauge wire leads from each of the three transmitting electrode stations to the transmitter at the truck.

Potential electrodes are ceramic "pots," which consist of a copper electrode inserted into a saturated solution of copper sulfate. The pots are planted in small holes, and the surrounding ground is moistened with fresh water in order to reduce the ground contact impedance. Copper sulfate solution diffuses through the unglazed, porous bottoms of the pots, providing a direct but unpolarizable current path between the ionic conduction in the ground and the electronic conduction in the wires. Insulated wires lead from the potential electrodes to the analog input jacks of the appropriate receivers for measurement of ground potential.

Receiver Synchronization and Calibration

While several crew members are setting up the line, the others bring together the three GDP-12 receivers, a spare receiver, a master transmitter controller and a spare transmitter controller for synchronization of their crystal oscillators (Figure 1.8). Each oscillator has a frequency of 5 MHz, which can be trimmed by up to ± 0.3 Hz by means of an external potentiometer. A timing cable connects the master transmitter controller to a receiver, and the receiver oscillator is trimmed such that its beat frequency is identical to that of the controller's oscillator. This process is

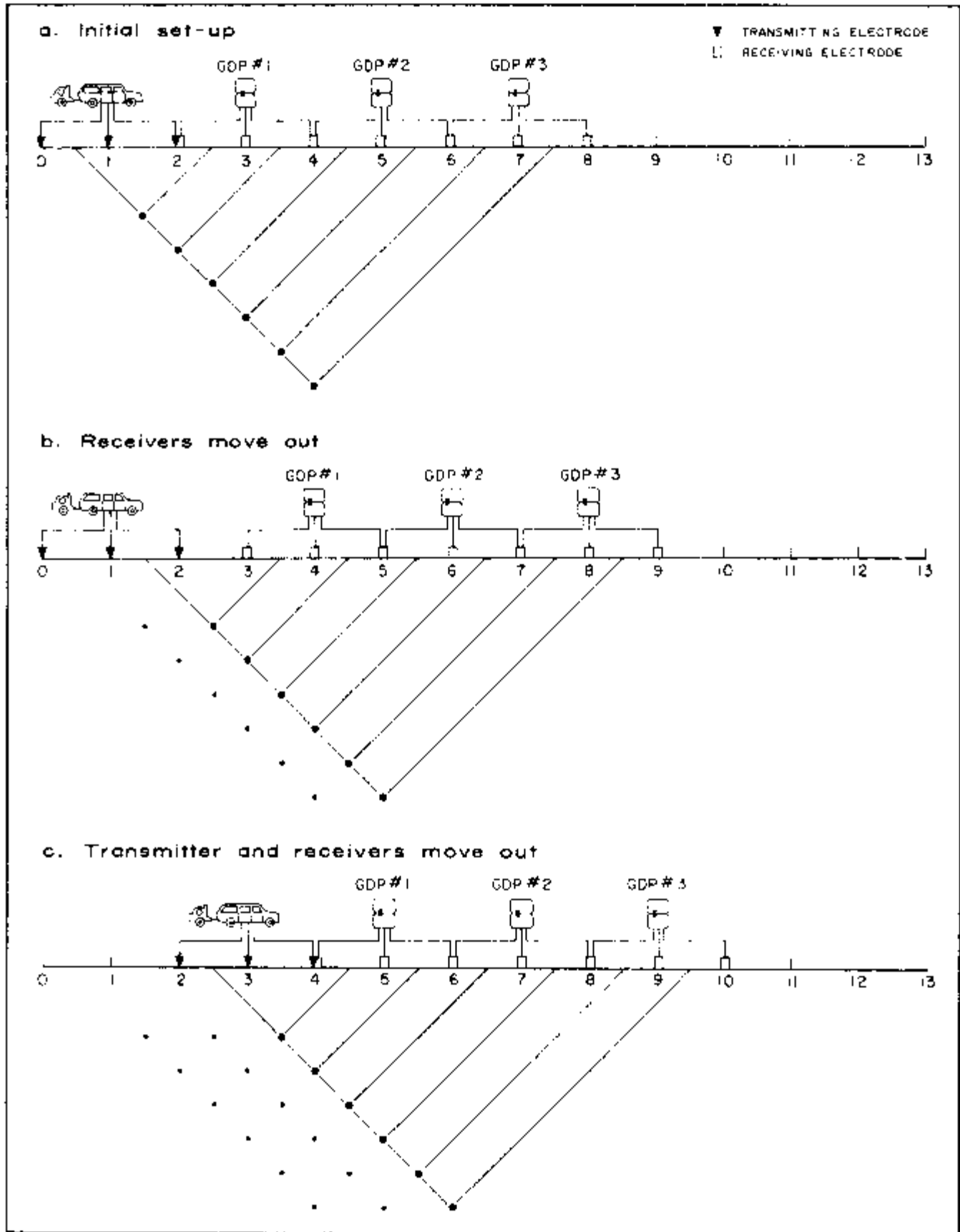


Figure 1.7. Logistical procedure in three-receiver, roll-along, resistivity/phase data acquisition.



Figure 1.8, Synchronization of receivers at the start of production, Lisbon Field project.

facilitated by a display on the controller's analog meter of the beat frequency between the two oscillators. Each receiver and the spare controller is trimmed in this manner. The oscillator ports of all units are then connected to a junction box, and a reset button is pushed in order to synchronize all oscillators in time. Hence, with all oscillators beating at the same frequency and starting at the same time, they all have the same timing reference for accurate phase angle measurements. The oscillators are all oven-controlled in order to prevent desynchronization due to thermal effects, but other effects, primarily minor impurities in the crystal lattice structures, cause the oscillators to "drift" by up to ± 0.2 milliradian at 1 Hz during a normal 10 to 14 hour field day. This lies within acceptable limits.

After the equipment is trimmed and synchronized, the receivers are calibrated using the internal signal of the master transmitter controller. This serves three purposes: it provides a check on the precision of synchronization, it establishes proper functioning of the equipment by repeating calibration values, and it provides an opportunity to store calibration values in memory for later removal from the field data.

Data Collection

After calibration, the three receivers are packed up and moved by truck or foot to the appropriate locations, as shown in Figure 1.7. The receiver nearest the transmitter truck is set up to read the $n=1$ and $n=2$ data, the middle receiver is set up to read the $n=3$ and $n=4$ data, and the far receiver reads the $n=5$ and $n=6$ data. The

$n=5/n=6$ receiver is the master receiver. Its operator is in charge of coordinating the data acquisition, since his data have the weakest signal and are most strongly affected by noise.

The transmitter operator is instructed to transmit current into dipole 0,1, at a frequency of 0.125 Hz. The current level depends upon the electrode resistance and the power range of the transmitter, but generally the maximum possible current is transmitted. Current linearity checks are done to confirm that the ground is not in a state of current saturation, that is, that it shows a strictly linear or ohmic response. This is done by measuring the voltage at two different currents, for example, at 18 amperes and at 9 amperes. If the ground function is linear, the receiver voltage at 9 amps should be half what it was with 18 amps, and the phase angle should be unchanged.

Examining the received voltage waveform on a portable oscilloscope, each receiver operator determines if noise levels are acceptable, verifies the proper operation of his equipment, determines appropriate gains, and selects the proper n -spacing, a -spacing, receiver station number, filter setting, and current level on the front panel thumbwheel registers. When the reset-continue button is pressed, the receiver begins to collect data automatically. The first waveform is digitized and stored in memory. Subsequent waveforms are digitized and added to memory, and with each successive addition, an averaged phase angle value and a standard error of the mean (SEM) value are displayed for channel 2 in the receiver's liquid crystal display window. This permits the operator to observe how well the data are converging. Data acquisition is stopped manually when convergence has reached an acceptable level, and the receiver proceeds to process the data automatically. A Fast Fourier Transform (FFT) is performed for each channel, apparent resistivity is calculated from the parameters selected on the thumbwheels, and phase angles are decalibrated. The final output is sent to a cassette/printer device, although it can also be recorded by hand. Output for each channel consists of raw magnitude, raw phase angle, apparent resistivity, decalibrated phase angle, and standard error of the mean.

This initial sequence of data collection is called a "stack." Several stacks are often taken to ensure sufficient data repeatability. Once all three receiver operators have obtained acceptable data, the master receiver operator instructs the transmitter operator to increment the frequency to 0.25 Hz. Stacking and averaging proceeds in a similar manner for the 0.25, 0.5, and 1.0 Hz data. Following this, the receivers are moved forward one a -spacing; data are acquired at $n=1$ to $n=6$ using dipole 1,2 as a transmitter dipole. The receivers are then moved forward one a -spacing, and the transmitting electrodes are moved forward two a -spacings. This procedure is repeated until adequate coverage has been obtained.

The crew chief is responsible for monitoring the data collection, and he keeps updated field pseudosections. This is done for several reasons. First, subtle problems and errors which have not been detected by the equipment operators can often be detected on pseudosections. Second, the pseudosections can be used to alter survey logistics as needed, depending upon the trends shown in the data. Third, the pseudosections are an invaluable aid to interpretation. Both the apparent resistivity and three-point decoupled phase angle can be used for interpretation in the field. REM data are not generated until after the data are returned to the office.

1.6 HARMONIC COMPLEX RESISTIVITY DATA ACQUISITION AND FIELD LOGISTICS

Data from two of the projects contained in this volume, Desert Springs (Chapter 4) and Garza (section 2.5), were obtained with a harmonic complex resistivity system in which squarewave current at a single frequency is transmitted and data at higher frequencies are calculated from a Fast Fourier Transform (FFT) of the waveform. The instrumentation is somewhat similar to that used for resistivity/phase. The GDP-12 receiver is merely programmed for complex resistivity data acquisition, and the necessary peripheral devices are added to the field set-up. The field data are very similar to the resistivity/phase data; only the frequencies at which they are acquired are different.

The advantages of harmonic data acquisition are two-fold. First, it is much faster, since data are not acquired discretely at every frequency desired, but are calculated from the measured waveform. A complex resistivity system acquiring harmonic data at 0.125, 0.375, 0.625, 0.875, 1.125, and 1.375 Hz on one dipole is about twice as fast as an equivalent, single-receiver resistivity/phase system acquiring discrete frequency data at 0.125, 0.25, 0.5, 1.0, and 2.0 Hz on two dipoles. The second advantage of complex resistivity is that any output irregularities in the transmitted waveform are monitored and deconvolved from the data. This is of crucial importance; many of the resistivity/phase surveys run in the past have been plagued by current instabilities from the effects of geology on the transmitter electrodes, resulting in peculiar diagonal effects. Such effects may be hand-corrected at times, but this process is tedious and injects unwanted elements of ambiguity into the data.

Instead of reading data with a receiver placed directly at the receiving dipole, as in resistivity/phase, the receiver and transmitter are mounted in a recording truck for complex resistivity work. The voltage drop across a remote receiving dipole is sensed by a small preamplifier, which also provides some noise rejection; the signal is sent down a communications cable (the analogue of a seismic cable) to the receiver in the recording truck. The cable replaces the crystal oscillator for purposes of synchronization of transmitted and received signals.

Setting Up the Survey Line

As with resistivity/phase work, a dipole-dipole array is used for complex resistivity. There are two modes of operation, and which one is used depends upon terrain, truck access to the line, etc. The two methods of operation are shown in Figures 1.9 and 1.10. The "roll-along" mode (Figure 1.9) involves a set-up similar to roll-along resistivity/phase. Three to seven transmitting electrodes are set out, and data are obtained one dipole at a time in a forward direction. After the receiver dipole has been advanced sufficiently to obtain the first "spread" of pseudosection data, the transmitting electrode array is advanced, and the survey continues in this fashion. The second mode (Figure 1.10) is called the "center-spread" mode. This involves setting up seven to ten transmitting electrodes, with the transmitting truck at the center of the spread. Data are obtained first on one side of the spread by advancing the receiving dipole from the center to well past the last transmitting electrode; the receiving dipole is then flipped to the other side and data are obtained by moving the receiving dipole in a reverse direction. Suitable repeat points are obtained to check the effects of reversing the relative positions of transmitting and receiving dipoles (this is called a reciprocity check).

As a matter of convenience, the center-spread mode is described in detail in this discussion, although the same principles apply almost universally to the roll-along mode. The field layout is illustrated in Figure 1.11.

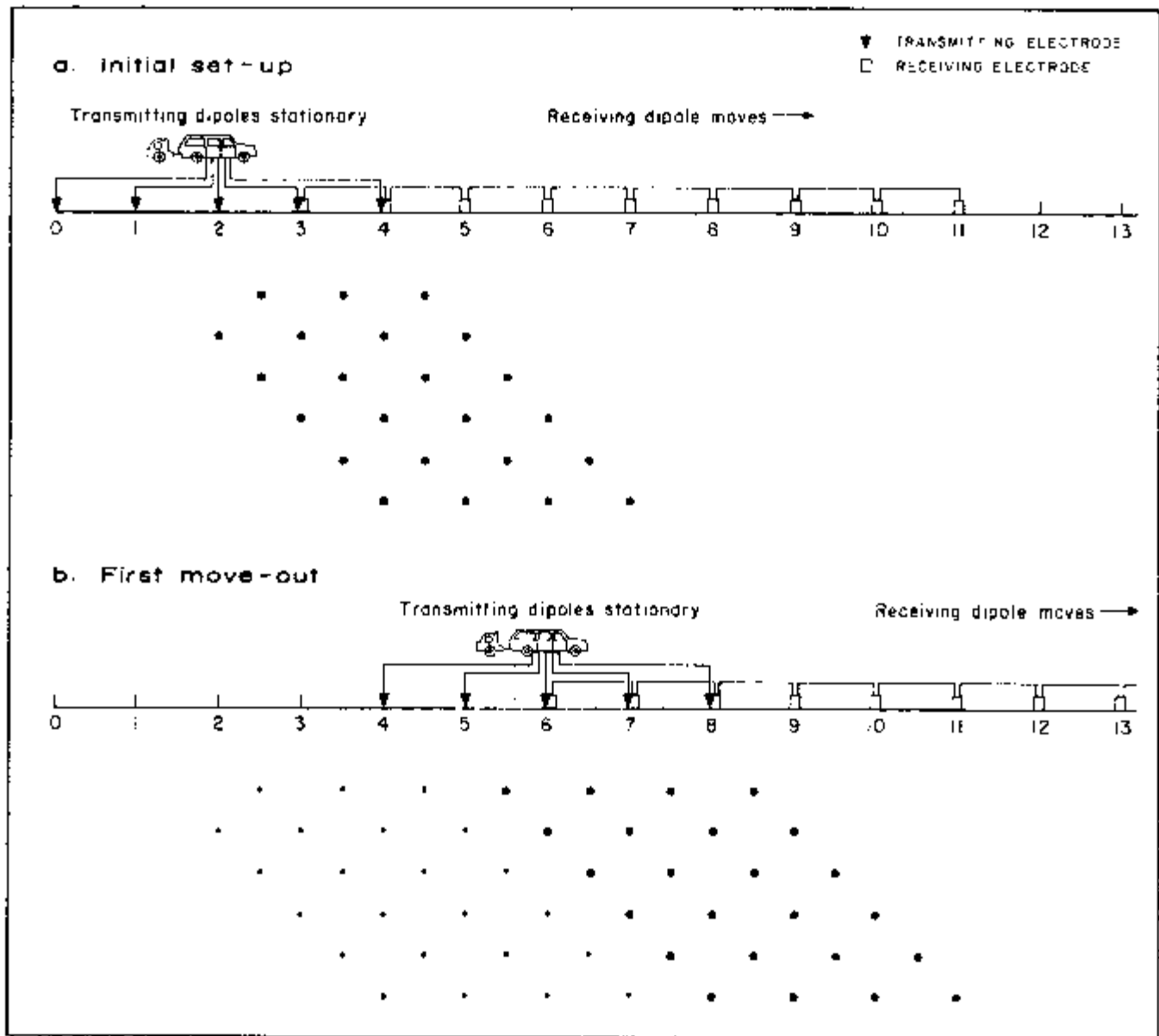


Figure 1.9. Logistical procedure in roll-along complex resistivity data acquisition.

Receiver Calibration

While the wires are being set out by the line crew, the crew chief assembles the GDP-12 instrumentation for a system calibration. This is done to confirm proper system operation and is performed every day prior to data acquisition. The goal in this procedure is to measure the resistance and phase shifts of the system for later removal from the data. A low-current squarewave signal, obtained from the GDP-12 receiver lid, is split into a single-ended and double-ended output via a voltage divider box. The double-ended (differential) signal is fed through a field preamplifier and isolation amplifier combination into channel one of the GDP-12 (this is the side that monitors the field signal). The single-ended source is fed through the isolation amplifier and into channel two of the GDP-12 (this is the side that monitors the transmitted signal). The two waveforms thus pass through similar electronic paths and through the same array of amplification and filtering devices into the GDP-12. In

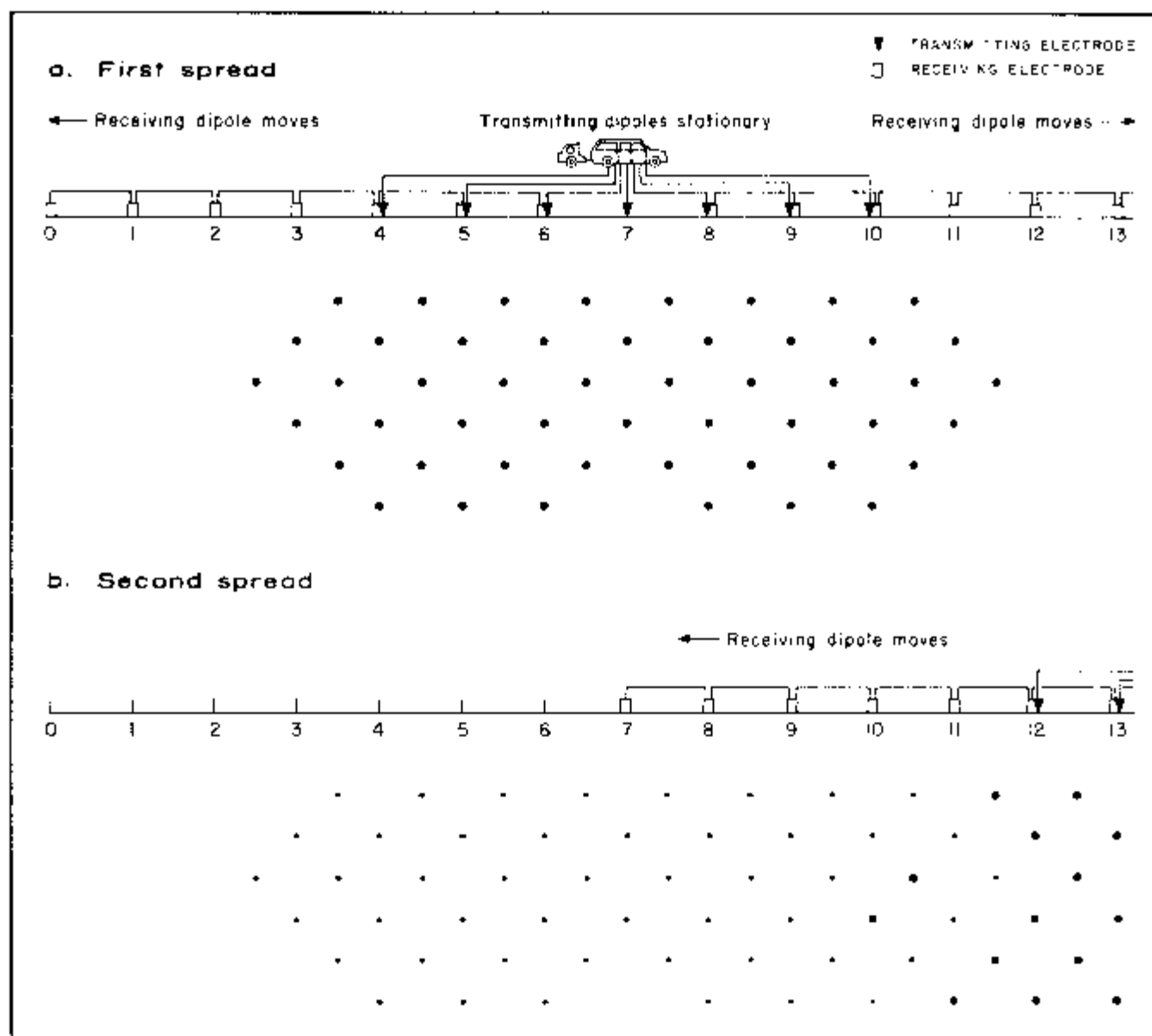


Figure 1.10. Logistical procedure in center-spread complex resistivity data acquisition. Several data points are often repeated between multiple spreads in order to provide a check of data continuity and reciprocity.

order to find the minor differences in the two paths (due to filtering in the field preamplifier and slight differences in electronic components), the two waveforms are deconvolved, as they are in the field measurements, with voltages being divided and phase angles subtracted. The deconvolved magnitude/phase data are known as the final system calibration, and are stored and later removed from the field data.

Field Processing Techniques

Two standard signal processing techniques are used in data acquisition: the Fast Fourier Transform (FFT), and deconvolution. While both of these are described in standard electrical engineering texts, a brief treatment is provided here for the benefit of the reader.

The FFT is a method by which a periodic signal may be represented by the sum of a series of sinusoids. A squarewave, which is normally used in complex

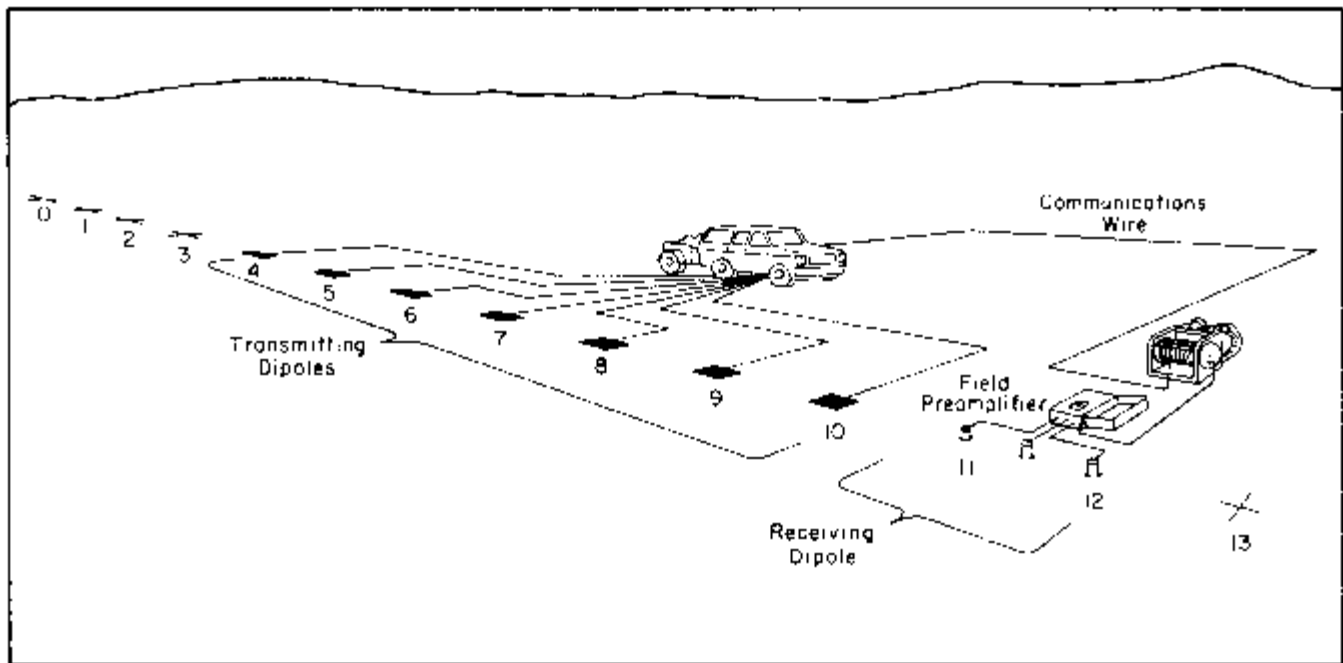


Figure 1.11. Field layout of a center-spread complex resistivity survey.

resistivity work, can be represented by the sum of a series of odd Fourier harmonics:

$$V = A \sin \omega t + \frac{A}{3} \sin 3\omega t + \frac{A}{5} \sin 5\omega t + \cdots + \frac{A}{n} \sin n\omega t + \cdots \quad (1.1)$$

(n odd)

in which V is the voltage or amplitude of the squarewave, $A=4/\pi$ is the amplitude of the first Fourier harmonic (i.e., the first term in the equation), ω is the angular frequency, and t is some arbitrary point in time. The first term is the first Fourier harmonic, or fundamental; the second term is the third harmonic, the next term is the fifth harmonic, and so forth. The even harmonics are zero for an ideal squarewave. Note that each successive harmonic is decreased in amplitude by the inverse of its harmonic number. Figure 1.12 shows the squarewave and its first few odd harmonics; if all harmonics are added together, their sum takes on the appearance of the original squarewave.

Since the n th harmonic has a frequency of n times the fundamental frequency, one can see that, by transmitting a squarewave with a frequency of f , one can use the FFT to obtain amplitude and phase data for frequencies $f, 3f, 5f, \dots, nf$. In other words, instead of transmitting and receiving data at every frequency desired, a single frequency is transmitted and a suite of data at higher frequencies is obtained automatically. The only limitation to this approach is that, since harmonic amplitudes decrease according to their harmonic number, the signal to noise ratio becomes much worse for the higher harmonics. In practical applications, harmonics 1 through 11 are normally obtained; harmonics higher than the 11th are too noisy to be obtained economically.

The lowest frequency normally used in complex resistivity work is 0.125 Hz. From this, data at frequencies of 0.125 to 1.375 Hz are obtained. In order to extend this range to higher frequencies, fundamental frequencies of 1.0 Hz and 8.0 Hz are

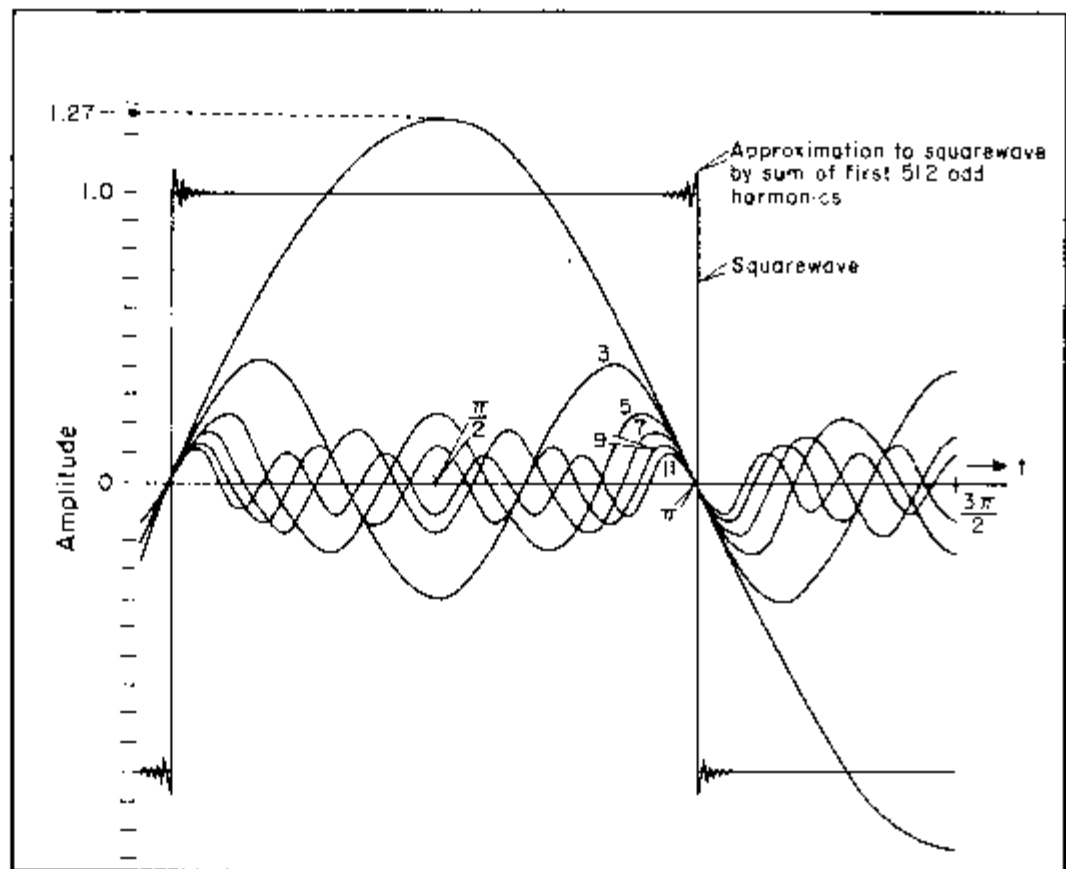


Figure 1.12. Representation of a squarewave by a series of odd Fourier harmonics.

also used, and non-zero odd harmonics from 1 to 11 are obtained for each of these. The result is a discrete frequency spectrum from 0.125 to 88 Hz, composed of three "blocks" of data (Table 1.1). The overlap between these "blocks" allows for a check of data quality through "bracketing."

Deconvolution is a process by which a given effect present in two Fourier transformed signals is removed from them by division. In complex resistivity, the squarewave signal transmitted into the ground is measured on channel 2 of the receiver, and the squarewave voltage which has been modified by the ground's electrical characteristics is measured on channel 1. While the original squarewave is needed to initiate a ground response, this waveform itself is of no interest to us, and

TABLE 1.1: COMPLEX RESISTIVITY FREQUENCIES

	0.125 Hz Data Block	1.0 Hz Data Block	8.0 Hz Data Block
Fundamental frequency	0.125 Hz	1.0 Hz	8.0 Hz
3rd harmonic	0.375	3.0	24.0
5th harmonic	0.625	5.0	40.0
7th harmonic	0.875	7.0	56.0
9th harmonic	1.125	9.0	72.0
11th harmonic	1.375	11.0	88.0

it must be removed from the total received response. This is accomplished by deconvolution, in which the Fourier transform of the received voltage is divided by the Fourier transform of the transmitted current, and the transmitted phase angle is subtracted from the received phase angle. The result of this is what we want: the ground response, or transfer impedance, for a given frequency.

Deconvolution serves another very important purpose. Any current or phasing instabilities due to the transmitter or due to peculiar electrode effects will be reflected in the received data; they will also be present in the data from the transmitted waveform. By deconvolving received and transmitted data, these effects will be removed. In making milliradian-accuracy measurements, this process is indispensable.

Data Collection

Following calibration, the field preamplifier is moved to the center of the receiving dipole. Three porous pots, planted at the ends and the center of the dipole, are connected to the preamplifier input. The signal is measured across the end pots; the center pot is used for common mode noise rejection. The crew checks proper preamplifier operation, selects a gain of 1 or 10, and determines the pot contact resistance. The communications cable, which has been laid out between the recording truck and the receiving dipole, is connected to the preamplifier.

Setting up the equipment in the recording truck, the crew chief disengages all filtering at the GDP-12 and examines the natural ground noise via a two-channel portable oscilloscope. This provides a check on types of noise present and provides information necessary to avoid signal saturation. Next, current is transmitted into one of the transmitting dipoles at the highest fundamental frequency being used on the survey, which typically is 1 or 8 Hz. After both the received and transmitted waveforms are carefully examined on the oscilloscope, appropriate filtering, gains, current level, n-spacing, a-spacing, and receiver station number are selected on the front-panel thumbwheels of the GDP-12. Stacking and averaging is then commenced by pressing the reset and continue buttons. Each successively measured waveform is digitized and is added to memory, and real-time raw phase angle and standard error of the mean values are calculated and displayed on the GDP-12's liquid crystal displays. These values are used to determine proper convergence of the data; stacking and averaging is terminated manually by the crew chief when data of the required precision have been acquired. The data set obtained from this process is called a "stack."

After termination of data collection, the GDP-12 begins processing the data. The digitized, summed waveforms are divided by the number of stacks in order to determine the averaged waveform, and a fast Fourier Transform is performed to obtain the harmonic data. The harmonics for the received and transmitted waveforms are then deconvolved, harmonic-for-harmonic, in order to derive the ground response, which is independent of the type of waveform. The apparent resistivity is calculated and all the input parameters and harmonic data are recorded on a mini-cassette and on paper by an electrostatic printer. The operator determines the quality of the data by examining the smoothness of the data changes and by examining the bracketing between data blocks, and by monitoring the real-time standard of the mean calculation provided for 0.125 and 1.0 Hz. At the outset of the project, a second stack is usually taken in order to relate absolute repeatability to the smoothness, bracketing, and standard of the mean checks.

Once acceptable data have been obtained, the next-lowest fundamental frequency is selected. Data are taken as before, and once data at all the required

frequencies have been obtained, the next transmitting dipole is selected. The process is continued until the desired pseudosection coverage has been obtained.

The crew chief keeps an updated data inventory list and updated pseudosections as the data are acquired in order to identify problems, and to provide preliminary in-the-field interpretation of the results.

1.7 CONTROLLED SOURCE AMT DATA ACQUISITION AND FIELD LOGISTICS

Description of the Technique

Having been used in massive sulfide detection for more than five years, the controlled source audiofrequency magnetotellurics (CSAMT) technique was applied to petroleum exploration in 1982. This technique is substantially different from resistivity/phase or complex resistivity.

While it is beyond the scope of this project to describe the CSAMT technique in detail, a brief discussion is provided in order to familiarize the reader with the basic principles. As shown in Figure 1.13, a long transmitting dipole is laid out on the ground several miles away from the site to be investigated. Four quantities are measured: 1) the potential drop across a grounded electric dipole which is oriented parallel to the transmitting dipole, 2) the magnetic field pickup in an antenna which is oriented perpendicular to the transmitting dipole, 3) the phase lag of the electric field waveform with respect to the transmitted waveform, and 4) the phase lag of the magnetic field waveform. The ratio of the horizontal electric field

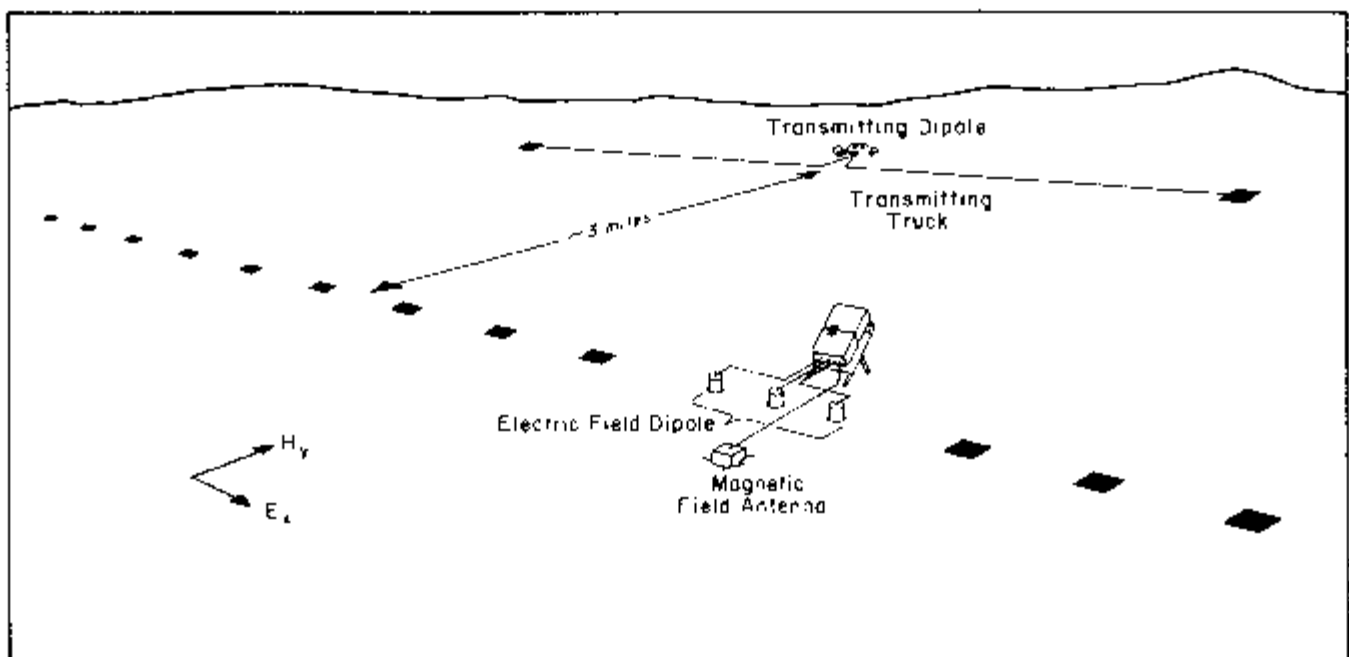


Figure 1.13. Field layout of a CSAMT survey.

voltage (E_x) and the perpendicular, horizontal magnetic field strength (H_y) is related to the apparent resistivity (ρ) of the ground at a given signal frequency (f):

$$\rho = \frac{1}{2\pi f \mu_0} \left(\frac{E_x}{H_y} \right)^2 \quad (1.2)$$

The depth of penetration is related to skin depth (δ), which is given by equation (9.87):

$$\delta = 503 \sqrt{\frac{\rho}{f}} \quad (\text{meters}) \quad (1.3)$$

Equation (1.3) shows that signal penetration increases with lower frequency signals and with higher resistivity ground. In contrast with resistivity/phase and complex resistivity techniques, penetration is not affected by geometric factors (i.e., dipole sizes or separations), since the ground sensed by the dipole-antenna combination is being subjected to a near-plane wave from the distant transmitter. As a result, the CSAMT pseudosection is not affected by diagonally-controlled geometric effects which are seen in dipole-dipole pseudosections.

CSAMT has a distinct advantage in that lateral resolution across a traverse is approximately equal to the size of the electric dipole. By using a sufficiently small dipole, the boundaries of a buried conductive or resistive feature can be determined to within a few feet. The chief disadvantage of CSAMT is that, at this time, it is difficult to determine accurate depth to a responsive zone when it falls within the "near-field" or "transition" frequency zones of CSAMT data acquisition. Computer modeling may eventually help resolve this problem.

Controlled source AMT differs in several respects from natural source MT methods, which have been used with mixed success in structure mapping for petroleum applications over the past three or four decades. The chief difference is that CSAMT has a dependable fixed signal source, while MT does not. This accounts for the enormous cost difference between the two systems: while a single MT station may require up to a day of data collection, CSAMT stations typically require less than 45 minutes. The CSAMT method also has a shallower penetration—typically less than 10,000 feet (3,000 m)—while MT penetrates up to many miles. Hence CSAMT is better suited to examining the alteration patterns which exist in sediments overlying hydrocarbon traps. CSAMT also requires a far less sophisticated and less expensive data acquisition system. The GDP-12 system is used for all data acquisition.

CSAMT Pseudosections

Apparent resistivity is the primary parameter of interest in CSAMT work. This is plotted as a function of signal frequency versus station number in pseudosection form, as shown in Figure 1.14. The rationale behind this approach is found in equation (1.3): higher frequencies result in shallower penetration, so the pseudosection is plotted with high frequency data at the top and low frequency data at the bottom.

Further Information

More detailed information on CSAMT can be found in the work of Goldstein and Strangway (1975), Zonge, Emer, and Ostrander (1980), Ostrander (1981), Bartel (1982), and Sandberg and Hohman (1982). An informational brochure (Zonge Engineering, 1981) describes the field logistics used by Zonge Engineering.

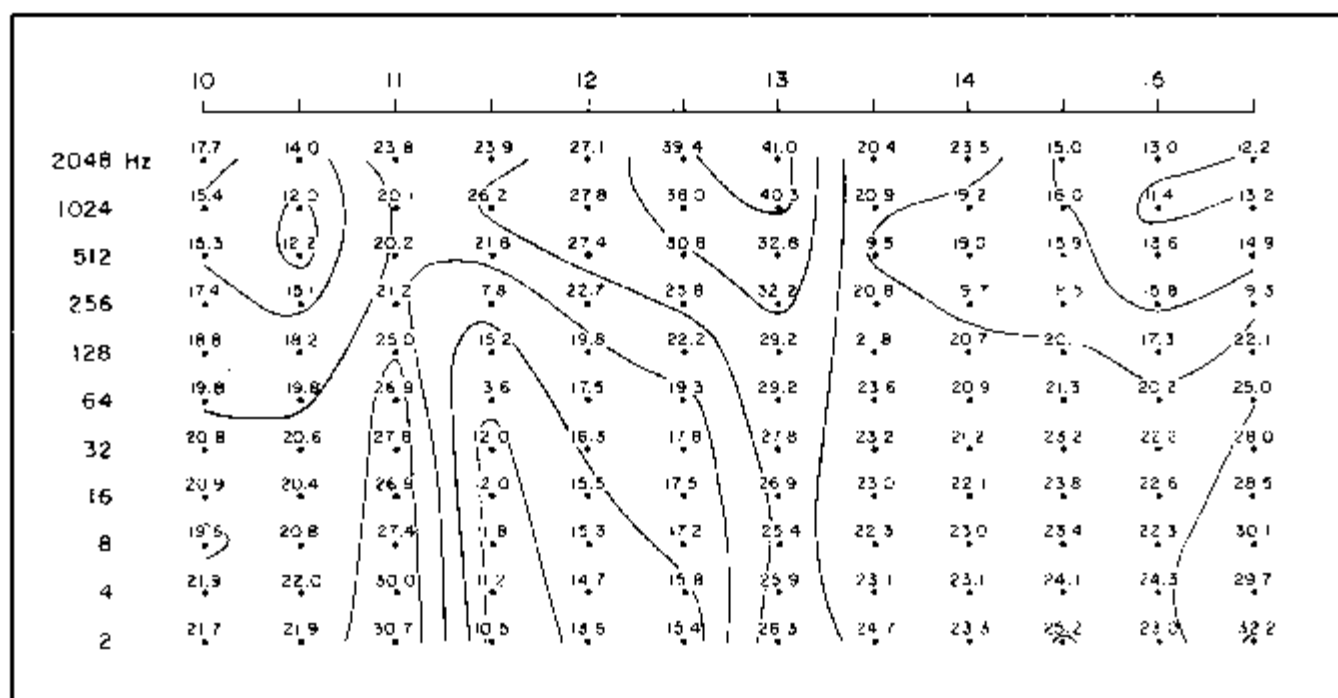


Figure 1.14. Apparent resistivity data from CSAMT data over Cowboy Field, San Juan County, Utah. Contour interval: 10.0, 12.6, 15.9, 20.0, 25.1, 31.6, 39.8 ohm meters.

1.8 DATA PROCESSING TECHNIQUES, RESISTIVITY/ PHASE AND COMPLEX RESISTIVITY DATA

Interfacing with the PRIME 750

Data are sent to the office by registered mail on a biweekly basis. The field data are stored on cassette tapes and electrosensitive paper; "inventory sheets" are kept as notes on acquisition of the data.

Cassette data are read into the memory of Zonge Engineering's PRIME 750 by means of a cassette reader device. A number of checks are made to ensure the proper transfer of the data. The bulk of the resistivity/phase data presented in this volume was obtained during the development of the CAP-12 Cassette/Printer, and consequently these data were recorded by hand. This required manual entry of the data into the computer.

Editing and Pre-Processing

Upon transfer of the raw data to the PRIME, a thorough check of data quality is made by data processing personnel. Data glitches and inconsistencies are corrected, incompletely transferred data blocks are identified, and the magnitude and phase data are averaged to produce a final set of raw data. These data are then decalibrated, and, if the data were acquired by means of complex resistivity, a correction factor is made for the resistance of the communications wire.

The apparent resistivity at 0.125 Hz is calculated for the dipole-dipole array data from equation (9.55):

$$\rho_a = \frac{V}{I} \pi a n (n+1) (n+2) \quad (1.4)$$

in which V is the voltage measured across the receiving dipole, I is the transmitted current, a is the dipole size, and n is the dipole separation. Corrections for gain settings are made automatically.

Decoupling the Field Data

At this point, the data consist of magnitude and raw phase angle measurements for each frequency obtained on the survey. The raw phase angle data consist of two distinct responses: induced polarization and electromagnetic coupling. In order to make use of these two responses in interpretation, they must be separated from each other. The processing required for this separation is called "decoupling."

As explained in section 9.8, decoupling is a very difficult process. The exact solution of the complex impedance equation is essentially untenable, so the normal approach is to make a few initial assumptions about the response of the earth and to invert the data iteratively by means of theoretical and empirical constraints. One of two types of solutions are normally obtained for Zonge Engineering data. The first is a "quick solution," which employs a quadratic extrapolation approach of the type developed by Kennecott and published by Hallof (1974). The second is a more exact solution developed and held proprietary by Zonge Engineering (Wynn and Zonge, 1975). All data which are presented in this volume have been decoupled by means of the latter technique.

QUADRATIC EXTRAPOLATION SOLUTION

The quadratic extrapolation technique is an arbitrary graphical approach which makes use of three assumptions: 1) induced polarization phase response is constant (independent of frequency) and is defined at DC; 2) electromagnetic coupling varies smoothly with frequency and is exactly zero at DC; 3) the two effects are additive. A fourth, implied assumption is that the extrapolation occurs over a relatively unchanging portion of the complex plane curve, and that the total coupling phase shift is relatively small (e.g., less than 100 milliradians).

Figure 1.15 shows the basic approach. A quadratic fit is made using data at three low frequencies on the curve, and an extrapolation is made to DC. If the extrapolated value is zero, the curve is assumed to be generated by electromagnetic coupling exclusively. If the extrapolated value is non-zero, the curve is assumed to be generated by both electromagnetic coupling and polarization, and the DC extrapolated value is supposed to represent the polarization response at DC. The equations used for the extrapolation are developed in section 9.8. For the resistivity/phase frequencies, which differ by binary intervals, the 3-point extrapolation equation is:

$$\phi_c = -\frac{8}{3} \phi_{.125} - 2\phi_{.25} + \frac{1}{3} \phi_{.50} \quad (1.5)$$

in which:

- ϕ_c is the three-point phase angle
- $\phi_{.125}$ is the phase angle at 0.125 Hz
- $\phi_{.25}$ is the phase angle at 0.25 Hz
- $\phi_{.50}$ is the phase angle at 0.50 Hz

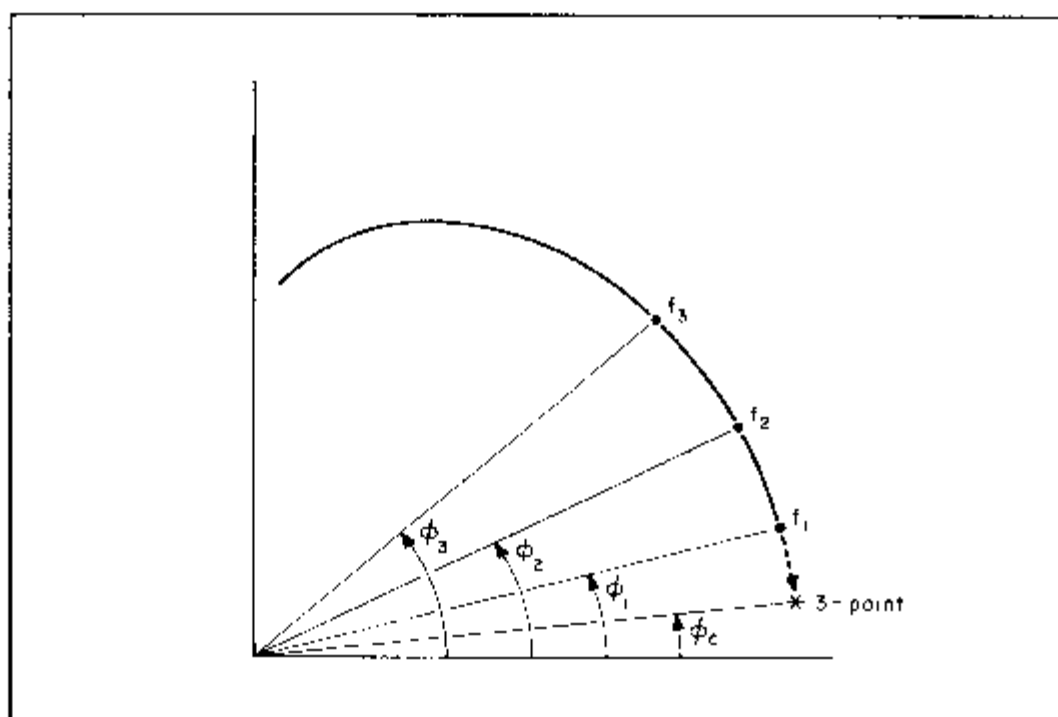


Figure 1.15. Three-point quadratic extrapolation.

In order to determine the separate polarization and coupling values at all frequencies, the polarization value is assumed to be independent of frequency, and the three-point value is subtracted from coupling values at each frequency. This approach has obvious drawbacks, since the inherent frequency response of polarization is ignored.

While the quadratic extrapolation technique is useful for a quick look at gross changes in polarization effects at a single frequency, it almost always produces either an artificial undercorrection or overcorrection to the data. An example of this is provided by examining the coupling for a dipole-dipole array over a homogeneous earth. An electromagnetic coupling routine called "TWOLAY" was used for this purpose, using a standard dipole spacing of 2,000 feet (610 m) and a ground resistivity of 30 ohm-meters. Only electromagnetic coupling effects were included; the ground was assumed to be nonpolarizable and homogeneous.

Three-point extrapolations of data at 0.125, 0.375, and 0.625 Hz were made for coupling curves at n -spacings of 1 through 6. Now, if the three-point extrapolation were correcting properly for coupling, we would expect all extrapolated values to be zero, since no polarization is assigned to the homogeneous half-space. However, the three-point data calculated from the model results are all non-zero, increasing in value from 0.4 milliradians at $n=1$ to 21.8 milliradians at $n=6$. This produces an artificially layered effect when plotted in pseudosection form, an effect which would artificially enhance an isolated polarization anomaly, as well as making it appear to be lower in the pseudosection than it really is. The reason for the failure of three-point calculations to match expected values is related to the non-validity of the fourth assumption behind the technique, i.e., the phase shifts are too large to be valid for a small angle approximation. Figure 1.16 illustrates the difference between the $n=1$ and $n=6$ extrapolations. For $n=1$, the coupling curve is small since the geometric separation is small (refer to section 9.8), and extrapolation occurs along

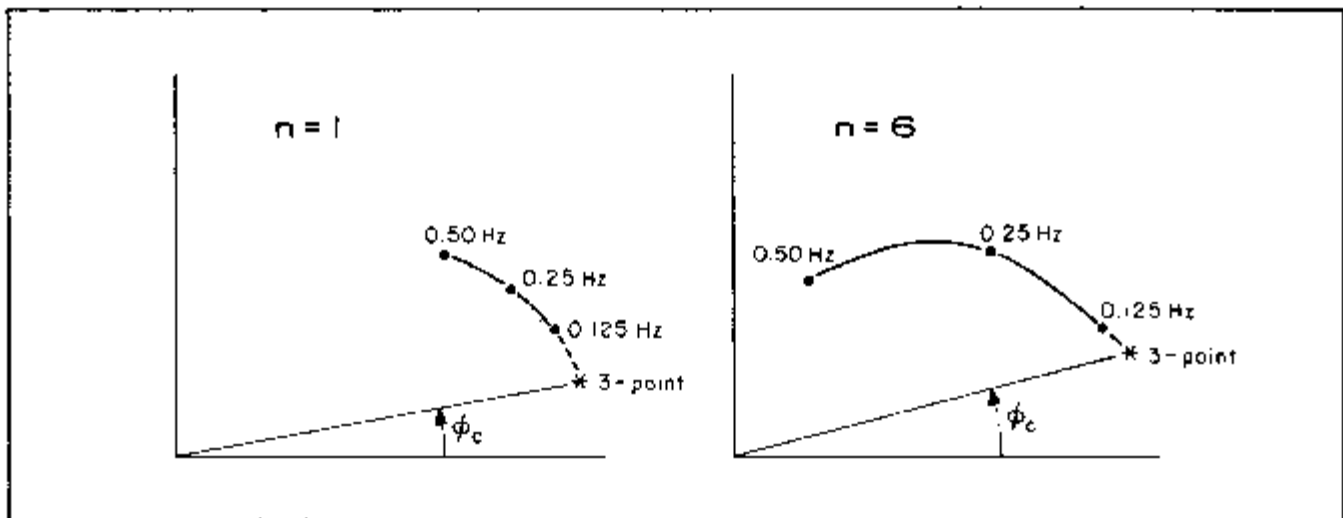


Figure 1.16. Comparison of the extrapolated 3-point phase angles for $n=1$ and $n=6$ on an arbitrary coupling curve.

the more linear portion of the curve. However, at $n=6$, the coupling curve is greatly extended due to the larger geometric separation, and the extrapolation is made from data points on the strongly curved portion of the coupling curve, resulting in an "undercorrection" or stronger residual phase calculation. The situation is even worse in high-over-low resistivity layering, where the coupling curve is even more strongly curved.

In-house research has shown that many subtle, polarizable anomalies over oil and gas fields can be lost in the three-point layering effect, especially in geologically complicated environments. As a result, it is advisable to use the more exact technique for decoupling the field data. Additional frequencies are usually required for this approach.

ZONGE ENGINEERING DECOUPLING TECHNIQUE

At this point, it would be useful for the reader to review the discussion of electromagnetic coupling in section 9.8. The following approach was developed by Ken Zonge in early 1973, and has been used successfully for mining and petroleum applications. The descriptions and explanations of the decoupling technique are provided solely for the understanding of the reader and are considered to be held under the proprietary agreement under which this volume has been distributed.

The sequence of decoupling is: 1) establish starting parameters of magnitude and phase angle, 2) select the number of levels or resistivity layers upon which to iterate, 3) curve-match the starting parameters with the field data until an acceptable decoupled response curve has been established.

The first step in decoupling is to establish initial IP parameters. The magnitude (M) and phase (ϕ) are determined by:

$$M = e^{-\frac{2\phi}{\pi} \ln \omega} \quad (1.6)$$

$$\phi = \phi_c \quad (1.7)$$

in which ω is the angular frequency and ϕ_c is the three-point extrapolated phase angle.

A layered-earth model is run in order to establish the minimum number of major resistivity layers which fit the apparent resistivity and electromagnetic coupling data. Usually the number of layers (i) is kept to one or two for the initial iterations, and is expanded to more than two if needed. The so-called coupling coefficients (CC i) for each layer (i) are roughly correlatable to resistivity contrast at each interface. The first coupling coefficient (CC1) determines the first level of layering:

$$\begin{aligned} \text{CC1} > 1 & \quad \text{low-over-high interface} \\ \text{CC1} = 1 & \quad \text{homogeneous earth} \\ \text{CC1} < 1 & \quad \text{high-over-high interface} \end{aligned}$$

The second through fifth coupling coefficients determine additional levels of layering:

$$\begin{aligned} \text{CC2-5} > 0 & \quad \text{low-over-high interface} \\ \text{CC2-5} < 0 & \quad \text{high-over-low interface} \end{aligned}$$

The extension of the coupling curve (θ) which results from each layer is given by

$$\theta = 8.564 \times 10^{-4} a \sqrt{\frac{f}{\rho_i}} \quad (1.8)$$

in which a is the dipole spacing and ρ_i is the resistivity of the i th-level layer. The magnitude and phase angle are given by

$$M = e^{-x} \quad X = \frac{2\phi_c}{\pi} \left[\ln \omega + \frac{A}{1+q} \left(\ln \frac{\omega}{\omega_{.125}} \right)^{1+q} \right] \quad (1.9)$$

$$\phi = \phi_c \left[1 + A \left(\ln \frac{\omega}{\omega_{.125}} \right)^q \right] \quad (1.10)$$

in which $\omega_{.125}$ is the angular frequency at 0.125 Hz. The quantities "A" and "q" are the Hilbert transform slopes, which are empirically determined. These quantities specify the shape of the iterated polarization curve.

Decoupling consists of an inversion routine which fits the starting data (layered-earth coupling plus Hilbert transform) to the raw field data in an iterative fashion. The success of the iterative process is determined by comparing the results to empirical observations of responses observed in field and laboratory measurements. The simplest initial assumptions which yield a successful inversion are adopted as the final solution. If an acceptable polarization response curve is not obtained, the complexity of the initial assumptions is increased until a proper inversion is achieved. Hence, decoupling results are not unique in a strict sense, but they represent the simplest possible solution which adequately fits the field data.

Calculation of REM Data

Following the decoupling process, four parameters are available for interpretation: apparent resistivity, apparent polarization as a function of frequency (spectral type), coupling coefficients, and total electromagnetic coupling data. In typical petroleum projects, the coupling data make up most of the response. The bulk of this response is simply the general response one would see using a large dipole array over a homogeneous earth with low resistivities. Hence, it would be useful to remove the homogeneous response from the total response in order to yield a residual response which is indicative of inhomogeneities in the ground—which are the things we want to detect. This is the logic behind the calculation of residual electromagnetic (REM) data.

The process is essentially a matter of straight algebraic subtraction and normalization. Pure electromagnetic coupling data are calculated for a homogeneous earth of the measured apparent resistivity and for the a and n-spacings. These data are subtracted on a frequency-by-frequency basis from the total coupling data to yield the unnormalized REM data. Since coupling is proportional to frequency, the frequency at which each data point is obtained is normalized to the highest frequency which has been obtained in field surveys (110 Hz). Next, since coupling is proportional to n-spacing, it must be normalized according to n-spacing in order to generate inter-comparable pseudosection data. The n-spacing normalizing factors are empirically determined, and are based upon the deepest data normally obtained (n=6).

The final, normalized REM data consist of real ("in-phase") and imaginary ("quadrature") components. Both contain valuable information, but usually the quadrature component is the most diagnostic in terms of detecting lateral effects in the earth. Only the quadrature components are presented in this volume. A brief description of these data is offered in the following section.

1.9 PARAMETERS USED IN RESISTIVITY/ PHASE AND COMPLEX RESISTIVITY INTERPRETATION

As noted earlier, three parameters are normally used for resistivity/phase interpretation: apparent resistivity, apparent polarization, and residual electromagnetic or REM. Other, additional parameters, such as raw phase angle, spectral type, and coupling coefficients are used in high resolution complex resistivity work, but they are not discussed here.

Apparent Resistivity

Apparent resistivity is a measurement of how well the earth conducts electricity. The dipole-dipole equation for apparent resistivity is derived in section 9.6, and the equation most useful for field work is given in equation (1.4):

$$\rho_a = \frac{V}{I} \pi a n (n+1) (n+2)$$

in which "a" is the dipole size (meters), "n" is the separation between receiving and transmitting dipoles (expressed as a multiple of "a"), I is the transmitted current (amperes), and V is the voltage drop measured across the receiving dipole (volts). The units for apparent resistivity are ohm-meters. Apparent resistivity is the direct inverse of apparent conductivity, whose units are mhos per meter or siemens per meter.

Apparent resistivity data are most sensitive to a conductive object lying in a resistive environment. The data are normally plotted in pseudosection form at 0.125 Hz. Modeling and field experience show that the depth of penetration of apparent resistivity data, obtained from n=1 to n=6 by means of the dipole-dipole array, is about twice the a-spacing. Given typical a-spacings of some 1,000 to 2,000 feet (300-600 m) for hydrocarbon surveys, it can be seen that apparent resistivity data typically respond to features whose depth of burial is less than 2,000 to 4,000 feet (600-1,200 m).

Apparent Polarization

Apparent polarization data represent the ability of the ground to store electrical charge in a capacitive way. Ground capacitance can result from any interface in which the mode of current transport changes from electronic to electrolytic or

when certain ions are restricted in motion by electrical or mechanical forces (see Chapter 8 for a more complete discussion of polarization). The most common sources of polarization in the earth are metallic minerals such as pyrite and chalcopyrite, or clays and graphitic shales.

Apparent polarization is usually plotted in pseudosection form. If the data have been decoupled, as is the case with all the data in this volume, the plotted values are called "decoupled phase angle": they are plotted at 0.125 Hz. If a quadratic extrapolation has been used, the plotted values are called "three-point phase angle" and they represent extrapolated DC (0 Hz) values. Apparent polarization penetration is about the same as that for apparent resistivity—roughly twice the a-spacing.

Residual Electromagnetic (REM)

As seen in the previous section, REM data represent how much the electromagnetic coupling in the ground differs from the calculated homogeneous earth coupling. In practical terms, REM data sense lateral resistivity changes in the ground, usually at depths greater than those probed by apparent resistivity and apparent polarization data. Due to the complex nature of the coupling observed for a dipole-dipole array, it is not possible to establish a firm, theoretically-derived value for the depth penetration of REM data. Modeling would help greatly in this effort, and a three-dimensional electromagnetic algorithm is currently under development. On a strictly empirical level, it has been observed that REM penetration is about 2 to 3 a-spacings, or up to 50 percent greater than the penetration of standard galvanic data. Several of the case histories illustrate this observation. Theoretical calculations show that the effective depth of penetration can be extended past 4 a-spacings with proper estimation of the inductive coupling term.

Only the imaginary or quadrature component of REM is presented in this volume. The numbers are normalized and hence do not have any physical units associated with them. The numbers are not normalized to a-spacing, so data taken with 1,000-foot (305 m) dipoles (for an example) will be lower in magnitude by a factor of 4 than data taken with 2,000-foot (610-m) dipoles. In these data, numbers vary from positive to negative, according to whether the homogeneous earth coupling curve is larger or smaller than the field coupling curve, respectively. Numbers near zero indicate the two curves are nearly identical (i.e., the response resembles a homogeneous earth). Positive numbers indicate a low-over-high resistivity layering, while negative numbers indicate high-over-low layering. Since negative REM values indicate low resistivities at depth, they may be specifically indicative of hydrocarbon-induced alteration, which is typically conductive.

REFERENCES

- Bartel, L.C., 1982, Evaluation of the CSAMT technique for mapping enhanced oil recovery processes (abs.): *Geophysics*, v. 47, p. 452.
- Goldstein, M.A., and Strangway, D.W., 1975, Audio-frequency magnetotellurics with a grounded electric dipole source: *Geophysics*, v. 40, p. 669-683.
- Hall of, P.G., 1974, The IP phase measurement and inductive coupling: *Geophysics*, v. 39, p. 650-665.
- Ostrander, A.G., 1981, Controlled source AMT—application and advantage (unpublished): 87th Annual Northwest Mining Association Convention, Spokane, Dec. 4. Reprints available from Zonge Engineering.
- Sandberg, S.K., and Hohmann, G.W., 1982, Controlled-source audiomagnetotellurics in geothermal exploration: *Geophysics*, v. 47, p. 100-116.
- Wynn, J.C., and Zonge, K.L., 1975, EM coupling, its intrinsic value, its removal and the cultural coupling problem: *Geophysics*, v. 40, p. 831-850.
- Zonge, K.L., Emer, D.F., and Ostrander, A.G., 1980, Controlled source audiofrequency magnetotelluric measurements: Technical papers, 50th Annual International Meeting and Exposition, SEG, Houston, v. 5, p. 2491-2521.
- Zonge Engineering, 1981, Controlled source AMT: information brochure.

Chapter 2

Interpreting Hydrocarbon Anomalies

2.1 INTRODUCTION

This chapter is dedicated to analyzing the characteristics of electrical anomalies measured over known hydrocarbons, to determining an explanation for them, and to demonstrating how the data are interpreted. The discussion will be confined primarily to resistivity/phase and complex resistivity measurements.

It shall be simply stated that the measurements themselves are both valid and repeatable. The validity of the induced polarization technique in general has been well demonstrated in a number of spectacular exploration successes in the mining industry since the 1950s, and by extensive theoretical investigations over the past 50 years. The utility of Zonge Engineering complex resistivity and resistivity/phase surveys has been firmly established in exploration programs over the last 10 years of contract field services. Repeatability of field measurements over periods of months and years has also been established on a number of projects by re-occupying lines for experimental or developmental projects. Quality control over the data is maintained by techniques outlined in Chapter 1.

2.2 STATISTICAL ANALYSIS OF ZONGE ENGINEERING HYDROCARBON SURVEYS, 1977-1982

This section summarizes all Zonge Engineering hydrocarbon projects conducted during the past five years, ending December 31, 1982. The current study involves 879 surface line-miles (1,414 line-km) of data, or 561 subsurface line-miles (903 line-km), obtained over 57.1 crew-months. The total cost of these surveys was \$2.6 million, with the resulting average cost of just under \$3,000 per surface line-mile. As shown in Figure 2.1, the surveys have been conducted in 10 states and two provinces, all in the western and midwestern area of the North American continent. A total of 55 lines have been run over 29 oil and gas fields, which vary in size from very small (less than 8 barrels of oil per day) to gas giants. Production varies from heavy oils to gas, at depths from 200 to over 16,000 feet (60-4,900 m). About 45% of the fields are structural traps, and 55% are stratigraphic; 20% involve primarily gas production, 60% primarily oil, and 20% have both oil and gas. In addition, 101 lines of data have been run over 49 prospects, 20 of which have been or are currently being drilled.

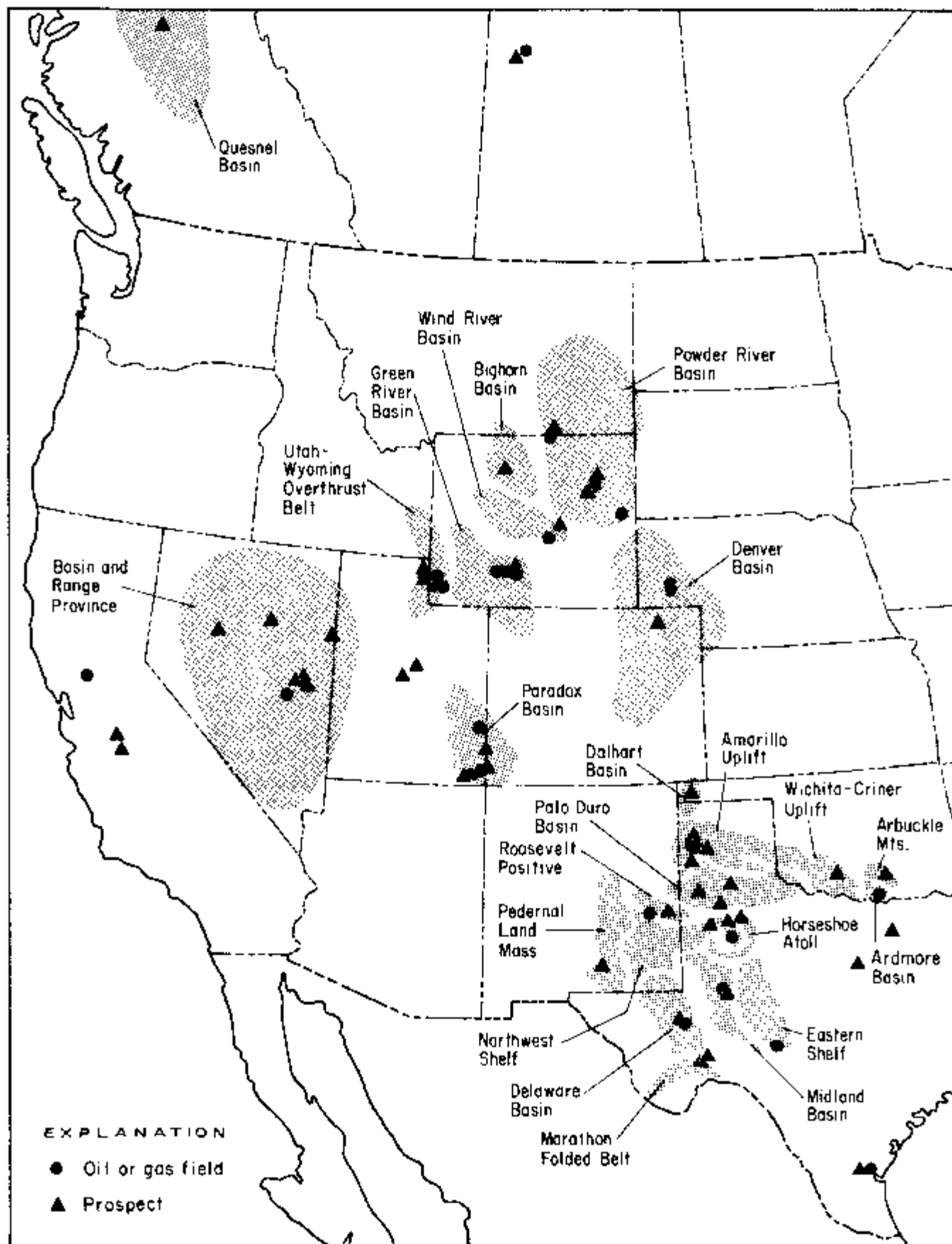


Figure 2.1. Locations of Zonge Engineering petroleum projects. 1977-1982.

Statistical Analysis of the Data

Almost all surveys run to date have used the dipole-dipole array to obtain either discrete-frequency resistivity/phase data or harmonic-frequency complex resistivity data. Frequencies as low as 0.01 Hz and as high as 110 Hz were used on some surveys, but the most commonly obtained frequencies are generally 0.125 to 1.375 Hz.

Three interpretational parameters--apparent resistivity, apparent polarization, and residual electromagnetic (REM) data--were analyzed in early 1983 for patterns in the data which resemble bonafide hydrocarbon responses. The data from existing oil and gas fields were specifically examined for the correlation of conductive apparent resistivity and REM anomalies, and of high polarization anomalies, with the lateral extent of the hydrocarbons. The anomalies were classified as follows:

1. Fair to excellent: moderately well-defined to classically shaped anomaly, well-correlated in plan view to the lateral extent of the hydrocarbons; would be recommended as a favorable drilling target if it were a prospect.
2. Absent to poor: poorly defined or poorly correlated anomaly, or one in which the definition is severely complicated by cultural, topographic, or structural effects; would not generally be recommended as a favorable drilling target, even though it may show subtly favorable trends.
3. Negatively correlated: distinct high resistivity, low polarization, or positive REM anomaly associated with the lateral extent of the hydrocarbons.
4. Data uninterpretable: severe cultural, structural, topographic, or other effects contaminating data.

Data from rank prospects were evaluated in a similar manner, with the obvious exception that correlation considerations were omitted. All statistics were compiled on a line-by-line basis; the statistics compiled on a field-by-field basis were quite similar. All lines run up through December, 1982 are included.

It should be stressed that the following statistics are to be regarded with some degree of caution, since any statistical summary of such widely varying field projects is subject to considerable ambiguity. Evaluations of a given anomaly are based upon interpretation, which is highly dependent upon the proper recognition of effects due to well casings, surface culture, topography, surface high resistivity materials, structure, etc. While care has to be taken to distinguish these spurious effects from true hydrocarbon alteration responses, it is not always possible to make the differentiation with absolute assurance. Hence, it is possible that some of the so-called "favorable" anomalies are merely unrecognized cultural or other spurious anomalies; conversely, it is also possible that some anomalies which were attributed to spurious effects may actually be partly due to bonafide hydrocarbon alteration responses. Great care has been taken to minimize the uncertainty in these regards. It is also important to recognize that the statistical sample in these compilations is rather small. In general, however, the statistics of Tables 2.1, 2.2, and 2.3 represent in a *qualitative* way the results of Zonge Engineering work to date.

An additional statement must be made in regard to these statistics: they merely represent a *statistical correlation* between electrical anomalies and hydrocarbons, prospects, and drilling. In no way can it be assumed *a priori* that a causal link exists; causality must be established by evidence which is independent of a simple statistical summary. For the present, we present these statistics merely for observation. Later sections will attempt to explain the origin of these anomalies.

Table 2.1 shows the correlation of electrical anomalies with the location of established hydrocarbon production. The parameters of apparent resistivity and REM are statistically correlated with hydrocarbons about one-half to two-thirds of

TABLE 2.1: CORRELATION OF ANOMALIES TO OIL AND GAS FIELDS

ALL PROJECTS (55 lines, 29 fields)

	Apparent Resistivity	Apparent Polarization	REM	At Least One Parameter
Fair to excellent	58%	24%	65%	66%
Absent to poor	31	58	24	27
Negative correlation	0	0	0	0
Uninterpretable or ambiguous	11	18	11	7

CASE HISTORIES (14 lines, 9 fields)

	Apparent Resistivity	Apparent Polarization	REM	At Least One Parameter
Fair to excellent	58%	29%	64%	64%
Absent to poor	21	64	15	29
Negative correlation	0	0	0	0
Uninterpretable or ambiguous	21	7	21	7

the time and are non-correlated about one-fourth of the time. In many cases, lack of correlation occurred over fields which had minimal production, spotty lateral production (e.g., discontinuous channel sand facies), or which produced only heavy oil. However, in several other cases, lack of correlation could not be readily associated with any particular field characteristics.

About one-tenth of the resistivity and REM data sets were rendered uninterpretable by cultural or structural effects, and at least half of the projects showed some signs of such contamination. Apparent polarization shows a lower statistical correlation with hydrocarbons; in fact, it is more often uncorrelated than it is correlated. Many of the incidences of non-correlation cannot be related to field characteristics, a fact which will be discussed later in regard to proposed anomaly mechanisms. At least one of the three interpretational parameters was correlated to producing fields in two-thirds of the projects.

Several items are of interest here. First, while apparent resistivity and REM show roughly similar correlations with oil and gas fields, it was noted that REM almost always provides better definition and lateral correlation to the producing field than does the resistivity parameter. Several examples of this are presented in the case histories. Second, all anomalous responses are low in resistivity, high in polarization, and negative (conductive) in REM; none of the fields show distinct negative correlations, i.e., high resistivity, low polarization, or positive (resistive) REM.

Table 2.1 also contains statistics for the case histories contained specifically in this volume: Garza, Ryckman Creek, Whitney Canyon, Desert Springs, Playa-Lewis, Desert Springs West, Little Buck Creek, Lisbon, and Trap Spring. The statistics for these fields show a very similar "success rate" to that of the larger group of 29 fields.

A useful supplement to this information is the results of work done over undeveloped prospects, summarized in Table 2.2. These statistics show similarities with results obtained over known fields. Some 20% of the prospects surveyed show some sort of an anomaly. Note that apparent resistivity and REM parameters show anomalies at roughly three times the rate of the polarization anomaly, comparing

TABLE 2.2: ANOMALIES OBSERVED OVER UNDEVELOPED PROSPECTS

	Apparent Resistivity	Apparent Polarization	REM	At Least One Parameter
Fair to excellent	16%	6%	19%	22%
Absent to poor	72	80	68	67
Uninterpretable or ambiguous	12	14	13	11

favorably with the results of Table 2.1. Most of the "uninterpretable" anomalies occurred on the ends of survey lines, where proper interpretation is not possible. Only about 5% of the projects were severely contaminated by cultural or structural effects.

A total of 35 wells have been drilled within one dipole length of Zonge Engineering survey lines, and the production results are tabulated in Table 2.3. The numbers represent the original interpretation prior to drilling. The drilling results from non-anomalous projects essentially reflect numbers just a bit better than those one might expect from grid-drilling a petroliferous basin, so one should be careful not to overinterpret them. However, the drilling results over previously established anomalies are really quite encouraging, despite the low statistical sample. These results also provide an early indication that a *perfect* success record is not necessarily guaranteed by using this technique; success is greatly enhanced by judicious use of information from other sources. For example, two dry holes were drilled on apparently favorable anomalies; computer modeling later showed the anomalies were probably artifacts of discontinuous high resistivities at the surface.

TABLE 2.3: PROSPECTS SUBSEQUENTLY DRILLED

	Producing Wells	Shows, Uneconomic	Dry Holes, No Shows
Drillholes on favorable anomalies (14)	79%	7%	14%
Drillholes on questionable anomalies (6)	33	50	17
Drillholes on non-anomalous areas (15)	0	0	100

The Origin of the Anomalies

It is important to recognize that the statistics of Table 2.1 merely point out an apparent correlation between electrical anomalies and the presence of hydrocarbons. There is considerable debate at present as to whether this is a matter of coincidence or whether there is an actual causal link between the anomalies and the hydrocarbons. The resolution of this issue will help determine whether or not electrical techniques can be used as a viable exploration tool in the petroleum industry.

There have been a number of ideas suggested to explain the anomalies observed by electrical contractors in general. These ideas generally fall into four categories:

1. Hydrocarbons are being detected directly by virtue of their high electrical resistivity.
2. Anomalies are partly or totally due to the presence of saline waters and zones of electrochemical alteration caused by upward migration from deep hydrocarbon accumulations.

3. Conductive and polarizable anomalies measured over established hydrocarbon production are due (at least in part) to spurious effects arising from the presence of conductive well casings, pipelines, or other cultural features.
4. Anomalies are partly or totally due to topography or subsurface structure effects.

The following discussion will deal with each of these four categories as possible sources of the anomalous responses reported in the literature and in this study.

2.3 THE DIRECT DETECTION OF HYDROCARBONS

Introduction

As is discussed in Chapter 10, the search for oil and gas by electrical methods has long concentrated on attempts at direct detection of the hydrocarbons at depth. A number of groups have claimed success in this effort, but invariably the evidence for these claims has been clouded by vagueness or misapplication of the fundamental laws of electromagnetism. As a result, electrical methods in general, and direct detection methods in particular, have earned a rather poor reputation with the petroleum industry.

This discussion briefly outlines the reasons why most claims of direct detection in the past have almost certainly been misdirected, and why direct detection in the near future is rather unlikely.

Oil as an Insulator

Many of the proponents of direct detection have claimed that oil, whose resistivity is some 3×10^{11} ohm-meters, should be distinguished quite easily by electrical data from sedimentary rocks, whose resistivities are typically less than 100 ohm-meters. These proponents claim that gas, as a nearly perfect insulator, should be an even better target.

This argument suffers from several rather substantial problems. A surface electrical measurement technique responds not only to oil and gas, but also to lithology, mineralogy, and especially pore fluid content. In a trap, interstitial pore spaces in the reservoir rock are typically filled not only with hydrocarbons but with saline (and therefore conductive) waters. As a result, the resistivity of a trap can be much lower than the resistivity of oil or gas, varying according to pore water salinity, pore space saturation, and type of permeability. Resistivity logs often show highly variable responses in hydrocarbon reservoirs, and it is not uncommon for the reservoir to actually show up as conductive due to the influence of pore fluids. Therefore, it is difficult to see the validity in searching for oil and gas as insulators, if their insulating properties are often overridden by the dominant effects of more conductive materials.

Detection of an Insulator with DC Resistivity

Assuming for the sake of argument that a given reservoir rock is much more resistive where hydrocarbons are present than where only pore fluids are found, what are the chances that the hydrocarbon-producing zone can be detected by means of DC resistivity measurements? In order to answer this question, a computer modeling routine known as "2DIP" (described in section 2.7) was used to model the dipole-dipole response to a buried insulator. The results, illustrated in Figure 2.2,

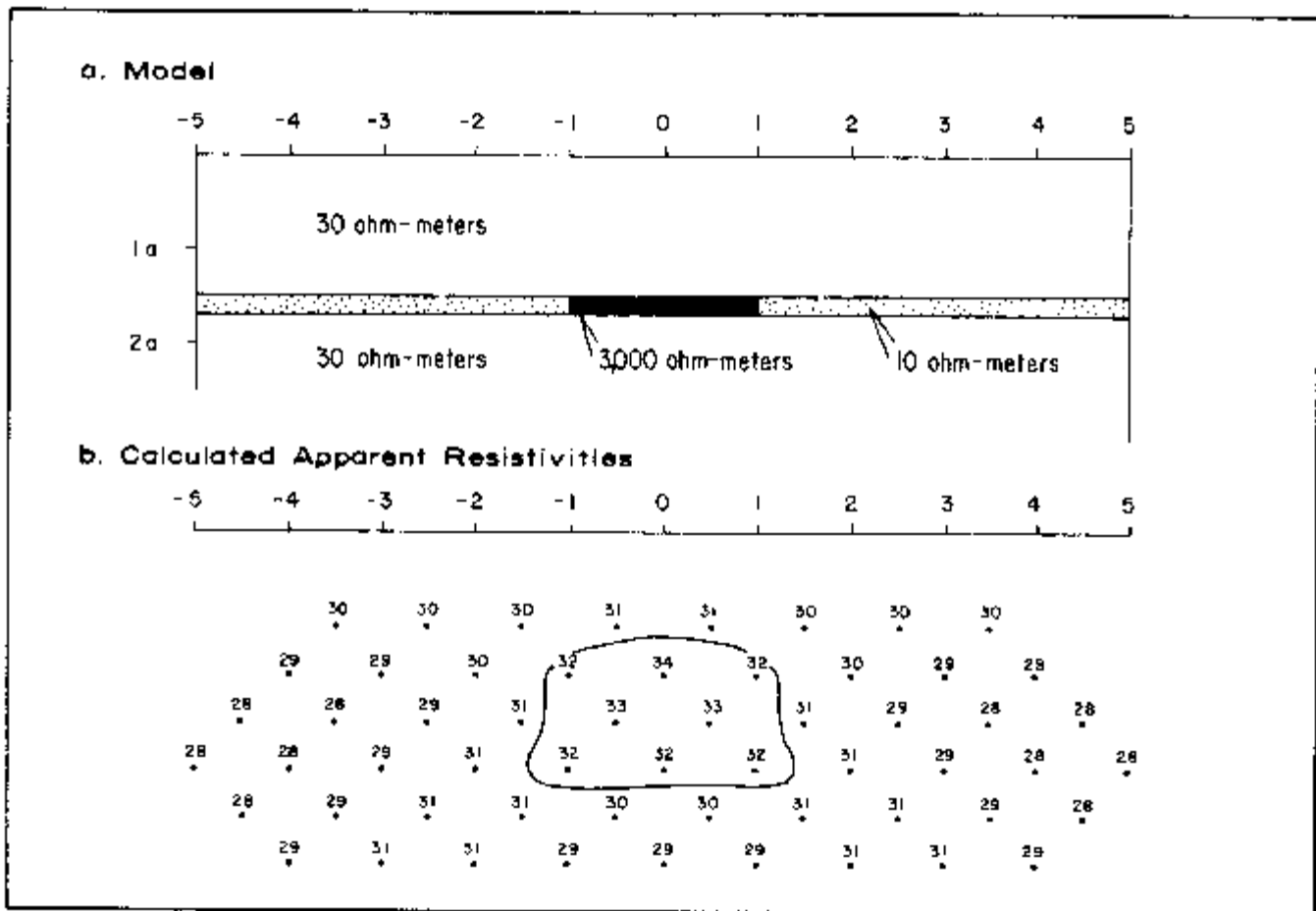
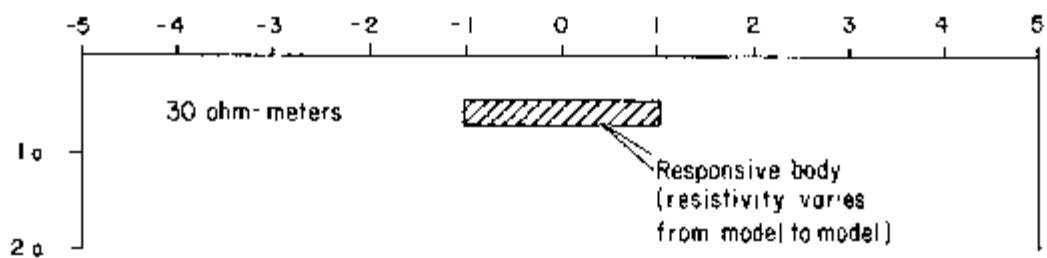


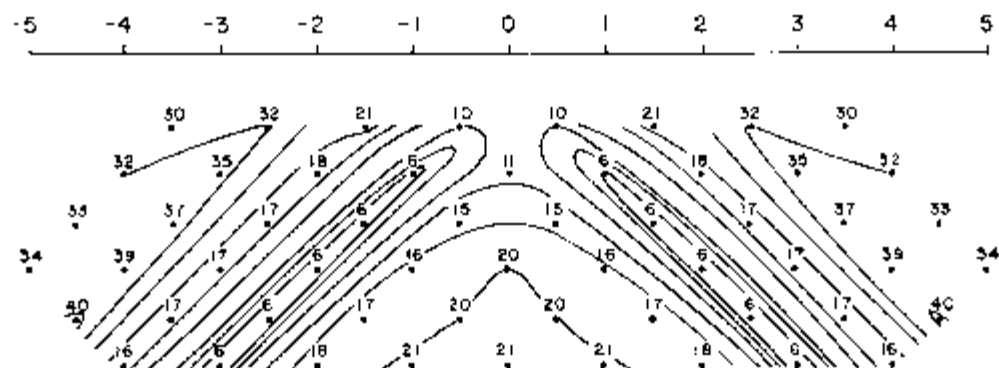
Figure 2.2. Two-dimensional resistivity model of a shallow resistive body. The model simulates the DC effects of an oil-saturated zone in a thin, porous reservoir sand. Contour interval: 10.0, 12.6, 15.9, 20.0, 25.1, 31.6, 39.8, 50.1, 63.1, 79.4, 100.0, . . . ohm-meters.

show that a resistive body could be identified as a subtle feature in a homogeneous earth environment, providing that the body is shallow and has sufficient thickness and lateral extent. This, unfortunately, is not a typical hydrocarbon exploration target, but is the exception. Further, the response from even such a shallow target as this would be obliterated by the mildest of effects from variations in surface and subsurface geology. Therefore, the direct detection of a hydrocarbon reservoir, even if it happens to be highly resistive as a whole, is unlikely using the dipole-dipole array.

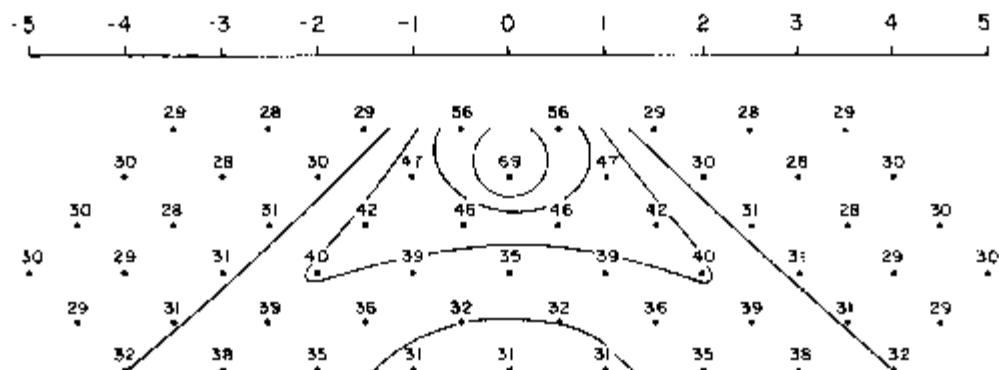
The rather pessimistic conclusion regarding direct detection with resistivity measurements should not be too surprising. Since the strength of a measured electrical signal is determined by the flow of current through the path of least resistance, i.e., through the conductive portions of the ground, it seems reasonable that a conductor in a homogeneous half-space would show a much stronger effect than an equivalent resistor. This is demonstrated by the "2DIP" models of Figure 2.3, in which the resistivity of a thin, buried body is varied from conductive to resistive to very resistive. When conductive, the body produces an anomaly whose maximum strength differs from background by a factor of 1:5; when resistive, it produces a maximum anomaly of less than 2:1. As pointed out some 50 years ago (Hedstrom, 1930), making the resistor even more resistive does not change the strength of the



a. Calculated Data: 0.3 ohm-meter body



b. Calculated Data: 3,000 ohm-meter body



c. Calculated Data: 30,000 ohm-meter body

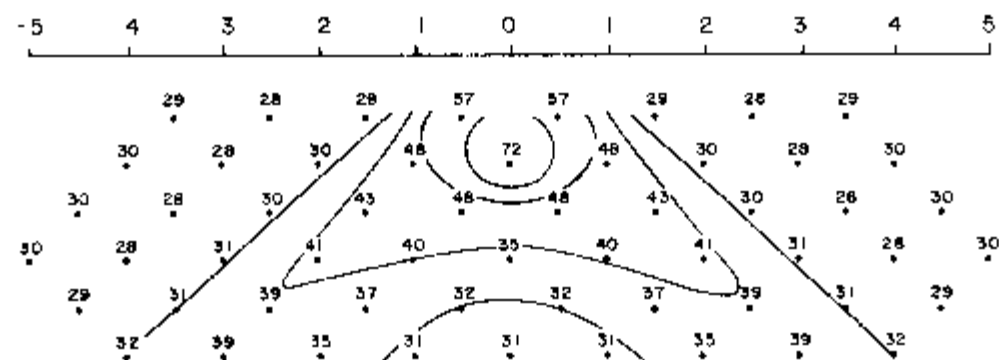


Figure 2.3. Two-dimensional resistivity model of a shallow body: a) a conductive body, with 1:100 resistivity contrast with respect to background; b) a resistive body, with 100:1 resistivity contrast; c) a resistive body, with 1,000:1 resistivity contrast. Contour interval: same as in Figure 2.2.

resistive anomaly significantly. This fact can be appreciated by comparing the model of Figure 2.3b to that of Figure 2.3c. Hence, the absolute value of the resistivity of oil and gas is irrelevant in regard to resistivity measurements, as long as the contrast is at least 100:1 with respect to background.

Detection of an Insulator with Magnetotellurics

Not only are insulators difficult to detect with resistivity methods, they are also difficult to detect with magnetotellurics (MT). The MT method represents a parametric sounding technique in which penetration is a function of signal frequency, as opposed to the dipole-dipole induced polarization method, in which penetration is a function of array dimensions. An MT modeling routine ("EMCDC") was used to compute the theoretical effects of the resistive slab of Figure 2.2. The results (Figure 2.4) again show a subtle anomaly which would be easily lost in a normal geologic environment. Hence, MT does not appear to offer significant advantages over resistivity methods in regard to direct detection of hydrocarbons.

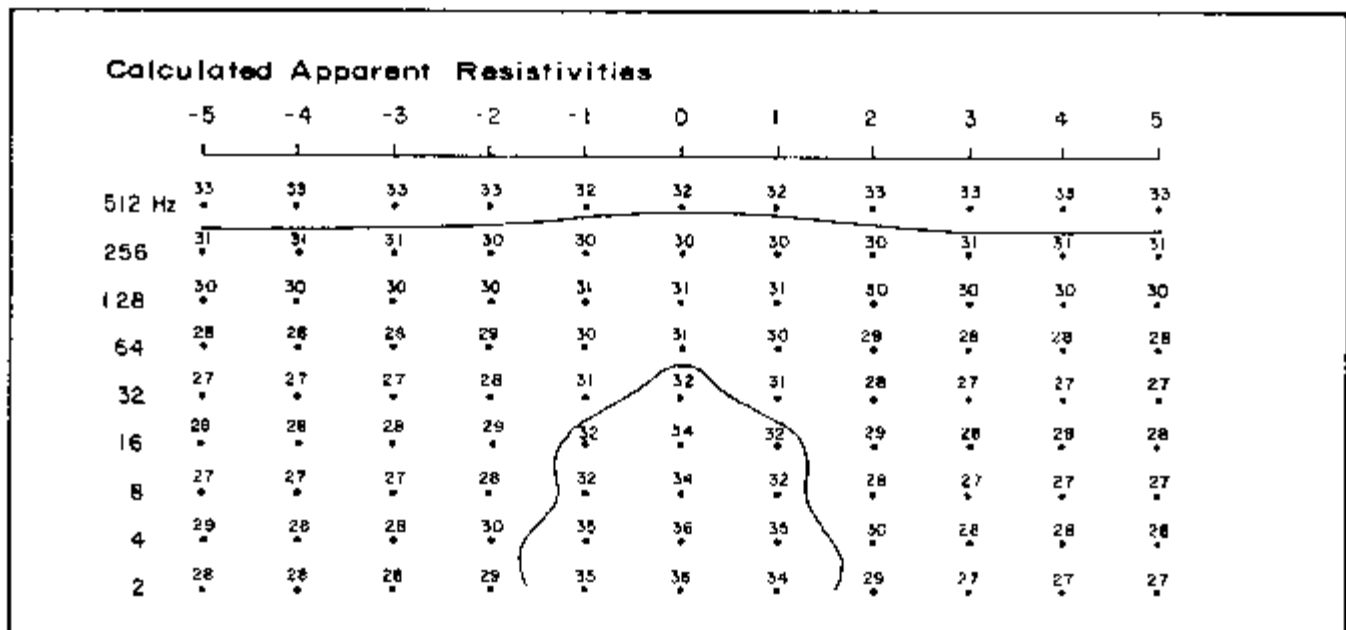


Figure 2.4. Two-dimensional MT resistivity model of a shallow resistive body. The model parameters and contour interval are the same as shown in Figure 2.2.

Transient "Reflections" from an Insulator

The preceding discussion has shown qualitatively some of the problems in the direct detection of hydrocarbons by processes which rely on measurement of the electric field at DC or low AC frequencies. There are also strong quantitative arguments against direct detection of "reflections" from the surface of an insulator.

An example of "transient reflection" methods is provided in the work by Electraflex, which is discussed briefly in Chapter 10. Electraflex uses a Schlumberger array, whose transmitting dipole is 2,640 feet (805 m) long and whose receiving dipole is 500 feet (152 m) long. In his numerous discussions of the technique, Jamil Azad states that a time-domain waveform of the type illustrated in Figure 2.5 is used for the measurements. The decay waveform during the "off" cycle is measured following a gap time; although it is never said what that gap time is, it is understood that measurements commence after 0.05 cycle has elapsed from the time of signal shut-off.

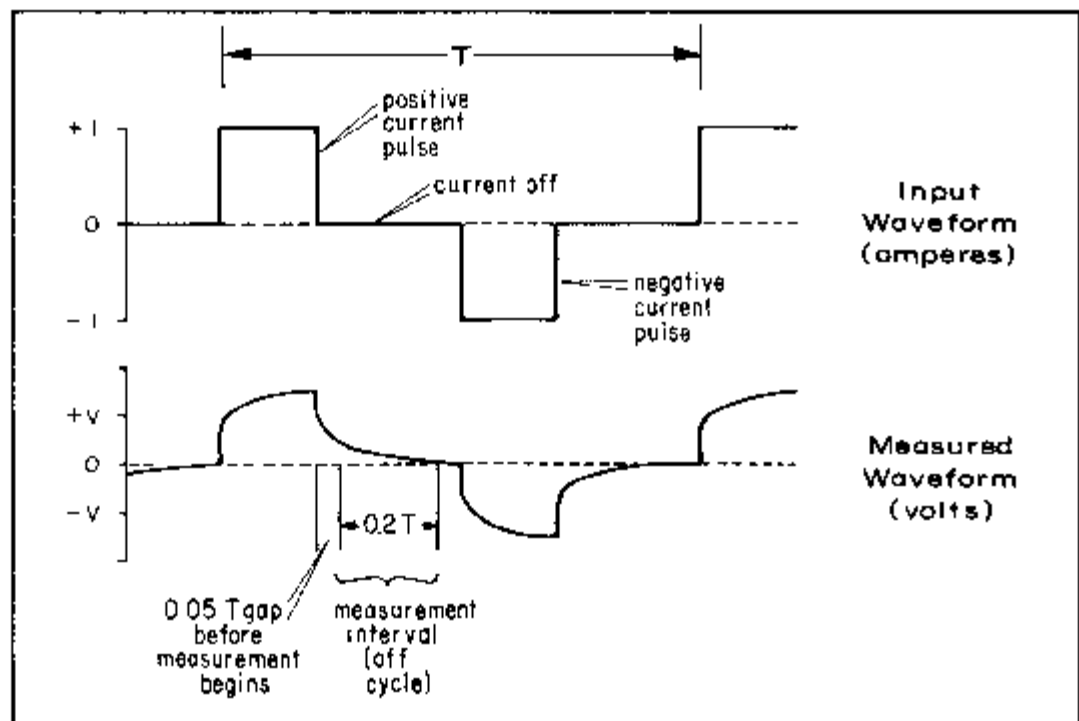


Figure 2.5. Typical Electraflex time-domain signal. Measurements are made after both positive and negative pulses.

Azad (1973) states that the gap is necessary to allow time for the IP response and near surface reflections ("first break") to decay, allowing deep electromagnetic effects to come through. However, Newmont scientists (Dolan, 1967), working with an almost identical waveform for some 30 years, have experimentally determined that a 0.055 cycle gap rejects most of the rapidly decaying electromagnetic effects and permits optimum measurement of the induced polarization effect. Also, note that the fixed dimensions of the Electraflex array dictate the penetration depth of the surveys in regard to induced polarization effects. That depth is not much greater than half the transmitting dipole length, or about 1,300 feet (400 m). Hence, it is likely that Electraflex measurements are not responding to deep "transient reflections" from hydrocarbons, as claimed by Azad, but are primarily measuring shallower induced polarization effects. This conclusion has recently been reached by Elfex (Powell, 1981), which had previously claimed to make transient measurements similar to those made by Electraflex.

Theoretical Problems with Reflection Measurements

Is it possible to measure the electromagnetic reflections from a buried insulator? In order to determine the answer to this question, consider the effects of a plane wave which is propagating through the earth in the z -direction, a subject which is treated in Chapter 9. Ignoring sinusoidal variations, the electric field amplitude E_x for a plane wave traveling downward in the earth (the z -direction) is related to the maximum field strength E_0 by equation (9.82):

$$E_x = E_0 e^{-kz} \quad (2.1)$$

in which k is the so-called propagation constant:

$$k = \alpha + i\beta \quad (2.2)$$

The quantities α and β are, respectively, the phase constant and the attenuation constant, which for conductive materials are given by equation (9.80):

$$\alpha = \beta = \sqrt{\mu\sigma\omega/2} \quad (2.3)$$

in which ω is the angular frequency, σ is the ground conductivity, and μ is the magnetic permeability. The effective depth of penetration, δ , from equation (9.85) is

$$\delta = 1/\alpha = \sqrt{2/\mu\sigma\omega} \quad (2.4)$$

and the wavelength of the plane wave is, from equation (9.88):

$$\lambda = 2\pi\delta \quad (2.5)$$

The attenuation of a downward travelling plane wave, expressed as a function of wavelength, can be rewritten from equation (2.1) as

$$E_x/E_0 = e^{-\alpha\lambda} \quad (2.6)$$

which reduces to

$$E_x/E_0 = e^{-2\pi} = 0.001867 \quad (2.7)$$

This can be expressed in terms of db by

$$20 \log_{10} (0.001867) = -54.6 \text{ db} \quad (2.8)$$

In other words, a plane wave is attenuated by a factor of about 55db per wavelength.

Now, consider the fact that, in order for a reflection to be resolved by a correlation-type receiver system, the object being measured must be separated from the receiving dipole by at least one and preferably two wavelengths. This immediately implies that the receiver system must have a dynamic range better than 100 db in order to resolve an electromagnetic reflection from an object one wavelength deep. However, it is doubtful that the Electraflex equipment has a dynamic range much better than 80 db. Hence, true transient reflections would be missed no matter what the depth of the target is: at large depths, attenuation would exceed the 80 db dynamic range and the receiver could not detect the minimal signal level, while at small depths, the target would be too shallow with respect to wavelength to be resolved. Given considerations of layering and subsurface structure, a dynamic range of at least 150 db would be required to reliably detect transients from a hydrocarbon layer at depth. Such a receiver system has yet to be built.

We can conclude from this discussion that resistivity soundings for direct detection of oil and gas are unlikely to succeed except for very shallow, thick targets. We can also conclude that detection of transient reflections from a hydrocarbon interface using currently available equipment is extremely unlikely.

**Zonge
Engineering
Data**

There is not the slightest chance that the Zonge Engineering data are responding to hydrocarbons directly. This can be stated not only for the arguments just outlined, but also for two other reasons. First, all anomalies which have been linked statistically to the presence of hydrocarbons at depth are electrically conductive. None are resistive, as might be expected at least part of the time if hydro-

carbons were being directly detected. Secondly, nearly all the hydrocarbon deposits measured to date have been much deeper than the galvanic penetration depth of the surveys. What is being measured are clearly conductive and occasionally polarizable effects which are much shallower than the hydrocarbons themselves.

2.4 THE ORIGIN OF ELECTRICAL ANOMALIES OVER HYDROCARBONS

Introduction

There is little doubt that light hydrocarbons migrate in meager amounts from their traps at depth to the surface of the earth. The evidence for vertical migration is provided by a number of studies over the past 50 years by geochemists, microbiologists, hydrologists, engineers, and geologists.

A general, intensive investigation of "tertiary migration," or leakage from hydrocarbon traps, has yet to be undertaken. Very little is understood about the mechanics and electrochemical results of migration through a complex sedimentary section. It is the purpose of this discussion to present some of the ideas currently in circulation and to relate these ideas to the origin of electrical anomalies over hydrocarbon deposits.

Evidence for Vertical Migration

The first evidence of hydrocarbon migration from depth was the observations of tar seeps, which go back several thousand years. A number of seeps are known throughout the world, although they probably occur over only a fraction of the known oil and gas fields. Color alteration of sediments (Donovan, 1974), vegetation changes (Richers, et al., 1982), and other effects are sometimes related to seepage areas.

Geochemists have presented convincing evidence of vertical migration in direct measurements of hydrocarbons in near-surface soils and in measurements of isotopic carbon ratios of near-surface, methane-altered carbonates. Horvitz (1969, 1982) and Duchscherer (1980, 1981) provide some general discussions and reading lists on geochemical methods. Pirson (1969, 1980) also contributes some interesting ideas from an electrochemical point of view. Roberts (1982) discusses vertical migration of helium from hydrocarbon traps. Davis (1969) presents evidence of hydrocarbon migration through a study of bacterial activity, which causes the precipitation of metallic sulfides in the overlying sediments. Ferguson (1979) outlines a number of near-surface mineralogic changes which appear to result from vertical migration.

Roberts (1980b) summarizes numerous observations of high-temperature anomalies over hydrocarbons, which he attributes to vertical migration processes. Roberts (1980a) also advocates some hydrodynamic theories which are designed to explain primary migration processes but which relate to tertiary migration as well.

Theory of Electrical Anomaly Generation

Due to the paucity of work on the mechanisms which result in the electrical anomalies observed over oil and gas fields, this discussion is by nature incomplete. However, the more likely possibilities in regard to induced polarization work will be discussed in this section.

As noted in section 2.2, the work conducted by Zonge Engineering shows

relatively consistent conductive anomalies but variable polarization anomalies in data obtained over hydrocarbon traps. Some of these anomalies are believed to be enhanced or caused by cultural, topographic, or structural interferences, as will be discussed in later sections of this chapter. However, many of these anomalies cannot be attributed to these effects, and instead are believed to arise from alteration of the sediments and changes in the pore fluids above the traps. The alteration patterns are highly variable in terms of their origin and magnitude, judging by the variability of the electrical anomalies. This should not be surprising, considering the complexities of hydrologic, mineralogic, chemical, and physical conditions present in the ground.

Anomalies measured by Zonge Engineering can often be placed in two categories: "deep" and "shallow." The "deep anomaly" is believed to be due to migration of saline water vertically out of the trap. It is detected as a deep, conductive zone by means of REM and apparent resistivity data. The "shallow anomaly" is probably due to mineralization and alteration which result from vertical migration of lighter hydrocarbons and possibly connate waters from the trap at depth. It is detectable as a shallow, polarizable anomaly with variable resistivities.

The "Deep Anomaly"

The "deep anomaly" is the most consistently observed feature in electrical surveys over existing oil and gas fields. Only a few characteristics of the "deep anomaly" can be stated unequivocally. When it exists, it is always electrically conductive, showing an apparent resistivity contrast of roughly 1 to 2 with respect to background. No deep resistive feature has yet been seen directly over a hydrocarbon trap, although, as noted in section 2.2, the conductive feature is occasionally absent. The "deep anomaly" rarely has an associated polarization response. It appears to be quite deep in extent, possibly extending to the depth of the trap itself. It does not often extend shallower than 1,000 feet (300 m) or so.

Due to resolution limitations of dipole-dipole data, not much can be said regarding the vertical or lateral structure of the "deep anomaly." It is roughly in the shape of a cylindrical column or plume which is, in general, reasonably well correlated with the lateral extent of the hydrocarbons. Computer modeling has suggested that the column is most conductive at depth, decreasing to nonanomalous values closer to the surface. This conclusion is only a preliminary one at this time, due to the small number of fields analyzed with high-resolution techniques such as controlled source AMT. Lateral structure is even less well-known. Computer modeling shows that it is difficult to distinguish between a solid cylindrical conductor and a hollow-cylinder conductor in typical dipole-dipole field data. Again, the detailing of structure in the "deep anomaly" is best left to techniques with better resolution.

THE "DEEP ANOMALY" MECHANISM

The "deep anomaly" is believed to be a direct result of brine discharge from hydrocarbon traps. As summarized by Meinhold (1971), Tóth (1980), and Roberts (1980a), the accumulation of many oil and gas deposits in traps in mature sedimentary basins may have been controlled by hydrodynamic factors which are often still active today. Roberts (Figure 2.6) views hydrocarbon traps as a "forced-draft" system in which organic material is carried from compacting shales (the source beds) to the ultimate trap by waters whose flow characteristics are controlled primarily by regional patterns of recharge and discharge. When water nears a trap with some vertical extent, its essentially horizontal movement is changed to vertical movement by the hydraulic gradient in the vicinity of the trap. If the trap is an effective one, Roberts argues that it acts as a filtering mechanism, discharging water but retaining the organic material or hydrocarbons as well as much of the dissolved salts. Whether

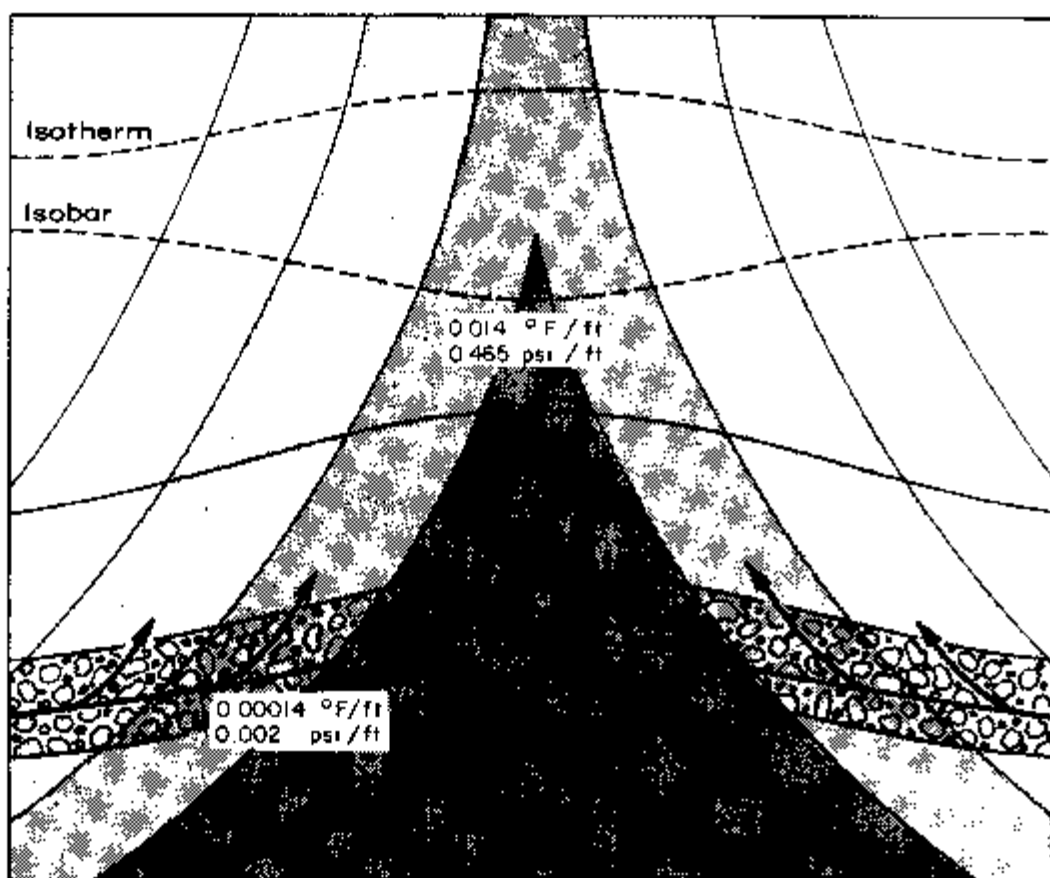


Fig. 2.6. Temperature, pressure, and salinity changes imposed upon convergent, upward-moving waters and their contents. Shaded zones show areas of higher salinity. Composite drawing from Roberts (1980a).

or not the hydrodynamic theory of hydrocarbon accumulation is correct is currently a matter of debate (Magara, 1981), but it is an idea which might help explain the origin of electrical anomalies. Other theories of petroleum migration may be equally compatible with the electrical data.

It is likely that any "impermeable" seal above the hydrocarbons will allow a small percentage of brine to be passed vertically out of the trap, especially in systems which have strong hydraulic gradients. Since the water originates from depth, it will have a higher temperature than the surrounding waters (Meinhold, 1971; Roberts, 1980b) and will therefore retain salts in solution more readily than the cooler waters which surround it. The volume of brine will be forced upwards by the continuous discharge from the trap beneath it, by virtue of its higher temperature, by decreased local pressure directly over the trap, and because of hydrostatic pressure considerations. Eventually, a decrease in temperature and pressure will cause salts to precipitate out of the water. The salts are subject to four competing influences: movement by horizontal groundwater flow, statistical diffusion, gravitational sink, and hydraulic lift from the discharge area of the trap. The relative importance of these four influences is not known and may vary considerably. However, in a dynamic system, brine is continually supplied through the trap, replacing the dispersing column above. Therefore, the "deep anomaly" might only be present in a dynamic system: as soon as the hydraulic water flow (and the supply of

hydrocarbons) through the trap ceases, the brine supply is terminated, the saline zone dissipates, and no anomaly can be measured.

Several substantial problems are associated with the brine discharge theory. First, it is an open question as to whether or not typical capping sediments are partly permeable to saline water. Neglia (1979) notes that no rock unit is completely impermeable, with the exception of evaporites and salts, but the relative permeability of the trap seal must allow enough brine to be discharged in order to supply the overlying sediments with salts faster than they are being dispersed. No studies into this matter have been found. Questions closely related to this involve the expected transport speed of the brines and the relative strengths of forces which tend to increase or decrease the salinities. For example, it might be argued that horizontal groundwater movement would tend to carry salts away faster than they could be resupplied. One encouraging bit of evidence in this regard comes from Bredehoeft and Papadopoulos (1965) who note that the *minimum* vertical movement of water needed to support the lowest-level observed geothermal anomalies would be about one foot (0.3 m) per year. This is roughly the same magnitude as the flow rate through compacted sedimentary units, indicating that *total* dispersion of vertically migrating brines is unlikely.

A significant problem with the observation of conductive material at depth is that insufficient work has been done to compare the field measurements to borehole resistivity logs. If a preferentially conductive zone often existed over hydrocarbon traps, one would think that fact would have been noted in well logs long ago (unless clays have complicated the well log data). The problem here is that ground resistivity measurements are made at around 0.1 Hz, and resistivity logs are made at frequencies above 1 kHz, hence, the two measurements differ in frequency by four to five orders of magnitude. Work by Clavier, Heim, and Scala (1976) suggests that a frequency difference of this magnitude would significantly influence the measurements. However, one would need to determine whether such a difference would result in a preferential insensitivity of well logs to changes in pore fluid salinity or clay alteration, a point which is currently hard to accept.

There are alternatives to the brine discharge theory which may be important in some or all environments. The main alternative involves alteration of clays at depth due to preferential cation exchange from waters rich in calcium or sodium. This possibility involves a number of questions and very few answers at present. However, ion exchange involves an influx of water-borne ions, and that almost certainly relates to the "forced-draft" ideas just considered; hence, the clay-alteration theory may have a driving force similar to the brine-discharge theory.

EXPLORATION LIMITATIONS

If the brine-discharge theory is substantively correct, what would the resulting anomaly be expected to look like? A roughly vertical column of brine, becoming more diffuse toward the edges and upward, would be expected. Maximum dissolved salts would be contained in regions of highest pressure and temperature, i.e., at depth near the discharge area. This is consistent with the interpretation of field data.

It is useful to engage in a few "thought experiments" in order to evaluate several possible limitations of the "deep anomaly" mechanism theory, as shown in the following discussion.

1) *Possibility of "false" anomalies.* An anomaly would be expected wherever a zone of brine is subject to upward movement. Presumably this would include zones in which hydrocarbons are just beginning to accumulate or even those in

which hydrocarbons will never accumulate due to the lack of organic material or a suitable trap. In other words, "false" anomalies might be measured in areas of discharge, regardless of whether or not hydrocarbons are present. In order to test this possibility, a large number of electrical anomalies would have to be drilled. Drilling to date has not favored the "false" anomaly hypothesis, but the small number of wells actually drilled prevents any firm conclusion to be made in this matter.

2) *Limitation as a function of trap design.* Whether or not the proposed mechanism would be similar for both stratigraphic and structural traps cannot be determined at this point. A difference in the magnitude of the conductive effect might be expected; however, since both types of traps involve changes in porosity and permeability, vertically as well as horizontally, both would be expected to produce some sort of anomaly. Indeed, "deep" anomalies have been measured over both types of traps.

3) *Depressurized reservoirs.* An anomaly over a depressurized reservoir might be expected to be weaker than an anomaly over a fully pressurized reservoir, due to solubility considerations. Lower pressures would mean lower solubility of salts; hence, waters migrating out of the trap would contain less total dissolved solids, and their resistivity would be higher than if the reservoir were more highly pressurized. The case histories of Desert Springs (Chapter 4) and Little Buck Creek (Chapter 5) tend to support this idea. In addition, low reservoir pressures would certainly have an effect upon flow velocity in and near the trap, but it is difficult to say what this effect would be.

4) *Depletion of hydrocarbons.* The role of upward-migrating hydrocarbons upon the "deep anomaly" is extremely difficult to understand at this point. It is possible that the invasion of clays and shales by low molecular weight hydrocarbons might alter the electrochemical characteristics of these sediments in some appreciable manner. Physical changes, such as evaporation of interstitial waters (Nisile, 1941), should also be considered, but again it is difficult to say what the electrical effects of these changes would be. Fortunately, depleted reservoirs are of no direct relevance to the use of electrical techniques in rank exploration, so the question is of academic interest.

5) *Cessation of hydrodynamic flow.* If the primary control on hydrocarbon accumulation is hydrodynamic, as Roberts (1980a) suggests, an anomaly might not be expected if the hydrodynamic flow of meteoric waters into the trap has ceased due to age. Hence, anomalies might be measured preferentially as a function of age: young traps, which might statistically involve gas more often than oil (Meinhold, 1971), would be more commonly detected than older traps on a statistical basis. Insufficient information is available to evaluate this possibility. Indeed, at this stage it is not even possible to judge the validity of the hydrodynamic hypothesis itself.

6) *Impermeable barrier above trap.* As suggested by Neglia (1979), shales and evaporites often pose permeability barriers to the cross-formational movement of waters and gases. In fact, shale layers may act as "filters" above the trap, retaining salts and organic material while passing water (Roberts, 1980a). It might be expected, then, that a thick shale or evaporite sequence might limit the strength of the "deep anomaly" by diminishing the amount of brine which passes through it. The almost universal presence of shales in petroliferous areas makes this hypothesis difficult to test, but some of the field data obtained by Zonge Engineering may support the idea. It is interesting to note that a strong conductive anomaly was measured at Lisbon Field (Chapter 6) in the shallow sediments despite a 3,000-foot (900 m) layer of salts which lie between these sediments and the hydrocarbon trap at depth.

7) *Contrast effects.* The relative effect of a buried body upon the apparent resistivity data depends partly upon the resistivity contrast of the body with respect to background. Hence, the invasion of highly saline waters into high resistivity ground will, by virtue of a high resistivity contrast, result in a pronounced anomaly. Conversely, the invasion of only moderately saline waters into low resistivity ground will result in a much weaker anomaly.

8) *Dipole size.* When the conductive zone is small with respect to the dipole size, the anomaly will be weakened (regardless of contrast) because the large dipole measures a bulk resistivity, averaging the conductive anomaly with resistive host rock. When the dipole is too small relative to target depth, the penetration will be insufficient and only the top of the column may be sensed, resulting in a weakened anomaly. Hence, it is fairly important to select a dipole size which is compatible with the target size and depth, as discussed in more detail in section 2.5.

The "Shallow Anomaly"

The "shallow anomaly" is found less consistently than the "deep anomaly", and its characteristics are more variable. When it is well defined, it is highly polarizable, but this occurs over only about one-fourth of the fields surveyed to date. It may involve high or low apparent resistivities near the surface, depending upon a number of specific geologic circumstances. The "shallow anomaly" is usually near the surface, but it can also extend to considerable depths.

THE "SHALLOW ANOMALY" MECHANISM

While the character of the "shallow anomaly" is inconsistent, its origin is probably better understood than is the origin of the "deep anomaly." The mechanisms for both are believed to have the same initial drive: vertical, hydraulic transport of material from the trap into the overlying sediments. However, the "shallow anomaly" is probably determined more by migration of light hydrocarbons than by migration of water.

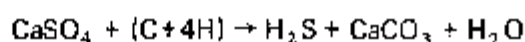
When saline waters are discharged from the trap, light hydrocarbons (predominantly methane through propane) are also discharged, either in solution or in separate phases. It seems likely that these hydrocarbons, if they are ever in solution, come out of solution before they emerge from the trap. One of the reasons for this assumption is that hydrocarbons are usually detected in surface soils *directly above* the trap; hydrocarbons dissolved in water would move partly by diffusion, moving horizontally as well as vertically and hence resulting in a broad, diffuse anomaly, whereas hydrocarbons in a separate phase would migrate primarily in a vertical direction as a result of the hydrostatic pressure gradient, resulting in the more focused anomalies seen in geochemical surveys. Another way of looking at this question is to consider that, if "salting out" caused deposition of hydrocarbons in the trap in the first place, these hydrocarbons would probably not go back into a brine solution above the trap, especially considering the decreased aqueous solubility of hydrocarbons in the much lower pressures above the trap. Although the light hydrocarbons might pass through the seal in solution, this decreased aqueous solubility and the lower pressures would soon result in the separation of phases above the trap. The slight increase in solubility with the lower temperatures above the trap would probably not offset the opposite effect of lower pressure and sustained salinity, but, as pointed out by Barker (1980), studies of the solubility of methane in brines at commonly encountered subsurface temperatures, pressures, and salinities are not available.

In any case, hydrocarbons are probably in separate-phase migration while rising through the sedimentary column. As such, they have higher mobilities than

water. Their migration rate is subject to considerable debate. The close plan-view correlation of hydrocarbons in near surface soils and traps at depth argues for a fairly rapid ascent. The fact that hydrocarbons make it to the surface at all also argues for a rapid ascent, since bacterial degradation from microorganisms in the sedimentary column would destroy any slow-moving hydrocarbons. Duchscherer (1980) quotes an AEC study in which vertical methane movement of rates of over 70 feet (20 m) per day were noted, but he provides no bibliographic reference.

Bacterial Degradation

As methane and small quantities of ethane and propane rise through the sedimentary column, they are usually subjected to biodegradation by anaerobic bacteria. The characteristics of these bacteria vary widely, but in general the result is the reduction of sulfatic waters through the action of *Desulfovibrio desulfuricans*:



The sensitivity of bacteria to hydrocarbons depends upon various factors, including the level of hydrocarbons present. If a certain threshold level of hydrocarbons is not present in the ground, microbial action will be of minimal importance. Hence, over the center of the field, where methane concentration would be expected to be highest, microbial activity would be most intense; somewhere toward the edge of the field, the sensitivity threshold would be reached, and hydrocarbons would continue up the sedimentary column unaltered, albeit in greatly diminished quantity. Mogilevskii (1940) and Soli (1957) suggested that this may explain the geochemical halos, in which surface hydrocarbons form a ring or halo around the producing field—a halo which is observed quite frequently, according to Horvitz (1969) and Duchscherer (1980). This explanation seems much more plausible than the one favored by Duchscherer, who proposes that carbonate precipitation causes an impermeable blockage to the hydrocarbons, which bypass the blockage, forming a halo. This writer sees no reason why the blockage would not continue to grow ever larger in lateral extent, eventually sealing off hydrocarbon migration completely.

Davis (1969), in a very interesting discussion of effects due to bacteria, describes a number of species which utilize straight-chain paraffinic hydrocarbons. Most of these consume methane; others have a preference for ethane or propane. This is useful since methane is both consumed and produced biogenically, but the presence of, say, ethane-oxidizing bacteria indicates the presence of an ethane source, which is normally a hydrocarbon trap at depth.

In general, anaerobic bacteria are found at temperatures less than about 140°F (60°C). The maximum practical depth limit is around 4,500 feet (1,500 m), and they often extend up the entire sedimentary column. Aerobic bacteria may be found near the surface or where the dissolved oxygen content of the waters is greater than about 8 milligrams per liter (Harwood, 1973); they typically inhabit sediments within the 68° to 122°F (20° to 50°C) range.

Hydrocarbons which survive bacterial degradation migrate up the sedimentary column and escape from the surface into the atmosphere. The concentration of hydrocarbons in surface soils is usually very low, indicating either a low rate of supply or a high rate of dissipation. It is widely believed that hydrocarbon accumulation in subsurface soils is a rather slow process. Transport is aided by microfractures and faults, but it is very possible that vertical transport through an unfractured, unfaulted section can also occur.

Near-Surface Mineralization

Within the top few thousand feet of sediments, the by-products of bacterial degradation—chiefly hydrogen sulfide, carbon dioxide, and calcium carbonates—interact with the sedimentary materials or meteoric waters to precipitate metallic sulfides and other substances. Chemical reactions account for much of this activity, but precipitation due to low temperature and pressure also occurs.

Pyrite is commonly found in sediments directly above some oil and gas fields. Ferguson (1979) shows a good correlation of pyrite with the planar extent of three fields in southwestern Oklahoma, and many other workers have noted pyrite over other fields as well. The mechanism which creates pyrite involves the reaction of hydrogen sulfide with iron. Hydrogen sulfide is derived either through microbial degradation of hydrocarbons or through upward migration of hydrogen sulfide from sour gases or oils in the trap at depth. Iron may be derived from two primary sources. One source is hematitic grain coatings and bonding agents in sandstones, in which case the following action may occur:



The stability of the results of this reaction is quite variable, since oxidation of pyrite can occur in the oxidizing zones near the surface or in the environments of oxygenated water recharge. A second source of iron is from meteoric waters, but this is probably not of primary importance.

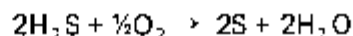
Snyder, et al. (1981), Oehler and Sternberg (1982), and a number of other researchers attribute induced polarization anomalies measured over hydrocarbon traps to pyrite generation. This is a natural assumption because of the inherent electrical response of disseminated pyrite and its relative abundance in the earth. Oehler and Sternberg showed a strong correlation between in-hole polarization responses and concentrations of pyrite over Ashland Field in southeastern Oklahoma. However, work by Carlson, Hughes, and Zonge (1982) shows that polarization responses over oilfields are quite variable, suggesting that the pyrite precipitation process is strongly affected by localized conditions.

It is interesting to note that, while micron-sized, unconnected pyrite grains will normally produce a strong polarization effect, the effect on apparent resistivities is quite variable. It is true that pyrite, as a metallic sulfide, is an efficient conductor of electrical current, but the effective conduction in a water-saturated rock usually occurs through pore fluids, not through disseminated metals. Unless the pyrite occurs in truly massive quantities, with interconnected grains, it will not usually supplant pore fluids as the chief conductive mechanism in the rock. Massive pyrite in a petroliferous environment is extremely rare; hence, pyrite probably has minimal effect on resistivities in most oilfield environments. Indeed, work by Duckworth (1981) at the University of Calgary indicates that, for pyrite quantities normally found in sedimentary environments (0 to 5%), interfacial impedance overwhelms the high conductivity of pyrite grains, yielding a *higher* resistivity for the rock as a whole. Laboratory measurements of artificial rocks (Ostrander and Zonge, 1979) show that the presence of disseminated pyrite has little effect on overall rock resistivity, although overall rock resistivity does have an effect on the polarization response of pyrite. Hence, one should not specifically expect either high or low apparent resistivities in the disseminated pyritic zones occasionally found over hydrocarbon deposits.

Resistivity anomalies can, however, result from carbonate cementation in near-surface sediments. It was noted earlier that organic reduction processes may

yield calcium carbonate, but calcite and dolomite can also result from inorganic processes. Oehler and Sternberg (1982) show high resistivities at the surface over hydrocarbon traps, and they attribute this to carbonate cementation. Note that this is a *very* near-surface effect; it has little to do with the "deep anomaly" unless calcification forms a physical barrier to salt discharge from the trap. Surface high-resistivity anomalies are not normally observed in Zonge Engineering surveys, since they tend to be overwhelmed by more conductive features and "averaged out" by the large dipole sizes used to achieve deep penetration.

Many other minerals are found over hydrocarbons and are attributed to leakage or migration processes. Most of these minerals occur in such meager amounts that they have little effect upon electrical measurements, so they are mentioned here only briefly as further evidence of migration. Sulfur may be found in oxidizing environments due to the instability of hydrogen sulfide there:



Ferguson (1979) found sulfur over three Oklahoma Fields, and many others have also noted the correlation of sulfur mineralization and petroleum. Donovan, Forgey, and Roberts (1979) have noted the presence of magnetite over some fields. They envision the production of magnetite to be related to reduction of hydrated iron oxides, which are found as grain coatings and bonding agents in sandstones. Other metallic minerals noted over oil and gas fields are lead, zinc, uranium, vanadium, manganese, nickel, chromium, and cobalt. In addition to these metal precipitates, rare gases, especially helium (Roberts, 1982), have been associated with some fields.

Clay Effects

One process which has not been mentioned in the literature in regard to resistivity and polarization anomalies is the role of clays. This is surprising in one sense, as clays are an extremely common source of low resistivity and high polarization anomalies in many areas of the world. In another sense, the lack of research into clay effects is not surprising due to the apparent unpredictability of clay responses. The properties of cation exchange, membrane polarization, and surface conduction in clays may be a major, but as yet unrecognized contributor to anomalies measured in sediments overlying hydrocarbons. If this is so, understanding the reaction of clay to an ascending column of hydrocarbons, biodegraded materials, and ion-filled waters may be of crucial importance to the successful use of electrical methods as a hydrocarbon exploration technique.

EXPLORATION LIMITATIONS

If the hydrocarbon migration mechanism is essentially correct, what might we expect "shallow" anomalies to look like? First, we would expect the maximum polarization effect to occur where the maximum iron and hydrogen sulfide supplies coincide. In a symmetrical anticline, maximum hydrocarbon leakage would occur from the center of the trap; microbial action would also be highest in the center of the migration column, and so would the produced hydrogen sulfide. Hence, anomalies in such a situation would be symmetrically centered over the oilfield. In addition, if clay alteration plays a significant role, one might expect a maximum anomaly where clays are present and where ion-rich waters and reducing hydrocarbons are found.

Some of the possible limitations noted earlier in conjunction with the discussion of the "deep anomaly" also apply to the "shallow anomaly." The possibility of "false" anomalies is not to be ignored, since the precipitation of pyrite and the

alteration of clays can be attributed to a number of sources separate from vertical migration from hydrocarbon traps. This problem is illustrated by the work by Oehler and Sternberg (1982), who present an example of a "false anomaly."

1) *Absence of iron or clays.* If the sediments through which the hydrocarbons and waters rise contain no available iron or clays for mineralization or alteration, no "shallow anomaly" will occur. While it is rare for a thick sedimentary sequence to lack both iron and clays, these materials may be poorly configured to produce an electrical response. For example, the iron may not be free to combine with hydrogen sulfide, or the clays may have a low cation-exchange capacity or peculiar geometry-pore fluid dynamics. Clays in particular are an infamous source of unpredictable electrical responses, largely because conductive and polarizable effects are so heavily dependent upon membrane and surface effects. This topic is treated in more detail in Chapter 8, and by Sumner (1967) and Madden and Cantwell (1967).

2) *Impermeable barrier above trap.* The smaller size and greater buoyancy of hydrocarbon gases allows them to pass through low-permeability layers such as shales and evaporites more effectively than saline waters. However, the upward migration process is probably considerably impeded by such layers. This has led many geochemists to the conclusion that hydrocarbons migrate upward by means of interconnected micro-fractures, faults, and geologic contacts. However, if this fracture-dependence is true, it is difficult to explain why geochemical and electrical anomalies are so well correlated in plan view with the lateral location of the hydrocarbons at depth, unless micro-fractures are so pervasive that faults and contacts provide only minor impedances to the migration. Hence, it is likely that most commonly encountered sedimentary units are, to one degree or another, significantly permeable to hydrocarbons of low molecular weight, regardless of fracturing.

3) *Depletion of hydrocarbons.* The low levels of hydrocarbons which migrate to the surface may decrease significantly as the trap is depleted of hydrocarbons, perhaps to the point of undetectability. Such an effect appears to have been observed by Horvitz (1969), who documented the disappearance of a geochemical anomaly over Hastings Field in Texas as the reserves were slowly diminished. Depletion of hydrocarbon reserves would slow the refueling process for the "shallow anomaly." It should then remain as a "fossil" anomaly or would disappear due to disruptive effects.

4) *Anomaly disruptive effects.* As noted earlier, hydrogen sulfide is unstable in an oxidizing environment, precipitating sulfur. If hydrogen sulfide oxidizes before it encounters a source of iron, no pyrite will be precipitated. Further, pyrite may also be unstable in an oxidizing zone, degenerating to iron oxide. Clay alteration is similarly sensitive to local conditions, especially to ion content of the waters and the degree of pore-fluid saturation.

A number of other limitations to the presence of "shallow" anomalies can also be raised. Therefore, a rather unpredictable anomaly of varying size, depth, and magnitude might be expected. This is precisely what is observed in the field. Hence, it is important to evaluate the absence or presence of the "shallow anomaly" in the light of the absence or presence of the "deep anomaly."

Conclusions on Mechanisms

It is clear from the preceding discussion that, while there is ample evidence for the existence of vertical migration and its effects on the sedimentary column, a great deal of work remains to be done. Therefore, any generalized theory of the origin of observed electrical anomalies must be largely speculative in terms of details. It is useful, however, to summarize the more important aspects of the problem.

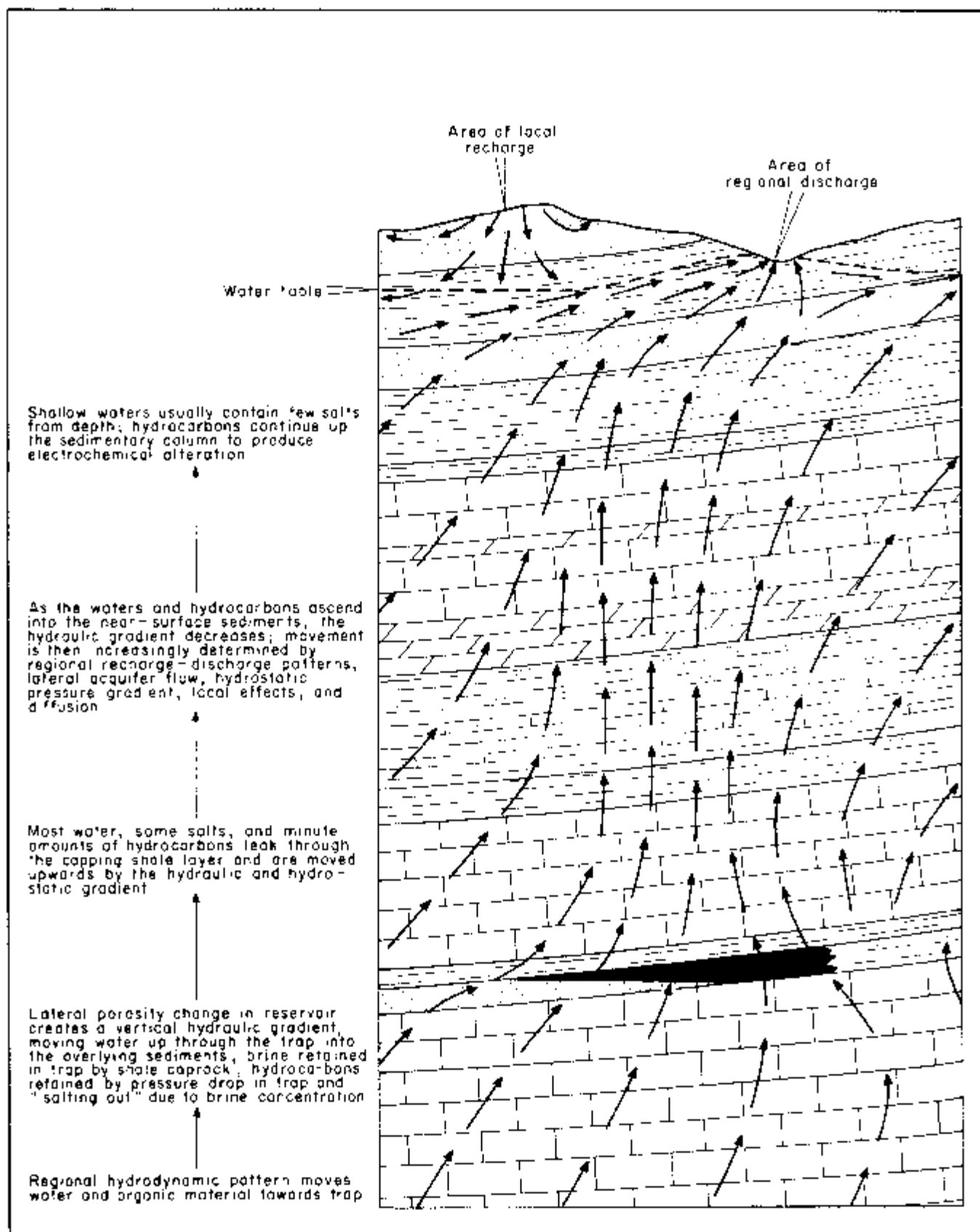


Figure 2.7. Hydrodynamic considerations in the origin of electrical anomalies. The figure is highly idealized for purposes of illustration. Figure 2.8 shows how the anomalies result from this pattern of water flow.

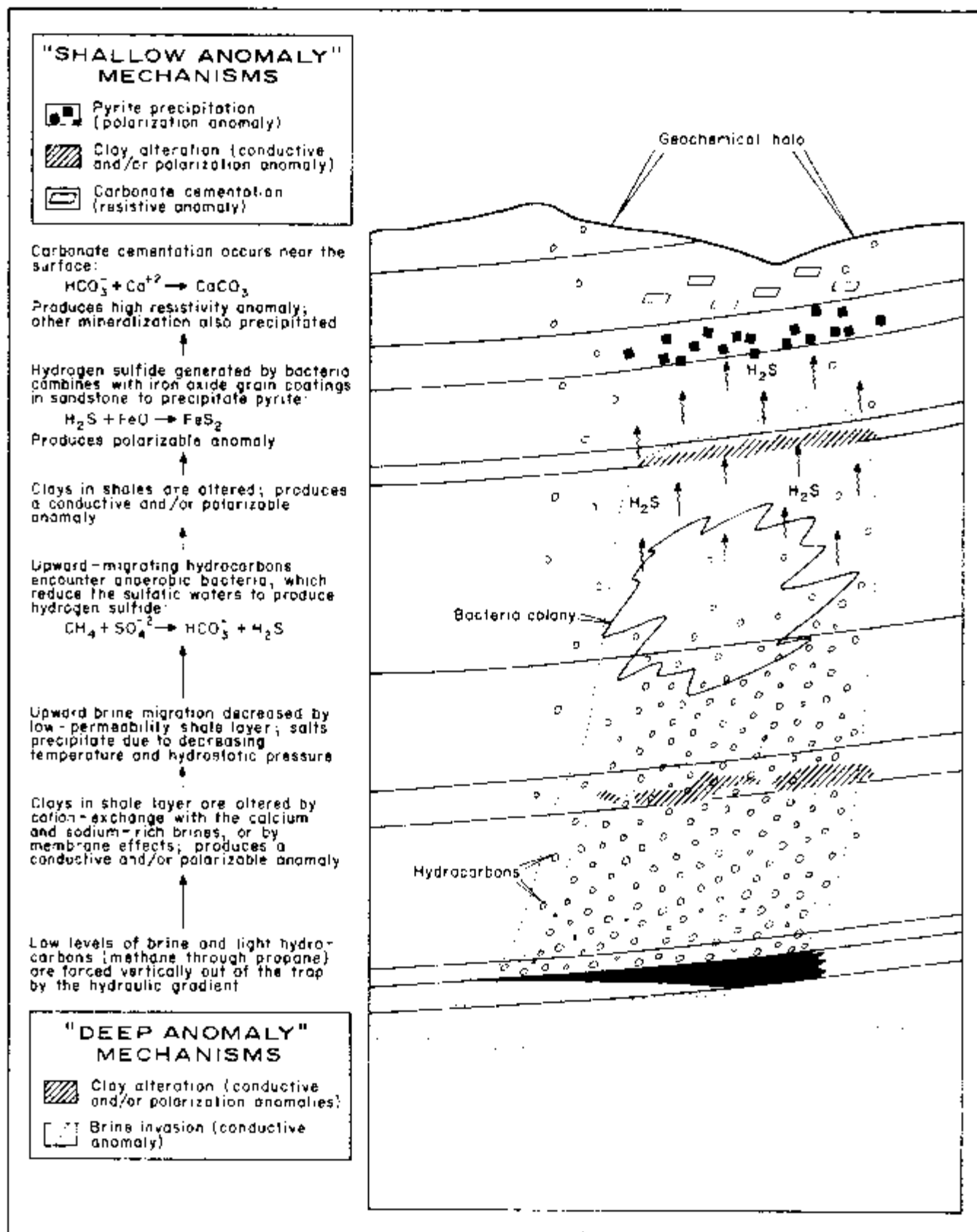


Figure 2.8. Proposed origin of the "deep" and "shallow" anomalies based upon the hydrodynamic considerations of Figure 2.7. The circumstances under which the proposed anomaly mechanisms are effective depend heavily upon geology; hence, the figure is highly idealized for purposes of illustration.

The theory presented in this chapter is based upon the upward migration of both saline waters and hydrocarbons from their trap at depth, both by hydraulic/hydrostatic means and by high-angle faults and fractures in the sedimentary column. Figure 2.7 shows a schematic representation of possible water flow patterns suggested by the theory, with specific reference to hydrodynamic processes (which may or may not be applicable in any given area). Figure 2.8 shows the resultant anomaly processes.

The theory helps explain two common types of electrical anomalies which are frequently encountered over oil and gas fields. The so-called "deep anomaly," a conductive, usually nonpolarizable feature, is attributed to vertical hydraulic discharge of brine from the top of the trap. The increased temperature of the discharged water enables it to retain a higher level of dissolved salts than surrounding waters, making it more electrically conductive. As the brine rises, cools, and enters areas of lower hydrostatic pressure, the salts are precipitated. Hence, the conductivity is greatest at depth, decreasing towards the surface. The so-called "shallow anomaly," a highly variable, polarizable feature, is probably related to pyrite or clay alteration. Pyrite is formed by the combination of hydrogen sulfide and iron in sediments at medium and shallow depths. The hydrogen sulfide is derived from leakage from sour hydrocarbon accumulations or through microbial degradation of lighter hydrocarbons; iron is derived from cementing material in sandstones or from free iron in meteoric waters. Clay alteration may have major effects on the data in some areas, due to ion exchange or membrane polarization effects. It remains to be seen how rising hydrocarbons in a reducing environment can affect the electrical properties of clays, but the subject should not be neglected. Minor resistivity anomalies near the surface may be due to mineralization, clays, or clastic cementation.

Future work in understanding the anomaly mechanisms is strongly advised, since this knowledge may eventually enable the geologist to extract more information from electrical data, such as depth and economic potential (two quantities which cannot be ascertained today). Research should be multidisciplinary, involving studies of geology, hydrology, fluid mechanics, geochemistry, and electrochemistry.

2.5 WELL-CASING EFFECTS

Introduction

In 1980 and 1981, Educational Data Consultants (EDCON) (Snyder et al., 1981) and Zonge Engineering (Zonge and Hughes, 1981) disclosed that they had measured apparent resistivity, apparent polarization, and electromagnetic coupling anomalies over several known hydrocarbon-producing fields. They claimed that these results indicated the presence of an alteration zone in the sediments above the hydrocarbons, a conclusion which suggested the induced polarization technique as a viable exploration tool in the search for oil and gas.

Almost immediately, Scott Holladay and Gordon West (1982) argued that the anomalies were not necessarily caused by true ground effects, but could very well be due to current channeling due to cased production wells. Using a modeling routine ("PIPE") developed at the University of Toronto, Holladay and West successfully simulated an apparent resistivity anomaly measured by EDCON over Lambert Field in Texas.

The well-casing problem can be illustrated by comparing the modeling results from a two-dimensional model of a "deep anomaly" to the results of a three-

dimensional model of well-casing effects. Figure 2.9 shows such a comparison for an idealized, elliptical-shaped oil field in which the producing wells are placed at regularly spaced locations. The first set of data (Figure 2.9a) was calculated for an idealized, cylindrical conductor extending vertically from the trap to 0.8 a-spacing of the surface. The results show a pronounced anomaly centered about the field. The second set of data (Figure 2.9b) was calculated for 7 well-casings placed symmetrically about the center of the field. The strong similarity in the results of these two widely differing models shows that, in this particular case, it would be difficult to distinguish well-casing effects from alteration effects. Obviously, then, one would be ill-advised to ignore well-casing effects in interpreting field data.

The issue of well-casing effects versus ground-alteration effects is still wide open to debate, and the applicability of the "PIPE" algorithm to field data figures prominently in the discussion of the case histories in this volume. Therefore, it is appropriate to describe the model, and to demonstrate some possible problems in its application.

Description of the Model

"PIPE" is an integral equation technique which calculates the effects at DC of infinitely long, hollow, cylindrical conductors lying vertically in a homogeneous half-space. The effects of each conductor are summed, and the net apparent resistivity and induced polarization effects are calculated as a function of field position for any four-electrode array. The details of the algorithm are scheduled for publication in an upcoming issue of *Geophysics*.

The input parameters for "PIPE" are: inner casing diameter, outer casing diameter, longitudinal conductance of the casing, wave number, complex impedance at the surface of the casing, planar location of the casings with respect to the survey line electrodes, and homogeneous half-space resistivity. Output consists of apparent resistivity and apparent polarization. For purposes of this volume, data are plotted in pseudosection form for the dipole-dipole array.

A number of tests were undertaken to ensure logical self-consistency of the model and to determine its limitations. The material presented in this volume represents modeling within those limitations.

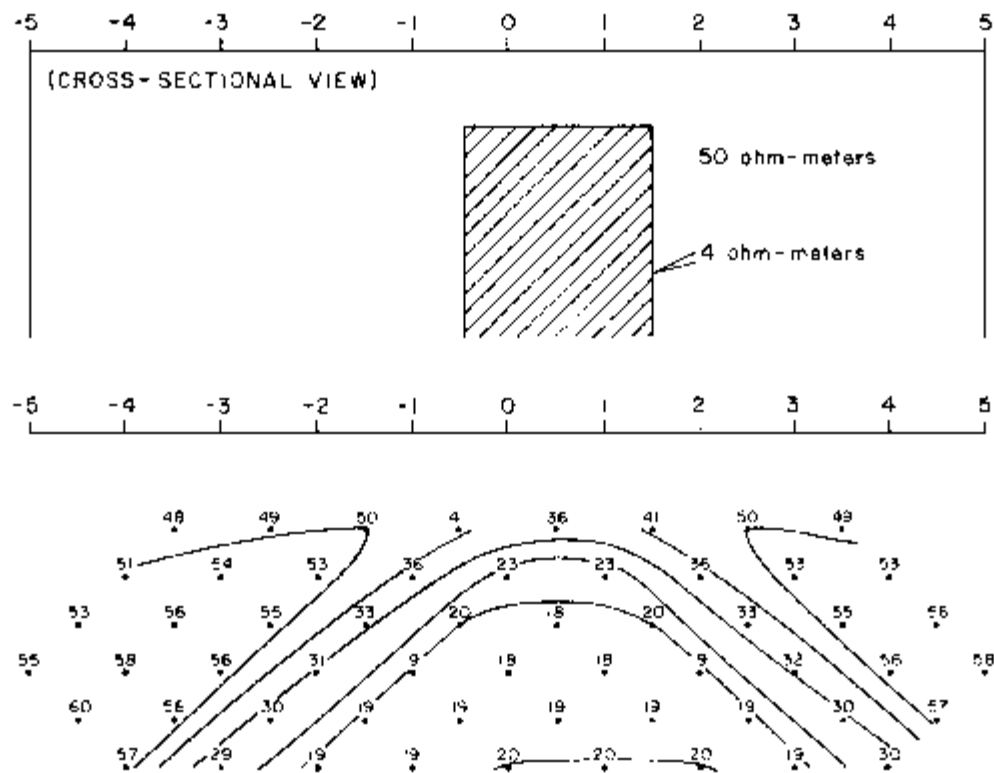
Problems with Using "PIPE"

There are some significant limitations to applying "PIPE" to data measured in the field, limitations which must be borne in mind when evaluating data calculated by the model. The object here is not to discredit the model, but to qualify its use in this volume. The work of Holladay and West is an achievement of fundamental importance in understanding induced polarization data, and those who seek to understand those data are indebted to these workers for their pioneering achievement. This section sets the context in which the model results can be used most successfully.

VARIABILITY OF WELL-CASING RESPONSE: A CASE HISTORY

The main problem with "PIPE" is not related to the algorithm at all, but is really a problem with the unpredictability of well-casing effects. It has been observed in field work that drill stem, which from an electrical standpoint should behave similarly to well casings, has usually (but not always) failed to produce any noticeable effects in the data. It has also been observed that many cased wells which lie close to receiving electrodes often show no strong effects. On the other hand, some cased wells cause extreme effects (see, for example, the Desert Springs case history of Chapter 4). In some field studies, wells of the same diameter, depth, and age respond in a radically different manner along the same survey line. This recalls

a. Conductive Alteration Column Model



b. Well - Casing Model

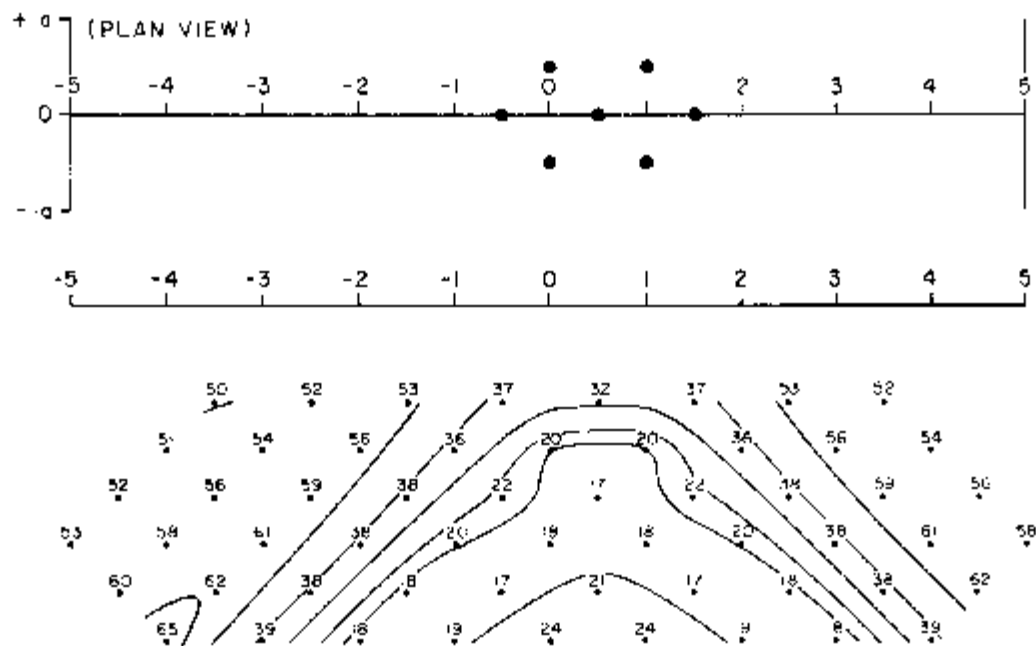


Figure 2.9. Results of computer modeling of apparent resistivity which compare the effects of a conductive alteration column over a hydrocarbon trap to the effects of well casings. a) Location of the conductive column (cross-sectional view), and results of the two-dimensional IP model "2DIP." Background resistivity = 50 ohm-meters. b) Location of the well casings (plan view), and results of the well-casing model "PIPE". Model parameters: well-casing diameter = 5.5 inches (14.0 cm), casing resistivity = 2.0×10^{-7} ohm-meters, surface impedance = $0 - 0i$, background resistivity = 50 ohm-meters. Refer to the text for an explanation of these parameters.

the extreme variability of responses from other grounded metal features such as pipelines, fences, and powerlines. If well-casing responses are unpredictable, it is impossible to model them successfully with confidence.

An example of the variability of well-casing response is provided by complex resistivity data obtained over Garza Field, located just east of the town of Post, in Garza County, Texas. The field has been producing oil from the San Andres and Glorieta formations of the lower Permian since the discovery well was drilled in 1935 (Myres, 1977). Drilling has continued up to the present. The field produces 36° API gravity oil primarily from the fine-grained, crystalline dolomites of the San Andres Formation between 2,910 and 3,260 feet (887-994 m). The trap is stratigraphic in nature; permeability is primarily intercrystalline.

Three lines of complex resistivity were obtained over Garza Field, using an a-spacing of 1,000 feet (304 m). Line 1, whose location is shown in Figure 2.10, is of particular interest in that data were obtained over it on three separate occasions. The first work involved a standard center-spread arrangement using nine transmitting electrodes. The second set of data was obtained over line 1, but with all dipoles shifted by 0.5 a-spacing. After these data were collected, four new producing wells were drilled in the vicinity of the line. About one month after drilling, line 1 was reoccupied in order to provide a check on well-casing effects. In order to distinguish the three sets of data, the following terminology will be used in this discussion.

1. Original data set: electrodes at integral-numbered stations.
2. Second data set: electrodes shifted half a dipole spacing to non-integral numbered stations.
3. Third data set: after drilling, electrodes at integral-numbered stations.

Apparent resistivities are about 10 ohm-meters on the line (Figure 2.11). A distinctive but low-amplitude conductive anomaly is superposed upon the low-over-high resistivity layering. This anomaly is well correlated with the producing zone; modeling strongly indicates that it is not due to well-casing effects, although some question remains about the effects of surface pipelines and powerlines. The low overall resistivities in the area make it difficult to perform a before-and-after well casing comparison for the apparent resistivity parameter, but the high phase response measured over the field shows more diagnostic effects.

Figure 2.12 shows both the field data and well-casing model data for apparent polarization, plotted at 0.125 Hz. The field data (Figure 2.12a) show a very strong polarization anomaly which is well correlated with the location of oil production. The peak response has the appearance of an inverted chevron centered on station 6, with a weaker response zone flanking it towards the southeast. The diagonal effects within this anomalous zone suggest the possibility of cultural contamination. The well-casing model of Figure 2.12b shows a similar chevron-shaped anomaly, with two substantial differences: first, the model anomaly is shifted with respect to the field anomaly by about 1,000 feet (300 m), and second, the strong polarization increases at depth which are evident in the field data are not reproduced by the model. However, the model does reproduce the general outline of the anomaly.

After the initial phase of field work was completed, four new wells were spudded near the line. All four were completed in the San Andres. In order to provide a direct before-and-after study of well casing effects, the Zonge Engineering crew returned to Garza Field, re-occupied the original stations exactly, and re-ran part of the original line. The data are compared to the original data set in Figure 2.13.

A comparison of the before-drilling and after-drilling data is very interesting. Most of the phase values compare relatively well. Some phases in the after-drilling

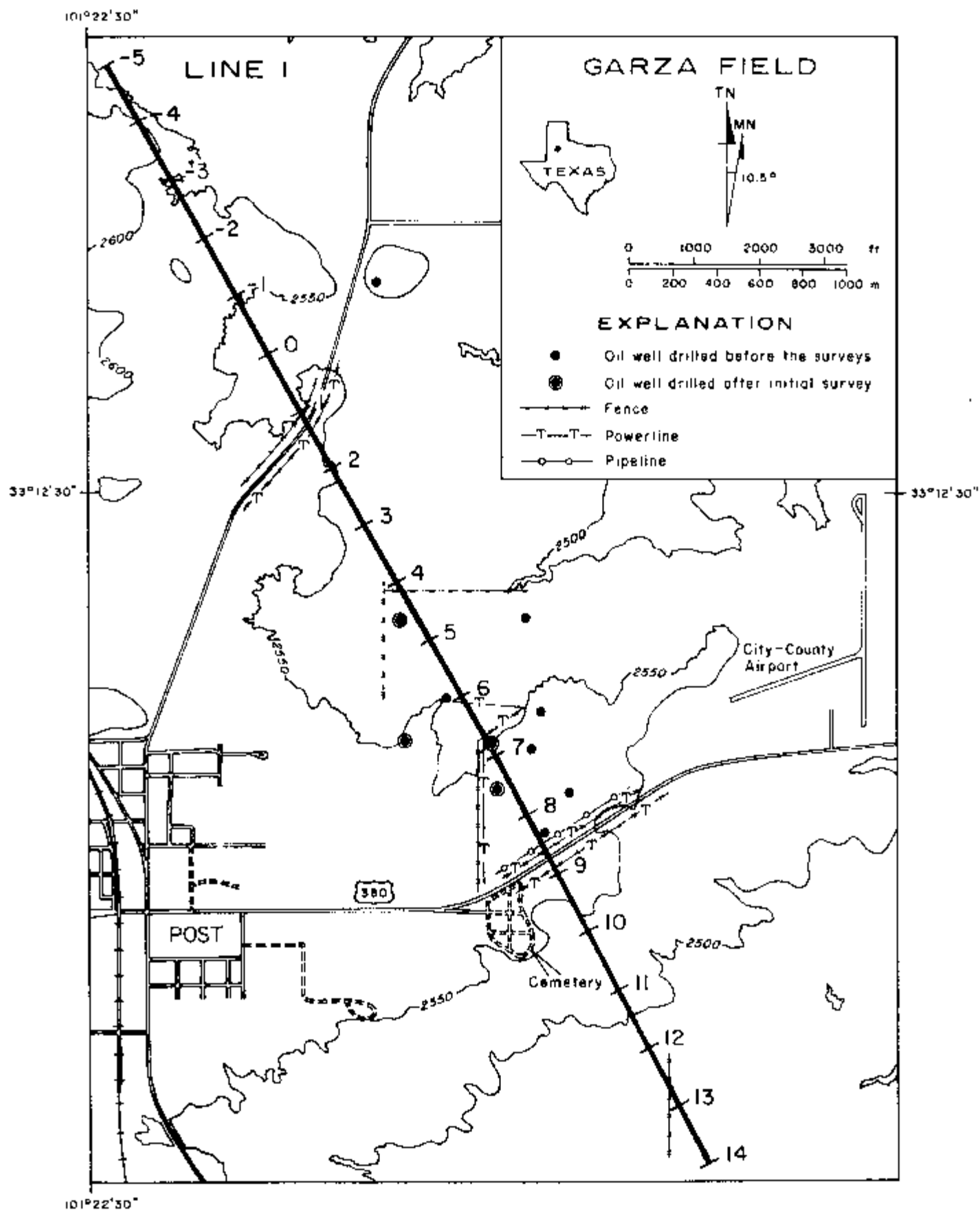


Figure 2.10. Location map of line 1, Garza Field, Garza County, Texas.

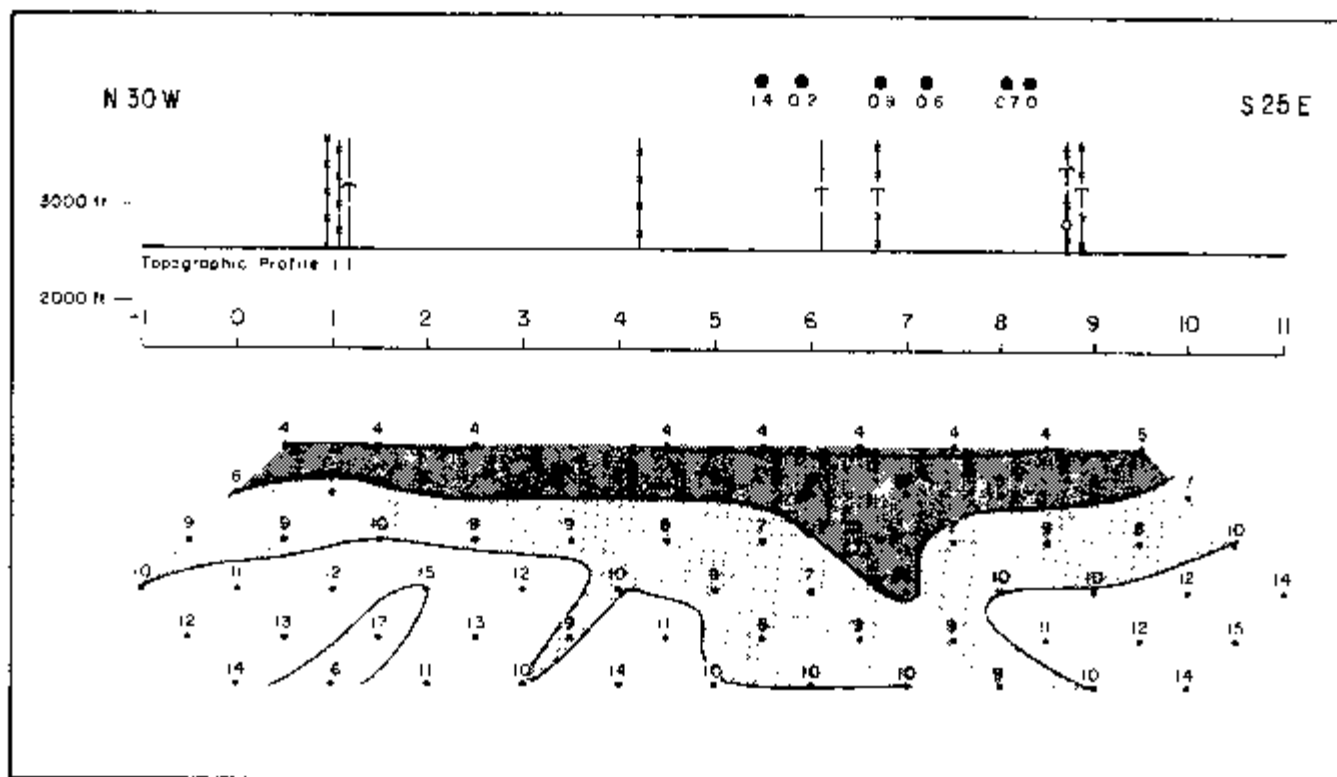


Figure 2.11. Apparent resistivity field data, Garza Field, for the original data set (see text). Contour interval: 1.0, 1.6, 2.5, 4.0, 6.3, 10.0, ... ohm-meters. For explanation of symbols, see Figure 2.10.

survey are lower, but none are significantly higher. Now compare these data to the before-and-after well-casing model simulation of Figure 2.13b. These model data predict strong near-surface responses from the new well casings, especially at the $n=1$ position beneath station 4.5 and along the left-plunging 7,8 diagonal. None of these predicted changes are evident in the field data, however.

At this point, we are faced with three possibilities: 1) the polarization response at Garza is primarily due to the well casings, but they respond in an erratic and unpredictable manner; 2) the response has very little to do with well casings, but is due to surface culture and alteration of the sediments overlying the oilfield; 3) the response is a combination of both the above. In examining the first possibility, we would initially suspect that the well casing near station 5.9 is easily the strongest responder; yet, well-casing modeling shows much too strong a surface response and too weak a deep response to support such a conclusion. Clearly, the data are affected by more than well-casing effects, since the character of the data and the character of well-casing effects are fundamentally different. The second possibility, i.e., that well-casing effects have no effect on the data, is also unlikely, since modeling does resemble some of the trends seen in the data. It is therefore believed that non-casing effects are more important than casing effects, although both are present in the field data.

Additional evidence that well casings do not produce the bulk of the anomaly is provided in Figure 2.14, which compares the original set of resistivity data with the second set of data, in which the line was shifted by exactly half a dipole spacing. It is known that when electrodes are moved with respect to a surface feature, the character of the anomaly changes substantially (see, for example, the apparent resistivity changes in Figures 2.15a and 2.15b in section 2.6). However, the only major change between the original and the shifted data at Garza Field is the elevation of mid-pseudosection phases beneath station 8.5 and the drastic lowering

of the left-plunging 8,9 diagonal; otherwise, the two sets of data merge quite satisfactorily. Modeling indicates that the intense powerline-pipeline-fence cluster at station 8.5 is responsible for the variations between the two data sets. Note, however, that the well casings do not produce a similar change. This suggests that well casings do not cause the majority of the response at Garza Field.

The conclusion to this investigation is that extreme variability in individual casing responses makes modeling very difficult. Therefore, one should be cautious in drawing unwarranted conclusions based upon the "PIPE" modeling alone.

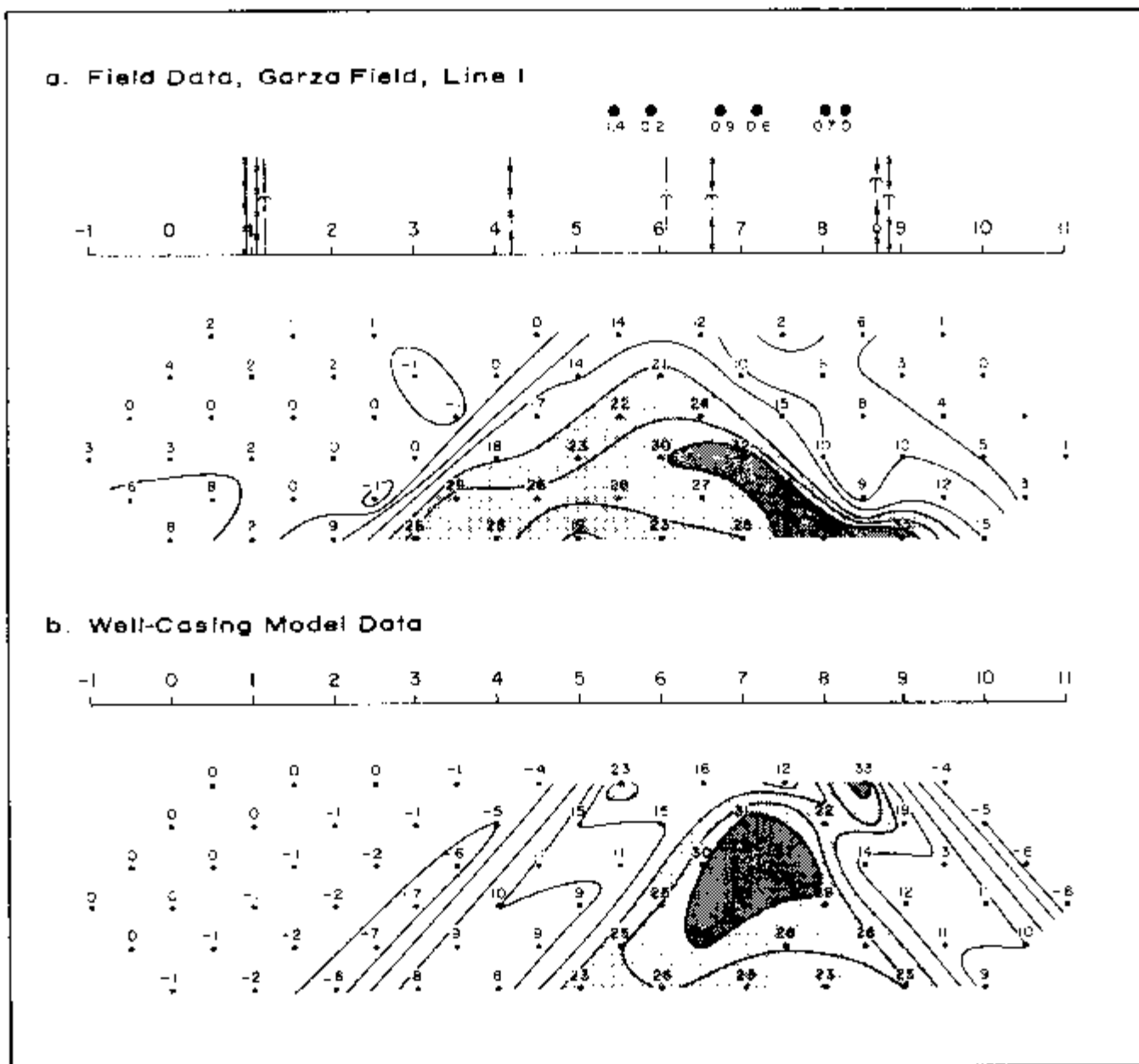


Figure 2.12. Apparent polarization field and well-casing model data, Garza Field, for the original data set (see text). Contour interval: 0, 5, 10, . . . milliradians. Model parameters: 6 well-casings, casing diameter = 4-1/2 inches (11.4 cm), casing resistivity = 2×10^{-3} ohm-meters, surface impedance = $1.0 + 1.8i$, background resistivity = 10 ohm-meters. For explanation of symbols, see Figure 2.10.

Figure 1 is a map showing the locations of new wells and the resulting phase values. The map features a horizontal axis from 2 to 9. Above the axis, four well locations are marked with circles and labeled 0.2, 1.0, 0, and 0.2. Below the axis, a series of rectangular boxes represent phase values at various locations. A legend in the bottom right corner explains the values: a box with '29' above it represents the 'Phase Value Before New Wells', and a box with '27' inside it represents the 'Phase Value After New Wells'.

Figure 1 is a schematic diagram of a water distribution system, showing a 9x9 grid of nodes. Each node contains a numerical value representing a phase. The grid is divided into four quadrants by a vertical line between columns 4 and 5, and a horizontal line between rows 4 and 5. The values are as follows:

Row \ Column	1	2	3	4	5	6	7	8	9
1	-1	-4	23	16					
2	-1	-5	15	15					
3	-2	6	19	57					
4	-3	2	14	42					
5	0	11	35						
6	10	29							
7	27								

A legend in the bottom right corner indicates that the values represent the 'Modeled Phase Before New Wells' (indicated by a small circle) and the 'Modeled Phase After New Wells' (indicated by a small square).

Figure 2.13. Apparent polarization for field and well-casing model data, Garza Field, comparing the original data set to the third data set, which was obtained after development drilling (see text). Contour interval: 0, 5, 10, ... milliradians. Model parameters: 10 well-casings; other parameters same as in Figure 2.12. For explanation of symbols, see Figure 2.10.

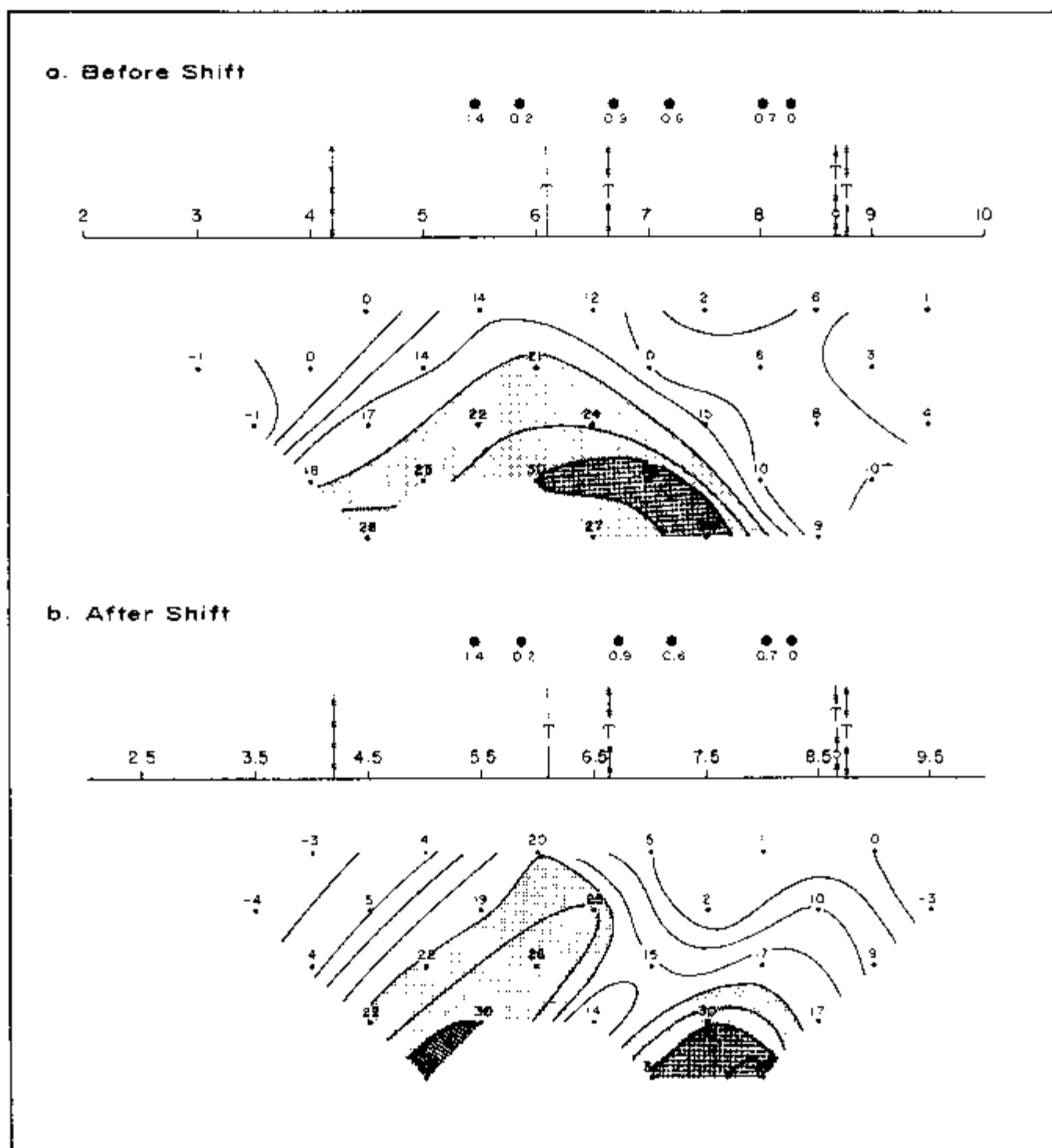


Figure 2.14. Apparent polarization field data, Garza Field, comparing the first data set to the second data set, in which the electrodes were shifted by 0.5 a-spacing (see text). Contour interval: 0, 5, 10, ... milliradians. For explanation of symbols, see Figure 2.10.

PROBLEMS WITH SURFACE IMPEDANCE DETERMINATION

The well-casing modeling of Garza Field was accomplished by adjusting the complex surface impedance assigned to the casings in order to achieve a best fit with the polarization data. In a very real sense, this is forcing the model to look like the data, and it injects a note of arbitrariness into the modeling process.

The solution to this is to measure the impedance of each well casing within at least one a-spacing of the line. This is not at all a trivial task, since it is difficult to measure a complex surface impedance to any degree of accuracy, and modeling shows that the figure must be very accurate. Some research is underway at Zonge Engineering to measure the real component of the surface impedance of a well casing in order to compare it to field data; initial indications are that this process would be prohibitively expensive if numerous well casings had to be measured in a typical survey.

The surface impedance problem indicates that, in most instances, the best use of modeling data is to evaluate overall trends in the field data, not specific features or magnitudes of responses.

PROBLEMS WITH THE HOMOGENEOUS EARTH ASSUMPTION

Layering effects can radically alter the appearance of data affected by lateral features such as well casings. Unfortunately, since "PIPE" does not permit layering effects to be included in the modeling, the model data and the field data are often difficult to compare properly. Holladay (1983) is developing an improved algorithm which may alleviate this problem.

PROBLEMS WITH VARIATIONS IN WELL-CASING GEOMETRY

The present modeling routine accepts only a single casing diameter, whereas wells are normally set with several sizes of surface and production casing. Modeling indicates that casing size has an appreciable effect upon the magnitude of the calculated effect. A related problem is that "PIPE" assumes an infinitely long casing, which may not be a viable assumption.

Well casings are often interconnected mechanically and electrically by supply pipelines. Considering the dramatic effects which pipelines alone can have on field data, connections with well casings could produce an overwhelming effect, as noted over Desert Springs Field (Chapter 4). Unfortunately, the solution of this kind of a problem is unlikely with an integral equation technique like "PIPE" (Wait, 1983).

PROBLEMS WITH THE DC APPROACH

"PIPE" calculates a strictly DC galvanic effect. It involves no electromagnetic effects whatever. This is an inconvenience, particularly when REM effects are interpreted, but a minor one when compared to other restrictions of the model.

Use of "PIPE" in the Case Histories

The preceding discussion urges great caution when using "PIPE" or any other model which oversimplifies a situation being modeled. However, it is beyond question that well casings have an effect on some data sets, despite the extreme variability of response from well to well. Therefore, we have elected to use "PIPE" in this volume of case histories under the very restrictive condition that only the *qualitative* aspects of the calculated data be used for interpretation. Again, we summarize the restrictions of the model:

1. "PIPE" treats all casings alike, despite field evidence that casing effects are highly variable.
2. The surface impedance of the model is arbitrary, i.e., unless surface impedance measurements are made in the field, the parameters must be varied

- arbitrarily to resemble the field data, especially in modeling apparent polarization data.
- 3. Geoelectric layering effects cannot be accommodated by the model.
- 4. Different well-casing sizes, interconnection of casings via surface pipelines, or finite-length casings cannot be modeled.
- 5. "PIPE" applies strictly to the DC case—no EM effects are calculated.

As a result of these problems, and the fact that "worst-case" parameters are often used to force an anomaly, "PIPE" often tends to "overmodel" field data by calculating a larger effect than is observed. Its chief utility, therefore, is to estimate the overall shape of the model data for comparison to the overall shape of the field data.

CALCULATION OF "RESIDUAL" DATA

In order to facilitate comparison of these data sets, a simple superposition technique has been used for apparent resistivity data in the case histories. The technique involves a point-for-point calculation of the ratio of the background resistivity (ρ_b) used in the model to the calculated apparent resistivity (ρ_c), and then multiplying it by the corresponding apparent resistivity (ρ) measured in the field, to yield the "residual" apparent resistivity (ρ_{residual}):

$$\rho_{\text{residual}} = \rho (\rho_b / \rho_c) \quad (2.9)$$

The residual data, then, represent what is left over when calculated well-casing effects are removed from the field data. This in no way implies total acceptance of the well-casing model; it merely shows a residual under the temporary assumption that the well-casing model is correct. The chief restriction of the residual calculation itself is that apparent resistivities measured in the field are close to the background resistivity used in the model; extreme differences will cause too large or small a correction to be applied to the data. In general, however, the residual calculation represents the difference between modeled and field data fairly, as long as field resistivities are within 50 to 100 ohm-meters of the assumed background resistivity used in the model.

MODELING PARAMETERS USED

Our approach in using "PIPE" is to try to show the *worst* effects which can reasonably be calculated with the model. If worst-case effects are removed from the data, and a residual anomaly remains, then one would be inclined to conclude that the anomaly cannot be caused entirely by well-casing effects, especially if the character of the field data differs from the character of the model data in a fundamental way. It should be borne in mind that this is really an extreme perspective taken only to argue a point of logic; in actuality, the well-casing effects observed in the field are frequently much less than those calculated by the model. This is demonstrated in several of the case histories.

In order to achieve a reasonable worst-case model, the following parameters were used:

1. Well-casing diameter is the diameter of the largest well casing used in the field at depths greater than 0.25 a-spacing. Inner diameters are, by industry convention, fixed by the outer diameter.
2. Well-casing resistivity is 2.0×10^{-3} ohm-meters, the value of the most conductive material normally used for casing and drill stem (U.S. Steel, 1983).
3. All cased wells within three a-spacings of the line were included in the model. All are assumed to have a maximum electrical response.

4. Real and imaginary coefficients for the complex surface impedance were usually set equal, and the value was adjusted in order to force the polarization model into a best fit of the field polarization data.
5. No attempt was made to model cementation effects, since modeling indicated that these were relatively minor, and since cementation practices vary with depth in many of the wells included in the case histories.
6. Wave number bounds were set between zero and -17 , as suggested by Holladay and West.
7. Wells were located by Petroleum Information lease-ownership maps. All wells in progress at the time of the survey were included, under the assumption that the electrical effects due to drill stem should be similar to those of cased wells.

2.6 SURFACE CULTURE EFFECTS

Surface Pipelines

Well casings are by no means the only source of cultural contamination in surface electrical measurements over oil and gas fields. Perhaps the worst offenders are grounded metal pipelines, which are common in most producing fields. Pipelines may produce artificial low resistivities, high polarization values, both, or neither; responses are generally unpredictable. Usually, a pipeline effect is strongest at the surface, with strong diagonals in an inverted chevron shape, as shown in the model data of Figure 2.15. The appearance varies considerably, depending upon the relative location of the pipeline with respect to the electrodes, as shown by the comparison of Figures 2.15a and 2.15b. An example of pipeline contamination of apparent resistivity data is provided in the discussion of Desert Springs Field in Chapter 4; an example of pipeline contamination of apparent polarization data is provided in the discussion of Line 2 at Lisbon Field in Chapter 6. Multiple pipeline effects are shown in the discussion of line 1 at Little Buck Creek, presented in Chapter 5.

As pointed out by Wynn and Zonge (1975), cathodic protection on pipelines can produce an additional coupling effect, especially at higher frequencies. Consequently, it is often advisable to have the protection turned off for the duration of the survey, especially to avoid the noise effects due to the unstable rectified waveform.

The situation to be avoided most is locating the survey line close to a parallel, grounded pipeline. This arrangement may cause severe coupling contamination of the data, wiping out any useful interpretation. The reason for this is that two parallel line elements are in a maximum coupling configuration. It is best to run survey lines perpendicular to pipelines—the minimum coupling configuration.

The extreme variability of pipeline effects is not understood, but it is a commonly encountered phenomenon and may be related to the quality of contact a given pipeline makes with the ground. Data on a number of survey lines have shown strong effects due to one pipeline but not the other. Effects cannot be predicted without making detailed surface impedance measurements. However, it is important to note that pipeline effects, when they are present in a set of data, can be recognized for what they are and are not easily confused with true alteration anomalies.

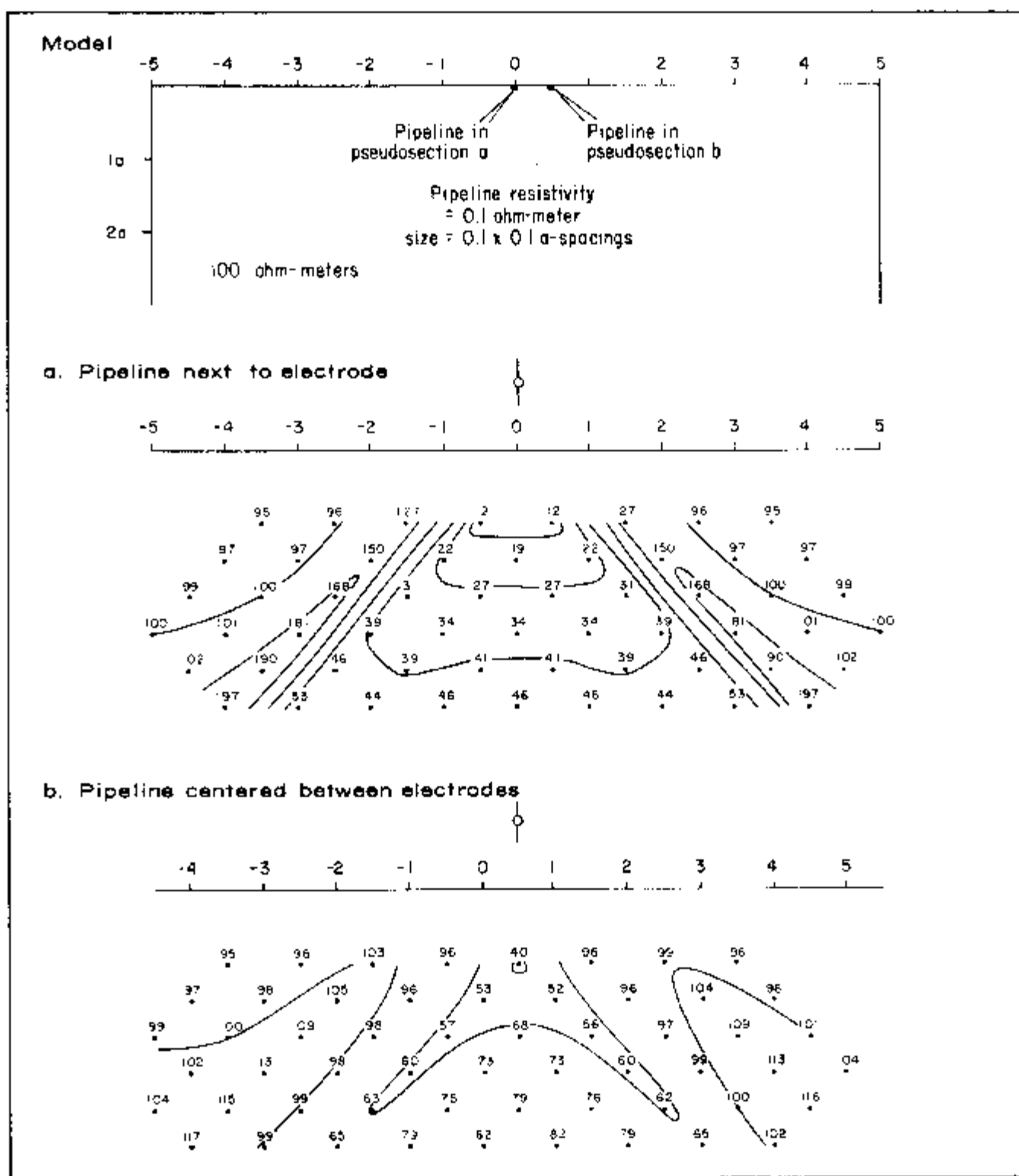


Figure 2.15. Two-dimensional resistivity model ("2DIP") of a pipeline, simulated by a very small solid conductor with rectangular cross-section, crossing the line at right angles. The pseudosections show the data resulting from a pipeline crossing the line at an electrode and crossing between two electrodes. Contour interval: 10.0, 15.9, 25.1, 39.8, 63.1, 100.0, . . . ohm-meters.

Powerlines

Powerlines, especially high-voltage, grounded ones, can produce fairly large effects on apparent resistivity and apparent polarization data. An example of powerline effects is noted above in the discussion of Garza Field (section 2.5). Powerline effects are less frequently seen in the data than are pipeline effects, and these effects are often (but not always) less than those due to pipelines. Powerline effects take on the expected diagonal or chevron appearance exhibited by other cultural features. The exception to this is a powerline running parallel to the survey line within one a-spacing. This kind of a situation is avoided in the field whenever possible due to the peculiar data contamination it often produces.

Fences

Fences can also produce strong diagonal effects in the data. The response or non-response of the fence is not predictable without making the necessary impedance measurements (Nelson, 1977); however, fence effects are usually easily recognized as such when they do appear. The worst effects are associated with well-grounded, metal-stake fences which extend over large distances and fall close to electrode stations. Fences which run parallel to the line within one a-spacing may severely compromise the integrity of the data. If possible, lines are oriented so that the fences cross at high angles and between electrodes.

**Other
Cultural
Features**

Other cultural features encountered in oilfield surveys involve buried cables, metal buildings, irrigation ditches, and so forth. These features may occasionally produce spurious responses in the data, but no examples of such are present in any of the case histories of this volume.

**2.7
TOPOGRAPHIC
EFFECTS****Introduction**

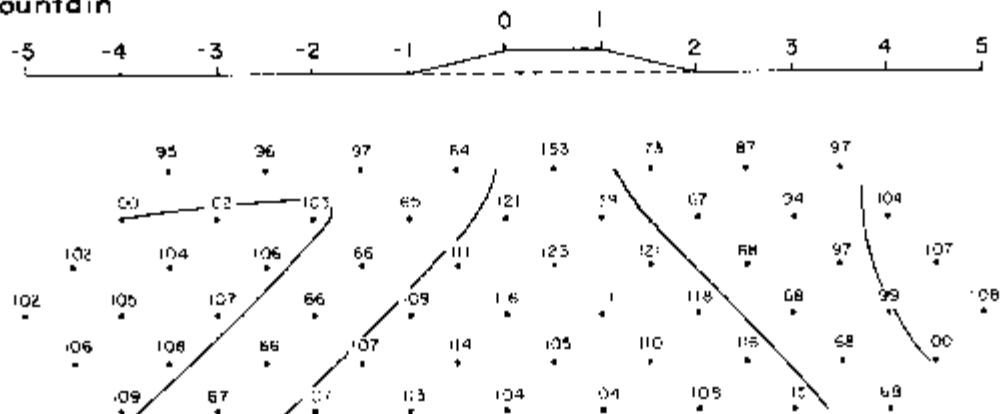
Apparent resistivity calculations, and to a lesser extent REM calculations, are affected by topography in that the relative dipole orientations are changed, as are the current distribution patterns in the earth. Strong effects can result from slopes of over 10 degrees, as described by Fox, Hohmann, and Rijo (1978). The approach taken in this study to deal with topography is to process the data normally, as if it were obtained from a strictly collinear, flat-earth dipole-dipole array, and then to interpret the nature of topographic effects by computer modeling.

**The "2DIP"
Algorithm**

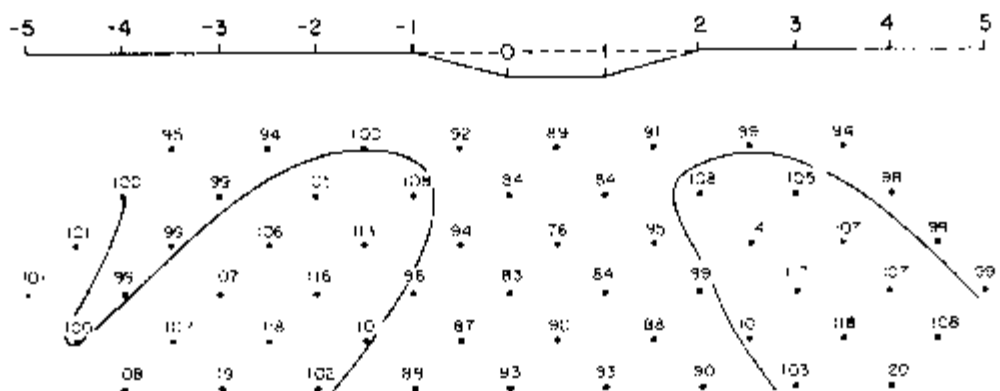
The algorithm used for all two-dimensional IP modeling in this volume is "2DIP," a finite-element routine which calculates apparent resistivity and apparent polarization effects for the dipole-dipole array. The model can include topography as well as buried structures and layers. Up to nine finite bodies can be modeled. A fine triangular mesh (69 x 20) is normally used for modeling in order to minimize edge-boundary effects.

The "2DIP" algorithm has shown its reliability in in-house modeling at Zonge Engineering for about two years. A number of reliability and limitations tests have been performed. The only significant problem which has been discovered is an artificial, low-over-high layering imprint upon all data, including a homogeneous earth model. Resistivities vary about 10 percent from $n=1$ to $n=6$, and the reader should bear this in mind when considering the model results. Two modeling limitations should also be borne in mind. One problem is that any off-line effects, such as those due to mesas and cliffs, cannot be modeled. This also means off-line

a. Mountain



b. Valley



c. Slope

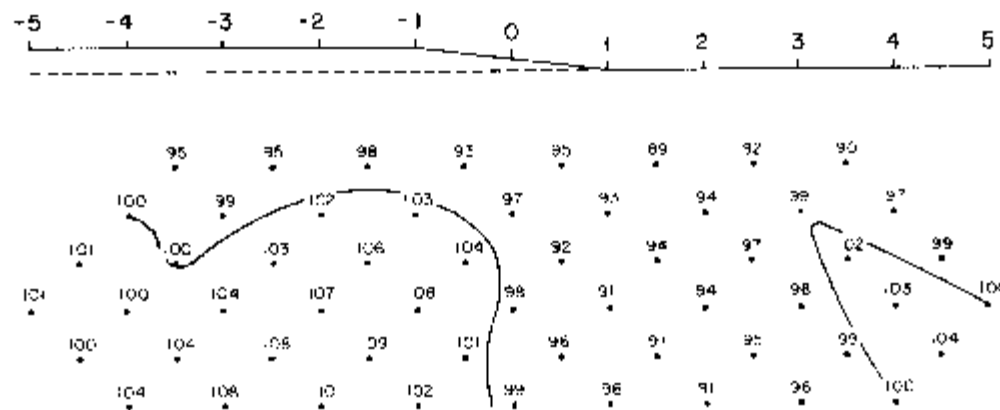


Figure 2.16. Two-dimensional resistivity model ("2DIP") of topographic effects due to a mountain, a valley, and a monoclinical slope change. The elevation change in each model is 0.25 a-spacing. Contour interval: 10.0, 15.9, 25.1, 39.8, 63.1, 100.0, ... ohm-meters. Background resistivity is 100 ohm-meters.

buried structural changes and non-perpendicular structures, such as subparallel faults and plunging folds, cannot be modeled accurately. Another limitation of "2DIP" is that model parameters are completely arbitrary and non-unique. Since resistivities and phase angles of each body may be adjusted in order to force-fit the model data to a set of field data, "2DIP" models present only one possible geoelectrical solution, not a unique geoelectrical solution.

Examples of Topographic Effects

The effects of topography on apparent resistivities of a homogeneous earth are predictable in the two-dimensional case. A mountain (Figure 2.16a) will produce a high resistivity feature beneath it in the pseudosection, flanked by low resistivity diagonals extending to depth. A valley (Figure 2.16b) will produce essentially the opposite effect, i.e., a central, low resistivity zone flanked by high resistivity diagonals. Note that a "valley effect" of this type could conceivably enhance or even produce a false low resistivity anomaly at depth. This emphasizes the importance of careful topographic modeling on projects with appreciable topography. A third example of topographic effects involves a change in slope from a high area to a lower area (Figure 2.16c). In this case, one obtains an asymmetric pseudosection in which a low resistivity diagonal points in the direction of the change in slope.

Additional complicating factors arise when a layered or dipping stratigraphic section of alternating resistivities intersects a surface of varying topography. In this case, it is often necessary to model both the effects of topography and geology. An example is shown in the following discussion.

2.8 SUBSURFACE GEOLOGIC EFFECTS

Stratigraphic and structural changes in the subsurface often influence the data significantly, and this is often an aid to interpreting data in areas with poor geologic control. While it is true that electrical techniques typically detect only changes in conductivity and polarizability, these properties are often intimately tied to lithology. Good examples of geoelectric mapping are presented in the case histories.

The main goal in making electrical measurements, however, is not to map lithology, since this can be done in greater detail and with much better depth control using reflection seismic techniques. Rather, the real utility of electrical measurements in petroleum applications is the detection of anomalous behavior which is indicative of oil or gas at depth. In this context, the imprint of subsurface geology must be well understood in order to avoid confusing it with true hydrocarbon responses.

There are several commonly encountered situations which make interpretation difficult. The first, and perhaps the worst, is the problem of a discontinuous high resistivity surface cover, such as volcanics. Resistive blocks tend to channel current flow around them, creating an artificial low resistivity zone below them in the pseudosection. This kind of an effect is illustrated in Figure 2.17. Since one of the features being looked for in hydrocarbon surveys is low resistivities at depth, it is critical to evaluate whether such features are due to surface effects or to hydrocarbon-related "deep" anomalies. This kind of an evaluation is best done with the aid of computer modeling and geologic information.

Another situation which engenders some difficulties involves selective topographic exposures of layered stratigraphy. The effects which are observed from such a situation depend upon the resistivities of the layers and their outcrop positions with respect to the electrodes. Figure 2.18 shows a typical example of the problems

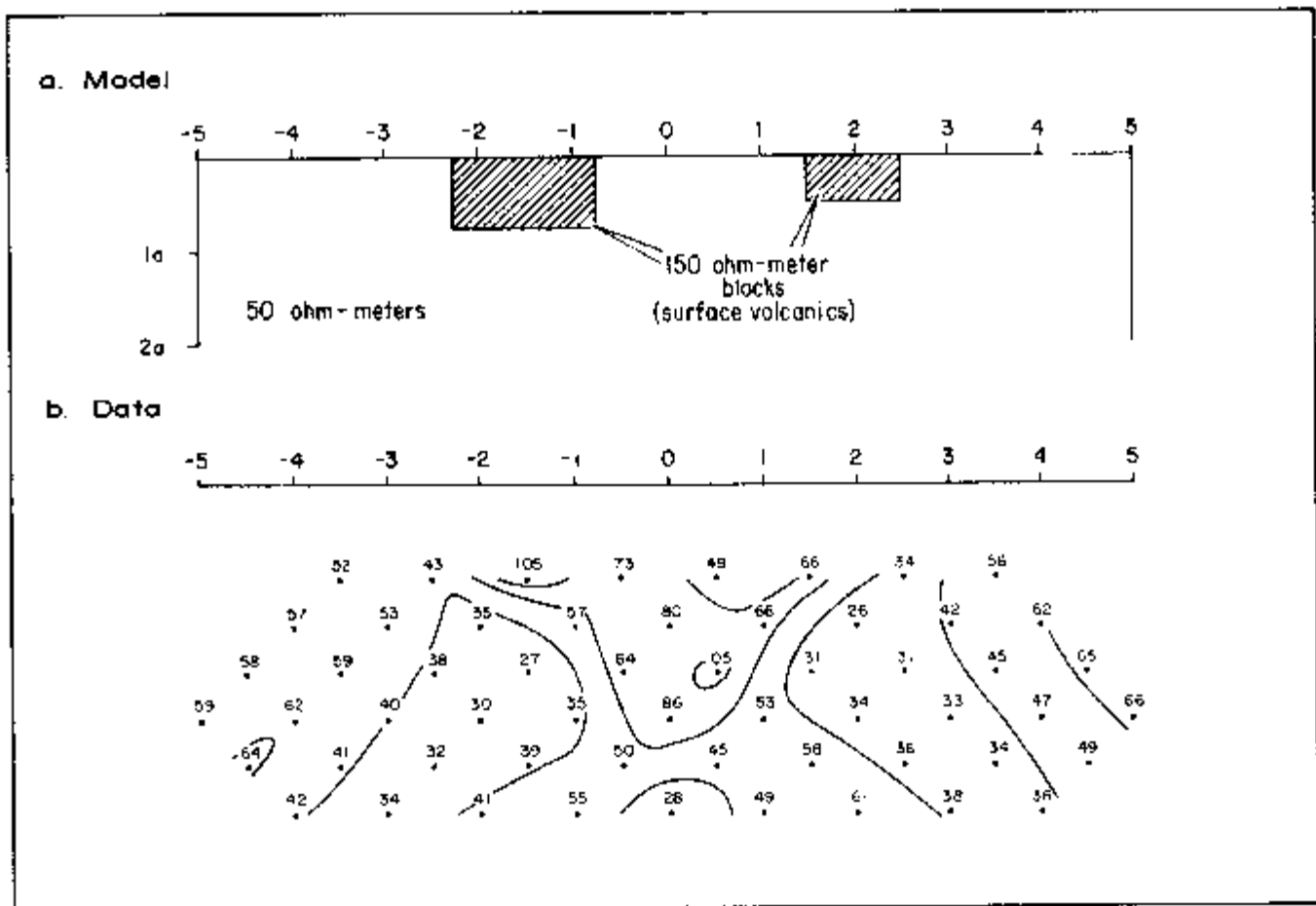


Figure 2.17. Two-dimensional resistivity model ("2DIP") of the effect of two discontinuous high resistivity blocks at the surface of a homogeneous earth. The geometric low resistivities produced by current channeling around those blocks could be misinterpreted as "deep anomalies" if care is not taken in evaluating the data. Contour interval: 10.0, 15.9, 25.1, 39.8, 63.1, 100.0, ... ohm-meters.

which can arise. The model shows the effects when topography cross-cuts horizontally-layered stratigraphy. In this case, some complexity is evident in the data, and a strong low resistivity anomaly at depth is apparent. Without adequate geologic knowledge, interpretation experience, and modeling facilities, there can be serious difficulties in distinguishing this topographic-structural anomaly from a "deep anomaly" due to conductive alteration above a hydrocarbon trap. In order to deal effectively with this problem, extensive two-dimensional modeling is quite useful.

Obviously, complicated geologic stratigraphy and structure make interpretation more difficult when no geologic information on the field site is available. Without geologic knowledge, it is certainly possible to come up with a geoelectric interpretation, but that interpretation will be unconstrained by geology and might include assumptions which are unrealistic. Hence, it is important to combine the geophysical and geologic data in order to arrive at a reasonably useful electrical model of the subsurface.

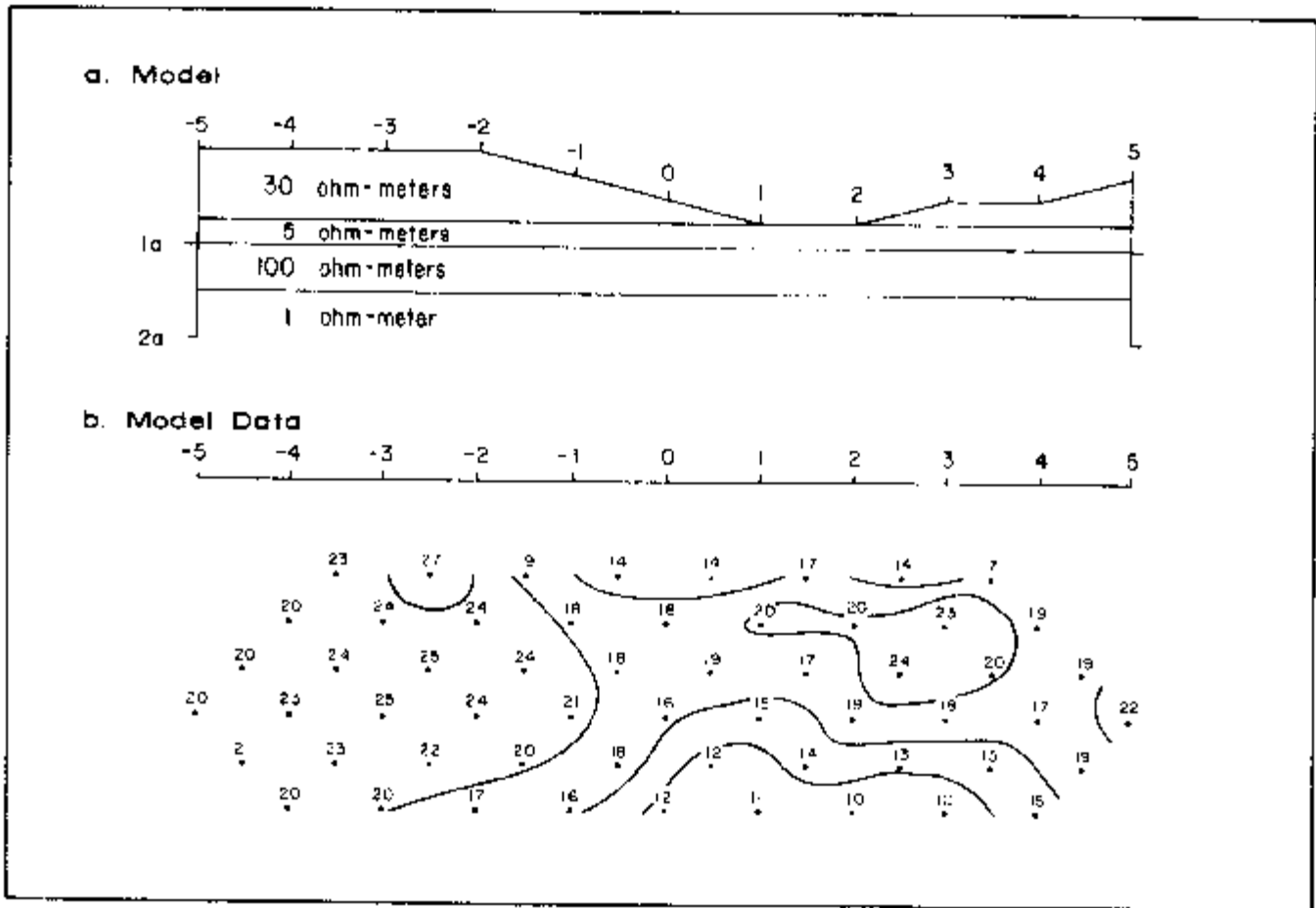


Figure 2.18. Two-dimensional resistivity model ("2DIP") of the effects due to layering which is cross-cut by varying topography. Note the artificial low resistivity zone at depth, which spuriously resembles a "deep anomaly." Contour interval: 10.0, 12.6, 15.9, 20.0, 25.1, 31.6, 39.8, 50.1, 63.1, 79.4, 100.0, . . . ohm-meters.

2.9 ANOMALIES DUE TO HYDROCARBON ALTERATION— WHAT TO LOOK FOR

We have seen some examples of spurious effects due to culture, topography, and geology in the preceding sections, but what should anomalies due to alteration by hydrocarbons look like? There is no simple answer. While endless speculations can be made regarding what alteration anomalies should look like based upon preconceived notions about the mechanisms which produce them, it is more useful to review some empirical observations which have been made over the past five years of Zonge Engineering surveys.

Conductive anomalies are often found over existing oil and gas fields. The responsive material is usually rather deep, but it can sometimes have a near-surface expression as well. An increased conductivity with depth has been indicated on some surveys. The conductive material is generally column-shaped; electrical structure within the column has not yet been resolved. The appearance of the conductor may change substantially, depending upon whether the ground shows high-over-low or low-over-high layering, what the background resistivities are, what kind of structure exists, and so forth. However, the main thing to look for is a lateral change at depth to lower resistivities which is well-bounded and cannot be explained by culture, topography, structure, or other effects. A good example of this type of anomaly is provided in the Whitney Canyon case history (Chapter 3).

Polarizable anomalies over hydrocarbons are much less common than conductive anomalies. Deep, strong, diagonally-controlled anomalies of the type seen at Garza Field (section 2.5) are generally regarded with some suspicion due to the possibility of cultural effects; shallow, well-bounded anomalies of the type seen at Ryckman Creek Field (Chapter 3) are more easily related to near-surface alteration. The strongest polarization anomalies in the Rocky Mountain and midwestern United States are often found in Texas and Oklahoma, so the polarization parameter may be more indicative of hydrocarbons in that province than elsewhere. However, it is important not to be tied too strongly to observations such as this, for they are made at a point in time when few hard facts are available on what hydrocarbon-related anomalies should really look like.

The case histories provide some interesting and illustrative examples of how oilfield anomalies can be interpreted in light of current understanding.

REFERENCES

- Azad, J., 1973, Direct oil prospecting with electrical transient reflections: *Canadian Jour. of Geophysics*, v. 9, Dec., p. 1-11.
- Barker, C., 1980, Primary migration: the importance of water-mineral-organic matter interactions in the source rock, *in* Problems of petroleum migration: AAPG studies in geology, no. 10, p. 19-31.
- Bredehoeft, J.D., and Papadopoulos, I.S., Rates of vertical groundwater movement estimated from the earth's thermal profile: *Water Resources Research Jour.*, v. 1, p. 325-328.
- Carlson, N.R., Hughes, L.J., and Zonge, K.L., 1982, Hydrocarbon exploration using induced polarization, apparent resistivity, and electromagnetic scattering (abs.): *Geophysics*, v. 47, p. 451. Full paper available in Technical papers, 51st Annual International Meeting and Exposition, SEG, Los Angeles, v. 3, p. 1339-1358.
- Clavier, C., Heim, A., and Scola, C., 1976, Effects of pyrite on resistivity and other logging measurements, *in* SPWLA 17th Annual Logging Symposium, Jun. 9-12, p. 1-34.
- Davis, J.B., 1969, Microbiology in petroleum exploration, *in* Unconventional methods in exploration for petroleum and natural gas: Dallas, Southern Methodist University, p. 139-157.
- Dolan, W.M., 1967, Considerations concerning measurement standards and design of pulsed I.P. equipment: *Proc. of the Symposium on Induced Electrical Polarization*, University of California, Berkeley.
- Donovan, T.J., 1974, Petroleum microseepage at Cement, Oklahoma—evidence and mechanism: *AAPG Bull.*, v. 58, p. 429-446.
- Donovan, T.J., Forgey, R.L., and Roberts, A.A., 1979, Aeromagnetic detection of diagenetic magnetite over oil fields: *AAPG Bull.*, v. 63, p. 245-248.
- Duchscherer, W., Jr., 1980, Geochemical methods of prospecting for hydrocarbons: *Oil & Gas Jour.*, Dec. 1, p. 194-208.
- , 1981, Nongasometric geochemical prospecting for hydrocarbons with case histories: *Oil & Gas Jour.*, Oct. 19, p. 312-327.
- Duckworth, K., 1981, Paradoxical resistivity anomalies due to sulphides in sedimentary rocks associated with hydrocarbons: *Jour. Canadian Soc. of Exploration Geophysicists*, v. 17, p. 72-74.
- Ferguson, J.D., 1979, The subsurface alteration and mineralization of Permian red beds overlying several oil fields in southern Oklahoma: *The Shaleshaker*, v. 29, Apr., p. 172-178, and May, p. 200-208.
- Fox, R.C., Hohmann, G.W., and Rijo, L., 1978, Topographic effects in resistivity surveys: Salt Lake City, Earth Science Laboratory, University of Utah Research Institute.
- Harwood, R.J., 1973, Biodegradation of oil, *in* The geology of fluids and organic matter in sediments: National Conference on Earth Science, Banff, Alberta, p. 149-156.
- Hedstrom, H., 1930, Geo-electrical exploration methods: *Oil Weekly*, v. 58, no. 6, Jul. 25, p. 34-36.
- Holladay, J.S., 1983: personal communication.
- Holladay, J.S., and West, G.F., 1982, Effect of well casings on surface electrical surveys (abs.): *Geophysics*, v. 47, p. 439. Full paper available in Technical papers, 51st Annual International Meeting and Exposition, SEG, Los Angeles, v. 2, p. 815-838.

- Horvitz, L., 1969, Hydrocarbon geochemical prospecting after thirty years, in *Unconventional methods in exploration for petroleum and natural gas*: Dallas, Southern Methodist University, p. 205-218.
- , 1982, Hydrocarbon geochemical prospecting after forty years, in *Unconventional methods in exploration for petroleum and natural gas*: Dallas, Southern Methodist University, p. 83-95.
- Madden, T.R., and Cantwell, T., 1967, Induced polarization, a review: in *Mining geophysics*, v. 2, p. 373-400.
- Magara, K., 1981, Hydrodynamics—does it trap oil?: *Jour. Petroleum Geology*, v. 4, p. 177-186.
- Meinhold, R., 1971, Hydrodynamic control of oil and gas accumulation as indicated by geo-thermal, geochemical, and hydrological distribution patterns: 8th World Petroleum Congress (Moscow), v. 2, p. 55-56.
- Mogilevskii, G.A., 1940, The bacterial method of prospecting for oil and natural gas (in Russian): *Razvedka Nedr.*, v. 12, p. 32-43. Trans., (RJ-1372) Associated Technical Services, East Orange, N.J., 1953.
- Myres, S.D., 1977, The Permian Basin, era of advancement: El Paso, Texas, Permian Press, p. 266.
- Neglia, S., 1979, Migration of fluids in sedimentary basins: *AAPG Bull.*, v. 63, p. 573-597.
- Nelson, P.H., 1977, Induced polarization effects from grounded structures: *Geophysics*, v. 42, p. 1241-1253.
- Nisle, R.G., 1941, Consideration of the vertical migration of gases: *Geophysics*, v. 6, p. 449-454.
- Oehler, D.Z., and Sternberg, B.K., 1982, Induced polarization for hydrocarbon exploration: geochemical/geological interpretation (extended abs.), in *Technical program abstracts and biographies*: 52nd Annual International Meeting and Exhibition, SEG, Dallas, p. 445-448.
- Ostrander, A.O., and Zonge, K.L., 1979, Complex resistivity measurements of sulfide-bearing synthetic rocks (abs.): *Geophysics*, v. 44, p. 409. Full paper available in *Induced polarization for exploration geophysicists* (short course): Johannesburg, South Africa, University of Witwatersrand, p. 71.
- Pirson, S.J., 1969, Geological, geophysical and chemical modifications of sediments in the environment of oil fields, in *Unconventional methods in exploration for petroleum and natural gas*: Dallas: Southern Methodist University, p. 159-186.
- , 1980, Pirson, oil is confined in the earth by redox potential barriers: *Oil & Gas Jour.*, Jul. 7, p. 153-158.
- Powell, J.A., 1981, Electrical transient surveys for hydrocarbon (abs.): *Geophysics*, v. 46, p. 432. Full paper available in *Technical papers*, 50th Annual International Meeting and Exhibition, SEG, Houston, v. 3, p. 1773-1794.
- Richers, D.M., Reed, R.J., Horstman, K.C., Michels, G.D., Baker, R.N., Lundell, L., and Marrs, R.W., 1982, Landsat and soil-gas geochemical study of Patrick Draw Oil Field, Sweetwater County, Wyoming: *AAPG Bull.*, v. 66, p. 903-922.
- Roberts, A.A., 1982, Helium emanometry in exploring for hydrocarbons: part II, in *Unconventional methods in exploration for petroleum and natural gas*: Dallas, Southern Methodist University, p. 135-149.
- Roberts, W.H., III, 1980a, Design and function of oil and gas traps, in *Problems of petroleum migration*: AAPG studies in geology no. 10, p. 217-240.
- , 1980b, Some uses of temperature data in petroleum exploration, in *Unconventional methods in exploration for petroleum and natural gas*: Dallas, Southern Methodist University, p. 8-49.
- Snyder, D.D., Kolvoord, R.W., Frangos, W., Bajwa, Y., Fleming, D.B., and Tasci, M.T., 1981, Exploration for petroleum using complex resistivity measurements, in *Advances in induced polarization and complex resistivity*: Tucson, short course reprints, University of Arizona, p. 209-253.
- Soti, G.G., 1957, Microorganisms and geochemical methods of oil prospecting: *AAPG Bull.*, v. 41, p. 134-140.
- Sumner, J.S., 1967, Principles of induced polarization for geophysical exploration: New York, Elsevier Scientific Publishing Co., 277 p.
- Toth, J., 1980, Cross-formational gravity-flow of groundwater: a mechanism of the transport and accumulation of petroleum (the generalized hydraulic theory of petroleum migration), in *Problems of petroleum migration*: AAPG studies in geology, no. 10, p. 121-178.
- U.S. Steel, 1983: personal communication with materials experts.
- Wait, J., 1983: personal communication.
- Wynn, J.C., and Zonge, K.L., 1975, EM coupling, its intrinsic value, its removal, and the cultural coupling problem: *Geophysics*, v. 40, p. 831-850.
- Zonge, K.L., and Hughes, L.J., 1981, The complex resistivity method, in *Advances in induced polarization and complex resistivity*: Tucson, short course reprints, University of Arizona, p. 163-208.

PART THREE

CASE HISTORIES

Chapter 3

Ryckman Creek and Whitney Canyon Fields Uinta County, Wyoming

3.1 INTRODUCTION

The Ryckman Creek and Whitney Canyon fields are located in the Western Wyoming Overthrust Belt, some ten miles (6 km) north of Evanston, Wyoming (Figure 3.1). Both fields occupy a prominent position in the hydrocarbon production of the Rocky Mountain states. Ryckman Creek, a prolific oil producer which has reserves of over 50 MMB of oil and over 150 BCF of gas, was the first substantial discovery in the Overthrust area. Whitney Canyon's estimated reserves of 3.1 TCF of gas place it firmly in the category of gas giant. These statistics, plus the extremely complex geology of the area, make the two fields an interesting target for electrical exploration.

Production at both Ryckman Creek and Whitney Canyon fields is from anticlinal traps on the hanging wall of the Absaroka Thrust Fault. As shown in Figure 3.2, the fields lie at the northern end of a roughly north-south trending line of oil and gas fields. This trend is directly controlled by the thrust faulting in the area.

A single line of resistivity/phase data was obtained over Ryckman Creek and Whitney Canyon, using a dipole spacing of 1,700 feet (520 m). The data were obtained on two separate occasions, during October, 1979, and August, 1980.

3.2 GEOLOGIC BACKGROUND

Exploration History of the Overthrust Belt

While oil springs in the Overthrust Belt were probably known by native Americans and trappers for some time, the first published account of the occurrence of oil is by Clayton (1848), who described the 1847 passage of the Mormons through Wyoming in their journey to Salt Lake City. Clayton noted the Hilliard oil spring in southern Uinta County, and commented:

"When the oil can be obtained free from sand, it is useful to oil wagons. It gives a nice polish to gunstocks and has been proved to be highly beneficial when applied to sores on horses, cattle, etc."

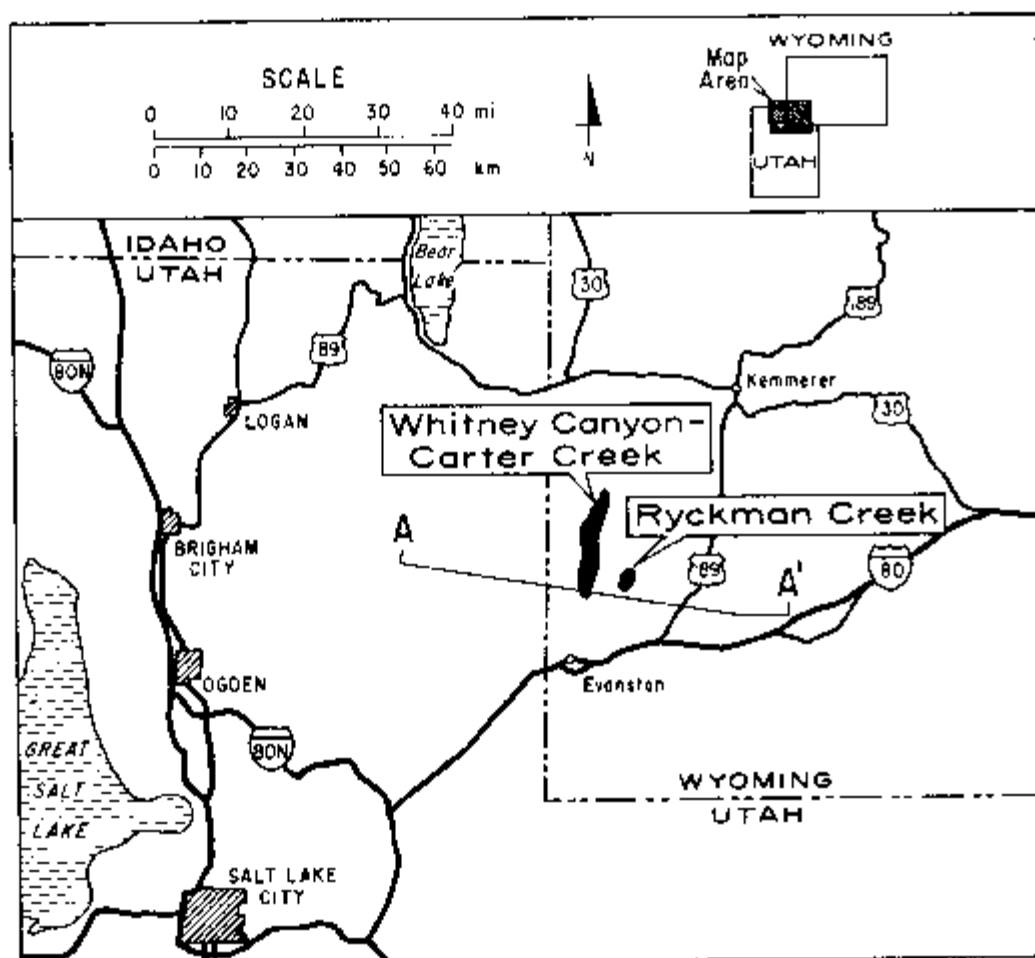


Figure 3.1. Location map of Ryckman Creek and Whitney Canyon-Carter Creek Fields.

A shallow well was drilled on the spring and the oil was sold locally to pioneers and settlers.

Oil springs like the one at Hilliard spurred a fair amount of interest in the area by small oil companies and individuals. The first significant drilling activity occurred in 1867 at the present-day Stove Creek Field and in 1868 at the nearby Carter Spring Field, both of which produced less than 20 barrels per day. Similar production was encountered at Twin Creek and Spring Valley in 1885, and at Fossil in 1902.

The discovery of the Labarge oil seep in 1907 generated a good deal of excitement in the area, but the first significant oil production in the Overthrust did not occur until 1924, when the Texas Production Company discovered Labarge Field. The discovery well was completed in Paleocene sands at 568 feet (173 m), and while the production rate of ten barrels per day was not very exciting by today's standards, the well nonetheless set off an oil boom in the general area. By 1928, some 85 new wells had been completed.

At the end of World War II, only Labarge and North Labarge Fields were producing, and for many years the combination of regionally low production, complex geology, high drilling costs, and lack of transportation outlets discouraged the major oil companies from entering the area. A turnaround in this situation began in

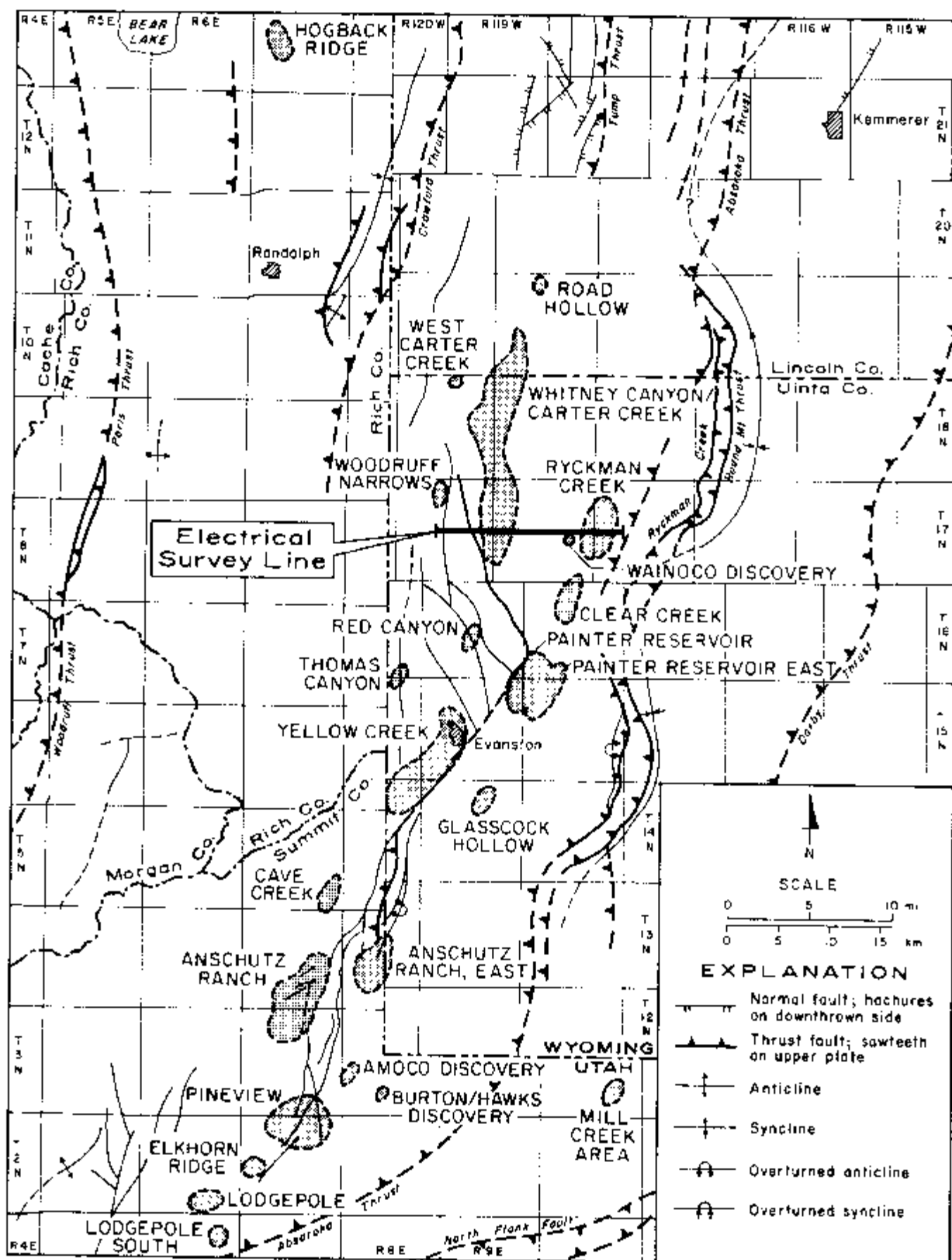


Figure 3.2. Utah-Wyoming Overthrust Belt fields and discoveries. Some information on these fields is provided in Table 3.1. Geology from Blackstone and VerPloeg (1981).

1949 with the entry of the first major into the area (Shell Oil Company), and with General Petroleum Corporation's discovery of oil at Tip Top in the North Labarge area in 1951. A number of exploration wells were drilled in the Overthrust during the next 25 years. Almost all of these were dry, but they served to help define the subsurface structure and to delineate potential reservoirs. A few were moderately successful: Willow Creek was discovered in 1957 and extended in 1974, and Mickelson Creek was discovered in 1960.

In 1975, the lackluster performance of Overthrust production came to a spectacular end with the American Quasar discovery at Pineview in Summit County, Utah. The discovery well, #1 Newton Sheep Co., established the first Overthrust production from the important Nugget Sandstone reservoir, flowing 550 BOPD and 270 MCFGPD between 9,928 and 9,936 feet (3,026 and 3,028 m). Later drilling established production in the Twin Creek, Stump, and Frontier formations as well.

It was at this time that congressional legislation passed over a century earlier came into play. In 1862 and 1864, Congress had granted the mineral rights to an extensive swath of land to the Union Pacific Railroad as an incentive to complete the western leg of the nation's first transcontinental railroad. As a result of this legislation, Union Pacific controlled every other square mile for 20 miles on each side of its track, with the federal government retaining the rights to the remaining sections. In 1969, prior to any significant Overthrust discoveries, Union Pacific granted exclusive exploration rights to Amoco Production Company for approximately 7.4 million gross acres (30,000 sq km), extending from northeastern Colorado to northeastern Utah and including much of the now productive Wyoming-Utah Overthrust area. Amoco was given access to odd-numbered sections, and Champlin Petroleum Company, a company Union Pacific had acquired in 1970, had access to the even-numbered sections. As a result of these events, Amoco and Champlin have played a dominant role in exploration and production in the Overthrust; Amoco alone owns an interest in 24 of the 26 producing fields in the Overthrust Belt. Farmouts and lease acquisitions account for the numerous secondary participants in the area.

In 1976, Amoco made a major discovery at Ryckman Creek on acreage obtained from Union Pacific. The discovery propelled the Overthrust region to the forefront of petroleum exploration in the United States. The discovery well, #1 Champlin-224-Amoco A, was drilled on a seismically-defined anticline by Amoco, Chevron, and Champlin Petroleum. After extensive testing for potential reservoirs, the well was completed in the Nugget sandstone, flowing an initial 288 BOPD from a 200-foot (60 m) oil column and 310 MCFGPD from a 300-foot (90 m) gas-condensate column. A second Nugget well was completed in March 1977, confirming the discovery, and production was extended to the Thaynes in December 1979 with the completion of a third well, 23 Ryckman Creek. Gas was noted in two zones of the Thaynes at 23 Ryckman Creek, and the well was dually completed in the Nugget and Thaynes. Subsequent development of Ryckman Creek has firmly established it as a major oil producer and as a respectable gas producer. Total reserves are estimated to be 150 billion cubic feet of gas and 50 million barrels of oil and condensate.

Since the Pineview and Ryckman Creek discoveries, development of Overthrust production has continued unabated. In March 1977, the discovery well was completed in the Twin Creek at Lodgepole Field, just eight miles southwest of Pineview. Production is currently from the Twin Creek and the Nugget.

Whitney Canyon was the next discovery. Several shallow dry holes had been drilled in the area in 1903 and 1945, but it was not until October 1976 that the area was committed to a deep test. The discovery well, #1 Amoco-Chevron-Gulf W1 Unit,

was originally projected to the Phosphoria at 13,400 feet (4,080 m) as a test of a subsurface seismic structure. However, a jammed core barrel and a break in the drill pipe due to high hydrogen sulfide gases prevented completion in the Phosphoria, and the hole was sealed off above that formation. The hole was then completed in the Thaynes in August 1977. Perforated between 9,178 and 9,266 feet (2,792-2,824 m), the well flowed gas at the rate of 4.7 MMCFGPD along with 196 bbls of condensate and 9 bbls of water. A second Whitney Canyon well, #2 Amoco-Chevron-Gulf W Unit, was drilled in May 1977 some 1,900 feet (580 m) northeast of the discovery well. Initial production was from the Thaynes. An extensive testing program for other promising formations established production in the Bighorn, which had not yet been productive in the Overthrust. The Madison and Weber also proved to be good reservoirs in these tests. A third well, #1 Champlin-457 Amoco-A, was spudded in October 1977. It had shows or production in the Phosphoria, Weber, Thaynes, Frontier, Bighorn, Darby, and Mission Canyon.

In February 1978, Chevron spudded its #1-32 Chevron Federal well north of Whitney Canyon in Lincoln County. Gas was produced in the Madison and Weber, opening up Carter Creek Field. Amoco then redrilled #1 Kewanee-Federal, which had been abandoned by Chevron at 8,550 feet (2,606 m) in 1976, and found production in the Bighorn. Located between Whitney Canyon and Carter Creek, this well unitized the two fields to a single, north-south oriented gas field.

Table 3.1 lists the major Overthrust discoveries of the past seven years. Many of these fields have enormous potential reserves, and the prospect for future discoveries is quite bright.

TABLE 3.1: OIL AND GAS FIELDS OF THE OVERTHRUST BELT¹

Field	Location	Operator	Discovery Well Completion Date	Production ²	Producing Formations
Pineview	Summit Co., Ut.	American Quasar	1/75	O,G	Frontier Stump Twin Creek Nugget
Ryckman Creek	Uinta Co., Wyo.	Amoco Prod.	9/76	O,G	Nugget Thaynes
Yellow Creek	Uinta Co., Wyo.	Amoco Prod.	7/76	G,C	Twin Creek Phosphoria
Lodgepole	Summit Co., Ut.	American Quasar	3/77	O,G	Twin Creek
Whitney Canyon	Uinta Co., Wyo.	Amoco Prod.	8/77	G,C	Thaynes Phosphoria Weber Mission Canyon Lodgepole Darby Bighorn
Elkhorn Ridge	Summit Co., Ut.	American Quasar	9/77	O,G	Twin Creek
Painter Reservoir	Uinta Co., Wyo.	Chevron USA	10/77	O,G	Nugget
Hogback Ridge	Rich Co., Ut.	American Quasar	10/77	G	Dinwoody Phosphoria
Anschutz Ranch	Summit Co., Ut.	Anschutz Corp.	10/78	G,C	Twin Creek Nugget
Clear Creek	Uinta Co., Wyo.	Chevron USA	6/78	O,G	Nugget
Lodgepole South	Summit Co., Ut.	Colorado Energetics	9/78	G	Kelvin
Carter Creek	Uinta Co., Wyo.	Chevron USA	7/79	G,C	Weber Madison
East Painter Reservoir	Uinta Co., Wyo.	Chevron USA	8/79	G,C	Nugget

TABLE 3.1 Continued

Field	Location	Operator	Discovery Well Completion Date	Production ²	Producing Formations
Cave Creek	Uinta Co., Wyo.	Amoco Prod.	10/79	G,C	Weber Madison Phosphoria
Red Canyon	Uinta Co., Wyo.	Amoco Prod.	12/79	G,C	Weber
Anschutz Ranch East	Summit Co., Ut.	Amoco Prod.	12/79	O,G	Nugget
Two Medicine Creek	Glacier Co., Mont.	Rainbow Resources	1/80	O	Sun River
Mill Creek	Summit Co., Ut.	Exxon	7/80	O	Three Forks Darby
Glasscock Hollow	Uinta Co., Wyo.	Amoco Prod.	9/80	G,C	Nugget
[SE-SW-8-T29N-R114W]	Sublette Co., Wyo.	American Quasar	10/80	G	"Mississippian" Bighorn
Blackleaf Canyon	Teton Co., Mont.	Rainbow Resources	12/80	G	Sun River
Woodruff Narrows	Uinta Co., Wyo.	Chevron USA	4/81	G,C	Bighorn
Thomas Canyon ³	Uinta Co., Wyo.	Chevron USA	7/81	G	Madison
[NW-NW-28-T3N-R8E]	Summit Co., Ut.	Burton/Hawks	mid '81	O	Kelvin Stump
[NW-SE-19-T3N-R8E] ⁴	Summit Co., Ut.	Amoco Prod.	mid '81	G	Preuss
Road Hollow	Lincoln Co., Wyo.	Exxon	10/81	G	Bighorn
[NW-SE-23-T17N-R119W]	Uinta Co., Wyo.	Wainoco	early '82	O,G	Ankareh
West Carter Creek ⁵	Uinta Co., Wyo.	Amoco Prod.	11/82	G,C	Bighorn Madison

¹ Updated to 12/31/82; includes significant discoveries² O=oil, G=gas, C=condensate³ Abandoned due to high hydrogen sulfide content⁴ Temporarily abandoned due to high water production⁵ Preliminary designation

Particularly germane to the discussion of the Ryckman Creek/Whitney Canyon electrical data are the recent discoveries at Woodruff Narrows (also called Woodruff Mountain Field) and the unnamed discovery by Wainoco at NW-SE-23-T17N-R119W. The Woodruff Narrows discovery well, #1-4H Amoco-Federal, was completed in the spring of 1981 as the deepest producer in the Overthrust Belt. The well flowed 2.8 MMCFGPD and 15 BPD of condensate from the Bighorn at 16,736-16,780 feet (5,101-5,115 m). Note that this well is 2.4 miles (3.9 km) north of the western end of the electrical survey line. The data there show a very strong anomaly, as will be discussed later. To date no deep wells have yet been drilled south of Woodruff Narrows; Chevron spudded its #1-16H Chevron-State well, SE-SW-16-T17N-R120W, on April 24, 1982, but the well was abandoned after reaching a total depth of only 3,215 feet (980 m). Amoco is currently drilling its #1 Champlin-804 Amoco-C in SE-NW-9-T17N-R120W, but this site is still two miles (3 km) north of the survey line.

The Wainoco discovery is located just west of Ryckman Creek, approximately half a mile (1 km) south of station 10 on the electrical survey line. The discovery well, B-1 Amoco-Champlin 370, flowed 230 BOPD and 840 MCFGPD from the Triassic Ankareh Formation between 12,418 and 12,602 feet (3,785-3,841 m). Production is from a structural unit separate from that of the Ryckman Creek Field. A second well, Chevron #1-14E, was drilled and abandoned one mile (1.6 km) north of the Wainoco discovery well, or 2,000 feet (610 m) north of the survey line. Total depth was 12,800 feet (3,900 m) in the Ankareh.

Geologic History of the Wyoming Overthrust Belt

Although a complete description of Overthrust geologic history cannot be reasonably presented here, a brief outline is offered for purposes of general understanding. A number of interesting papers on this subject are published or referenced in the 1977 Wyoming Geologic Association's Guidebook.

As described by Peterson (1977), Blackstone (1977), Rose (1977), and others, western Wyoming was the location of the western margin of the North American craton during Precambrian time. West of the craton there existed a miogeosynclinal depositional shelf, in which several depositional troughs were located (Figure 3.3). These troughs were formed as a result of rifting some 850 million years ago, and they show a remarkable similarity in shape to the modern-day Thrust Belt of the western United States.

During Precambrian time, western Wyoming received clastic deposition from erosion of the craton to the east. Erosion came to an end during the early Cambrian, when a prolonged era of subsidence brought a sequence of marine and littoral rocks. Deposition continued throughout the Paleozoic except for an erosional episode during the Silurian. Devonian and Mississippian sedimentation involved mostly deep marine carbonates, changing to shallower environments during the Pennsylvanian and the Permian. Post-Devonian deposition was significantly affected by the Antler Orogeny to the west. By the end of the Paleozoic, some 35,000 feet (10,670 m) of sediments had been deposited in the area.

Early Triassic sedimentation consisted primarily of clastics. Deposition was minimal during the middle Triassic. The Sevier Orogeny in northeastern Nevada and northwest Utah elevated most of present-day Idaho during Jurassic time, disrupting the sedimentation pattern established in the Cambrian. The western Overthrust area received no Jurassic sediments, and coarse clastics were deposited toward the east.

The major thrust faulting of western Wyoming began in early Cretaceous time. The mechanism for this activity is not fully understood. Two hypotheses exist, one that the upper plate was shoved over the lower one, and the other that the lower plate slid underneath the upper one due to gravitational forces. Rubey and Hubert (1959) suggested that abnormal fluid pressures may have had a major contribution to the overthrusting activity. Tectonic activity continues today, as judged by seismicity in the area.

Current Geology

Table 3.2 summarizes the stratigraphy of the Ryckman Creek/Whitney Canyon area. Several thousand feet of Tertiary sediments overlie the overthrust strata, as shown in the generalized cross-section A-A' of Figure 3.4. Detailed cross-sections of Ryckman Creek and Whitney Canyon are shown in Figures 3.5 and 3.6, respectively. The electrical line location with respect to these fields is shown in Figure 3.7. Figure 3.8 is a structure map of Ryckman Creek, contoured on the top of the Nugget Sandstone; Figure 3.9 is a structure map of Whitney Canyon, contoured on top of the Mission Canyon Formation.

Reservoir Geology

Reservoir data on Ryckman Creek and Whitney Canyon fields are presented in Tables 3.3 and 3.4, respectively.

The structure at Ryckman Creek is an asymmetric, overturned, north-south trending anticline on the hanging wall of the Absaroka Thrust Plate (Figure 3.4). The structure has some 1,500 feet (460 m) of closure. A total hydrocarbon column of 515 feet (157 m) is found in the prolific Nugget Sandstone, including a 215 foot (66 m) column of oil and a 300 foot (90 m) gas cap. The Nugget is some 800 feet (240 m) thick at Ryckman Creek. It consists of a massive, cross-bedded, cross-laminated, white to red-brown, porous, quartzose sandstone with well rounded, well

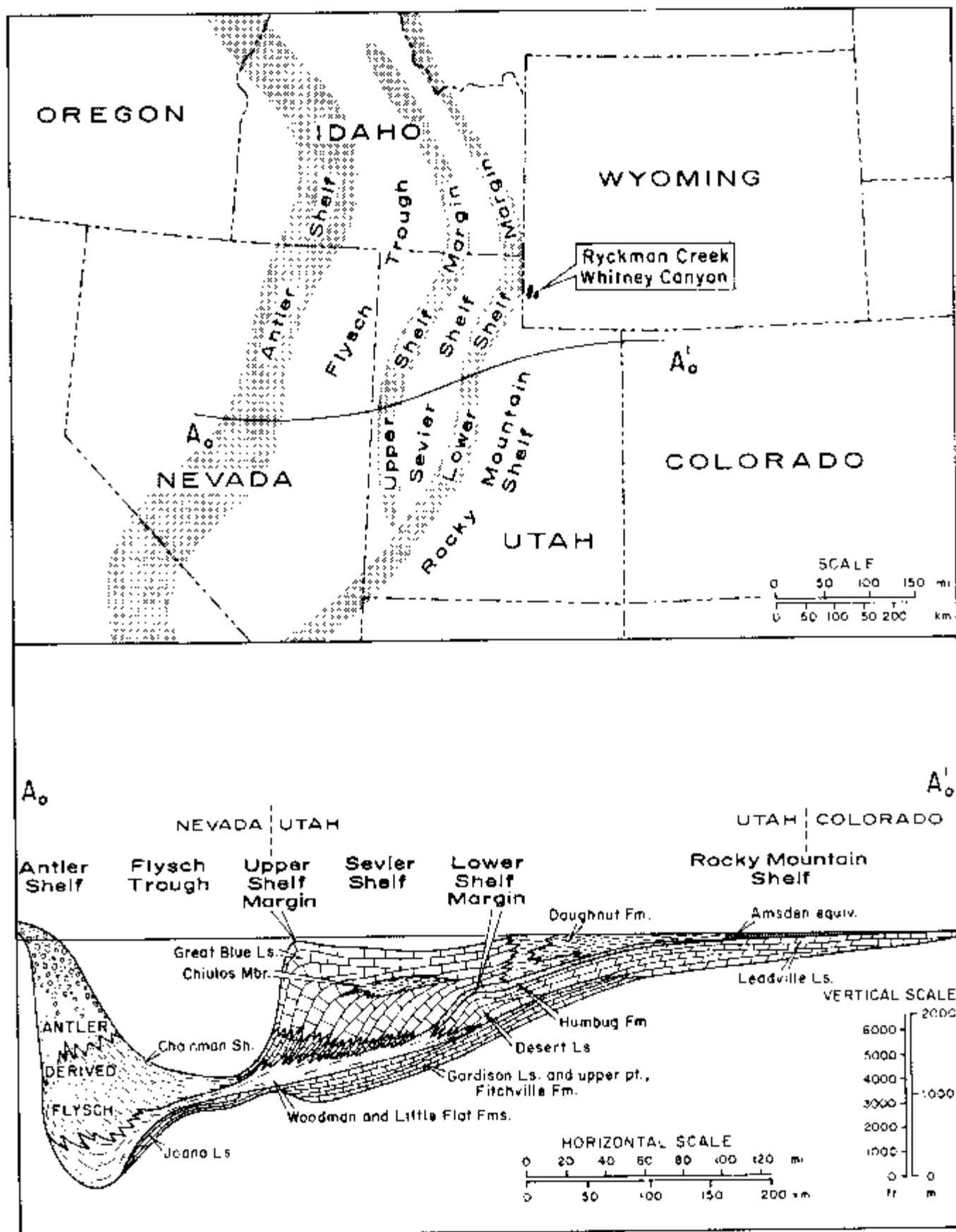


Figure 3.3. Paleozoic depositional environment in the west-central United States. From Rose (1977).

TABLE 3.2: STRATIGRAPHIC DESCRIPTION OF RYCKMAN CREEK AND WHITNEY CANYON FIELDS

System	Symbol	Formation	Lithologic Description
CENOZOIC ROCKS			
Tertiary			
Eocene	—	Wasatch-Green River Fms. (undifferentiated) (unconformity)	Shales and sandy shales with a basal conglomerate
Paleocene	Te	Evanson Fm. upper part	Shale
MESOZOIC ROCKS			
Cretaceous			
		conglomerate lower part	Conglomerate Silty shale
	Ka	Aspen Sh.	Sandy shale
	Kbr	Bear River Fm. (unconformity)	Shales with a basal sandstone
	KJg	Gannett Group (unconformity)	Interbedded shales and sandy shales with a basal unit of fossils and conglomerates
Jurassic			
	Jst	Stump Ss.	Calcareous sandstones, shales, and sandy limestones
	Jp	Preuss Ss.	Shale
	Jtc	Twin Creek Fm.	Interbedded limestones, conglomeratic limestones, and shales
Triassic			
	Trn	Nugget Ss.	Fine to medium grained, well rounded, well sorted, quartzose sandstone with 5-10% feldspar; <i>hosts oil and gas at Ryckman Creek</i>
	Trs	Ankareh Sh.	Sandy shale with middle conglomeratic unit; <i>hosts oil at the Wainoco discovery well, NW-SE-23-T17N-R119W</i>
	Trt	Thaynes Ls.	Limestone with dolomitic and shale sections; <i>hosts gas at Ryckman Creek and at the fractured southern portion of Whitney Canyon</i>
	Trws	Woodside Sh.	Sandy shale
	Trd	Dinwoody Fm.	Sandy shale; <i>hosts non-commercial gas at Whitney Canyon</i>
PALEOZOIC ROCKS			
Permian			
	Pp	Phosphoria Fm.	Interbedded shales and fossiliferous limestones; <i>hosts sour gas at Whitney Canyon</i>
Pennsylvanian			
	Pw	Weber Ss.	Sandstone with minor siltstone, shale, and carbonate beds; <i>hosts gas at Whitney Canyon</i>
	Pm	Morgan Fm. (Amsden Fm.)	Interbedded sandstones, shales, and dolomites
Mississippian			
	Mmc	Mission Canyon Fm. (Madison Ls.) Upper unit	Limy dolomites and dolomites with nodular anhydrite
		Middle unit	Limy dolomite, bioclastic; <i>hosts extensive gas at Whitney Canyon</i>
		Lower unit	Shaly micritic limestones and dolomite limestones
	MI	Lodgepole	Dolomitic limestones and limy dolomites; <i>hosts gas at Whitney Canyon</i>

TABLE 3.2 Continued

System	Symbol	Formation	Lithologic Description
Devonian	Dd	(unconformity) Darby Fm.	Carbonates, anhydrites, siltstones, and shales; <i>hosts gas in the highest portion of the Whitney Canyon structure</i>
Ordovician	Obh	(unconformity) Bighorn Dol.	Thinly bedded dolomite with minor shale beds; <i>hosts gas at Whitney Canyon and Woodruff Narrows</i>
Cambrian	Eg	Gallatin Ls.	Limestone

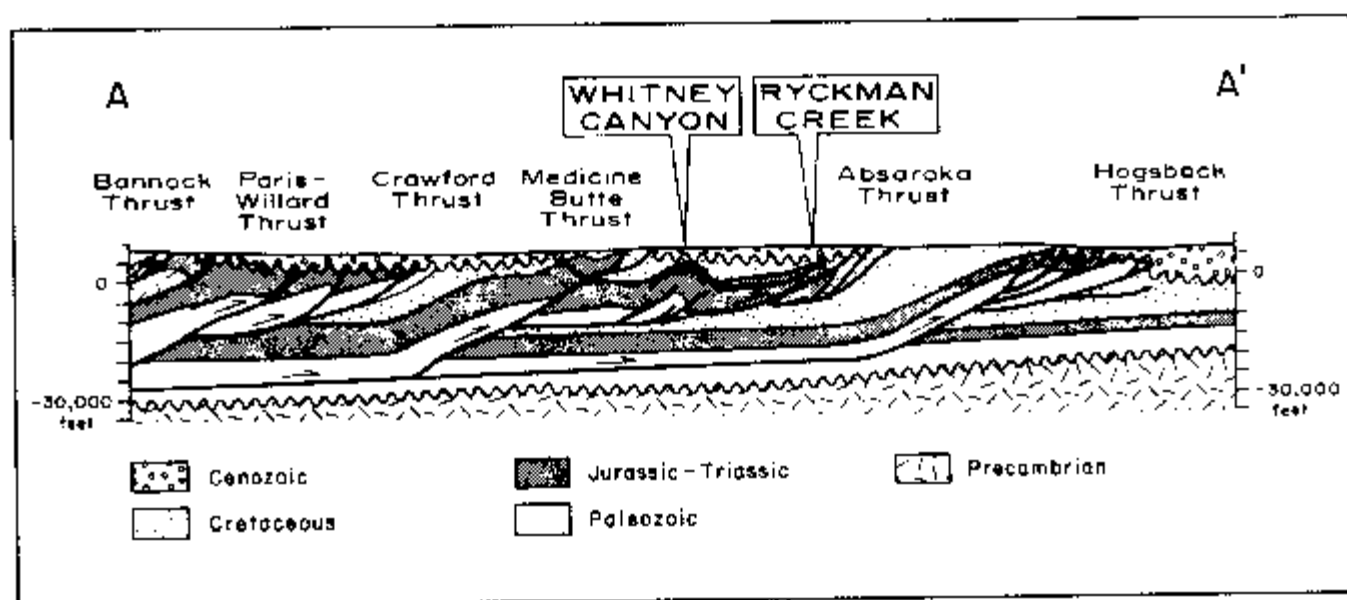


Figure 3.4. Generalized geologic cross-section A-A' across the Utah-Wyoming Overthrust Belt, with no vertical scale exaggeration. Figure 3.1 shows the map location. After Dixon (1982).

sorted, fine grains. Porosity is quite high throughout the unit at the discovery well; permeability is anisotropic, being highest in a vertical direction. Oils are paraffinic, high in gravity, and low in sulfur; gas is similarly low in sulfur.

Ryckman Creek has an active water drive. At present, only oil is produced. Stripped natural gas has been re-injected back into the gas cap since 1977 in order to maintain reservoir pressure, supplemented by nitrogen injection beginning in 1981. Total oil production varies from 100 to 1,200 BOPD per well. Low-sulfur gas and condensate are also obtained from the Thaynes, which has primarily fracture porosity.

The Whitney Canyon-Carter Creek complex, now considered a gas giant, produces gas and condensate from eight pay zones in a large, north-south trending anticline on the hanging wall of the Absaroka Thrust Plate. The Whitney Canyon-Carter Creek structure is about 4x15 miles (6x24 km) in size and has some 4,500 feet (1,400 m) of closure.

Some 70 to 80 percent of the field's reserves are found in the Mission Canyon Formation, a regressive carbonate and evaporite sequence. As indicated in

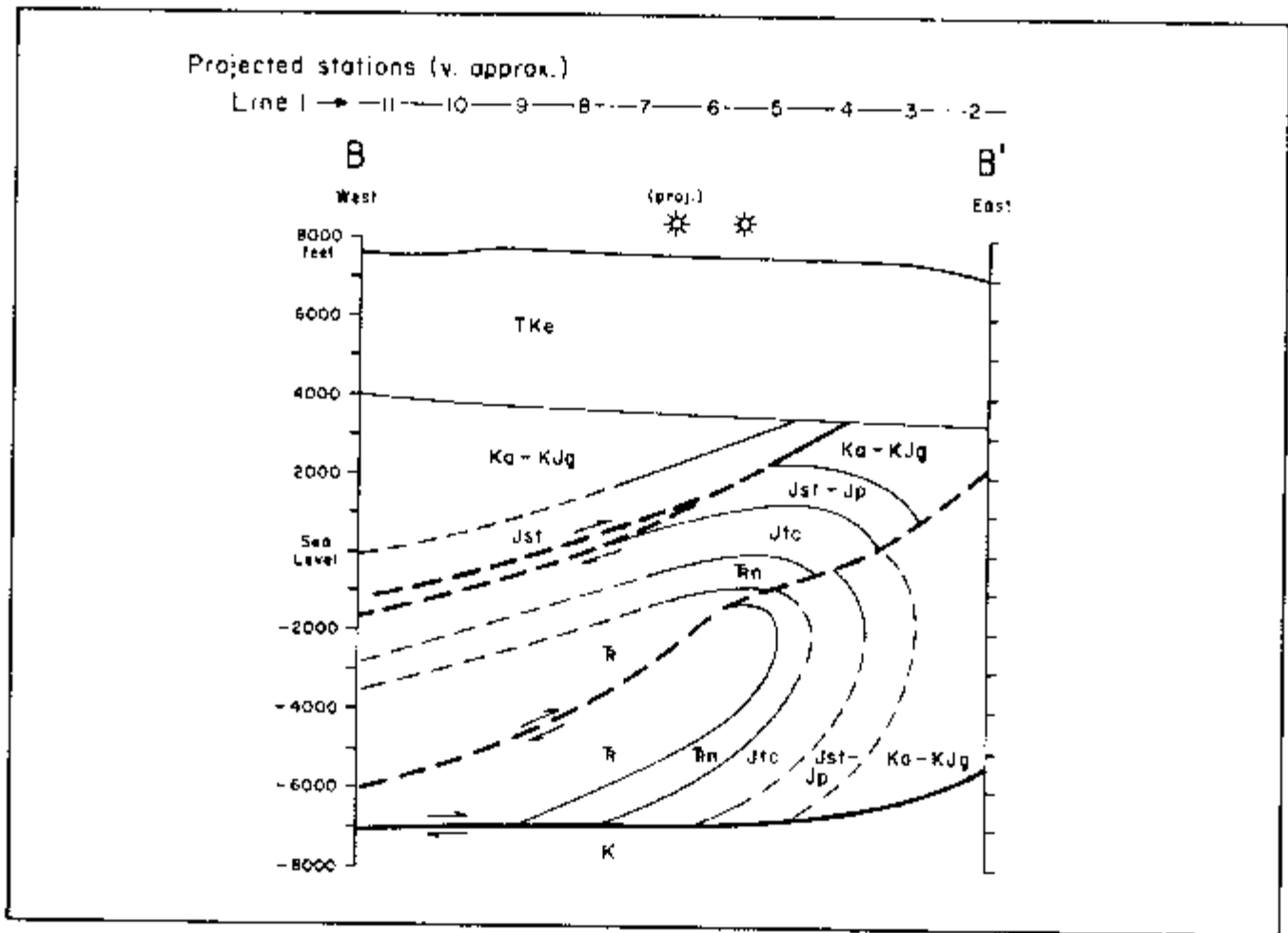


Figure 3.5. Geologic cross-section B-B' across Ryckman Creek Field, with no vertical scale exaggeration. Refer to Figure 3.7 for map location. Geology from Kelly and Hine (1977).

the stratigraphic description of Table 3.2, the producing zone is a bioclastic limy dolomite which was deposited in a high-energy shoreline environment. Porosity is primarily matrix type, with some fracturing enhancement. Gas is high in sulfur.

Other commercial producing formations at Whitney Canyon are the Thaynes, Phosphoria, Weber, Lodgepole, Darby, and the Bighorn. The carbonates and shales of the Thaynes have both matrix and porosity permeability. Production is from interbedded dolomites; as of 1981, production had only been established in the more fractured southern flank of the Whitney Canyon anticline. The Thaynes hosts the only sulfur-free gas in the field. The Phosphoria shales and limestones host an undetermined amount of sour gas, which Hoffman and Kelly (1981) call non-commercial. The Weber shows matrix and fracture porosity, and the gas has a very high hydrogen sulfide content. The Lodgepole Formation, a transgressive sequence of limy dolomites and dolomitic limestones, has primarily matrix porosity with some fracture porosity evident. Production may prove to be favorable across the full area of the field. Gas is high in hydrogen sulfide. The Darby production is from a limy dolomite zone near the top of the formation. Since the top of the Darby is substantially eroded toward the north end of Whitney Canyon, production is limited

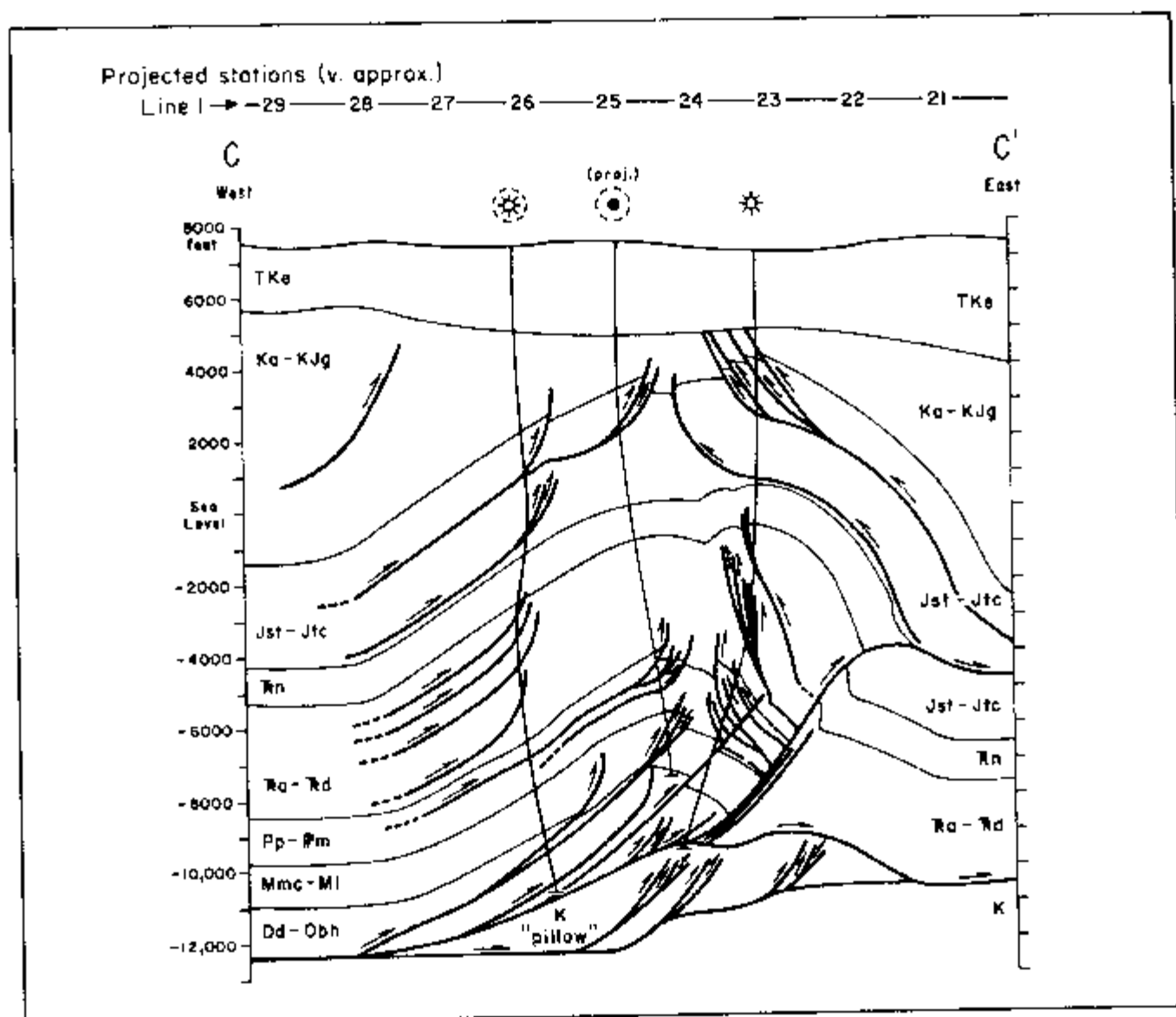


Figure 3.6. Geologic cross-section C-C' across Whitney Canyon Field, with no vertical scale exaggeration. Refer to Figure 3.7 for map location. Geology from Hoffman and Kelly (1981).

to the highest portion of the Whitney Canyon structure, and the Darby is therefore not expected to be a major reservoir. Porosity in the Darby is due to fracturing, and gas is fairly low in hydrogen sulfide (1.0%). The Bighorn Dolomite produces gas from two zones of fracture type porosity, located at the top of the formation. Gas is relatively low in hydrogen sulfide (0.63%).

The source of the hydrocarbons at Whitney Canyon has been determined by chromatography to be the subthrust Cretaceous strata. Hence, primary migration can be dated as post-Cretaceous.

Due to the high hydrogen sulfide content of the gas, most of the wells which had been drilled at the time of the electrical survey had been shut in pending completion of a gas-sweetening plant, which was begun in 1980 and came on line in October 1982. The \$340 million plant has now reached its total capacity of 12,600 barrels per day of natural gas liquids and 6,000 barrels per day of condensate. The

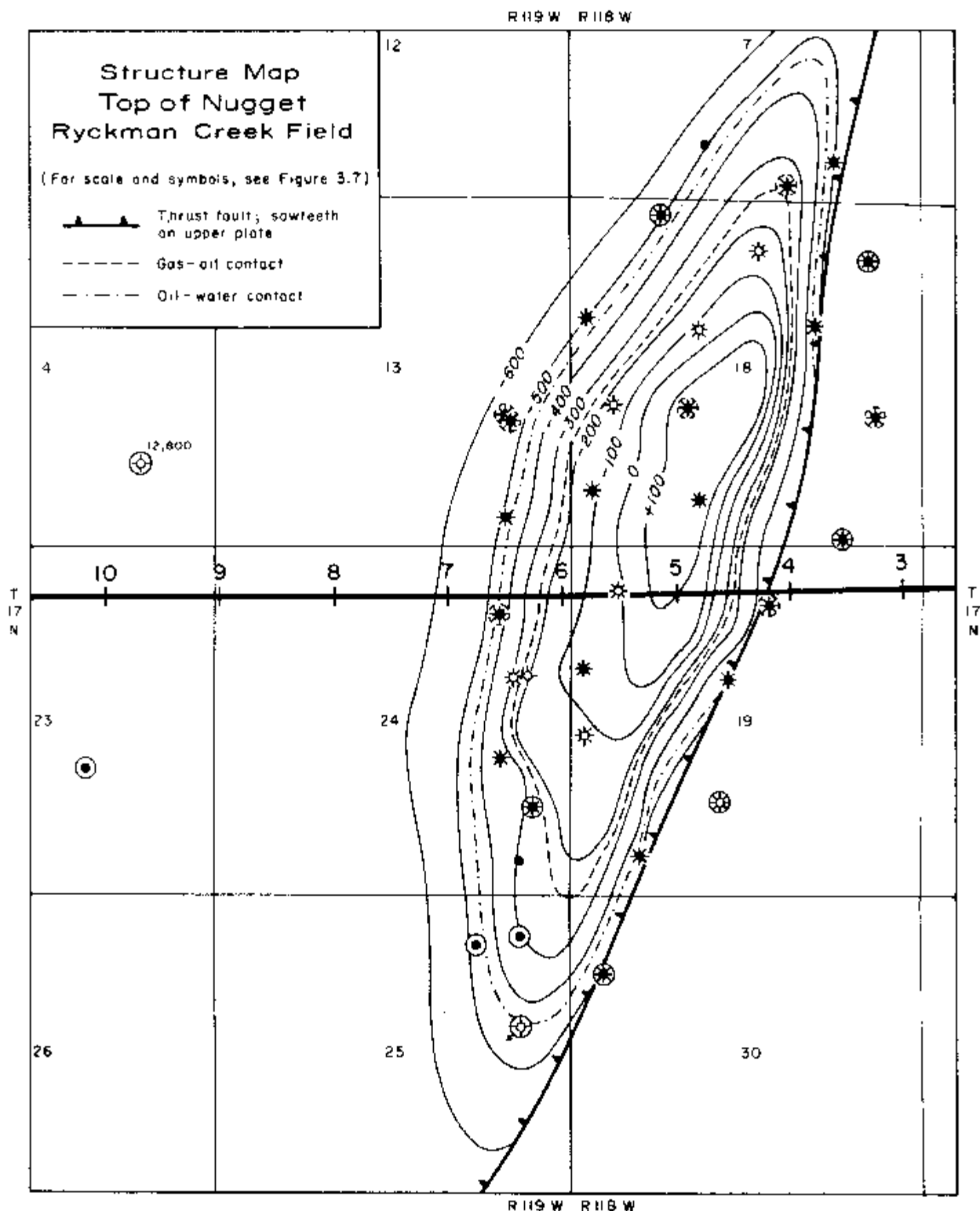


Figure 3.8. Structural map of Ryckman Creek Field, contoured on top of the Nugget Sandstone. Contour interval: 100 feet (30 m). Geology from *The Overthrust Belt, 1981 (Petroleum Information)*.

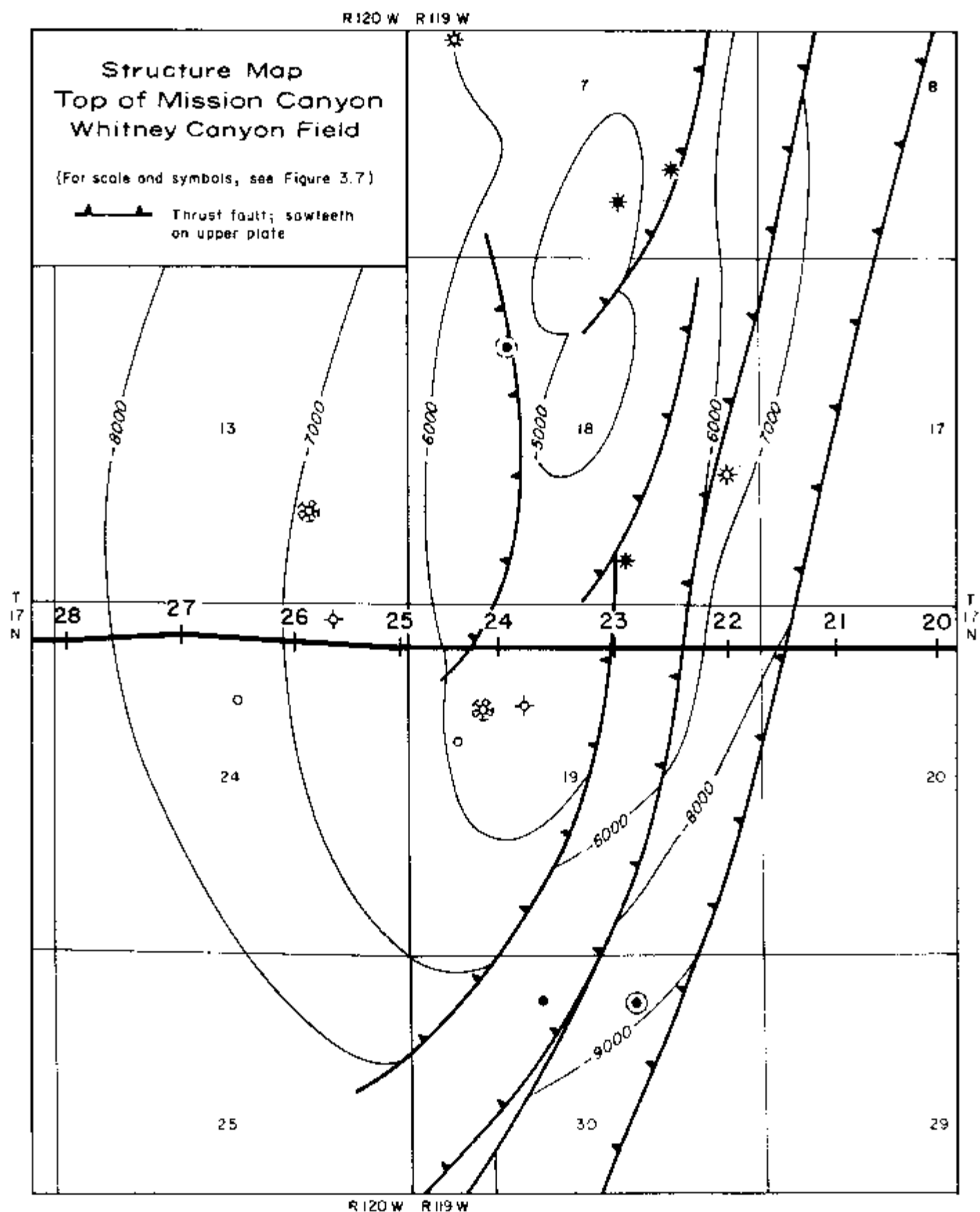
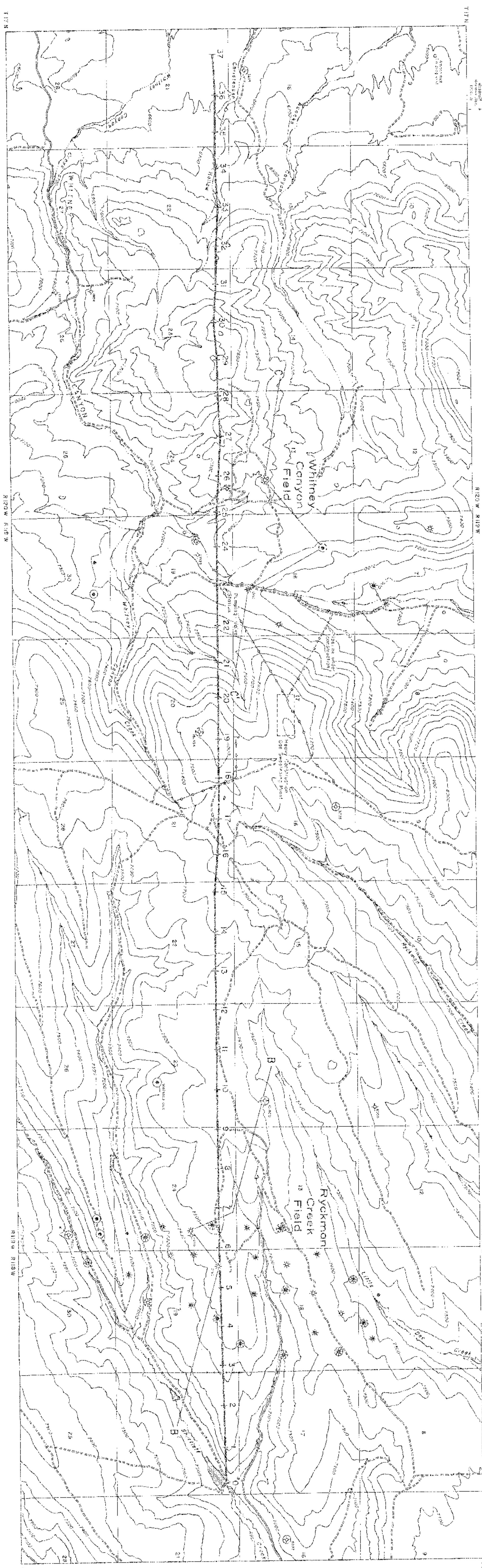
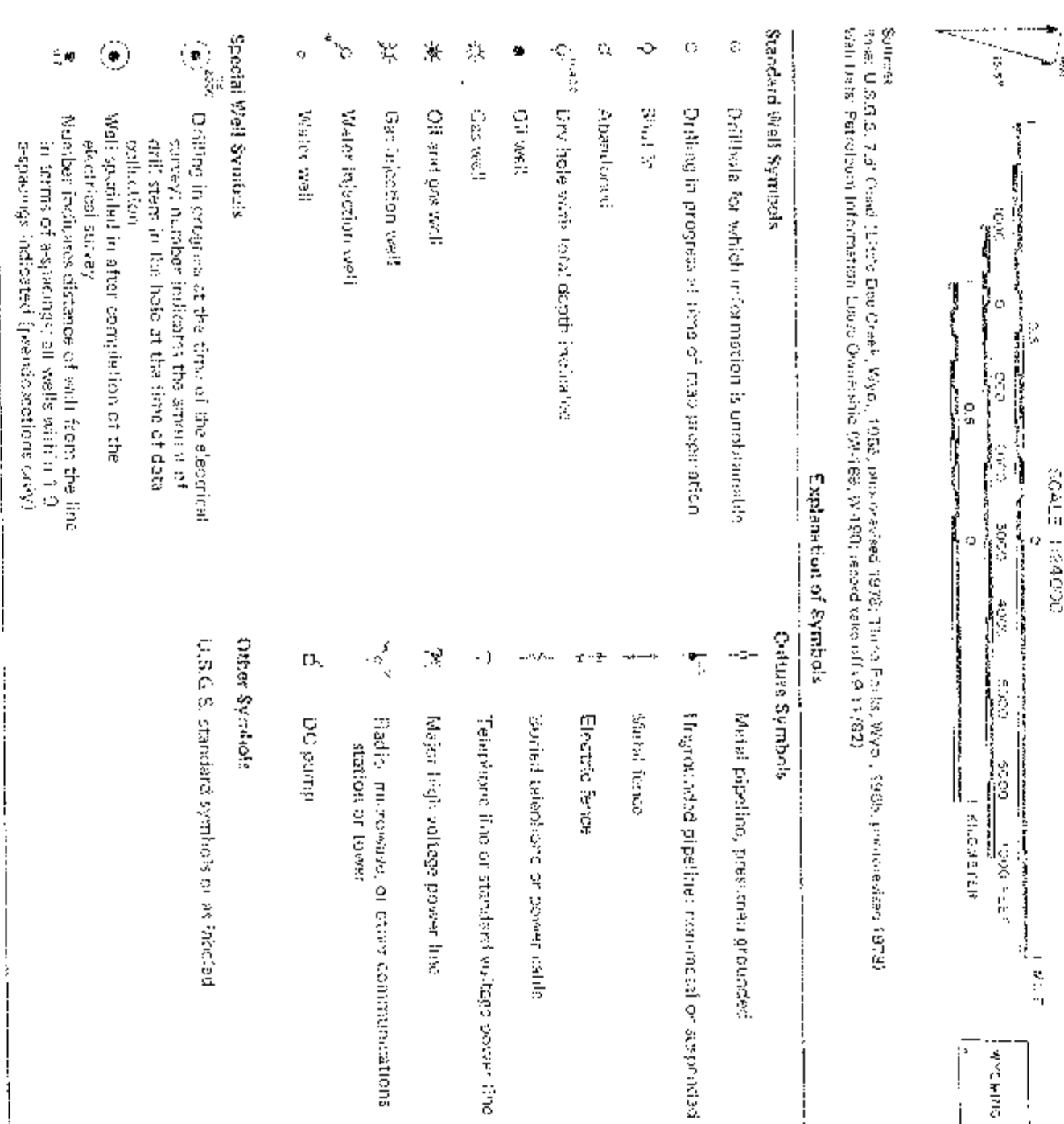


Figure 3.9. Structural map of Whitney Canyon Field, contoured on top of the Mission Canyon Formation. Contour interval: 1,000 feet (305 m). Geology from Hoffman and Kelly (1981).

Figure 3.7
LINE LOCATION MAP
Hydrus Creek and Whitney Canyon Fields
Upper San Joaquin



General Field Data

Region: Western Wyoming Overthrust Belt
Production: Oil, gas
Type of Trap: Structural; thrust-faulted anticline
Producing Formations and Depths: Nugget Ss., 7,800 ft
Thaynes Ls., 9,800 ft
Other Significant Shows: None
Total Reserves: 150 BCFG, 50 MMBO
Productive Area: 1,000 acres
Field Operator: Amoco
Number of Producing Wells (10/79): 18
Number of Shut-in Wells (10/79): 0
Number of Dry or Abandoned Wells (10/79): 1
Well Casing Data: 13-3/8 inch at 1,962 ft, 9-5/8 inch at 8,422 ft (discovery well)

Discovery Well

Name: 1 Ryckman Creek WI Unit
Location: NW-NW-19-T17N-R118W
Completion Date: 9/22/76
Total Depth: 14,795 ft
Perforations: 7,804-7,808 ft, 7,860-7880 ft (Nugget)
Initial Potential: 310 MCFGPD, 28B BOPD
Treatment: Breakdown perforations with KCl water; acidize with 500 gals of 15% HCl

Reservoir Data: Nugget Sandstone

Discovery: 9/22/76, 1 Ryckman Creek WI Unit, NW-NW-19-T17N-R118W
Lithology: Quartzose sandstone
Age: Triassic/Jurassic
Type of Trap: Structural; thrust-faulted anticline
Drive Mechanism: Active water drive
Initial Pressure: BHP 2,900 psi at gas/oil contact in discovery well
Recent Pressure (12/78): BHP, 2,881 psi at gas/oil contact in discovery well
Reservoir Temperature: 140°F at gas/oil contact in discovery well
Gross Thickness of Reservoir Rock: 815 ft
Porosity: 15% average
Permeability: Average 76 millidarcies, range 1.5-945 millidarcies. Primarily matrix porosity and permeability, relatively constant across the field, minor fracture porosity.
Oil/Gas Column: Maximum of 515 ft: 215 ft oil column, 300 ft gas cap
Gas/Oil Ratio: 1,108:1 on the discovery IP
Original Gas/Oil Contact: -235 ft true vertical depth
Original Oil/Water Contact: -450 ft true vertical depth
Gas Character: 1,238 BTU/cu ft
Gas Analysis:

Methane	77.86%
Ethane	11.27
Propane	5.25
Iso-Butane	1.11
n-Butane	0.33
iso-Pentane	0.25
Hexanes	0.19
Heptanes +	0.21
Nitrogen	2.31
Carbon dioxide	0.05
Hydrogen sulfide	nil

Oil Character: Low sulfur, paraffin base crude; gravity 47.4° API; pour point 30°F
Oil Analysis:

Sulfur (wt %)	0.026%
Hydrogen sulfide	nil

TABLE 3.3 Continued

Water Saturation: 21%	
Water Salinity: 12,800 ppm NaCl	
Cumulative Production (9/76-12/78): 1,558,669 BO; 2,338 BCFG	
Estimated Primary Recovery: Not reported	
Type of Secondary Recovery: Not reported	
Estimated Ultimate Recovery: 40-50 MMBO; 100-150 BCFG	
Reservoir Data: Thaynes Limestone	
Discovery: 12/79, 23 Ryckman Creek, NE-NE-24-T17N-R119W	
Lithology: Carbonates and shales	
Age: Triassic	
Type of Trap: Structural; thrust-faulted anticline	
Reservoir Temperature: 155° F (est.)	
Gross Thickness of Reservoir Rock: 1,100 ft	
Porosity: Not reported	
Permeability: Natural fractures	
Oil/Gas Column: Not reported	
Gas/Oil Ratio: 26,000:1	
Gas Character: 1,239 BTU/cu ft	
Gas Analysis: Methane	78.80%
Ethane	10.20
Propane	5.20
iso Butane	1.10
n-Butane	0.30
iso-Pentane	0.20
Hexanes	0.20
Heptanes +	0.20
Nitrogen	2.30
Carbon dioxide	0.05
Hydrogen sulfide	nil
Condensate Character: Low sulfur; gravity 47.4° API; pour point 30° F	
Condensate Analysis: Sulfur	0.026%
Hydrogen sulfide	nil
Estimated Primary Recovery: Not reported	
Type of Secondary Recovery: Not reported	
Estimated Ultimate Recovery: Not reported	

TABLE 3.4: RESERVOIR CHARACTERISTICS OF WHITNEY CANYON FIELD

General Field Data**Region:** Western Wyoming Overthrust Belt**Production:** Gas, oil**Type of Trap:** Structural; thrust-faulted anticline

Producing Formations and Depths:

Thaynes Ls.,	9,200 ft
Phosphoria Fm.,	11,800 ft
Weber Ss.,	11,200 ft
Mission Canyon Fm.,	12,600 ft
Lodgepole Ls.,	13,000 ft
Darby Fm.,	13,500 ft
Bighorn Dol.,	14,200 ft

Other Significant Shows: Dinwoody Fm., 11,200 ft**Total Reserves:** 3.1 TCFG, 66 MMBO**Productive Area:** 38,000 acres

TABLE 3.4 Continued

Field Operator: Amoco
 Number of Producing Wells (8/80): 0 (shut in awaiting completion of gas-sweetening plant)
 Number of Shut-in Wells (8/80): 7
 Number of Dry or Abandoned Wells (8/80): 0
 Well Casing Data: 20 inch at 80 ft, 13-3/8 inch at 2,500 ft, 9-5/8 inch at 12,500 ft, 7 inch at 16,500 ft (typical Chevron wells)

Discovery Well

Name: 1 Amoco-Chevron-Gulf W1 Unit
 Location: SW-SE-18-T17N-R119W
 Completion Date: 8/18/77
 Total Depth: 10,691 ft, plugged back to 9,503 ft
 Perforations: 9,178-9,182 ft, 9,183-9,221 ft, 9,221-9,266 ft (Thaynes Ls.)
 Initial Potential: 4,713 MCFGPD, 196 BCPD, 9 BWPD
 Treatment: Acidized with 2,000 gals of 15% HCl

Reservoir Data: Thaynes Limestone

Discovery: 8/18/77, 1 Amoco-Chevron-Gulf W1 Unit, SW-SE-18-T17N-R119W
 Lithology: Carbonates and shales
 Age: Triassic
 Type of Trap: Structural; thrust-faulted anticline
 Drive Mechanism: Gas expansion
 Initial Pressure: BHP 3,685 psi (DST) with 5/8 ck
 Recent Pressure (4/79): BHP 3,713 psi (DST)
 Reservoir Temperature: 195°F
 Gross Thickness of Reservoir Rock: 1,100 ft
 Porosity: 3.7% average, range 0-8%; fracture porosity dominates matrix porosity
 Permeability: Unknown
 Oil/Gas Column: 75 ft gas
 Gas/Oil Ratio: 48,000:1
 Original Gas/Water Contact: Undetermined
 Gas Character: Low sulfur gas; 1,210 BTU/cu ft; gravity 0.76° API
 Gas Analysis:

Methane	79.50
Ethane	6.68
Propane	2.62
iso-Butane	1.06
n-Butane	0.64
iso-Pentane	0.44
n-Pentane	0.32
Hexanes	0.33
Heptanes +	1.80
Nitrogen	6.51
Carbon dioxide	0.10
Hydrogen sulfide	nil (150 ppm)

Water Salinity: 2,000 ppm NaCl (DST SW-SE-7-T17N-R119W)

Water Resistivity: 1.05 ohm meters at 195°F

Estimated Primary Recovery: Not determined

Type of Secondary Recovery: Not determined

Estimated Ultimate Recovery: Not determined

Reservoir Data: Phosphoria Formation

Discovery: 1977, 1 Amoco-Chevron-Gulf W1 Unit, SW-SE-18-T17N-R119W
 Lithology: Shales, limestones
 Age: Permian
 Type of Trap: Structural; thrust-faulted anticline
 Reservoir Temperature: 200°F
 Gross Thickness of Reservoir Rock: 800 ft

TABLE 3.4 Continued

Porosity: Not reported	
Permeability: Fairly tight	
Oil/Gas Column: Not reported	
Gas/Oil Ratio: 57,000:1	
Gas Character: Sour gas; 1,125 BTU/cu ft	
Gas Analysis: Methane	73.52%
Ethane	8.11
Propane	2.00
iso-Butane	0.80
n-Butane	0.80
iso-Pentane	0.18
n-Pentane	0.19
Hexanes	0.15
Heptanes +	0.15
Nitrogen	2.60
Carbon dioxide	4.80
Hydrogen sulfide	6.70
Estimated Primary Recovery: Not reported	
Type of Secondary Recovery: Not reported	
Estimated Ultimate Recovery: Believed to be substantial, but undetermined as of 1981	

Reservoir Data: Weber Sandstone

Discovery: 1978, 2 Amoco-Chevron-Gulf, NE-NE-SE-18-T17N-R119W	
Lithology: Sandstone	
Age: Pennsylvanian	
Type of Trap: Structural; thrust-faulted anticline	
Reservoir Temperature: 205°F	
Gross Thickness of Reservoir Rock: 750 ft	
Porosity: 4.6% average, range 2-12%; fracture porosity dominates matrix porosity	
Permeability: 0.02 to 150 millidarcies	
Oil/Gas Column: 180 ft gas	
Gas/Oil Ratio: 48,000:1	
Gas Character: Sour gas; 1,100 BTU/cu ft; gravity 1.09° API	
Gas Analysis: Methane	57.00
Ethane	5.82
Propane	2.02
iso-Butane	0.49
n-Butane	0.57
iso-Pentane	0.27
n-Pentane	0.20
Hexanes	0.22
Heptanes +	5.95
Nitrogen	1.01
Carbon dioxide	5.11
Hydrogen sulfide	21.34

Estimated Primary Recovery: Not reported
Type of Secondary Recovery: Not reported
Estimated Ultimate Recovery: Not reported

Reservoir Data: Mission Canyon Formation

Discovery: 1978, 2 Amoco-Chevron-Gulf, NE-NE-SE-18-T17N-R119W	
Lithology: Limy dolomites and limestones	
Age: Mississippian	
Type of Trap: Structural; thrust-faulted anticline	
Reservoir Temperature: 210°F	
Gross Thickness of Reservoir Rock: 1,500 ft	

TABLE 3.4 Continued

Porosity: 6.6% average; range 2-20%; both matrix and fracture porosity	
Permeability: 0.01-300 millidarcies; both matrix and fracture permeability	
Oil/Gas Column: 335 ft	
Gas/Oil Ratio: 51,000:1	
Gas Character: Sour gas; 1,150 BTU/cu ft; gravity 0.85° API	
Gas Analysis: Methane	67.16%
Ethane	6.30
Propane	1.87
iso-Butane	0.47
n-Butane	0.46
iso-Pentane	0.22
n-Pentane	0.17
Hexanes	0.25
Heptanes +	1.51
Nitrogen	0.60
Carbon dioxide	5.75
Hydrogen sulfide	15.24

Estimated Primary Recovery: Not reported**Type of Secondary Recovery:** Not reported**Estimated Ultimate Recovery:** Not reported**Reservoir Data: Lodgepole Limestone****Discovery:** 5/5/81, 1-6F Chevron-Federal, SW-SW-6-T18N-R119W**Lithology:** Dolomitic limestone, limy dolomite**Age:** Mississippian**Type of Trap:** Structural; thrust-faulted anticline**Reservoir Temperature:** 215°F (est.)**Gross Thickness of Reservoir Rock:** 500-750 ft**Porosity:** 5.3% average; range 2-12%**Permeability:** Not reported**Oil/Gas Column:** 113 ft**Gas/Oil Ratio:** Not reported**Gas Character:** Sour gas; gravity 0.85° API**Gas Analysis:** Hydrogen sulfide 15.5%**Estimated Primary Recovery:** Not reported**Type of Secondary Recovery:** Not reported**Estimated Ultimate Recovery:** Not reported**Reservoir Data: Darby Formation****Discovery:** 1979, 1 Champlin-457 Amoco-A, SW-SE-17-T17N-R119W**Lithology:** Carbonates, anhydrite, siltstone, shale; production from limy dolomite**Age:** Devonian**Type of Trap:** Structural; thrust-faulted anticline**Reservoir Temperature:** 215°F (est.)**Gross Thickness of Reservoir Rock:** 700-800 ft**Porosity:** 4.5% average; range 2-10%**Permeability:** 0.01-80 millidarcies; fracture permeability**Oil/Gas Column:** 21 ft**Gas/Oil Ratio:** Not reported**Gas Character:** Gravity 0.70° API**Gas Analysis:** Hydrogen sulfide 1.0%

(other figures, see data on Bighorn Dolomite)

Estimated Primary Recovery: Not reported**Type of Secondary Recovery:** Not reported**Estimated Ultimate Recovery:** Not reported

TABLE 3.4 Continued

Reservoir Data: Bighorn Dolomite**Discovery:** 12/29/78, 2 Amoco-Chevron-Gulf, NE-NE-SE-18-T17N-R119W**Lithology:** Limy dolomite**Age:** Ordovician**Type of Trap:** Structural; thrust-faulted anticline**Drive Mechanism:** Gas expansion**Initial Pressure:** BHP 6,300 psi (DST)**Recent Pressure (4/79):** BHP 6,300 psi (DST)**Reservoir Temperature:** 220°F**Gross Thickness of Reservoir Rock:** 600 ft**Porosity:** 0-7%, primarily fracture porosity, with some matrix porosity**Permeability:** None; fracture permeability**Oil/Gas Column:** 40 ft**Gas/Oil Ratio:** 55,000:1**Original Gas/Water Contact:** Variable**Gas Character¹:** Low sulfur gas, 1,135 BTU/cu ft

Gas Analysis¹:	Methane	84.86%
	Ethane	6.75
	Propane	2.02
	iso-Butane	0.48
	n-Butane	0.44
	iso-Pentane	0.27
	n-Pentane	0.23
	Hexanes	0.45
	Heptanes +	1.22
	Nitrogen	0.71
	Carbon dioxide	1.95
	Hydrogen sulfide	0.63

Water Salinity: 35,000 ppm NaCl (SW-SE-18-T17N-R119W)**Water Resistivity:** 0.12 ohm-meters at 220°F (SW-SE-18-T17N-R119W)**Estimated Primary Recovery:** Not determined**Type of Secondary Recovery:** Not determined**Estimated Ultimate Recovery:** Not determined¹Includes Darby production

daily production of some 1,200 long tons (1,220 metric tons) of sulfur makes the plant the second largest sulfur producer in the United States.

The Wainoco discovery well west of Ryckman Creek, which was spudded after completion of the electrical survey, produces from the Ankareh Formation. Few details are available on this new, unnamed field. Woodruff Narrows, located north of the western end of the electrical survey line, produces gas from the Bighorn.

Well-Casing Information

The discovery well at Ryckman Creek is set with 13-3/8-inch (34.0 cm) casing at 1,962 feet (598 m) with 250 sacks of cement. Production casing of 9-5/8-inch (24.5 cm) diameter is set at 8,422 feet (2,567 m) with 700 sacks of cement. It is assumed that most subsequent wells are cased in a similar way. The greater production depths at Whitney Canyon require a more complex arrangement. In typical Chevron wells, 20-inch (50.8 cm) surface casing is set at 80 feet (24 m). Production casing begins with 13-3/8-inch (34.0 cm) at 2,500 feet (760 m), then telescopes to 9-5/8-inch (24.5 cm) at 12,500 feet (3,800 m) and 7-inch (17.8 cm) at 16,500 feet (5,030 m).

The well-casing modeling for this chapter uses a casing diameter of 13-3/8 inches (34.0 cm) for both Ryckman Creek and Whitney Canyon.

3.3 DISCUSSION OF THE DATA

Introduction

A resistivity/phase crew of eight persons, headed by Zonge Engineering geophysicist Norman R. Carlson, was mobilized to the Ryckman Creek area October 27, 1979. Work progressed on schedule despite early snows, and data collection took only three days. Data were obtained on this phase of the survey for transmitter stations 0,1 to 8,9 (see Plate 3.1).

On July 30, 1980, data collection was resumed by extending the Ryckman Creek line across the Whitney Canyon gas field. Stations on the Ryckman Creek line were reoccupied, and the last transmitting dipole (8,9) was re-read in order to insure continuity in data collection. Data repeated well and the line was extended to transmitting dipole 29,30, just past the western edge of Whitney Canyon.

Data collection during this phase of the survey was significantly slower than during the Ryckman Creek phase due to frequent thunderstorm activity. Extremely long averages were necessary in order to assure research-quality data. In addition, strong cultural noise was present in the area due to the development of the Whitney Canyon gas processing plant and the area's pipelines and powerlines. These problems contributed to making the Whitney Canyon data four times as expensive per line mile as the Ryckman Creek data. The crew completed the survey August 24, 1980.

Topography on the survey was only moderate, and surface culture was fairly light. Numerous cased wells were in place at Ryckman Creek at the time of the survey, but Whitney Canyon was fairly undeveloped.

Data were obtained at the standard roll-along resistivity/phase frequencies: 0.125, 0.25, 0.5, and 1.0 Hz. The dipole spacing for these data was $a=1,700$ feet (518 m). Total surface coverage for the project is 11.9 line-miles (19.2 line-km); total subsurface coverage is 9.3 line-miles (15.0 line-km).

The apparent resistivity, apparent polarization, and REM data are presented in Plate 3.1 at the back of this Chapter. It may be unfolded for reference while reading the text.

Line Interpretation

A single east-west line traversed the Ryckman Creek and Whitney Canyon fields and a considerable amount of background. The field data are presented in Plate 3.1. The repeat diagonal (left-plunging 8,9 diagonal) shows data from the two field sessions; numbers on top are from the Ryckman Creek survey in 1979, and numbers on the bottom are from the Whitney Canyon survey in 1980. The "stretching out" of the data in the center part of Whitney Canyon is the result of a logistical move designed to avoid culture problems. A pipeline lies at station 23.0; in order to avoid placing an electrode near it, the crew chief elected to advance the electrodes one-half station such that transmitting dipole 22.5,23.5 was used instead of 22,23 and 23,24.

APPARENT RESISTIVITY DATA

The general trends in the apparent resistivity data correlate well with geologic trends in the Ryckman Creek/Whitney Canyon area, which are illustrated in the cross-sections of Figures 3.4, 3.5, and 3.6. Resistivity layering is high-over-low,

with high resistivities correlating quite well with upper Tertiary sediments of the Wasatch and Green River formations, and low resistivities correlating with lower Tertiary and upper Cretaceous sediments of the Evanston, Aspen, and Bear River formations. The very near surface layer is quite high in resistivity, possibly indicating lower water saturation in the surface sediments.

Superimposed upon the layering effects are three anomalously low resistivity areas. The eastern anomaly, centered on station 5.5, correlates with the Ryckman Creek production, although the anomaly extends both east and west well past the limits of the field. The second anomaly, centered between stations 23 and 27, correlates very well with the Whitney Canyon production. The third anomaly, the strongest of the three, lies on the extreme western end of the line. No hydrocarbon production has yet been established in that area.

In order to determine the cause of these anomalies, five possible sources are examined: well casings, surface culture, topography, subsurface structure, and electrochemical alteration due to the presence of hydrocarbons at depth.

Well-Casing Effects

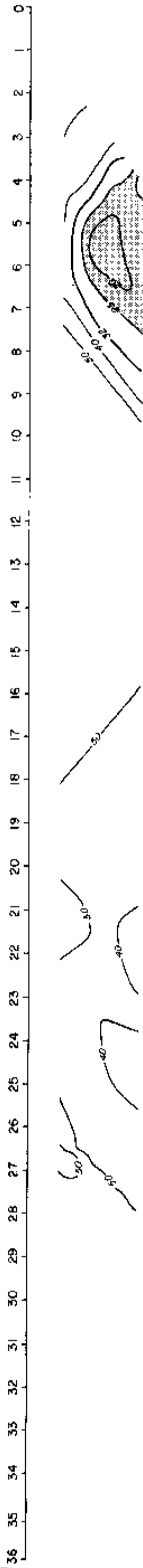
The effects of well casing on electrical survey data are extremely difficult to assess. The "PIPE" model of Holladay and West (1982) was developed to estimate the effects of well casings on IP data. Unfortunately, there are serious problems which limit the application of the model to field situations. These problems are discussed in some detail in Chapter 2 and in many of the case histories presented in this study, but briefly they involve ambiguities regarding assignment of surface impedances to the casings, the variability of casing responses, inability to specify multiple diameters for the casings, and an inability to take into account possible casing interconnection by collection pipeline networks. "Overmodeling" effects resulting from assumptions dictated by program limitations are presented in this and subsequent chapters.

Despite these difficulties, the "PIPE" model represents the first serious effort to deal with the effects of well casings, and it is useful as a starting point for discussing these effects in the Ryckman Creek/Whitney Canyon data. The map of Figure 3.7 shows wells in production, being drilled, and undrilled at the time of the electrical survey. At Ryckman Creek, seven producing wells fell within one a-spacing of the line, and two were being drilled. For the purposes of the model, all of these wells were treated identically, assuming that drill stem produces effects which are identical to those of production casing. At Whitney Canyon, only one cased well fell within one a-spacing of the line at the time of the survey. The deep hole at SE-NE-20-T17N-R119W was being drilled during the survey; mechanical problems forced its abandonment during completion of the west end of the line and the rig was moved 20 feet (6 m) or so, where it was drilled as a dry hole to a total depth of 16,434 feet (5,009 m). This well and the one at SW-NW-19-T17N-R119W were included in the model.

The well-casing model results for apparent resistivities are shown in Figure 3.10. A very strong effect has been calculated at Ryckman Creek; peak anomaly values reach two-thirds the background resistivity. The calculated residual (field data minus well-casing effects) shows no correlation with the field, but only a low resistivity, westward-dipping layer at depth. Evidence from other fields suggests that "PIPE" tends to "overmodel" field data, and there is some subtle evidence of overmodeling at Ryckman Creek. Note, for example, the depression of the 32 ohm-meter contour over the field, and the associated high resistivity, left-plunging 3,4 and right-plunging 7,8 diagonals. Unless one believes that anomalously *high* resistivities are actually present over the field at moderate depths, this is evidence of over-

Figure 3.10. Well casing model of apparent resistivity data for the Ryckman Creek/Whitney Canyon line. Model includes 22 wells at Ryckman Creek and 9 wells at Whitney Canyon. Model parameters: casing diameter = 13-3/8 inches (34.0 cm), casing resistivity = 2.0×10^{-7} ohm-meters, surface impedance = $0.5 + 0.5i$, background resistivity = 50 ohm-meters. Figure 3.7 shows well locations.

a. Well-Casing Model



b. Well-Casing Residual

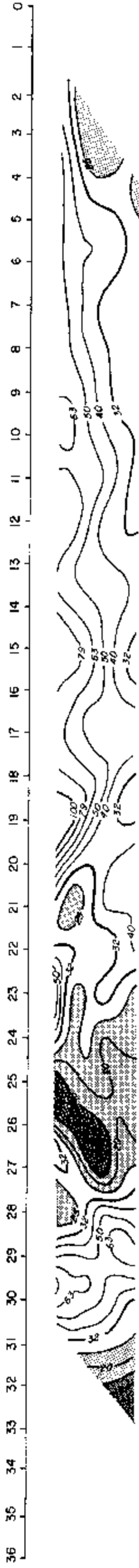


Figure 3.11. Topographic model of apparent resistivity data for the Ryckman Creek/Whitney Canyon line. Background resistivity = 50 ohm-meters. Plate 3.1 shows topography.

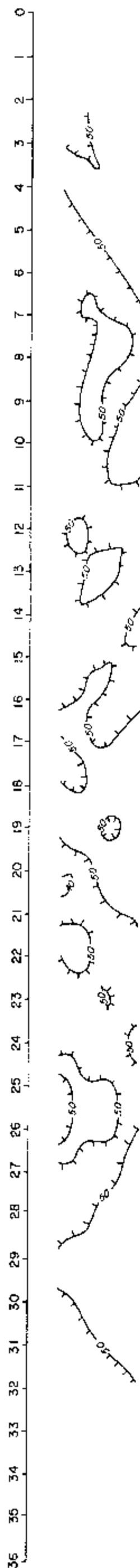
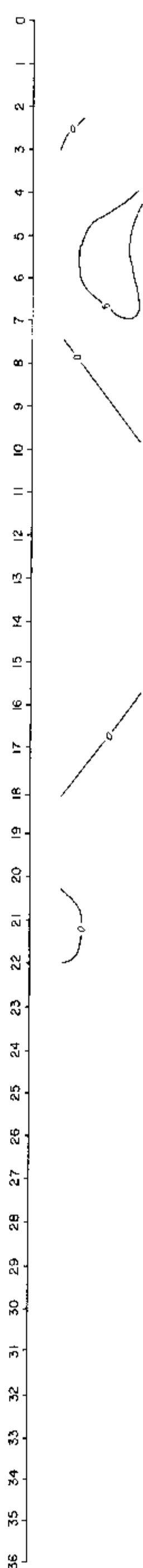


Figure 3.12. Well-casing model of apparent polarization data for the Ryckman Creek/Whitney Canyon line. Model parameters: same as in Figure 3.10. Figure 3.7 shows well locations.



modeling by "PIPE." Therefore, it is difficult to draw any quantitative conclusions regarding the effects of well casings at Ryckman Creek, based on the results of this modeling.

The situation over Whitney Canyon is different, if only because the field had not yet been fully developed when these data were collected. The calculated well-casing effect is broad and fairly subtle, on the order of 10 to 20 percent, and the residual bears a strong resemblance to the original field data. Since the model represents a worst-case approximation, it is safe to conclude that well casings have very little to do with the anomaly measured at Whitney Canyon.

The very strong anomaly on the west end of the line is unrelated to well-casing effects, since no producing wells were located there at the time of the survey.

Surface Culture Effects

Considering now the problem of surface culture, pipelines cross the line at stations 5.3, 6.2, 6.8, 17.8, and 23.0. These pipelines might be expected to behave similarly to those modeled in section 2.6. The pipeline at station 17.8 is connected to a pipeline which runs parallel to the survey line 0.5 spacing to the north. However, the data show no obvious effects from this feature. There are also no near-surface effects resulting from three pipelines which cross the line at Ryckman Creek. The data in the vicinity of the pipeline at station 23 are actually resistive—exactly opposite the sign which would be expected—so it is doubtful that it exerts any influence of a conductive nature upon the data. The only other surface culture on the line consists of two fences east of Ryckman Creek; these appear to have little or no influence on the data. Hence, we can conclude that surface culture probably does not cause any recognizable electrical effects on the line.

Topographic Effects

Topography on the Ryckman Creek/Whitney Canyon line is appreciable, as shown in Plate 3.1. In order to obtain an estimate of topographic changes on the apparent resistivity data, the topography was gridded with a very fine mesh and was modeled with the two-dimensional program "2DIP." The results are shown in Figure 3.11. As can be seen, topography can be expected to produce values of apparent resistivity which are slightly too high or low in isolated portions of the line. The changes are generally less than about 20 percent, however, and other effects in the data dominate topographic effects. Hence, the interpretation is not affected to any significant degree by topographic effects.

Subsurface Structure Effects

Subsurface structure appears to have a substantial influence on the data in portions of the pseudosection. As can be seen in the geologic cross-sections, a relatively undisturbed section of 2,000 to 4,000 feet (600-1,200 m) of Tertiary and upper Cretaceous sediments overlies some 10,000 to 15,000 feet (3,000-4,500 m) of overthrust Mesozoic and Paleozoic strata. Most of the features in the apparent resistivity pseudosection result from changes within the overburden. As noted earlier, these sediments contribute to high-over-low resistivity layering, with Tertiary units showing high resistivities and lower Tertiary to Cretaceous units showing low resistivities.

On the extreme east and west ends of the line, the Tertiary/Cretaceous overburden thins or disappears entirely due to thrust faulting. The thinning east of Ryckman Creek brings the low-resistivity Cretaceous sediments closer to the surface in that direction, resulting in a zone of low resistivities which extends eastward. This in no way explains the existence of the lateral, deep, conductive anomaly which

correlates with the lateral extent of the hydrocarbons, but it may help explain why the anomaly spreads out so far horizontally.

The influence of overthrust units underlying the Tertiary/Cretaceous overburden is minimal across most of the line (except, as noted, at the western and eastern ends of the line). This is because the zone of influence of apparent resistivity is about two a-spacings, or roughly 3,500 feet (1,100 m)—shallower than the top of the overthrust strata. An exception occurs near the Whitney Canyon Anticline (Figure 3.6), where the overthrust strata lie within 2,500 feet (750 m) of the surface. Here, there is a possibility that the data from the deeper n-spacings are partly influenced by overthrust structure. However, there is no likelihood that a significant portion of the broad conductive anomaly at Whitney Canyon is merely a structural effect.

Towards the far west end of the line, Cretaceous, Triassic, and Jurassic sediments are thrust all the way to the surface along the Medicine Butte Thrust Fault. The behavior of the apparent resistivities in this area strongly suggests that the shape and strength of the anomaly is at least partly due to the outcropping of these overthrust strata.

Alteration Effects

Having failed to explain away the Whitney Canyon and Ryckman Creek apparent resistivity anomalies as the result of well casings, surface culture, topography, and subsurface structure, we are left with the very likely possibility that these anomalies, which are so well correlated with the lateral extent of the hydrocarbons, are due to alteration effects in the sediments directly overlying the hydrocarbons. This conclusion is very uncertain for Ryckman Creek due to problems with the well-casing model, but is quite firm for Whitney Canyon, where only a few wells were cased at the time of the survey. A more detailed discussion of the alteration theory is given in the conclusions of this chapter.

APPARENT POLARIZATION (DECOUPLED PHASE ANGLE) DATA

When these data were originally obtained, a three-point quadratic extrapolation was applied to the raw phase data to separate polarization from electromagnetic coupling. The results showed a low-over-high polarization section due to undercorrection at depth, as described in section 1.8; this led to an appearance that anomalies extended to and became more pronounced at depth. The present set of data, which has been decoupled using proprietary techniques described in section 1.8, shows no pervasive, deep effects. Instead, isolated zones of moderate polarization are noted, the most interesting of which are due to features which are fairly shallow. This demonstrates the acute need for proper processing of this type of data.

The decoupled phase data of Plate 3.1 show two shallow zones of potential interest. At Ryckman Creek, a small bank of phase values which are twice the background value correlates well with the lateral extent of the hydrocarbons. The anomaly appears to be a near surface feature. A similar, but weaker anomaly is found at Whitney Canyon.

Well-Casing Effects

In order to gain some qualitative insight into the effects of well casings, a "PIPE" model was run, using a complex surface impedance which provided the best fit to the phase data, and including the effects calculated for both well casings and drill stem in wells being drilled at the time of the survey. The results of this model are shown in Figure 3.12. Note that the maximum anomaly at Ryckman Creek occurs at the n=3 plot point beneath station 5.5, and that the anomaly has a rounded, chevron-shaped appearance, with effects extending diagonally to depth. In

contrast, the field data show a maximum effect at $n=2$, and the shape of the field anomaly is more tabular and horizontal in appearance. A second model, including only casings in producing wells (i.e., including no drill stem) showed only a slightly better match with the data. A third model, including only drill stem effects (i.e., including no producing wells), showed a slightly poorer match to the data than the model of Figure 3.12. All three of these models suggest that well-casing effects, if they exist at all, tend to make the anomaly in the field data appear to be deeper than it really is. The conclusion, therefore, is that well casings do not cause the majority of the polarization at Ryckman Creek, although they may contribute to its overall strength at deeper n -spacings.

The second shallow polarization anomaly seen on the line is found over Whitney Canyon. It lies at about the same depth in the pseudosection as the anomaly at Ryckman Creek, but it has a more discontinuous shape due to the combination of thunderstorm-related noise and what may be localized changes in polarizability of the Tertiary and Cretaceous sediments. The well-casing model of Figure 3.12 shows a weak effect calculated for the drill stem in the hole being drilled south of station 19.2; note that the strength of the model anomaly and the trends (e.g., a left-plunging 18,19 diagonal) indicate that the drill stem probably does not cause much of a polarization anomaly, although a slight effect may be evident in the field data. A second model, calculated for well casings only (no drill stem), shows a barely detectable deep anomaly at the center of the producing field, while the field data show a contorted responsive zone near the surface (ignoring the $n=6$ data point beneath station 24, which appears to be noisy). Therefore, while well-casing effects may account for some of the isolated, deeper responses and for a portion of the shallower response beneath station 19, they do not account for the very shallow anomaly at Whitney Canyon. In fact, well-casing effects may explain why the anomaly is only moderately correlated with the lateral extent of the hydrocarbons. By subtracting calculated well-casing effects from the field data, one can see that the resulting high polarization areas would correlate even better with the hydrocarbons than do the anomalies in the field data.

Surface Culture Effects

Three pipelines cross the line over Ryckman Creek. Modeling suggests that the response of a pipeline would be strongest at $n=1$, expanding to depth in a very sharply-defined, chevron-shaped anomaly (see section 2.6). The anomalies would be predictably asymmetric, depending upon the position of the pipeline with respect to the electrode positions. The superposed effect would be strongest at the surface, but would show deeper, high-low, geometric diagonal effects. None of this character is evident in the data. Instead, the measured anomaly is strongest at $n=2$, not $n=1$, and it has a very horizontal, vertically-limited extent which is not indicative of geometric effects from surface features.

The pipeline which crosses the line at station 17.8 does not appear to produce an anomalous effect of any significant degree. Again, the strongest effect would be at the $n=1$ stations, where no recognizable effect is seen. The pipeline at station 23.0 may contribute somewhat to the diagonal effects which appear to emanate from that area, but the character of the data indicates that the pipeline's influence is of secondary importance.

The two fences east of Ryckman Creek do not appear to influence the field data at all.

Subsurface Structure Effects

The anomalies measured over Ryckman Creek and Whitney Canyon fields cannot be attributed to subsurface structure, since most structure lies well below the effective penetration of the apparent polarization data.

Alteration Effects

The fact that the shallow anomalies correspond in plan view to the lateral extent of the hydrocarbons implies, in the absence of other explanations, that there is alteration of some sort in the near-surface sediments, and that the alteration is causally linked to the presence of the hydrocarbons at depth. The polarization anomalies may be due to low-grade sulfide mineralization, changes in clay characteristics, or some unknown alteration effect due to vertical migration of hydrocarbons and/or waters from depth. More will be said of this in the conclusions of this chapter.

Other Polarizable Features

The zone of high polarization, found near the surface between stations 29 and 30, is very isolated and is therefore of little interest. It occurs near the surface expression of the Medicine Butte Thrust Fault; perhaps the overthrust sediments are slightly mineralized or altered at the surface. A second zone of high polarization is found at depth between stations 15 and 18. This feature is exceedingly difficult to explain by any theory other than that involving a localized facies change. It is believed that culture and structure have little to do with this feature.

One of the most interesting aspects of these data is the absence of high polarization in the conductive zone on the far west end of the line. If Ryckman Creek and Whitney Canyon can be used as examples of what a hydrocarbon anomaly should look like in this area, it is questionable that the conductive zone is due to hydrocarbons, since it lacks a polarization response. However, insufficient data have been obtained in this area to make such a judgement.

RESIDUAL ELECTROMAGNETIC (REM) DATA

The REM data show high-over-low resistivity layering, as do the apparent resistivity data. The somewhat contorted appearance of the high resistivity region (positive REM numbers) is primarily the result of the fact that numbers are quite small, and hence reflect minor subsurface and cultural effects. Superimposed on these effects are four anomalous areas: Ryckman Creek, west of Ryckman Creek, Whitney Canyon, and the west end of the line.

Ryckman Creek and Whitney Canyon Fields

The Ryckman Creek anomaly is highly conductive and appears to extend to considerable depth, much as observed in the apparent resistivity data. However, note that the REM anomaly is better bounded with respect to the location of the hydrocarbons. This is probably because REM quadrature data are less sensitive to resistivity layering, and the conductive Cretaceous sediments which broaden the resistivity anomaly are not being picked up as well by REM. This is a distinct advantage of REM quadrature data: they are more sensitive to lateral resistivity changes than they are to layering changes. We would still like to see a better cut-off at the edges of the anomaly, but at least the highest portion of the strongest portion of the anomaly corresponds to the producing field.

The Whitney Canyon REM anomaly is narrower than the resistivity anomaly, possibly because the REM data are affected by the lateral high resistivity change at the surface between stations 22 and 24. This tends to limit the eastern extension of the anomaly and to produce high resistivity diagonals (left-plunging 22,23, and right-plunging 23,24). It is interesting to note that the REM anomaly becomes significantly stronger at depth, and has a more consistent shape than the apparent resistivity anomaly.

Other Anomalous Features

The deep anomaly west of Ryckman Creek is unique to the REM data set. Hints of this feature are seen in the apparent resistivity and apparent polarization data, but only in the REM data is a definable anomaly seen. The reason for this is probably that REM data are penetrating below the zone of influence of the galvanic data, and hence are picking up a response from conductive material at depth. The anomaly appears to have two zones of maximum strength, beneath station 12 and beneath station 15. The zone beneath station 15 may be largely due to a localized high resistivity unit near the surface. An example of this is found in the discussion of section 2.8. The anomalous zone beneath station 12 may be similarly affected, but to a lesser degree. However, the region between stations 12 and 14 appears to be generally anomalous overall, and could possibly be associated with hydrocarbons.

The conductive anomaly on the far west end of the line is strongly correlated with the conductive anomaly found in the apparent resistivity data. The REM values are much more negative (conductive) than those observed anywhere else on the line. The most likely explanation for this feature involves the presence of highly conductive sediments which have been brought to the surface by thrusting along the Medicine Butte Thrust Fault. An alternative possibility is that the anomaly is connected with alteration due to hydrocarbons, but not enough data were gathered to comment further upon this possibility.

3.4 CONCLUSIONS

Ryckman Creek and Whitney Canyon

REVIEW OF THE DATA

The Ryckman Creek Field shows a strong conductive anomaly in the apparent resistivity and REM quadrature data. The anomaly extends from intermediate depths to below the pseudosection grid. Well-casing modeling was performed on the Ryckman Creek data, resulting in a residual, resistive anomaly which is interpreted as an "overmodeling" effect. This result, coupled with the inherent difficulties in applying the well-casing model, makes it impossible to determine quantitatively the extent of well-casing effects upon the data. However, the fact that well-casing effects calculated at Whitney Canyon do not even *qualitatively* model the anomaly measured there (i.e., the trends in the data and the trends in the modeled data are completely different), suggests by example that well casings may not play a major role in the anomaly at Ryckman Creek. Hence, there is a strong possibility that a conductive anomaly exists in the Ryckman Creek data which is independent of well-casing effects. This anomaly does not appear to be influenced significantly by surface culture or topography; subsurface structure tends to spread the anomaly out but cannot explain the lateral changes. Thus, there seems to be a columnar alteration zone which is relatively more conductive than the surrounding rocks. The REM data suggest that it extends to considerable depth.

The apparent polarization data at Ryckman Creek show a thin, flat-lying, polarizable zone lying less than 1,000 feet (300 m) deep. This anomaly cannot be reasonably explained by effects due to well-casings, surface culture, or subsurface structure. Instead, it appears to be due to alteration of near-surface sediments directly over the much deeper hydrocarbon trap.

The Whitney Canyon Field also shows strong apparent resistivity and REM anomalies which extend from very close to the surface to considerable depths. The apparent resistivity anomaly cannot be approximated either qualitatively (shape,

character, and location) or quantitatively (strength) by even a worst-case well-casing model. In fact, the data very strongly indicate that well casings, surface culture, topography, and subsurface structure have very little to do with the existence or shape of the conductive anomaly. Hence, it is difficult to avoid the conclusion that the anomaly is due to conductive alteration of the strata overlying the reservoir. The very good correlation of the anomaly with the lateral extent of the hydrocarbons suggests that the alteration is causally linked to the presence of the hydrocarbons at depth.

The apparent polarization anomaly at Whitney Canyon shows a very complex pattern, possibly due to a fair amount of thunderstorm-related noise. There is a slight suggestion of polarization responses over the field. These seem to be very near-surface features. Well-casing models suggest that effects due to well casings have little to do with the Whitney Canyon polarization anomaly, and in fact, the model data and the field data are quite different in general character. It is also extremely unlikely that the anomaly is influenced significantly by surface culture. Again, the conclusion is that the areas of higher polarization are due to alteration of near-surface sediments, although the overall effect is much less than that observed at Ryckman Creek.

POSSIBLE SOURCES OF THE ANOMALIES

Two distinctive effects are evident in the Ryckman Creek and Whitney Canyon data: a deep, conductive, relatively non-polarizable zone (the so-called "deep anomaly") lying just above the hydrocarbons, and a shallow, relatively non-conductive, polarizable zone (the "shallow anomaly") lying far above the hydrocarbons. Both are believed to be related to upward migration of material from the traps themselves, as described in section 2.4.

The deep conductive anomalies may be due to the upward leakage of saline water from the reservoirs, whose connate water resistivities are typically less than 1 ohm-meter. The active water drive at Ryckman Creek is an ideal candidate to transport the saline waters vertically out of the trap, as suggested by Roberts (1980), and the Whitney Canyon drive might be expected to behave in a similar manner. Energized by a strong hydraulic gradient due to the geometry of the traps and decreased hydrostatic pressures in the overlying sediments, the brine waters from the traps would rise vertically, making the overlying zones appear to be relatively conductive to an electrical survey. Eventually the decreased temperature and pressure would decrease the solubility of salts sufficiently that they would precipitate. This would determine the top of the conductive anomaly.

The conductive anomalies measured over the two fields are similar in magnitude, despite the enormous differences between them in terms of trap size and total reserves. Perhaps both anticlines are equally effective at expelling saline waters from the reservoirs. If the dissolved salt content of the reservoir waters of the two fields were roughly equal, and if the rate of expulsion were roughly equal, one might expect the two anomalies to be similar in magnitude, keeping in mind the difference in field size. The slightly stronger Ryckman Creek anomaly may reflect the fact that Nugget reservoir waters are apparently lower in total dissolved solids than the Whitney Canyon reservoir waters; alternatively, it may also reflect enhancement by well-casing and surface culture effects.

The fact that the Whitney Canyon anomaly extends all the way to the surface, and the Ryckman Creek anomaly does not, may be related to solubility considerations. Waters rising from traps at Whitney Canyon are hotter, in that they originate from greater depths. These higher temperature waters might be expected to

retain dissolved salts farther up the column of ascent than would cooler waters rising from Ryckman Creek. Other considerations may enter into this as well, and may even dominate the proposed temperature effect. A great deal of experimental work remains to be done regarding this subject.

The polarizable anomalies may be due to alteration of the near-surface sediments by vertically-migrating hydrocarbons of low molecular weight. The two most likely sources of alteration are pyrite precipitation and changes of the ion exchange characteristics of clays. Pyrite would be formed by the combination of free iron and hydrogen sulfide. Iron can usually be found to some degree in meteoric waters or in the matrix structure of sedimentary rocks, especially sandstones. Hydrogen sulfide can originate in the trap as a dissolved gas or it can be manufactured by reduction of hydrocarbons by anaerobic bacteria. The hydrogen sulfide content of the Nugget and Thaynes reservoirs at Ryckman Creek is extremely low; hence bacterial action is the more likely source of sulfur there. On the other hand, Whitney Canyon reservoirs are typically quite high in hydrogen sulfide, so either source is possible there. The Ryckman Creek polarization anomaly is significantly stronger than the Whitney Canyon anomaly, but it is difficult to understand why. Perhaps the shallower reservoirs at Ryckman Creek in some way contribute a greater supply of hydrocarbons available for reduction in the subsurface than do the deeper traps at Whitney Canyon. Also, the diffusion by horizontally flowing aquifer waters might tend to dissipate a tall column of ascending hydrocarbons more than a short column. The role of clays in this dynamic situation is not completely understood, but changes in cation-exchange capacity, absorption by clays of rising gases, etc., are subjects for future investigation.

A final note may be of interest here. There has been some discussion in the petroleum industry that hydrocarbons migration may be heavily influenced in its direction of motion by faults, and that electrical anomalies might therefore be displaced laterally from the location of the hydrocarbons. With its intermediate-angle thrust faulting, Ryckman Creek and Whitney Canyon provide a good test of this hypothesis. If any offset to the anomalies were to be observed, we would expect it to be towards the east of the hydrocarbons. Such an effect is not dominant in these data, suggesting that, in this case, upward migration of either light hydrocarbons or waters is not heavily influenced by the considerable thrust faulting present across the line.

Other Anomalies Observed on the Line

Two anomalies over non-producing areas are found on this line of data: one on the center of the line at depth, the one on the far west end of the line. Both are of possible interest in regard to hydrocarbons.

The anomaly towards the center of the line is best defined in the REM data as a conductive zone at great depth, although hints of it are seen in the apparent resistivity and apparent polarization data. Some high resistivity surface material probably tends to enhance the overall magnitude of this anomaly, especially towards the west. The electrical interpretation places the most inherently responsive zone between stations 11 and 15. Although no near-surface polarization anomaly occurs in conjunction with this feature, the variation between the polarization anomalies at Ryckman Creek and Whitney Canyon suggests that this may not be a critical consideration in terms of a hydrocarbon indicator. The anomaly is considered to be fairly well-defined overall.

Subsequent to completion of this survey line, Wainoco spudded in a discovery well some 2,500 feet (760 m) south of station 10.2. This well produces oil and gas from the Ankareh Formation at a depth of 12,418 to 12,602 feet (3,785 to

3,841 m). The well is too far away from the electrical line (1.5 a-spacings) to relate to the data. A second well was drilled by Chevron north of the survey line, but it was dry, with no shows; total depth was in the Ankareh at 12,800 feet (3,901 m). Since the line drawn between the two wells crosses a narrow resistive zone between the Ryckman Creek anomaly, and the deep, weaker anomaly west of Ryckman Creek, and since the second well is more than one a-spacing from the line, no conclusions can be drawn at this time regarding extension of the Wainoco production. However, the data suggest that drilling directly on the line would best be done in one of two spots: 1) on the deep anomaly between stations 11 and 15, ideally on station 13, and 2) on the western edge of the Ryckman Creek anomaly, which may be extended westward due to alteration from a second reservoir at depth. The second possibility is the less preferred of the two. The Ankareh production in the Wainoco well could be related to either possibility. Again, subsurface geology and seismic data should be used in conjunction with these electrical data to formulate the best exploration strategy. Several additional lines of data should ideally be obtained in order to define the planar extent of the anomaly.

A second area of interest lies on the extreme west end of the line. The extremely low resistivities (much lower than those observed over the two known fields), and the coincidence of this feature with the upthrown Mesozoic strata along the Medicine Butte Thrust do not tend to strongly favor it as a hydrocarbon target. However, the character of the anomaly cannot be ascertained since it lies on the extreme end of the line. The line would have to be extended about three miles (5 km) in order to evaluate this feature.

Some incentive for additional work in this area may be found in the 1981 discovery at Woodruff Narrows, 2.4 miles (3.0 km) north of the anomaly. This well flowed an initial 2.8 MMCFGPD from a Bighorn reservoir at 16,736 to 16,780 feet (5,101 to 5,115 m). Looking at the situation rather optimistically, a southward extension of Woodruff Narrows along the trend of overthrust fields would bring it across the west end of the survey line. The proper placement of several more electrical lines in the vicinity, and a combined interpretation of electrical, seismic, and subsurface geologic information should prove to be an optimum exploration strategy. Seismic and geologic data would establish the structural context for future drilling, and electrical data would establish the likelihood of hydrocarbons through the existence of overlying alteration patterns.

REFERENCES

- Blackstone, D.L., Jr., 1977, The Overthrust Belt salient of the Cordilleran Fold Belt, western Wyoming-southern Idaho-northeastern Utah, *in* Rocky Mountain Thrust Belt geology and resources: 29th annual field conference guidebook, Wyoming Geol. Assn., p. 367-384.
- Blackstone, D.L., Jr., and Ver Ploeg, A.J., 1981, Tectonic map of the Overthrust Belt, western Wyoming, southeastern Idaho and northeastern Utah: Geol. Survey of Wyoming.
- Clayton, W., 1848, Latter Day Saints emigrants' guide, p. 29.
- Dixon, J.S., 1982, Regional structural synthesis, Wyoming salient of western Overthrust Belt: AAPG Bull., v. 66, p. 1560-1580.
- (Editor), 1982, Seismics played big role in Ryckman Creek Field discovery: Oil & Gas Jour., Mar. 1, p. 46.
- Fernandez, M., and Andrews, J., 1979, Whitney Canyon, *in* Wyoming oil and gas fields symposium, Green River Basin, vol. 2: Wyoming Geol. Assn., p. 420-421.
- Hodgden, H.J., and McDonald, E., 1977, History of oil and gas exploration in the Overthrust Belt of Wyoming, Idaho and Utah, *in* Rocky Mountain Thrust Belt geology and resources: 29th annual field conference guidebook, Wyoming Geol. Assn., p. 37-69.

Plate 3.1
RESISTIVITY/PHASE PSEUDOSECTION DATA
Hickman Creek and Whitney Canyon Fields
Union Co., Wyoming

Line 1
a = 1,000 feet

Explanation of Symbols

Standard Well Symbols	Culture Symbols
① Driftless for which information is undeterminable	⬇ Metal pipeline, presumed grounded
② Drilling in progress at time of map preparation	⬇ Ungrounded pipeline, non-metal or suspended
③ Shut in	⬇ Metal fence
④ Abandoned	⬇ Electric fence
⑤ Dry hole with true casing indicated	⬇ Buried telephones or power cable
⑥ Oil well	T Telephone line or standard voltage power line
⑦ Gas well	⚡ Higher high voltage power line
⑧ Oil and gas well	⚡ Radio, microwave, or other communication station or tower
⑨ Gas injection well	⚡ U/G pump
⑩ Water injection well	
⑪ Water well	
⑫ Other Symbols	
⑬ (Drilling in progress at the time of the electrical survey; number indicates the amount of drill stem in the hole at the time of data collection)	U.S.G.S. standard symbols as indicated
⑭ Well spudded in after completion of the collection	
⑮ electrical survey	
⑯ Number indicates distance of well from the line in terms of a section; all wells within 100 feet are indicated (pseudosection only)	

ZONE ENGINEERING
& RESEARCH ORGANIZATION

West
3.5°
3A

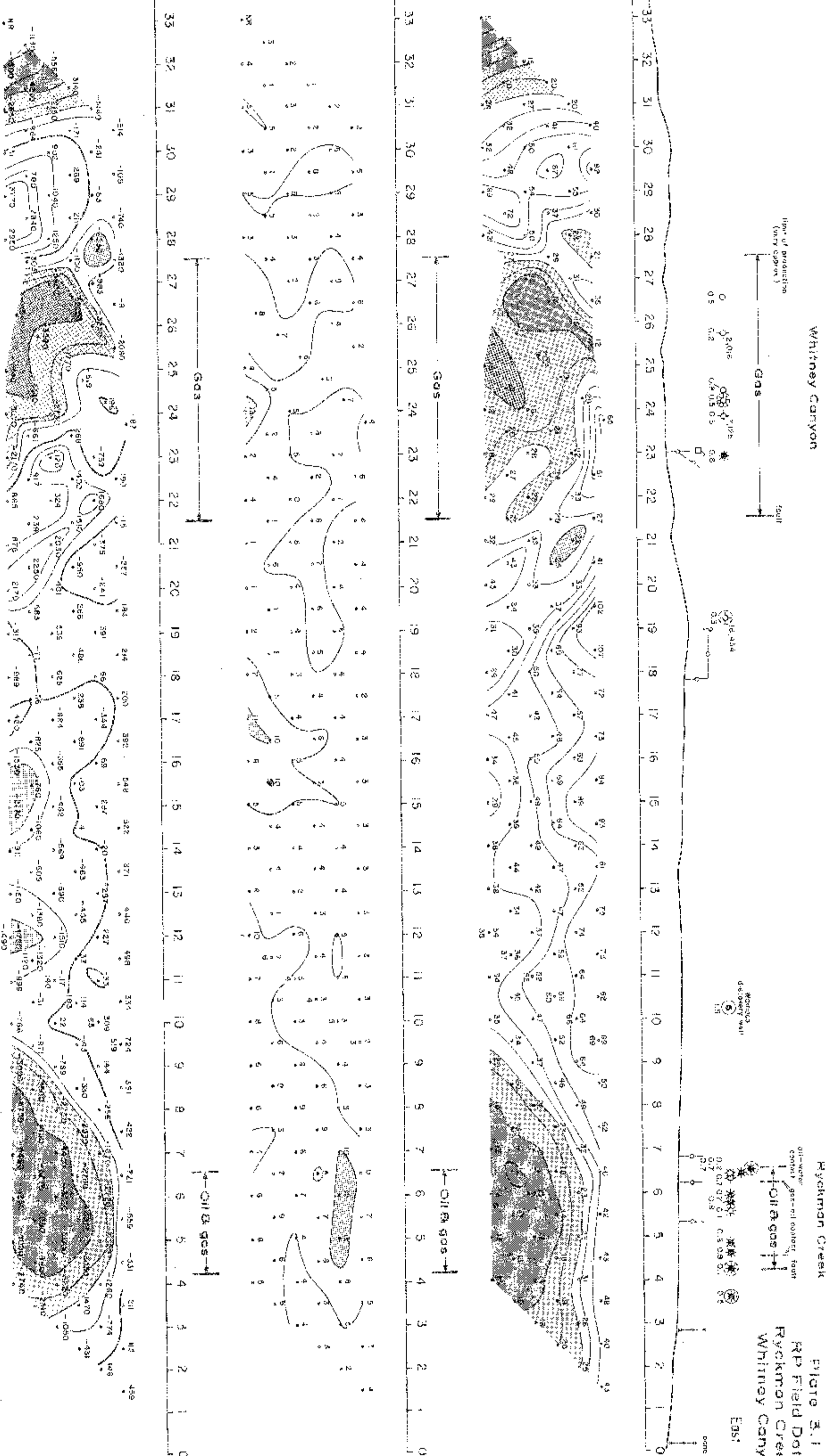
8000 ft. — Topographic profile, ft.
Apparent Resistivity
Units: ohm-meters
Frequency: 0.125 Hz
Logarithmic contour interval:



Decoupled Phase Angle
Units: milliradians
Frequency: 0.125 Hz
Linear contour interval:



REM Quadrature
Units: normalized imaginary
Frequency: 0.125 Hz
Logarithmic contour interval:



Chapter 4

Desert Springs, Playa-Lewis, and Desert Springs West Fields Sweetwater County, Wyoming

4.1 INTRODUCTION

The Desert Springs area fields are located about 30 miles (48 km) east of Rock Springs in the Wamsutter Arch area of south-central Wyoming (Figure 4.1). The fields are part of a large grouping of fields which produce gas from stratigraphic traps in Upper Cretaceous sandstones, located primarily in the Lewis Shale and the Almond Formation. As shown in Figure 4.2, the gas fields often connect with each other, so the distinction between Desert Springs Field and Patrick Draw, or between Playa-Lewis and Desert Springs West, is rather vague.

A single line was run in an east-west direction using 2,000-foot (610 m) dipoles. The line traversed the Desert Springs, Playa-Lewis, and Desert Springs West fields.

4.2 GEOLOGIC BACKGROUND

Exploration History of the Desert Springs Area

Although a few shallow holes were drilled north of the Wamsutter Arch during the early 1920s, exploration south of the arch was neglected until the 1940s due to the great depths to potentially productive sandstones and due to the lack of promising surface structures. The first productive well in the area was drilled into the crest of the Table Rock anticline in 1946. Gas was found at 3,300 feet (1,000 m) in the lower sandstone of the Hiawatha member of the Wasatch Formation, a Tertiary unit, but later drilling cast doubt upon the economic potential of Tertiary sands due to their discontinuous nature. Gravity and seismic methods were used extensively during the next decade, and while surface mapping was relatively unproductive, the combination of structural mapping and the search for production in deeper horizons known to be productive elsewhere led to a dramatic increase in leasing in the area. The result of these exploratory efforts was the 1954 Table Rock discovery well, which produced gas from sandstones in the Lewis Shale and the Almond Formation, both of Cretaceous age. This drilling, plus the success of a

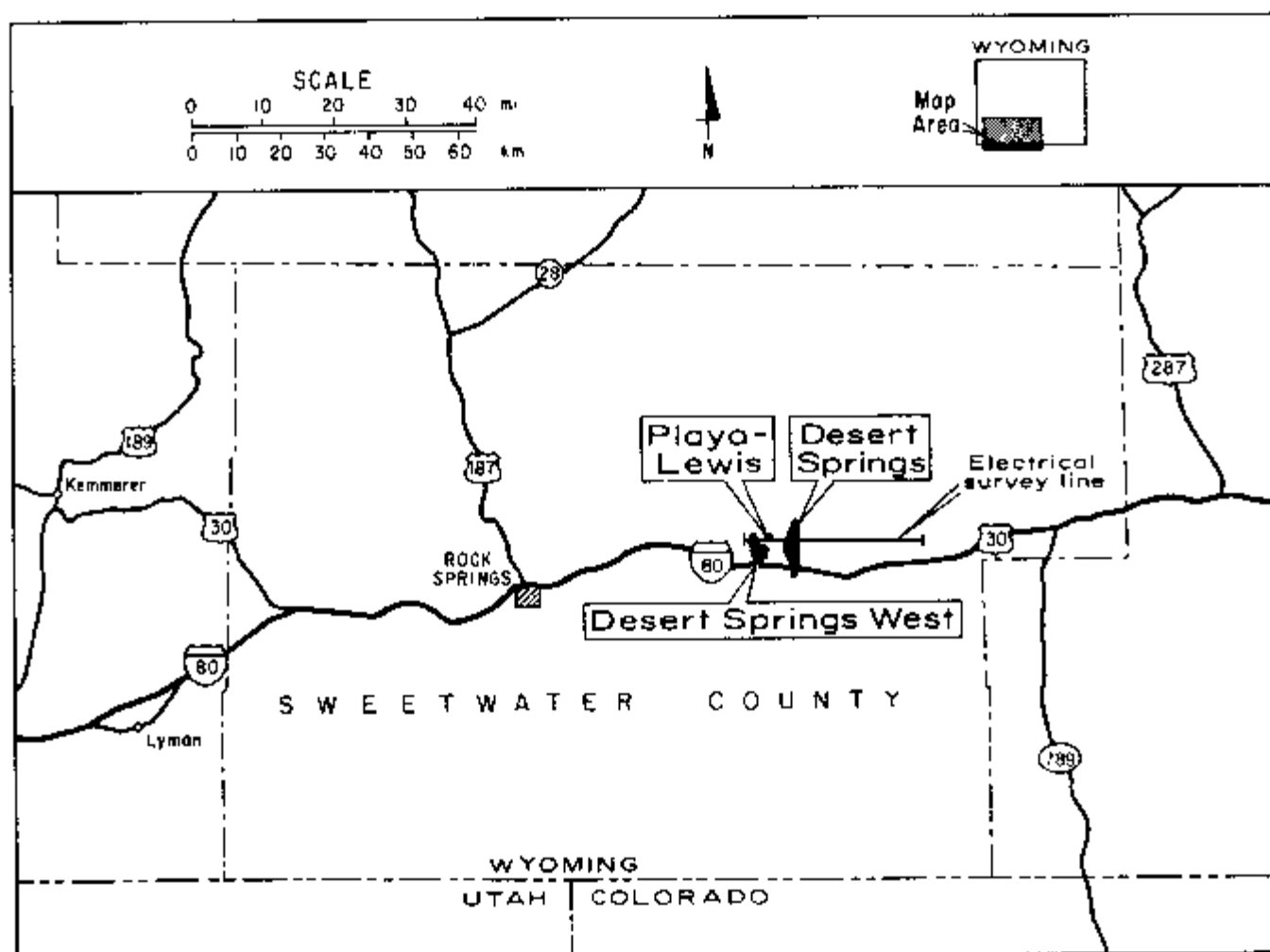


Figure 4.1. Location map of Desert Springs, Playa-Lewis, and Desert Springs West fields.

second well at Table Rock Southwest, constituted the first proof of stratigraphic reservoir potential in Cretaceous rocks in the Green River Basin.

In 1958, the El Paso Natural Gas Company drilled a well north of Table Rock based upon a seismic anomaly which was thought to represent a large, crescent-shaped fault closure. The seismic interpretation proved to be incorrect, but the well was fortuitously successful and produced gas from the Almond Formation from 5,887 to 5,954 feet (1,794-1,815 m). The new field, designated Desert Springs, was purely stratigraphic in nature. During 1959 and 1960, the Desert Springs production was rapidly extended southward (Arch Unit), and new discoveries were made at Patrick Draw, Playa-Lewis, and Beacon Ridge. Patrick Draw proved to be one of the most productive discoveries, and briefly ranked as the third most prolific producer in Wyoming. The discoveries of this period are summarized in Table 4.1, and are located on the map of Figure 4.2.

The future of gas production in the greater Green River Basin is fairly promising. McPeck (1981) estimates that more than 20 TCFG may be produced from a 3,000 square mile (7,800 sq km) geopressed zone of the eastern basin.

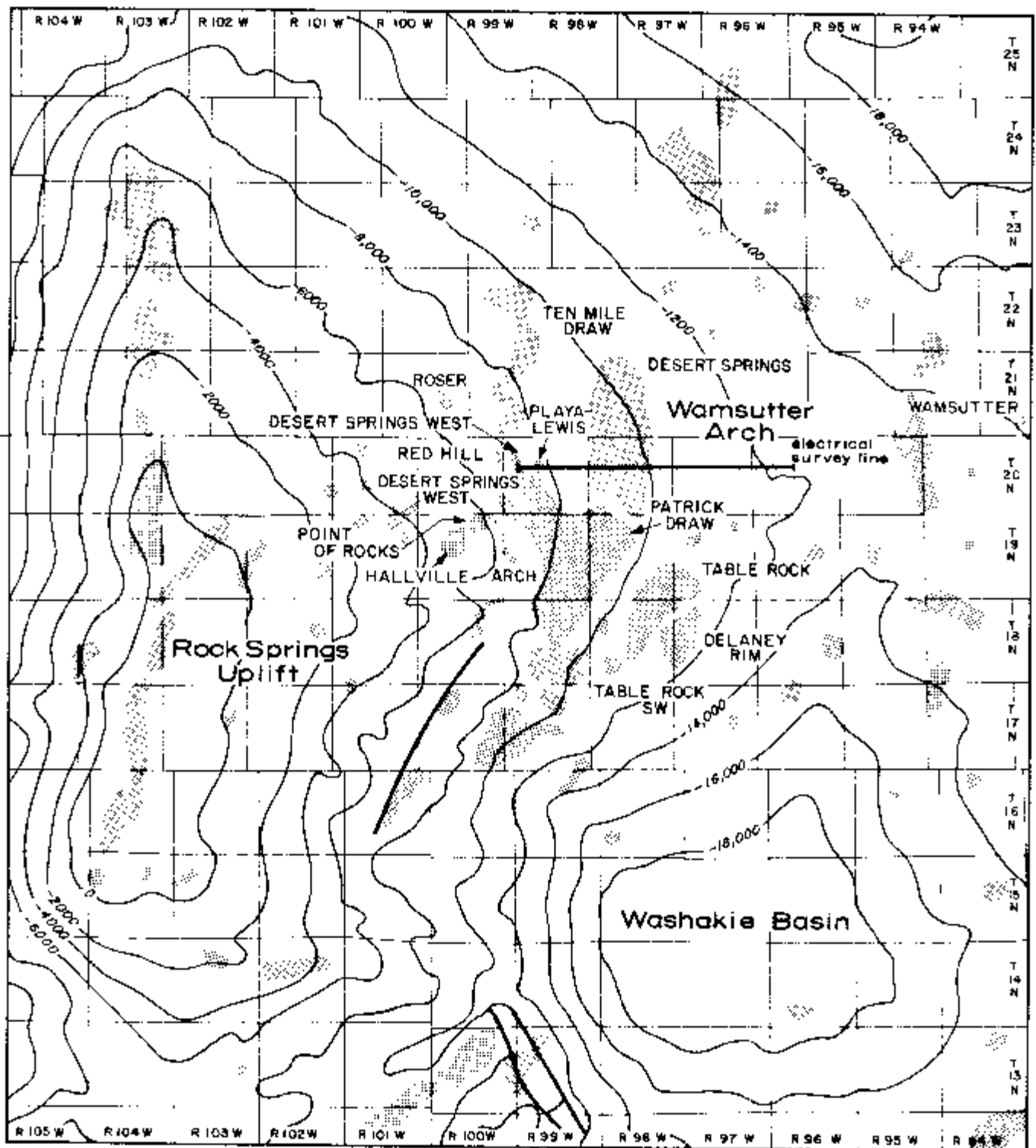


Figure 4.2. Map of oil and gas fields of the Wamsutter Arch area of southwestern Wyoming. Structure contours on top of the Phosphoria Formation. Contour interval: 2,000 feet (610 m). After Peppard-Soulders (1979).

TABLE 4.1
SOME OIL AND GAS FIELDS IN THE WAMSUTTER ARCH AREA

Field Name	Type of Trap	Productive Area (acres)	Producing Formation	Reserves	Discovery Date	Est. Ultimate Production	
						Gas (BCFG)	Oil (MMBO)
Delaney Rim	Strat	3,360	Lewis	Oil	8/30/75	1.3	3.57
			Almond	Gas	5/17/76	0.2	--
Desert Springs	Strat	28,800	Lewis "e"	Gas, oil	5/1/58	210	1.85
			Almond	Gas, oil	3/27/58	200	.65
Desert Springs West	Strat	3,880	Almond	Gas, oil	5/25/59	15	.74
Hallville	Struc-strat	80	Almond	Oil	12/20/62	--	.06
Patrick Draw	--	21,340	--	--	--	?	66.47
Arch Unit, west	Strat	8,010	Almond	Oil	4/18/59	--	23.43
Arch Unit, east	Strat	2,800	Almond	Gas	4/14/60	37	--
Monell Unit	Strat	8,530	Almond	Oil, gas	11/11/59	considerable	30.39
North Unit	Strat	2,000	Fox Hills	Gas	8/28/61	4.4	--
			Almond	Oil	5/22/61	2.6	3.65
Playa-Lewis	Strat	22,538	Almond	Gas	10/31/63	9	--
Point of Rocks	Strat	?	Blair	Gas	9/27/63	2.3	--
			Frontier	Gas	3/19/73	48	--
Robin	Strat	640	Almond (upper)	Oil, gas	4/16/72	0.3	.21
			Almond (lower)	Oil, gas	10/18/71	2	?
Roser	Strat	320	Almond	Gas	10/7/71	?	--
Table Rock, Table Rock SW	Struc-strat	15,000*	Wasatch	Gas	5/4/46	1	--
			Lewis	Oil, gas	3/9/54	50	.50
			Almond	Oil, gas	2/1/54	170	2.00
			Dakota	Gas	10/1/77	?	?
			Nugget	Gas	9/8/66	450	--
			Weber	Gas	11/18/76	75	--
			Madison	Gas	7/30/75	350	--
Ten Mile Draw	Strat	1,500	Lewis	Gas	6/27/72	6	--
			Almond	Gas	6/27/72	1.0	--
Wamsutter	Strat	12,160	Lewis	Gas	4/29/77	25	--
			Almond	Gas	8/13/58	118	0.4

Geologic History of the Desert Springs Area

The post-Jurassic geologic history of the Wamsutter Arch area of south-central Wyoming is dominated by major uplift and folding beginning in the late Cretaceous and by a succession of transgression-regression sequences of late Cretaceous seas. Since no wells have penetrated deeper than the upper-middle Cretaceous Ericson Sandstone in the area, little is known of the origins of the underlying rocks in the immediate vicinity. The stratigraphy common to the Wamsutter Arch fields is described in Table 4.2.

The Baxter Shale contains a sequence of silty shales and sandstones deposited on the floor of relatively shallow Cretaceous seas which crossed the North American continent in a relatively narrow north-south trough. Baxter deposition was accompanied by minor uplift in the area of southwestern Wyoming, resulting in a lenticular sandstone unit composed of reworked clastic sea sediments laid down in shallow waters. Subsequent fine-grained sandstones of the Blair Formation were deposited in connection with emergent sand islands and deltaic sands resulting from retreat of the Cretaceous seas.

**TABLE 4.2: STRATIGRAPHIC DESCRIPTION OF
DESERT SPRINGS, PLAYA-LEWIS, AND DESERT SPRINGS WEST FIELDS**

System	Symbol	Formation	Lithologic Description
GENOZOIC ROCKS			
Tertiary			
Eocene	Tw	Wasatch Fm.	Shales
	Twh	Hiawatha Mbr. (unconformity)	Claystones and fluvial sandstones
Paleocene	Tfu	Fort Union Fm.	Sandstones, siltstones, shales, and coal beds
MESOZOIC ROCKS			
(unconformity)			
Cretaceous	Kl	Lance Fm.	Sandstones, siltstones, shales, and coal beds
	Kfh	Fox Hills Ss.	Sandstones
	Kle	Lewis Sh.	Shallow marine and littoral shales and sandstones; sands form a major reservoir in Desert Springs area fields
	Kal	Mesa Verde Group	
		Almond Fm.	Shales, siltstones, and sandstones
		Zone I	No production, minor gas shows
		Zone II, "B ₁ sand"	Productive zone in Desert Springs area fields
		Zone III, "B ₂ sand"	Productive zone in Desert Springs area fields
		Zone IV (Lower Almond)	Shales, siltstones, and coal beds; no significant reservoir potential
	Ke	Ericson Fm.	Sandstones; numerous gas shows
	Kr	Rock Springs Fm.	Facies change from carbonaceous shales, sandstones and coal beds northwest of the field area to littoral and shallow marine sandstones and shales toward the southwest
	Kbl	Blair Fm.	Fine-grained sandstone lentils
	Kbs	Baxter Sh.	Silty shales with an intermediate sandstone and shale member (the "Airport Ss.")

The Rock Springs Formation consists of a sequence of non-marine to marine rocks deposited along the shoreline of the eastward-retreating late Cretaceous seas. The facies changes from sandstone/shale/coal-bed rocks in the northwest to fine-grained littoral, shallow marine sandstones and shales toward the southeast indicate that the seas deepened to the east. This depositional pattern was fairly stable until the uplift of the north-south trending Church Buttes Anticline. Uplifted material was eroded and carried away by braided streams in a large, fan-shaped delta which covered southern Wyoming, northwestern Colorado, and northeastern Utah. These deposits comprise the bulk of the Ericson Formation, which consists mostly of sandstones.

Deposition in a shallow embayment in the area of the future Rock Springs Uplift resulted in the Almond Formation, which consists of interbedded shales, siltstones, sandstones, and coal laid down in the low energy coastal plain, tidal flat, and swamp environments of the embayment. Littoral sands in the upper Almond constitute one of the two major reservoir rocks in the Desert Springs area.

After deposition of the Almond Formation, the seas began a final advance from the east, leaving the alternating sequences of shales, beach deposits, reworked Almond sands, and offshore bar sands which characterize the Lewis Shale. A single

sandstone reservoir in the Lewis Shale constitutes a second primary reservoir of the Wamsutter Arch area. As was the case with the Rock Springs deposition, deeper seas toward the east resulted in a facies change from western shoreline sands to eastern shales (see Figure 4.3 for an illustration of these environments).

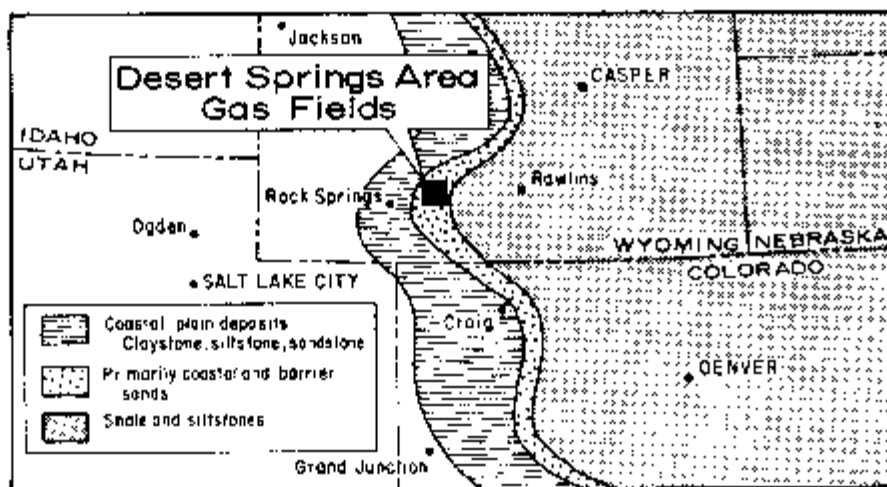


Figure 4.3. Map of the Cretaceous seas at the time of deposition of the Upper Almond Formation. The seaway formed a narrow corridor between the Gulf of Mexico and Canada. After Richers et al. (1982).

Beginning in the late Cretaceous, central Wyoming was subjected to extensive upwarping along a northeast trend extending from the Rock Springs uplift to northwestern Colorado. This trend was known as the Table Rock Platform or Anticline. The episode of uplift was followed by deposition of Lance (late Cretaceous) and Fort Union (Paleocene) sediments. These two units are virtually indistinguishable, and involve sandstones, siltstones, shales, and coal, all deposited in moist lowland environments. The gradual transition to higher, drier environments which resulted from continued sea regression and local uplift continued through the mid-Eocene. Sediments of this age include Hiawatha claystones and fluvial sandstones, which characterize flood plain and savanna environments.

During the early Eocene, the uplifting activity of the Table Rock Platform subsided, and structural activity shifted to the Overthrust Belt of western Wyoming and to the present-day locations of the Wind River Mountains and the Uinta Mountains. Sedimentation during this period of relative quiescence was characterized by the shallow lacustrine deposits of the Green River Formation. According to Ritzma (1963), sedimentation patterns were mostly unaffected by the Table Rock uplifting.

A resumption of structural activity began in the latter half of the Eocene and continued through the Oligocene. It was during this time that the Rock Springs Uplift and folding of the Wamsutter Arch occurred, possibly as a result of the emplacement of a batholith at depth. Folding was accompanied by a series of east-west normal faults extending along part of the fold axis. The Wamsutter Arch, which extends east-west from the Rock Springs Uplift past the Wamsutter gas field, plunges steeply toward the east. The structural relief is nearly 20,000 feet (6,000 m) from the deeper portions of the Washakie Basin to the projected crest of the Rock Springs Uplift. Rocks in the Table Rock Platform were tilted some five to eight

degrees toward the east and southeast, allowing previously emplaced hydrocarbons to escape into new stratigraphic traps. Ritzma (1963) notes that oil traps currently occupy a higher structural position on the Wamsutter Arch than do gas traps, and he concludes that the trapped hydrocarbons did not migrate significantly when the local dip of sediments was slowly reversed during the folding episode.

By the end of the Oligocene, the major portion of the structural uplift and folding had ended, although some minor activity may have continued through the Pliocene. Volcanic activity commenced during this time, resulting in lava and ash flows. The source of this material was located in the Leucite Hills to the northeast of the Rock Springs Uplift, and volcanism may have continued into the late Pleistocene.

Current Geology

The electrical line location with respect to the producing fields is shown in Figure 4.4. The structure of the top of the Almond Formation is shown in Figure 4.5. The eastward dip of the structure represents the east flank of the Rock Springs Uplift. The dip is about five degrees, as illustrated in the geologic cross-section A-A' of Figure 4.6. The fault running in an east-northeast direction near the Playa-Lewis and Desert Springs West fields is a tensional fault which is related to the Rock Springs Uplift. Richers et al. (1982) found high concentrations of light hydrocarbons in sub-parallel tensional faults towards the south.

Reservoir Characteristics

Desert Springs production occurs from the Almond Formation and the Lewis Shale, both of which are Upper Cretaceous in age. The reservoirs are stratigraphic and are located in sandstone units within the two formations. The producing zones from the two horizons are delineated in Figure 4.5; note that only Almond production occurs beneath the electrical survey line.

The Almond Formation is some 200 feet (60 m) thick at Desert Springs. The lower half consists primarily of carbonaceous shales, siltstones, and coal. The few sandstones in this section probably represent pinchouts of sand beneath a series of intraformational unconformities, an artifact of the erratic littoral depositional history of the Cretaceous seas. It is not surprising then, that this section of the Almond does not usually host hydrocarbons. The upper section consists of lagoonal and shallow marine facies, which include interbedded littoral marine sandstones that host most of the Almond gas. As shown in the stratigraphic description (Table 4.2), the Almond can be divided locally into Zones I, II, III, and IV, as done by May (1961). Most of the production is from the so-called "B₁ sand" of Zone II and the "B₂ sand" of Zone III. The two sand units are separated by a thin, impermeable shale layer which causes each to be associated with its own separate formation waters. Both sands pinch out on their updip sides by facies changes to impermeable lagoonal shale and siltstone sediments; they pinch out laterally (north and south) due to facies changes and structure. The gas production is limited downdip by the gas/water contact. The Almond drive involves pressure depletion.

The Lewis Shale in the vicinity of Desert Springs is approximately 1,500 feet (460 m) thick, and consists of marine shales and shallow marine sands. The so-called "e" sand, a north-south oriented off-shore bar sandstone, is the producing member of the Lewis Shale. The "e" sand has a maximum thickness of 38 feet (12 m). All production from the Lewis lies to the north of the survey line.

Other formations, such as the Wasatch, Fox Hills, and Ericson, have produced shows of gas in the Desert Springs area, but the discontinuous nature of their reservoir sands makes them uneconomical.

General Field Data

Discovery Well

Reservoir Data: Lewis Shale, "a" sandstone

El Paso Nat. Gas No. 7 Unit
C-SE-22-T2DN-R98W

Methane	88.94%
Ethane	5.85
Propane	1.96
Isobutane	0.29
Normal butane	0.32
Isopentane	0.16
Normal pentane	0.12
Hexanes +	0.33
Carbon dioxide	2.03
Hydrogen sulfide	0 (trace reported in some wells)

TABLE 4.3 Continued

Water Saturation: 50% of pore space	
Water Salinity: 70,000 ppm NaCl	
Water Resistivity: 0.11 ohm-meters at 68°F	
Daily Average Production (1980) ¹ : 35-40 MCFGPD	
Cumulative Production (1958-1978): 114,068 BCFG, 1,410,800 BO	
Estimated Primary Recovery: 210 BCFG, 1,850,000 BO	
Type of Secondary Recovery: None	
Estimated Ultimate Recovery: 210 BCFG, 1,850,000 BO	
Reservoir Data: Almond Formation, B-1 and B-2 sandstones	
Discovery: 3/27/58, El Paso Natural Gas 1 Unit, C SE-26-T21N-R98W	
Lithology: Sandstone	
Age: Cretaceous	
Type of Trap: Stratigraphic, facies pinchout of sands in a westerly updip direction	
Drive Mechanism: Pressure depletion	
Initial Pressure: 2,180 psi	
Recent Pressure (1980): 1,000 psi	
Reservoir Temperature: Unknown	
Gross Thickness of Reservoir Rock: B-1 sand, 18 ft; B-2 sand, 18 ft	
Porosity: 16% (cores)	
Permeability: 11.4 millidarcies average (cores), range 0.3 to 122 millidarcies	
Gas Column: B-1 sand, 1,174 ft; B-2 sand, 241 ft	
Gas/Oil Ratio: 166,000:1	
Gas/Water Contact: B-1 sand, 1680 ft; B-2 sand, +910 ft	
Gas Character: Condensate gravity 52.3° API	
Gas Analysis:	Methane 88.86%
	Ethane 5.14
	Propane 2.08
	Butane 1.0
	Other hydrocarbons 0.61
	Carbon dioxide 2.31
	Sulfur 0.03
Oil Character: Not reported	
Water Saturation: 45% of pore space	
Water Salinity: 8,000 to 10,000 ppm NaCl	
Water Resistivity: 0.6 to 0.78 ohm-meters at 68°F	
Cumulative Production (1958-1978): 98,529,195 MCFG, 583,148 BO	
Estimated Primary Recovery: 200 BCFG, 650,000 BO	
Type of Secondary Recovery: None	
Estimated Ultimate Recovery: 200 BCFG, 650,000 BO	

¹ Includes Almond productionTABLE 4.4: RESERVOIR CHARACTERISTICS OF
PLAYA LEWIS FIELD**General Field Data**

Region: Green River Basin
 Production: Gas
 Type of Trap: Stratigraphic
 Producing Formations and Depths: Lewis Sh., "c" sandstone, 3,500 ft
 Other Significant Shows: Almond Fm.
 Total Reserves: > 9 BCFG
 Productive Area: 2,000 acres
 Field Operator: Mesa Petroleum, Prenalta, K.D. Luff

TABLE 4.4 Continued

Number of Producing Wells (3/78): 7
 Number of Shut-in Wells (3/78): 0
 Number of Dry or Abandoned Wells (3/78): 3
 Well Casing Data: 5½ inch at 3,548 ft with 95 sx (discovery well); 10½ inch at 385 ft, 5½ inch at 3,898 ft (Almond well at SW-NE-NE-17-T20N-R99W)

Discovery Well

Name: Pubco Petroleum 15-22 Playa Unit
 Location: NW-NE 22-T20N-R99W
 Completion Date: 10/31/63
 Total Depth: 4,520 ft
 Perforations: 3,443-3,449 ft (Lewis "d" sand)
 Initial Potential: Flow 3,800 MCFGPD
 Treatment: None

Reservoir Data: Lewis Shale, "d" sandstone

Discovery: 10/31/63, Pubco Petroleum 15-22 Playa Unit, NW-NE-22-T20N-R99W
 Lithology: Sandstone
 Age: Cretaceous
 Type of Trap: Stratigraphic
 Drive Mechanism: Pressure depletion
 Initial Pressure: 1,459 psi (DST)
 Recent Pressure (1978): 675 psi
 Reservoir Temperature: 96-104° F
 Gross Thickness of Reservoir Rock: 9 ft average
 Porosity: 18 to 24% (logs)
 Permeability: Unknown
 Gas Column: 400 ft
 Gas/Oil Ratio: Dry gas
 Gas/Water Contact: Approx. +3,300 ft
 Gas Character: 1,121 BTU/cu ft dry gas at 60° F, 14.65 psi; 0.642 specific gravity; condensate gravity 59.6° API
 Water Salinity: 26,000 ppm NaCl
 Water Resistivity: 0.3 ohm-meters at 56° F
 Cumulative Production (1963-1977): 6,138,253 MCFG, 8,066 bbl condensate
 Estimated Primary Recovery: Not reported
 Type of Secondary Recovery: Not reported
 Estimated Ultimate Recovery: 9,000,000 MCFG

TABLE 4.5: RESERVOIR CHARACTERISTICS OF DESERT SPRINGS WEST FIELD

General Field Data

Region: Green River Basin
 Production: Gas, oil
 Type of Trap: Stratigraphic
 Producing Formations and Depths: Almond Fm., 3,800 ft
 Other Significant Shows: Lewis Sh.
 Total Reserves: Not reported
 Productive Area: 3,880 acres
 Field Operator: Texas National Petroleum, Kenneth Luff, Pubco, Union Pacific Railroad
 Number of Producing Wells (1/78): 39
 Number of Shut-in Wells (1/78): 1

TABLE 4.5 Continued

Number of Dry or Abandoned Wells: 21

Well Casing Data: 10½ inch at 385 ft with 250 sx cement, 5½ inch at 3,898 with 500 sx cement (discovery well)

Discovery Well

Name: Texas National Petroleum 1 UPRR

Location: NE-NE-17-T20N-R99W

Completion Date: 5/25/59

Total Depth: 7,589 ft

Perforations: 3,818-3,830 ft (Almond)

Initial Potential: Flow 9,200 MCFGPD

Treatment: SF with 500 gals MCA, 30,000 gals Petrogel, 60,000# sand

Reservoir Data: Almond Formation

Discovery: 5/25/59, Texas National Petroleum 1 UPRR, NE-NE-17-T20N-R99W

Lithology: Sandstone

Age: Cretaceous

Type of Trap: Stratigraphic

Drive Mechanism: Solution gas

Initial Pressure: 1,240 psi

Recent Pressure (1/78): Unknown

Reservoir Temperature: Unknown

Gross Thickness of Reservoir Rock: 10 ft

Porosity: 18%

Permeability: 10 millidarcies

Oil/Gas Column: Not determined for individual sandstone stringers

Gas/Oil Ratio: 500:1

Gas/Water Contact: +3,140 ft (north of fault contact; not determined south of fault contact)

Oil Character: Amber-green, gravity 43.0 to 45.5° API

Oil Analysis: Sulfur 0.03%

Water Salinity: 3,600 ppm

Water Resistivity: 1.65 ohm-meters at 88°F (DST)

Cumulative Production (5/59-1/78): 14,666,046 MCFG, 742,466 BO, 24,058 BW

Estimated Primary Recovery: Not reported

Type of Secondary Recovery: Not determined

Estimated Ultimate Recovery: Not determined

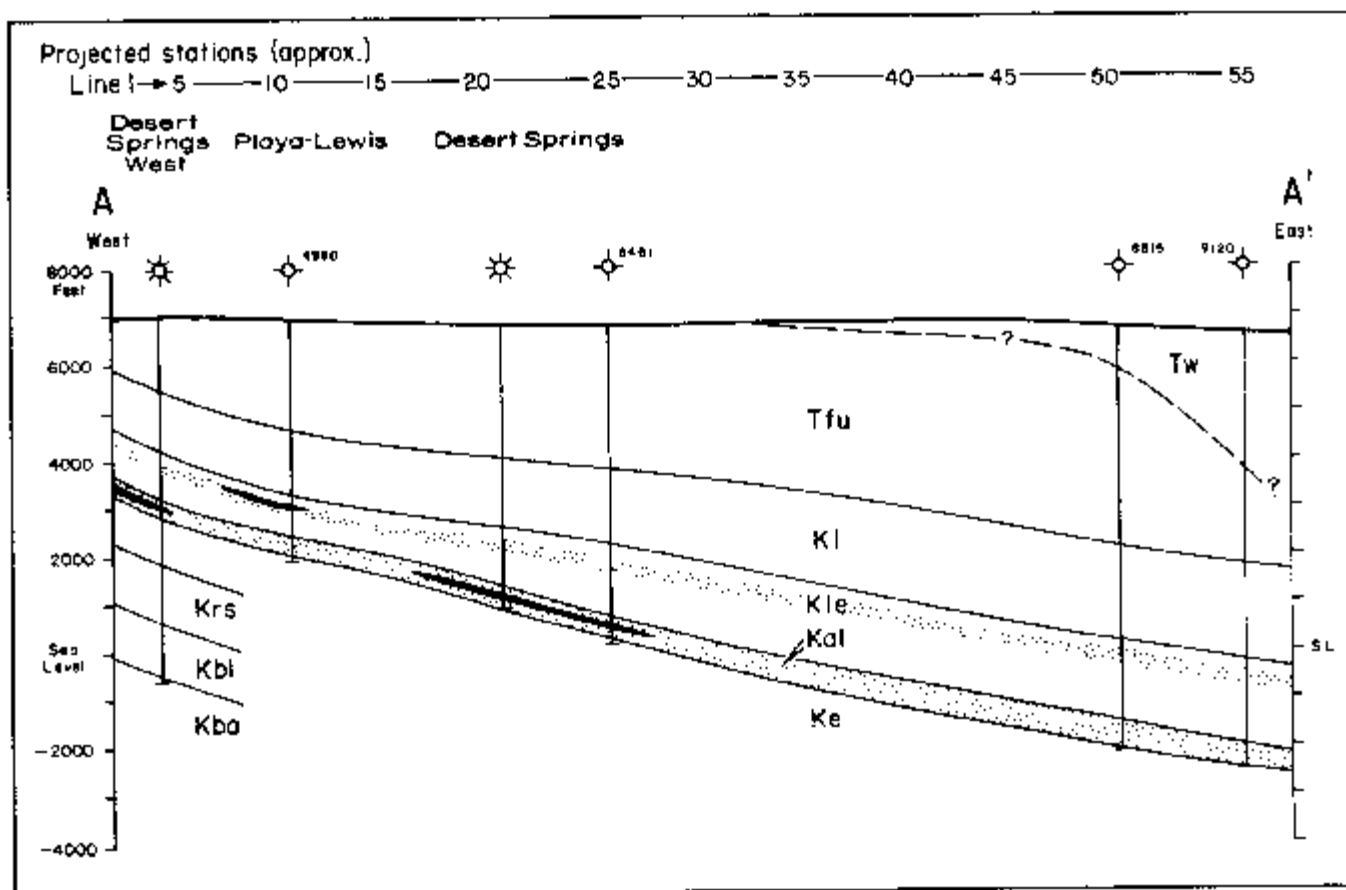


Figure 4.6. Geologic cross-section A-A' with 2:1 vertical scale exaggeration; this may be compared with the electrical data. Refer to Figure 4.4 for map location.

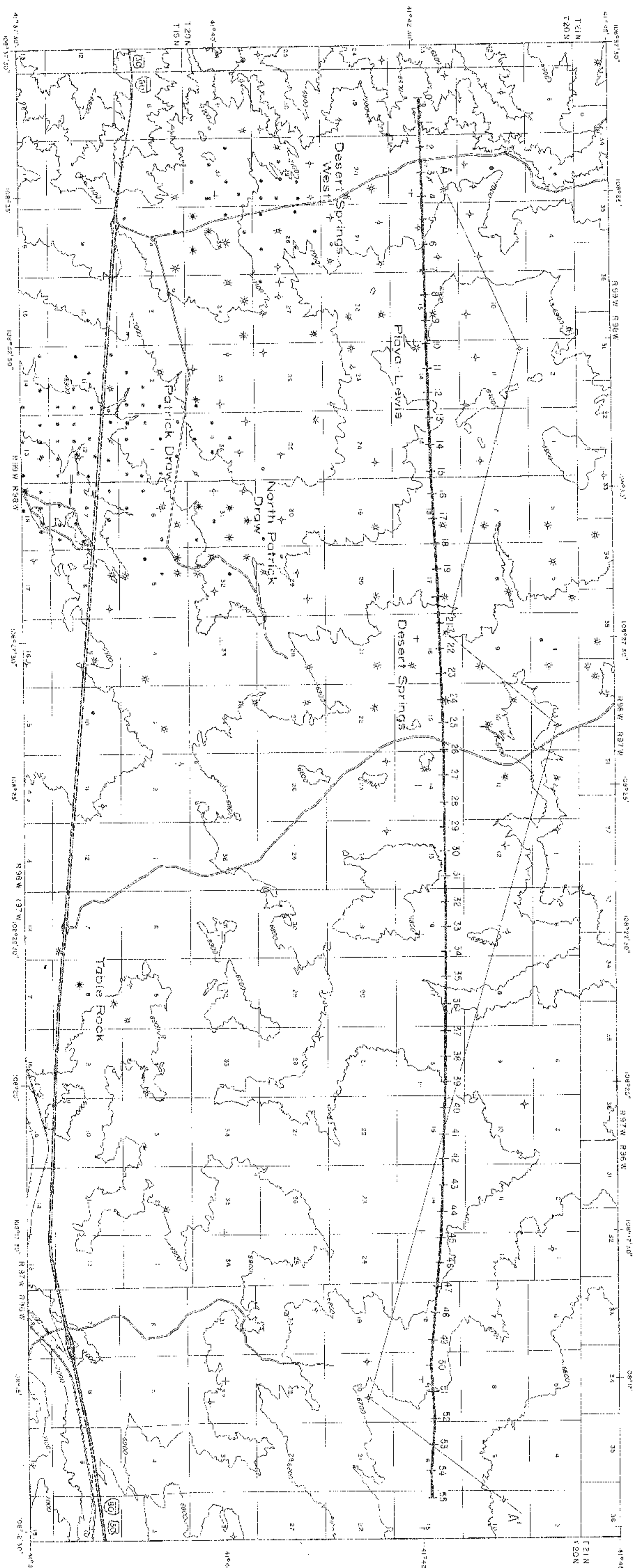
Playa-Lewis production is from Lewis "d" sands, whose plan view location is shown in Figure 4.4. The "d" sands are less than 10 feet (3 m) thick on the average. The driving mechanism is pressure depletion.

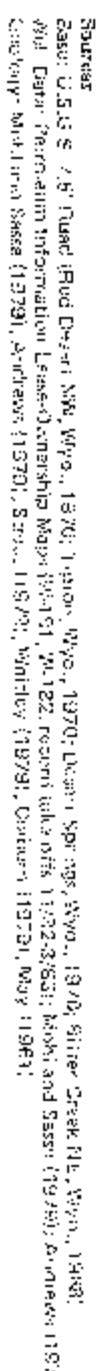
Desert Springs West produces gas and oil from the Almond Formation. The main productive unit lies south of the survey line; a narrow corridor of production extends north across the western end of the line. Production is from thin, discontinuous sands; the system has a solution gas drive.

An important consideration in evaluating the electrical data is that all three reservoirs over which the survey line is run are partially depleted in terms of pressure and gas reserves. As will be noted later, this appears to have a very significant impact upon the driving mechanism for electrochemical anomalies.

Well-Casing Information

Well casings in the Desert Springs, Playa-Lewis, and Desert Springs West fields are set with 10-3/8-inch (26.4 m) surface casing at about 400 feet (120 m), and 5-1/2-inch (14.0 cm) production casing at total depth. Well-casing models presented in this chapter use 5-1/2 inch diameter casings.



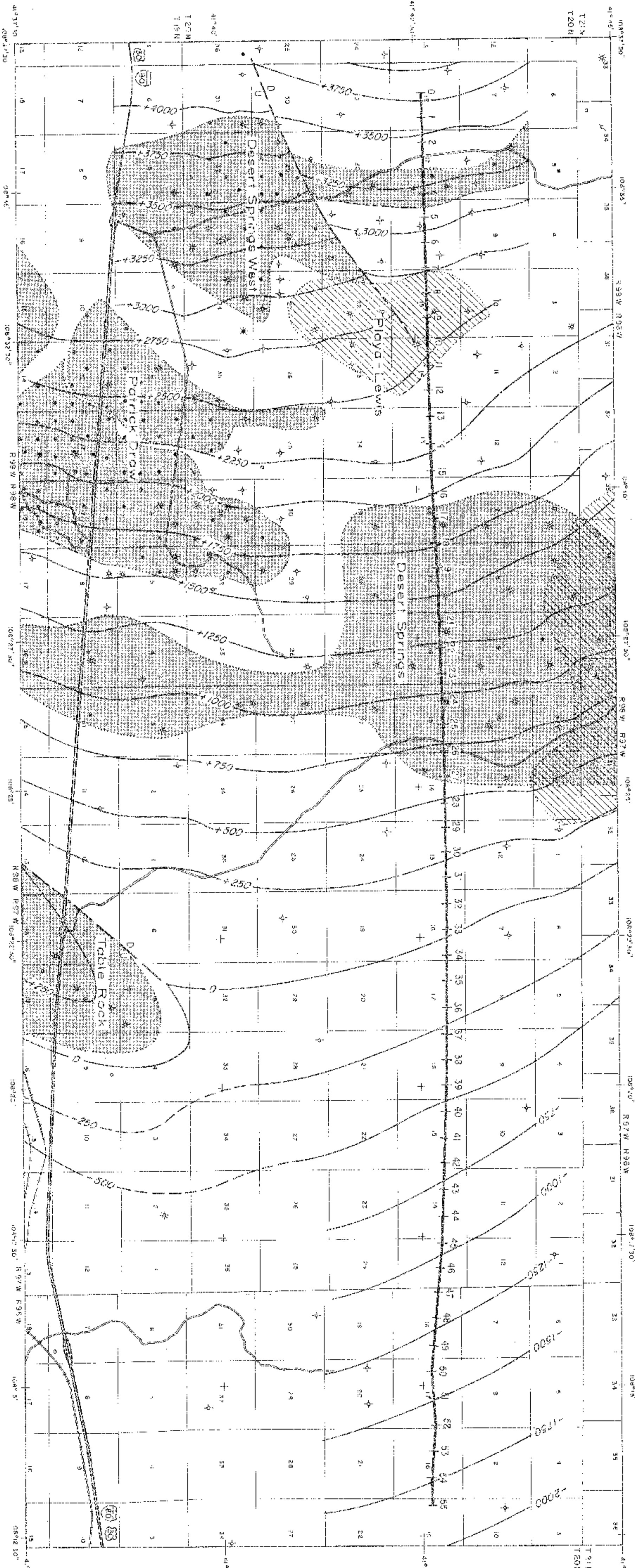


Standard Math Symbols Calculus Symbols

⑥	Drillhole for which information is unobtainable	↓	Metall pipeline, presumed grounded
⑦	Crilling in burjers at deep of met. penetration	↓	Ungrounded pipeline, common or suspect leak
⑧	Shut in	↓	Metall fence
⑨	Abandoned	↓	Elastic fence
⑩	Dry hole with total depth indicated	↓	Buried telephone or power cable
⑪	Oil well	↓	Telephone line or standard voltage power line
⑫	Gas well	↓	High-voltage power line
⑬	Oil and gas well	↓	Radio, microwave, or other communications station or tower
⑭	Gas injection well	↓	
⑮	Water injector well	↓	DC power
⑯	Water well	↓	

Symbol	Meaning
\mathbb{R}	Real numbers
\mathbb{C}	Complex numbers
\mathbb{Q}	Rational numbers
\mathbb{Z}	Integers
\mathbb{N}	Natural numbers
\mathbb{P}	Projective space
\mathbb{A}	Affine space
\mathbb{G}	Group
\mathbb{H}	Quaternion
\mathbb{O}	Octonion
\mathbb{S}	Sphere
\mathbb{B}	Ball
\mathbb{D}	Disc
\mathbb{E}	Euclidean space
\mathbb{F}	Field
\mathbb{K}	Field
\mathbb{L}	Lie algebra
\mathbb{M}	Manifold
\mathbb{N}	Natural numbers
\mathbb{O}	Octonion
\mathbb{P}	Projective space
\mathbb{Q}	Rational numbers
\mathbb{R}	Real numbers
\mathbb{S}	Sphere
\mathbb{T}	Torus
\mathbb{U}	Unitary group
\mathbb{V}	Vector space
\mathbb{W}	Weight space
\mathbb{X}	Space
\mathbb{Y}	Space
\mathbb{Z}	Integers
\mathbb{A}	Affine space
\mathbb{B}	Ball
\mathbb{C}	Complex numbers
\mathbb{D}	Disc
\mathbb{E}	Euclidean space
\mathbb{F}	Field
\mathbb{G}	Group
\mathbb{H}	Quaternion
\mathbb{I}	Interval
\mathbb{J}	Interval
\mathbb{K}	Field
\mathbb{L}	Lie algebra
\mathbb{M}	Manifold
\mathbb{N}	Natural numbers
\mathbb{O}	Octonion
\mathbb{P}	Projective space
\mathbb{Q}	Rational numbers
\mathbb{R}	Real numbers
\mathbb{S}	Sphere
\mathbb{T}	Torus
\mathbb{U}	Unitary group
\mathbb{V}	Vector space
\mathbb{W}	Weight space
\mathbb{X}	Space
\mathbb{Y}	Space
\mathbb{Z}	Integers
\mathbb{A}	Affine space
\mathbb{B}	Ball
\mathbb{C}	Complex numbers
\mathbb{D}	Disc
\mathbb{E}	Euclidean space
\mathbb{F}	Field
\mathbb{G}	Group
\mathbb{H}	Quaternion
\mathbb{I}	Interval
\mathbb{J}	Interval
\mathbb{K}	Field
\mathbb{L}	Lie algebra
\mathbb{M}	Manifold
\mathbb{N}	Natural numbers
\mathbb{O}	Octonion
\mathbb{P}	Projective space
\mathbb{Q}	Rational numbers
\mathbb{R}	Real numbers
\mathbb{S}	Sphere
\mathbb{T}	Torus
\mathbb{U}	Unitary group
\mathbb{V}	Vector space
\mathbb{W}	Weight space
\mathbb{X}	Space
\mathbb{Y}	Space
\mathbb{Z}	Integers
\mathbb{A}	Affine space
\mathbb{B}	Ball
\mathbb{C}	Complex numbers
\mathbb{D}	Disc
\mathbb{E}	Euclidean space
\mathbb{F}	Field
\mathbb{G}	Group
\mathbb{H}	Quaternion
\mathbb{I}	Interval
\mathbb{J}	Interval
\mathbb{K}	Field
\mathbb{L}	Lie algebra
\mathbb{M}	Manifold
\mathbb{N}	Natural numbers
\mathbb{O}	Octonion
\mathbb{P}	Projective space
\mathbb{Q}	Rational numbers
\mathbb{R}	Real numbers
\mathbb{S}	Sphere
\mathbb{T}	Torus
\mathbb{U}	Unitary group
\mathbb{V}	Vector space
\mathbb{W}	Weight space
\mathbb{X}	Space
\mathbb{Y}	Space
\mathbb{Z}	Integers
\mathbb{A}	Affine space
\mathbb{B}	Ball
\mathbb{C}	Complex numbers
\mathbb{D}	Disc
\mathbb{E}	Euclidean space
\mathbb{F}	Field
\mathbb{G}	Group
\mathbb{H}	Quaternion
\mathbb{I}	Interval
\mathbb{J}	Interval
\mathbb{K}	Field
\mathbb{L}	Lie algebra
\mathbb{M}	Manifold
\mathbb{N}	Natural numbers
\mathbb{O}	Octonion
\mathbb{P}	Projective space
\mathbb{Q}	Rational numbers
\mathbb{R}	Real numbers
\mathbb{S}	Sphere
\mathbb{T}	Torus
\mathbb{U}	Unitary group
\mathbb{V}	Vector space
\mathbb{W}	Weight space
\mathbb{X}	Space
\mathbb{Y}	Space
\mathbb{Z}	Integers
\mathbb{A}	Affine space
\mathbb{B}	Ball
\mathbb{C}	Complex numbers
\mathbb{D}	Disc
\mathbb{E}	Euclidean space
\mathbb{F}	Field
\mathbb{G}	Group
\mathbb{H}	Quaternion
\mathbb{I}	Interval
\mathbb{J}	Interval
\mathbb{K}	Field
\mathbb{L}	Lie algebra
\mathbb{M}	Manifold
\mathbb{N}	Natural numbers
\mathbb{O}	Octonion
\mathbb{P}	Projective space
\mathbb{Q}	Rational numbers
\mathbb{R}	Real numbers
\mathbb{S}	Sphere
\mathbb{T}	Torus
\mathbb{U}	Unitary group
\mathbb{V}	Vector space
\mathbb{W}	Weight space
\mathbb{X}	Space
\mathbb{Y}	Space
\mathbb{Z}	Integers
\mathbb{A}	Affine space
\mathbb{B}	Ball
\mathbb{C}	Complex numbers
\mathbb{D}	Disc
\mathbb{E}	Euclidean space
\mathbb{F}	Field
\mathbb{G}	Group
\mathbb{H}	Quaternion
\mathbb{I}	Interval
\mathbb{J}	Interval
\mathbb{K}	Field
\mathbb{L}	Lie algebra
\mathbb{M}	Manifold
\mathbb{N}	Natural numbers
\mathbb{O}	Octonion
\mathbb{P}	Projective space
\mathbb{Q}	Rational numbers
\mathbb{R}	Real numbers
\mathbb{S}	Sphere
\mathbb{T}	Torus
\mathbb{U}	Unitary group
\mathbb{V}	Vector space
\mathbb{W}	Weight space
\mathbb{X}	Space
\mathbb{Y}	Space
\mathbb{Z}	Integers
\mathbb{A}	Affine space
\mathbb{B}	Ball
\mathbb{C}	Complex numbers
\mathbb{D}	Disc
\mathbb{E}	Euclidean space
\mathbb{F}	Field
\mathbb{G}	Group
\mathbb{H}	Quaternion
\mathbb{I}	Interval
\mathbb{J}	Interval
\mathbb{K}	Field
\mathbb{L}	Lie algebra
\mathbb{M}	Manifold
\mathbb{N}	Natural numbers
\mathbb{O}	Octonion
\mathbb{P}	Projective space
\mathbb{Q}	Rational numbers
\mathbb{R}	Real numbers
\mathbb{S}	Sphere
\mathbb{T}	Torus
\mathbb{U}	Unitary group
\mathbb{V}	Vector space
\mathbb{W}	Weight space
\mathbb{X}	Space
\mathbb{Y}	Space
\mathbb{Z}	Integers
\mathbb{A}	Affine space
\mathbb{B}	Ball
\mathbb{C}	Complex numbers
\mathbb{D}	Disc
\mathbb{E}	Euclidean space
\mathbb{F}	Field
\mathbb{G}	Group
\mathbb{H}	Quaternion
\mathbb{I}	Interval
\mathbb{J}	Interval
\mathbb{K}	Field
\mathbb{L}	Lie algebra
\mathbb{M}	Manifold
\mathbb{N}	Natural numbers
\mathbb{O}	Octonion
\mathbb{P}	Projective space
\mathbb{Q}	Rational numbers
\mathbb{R}	Real numbers
\mathbb{S}	Sphere
\mathbb{T}	Torus
\mathbb{U}	Unitary group
\mathbb{V}	Vector space
\mathbb{W}	Weight space
\mathbb{X}	Space
\mathbb{Y}	Space
\mathbb{Z}	Integers
\mathbb{A}	Affine space
\mathbb{B}	Ball
\mathbb{C}	Complex numbers
\mathbb{D}	Disc
\mathbb{E}	Euclidean space
\mathbb{F}	Field
\mathbb{G}	Group
\mathbb{H}	Quaternion
\mathbb{I}	Interval
\mathbb{J}	Interval
\mathbb{K}	Field
\mathbb{L}	Lie algebra
\mathbb{M}	Manifold
\mathbb{N}	Natural numbers
\mathbb{O}	Octonion
\mathbb{P}	Projective space
\mathbb{Q}	Rational numbers
\mathbb{R}	Real numbers
\mathbb{S}	Sphere
\mathbb{T}	Torus
\mathbb{U}	Unitary group
\mathbb{V}	Vector space
\mathbb{W}	Weight space
\mathbb{X}	Space
\mathbb{Y}	Space
\mathbb{Z}	Integers
\mathbb{A}	Affine space
\mathbb{B}	Ball
\mathbb{C}	Complex numbers
\mathbb{D}	Disc
\mathbb{E}	Euclidean space
\mathbb{F}	Field
\mathbb{G}	Group
\mathbb{H}	Quaternion
\mathbb{I}	Interval
\mathbb{J}	Interval
\mathbb{K}	Field
\mathbb{L}	Lie algebra
\mathbb{M}	Manifold
\mathbb{N}	Natural numbers
\mathbb{O}	Octonion
\mathbb{P}	Projective space
\mathbb{Q}	Rational numbers
\mathbb{R}	Real numbers
\mathbb{S}	Sphere
\mathbb{T}	Torus
\mathbb{U}	Unitary group
\mathbb{V}	Vector space
\mathbb{W}	Weight space
\mathbb{X}	Space
\mathbb{Y}	Space
\mathbb{Z}	Integers
\mathbb{A}	Affine space
\mathbb{B}	Ball
\mathbb{C}	Complex numbers
\mathbb{D}	Disc
\mathbb{E}	Euclidean space
\mathbb{F}	Field
\mathbb{G}	Group
\mathbb{H}	Quaternion
\mathbb{I}	Interval
\mathbb{J}	Interval
\mathbb{K}	Field
\mathbb{L}	Lie algebra
\mathbb{M}	Manifold
\mathbb{N}	Natural numbers
\mathbb{O}	Octonion
\mathbb{P}	Projective space
\mathbb{Q}	Rational numbers
\mathbb{R}	Real numbers
\mathbb{S}	Sphere
\mathbb{T}	Torus
\mathbb{U}	Unitary group
\mathbb{V}	Vector space
\mathbb{W}	Weight space
\mathbb{X}	Space
\mathbb{Y}	Space
\mathbb{Z}	Integers
\mathbb{A}	Affine space
\mathbb{B}	Ball
\mathbb{C}	Complex numbers
\mathbb{D}	Disc
\mathbb{E}	Euclidean space
\mathbb{F}	Field
\mathbb{G}	Group
\mathbb{H}	Quaternion
\mathbb{I}	Interval
\mathbb{J}	Interval
\mathbb{K}	Field
\mathbb{L}	Lie algebra
\mathbb{M}	Manifold
\mathbb{N}	Natural numbers
\mathbb{O}	Octonion
\mathbb{P}	Projective space
\mathbb{Q}	Rational numbers
\mathbb{R}	Real numbers
\mathbb{S}	Sphere
\mathbb{T}	Torus
\mathbb{U}	Unitary group
\mathbb{V}	Vector space
\mathbb{W}	Weight space
\mathbb{X}	Space
\mathbb{Y}	Space
\mathbb{Z}	Integers
\mathbb{A}	Affine space
\mathbb{B}	Ball
\mathbb{C}	Complex numbers
\mathbb{D}	Disc
\mathbb{E}	Euclidean space
\mathbb{F}	Field
\mathbb{G}	Group
\mathbb{H}	Quaternion
\mathbb{I}	Interval
\mathbb{J}	Interval
\mathbb{K}	Field
\mathbb{L}	Lie algebra
\mathbb{M}	Manifold
\mathbb{N}	Natural numbers
\mathbb{O}	Octonion
\mathbb{P}	Projective space
\mathbb{Q}	Rational numbers
\mathbb{R}	Real numbers
\mathbb{S}	Sphere
\mathbb{T}	Torus
\mathbb{U}	Unitary group
\mathbb{V}	Vector space
\mathbb{W}	Weight space
\mathbb{X}	Space
\mathbb{Y}	Space
\mathbb{Z}	Integers
\mathbb{A}	Affine space
\mathbb{B}	Ball
\mathbb{C}	Complex numbers
\mathbb{D}	Disc
\mathbb{E}	Euclidean space
\mathbb{F}	Field
\mathbb{G}	Group
\mathbb{H}	Quaternion
\mathbb{I}	Interval
\mathbb{J}	Interval
\mathbb{K}	Field
\mathbb{L}	Lie algebra
\mathbb{M}	Manifold
\mathbb{N}	Natural numbers
\mathbb{O}	Octonion
\mathbb{P}	Projective space
\mathbb{Q}	Rational numbers
\mathbb{R}	Real numbers
\mathbb{S}	Sphere
\mathbb{T}	Torus
\mathbb{U}	Unitary group
\mathbb{V}	Vector space
\mathbb{W}	Weight space
\mathbb{X}	Space
\mathbb{Y}	Space
\mathbb{Z}	Integers
\mathbb{A}	Affine space
\mathbb{B}	Ball
\mathbb{C}	Complex numbers
\mathbb{D}	Disc
\mathbb{E}	Euclidean space
\mathbb{F}	Field
\mathbb{G}	Group
\mathbb{H}	Quaternion
\mathbb{I}	Interval
\mathbb{J}	Interval
\mathbb{K}	Field
\mathbb{L}	Lie algebra
\mathbb{M}	Manifold
\mathbb{N}	Natural numbers
\mathbb{O}	Octonion
\mathbb{P}	Projective space
\mathbb{Q}	Rational numbers
\mathbb{R}	Real numbers
\mathbb{S}	Sphere
\mathbb{T}	Torus
\mathbb{U}	Unitary group
\mathbb{V}	Vector space
\mathbb{W}	Weight space
\mathbb{X}	Space
\mathbb{Y}	Space
\mathbb{Z}	Integers
\mathbb{A}	Affine space
\mathbb{B}	Ball
\mathbb{C}	Complex numbers
\mathbb{D}	Disc
\mathbb{E}	Euclidean space
\mathbb{F}	Field
\mathbb{G}	Group
\mathbb{H}	Quaternion
\mathbb{I}	Interval
\mathbb{J}	Interval
\mathbb{K}	Field
\mathbb{L}	Lie algebra
\mathbb{M}	Manifold
\mathbb{N}	Natural numbers
\mathbb{O}	Octonion
\mathbb{P}	Projective space
\mathbb{Q}	Rational numbers
\mathbb{R}	Real numbers
\mathbb{S}	Sphere
\mathbb{T}	Torus
\mathbb{U}	Unitary group
\mathbb{V}	Vector space
\mathbb{W}	Weight space
\mathbb{X}	Space
\mathbb{Y}	Space
\mathbb{Z}	Integers
\mathbb{A}	Affine space
\mathbb{B}	Ball
\mathbb{C}	Complex numbers
\mathbb{D}	Disc
\mathbb{E}	Euclidean space
\mathbb{F}	Field
\mathbb{G}	Group
\mathbb{H}	Quaternion
\mathbb{I}	Interval
\mathbb{J}	Interval
\mathbb{K}	Field
\mathbb{L}	Lie algebra
\mathbb{M}	Manifold
\mathbb{N}	Natural numbers
\mathbb{O}	Octonion
\mathbb{P}	Projective space
\mathbb{Q}	Rational numbers
\mathbb{R}	Real numbers
\mathbb{S}	Sphere
\mathbb{T}	Torus
\mathbb{U}	Unitary group
\mathbb{V}	Vector space
\mathbb{W}	Weight space
\mathbb{X}	Space
\mathbb{Y}	Space
\mathbb{Z}	Integers
\mathbb{A}	Affine space
\mathbb{B}	Ball
\mathbb{C}	Complex numbers
\mathbb{D}	Disc
\mathbb{E}	Euclidean space
\mathbb{F}	Field
\mathbb{G}	Group
\mathbb{H}	Quaternion
\mathbb{I}	Interval
\mathbb{J}	Interval
\mathbb{K}	Field
\mathbb{L}	Lie algebra
\mathbb{M}	Manifold
\mathbb{N}	Natural numbers
\mathbb{O}	Octonion
\mathbb{P}	Projective space
\mathbb{Q}	Rational numbers
\mathbb{R}	Real numbers
\mathbb{S}	Sphere
\mathbb{T}	Torus
\mathbb{U}	Unitary group
\mathbb{V}	Vector space
\mathbb{W}	Weight space
\mathbb{X}	Space
\mathbb{Y}	Space
\mathbb{Z}	Integers
\mathbb{A}	Affine space
\mathbb{B}	Ball
\mathbb{C}	Complex numbers
\mathbb{D}	Disc
\mathbb{E}	Euclidean space
\mathbb{F}	Field
\mathbb{G}	Group
\mathbb{H}	Quaternion
\mathbb{I}	Interval
\mathbb{J}	Interval
\mathbb{K}	Field
\mathbb{L}	Lie algebra
\mathbb{M}	Manifold
\mathbb{N}	Natural numbers
\mathbb{O}	Octonion
\mathbb{P}	Projective space
\mathbb{Q}	Rational numbers
\mathbb{R}	Real numbers
\mathbb{S}	Sphere
\mathbb{T}	Torus
\mathbb{U}	Unitary group
\mathbb{V}	Vector space
\mathbb{W}	

● **Effect size:** Effect size is defined as a ratio computed by dividing the difference between the means of the two groups by the standard deviation of the dependent variable. Effect size is a measure of the magnitude of the effect of the independent variable on the dependent variable. Effect size is a ratio computed by dividing the difference between the means of the two groups by the standard deviation of the dependent variable. Effect size is a measure of the magnitude of the effect of the independent variable on the dependent variable.



4.3 DISCUSSION OF THE DATA

Introduction

A resistivity/phase crew of eight persons, headed by Zonge Engineering geophysicists Gary N. Young and Norman R. Carlson, was mobilized to the Desert Springs area on October 20, 1980. The survey line was begun with a dipole spacing of 1,900 feet (579 m), obtaining resistivity/phase data at 0.125, 0.25, 0.5, 1.0, 2.0, and 4.0 Hz up to transmitting dipole 33,34.

Beginning with the right-plunging 32,33 dipole, complex resistivity data were obtained in a four-electrode roll-along mode, at a harmonic frequency range of 0.125 to 1.375 Hz. The dipole spacing for this phase of the work was 2,000 feet (610 m). Two overlapping dipoles were measured in order to insure continuity between the two types of data collection. The final data were obtained on December 2.

A total of 20.2 surface line-miles (32.6 line-km) of data were obtained on the survey. Total subsurface coverage was 17.9 line-miles (28.7 line km).

Production on the survey was slowed by severe telluric noise, which may have been related to sunspot activity. Weather and equipment problems also caused some delays. Since the complex resistivity data represent the first time the GDP-12 complex resistivity system was used in petroleum exploration, the data were taken fairly slowly in order to verify proper operation.

The apparent resistivity, apparent polarization, and REM data are presented in Plate 4.1 at the back of this chapter. It may be unfolded for reference while reading the text.

Line Interpretation

As can be seen in Figure 4.5 and Plate 4.1, the electrical line traverses narrow zones of production from Lewis and Almond reservoirs at Playa-Lewis and Desert Springs West fields, and a wider Almond production zone at Desert Springs Field. Toward the east, the line traverses approximately 10 line-miles (16 line-km) of non-productive territory. Hence, the line provides an opportunity to evaluate data over fields of various plan-view sizes and to compare these data with an extensive amount of background data.

The field data are shown in Plate 4.1. The two repeat diagonals show resistivity/phase data above the plot point and complex resistivity below the plot point.

APPARENT RESISTIVITY DATA

The resistivity layering is low-over-high across the entire line. A slight easterly dip is suggested by the data. This is in agreement with the dip of subsurface lithology, as shown in Figure 4.6. The low-to-high resistivity interface appears to lie about 0.3 a-spacings deep, and the resistivity contrast is about 4:1. Since all available stratigraphic logs do not begin any shallower than 500 feet (120 m), or 0.25 a-spacings, these logs can provide no information on the nature of the conductive material at the surface.

The apparent resistivities of 50 to 55 ohm-meters at depth are uniform from the east end of the line up to about station 27 or so, where a significant change occurs. From station 27 to the west end of the line, the apparent resistivities at depth are lower by 5 to 15 ohm-meters. These lowered resistivities extend all the way across the western half of the line, and they show no correlation to the easterly dip of the stratigraphy. This abrupt change is therefore probably unrelated to subsurface stratigraphy per se, but is probably due to low-level brine water discharge

from the gas traps on the west end of the line. Note that the correlation here is very good: all of the high-resistivity portion of the line is in the non-producing area, and all of the lower resistivity portion of the line is in the proximity of wells with shows or production.

The apparent resistivity data show two specific zones of potential interest in hydrocarbon exploration. The first is a broad conductive zone between stations 19 and 25, which correlates with the Desert Springs production. The second zone is a very shallow, limited conductive zone between stations 8 and 11 which correlates with the Playa-Lewis Field. In addition, two very minor diagonal effects are correlated with the narrow zone of Desert Springs West production near station 4.

In order to examine the influence of well casings upon the data, the "PIPE" model of Holladay and West (1982) was run (Figure 4.7). As explained in section 2.5, this algorithm often provides a worst-case approximation of well-casing effects. Some ambiguity exists as to which wells were cased, and which wells had had their casing pulled at the time of the survey. For example, the well near station 21.4 is not listed on recent Petroleum Information maps, yet it is known to have existed sometime in the past. It is possible that this and other casings were pulled prior to the survey. The model data of Figure 4.7 include only producing wells on the Petroleum Information maps; all such wells within 3 a-spacings of the line were included. Modeling was done using 5-1/2-inch (14.0 cm) diameter casings.

The first thing to note about the residual data of Figure 4.7 is that the change to lower resistivities west of about station 27 is still evident. In other words, this change in character cannot readily be attributed to well-casing effects, even in a worst-case model. A look at the locations of other cultural features, such as pipelines, also suggests that these features do not cause the overall change in character, although we shall see that specific features on the line do appear to be related to culture.

Desert Springs Field

Almond production at Desert Springs Field lies approximately between stations 16.5 and 27. A substantial conductive zone is found in this portion of the pseudosection, although it is smaller in lateral extent than the productive sands. While this anomaly is very impressive at first glance, its character is very similar to what one would expect of cultural effects. The peak surface responses are centered at the surface near stations 20 and 24; strong diagonal effects plunge left and right from these positions, and their effects are superposed to form a low resistivity zone between them at depth.

The well-casing model of Figure 4.7 shows a fair qualitative match to the data. The model correctly shows the conductive diagonals, flanking resistive diagonals, and the conductive zone at depth beneath station 24. The magnitude of the calculated effect is lower than that shown in the field data, and the strong surface response seen in the field data is not reproduced by the model. However, one can envision considerable enhancement of the cultural contamination at the surface due to grounded metal pipelines which cross near electrodes 20 and 24, and which connect to the offending wells just north of the line. Hence, the apparent resistivity anomaly at Desert Springs appears to be a classic example of cultural effects, with both surface pipelines and well casings producing strong effects. If these effects are taken into consideration, there is little or no evidence that any bona fide conductive anomaly exists in the apparent resistivity data over Desert Springs Field, outside of the generally anomalous data over the entire western half of the line. The reason for this may be related to pressure reduction in the reservoir, as described later in this chapter.

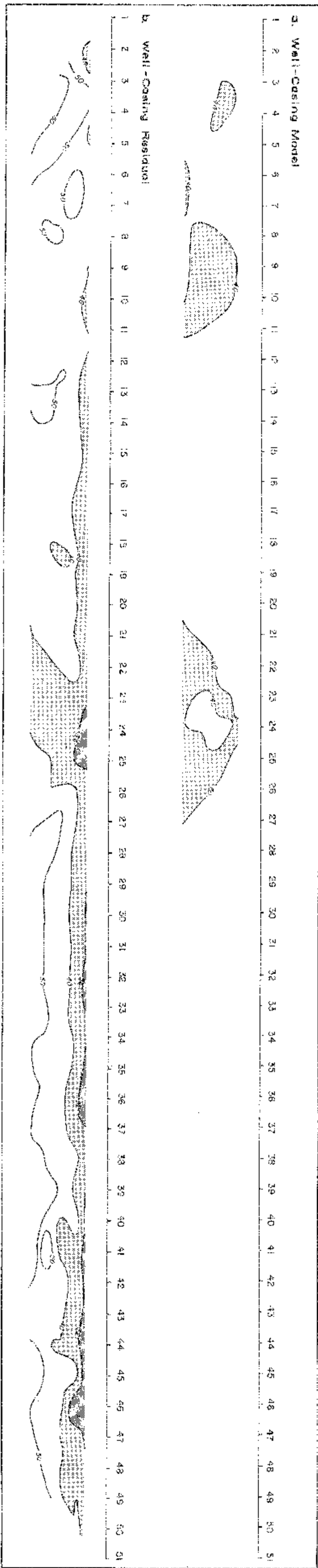


Figure 1.7. Well-casing model of apparent resistivity data for the Desert Springs area line Model parameters: 2m casing well, casing diameter = 6.75 inches (17.3 cm), casing resistivity = 2.0×10^{-7} ohm-meters, surface impedance = 0.5 ± 0.5 mV/ground resistivity = 45 ohm-meters. All wells within 3 kilometers of the line were included, except for the following wells not listed on previous information maps: C-HW-18, T20N-R8W, C-HW-18, T20N-R8W, C-HW-18, T20N-R8W. Figure 1.4 shows well locations.

Playa-Lewis Field

The Playa Lewis Field produces gas from the Lewis Formation. The literature (Whitley, 1979) shows two Almond wells near the line, but these are not shown on recent Petroleum Information maps. Hence, the issue of well-casing effects is rendered ambiguous. Only the wells which are listed on Petroleum Information maps are included in the well-casing modeling. The slight surface anomaly over the production may be partly caused by two pipelines which traverse the line at stations 9.2 and 10.0, but is more likely the result of a slight resistivity change in the near surface. There is no evidence that a "deep anomaly" of the type described in Chapter 2 is specifically correlated to Playa-Lewis production, aside from the generally conductive zone at depth.

Desert Springs West Field

Lewis production occurs at Desert Springs West in a narrow zone between stations 3 and 4.5. Two weak, conductive diagonals are seen plunging left and right from dipole 3,4. Considering the well-casing problems encountered over Desert Springs and Playa-Lewis, one might initially suspect that these diagonal effects are caused by the shut-in oil well which lies 0.4 a-spacing north of station 3.3. However, the effects from this well should consist of a sharp chevron-shaped zone centered at the $n=1$ position at station 3.5, as shown in the well-casing model data of Figure 4.7. The discrepancy between the model and the field data results only in enhancement of the right-plunging 2,3 diagonal on the residual section. This suggests that the well does not produce any noticeable effect on the data. Since no surface culture, topographic, or structural influences are to be expected in the data, this very subtle feature may reflect a slight change in the resistivity of the surface rocks. The fact that this alteration lies directly over the producing zone suggests that a causal link may exist between the anomaly and the hydrocarbons. However, this anomaly is far from being a classic hydrocarbon-type feature, and would represent a very poor target if found in the course of exploration work.

APPARENT POLARIZATION (DECOUPLED PHASE ANGLE) DATA

Polarization layering is low-over-high across the line. The data show more variability than the apparent resistivity data, and they show no evidence of the eastward dip of the sediments.

The data are not heavily influenced by well-casing or pipeline effects, which should be greatest near the top of the pseudosection and decrease toward the bottom. Some 1 to 2 milliradians of anomalous behavior may be generated by culture on the line, but no classic chevron-shaped features are visible.

There is no correlation between high apparent polarization values and the lateral extent of any of the three hydrocarbon-producing zones. Instead, most of the variability across the line may be due to noise, minor mineralization changes, or clay alteration in shaly units. Stratigraphic logs show that fine-grained pyrite is observed across the length of the line, but that the amount of pyrite and the location of the mineralized zones is quite variable. No "shallow anomalies" of the type described in Chapter 2 are evident in these data.

RESIDUAL ELECTROMAGNETIC (REM) DATA

Unlike the apparent resistivity data, the REM data show high-over-low resistivity layering. This is due to the fact that REM penetration on this line appears to be significantly greater than that of the galvanic data. The thin, conductive surface layer observed earlier in the apparent resistivity data is almost totally transparent to REM. The resistive unit seen below $n=1$ in the apparent resistivity data dominates

the top half of the REM pseudosection, and the conductive unit which is just barely sensed at depth by resistivity is shown extremely well by REM. Hence, a great deal of additional information can be discerned from the REM data.

One of the most important features shown by the REM data is the change in character of the data near station 27. Although a similar change was seen in the apparent resistivity data, it is particularly pronounced in the strong high-over-low (positive over negative numbers) effect seen in REM west of station 27. The data show a generally conductive area at depth in this region. The conductive material correlates with the region of gas production; the more resistive and rather homogeneous zone east of station 27 correlates with barren sands.

It is highly unlikely that culture causes this broad, conductive feature on the west side of the line, since the data are anomalous even in areas which are untouched by culture. In addition, contrary to what would be expected of culture, no strong effects are observed at the surface, and the anomaly is strongest at depth. This is not to say, however, that culture has no influence on the data. On the contrary, much of the diagonally-controlled data over Desert Springs Field seem to show clear indications of the pipeline-well casing combinations near stations 20 and 24. But the increasing conductivity at depth cannot be readily accounted for by cultural effects. So, while some details of the anomalies can be attributed to culture, the general conductive character of the region as a whole cannot be explained in this manner.

Since the broad anomaly cannot be explained by contamination due to culture, and does not correspond to the eastward dip of the stratigraphy, it can reasonably be concluded that it shows a deep, cross-formational zone of low resistivity which may be related to brine discharge from the gas traps. It is very interesting to note, however, that the specific fields in this area do not exhibit pronounced, classically-shaped anomalies which are well-bounded at the field perimeters (with the possible exception of a strong response at $n=6$ over Desert Springs). This may be related to depressurization of the reservoirs, as noted in the conclusions.

4.4 CONCLUSIONS

Review of the Data

The character of the apparent resistivity and REM data shows a distinct change near station 27. East of station 27, across 10 miles (16 km) of non-productive stratigraphy, resistivities are quite uniform, reflecting only the regional eastward dip of the sediments. West of station 27, a broad, cross-formational conductive zone is found at depth. This zone corresponds to the gas-producing portion of the line. The conductive zone is fairly subtle in the apparent resistivity data, but is much clearer in the REM data due to REM's increased depth of penetration. There are no apparent polarization anomalies on the line which correlate with the gas fields.

Possible Sources of the Anomalies

It is likely that the broad, conductive zone reflects low levels of brine water discharge from the reservoir sands. This would correspond to the "deep anomaly" described in Chapter 2. There is no corresponding "shallow anomaly" evident in either the apparent polarization or apparent resistivity data. Two possible explanations exist for this: 1) subsurface mineralization or clay alteration effects never resulted from upward migration of hydrocarbons, or 2) these effects diminished with depletion of the gas reserves due to oxidation or other disruptive effects.

Although the general region of gas production is clearly delineated in the apparent resistivity and REM data, the exact perimeters of the three distinct fields are not. Desert Springs Field shows the best apparent resistivity anomaly at first glance, but it is probable that these data are strongly influenced by pipelines and moderately influenced by well casings. The REM data, however, show significantly less contamination by culture, and they show a slight increase in the conductive zone at depth which correlates moderately well with Desert Springs production. Playa-Lewis and West Desert Springs fields cannot be specifically outlined on the basis of the data, except by very weak, low resistivity zones at the surface.

The lack of distinction between the three fields provides a good opportunity to learn something about the "deep anomaly" mechanism which seems to produce the strong anomalous responses seen over Ryckman Creek and Whitney Canyon Fields (Chapter 3). The first question one might raise is that, unlike the huge anticlinal traps at Ryckman Creek and Whitney Canyon, the Desert Springs area fields are purely stratigraphic in nature; therefore, little hydrostatic pressure difference would be found within the reservoirs themselves, limiting the hydraulic mechanism which drives the anomalies. However, a close look at the geology shows that, at least over Desert Springs, this is not true. Table 4.3, for instance, shows that the reservoir sands at Desert Springs are about 30 feet (9 m) thick in a down-dip direction. Considering the width of the field and the 5 degree dip of the stratigraphy there, the reservoir exhibits a total east-west relief of some 1,900 feet (580 m), which would certainly result in a reasonable hydrostatic gradient. Moreover, the hydraulic action which moved the hydrocarbons to their traps in the first place, if it is still active, would certainly be sufficient to discharge some saline water from the trap. This saline discharge seems to be the effect which is being measured with the REM data, although it is likely that the response is seriously diminished from what it was before the exploitation of the reservoir sands.

A much better explanation for the lack of separate, distinct anomalies in the three Desert Springs area fields is that the anomaly mechanism has been diminished in strength by pressure reduction in the reservoir sands. As summarized by Tables 4.3, 4.4, and 4.5, reserves at the time of the electrical survey had been seriously depleted. At Desert Springs, in the Lewis reservoir, over 50 percent of the gas and over 90 percent of the oil had been recovered. At the Playa-Lewis Field, some 70 percent of the gas reserves had been recovered. Desert Springs West is also believed to have been similarly developed. More importantly, reservoir pressures in the fields had dropped some 50 percent or more. Such drastic changes in reservoir pressure would result in a serious reduction of solubility of salts in the upward migrating waters; hence, the waters above the trap would have a lower brine concentration than before depressurization of the reservoir. This would result in three effects: 1) the overall salinity above the trap would decrease, resulting in a lesser anomaly; 2) the brine would not extend as far towards the surface, and 3) the brine would be more "spread out" at depth due to the increased importance of groundwater diffusion relative to the upward migration of brine water. All three of these effects are consistent with the data.

Hence, we might conclude that pressure depletion in the reservoirs has degraded the brine supply to the "deep anomaly," and that reduction of vertical hydrocarbon migration by depletion of reserves in the trap has limited the resupply of the "shallow anomaly," if indeed it existed at all. This provides important evidence which supports the anomaly mechanism outlined in Chapter 2.

REFERENCES

- Andrews, J.A., 1979, Desert Springs, West, *in* Wyoming oil and gas fields symposium, Green River Basin, vol. 2: Wyoming Geol. Assn., p. 132-133.
- Colburn, J.A., 1979, Table Rock, and Table Rock, Southwest, *in* Wyoming oil and gas fields symposium, Green River Basin, vol. 2: Wyoming Geol. Assn., p. 378-383.
- DeVoto, R.H., and Bitter, R.K. (editors), 1985, Sedimentation of late Cretaceous and Tertiary outcrops, Rock Springs Uplift: 19th annual field conference guidebook, Wyoming Geol. Assn.
- Earl, J.H., 1981, Desert Springs gas field, Sweetwater County, Wyoming: Geophysics, v. 26, p. 673-681.
- Holladay, J.S., and West, G.F., 1982, Effects of well casings on surface electrical surveys (abs.): Geophysics, v. 47, p. 439. Full paper available in Technical papers, 51st Annual International Meeting and Exposition, SEG, Los Angeles, v. 2, p. 815-838.
- May, B.E., 1981, The Desert Springs Field: 16th annual field conference guidebook, Wyoming Geol. Assn., p. 290-293.
- McPeck, L.A., 1981, Eastern Green River Basin: a developing giant gas supply from deep, over-pressured Upper Cretaceous sandstones: AAPG Bull., v. 65-66, p. 1078-1088.
- Mohl, K.L., and Sasse, C., 1979, Desert Springs, *in* Wyoming oil and gas fields symposium, Green River Basin, vol. 1: Wyoming Geol. Assn., p. 130-131.
- Peppard-Soulders, 1979, Hydrocarbon production map of the greater Green River Basin, *in* Wyoming oil and gas fields symposium, Green River Basin, vol. 2 (pocket): Wyoming Geol. Assn.
- Petroleum Information, 1982, Lease-ownership maps W-181, W-182 (record takeoff dates 11/82-3/83).
- Richers, D.M., Reed, R.J., Horstman, K.C., Michels, G.D., Baker, R.N., Lundell, L., and Marrs, R.W., 1982, Landsat and soil-gas geochemical study of Patrick Draw Oil Field, Sweetwater County, Wyoming: AAPG Bull., v. 66, p. 903-922.
- Ritzma, H.R., 1963, Geology and occurrence of oil and gas, Wamsutter Arch, Wyoming, *in* Backbone of the Americas: AAPG Memoir No. 2, p. 188-195.
- 1968, Geology and occurrence of oil and gas, Wamsutter Arch, Sweetwater County, Wyoming: AAPG Memoir No. 9, v. 1, p. 817-827.
- Street, B.A., 1979, Patrick Draw and Patrick Draw, North, *in* Wyoming oil and gas fields symposium, Green River Basin, vol. 2: Wyoming Geol. Assn., p. 274-277.
- Whitley, W.W., 1979, Playa-Lewis, *in* Wyoming oil and gas fields symposium, Green River Basin, vol. 2: Wyoming Geol. Assn., p. 290-291.

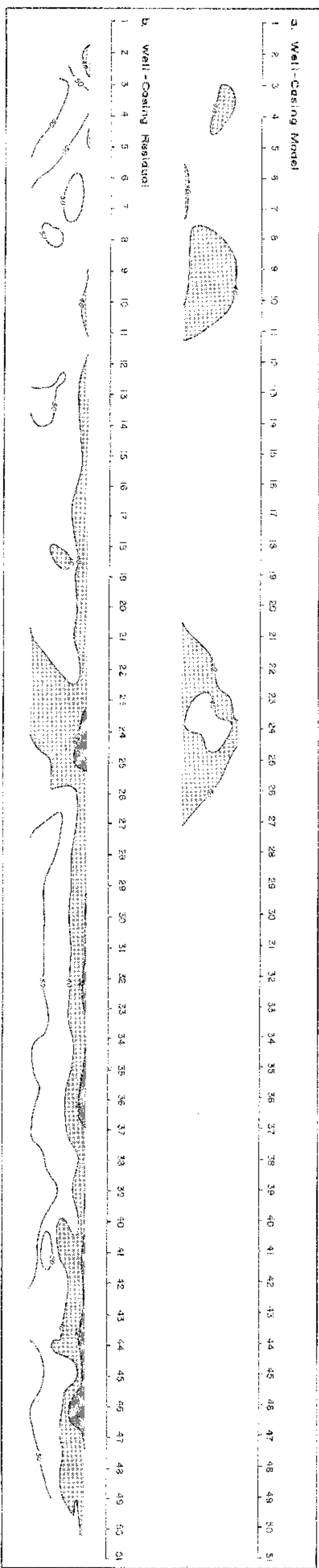


Figure A.7. Well-casing model of apparent resistivity data for the Desert Springs area line Model parameters: 2x casing wells, casing diameter = 6 1/2 inches (16.5 cm), casing resistivity = 2.0×10^{-7} ohm-meters, surface impedance = 0.5 ± 0.5 mV/ground resistivity = 45 ohm-meters. All wells within 3 kilometers of the line were included, except for the following wells not listed on previous information maps: C-HW-18-T20N-R8W, C-HW-18-T20N-R9W, C-HW-18-T20N-R10W. Figure A.4 shows well locations.

Chapter 5

Little Buck Creek Field

Niobrara County, Wyoming

5.1 INTRODUCTION

Little Buck Creek Field is located on the extreme southeast boundary of the Powder River Basin, some 20 miles (32 km) north of Lusk, Wyoming and about 6 miles (10 km) east of the prolific Lance Creek Field. The general location is shown in Figure 5.1. Production at Little Buck Creek is almost exclusively oil, trapped in sandstone members of the Cretaceous Fall River Sandstone and the Permian to Pennsylvanian Minnelusa Formation. The oil is retained by a north-south trending anticline. Production has totalled nearly 12 million barrels as of early 1983. Most of the oil has now been recovered, and a number of wells are shut in.

Two perpendicular lines of resistivity/phase data were obtained over Little Buck Creek, using a dipole spacing of 1,000 feet (305 m).

5.2 GEOLOGIC BACKGROUND

Exploration History of the Little Buck Creek Area

Although the occurrence of oil in Wyoming had been noted as early as 1833, commercial exploitation did not begin until the 1880s. The first producing oil well in the state was drilled in 1884 at Dallas Dome, near Lander. This was followed five years later by the first producing well in the Powder River Basin, drilled by the Pennsylvanian Oil and Gas Company north of the present-day Salt Creek Field. Other, minor discoveries followed at Moorcroft Field in 1887 and Shannon Field in 1889, and by 1895 enough oil was being produced to support the state's first refinery at Casper.

Development of the Powder River Basin was quite slow during the first 30 years of the twentieth century because of the remoteness of the producing fields. Raw crude had to be transported at first by 12- and 16-team coaches and later by truck, making the long trip to commercial centers in the East a profitless venture. This was especially true prior to World War II, when prices for crude dipped as low as ten cents per barrel.

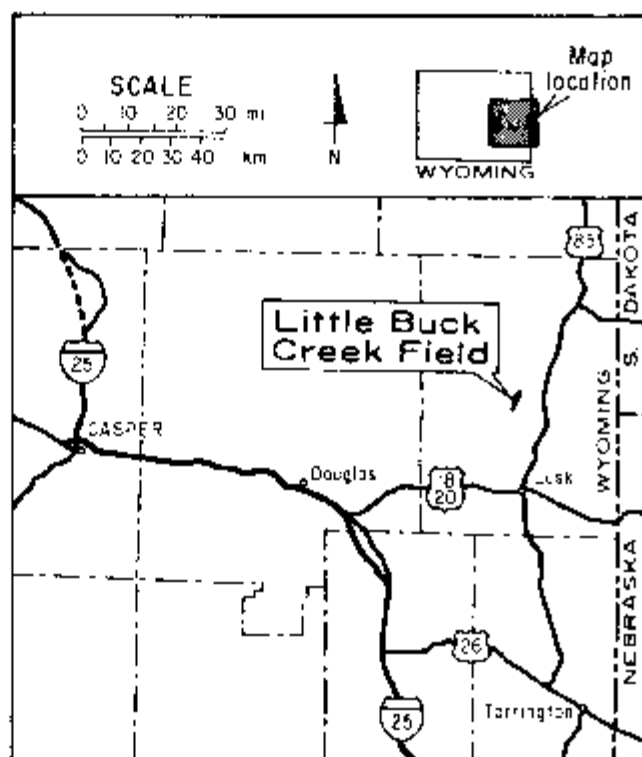


Figure 5.1. Location map of Little Buck Creek Field.

In spite of these difficulties, several discoveries during the early part of the century sparked a series of exploration booms. Salt Creek Field was the first and certainly the most prolific discovery in the early days of Powder River Basin exploration. The discovery well, drilled in 1908, was a gusher, and a dam had to be constructed in order to hold the uncontrolled oil (Maynard et al., 1981). Other finds of the era included Teapot Field in 1914, and Big Muddy in 1916. In 1918, the Ohio Oil Company completed a well at the crest of an east-west trending anticline at Lance Creek, producing oil from upper Cretaceous sands at 2,689 feet (820 m). This well, which was later deepened to a second producing horizon in the Fall River Sandstone at 3,663 feet (1,116 m), set off a boom in leasing activity from 1918 through the summer of 1921. In 1930, the upper unit of the Sundance Formation was found to be productive, followed in 1935 by a major discovery well which produced an initial 2,000 barrels per day from the lower Sundance. These events sparked a sustained boom in leasing and drilling activity in the area, leading to the extension of Lance Creek production to the Minnelusa Formation.

At this time, a single, east-west trending anticlinal structure was known in the Lance Creek area, with Lance Creek Field located at its crest. The crest of the anticline was known to plunge gradually toward the east, and in 1936, Conoco decided to search for new structural closures along that trend. True-dip data obtained from reflection seismic work indicated the presence of two such closures. In 1937, Conoco drilled the largest target, opening up the East Lance Creek Field in the Fall River Sandstone.

In 1942, a seismic correlation map of the Fall River Sandstone was made on the basis of the 1936 seismic data and Fall River wells in the area. This map, which is redrawn in Figure 5.2, more clearly outlined the second structural closure found

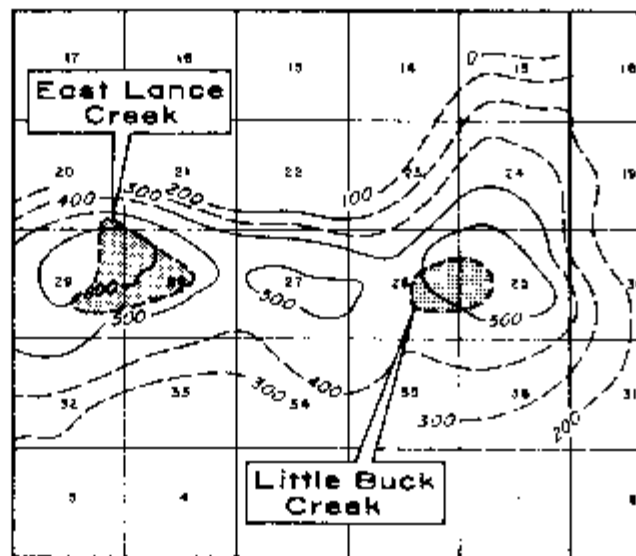


Figure 5.2. Reflection seismograph correlation map, contoured on top of the Fall River Sandstone (Dakota Sandstone), compiled by Conoco in 1942 in a re-interpretation of their 1936 seismic data. Contour interval: 100 feet (15 m). After Swan (1947).

earlier. Conoco followed this work by drilling the Little Buck Creek discovery well, #1 Wright, at NW-SW-NW-25-T36N-R64W. The well was completed in the Fall River on June 18, 1944, producing 43° API gravity oil at 3,850 feet (1,173 m). Development continued with the extension of production to the Upper Minnelusa in 1948 and to the first and second Leo sands of the Middle Minnelusa in 1949. Fall River production was extended southward in 1951 with the discovery of Little Buck Creek South. Total production at Little Buck Creek has totalled nearly 12 million barrels, making the field a respectable producer for the area, although it falls well short of the 100 million-plus barrels produced at Lance Creek.

The pattern of development in the Powder River Basin has been steadier since the 1940s due to increasing crude prices and more efficient transportation. By 1958, Powder River oil had accounted for 48 percent of Wyoming's total production, and while recent discoveries in the Overthrust area have shifted exploration emphasis toward the western part of the state, the Powder River Basin continues to play an important role in exploration activity today. Ver Ploeg and Oliver (1981) report that 46 percent of all exploratory wells drilled in Wyoming in 1979 were located in the Powder River Basin. Since most of the post-Mississippian structures along the basin margins have already been explored, the search for stratigraphic traps is being given increased importance. It is hoped that electrical exploration techniques such as the one presented in this volume will be more fully utilized in order to explore for the more subtle traps in this area.

Geologic History of the Powder River Basin

Table 5.1 provides a stratigraphic description of the Little Buck Creek area. As noted by some of the authors referenced at the end of this chapter, the formation nomenclature in the Powder River Basin is somewhat confused. Alternative formation names are placed in parentheses in Table 5.1. Please note that the Dakota Sandstone, which is widely present in the basins to the south and west, is known as the Fall River Sandstone in the Little Buck Creek area.

TABLE 5.1: STRATIGRAPHIC DESCRIPTION OF
LITTLE BUCK CREEK FIELD

System	Symbol	Formation	Lithologic Description
CENOZOIC ROCKS			
Tertiary			
Miocene	Ta	Arikaree Fm.	Buff to tan, very fine grained, poorly bedded sandstone containing tiny grains of magnetite
Oligocene	Twr	White River Fm.	Interbedded brown, pink, gray, and green tuffaceous siltstone and conglomerate
Eocene	Tw	(unconformity) Wasatch Fm.	Gray, brown, and reddish-pink conglomeratic to fine grained arkosic sandstones, siltstones, carbonaceous shales, and coal beds
Paleocene	Tfu	(unconformity) Fort Union Fm.	Light to dark gray, very fine grained to conglomeratic sandstone interbedded with siltstones, claystones, carbonaceous shales, and coal beds
	Tftr	Torque River mbr.	
	Tfl	Laho Sh.	
	Tft	Tullock mbr.	
MESOZOIC ROCKS			
Cretaceous			
	Kl	Lance Fm.	Gray carbonaceous shale and massive lenticular concretionary sandstone, with many thin coal beds in the lower half
	Kfh	Fox Hills Ss.	Light gray sandstone
	Kp	Pierre Sh.	Gray shale
	Kn	Niobrara Sh.	Gray calcareous shale; flecked with chalk near the top
	Kcl	Carlisle Sh.	Dark gray shales with shaly sands and calcareous matter
	Kg	Greenhorn Ls.	Dark gray shales with shaly sands and calcareous matter
	Klif	Belle Fourche Sh.	Dark gray shales and sandy shales
	Kmr	Mowry Sh.	Gray siliceous shale
	Knc	Newcastle Ss.	Light gray to buff, fine grained sandstone with numerous black shale partings; hosts oil at Lance Creek
	Ksc	Skull Creek Sh.	Dark gray to black shale
	Kfr	Inyan Kara Group	Fine grained gray to brown sandstone with interbedded mudstone, some coal beds; <i>hosts oil at Little Buck Creek</i> ; also hosts oil at Lance Creek, Lance Creek East, and other nearby fields
		Fall River Ss.	
		(Dakota Ss. in west Powder River Basin)	
		(unconformity)	
	Kfu	Fuson Sh.	Variegated shales with some yellowish sandstone
	Kla	Lakota Ss.	Coarse to conglomeratic, gray to brown sandstone containing coal beds
		(unconformity)	
Jurassic	Jm	Morrison Fm.	Variegated shales, thin sandstones, minor limestones; hosts minor amount of oil at Lance Creek

TABLE 5.1 Continued

System	Symbol	Formation	Lithologic Description
Triassic	Js	Sundance Fm. Upper unit	Slightly glauconitic, gray-green shales and sandstones, 1st Sundance sand productive at Lance Creek
		(unconformity) ----- Lower unit	Slightly glauconitic sandstone with some gray-green shale, lowermost part is the "basal Sundance sand," which hosts oil at Lance Creek and Lightning Creek
	Ts	(unconformity) ----- Spearfish Fm. (Chugwater Fm.)	Red-brown shale, with limestone and anhydrite near the base
		(unconformity) -----	
PALEOZOIC ROCKS			
Permian		Goose Egg Fm.	
	Pm	Minnekahta Ls. mbr.	Gray to pink limestone
	Pa	Opeche Sh. mbr.	Red-brown shale
		(unconformity) -----	
	Pml	Minnelusa Fm.	
		Upper mbr.	
	Pmc	Converse sands (1st and 2nd sands; also known as the "Tensleep" sands)	Red to buff sandstones; <i>hosts oil at Little Buck Creek</i> ; also hosts oil at Lance Creek
		Carbonates	Limestones, anhydrites and some dolomites; includes a prominent red shale marker bed, which is radioactive
Pennsylvanian		(unconformity) -----	
	Pml	Middle mbr.	Limestones, dolomites, and anhydrites, with up to four sandstone horizons (called the 1st, 2nd, 3rd, and 4th Leo sands, in order of increasing depth); <i>Leo sands host oil at Little Buck Creek</i> , also at Lance Creek
		(unconformity) -----	
		Lower mbr. Carbonates	Cherty limestones and dolomites, and dolomitic sands; hosts oil at Lance Creek
Mississippian	Pmb	Bell sand	Cross-bedded, pink to white shaly sandstone
		(unconformity) -----	
	Mm	Madison Ls.	
		Upper mbr.	Crystalline, light tan to light gray limestone with thin shale beds
Cambrian/Ordovician		(unconformity) -----	
		Lower mbr.	Dolomitized limestones, thin-bedded dolomites and thin-bedded limestones
		(unconformity) -----	
	Ed	Deadwood Fm.	
Precambrian		(unconformity) -----	
	pG		Metamorphics and intrusives

In general, the geologic record of the Powder River Basin does not show the extreme tectonic deformation which characterizes the Overthrust region of western Wyoming and eastern Utah, but the area was subjected to several periods of tectonism which strongly influenced sedimentation patterns. The first major activity seems to have occurred in the Precambrian. Micaceous shales, ferruginous sandstones, siltstones, and quartzose sandstones, deposited by several transgressions of Precambrian waters, were intensely folded and uplifted. Some of the rocks were strongly mineralized by intrusive events at this time.

Paleozoic sedimentation was largely controlled by the northerly dip which characterized the paleotopography in the area. Cambrian through Ordovician sedimentation involved an onlap of sediments across this shelf, with thicker sediments lying to the west and north of the Little Buck Creek area. The slow eastward transgression of the seas did not actually reach the southeast portion of the basin until Ordovician time. Several unconformities indicate breaks in the deposition of dolomites, shales, and limestones of the Ordovician and Mississippian.

During late Mississippian time, vast areas of the Rocky Mountains and the Ozark Highlands of Oklahoma and Arkansas were elevated. This event subjected them to erosion and solution, leading to the development of karst topography and soils which characterize the top of the Mississippian in many of the interior western states. The Mississippian uplift appears to have created a depressed area in Converse and Niobrara counties of eastern Wyoming. This depression, known as the Lusk Embayment, is the northwest extension of the broad depositional Denver-Julesburg Basin which covered western Nebraska and northeastern Colorado during Pennsylvanian time. It was in this embayment that the oil-productive rocks of the Minnelusa Formation were deposited. The basal unit is the Bell sandstone, probably eolian, which was laid down near the edge of the Pennsylvanian sea. Deposition of cherty carbonates of the Lower Minnelusa was followed by erosion. The Middle Minnelusa consists primarily of carbonates, shales, and clastics deposited in broad, shallow lagoons. Interbedded among these rocks are four sandstone horizons known as the "Leo sands"; according to Tromp, et al. (1981), these are probably at least partly eolian. The source of these sands was probably the uplifted areas to the west or north. The top two Leo sands host much of the oil production at Little Buck Creek and Lance Creek fields. An erosional unconformity separates the Middle Minnelusa from the carbonates and anhydrites of the Upper Minnelusa. The anhydrites are probably reworked materials of Pennsylvanian age transported from the west. The two Converse sands, which host some oil at Little Buck Creek and Lance Creek fields, lie near the top of the Minnelusa and also appear to have been derived from the west. A radioactive red shale marker lies atop these sands. The overlying shales, mudstones, carbonates, and anhydrites of the Goose Egg and Spearfish formations were deposited in lagoonal and shallow marine waters similar in nature to those which led to the Minnelusa sediments.

During the Jurassic, four transgressive pulses originated from waters to the north, the first two of which did not reach the area of the Powder River Basin. The third transgressive sequence inundated much of Utah, northwestern Colorado, and western Nebraska, depositing the Lower Sundance Formation, in which sand members host oil at Lance Creek. The fourth transgression covered more area than the third and resulted in deposition of the Upper Sundance strata.

The sequence of early Cretaceous rocks which form the Inyan Kara Group indicates variable depositional environments at the edge of the Cretaceous seas. The Lakota and Fuson formations were probably of littoral and non-marine origin. The Fall River Sandstone, in which oil was first discovered at Little Buck Creek, is a

fine-grained, occasionally massive sandstone deposited in a shallow, oscillating shelf environment. The source of the sands was probably from the south or southeast. Overlying Cretaceous strata are primarily marine, lagoonal, and coastal sediments. The Pierre Shale (equivalent to the Lewis Formation in the Green River Basin) consists of marine sediments deposited during the final transgression of the Cretaceous seas. The Fox Hills Sandstone was deposited during the regressive sequence, and the Lance Formation is attributed to continental deposition following this regression.

It was not until the late Cretaceous and early Tertiary that the Powder River Basin was formed, although the basic structural trend appears to have been in existence at least since Permian times (Strickland, 1958). As illustrated by the structure contour map of Figure 5.3, the axis of the basin has a north-northwest orientation and an asymmetrical shape. The asymmetry is due to intense folding and thrust faults with up to two miles (3 km) of vertical displacement. Many of the steep flanks to the south appear to be due to high-angle reverse faults which resulted from the Laramie, Hartville, and Black Hills uplifts. The reverse fault located north of the Hartville Uplift appears to have played a role in the oil accumulations found at Lance Creek, East Lance Creek, and Little Buck Creek.

Current Geology

Surface material at Little Buck Creek involves Mesozoic marine sediments of the Lance Formation, except toward the south and in some spotty areas, where the White River Formation of Oligocene age is exposed.

As indicated in the surface geology and structure map of Figure 5.4, the Lance Creek and East Lance Creek oil production is controlled by a meandering anticlinal trend. Little Buck Creek production is largely controlled by a similar anticline oriented roughly northeast-southwest—perpendicular to the Lance Creek anticline. The specific reason for this abrupt change is not known, although the deformation on this flank of the Powder River Basin is quite severe.

The locations of the resistivity/phase survey lines are shown in Figure 5.5; the Fall River structure is shown in plan view in Figure 5.6.

The geologic cross-section of Figure 5.7 shows that the sediments in the area of Little Buck Creek itself are relatively flat-lying. The close-up cross-section of Figure 5.8 is an electric log correlation cross-section which has been tied in to nearby stratigraphic logs. Formation resistivities are typically less than 10 ohm-meters in the top 4,000 feet (1,200 m) of sediments, which are Cretaceous in age. The underlying sediments are quite variable in resistivity, but these units are beyond the zone of influence of the electrical data reported here.

Stratigraphic logs in the field reveal the occasional presence of pyrite in the Niobrara and Muddy formations, but it is not possible to determine from the logs whether or not the pyrite occurs in sufficient quantity to produce a polarization response in the data. There is very little indication of pyrite in the near-surface formations, although micron-sized grains could have been missed in hand-sample analyses.

Reservoir Characteristics

As summarized by Wenger and Reid (1958), Powder River Basin oils can be divided into two types, based upon sulfur content and age. The first type is found in formations of Jurassic age or younger and has a low sulfur content, generally less than 0.5 percent. These oils are typically light in color, waxy, and are mainly paraffinic or naphthenic. The second type of oil generally comes from formations of Jurassic age or older. They generally are higher in sulfur content, have a dark color,

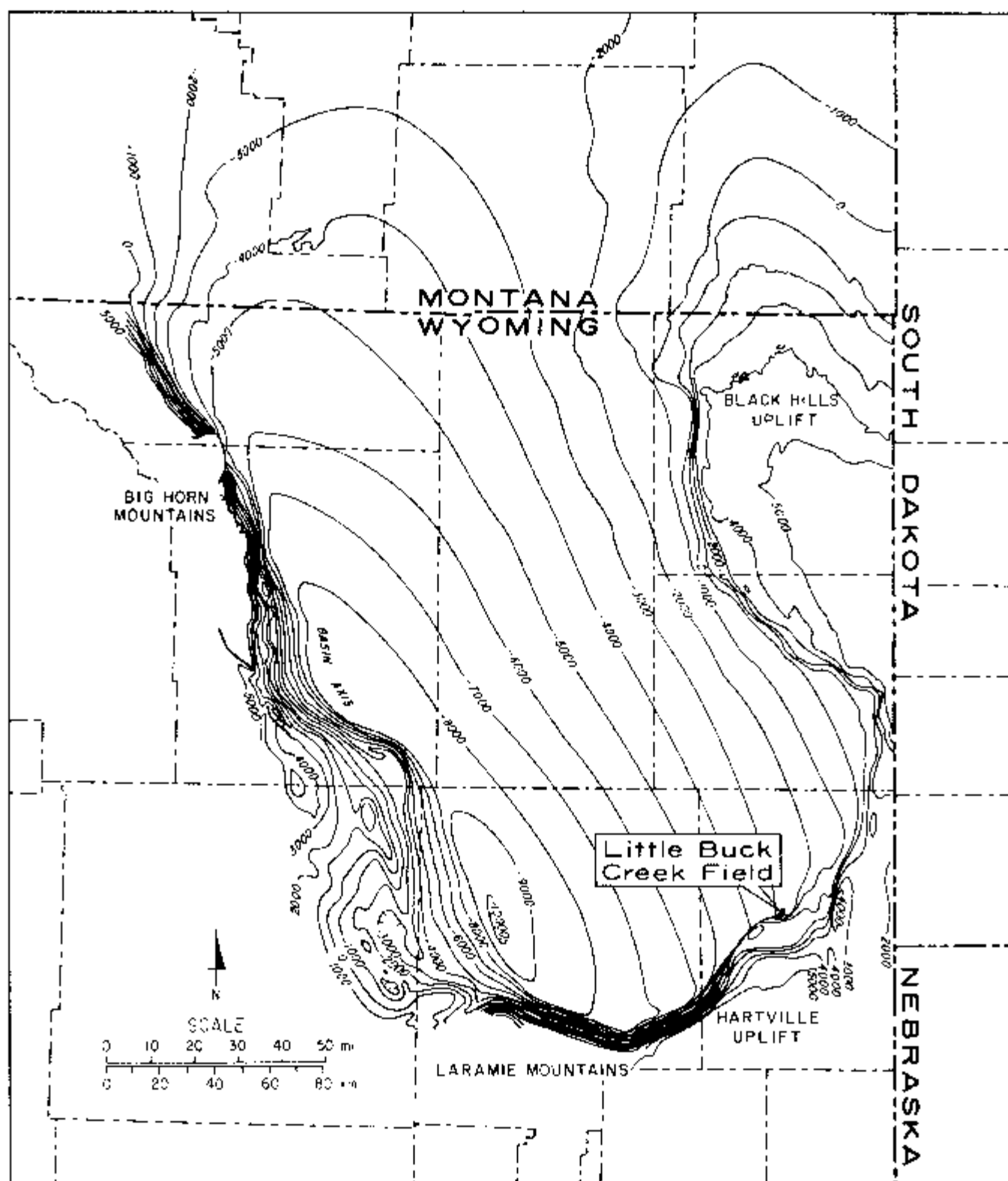


Figure 5.3. Structure map of the Powder River Basin, contoured on top of the Fall River Sandstone (Dakota Sandstone). Contour interval: 1,000 feet (305 m).

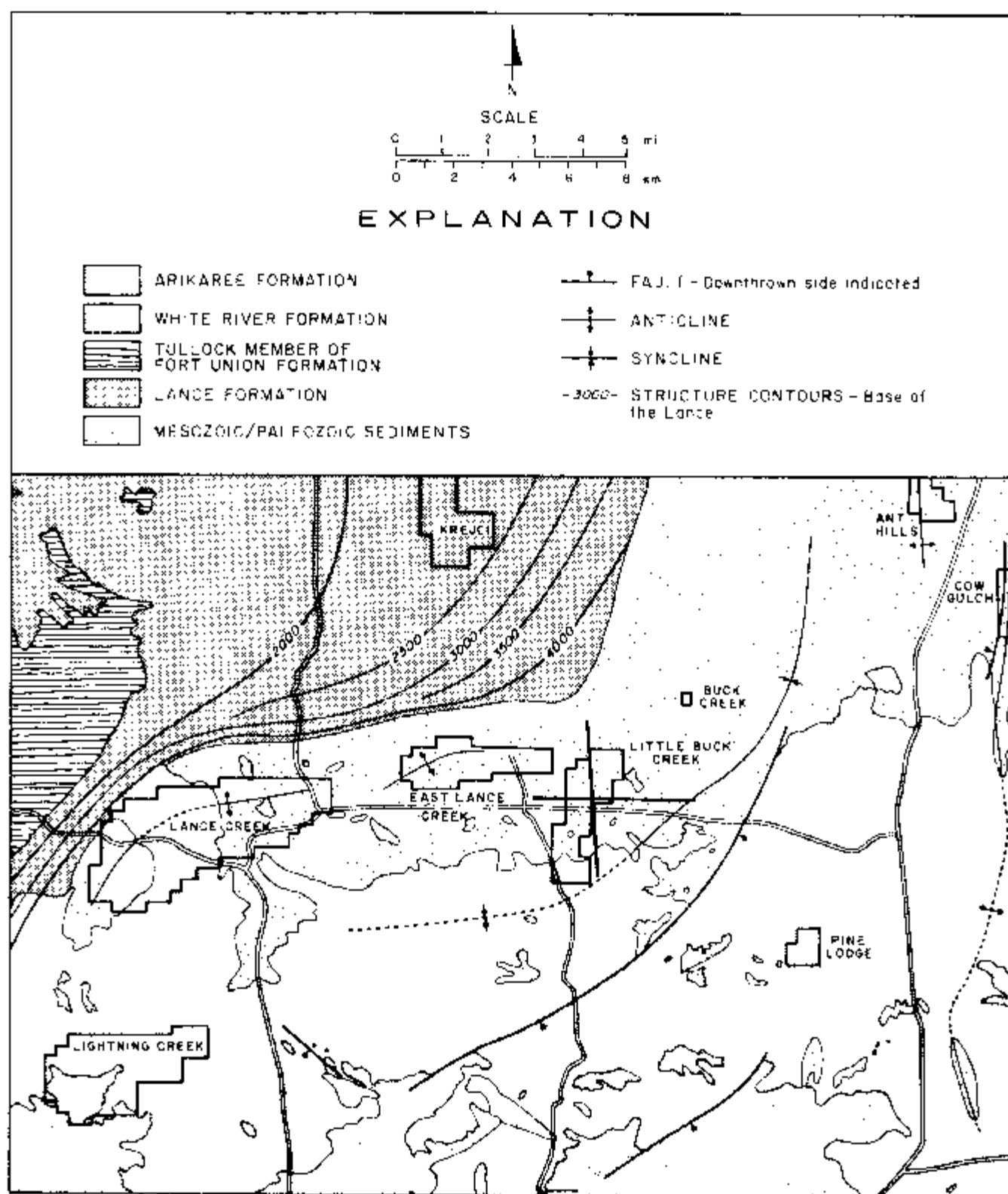


Figure 5.4. Surface geology and structure map of the Little Buck Creek area. After Denison and Horn (1975).

Plate 4.1
RESISTIVITY/PHASE AND COMPLEX RESISTIVITY PSEUDOSECTION DATA
Desert Springs, Playa-Lewis, and Desert Springs West Fields
Sweeney Co., Wyoming

Line 1
2 - 1,800 feet for resistivity/phase data
3 - 2,000 feet for complex resistivity data

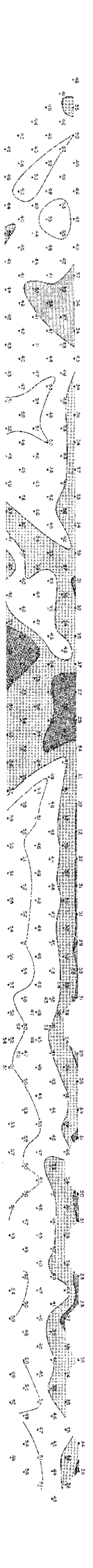
Standard Well Symbols	Exploration of Symbols	Native Symbols
Drillhole for which information is unavailable		Initial pipeline presumed grounded
Drilling in progress at time of map preparation		Ungrounded pipeline: not metal or suspended
Shut in		Metal fence
Abandoned		Elastic fence
Dry hole with total depth indicated		Buried telegraph or power cable
Oil well		Telephone line or standard voltage power line
Oil and gas well		Major high voltage power line
Gas injection well		Radio, microwave, or other communications station or tower
Water injection well		D.C. dummy
Water well		Other Symbols
Special Well Symbols		U.S.G.S. standard symbols or as labeled
Drilling in progress at the time of the electrical survey; number indicates the amount of d.i.t. stem in the hole at the time of C.A.S. operation		
Well spudded in after completion of the electrical survey		
Number indicates distance of well from the line at point of acquisition (all wells within 1.0 spacing indicated (pseudosection only))		

Desert Springs West
Playa - Lewis
Desert Springs



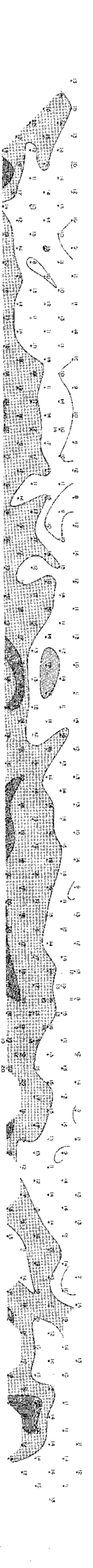
Apparent Resistivity

Units: ohm-meters
Frequency: 0.125 Hz
Layer thickness: 100 m
Layer resistivity: 100 ohm-meters



Decoupled Phase Angle

Units: millivolts
Frequency: 0.125 Hz
Layer thickness: 100 m
Layer resistivity: 100 ohm-meters



REM Quadrature

Units: microhms
Frequency: 0.125 Hz
Layer thickness: 100 m
Layer resistivity: 100 ohm-meters

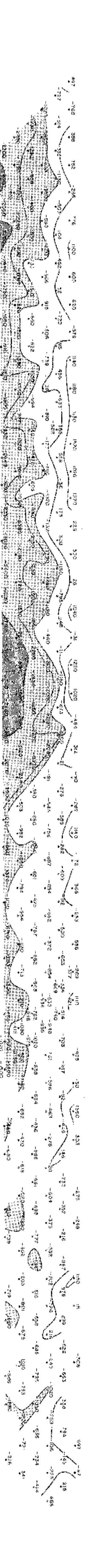
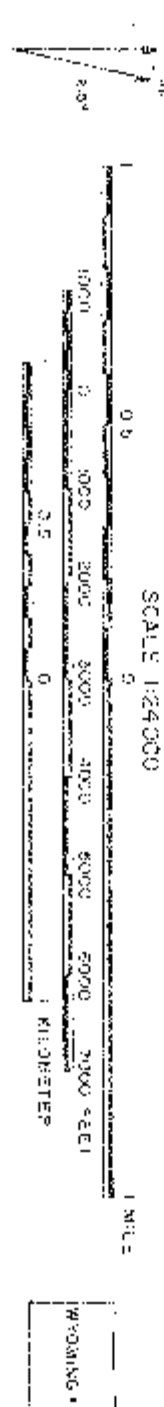


Figure 5.5
LINE LOCATION MAP
Little Buck Creek Field
NICHOLS CO., WYOMING



Source:
Data: U.S.G.S. 7.5' Quad (Telephone Dunes, Wyo., 1981; Rabbit Mountain, Wyo., 1991)
Well Data: Petroleum Information System (as of 12/01/90; W-80; record interval: 4.5/82)

Explanation of Symbols

Standard Well Symbols	Other Symbols
○ Drilling for which information is unobtainable	↓ Metal pipeline, pressurized groutings
○ Drilling in progress at time of map preparation	--- Ungrouted pipeline: run-in, or suspended
○ Shut in	↑ Metal fence
○ Abandoned	↑ Electric fence
○ Dry hole with total depth indicated	↓ Buried telephone or power cable
○ Oil well	↓ Telephone line or standard voltage power line
○ Gas well	↑ Major high voltage power line
○ Oil and gas well	↑ Radio, microwave, or other communications station or tower
○ Gas injection well	□ DC pump
○ Water injection well	
○ Water well	

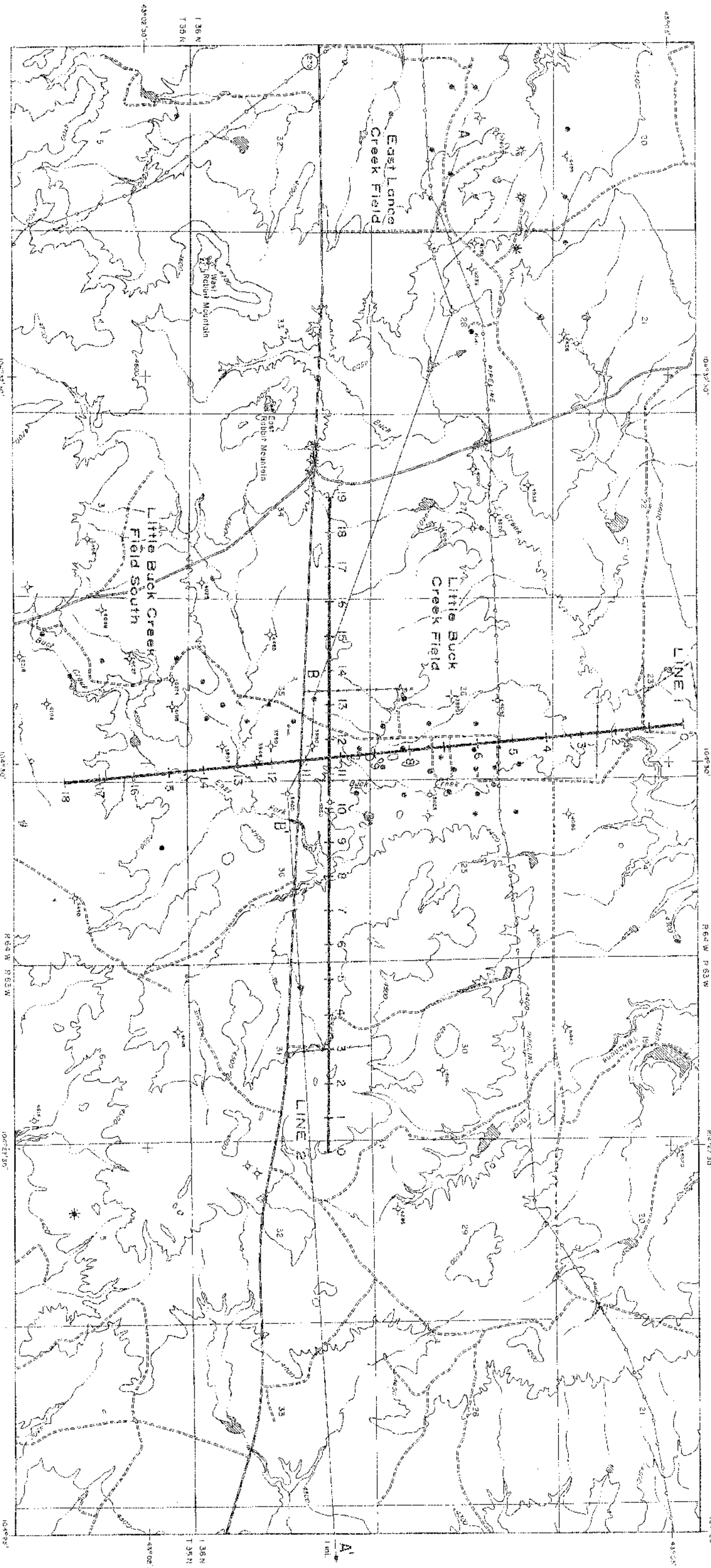
Special Well Symbols

- Drilling in progress at the time of the electrical survey; number indicates the amount of drilling in the hole at the time of data collection
- Well completed in after completion of the electrical survey
- Number indicates distance of well from the line in terms of 0-spaces; all wells within 1.0 spacing indicated (exceptions only)

Map-Specific Symbols

Topographic contour interval: 100 feet

Zone: Engineering & Research Organization, Inc.



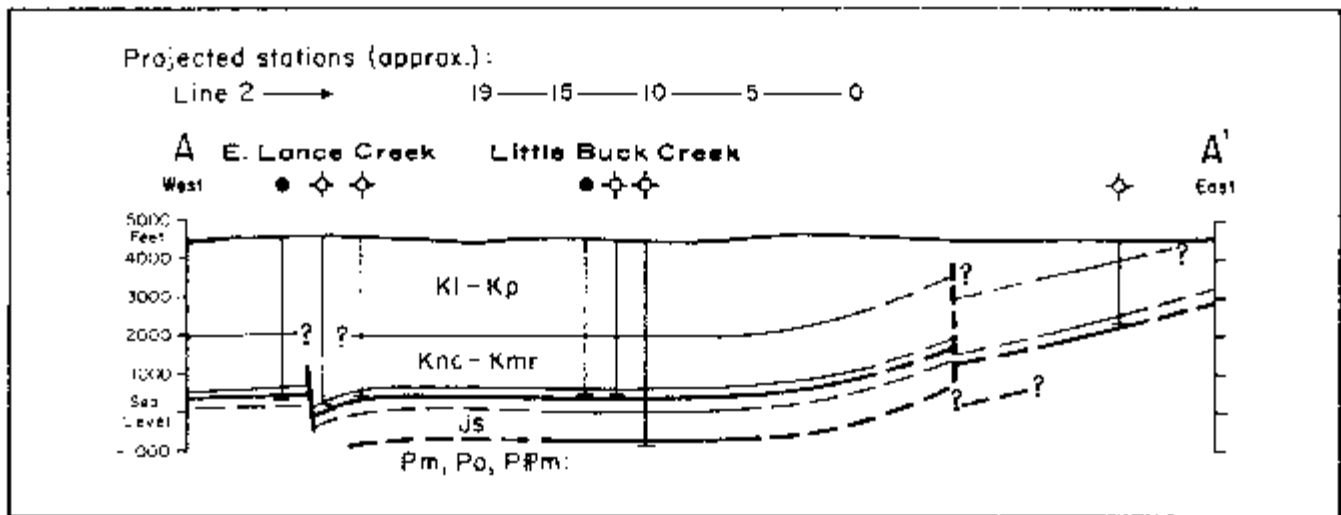


Figure 5.7. Geological cross-section A-A', with 2:1 vertical scale exaggeration; this may be compared with the data from line 2 of the electrical survey. Compiled from long-normal resistivity logs, which were correlated with stratigraphic logs. Refer to Figure 5.5 for map location.

and are asphaltic. As indicated in the tabulated reservoir data of Table 5.2, the Fall River oils at Little Buck Creek are of the first type, while the Minnelusa oils have characteristics between the two types.

The origin of Fall River oils is not certain, but Strickland (1958) notes that the source may be the black shales in the overlying Mowry and Skull Creek formations. The sulfur content at Little Buck Creek is about typical for Cretaceous oils in the Powder River Basin, and the specific gravity is somewhat higher. Connate water resistivities are about 0.1 to 0.3 ohm-meters.

Minnelusa oils, which are found exclusively in the Converse and Leo sands, are believed to have migrated from the carbonates and black shales which are interbedded with the sands. This opinion seems to be fairly widely held, and Strickland (1958) notes that maximum oil production in the Middle Minnelusa often corresponds to maximum thickness of the black shales. Converse oils at Little Buck Creek have a much higher specific gravity than is typical of Upper Minnelusa oils in the basin, which average 27° API, and the sulfur content of oils in the Converse is lower than that of oils from most other Permian reservoirs. Oils trapped in the Leo sands are fairly typical of most basin oils of Pennsylvanian age in terms of gravity and sulfur content. Connate water resistivities in the Minnelusa reservoirs at Little Buck Creek are uniformly low.

Both the Little Buck Creek and Little Buck Creek South oilfields have a water drive. The fields are nearly pumped out now; Little Buck Creek currently produces some 39 BOPD, with a total of 11.8 MMBO recovered, and Little Buck Creek South produces 9 BOPD, with a total of 0.01 MMBO recovered.

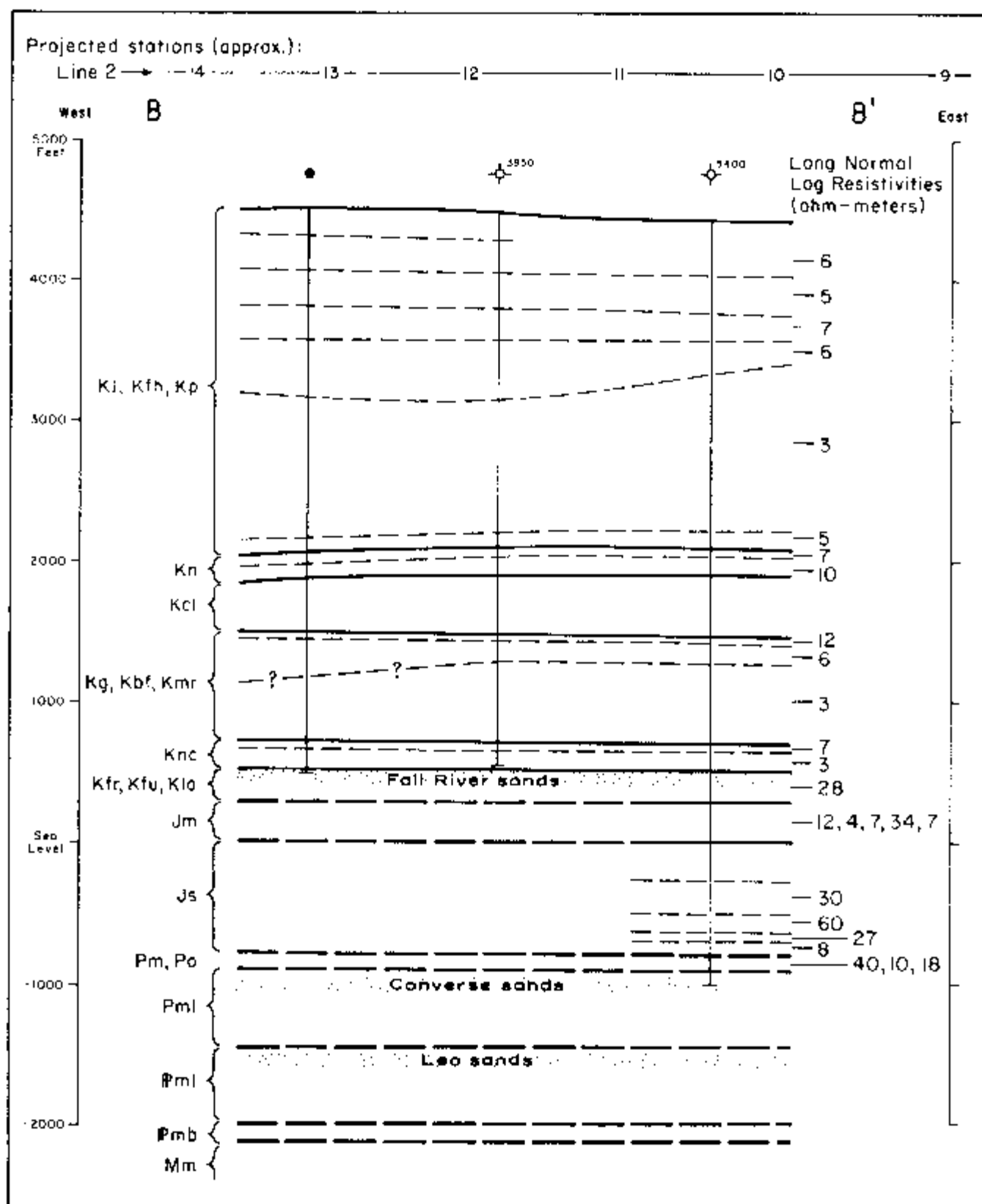


Figure 5.8. Geologic cross-section B-B', with no vertical scale exaggeration; this may be compared with the data from Line 2 of the electrical survey. Compiled from long-normal resistivity logs, which were correlated with stratigraphic logs. Refer to Figure 5.5 for map location.

TABLE 5.2: RESERVOIR CHARACTERISTICS OF
LITTLE BUCK CREEK FIELD¹**General Field Data****Region:** Southeast Margin of the Powder River Basin**Production:** Oil**Type of Trap:** Structural; anticline**Producing Formations and Depths:** Fall River Ss. (Dakota Ss.), 3,850 ft.

Upper Minnelusa Fm., 1st & 2nd Converse sands, 5,200 ft

Middle Minnelusa Fm., 1st & 2nd Leo sands, 5,900 ft

Other Significant Shows: None**Total Reserves:** 12 MMBO**Productive Area:** 740 acres**Field Operator:** Conoco**Number of Producing Wells (4/82):** 34**Number of Shut-in Wells (4/82):** 0**Number of Dry or Abandoned Wells (4/82):** 18**Well Casing Data:** Surface casing typically 13-3/8 inch at 200-350 ft, but sometimes 9-5/8 or 8-3/8 inch; production casing 5½ or 7 inch at 6,500 ft, all holes cemented**Discovery Well****Name:** Conoco #1 Wright**Location:** NW-SW-NW-25-T36N-R64W**Completion Date:** 6/18/1944**Perforations:** 3,850 ft (Fall River Ss.)**Reservoir Data: Fall River Sandstone****Discovery:** 6/18/44, Conoco #1 Wright, NW-SW-NW-25-T36N-R64W**Lithology:** Sandstone**Age:** Lower Cretaceous**Type of Trap:** Structural; anticline**Gross Thickness of Reservoir Rock:** 65 ft**Oil Character:** Brownish-green; gravity 41.9° API; pour point 50°F**Oil Analysis:** Light gasoline 7.5%

Naphtha 26.9

Kerosene & gas oil 30.2

Lubricating oil 17.1

Residuum 17.8

Nitrogen 0.027

Sulfur 0.06

Cumulative Production (1944-1958): 3,571,351 BO at Little Buck Creek; 294,288 at Little Buck Creek South**Estimated Primary Recovery:** Not reported**Type of Secondary Recovery:** Not reported**Estimated Ultimate Recovery:** Not reported**Reservoir Data: Minnelusa Formation, 1st & 2nd Converse Sands****Discovery:** 1948**Lithology:** Sandstone**Age:** Permian**Type of Trap:** Structural; anticline**Oil Character:** Brown to black; gravity 35.0° API; pour point less than 5°F

TABLE 5.2 Continued

Oil Analysis:	Light gasoline	8.6%
	Naphtha	25.4
	Kerosene & gas oil	33.0
	Lubricating oil	15.8
	Residuum	16.5
	Nitrogen	0.09
	Sulfur	0.77

Water Resistivity: 0.1 to 0.3 ohm-meters²

Cumulative Production (1948-1958): 792,585 BO

Estimated Primary Recovery: Not reported

Type of Secondary Recovery: Not reported

Estimated Ultimate Recovery: Not reported

Reservoir Data: Minnelusa Formation, 1st and 2nd Leo Sands

Discovery: 1949

Lithology: Sandstones interbedded with carbonates and clastics

Age: Pennsylvanian

Type of Trap: Structural; anticline

Oil Character: Brown to black; gravity 33.4° API; pour point less than 5°F

Oil Analysis ¹ :	Light gasoline	7.7%
	Naphtha	24.7
	Kerosene & gas oil	32.5
	Lubricating oil	16.3
	Residuum	18.5
	Nitrogen	0.136
	Sulfur	0.63

Water Resistivity: 0.1 to 0.3 ohm-meters²

Cumulative Production (1949-1958): 2,144,266 BO

Estimated Primary Recovery: Not reported

Type of Secondary Recovery: Not reported

Estimated Ultimate Recovery: Not reported

¹ Includes Little Buck Creek South

² Average for the entire Minnelusa

³ Refers to 1st Leo sand only

Well-Casing Information

Surface casing 8-3/8 to 13-5/8 inches (21.3-34.6 cm) in diameter is set to between 200 and 350 feet (61-107 m). Production casing is typically 5-1/2 or 7 inches (14.0 or 17.8 cm) in diameter, is set to total depth, and is cemented. Well-casing models use a worst-case 7-inch casing diameter. It should be noted, however, that there is considerable ambiguity as to how many and which wells were actually cased at the time of the survey. Since production from Little Buck Creek is in steep decline, many of the wells are shut in or abandoned, and some wells are pumped only periodically. Casings from other wells have probably been pulled. Hence, well-casing models should be regarded with even more caution than usual.

5.3 DISCUSSION OF THE DATA

Introduction

A resistivity/phase crew of eight persons, headed by geophysicist Norman R. Carlson, was mobilized to the Little Buck Creek area on August 22, 1979. Data were collected using 1,000 foot (305 m) dipoles along two lines which intersected near the center of the field. Frequencies of 0.125, 0.25, 0.5, and 1.0 Hz were used. Data acquisition was slowed by some unexpected permitting problems, afternoon thunderstorms, and noise due to culture. The field work was completed on September 3. Total surface coverage for the project was 7.0 line-miles (11.3 line-km); total sub-surface coverage was 4.0 line-miles (6.4 line-km).

Cultural effects were particularly troublesome on this survey. The numerous powerlines and cathodically-protected pipelines caused a significant amount of noise. Fortunately, the crew was able to have the cathodic protection on the pipelines turned off during most of the data acquisition. In addition to noise, surface culture at Little Buck Creek also created intensive current channeling effects which must be considered in the interpretation.

The apparent resistivity, apparent polarization, and REM data are presented as Plates 5.1 and 5.2 at the back of this chapter. They may be unfolded for reference while reading the text.

Line 1 Interpretation

Line 1 was run along the long axis of the Little Buck Creek Field at an orientation of N 5° W. The field data are presented in Plate 5.1.

APPARENT RESISTIVITY DATA

Background resistivities on line 1 are about 7 to 8 ohm-meters, and a subtle high-over-low resistivity layering situation can be seen. These observations are in substantial agreement with electric log resistivities, which are summarized in Figure 5.8.

A very dramatic, chevron-shaped anomaly is centered on station 7. The low resistivity, right-plunging 5,6 and 6,7 diagonals, and the even lower resistivity left-plunging 7,8 and 8,9 diagonals, are due to near-surface features. These features are almost certainly caused by culture, in the form of well casings, pipelines, powerlines, or fences. The data are so badly contaminated by cultural effects that they are severely restricted for purposes of hydrocarbon interpretation. As indicated in section 2.2, this kind of contamination occurs over roughly 10 percent of the lines run over oil and gas fields. This particular example is one of the most spectacular cases we have seen.

The source of the contamination is of relatively minor interest, so it will be discussed only briefly. As noted earlier, it is not known which of the many wells were cased at the time of the survey. It is assumed for the sake of well-casing modeling that all wells were cased. Figure 5.9 presents the modeling results from the Holladay and West (1982) "PIPE" algorithm; 30 wells within 2.2 a-spacings of the line were included in the model. The strongest calculated effect from these casings occurs at depth; the strong, near-surface, low resistivity zone and associated diagonals are not shown, even in a qualitative sense. The model grossly "overmodels" the field data, possibly because not all wells were cased at the time of the survey. Modeling selective well-casings shows a better qualitative match to the data, although the magnitude of the effect is much lower than that seen in the data. As an experiment, two specific well casings (0.3 a-spacings from station 7.2, and the one directly on line at station 7.4) were used in a model to achieve a best fit; the addition of any

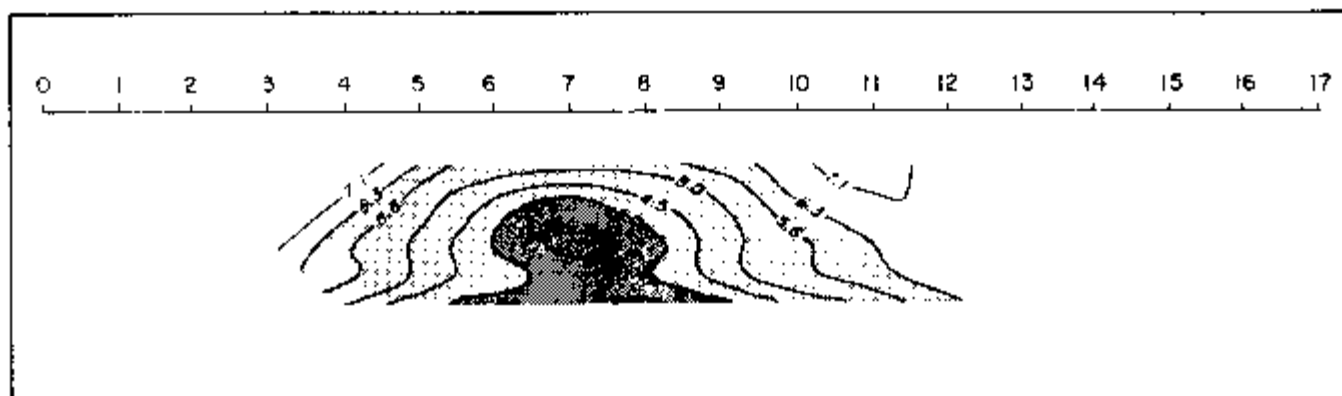


Figure 5.9. Well-casing model of apparent resistivity data for line 1, Little Buck Creek Field. Model parameters: 30 cased wells, casing diameter = 5-1/2 inches (14.0 cm), casing resistivity = 2.0×10^{-7} ohm-meters, surface impedance = $0.5 \pm 0.5i$, background resistivity = 7 ohm-meters. Figure 5.5 shows well locations.

other casings destroyed any resemblance to the field data. Therefore, it is unlikely that well-casing effects contribute heavily to contamination of the data.

The most likely explanation for the contamination is the combined effect of pipelines crossing the line at stations 6.3, 6.7, and 7.4. The pipeline effect appears to overwhelm any well-casing effects present in the data.

It is curious to note the unpredictability of contamination by surface culture on line 1. Effects due to the pipelines between stations 6 and 8 dominate the pseudosection, while the pipeline at station 4.3 seems to have no effect at all. Similarly, the fence at station 1.1 shows a strong near-surface response (right-plunging 1,2 diagonal), yet the fences at stations 2.6 and 11.2 show no response, despite the fact that all fences in the area are similar in construction. This illustrates the difficulty of modeling such features.

APPARENT POLARIZATION (DECOUPLED PHASE ANGLE) DATA

The relatively non-responsive background polarization on the line is dominated by effects due to surface culture. Modeling (Figure 5.10) suggests that surface pipelines, rather than well casings, cause the chevron-shaped anomaly. The data are heavily contaminated, but there is a slight indication of a mildly polarized zone which may be correlated with the lateral extent of the hydrocarbons. However, the case for this observation is rather weak, and the response seen in the data would represent a very poor drilling target if this project were a wildcat survey.

RESIDUAL ELECTROMAGNETIC (REM) DATA

The REM data are severely contaminated by culture, probably in the form of surface pipelines, and no residual anomaly which correlates with the hydrocarbons can be discerned. The broad, weaker conductive REM anomaly at depth could be due to hydrocarbon alteration, but the strong near-surface conductive feature tends to override the weak response at depth.

Line 2 Interpretation

Line 2 was run east to west, roughly perpendicular to line 1. The field data are presented in Plate 5.2.

APPARENT RESISTIVITY DATA

Resistivity layering is a very subtle high-over-low, with most apparent resistivities falling in the 6 to 8 ohm-meter range. This is in agreement with the results for line 1 and with the electric log resistivities of Figure 5.8.

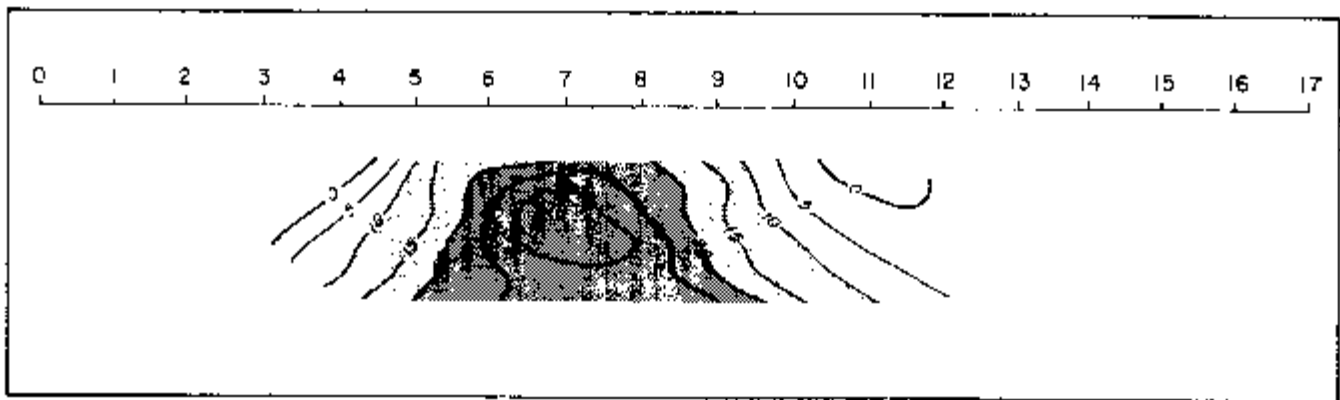


Figure 5.10. Well-casing model of apparent polarization data for line 1, Little Buck Creek Field. Model parameters: same as in Figure 5.9. Figure 5.5 shows well locations.

A 1 ohm meter (20 percent) depression in the observed apparent resistivities occurs at depth on the western end of the line. This low resistivity zone shows a moderately good correlation to the lateral extent of the hydrocarbons, although the zone of lowest resistivities is offset to the eastern edge of the field.

In order to obtain a qualitative estimate of well-casing effects, the "PIPE" program of Holladay and West (1982) was applied to the data. A total of 28 wells within 4.9 a-spacings of the line were included. As noted earlier, it is not known how many of these wells were cased at the time of the survey, so this modeling exercise is very subjective; hence, no well-casing residual data have been calculated.

Figure 5.11 shows the model results. The calculated well-casing effect is fairly symmetrical about the field, centered on station 12. The magnitude of the calculated well-casing effect matches the field data very well, and the appearance of the model data strongly resembles the appearance of the field data. However, note that the model calculates a maximum effect at depth which is approximately 1,500 feet (450 meters) west of the anomaly in the field data. In order to explain the anomaly completely in terms of well-casing effects, one would have to postulate that the shift is due to a much higher response from wells toward the east (a statistical improbability, since all wells are roughly the same age, and hence should have similar surface impedances), or that wells toward the west are mostly uncased (which is untrue, according to Conoco (1983)).

From the preceding discussion, it is probably safe to conclude that, while the match between model and field data suggests that a portion of the field response may be due to casing effects, there is a residual, low-amplitude response at depth on the eastern edge of the field which is probably not due to well casings. This response cannot be explained in terms of surface culture; indeed, there is no evidence that any of the surface culture encountered on line 2 affects the data at all. Neither can the response be explained by topographic effects, which are negligible on this survey, or by subsurface structure, which is horizontally layered over the field. Instead, the response is probably due to a very subtle, lateral resistivity change in the sediments above the field.

There are two points to be noted about the anomaly. First, its magnitude is so low that, assuming well-casings have had the effect described above, the residual target would probably be overlooked in rank exploration work. Hence, for all practical purposes, only a very poor anomaly is seen in the apparent resistivity data. Secondly, since the anomaly is not very well correlated with the lateral extent of the

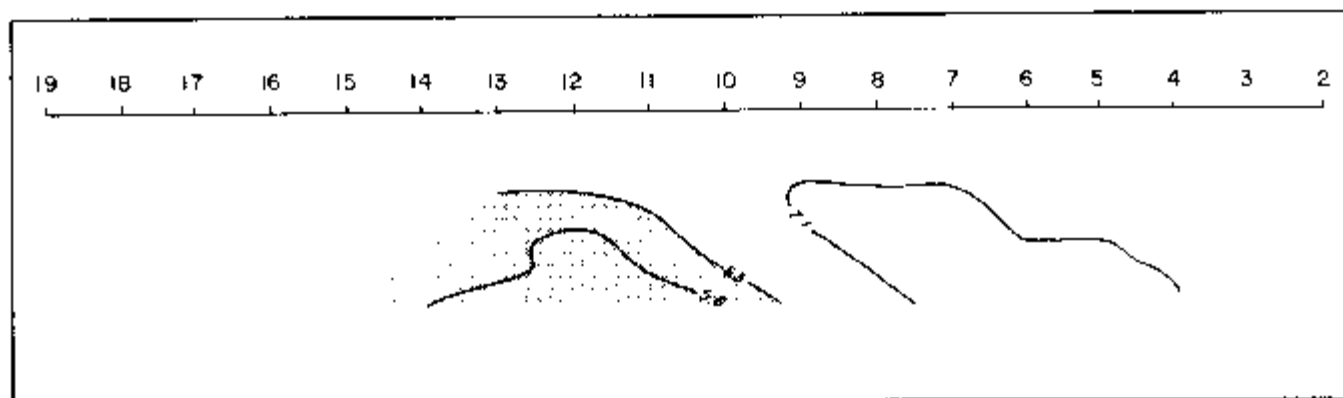


Figure 5.11. Well-casing model of apparent resistivity data for line 2, Little Buck Creek Field. Model parameters: 28 cased wells, casing diameter = 5-1/2 inches (14.0 cm), casing resistivity = 2.0×10^{-7} ohm-meters, surface impedance = $0.5 + 0.5i$, background resistivity = 7 ohm-meters. Figure 5.5 shows well locations.

hydrocarbons, it could easily be a slight facies variation within the Cretaceous shales and sandstones of the Fox Hills and Pierre formations—a variation which would have no causal link to the hydrocarbons at depth. Alternatively, the anomaly could be due to a column of weak, hydrocarbon-related electrochemical alteration which, perhaps due to local horizontal groundwater flow, is displaced from the oilfield to the east. Since no substantive information on groundwater flow has been found, this possibility cannot be confirmed or disproved.

The lack of a well-defined apparent resistivity anomaly on line 2 may be related to the fact that reserves at Little Buck Creek Field are nearly depleted and reservoir pressures are reduced. This matter is discussed in the Conclusions at the end of this chapter.

No other conductive features are found at depth. Two shallow zones whose resistivities are slightly lower than background are found between stations 8 to 9 and between stations 3.5 to 5. There is some chance that these are related to a conductive REM anomaly found at depth on the east end of the line, as will be noted in the discussion of the REM data.

APPARENT POLARIZATION (DECOUPLED PHASE ANGLE) DATA

Polarization layering is low-over-high on line 2, although the background rocks are all considered to be relatively non-polarizable. A slight amount of noise is evident in the pseudosection, although the overall interpretation is not affected. Only the small zone of values in the 10 to 15 milliradian range on the west-central portion of the line is of much interest. This zone corresponds to the low-resistivity zone noted earlier; it lies on the eastern edge of the producing field.

A well-casing model of the polarization data was run, and the results are shown in Figure 5.12. Although the model shows too high a polarization effect, note that the calculated response is centered at depth between stations 11 and 13, or between stations 10 and 14 near the surface. The model response is thus shifted 2,000 to 3,500 feet (600-1,100 m) to the west of the peak field response. Thus, it seems that a small polarization effect independent of well-casing effects is observed on the eastern edge of the field. Again, there are no obvious effects due to surface culture or subsurface culture, so the remaining possibilities are either that the slight rise in polarization is due to a slight facies change which is unrelated to the hydrocarbons at depth, or that it is due to alteration of Cretaceous sediments by upward migrating hydrocarbons from their traps below.

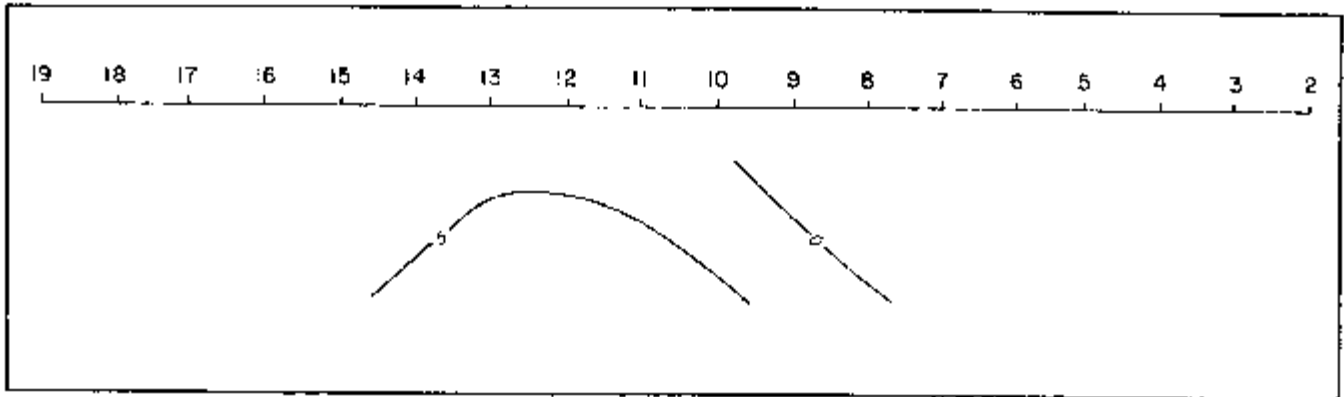


Figure 5.12. Well-casing model of apparent polarization data for line 2, Little Buck Creek Field. Model parameters: same as in Figure 5.11. Figure 5.5 shows well locations.

In any case, the polarization anomaly, while better defined than the apparent resistivity anomaly, is considered poor to fair at best. It would not make a strong exploration target if found on a line run over a prospect. The lack of a good anomaly may be due to depletion of the reservoir at depth, as discussed in the Conclusions.

RESIDUAL ELECTROMAGNETIC (REM) DATA

The REM data show a high-over-low resistivity layering picture, as seen in the apparent resistivity data. Superimposed upon this layering are two conductive zones at depth, one in the west-central portion of the line, and the other on the eastern end of the line.

The anomaly in the west-central portion of the line is fairly well defined but its magnitude with respect to background is not very impressive except at the $n=6$ level. The most conductive zone lies on the eastern edge of Little Buck Creek Field, and therefore the correlation to the hydrocarbons is not particularly good. This displacement is identical to the displacement of the apparent resistivity and polarization anomalies. The conclusion is the same as before: even assuming that the calculated well-casing effect is correct, a very subtle, residual anomaly unrelated to well casings lies at depth on the eastern edge of the field. Since the REM data appear to have a greater depth of penetration on this survey than do the galvanic data, it is not surprising that the REM anomaly is better defined than the galvanic anomalies, although it is no better than "fair" in quality. The lack of evidence for cultural or structural effects in the data indicates that the anomaly is due to some lateral resistivity change in Cretaceous sediments. This change could involve a minor facies change which is unrelated to the presence of hydrocarbons at depth, or it could be due to an alteration column caused by upward migration of hydrocarbons from the trap at depth.

The most interesting REM feature on line 2 is found on the east end of the line, in a region in which hydrocarbon production has not been established. The anomaly is fairly well defined; if well-casing effects on the REM data to the west could be removed, the relative definition of this feature would appear to be even better. There is little evidence of an associated anomalous response in the apparent resistivity or apparent polarization data. The very subtle, near-surface, low-resistivity zone between stations 3.5 and 5 may be due to some sort of alteration which is associated with the deeper data.

5.4 CONCLUSIONS

Little Buck Creek Field

REVIEW OF THE DATA

The data for line 1 of the Little Buck Creek survey are overwhelmingly contaminated by strong effects due to surface pipelines, with possible secondary contributions from well-casings, a fence, and a powerline. The apparent resistivity and REM data are virtually impossible to use for hydrocarbon interpretation. The apparent polarization data are also severely affected, but there is some indication that slightly high polarization values may be associated with the sediments which overlie the hydrocarbon trap.

The situation from a cultural standpoint is better on line 2. Apparent resistivity, REM, and polarizable anomalies are seen at depth on the eastern edge of the producing field. These features cannot be explained by well-casing effects, although such effects may very well increase the magnitude of these anomalies. Surface culture appears to have a minimal impact on these data. The effects of subsurface structure and topography are also minimal due to the flat-lying stratigraphy and the essentially flat ground. Therefore, it is believed that lateral alteration features in Cretaceous sediments between 1,000 and 2,000 feet (300-600 m) produce the very subtle, low resistivity anomaly and the slightly more obvious polarization and REM anomalies.

The changes in the data may or may not be related to the presence of hydrocarbons at depth. For example, they might be due to a lateral facies change. However, the limited lateral size, substantial depth extent, high correlation of low resistivities to high polarizations, and proximity of the anomalies to the producing oilfield make this explanation somewhat unlikely. Instead, it is more probable that the lateral electrical changes in Cretaceous sediments are causally connected to the hydrocarbons at depth.

GEOLOGIC INTERPRETATION

The subtlety of the anomalies measured over Little Buck Creek may provide important confirming information regarding the anomaly mechanisms discussed in section 2.4. As noted in the geologic description, some 12 million barrels of oil have been recovered from Little Buck Creek and Little Buck Creek South over the past 39 years. Currently, 34 intermittently producing wells yield a field total of less than 50 barrels of oil per day. Hence, the recoverable reserves in the field are nearly exhausted.

The decrease in reservoir pressurization which certainly accompanies the depletion of oil has probably greatly diminished the driving mechanism for vertical migration. As noted in section 2.4, the chief mechanism for expelling light hydrocarbons and saline waters from a trap is believed to be hydraulic in nature. With decreased reservoir pressure, the solubility of salts in the local water system would be greatly reduced. The result would be salt precipitation and a consequent increase in pore fluid resistivity. Hence, the apparent resistivities would be increased over the trap. On the other hand, the shallower anomaly, which consists of mineralization and alteration phenomena, might remain as a fossil anomaly, providing it were not subject to disruptive effects, such as oxidation from surface water recharge.

The subtle anomalies on the eastern edge of the Little Buck Creek Field may reflect the final phase of vertical migration from the field, calling to mind the disappearing geochemical anomaly measured by Horvitz (1969) over Hastings Field in Texas. The remnants of the deep anomaly are picked up in a weak REM response

and a weaker resistivity response; these data suggest that the anomaly mechanism is not yet completely neutralized. The polarization anomaly may reflect some low-grade mineralization or clay alteration over the field. The fact that the anomalies are shifted toward the east side of the field is enigmatic; perhaps local trends in ground-water flow have contributed a slight horizontal component to the otherwise vertical migration pattern.

The Undrilled Anomaly

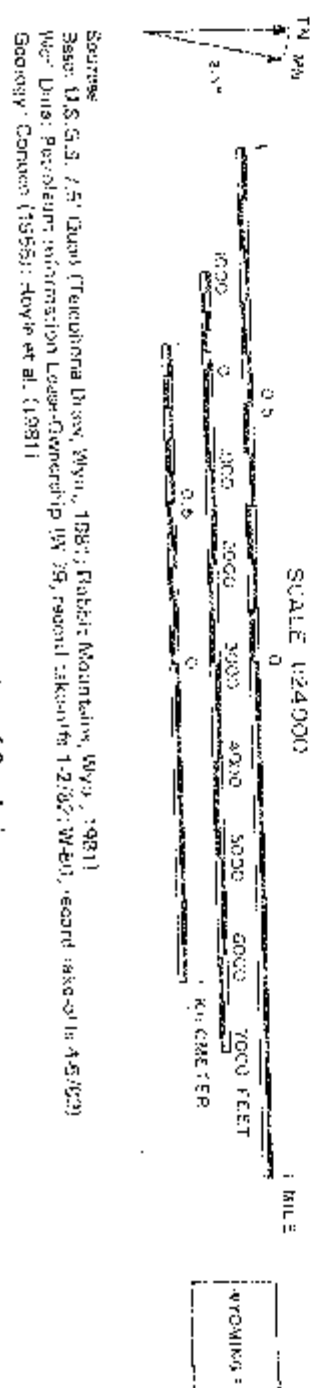
The conductive REM anomaly between stations 3 and 6 on line 2 represents a potentially attractive drilling target on the basis of this set of data. The anomaly has a fairly well defined pattern and shows a 2:1 contrast with respect to background. It is not associated with any anomalous polarization values, but there may be a subtle conductive surface expression in the apparent resistivity data.

In order to exploit this target properly, we would suggest running a north-south cross line, intersecting line 2 at station 4. The data should then be correlated with subsurface geology and seismic data in order to determine the attractiveness of a drilling program. On the basis of the electrical data alone, the best drilling location would probably be directly on station 4.

REFERENCES

- Conoco, 1983, personal communication from company geologists.
- Denson, N.M., and Horn, G.H., 1975, Geologic and structure map of the southern part of the Powder River Basin, Converse, Niobrara, and Natrona Counties, Wyoming (east part): Dept. of the Interior/U.S.G.S. misc. investigations series map I-877, sheet 2.
- Foster, D.L., 1958, Summary of the stratigraphy of the Minnelusa Formation, Powder River Basin, Wyoming, *in* Powder River Basin: 13th annual field conference guidebook, Wyoming Geol. Assn., p. 39-44.
- Holladay, J.S., and West, G.F., 1982, Effects of well casings on surface electrical surveys (abs.): *Geophysics*, v. 47, p. 439. Full paper available in Technical papers, 51st Annual International Meeting and Exposition, SEG, Los Angeles, v. 2, p. 815-838.
- Horvitz, L., 1969, Hydrocarbon geochemical prospecting after thirty years, *in* Unconventional methods in exploration for petroleum and natural gas: Dallas, Texas, Southern Methodist University, p. 135-149.
- Hoyle, B.L., Kraus, G.P., and Swanson, J., 1981, Lance Creek East, *in* Oil and gas fields of the Powder River Basin, vol. 2: Wyoming Geol. Assn., p. 242-243.
- Maynard, J.L., Rickles, S.E., Sackreiter, D.K., and VerSteeg, D.J., 1981, Salt Creek, *in* Oil and gas fields of the Powder River Basin, vol. 2: Wyoming Geol. Assn., p. 358-361.
- Petroleum Information, 1982, Lease-ownership maps W-79, W-80 (record takeoff dates 1/82-5/82).
- Strickland, J.W., 1958, Habitat of oil in the Powder River Basin, *in* Powder River Basin: 13th annual field conference guidebook, Wyoming Geol. Assn., p. 132-147.
- Swan, B.G., 1947, Geophysical history of East Lance Creek and Little Buck Creek fields, Niobrara County, Wyoming: *Geophysics*, v. 12, p. 153-158.
- Tromp, P.L., Cardinal, D.F., and Steidtmann, J.R., 1981, Stratigraphy and depositional environments of the "Leo Sands" in the Minnelusa Formation, Wyoming and South Dakota, *in* Energy resources of Wyoming: 32nd annual field conference guidebook, Wyoming Geol. Assn., p. 11-22.
- Ver Ploeg, A.J., and Oliver, R.L., 1981, Wyoming's oil and gas industry—past, present, and future, *in* Energy resources in Wyoming: 32nd annual field conference guidebook, Wyoming Geol. Assn., p. 65-81.
- Waage, K.M., 1958, Regional aspects of Inyan Kara stratigraphy, *in* Powder River Basin: 13th annual field conference guidebook, Wyoming Geol. Assn., p. 71-76.
- Wenger, W.J., and Reid, B.W., 1958, Characteristics of petroleum in the Powder River Basin, *in* Powder River Basin: 13th annual field conference guidebook, Wyoming Geol. Assn., p. 148-156.
- Wyoming Geol. Assn., 1955, Little Buck Creek and Little Buck Creek South, *in* Wyoming oil and gas fields: Wyoming Geol. Assn., p. 262.

Figure 5-B
STRUCTURE MAP-TOP OF FALL RIVER SANDSTONE
Little Buck Creek Field
Madison Co., Wyoming



Source: U.S.G.S. 7.5' Quad (Treadwell, Wyo., 1981); Public Mountain, Wyo., 1981
Well Data: Petroleum Information Cooperation (WIC) Report (WIC-1), record (WIC-1) 451021
Geology: Canyon (1955); Hoyt et al. (1981)

Explanation of Symbols

Standard Well Symbols

- Drilling for which information is undetermined
- Drilling in progress at time of map preparation
- Shut in
- Abandoned
- Dry hole with total depth indicated
- Oil well
- Gas well
- Oil and gas well
- Gas injection well
- Water injection well
- Water well

Captive Symbols

- Meter pipeline, presumed grounded
- Ungrounded pipeline non-metal or suspended
- Metal fence
- Electric fence
- Buried telephone or power cable
- Telegraph line or standard voltage power line
- Major high voltage power line
- Radio, microwave, or other communications station or tower
- DC jump

Special Well Symbols

- Drilling in progress at the time of the electrical survey; number indicates the amount of cello tape in the hole at the time of data collection
- Well spudded in after completion of the electrical survey
- Number indicates distance of well from the line in terms of 2500 ft. at wells within 1000 ft. boundaries indicated (randomness only)

Other Symbols

- U.S.G.S. standard symbols or as labeled

Map Specific Symbols

Structure contour interval: 10 feet

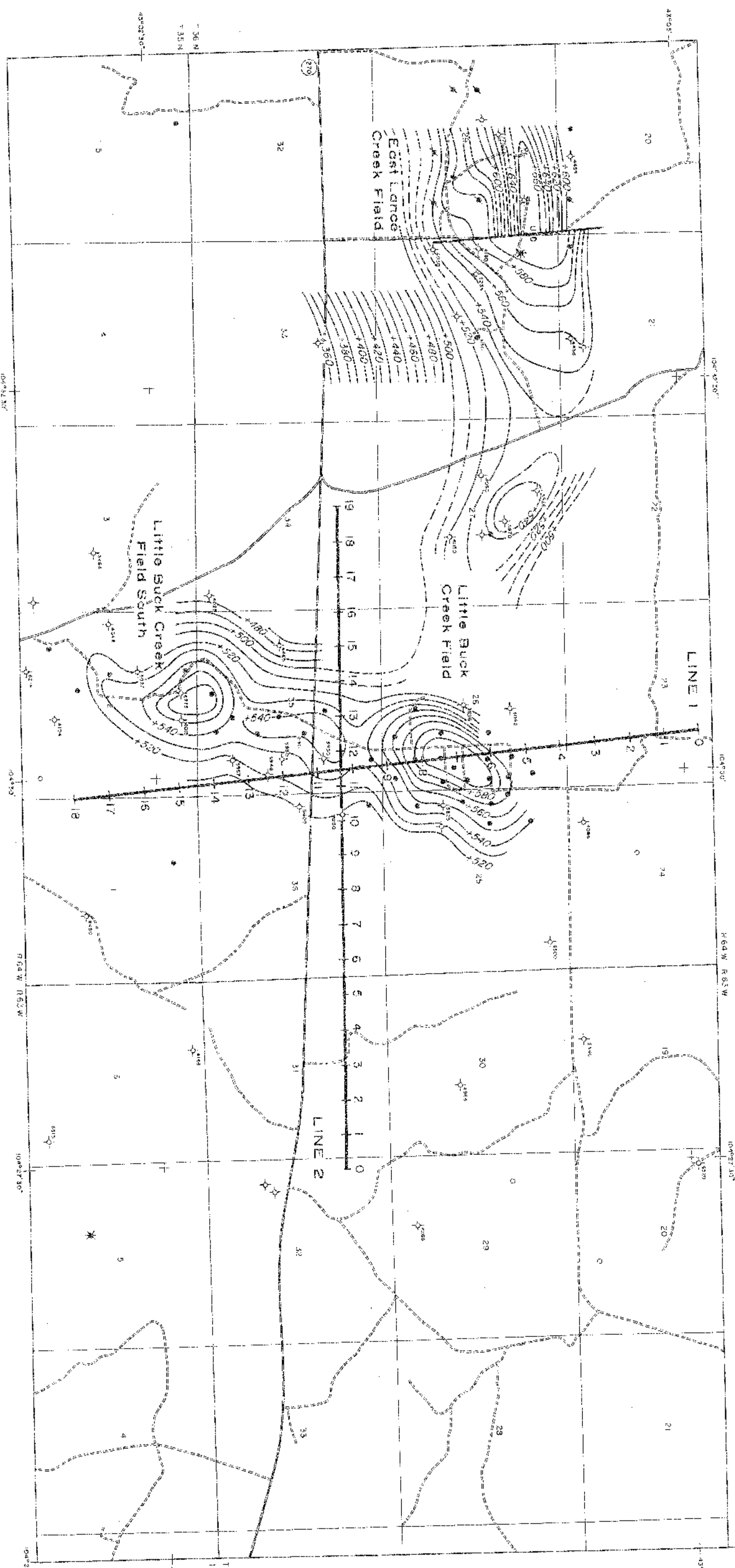
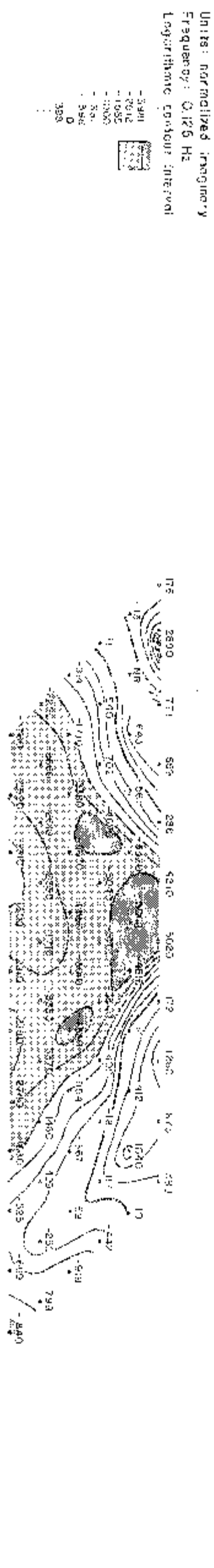
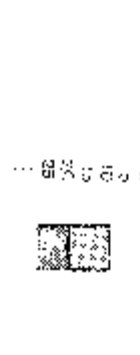
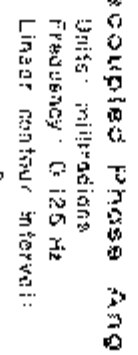
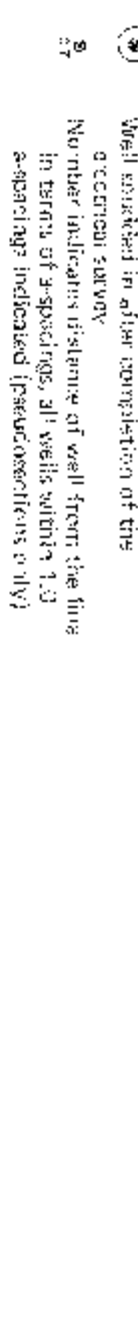
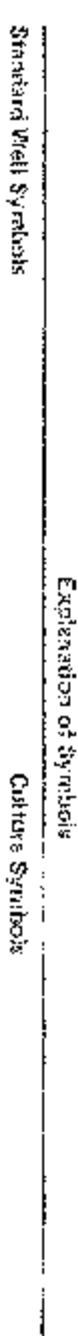


Plate 5.1
RP Field Data
Little Buck Creek Field
Line 1



Chapter 6

Lisbon Field

San Juan County, Utah

6.1 INTRODUCTION

Lisbon Field is located in the Paradox Basin, some 32 miles (51 km) south of Moab, Utah (Figure 6.1). The field lies on the western flank of the northwest-trending Lisbon Valley-Dolores Anticline, one of the five major salt folds in the basin. Oil and gas are produced from the Mississippian Leadville Formation, with some of the wells acting as gas injection wells as a part of a pressure-maintenance program. Hydrocarbon accumulation is controlled by a faulted anticline in the Paleozoic rocks, a structure which is not directly related to the structure in the overlying salt.

Lisbon Field is a major producer for the area and was an important discovery by Pure Oil Company in 1960 not only because of its size, but also because it proved the reservoir potential of Mississippian and Devonian rocks in the Paradox Basin. Ultimate production is expected to be about 42 million barrels of oil and 250 billion cubic feet of gas, of which most of the oil and a small fraction of the gas have now been recovered.

Three lines of resistivity/phase data were run across Lisbon Field using a dipole spacing of 2,000 feet (610 m).

6.2 GEOLOGIC BACKGROUND

Exploration History of Lisbon Field

The Paradox Basin has had an erratic and not always successful exploration history. The first indication of hydrocarbons dates back to 1879, when E.L. Goodridge noted an oil seep near Mexican Hat, Utah. This was not developed commercially until a well was completed in the Rico Formation in 1908. After an initial surge of development, the Mexican Hat field was eventually abandoned, and subsequent activity in the Paradox Basin was sparse despite discoveries in adjoining provinces. Southeast Utah did not see another producer until the discovery of Crescent Junction Field in 1946.

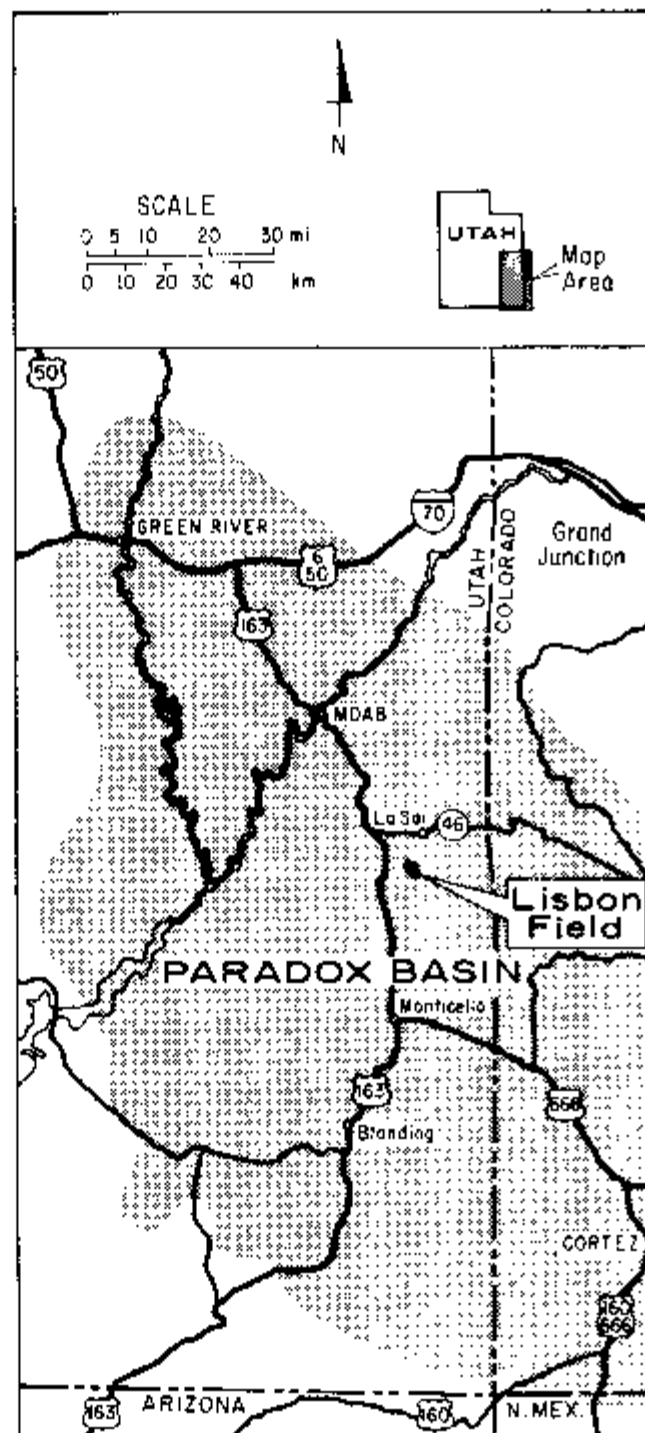


Figure B.1. Location map of Lisbon Field.

Exploration activity did not really pick up until it was realized that Pennsylvanian rocks constituted potentially attractive petroleum targets. The first significant Pennsylvanian production in Utah was recorded at Boundary Butte in 1948, followed by a Shell Oil discovery at Desert Creek six years later. A third, very significant discovery by Texaco in 1956 at Aneth Field finally erased the Paradox Basin's stigma of being a poor producing province.

While most of the industry focused attention on Pennsylvanian targets, the Pure Oil Company (now merged with Union Oil Company of California) began to explore for traps of Mississippian age. Pure's Big Flat discovery in 1957, which followed a program of geologic and seismic studies, was the first Mississippian discovery in the Paradox Basin. Although it proved to be a mediocre producer, the Big Flat find sparked a flurry of Mississippian tests during the next several years, none of which were successful.

Pure Oil was not deterred, and an ambitious program of geologic structure and seismic mapping was undertaken with the intent of finding promising anticlinal structures in Mississippian strata. This program identified two good targets southwest of the Lisbon Valley-Dolores salt anticline. The anticline had been mapped as early as the 1900s, and it was first drilled in 1927, but exploration for Paleozoic targets had been made difficult by the effects of the overlying Paradox Salt. Gravity methods were ineffective in the area, and seismic interpretation in the 1950s could not always distinguish reflections from the various lithologic units; indeed, the fault which bounds Lisbon Field to the northeast could not be distinguished on the basis of seismic data, but was inferred by correlation. In any case, Pure persevered and spudded wells on both of its targets in 1959. The discovery well at Lisbon was completed January 4, 1960, flowing 587 BOPD from the McCracken Sandstone of Devonian age. Declining production led to its recompletion in the Leadville Formation, a Mississippian unit, and the well was later reconverted to a McCracken oil producer and a Leadville gas injection well.

The discovery at Lisbon was marked as one of the most significant of 1960 in the United States. It proved the potential of Mississippian and Devonian strata in the Paradox Basin, although the promise of these strata has never been completely fulfilled. In addition to Lisbon Field, current Leadville producers in San Juan County include Big Indian (1961), Little Valley (1961), Cleft (1962), and Hook and Ladder (1977). None of these has been as successful as Lisbon, which continues to be a major producer in the area.

Recent exploration in the Paradox Basin has focused attention primarily on Pennsylvanian strata, especially the Ismay and Desert Creek zones of the Paradox Formation, which are easily the most productive in the area. The traps in these strata are both structural and stratigraphic in nature.

Geologic History of the Paradox Basin

The stratigraphic sequence at Lisbon Field is listed in Table 6.1. Most of the sediments were deposited in shallow water environments during episodes of tectonic subsidence. Local sedimentation patterns were heavily dependent on Precambrian, continental-scale rift development, and on the formation and flowage of Pennsylvanian salts.

About 1.5 billion years ago, a series of major rift systems developed in the western United States as a result of crustal compression from the north. As shown in Figures 6.2 and 6.3, two of these lineaments intersected one another on the northeastern boundary of the present-day Paradox Basin. The northeast trend, known as the Colorado Lineament, extended from the Grand Canyon area to Minnesota and was characterized by left-lateral normal faults. Its conjugate trend, the Olympic-Wichita Lineament, extended from Washington to southern Oklahoma, running northwest to southeast with right-lateral strike-slip displacement. Together these two trends produced Precambrian faults running northwest-southeast and folds running northeast-southwest. The faulting which developed during this time heavily influenced the later geologic history of the Paradox Basin.

TABLE 6.1: STRATIGRAPHIC DESCRIPTION OF LISBON FIELD

System	Symbol	Formation	Lithologic Description
MESOZOIC ROCKS			
Cretaceous	Kmc	Mancos Sh.	Shales, mudstones, and siltstones
	Kd	Dakota Ss.	Sandstones, conglomerates, shales, mudstones, and coal beds
(unconformity) -----			
Jurassic	Kbc	Burro Canyon Fm.	Sandstones, conglomerates, and mudstones
	Jm	Morrison Fm.	
	Jmb	Brushy Basin mbr.	Mudstones; minor limestones and shales
	Jms	Salt Wash mbr.	Sandstones and mudstones
	San Rafael Group		
	Js	Summerville Fm.	Sandy mudstones, shales, and fine-grained sandstones
	Je	Entrada Ss. Moab mbr. Slick Rock mbr.	Fine-grained eolian sandstone Fine-grained eolian and shallow marine sandstone with occasional coarse grains
Jurassic/Triassic	Jca	Carmel Fm. (Dewey Bridge mbr. of Entrada Ss.)	Siltstones, silty shales, gypsum, and thin beds of fossiliferous limestone
	(unconformity) -----		
	JTna	Glen Canyon Group Navajo Ss.	Cross-bedded eolian sandstone with a few cherty limestone beds
	JTka	Kayenta Fm.	Fine-grained sandstones, mudstones, and lacustrine limestones
	JTw	Wingate Ss.	Massive, cliff-forming, cross-bedded eolian sandstone
(unconformity) -----			
Triassic	Tc	Chinle Fm.	
	Tcc	Church Rock mbr.	Siltstones and fine-grained sandstones with no bentonite
	Tco	Owl Rock mbr.	Mudstones and thin lacustrine limestones with no bentonite
		Petrified Forest mbr.	Claystones, mudstones, siltstones, and some sandstones; bentonitic
	Tcm	Moss Back mbr.	Cross-bedded sandstone with conglomeratic limestone-chert-quartzite lenses, silicified wood, and bentonite; hosts uranium in Lisbon Field area
	Tcb	Monitor Butte mbr.	Claystones and clayey-micaceous sandstones; bentonitic
	Tcs	Shinarump mbr.	Conglomeratic basal sandstone with bentonite; hosts uranium in Monument Uplift area
	(unconformity) -----		
	Tm	Moenkopi Fm.	Fine-grained, cross-bedded sandstones, siltstones, and mudstones
PALEOZOIC ROCKS			
Permian	(unconformity) -----		
	Pc	Cutler Fm. Upper unit	Conglomerates, siltstones, mudstones, and arkosic sandstones; local cherts and limestones
	(unconformity) -----		
Permian	Lower unit		Mudstones and sandstones
	(unconformity) -----		

TABLE 6.1 Continued

System	Symbol	Formulation	Lithologic Description
Pennsylvanian	Phu	Hermosa Group	
		Honaker Trail Fm. (Upper Hermosa)	Fossiliferous limestone with sandstones, siltstones, mudstones, and shales; hosts minor amounts of hydrocarbons in the Paradox Basin
		Paradox Fm. Ismay zone	Dolomites, siltstones, shales, and anhydrites; hosts major amounts of hydrocarbons in the southern Paradox Basin
		Desert Creek zone	Hosts major amount of hydrocarbons in the southern Paradox Basin
		Paradox Salt (Akah and Barker Creek zones)	Salt with thin beds of shale, anhydrite, siltstone, and dolomite; fractured; <i>non-commercial oil in a 15-foot bed at Lisbon Field</i>
		Pinkerton Trail Fm. (Lower Hermosa)	Dolomites and limestones with some dolomitic siltstones, shales, and anhydrites
	Pm	Molas Fm. (unconformity)	Silty and sandy shales
Mississippian	MI	Leadville Fm. (Redwall Ls.)	Dolomitic and fossiliferous limestone with a weathered karst-type upper boundary; <i>dolomites host most of the hydrocarbons at Lisbon Field and at a few other Paradox Basin fields</i>
Devonian	Do	(unconformity)	
		Ouray Ls.	Limestone with poor porosity; <i>hosts non-commercial gas and condensate in more porous zones at Lisbon Field</i>
		Upper unit Lower unit	Dense lithographic limestone Medium crystalline limestone with thin beds of dolomite
	De	Elbert Fm. Upper mbr. McCracken Ss. mbr.	Arenaceous limestone with thin beds of shale Dolomitic sandstones, sandy dolomites, and dolomitic shales with erratic porosity and permeability; <i>hosts minor amount of oil at Lisbon Field</i>
	Da	Aneth Fm.	Glaucconitic dolomite with siltstone partings; hosts oil primarily at Aneth Field
Cambrian		(unconformity)	
	Cl	Lynch Dol.	Argillaceous dolomite with thin shale beds
	Clm	Maxfield Ls. (Muav Ls.)	
	Co	Ophir Sh. (Bright Angel Sh.)	Shale and siltstone
	Ct	Tentic Qtzite. (Tapeats Ss.)	Shale and siltstone at top grades downward to coarse-grained sandstone
PRECAMBRIAN ROCKS			
Precambrian	pC	(unconformity)	Granitic and metamorphic rocks

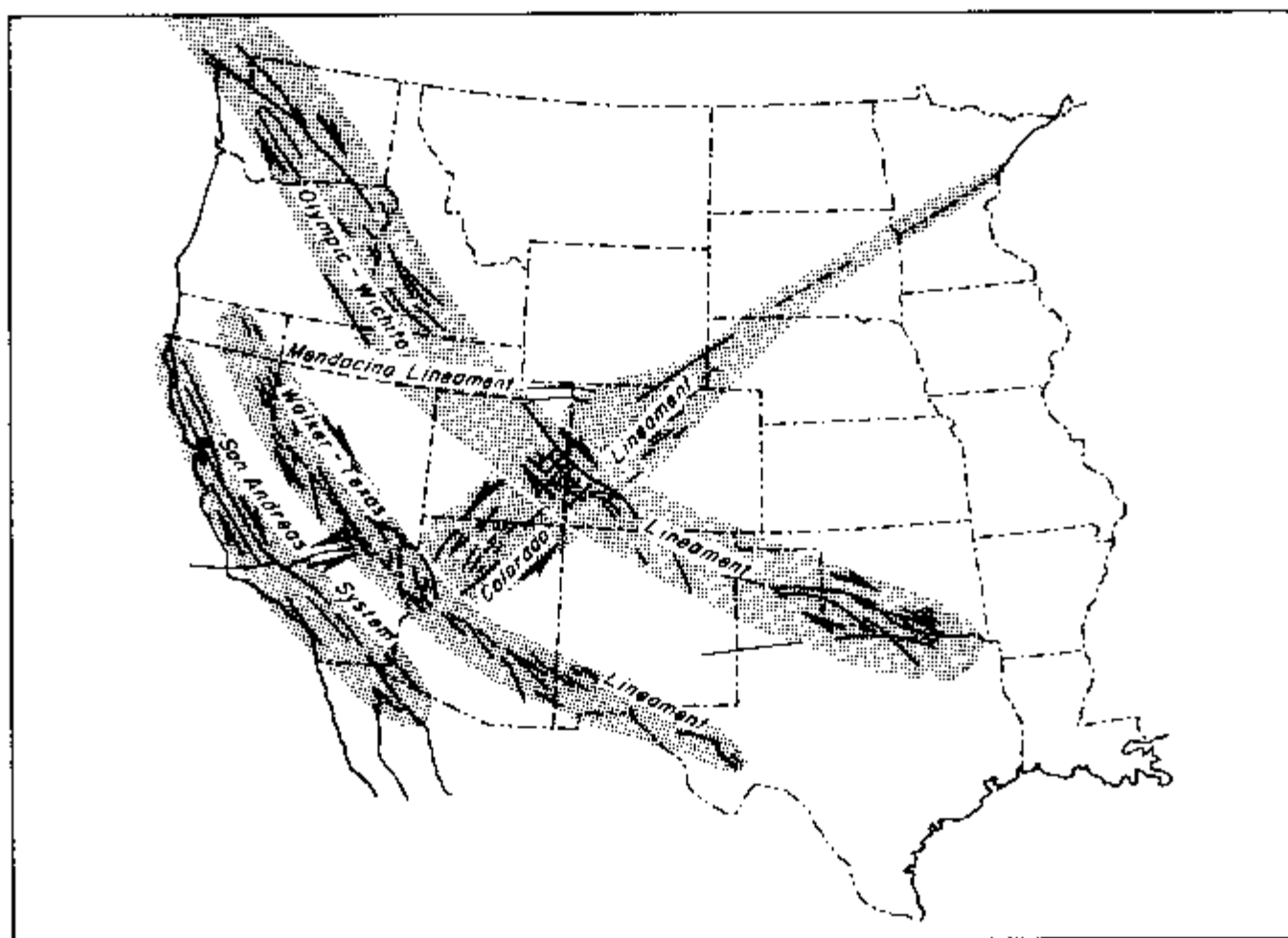


Figure 6.2. Major Precambrian lineaments. Arrows show the sense of strike-slip offset. After Baars and Stevenson (1981).

The early Paleozoic period in the Paradox Basin area was relatively quiescent tectonically, although minor fault movement, subsidence, and uplift contributed to local changes in depositional patterns. The first Paleozoic sediments were laid down in the middle-to-late Cambrian as a transgressive marine and littoral sequence advancing from the west. Uplift during the early Ordovician resulted in non-deposition or complete erosion of sediments from Ordovician to mid-Devonian in age. The only exception appears to be the Aneth Formation, a thin lens of siltstones and dolomites of mid-Devonian age which extends over the south central portion of the Paradox Basin. The Aneth is a producing zone at Aneth Field but is not present at Lisbon Field.

Subsidence during the late Devonian and early to middle Mississippian permitted the transgression of waters from the west and the south, resulting in deposition of the reservoir rocks at Lisbon Field. Devonian sediments in the area involve three units. The McCracken Sandstone, which is the basal unit of the Elbert Formation, consists of sandstones, dolomites, and shales. The Upper Elbert consists of limestones, shales, and dolomites. The Ouray Limestone is made of relatively dense limestones. Shows of gas have been found in all three units, but only the McCracken

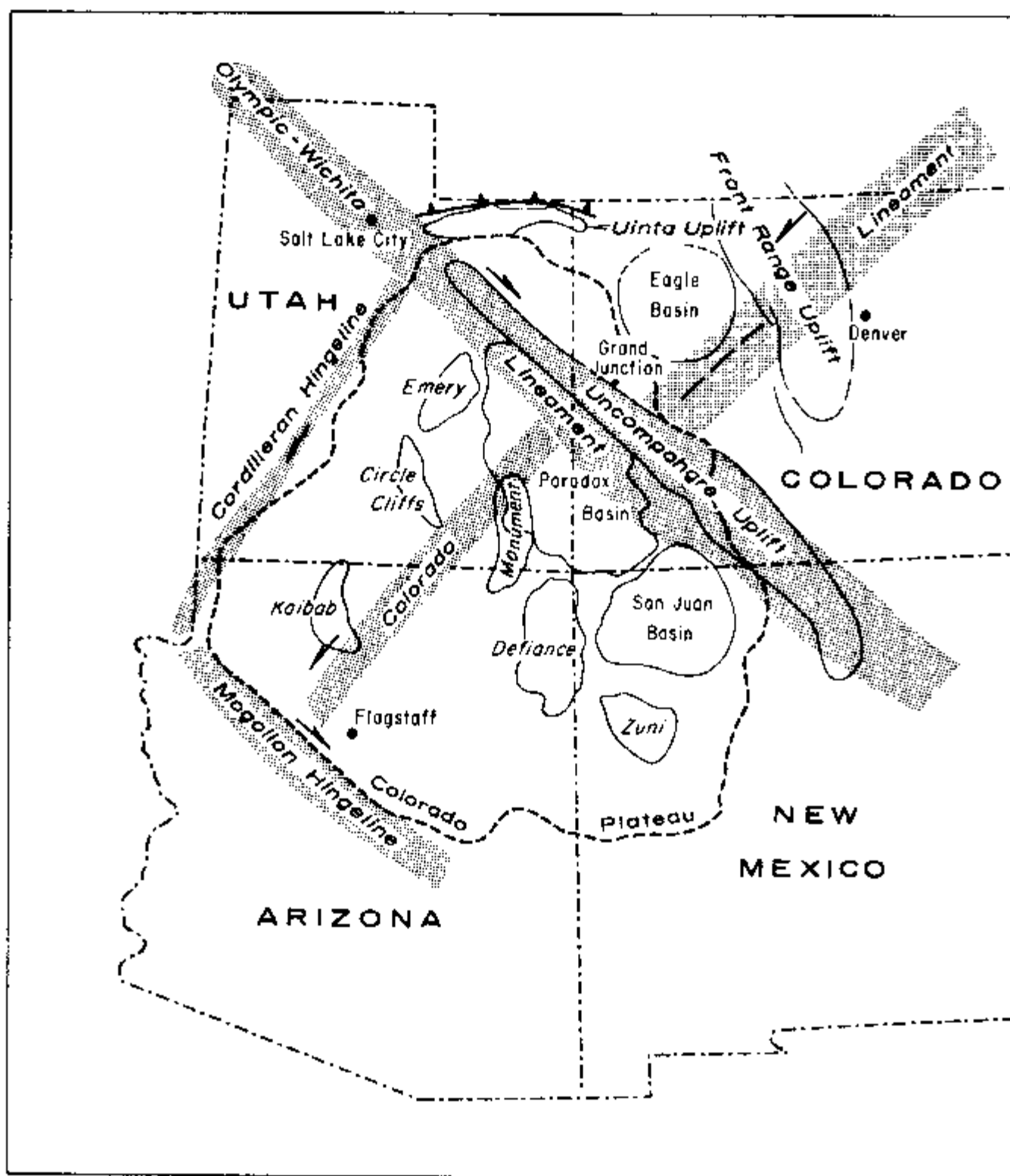


Figure 6.3. Map of the major structural features affecting Paleozoic sedimentation in the west-central United States. Compare this with Figure 6.2. After Baars and Stevenson (1981).

has proved productive (and only marginally, at that). Mississippian sediments were deposited on a broad, shallow marine shelf which dipped gently to the northwest. The single Mississippian unit in the Paradox Basin is the Leadville Formation (known elsewhere as the Redwall Limestone) which constitutes the chief economic reservoir at Lisbon Field.

Tectonic activity slowly increased in late Mississippian time, accelerating in the Pennsylvanian to form the basis of the Rocky Mountain uplift. In the Paradox Basin, the most important features of this event were the Uncompahgre Uplift to the northeast and the Defiance Uplift to the south (Figure 6.3). These features, plus concurrent right-lateral offset along the Olympic-Wichita Lineament, contributed to the formation of the first major topographic expression of the Paradox Basin. Mississippian rocks, which formed the tops of the uplifted areas, were severely eroded, and clastic debris up to 20,000 feet (6,000 m) in thickness was deposited in the low-lying areas from source materials in the Uncompahgre Uplift. The eroded surface of the Mississippian rocks developed a karst topography which is preserved at depth today, and which is also found in much of the central United States.

During the middle Pennsylvanian, the area underwent a period of subsidence due to continued fault movement and clastic deposition, allowing great thicknesses of evaporites to be accumulated. This material is known as the Paradox Salt, and its importance to the local geology is chiefly due to its flow characteristics. It is believed that lateral salt flow was initiated during deposition by the continued loading of arkoses and clastics from the northeast. The salt appears to have flowed laterally to the southwest at first, but this motion was inhibited by the succession of northwest-trending basement faults of the Precambrian Olympic-Wichita Lineament. The salt was then directed upward toward the surface along the fault faces, forming salt diapirs. Areas from which the salt had flowed became depressed and continued to be filled with erosional debris, maintaining the flow mechanism through Permian time.

Permian sediments consist of the Cutler Formation, derived at first from erosion of local hills and ridges, which were generally of low relief, and later from more distant sources. Tectonic activity ceased during Permian time, and the area remained relatively quiescent during the deposition and erosion cycles of the Mesozoic. Salt flow also slowed considerably at this time, although secondary flow from diapirs produced salt "pillows" in the basin.

A minor marine transgression occurred over the Colorado Plateau at the beginning of the Triassic. Waters were shallow and of low energy, producing the siltstones, fine-grained sandstones, ripple marks, and dessication features of the Moenkopi Formation. A change to primarily fluvial and lacustrine environments led to the deposition of Chinle sediments, beginning with bentonitic claystones, mudstones, siltstones, and sandstones, and ending with non-bentonitic units of otherwise similar lithology. The uranium deposits found at Lisbon Field are found in one of the bentonitic units of the Chinle, the Moss Back Member.

The Jurassic-Triassic Glen Canyon Group, consisting of the Wingate, Kayenta, and Navajo formations, probably represents a change to eolian and fluvial environments. The massive, cliff-forming, fine-grained Wingate Sandstone appears to be wholly eolian. The subsequent Kayenta Formation derives its sediments of sandstones, mudstones, and limestones from shallow lacustrine and fluvial sources. The spectacularly cross-bedded Navajo Sandstone is probably mainly eolian, but it also includes some playa-lake beds of cherty limestone.

A second transgression of Mesozoic seas during Jurassic time deposited the silty shales and silty sandstones of the San Rafael Group. Again, depositional environments were of low energy, involving shallow sea-floor sedimentation. Some

units appear to be eolian; particularly noteworthy among these is the Slick Rock Member of the Entrada Sandstone, which forms the beautiful and intricate arches and bridges at Arches National Park. Late Jurassic time brought the cross-bedded eolian sandstones, fluvial mudstones, and lacustrine limestones and shales of the Morrison Formation. Similar rocks were laid down to form the Burro Canyon Formation.

Transgression of the Jurassic-Cretaceous seas across the interior of the United States produced the mudstones, shales, and siltstones which characterize the Dakota Sandstone and the Mancos Shale of the Paradox Basin. Marine deposition was concurrent with the onset of the Laramide Orogeny. In most areas of the western United States, the Laramide was an extremely important event which shaped many of the geologic patterns we see today. It was also important in the Paradox Basin area, producing normal faulting with reverse drag on reactivated Precambrian fault patterns. Most of these faults were also overturned to the east, and the uplift of the Colorado Plateau caused streams to flow toward the southwest, cross-cutting the salt anticlines (hence the name "Paradox Basin"). Baars and Stevenson (1981) suggest that the elastic Paradox Salt was crucial in the area's resistance to the severe overthrusting and folding which characterizes the Cordilleran-Mogollon hingelines of Arizona and central Utah.

Salt flow in the Paradox Basin has continued unabated to this date, although not at the original rate established in Pennsylvanian time. It is important to note that the effects of salt flow have caused a wide difference in Paleozoic and post-Paleozoic structure. This fact has made successful seismic interpretation for anticlinal Paleozoic traps a challenging enterprise in the Paradox Basin.

Current Geology

The line location map, topography map, and geologic maps for the Lisbon Field project are presented in Figures 6.4 to 6.8. These maps may be compared to the cross-sections of Figures 6.9 and 6.10.

It is clear from the preceding discussion that the structure of the Paradox Salt is a dominant pattern in Paradox Basin geology. Figure 6.6 is a structural contour map of the top of the Paradox. The prominent northwest-southeast basement fault is flanked to the southwest by the Lisbon Valley-Dolores Anticline. Figure 6.7 shows that the anticline is due primarily to a thickening of the Paradox Salt unit, which is the result of Pennsylvanian and post-Pennsylvanian flowage.

The Paleozoic structure does not correspond directly to the Pennsylvanian structure, which is illustrated by the Mississippian structure map of Figure 6.8. Note the block faulting which is controlled by two high angle, northwest-southeast trending normal faults. The upthrown block on the southwest flank of the southwest fault forms several anticlinal closures which host hydrocarbons at the Lisbon, Hook and Ladder, and Little Valley fields. Big Indian and Wilson Canyon are found on the upthrown block of the northeast fault. It is worthwhile to note that there are alternative views of the secondary fault patterns depicted here (Smith and Prather, 1981).

The cross-sections A-A' of Figure 6.9 and B-B' of Figure 6.10 show the Lisbon Field structure from south to north and from southwest to northeast. The cross-section A-A' corresponds to the data of electrical line 1. The cross-section B-B', which can be compared to the data of electrical lines 2 and 3, clearly shows the thickening of the Paradox Formation northeast of the Mississippian anticline.

Plate 5.2
RESISTIVITY/PHASE RESOLUTION DATA
Little Buck Creek Field

Normal Co. Wyoming

Line 2
a - 1.000 feet

Separation of Symbols

Standard Well Symbols	Custom Symbols
○ Drilling for which information is unobtainable	⌋ Metal pipeline, presumed grounded
○ Drilling in progress at time of map preparation	⌋ Ungrounded pipeline, with metal or aluminum
△ Shot in	⌋ Metal fence
○ Abandoned	⌋ Electric fence
○ ^W Dry hole with total depth indicated	⌋ Buried telephone or power cable
○ Oil well	⌋ Telephone line or standard voltage power line
○ Gas well	⌋ Major high voltage power line
○ Oil and gas well	⌋
⋆ Gas injection well	⌋ Radio microwave or other communications station or tower
○ Water injection well	⌋ DC pump
○ Water well	⌋

Special Well Symbols

- ^W Drilling in progress at the time of the electrical survey; number indicates the amount of drill stem in the hole at the time of data collection
- Well studied in after completion of the electrical survey
- Number indicates distance of well from the line in terms of spacings; all wells within 1.0 spacing indicated (pseudocontact only)

Other Symbols

U.S.G.S. standard symbols or as labeled

ZIONGE ENGINEERING & RESEARCH ORGANIZATION

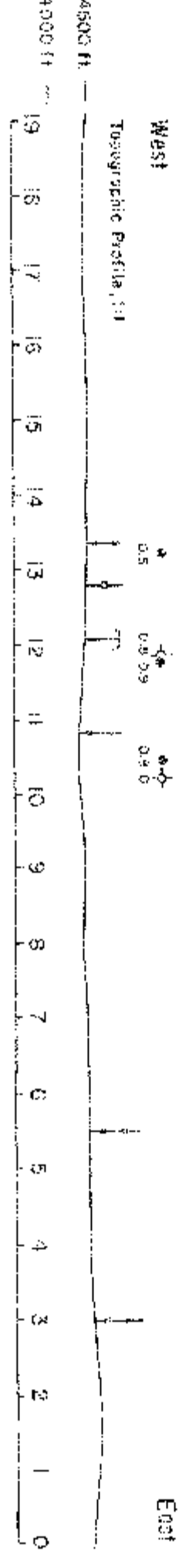
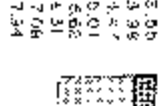
Plate 5.2
R.P. Field Data
Little Buck Creek Field
Line 2

Apparent Resistivity

Units: ohm-meters

Frequency: 0.125 Hz

Logarithmic colour interval:

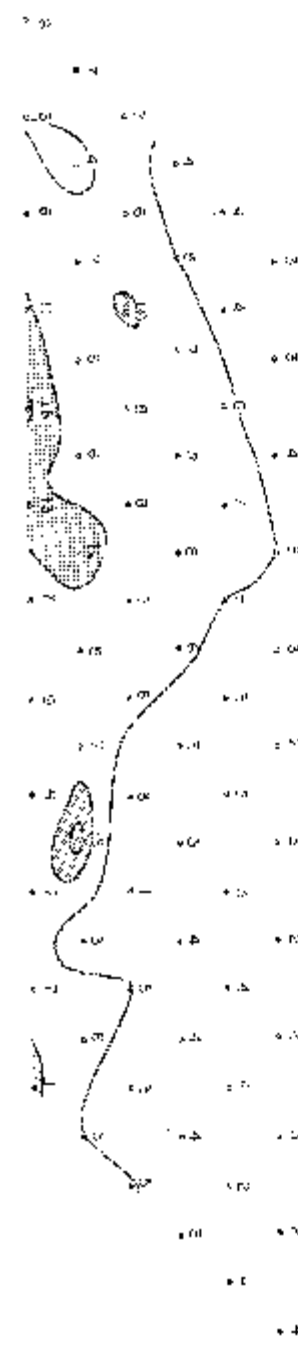
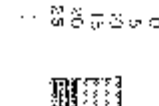


Decoupled Phase Angle

Units: milliradians

Frequency: 0.125 Hz

Linear colour interval:

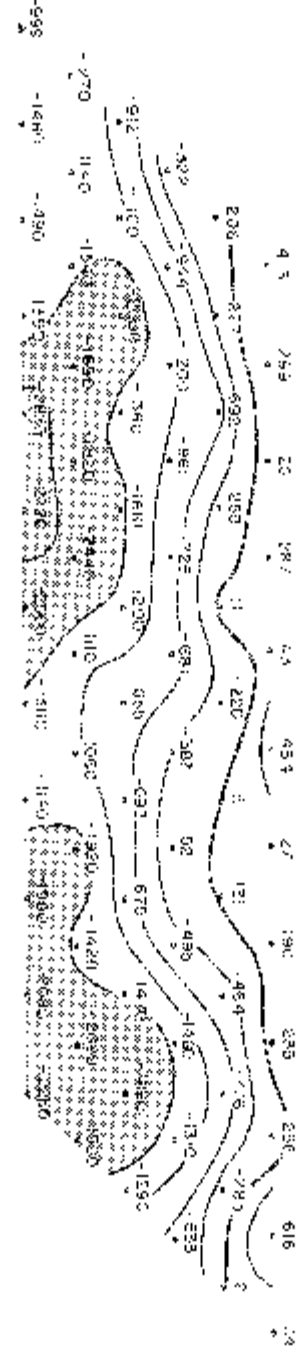
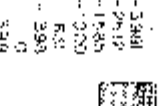


REM Quadrature

Units: normalized imaginary

Frequency: 0.125 Hz

Logarithmic colour interval:



10.5

4.0

5.0

2.0

10.5

4.0

5.0

2.0

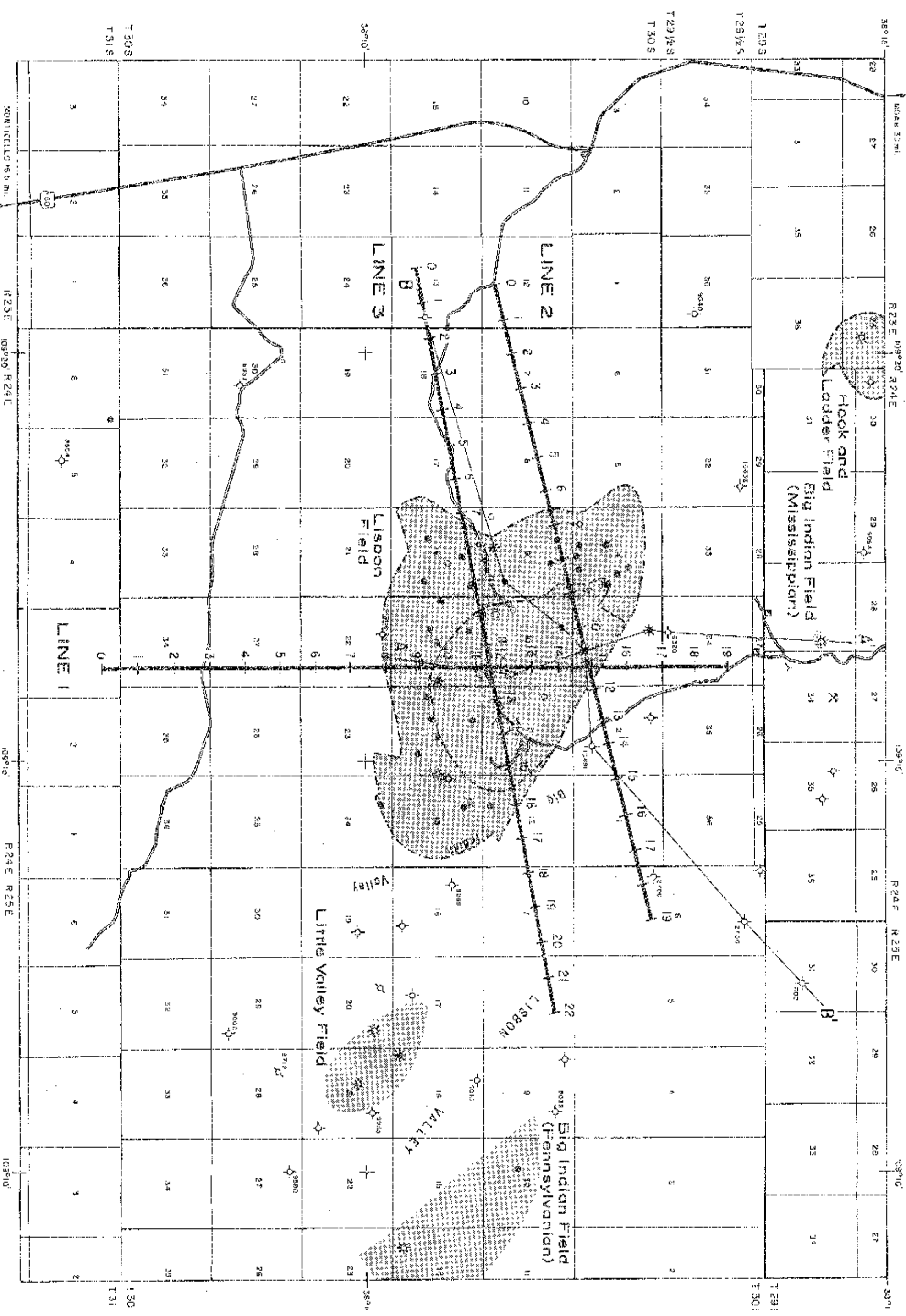
PLATE F 100505

J-FAB

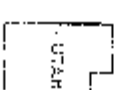
Source#
Brew, U.S.C. 9, 16 "Dund & Ibbot, Valley, Ut., 1964; Hatch Pond, Wt., 1964
Well Data: Pennsylvania Insurance-Lake-Ownership 13-6, U.S. record 100-015-B-121-33; Bowley (1972), Budd (1960), Clark (1978); Latch
(1978); J. J. J. Mitchell (1961); Parker (1961, 1968); Smith (1978)

Standard Well Symbols	Culture Symbols
① Aritholia for which information is inadequate	① Metal pipelines, presumed grounded
② Drilling in progress at time of map preparation	② Ungrounded pipelines: non-metal or suspected
③ Shut in.	③
④ Abandoned	④ Metal fence
⑤ Dry hole with total depth indicated	⑤ Electric fence
⑥ Oil well	⑥ Buried telephone or power cable
⑦ Gas well	⑦ Telephone line or standard voltage power line
⑧ Oil and gas well	⑧ Major high voltage power line
⑨ Gas inspection well	⑨ Radio, microwave, or other communications station or tower
⑩ Water injection well	⑩ DC pump
⑪ Water well	

Special Well Symbols	Other Symbols
① Drilling in progress at the time of the electrical survey; number indicates the amount of well stem in the hole at the time of sale	① U.S.G.S. standard symbols or as needed
② Well completed in after completion of the electrical survey	
③ Number indicates distance of well from fire line in terms of seconds; all wells within 1.0 seconds indicated (precaution only)	



San Juan Co., Utah

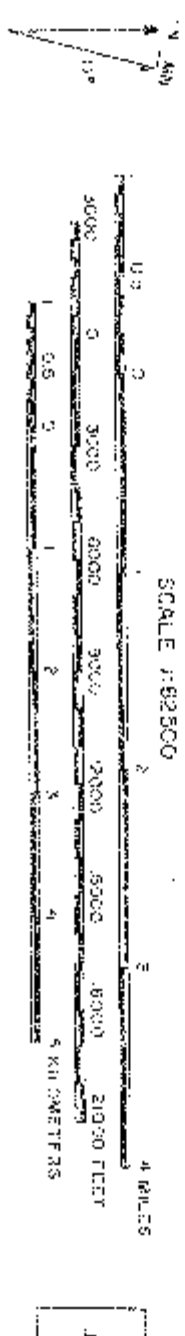


Base: U.S.C.S. 15 Quad Elsthor Valley, Ut. 1954; Miller Box, Lt., 1954)

$$\frac{d}{dt} \left(\frac{\partial L}{\partial \dot{x}} \right) = \frac{\partial L}{\partial x}$$


Figure 6.6
STRUCTURE MAP—TOP OF UPPER PARADOX

Lisbon Field
San Juan Co., Utah



Source:
From U.S.G.S 1:62,500 Quad (Lisbon Valley, UT, Sheet: Hatch Peak, UT, 1964)
Well Data: Petroleum Information Library—Ownership (U373, 1988; record labels: 8-12-82); Standley (1975); Smith (1960); Clark (1970); Smith
(1973); Smith; Mitchell (1951); Powell (1961); 1968; Smith (1978)
Geology: Parker (1981, 1986); Clark (1978); Lamb (1976); Jones Smith (1978)

Explanation of Symbols

Standard Well Symbols

- | | |
|---|--|
| 1 Drillhole for which information is undependable | φ Metal pipeline, presumed grounded |
| 2 Drilling in progress at time of map preparation | φ _u Unspaced pipeline: horizontal or suspended |
| 3 Shut in | ⊥ Metal fence |
| 4 Abandoned | ⊥ Electric fence |
| 5 Dry hole with total depth indicated | ⊥ Buried telephone or power cable |
| 6 Cui well | ⊥ Telephone line or standard voltage power line |
| 7 Gas well | ⊥ Major high voltage power line |
| 8 Oil and gas well | ⊥ Radio, microwave, or other communications station or tower |
| 9 Gas injection well | ⊥ DC pump |
| 10 Water injection well | |
| 11 Water well | |

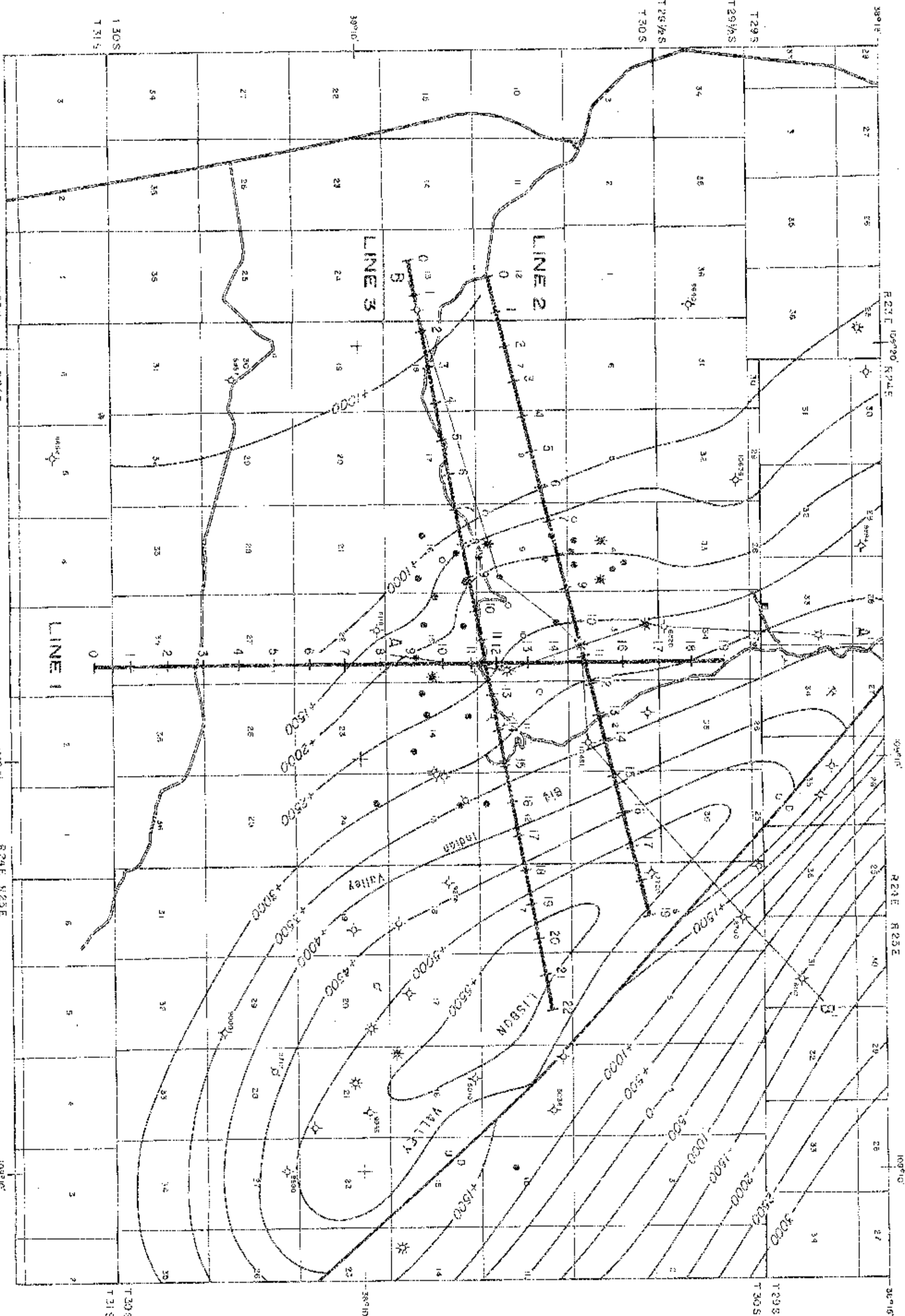
Special Well Symbols

- | | |
|--|---|
| 12 Drilling in progress at the time of the electrical survey; number indicates the amount of drill stem in the hole at the time of data collection | Other symbols |
| 13 Well standard in after completion of the electrical survey | (U.S.G.S. standard symbols or as labeled) |
| 14 Number indicates distance of well from the line in terms of sections; all wells within 1/2 section are indicated (pseudoregions only) | |

Map-Specific Symbols

Structure contour interval: 500 feet

Zenith Engineering & Research Organization, Inc.



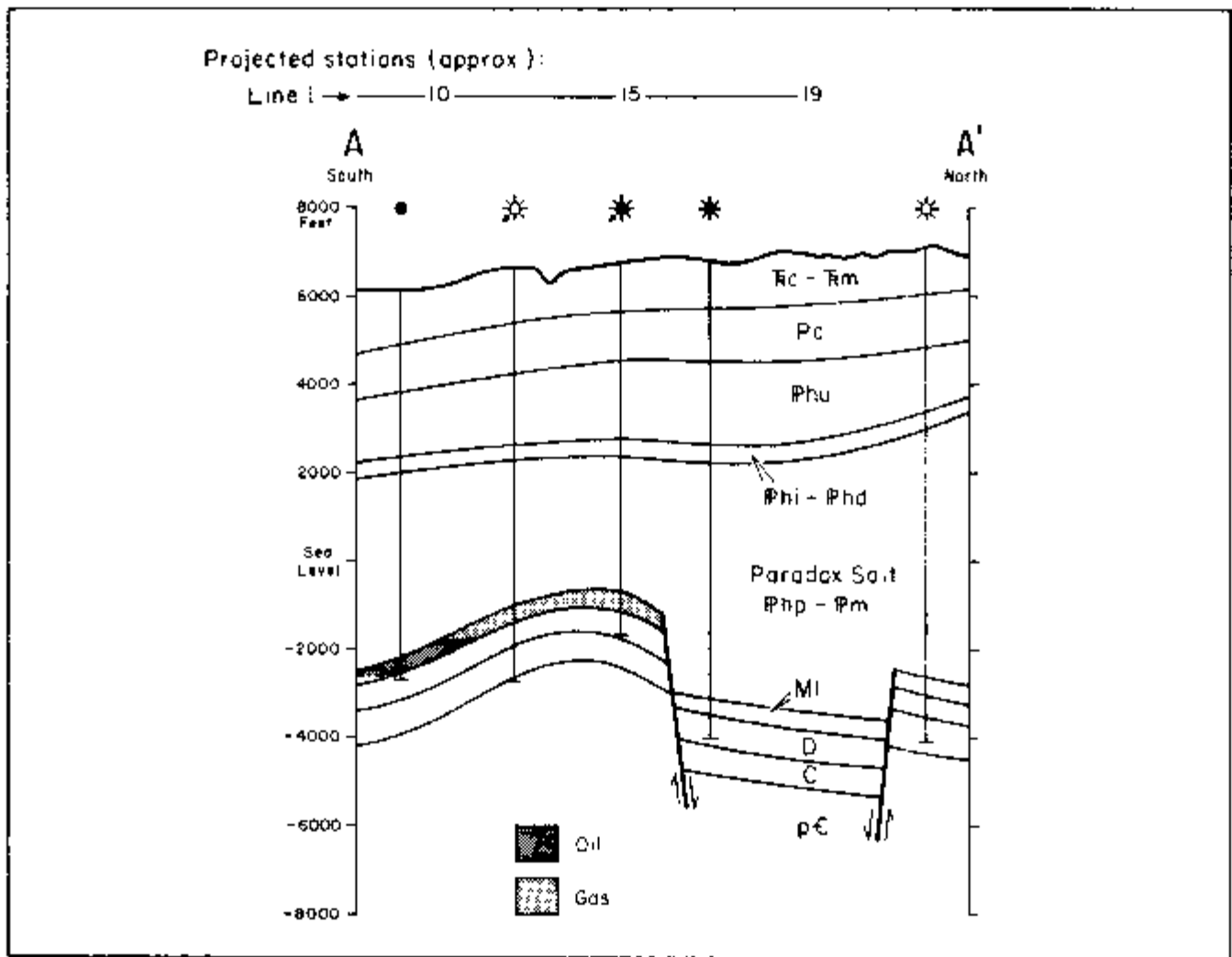


Figure 6.9. Geologic cross-section A-A', with no vertical scale exaggeration; this may be compared with the data from line 1 of the electrical survey. Refer to Figure 6.4 for map location. Geology from Parker (1961).

Reservoir Geology

Although some shows have been observed in the Paradox Salt at Lisbon Field, the only economic production has come from Devonian and Mississippian rocks. The Devonian reservoir is the McCracken Sandstone Member of the Elbert Formation. McCracken porosity and permeability vary erratically, and the unit is only a secondary oil producer. Some production has also come from the Upper Devonian Ouray Limestone. The Mississippian reservoir is the Leadville Formation, the stratigraphic equivalent of the Redwall Limestone, which outcrops prominently in the Grand Canyon of Arizona. Leadville production accounts for most of the production at Lisbon. Both oil and gas are found in the more porous zones of dolomite beds. The trap is formed by a faulted anticline; oil is found in a ring-shaped feature due to the high relief of the enclosing structure, and gas is found in the

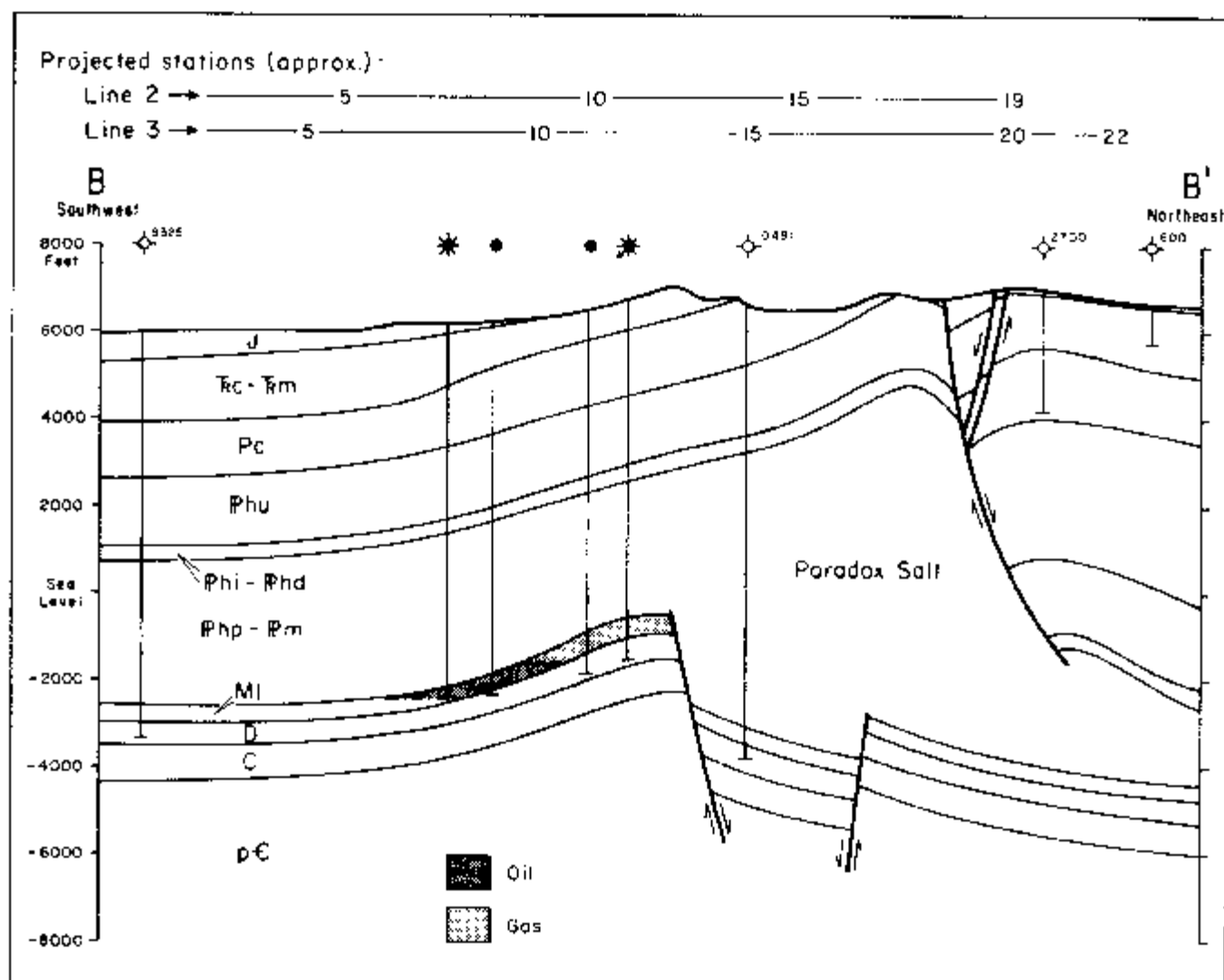


Figure 6.10. Geologic cross-section B-B', with no vertical scale exaggeration; this may be compared with the data from lines 2 and 3 of the electrical survey. Refer to Figure 6.4 for map location. Geology from Parker (1961).

structural cap (see Figures 6.9 and 6.10). The trap has a closure about equal to the total hydrocarbon-condensate column; hence, it is filled nearly to the spill point. The recovered oil, gas, and water are separated at each well, measured, and piped under pressure to a central plant. The constituents are then stage-separated. Oil is stabilized and marketed, gas is stripped, compressed, and reinjected back into the gas cap, and salt water is injected back into the Leadville through a dry well south of the field.

Table 6.2 presents statistical information on the Leadville and McCracken reservoirs. The differences in BTU and other characteristics have suggested to some that the hydrocarbons in the two reservoirs have two distinct source beds. These source beds are unknown, although the black shale section of the Paradox Forma-

**TABLE 6.2: RESERVOIR CHARACTERISTICS OF
LISBON FIELD**

General Field Data

Region: Paradox Basin

Production: Oil, gas

Type of Trap: Structural; faulted anticline

Producing Formations and Depths: Leadville Fm., 7,500-8,500 ft
Elbert Fm., McCracken Ss. mbr., 8,300 ft

Other Significant Shows: None

Total Reserves: 250 BCFG, 44.3 MMBO

Productive Area: Proved 5,120 acres in Leadville and 1,050 acres in McCracken

Field Operator: Union Oil

Number of Producing Wells (12/80): 12 (plus 3 injection wells)

Number of Shut-in Wells (12/80): 12

Well Casing Data: Surface casing 13-3/8 inch to about 73 ft; 9-5/8 to 10 1/2 inch casing to between 700 and 1,200 ft; production casing 5 1/2 or 7 inch to total depth (typical well). Paradox section is cemented.

Discovery Well

Name: Pure Oil No. 1 SW Lisbon USA

Location: NE-NW-10-T30S-R24E

Completion Date: 1/5/60

Total Depth: 8,440 ft

Perforations: 7,567-7,970 ft (Leadville); 8,261-8,293 ft, 8,310-8,348 ft (McCracken)

Initial Potential: Flow 179 BOPD, 4,376 MCFGPD (Leadville); 586 BOPD (McCracken)

Treatment: HyFlo, acid, sand-oil fracture

Reservoir Data: Leadville Formation

Discovery: 1/5/60, Pure Oil No. 1 SW Lisbon USA, NE-NW-10 T30S-R24E

Lithology: Dolomite and limestone

Age: Mississippian

Type of Trap: Structural; faulted anticline

Drive Mechanism: Expanding gas cap and gravity drainage

Initial Pressure: 2,982 psi at -2,400 ft

Reservoir Temperature: 127°F (est.)

Gross Thickness of Reservoir Rock: 225 ft

Porosity: 5.5% average; highly variable, 1 to 21%; mainly fracture porosity

Permeability: 22 millidarcies average; highly variable, 0.01-1,100 millidarcies

Oil/Gas Column: 1,870 ft

Gas/Oil Ratio: 1:1,200 at base of oil ring, 37,500:1 at top of gas cap

Original Gas/Oil Contact: -1,800 ft

Original Oil/Water Contact: -2,570 ft

Gas Character: Sour; 740 BTU (1,207 BTU in oil ring); specific gravity 0.97

Gas Analysis:

	Lisbon No. 1 USA C-4-T30S-R24E -2,200 ft	Lisbon No. 2-21-F 21-T30S-R26E -2,450 ft
Methane	40.1%	61.03%
Ethane	8.5	5.19
Propane	5.2	1.38
Nitrogen	15.5	13.03
Oxygen	trace	not analyzed
Argon	0.1	not analyzed
Helium	1.0	not analyzed
Hydrogen	0.1	not analyzed
Carbon dioxide	26.7	15.42
Hydrogen sulfide	0.0	2.17

TABLE 6.2 Continued

Oil Character: Sour, yellow to red; gravity 54° API (71° API in gas cap)
Oil Analysis: Carbon dioxide 20%
Water Saturation: 39%
Water Salinity: High, 70,000 to 100,000 ppm TDS
Water Resistivity: 0.045 to 0.06 ohm-meters at 127°F
Daily Average Production (12/80): 53,230 MCFGPD, 1,894 BOPD, 3,729 SWPD
Cumulative Production (1/60-12/80): 363 BCFG, 42.7 MMBO, 11.4 MMB liquids
Estimated Primary Recovery¹: 250 BCFG (70%), 26.7 MMBO (30%)
Type of Secondary Recovery: Controlled pressure decline by crestal gas injection
Estimated Ultimate Recovery¹: 250 BCFG (70%), 42.9 MMBO (47%)

Reservoir Data: Elbert Formation, McCracken Sandstone member

Discovery: 1/5/60, Pure Oil No. 1 SW Lisbon USA, NE-NW-10-T30S-R24E
Lithology: Dolomitic sandstones and shales, sandy dolomites
Age: Devonian
Type of Trap: Structural; faulted anticline
Drive Mechanism: Solution gas
Initial Pressure: 2,713 psi at 8,271 ft
Reservoir Temperature: 131°F
Porosity: 8%
Permeability: 2.6 millidarcies
Original Oil/Water Contact: -2,300 ft
Gas Character: Sweet; 1,300 BTU
Oil Character: Red, waxy; gravity 43° to 50° API
Water Saturation: 43%
Water Salinity: High, 70,000 to 100,000 ppm TDS
Water Resistivity: 0.043 to 0.058 ohm-meters at 131°F
Daily Average Production (1981): 26 BOPD
Cumulative Production (1952-9/65): 202,838 MCFG, 110,805 BO, 4,552 BW
Estimated Primary Recovery: 1,375,800 BO (20%)
Type of Secondary Recovery: None
Estimated Ultimate Recovery: 1,375,800 BO (20%)

¹ Initial estimates for oil, which are apparently much too low.

tion, where stains are found today, has been suggested as a likely candidate. Accumulation in the present-day traps may have occurred in the late Mississippian or Pennsylvanian times, according to Parker (1968).

Groundwater Characteristics

The groundwater regimes of the Paradox Basin can be divided into three distinct hydrostratigraphic units (Thackston, McCulley, and Preslo, 1981). The upper unit, which lies above the Paradox Formation, is high in calcium, magnesium, and bicarbonates. It also contains a variable level of sodium chloride, much of which appears to originate in the upper Pennsylvanian Honaker Trail Formation. No sodium-rich evaporites have been reported in the Paradox Basin, and Thackston, McCulley, and Preslo (1981), speculate that most of the sodium is supplied by "ion exchange in clay-rich strata and alteration of plagioclase." The flow characteristics of the upper unit are controlled primarily by gravity. At Lisbon, this would mean that flow would be into Hatch Wash, immediately south and west of the producing field.

The middle flow regime is in the Paradox Formation. The high evaporite content in the Paradox causes it to behave as an aquitard. Permeability is usually

very limited, and although some shows of brine water and hydrocarbons have been observed in the Paradox, these pockets are quite isolated. It is not surprising, therefore, that water composition in the middle regime is quite variable. In general, the total count of dissolved solids is high; principal ions are sodium, chlorine, potassium, calcium, and magnesium.

The lower flow regime lies primarily in the Mississippian Leadville Formation. Flow is generally unrestricted and is very extensive due to good permeabilities. The flow direction is primarily controlled by subsurface structure, but the general regional flow in the basin is toward the southwest. The salinity of these waters is quite high, about 66,000 to 82,000 parts per million of total dissolved solids. Areas overlain by the Paradox Salt appear to be more saline than areas outside the basin which are not overlain by salts, indicating that some solution of the Paradox salts is occurring. However, it is unlikely that any significant mixing of the middle and lower hydrostratigraphic units occurs. Instead, most of the salt contribution from the Paradox probably occurs by means of mechanical solution in the vicinity of fractures and faults in the salt body.

Well-Casing Information

Normal drilling practice at Lisbon is to set a 13-3/8-inch (34.0 cm) casing from the surface to as deep as 73 feet (22 m) depending upon surface conditions. Casing of 9-5/8 to 10-3/4 inches (24.5-27.3 cm) diameter is then set to 700 to 1,200 feet (210-365 m). The well is then drilled to total depth, 5-1/2 or 7-inch (14.0 or 17.8 cm) production casing is set, and the Paradox Salt section is cemented. Well-casing models used for interpretation use a casing diameter of 10-3/4 inches.

6.3 DISCUSSION OF THE DATA

Introduction

A resistivity/phase crew of eight persons, headed by Zonge Engineering geophysicist Norman R. Carlson, was mobilized to the Lisbon Field project on April 11, 1980. Two subparallel lines and one cross-line were run using a dipole length of 2,000 feet (610 m); data were obtained at 0.125, 0.25, 0.5, and 1.0 Hz. Work continued through May 2. A total of 22.6 surface line-miles (36.3 line-km) were covered; total subsurface coverage was 13.6 line-miles (22.0 line-km).

The Lisbon project presented a number of difficulties typical of those which can confront an electrical survey of this type. Topography was significant, involving numerous mesas with steep cliffs. This slowed production at times and produced topographic effects in the data. Heavy electrical noise was encountered from electrical storms during most of the survey, and extensive stacking and averaging were required to obtain acceptable data. Production had to be terminated on several days due to danger of electrical shock from lightning. Another source of noise was the workings in the subsurface uranium mines at Lisbon. Mine machinery and railways powered by direct electrical current produced large shifts in the ground potential observed at the surface, necessitating strategic planning of data acquisition. Culture was a significant problem at Lisbon Field. Cultural features consisted of numerous cased wells, grounded surface collection pipelines, telephone lines, medium to heavy duty powerlines, and fences. Pipelines and well casings produced the majority of cultural contamination in the data, while powerlines contributed significant amounts of 60 and 180 cycle noise.

The apparent resistivity, apparent polarization, and REM data for lines 1, 2, and 3 are presented as Plates 6.1, 6.2, and 6.3 at the back of this chapter. They may be unfolded for reference while reading the text.

Line 1 Interpretation

As shown in Figure 6.4, line 1 traversed Lisbon Field from south to north. Permit restrictions prevented the acquisition of data off the northern end of the field, but a fair amount of background information was obtained to the south. The field data are presented in Plate 6.1.

APPARENT RESISTIVITY DATA

The apparent resistivity layering is high/low/high on line 1. The data show a shallow southerly dip similar to that depicted in the cross-section A-A' (Figure 6.9). The high resistivities at the surface, which pinch out north of the middle of the line, may be correlated with lower Jurassic and upper Triassic sediments which outcrop south of the oilfield. There is probably a general trend toward high resistivities at the surface across the entire line, indicating that the surface rocks are probably dry. The middle, low resistivity layer can be correlated quite well to the lower Triassic Chinle and Moenkopi formations and the Permian Cutler Formation. As shown in Table 6.3, well logs show these units to be low in resistivity. The high resistivity layer at depth corresponds to Pennsylvanian sediments, particularly the highly resistive Paradox Salt.

TABLE 6.3: WELL LOG RESISTIVITIES,¹ LISBON FIELD

Formation	Lisbon Unit #B-616 SE-NE-NW-16-T30S-R24E		Lisbon Unit #B-99 SE-SW-9-T30S-R24E	
	Average Resistivity (ohm-meters)	Range in Resistivities (ohm-meters)	Average Resistivity (ohm-meters)	Range in Resistivities (ohm-meters)
Chinle, Moenkopi (Triassic)	20	8-30	20	8-32
Upper Cutler (Permian)	35	10-250	30	10-150
Lower Cutler (Permian)	50	15-250	45	15-100
Honaker Trail (Pennsylvanian)	80	15-≥250	100	10-≥450
Upper Paradox (Pennsylvanian)	100	40-≥250	100	20-≥250
Paradox Salt (Pennsylvanian)	≥250	5-≥250	≥250	10-≥250
Leadville (Mississippian)	80	20-500(?)	60	20-1000(?)
Ouray, Elbert (Devonian)	500(?)	250-1000(?)	500(?)	250-1000(?)

¹Schlumberger Laterolog 3

Superimposed upon the layering effects is a broad zone of low resistivities extending from the surface to moderate depths. The southern edge of the low resistivity zone corresponds roughly to the southern edge of the producing field. The right-plunging, high resistivity diagonal 10,11 and premature data cut-off towards the north prevent drawing any conclusions as to how well the data correlate with the northern edge of the producing field.

In order to determine the origin of the conductive anomaly, four possibilities will be examined: culture, surface topography, subsurface structure, and hydrocarbon-related electrochemical alteration.

There is an extensive amount of culture near line 1, including five cased wells within one dipole spacing of the line. A well-casing model was constructed to simulate the apparent resistivity data, using the "PIPE" algorithm of Holladay and West (1982). Despite serious qualifications regarding application of this model to field data (section 2.5), the algorithm is useful in presenting a *worst-case* scenario regarding well-casing effects. A well-casing diameter of 10-3/4 inches (27.3 cm) was assumed, even though many casings are only 9-5/8 inches (24.5 cm) in diameter at Lisbon, and despite the fact that all casings are only 5-1/2 to 7 inches (14.0-17.8 cm) in diameter at depths greater than about 1,000 feet (300 m).

The well-casing model data and residual data are presented in Figure 6.11. The model data show a chevron-shaped, low resistivity zone centered between stations 9 and 10; the strongest effect occurs along the 8,9 right-plunging diagonal. Note that while the field data show the low resistivity zone at intermediate to shallow depths, the well-casing model shows a significant effect at all depths. Hence, it is not surprising that the residual data, which show the residual of the field data after removal of calculated well-casing effects, show an anomaly very similar to that seen in the original field data. Therefore, one can conclude that, even in the most severe application of the "PIPE" model, well casings do not account for all the conductive anomaly observed on line 1.

The potential effects of other culture along line 1 should also be considered. There is no evidence that the fence at station 6 has any effect on the apparent resistivity data. There is also no evidence of effects from the powerlines at stations

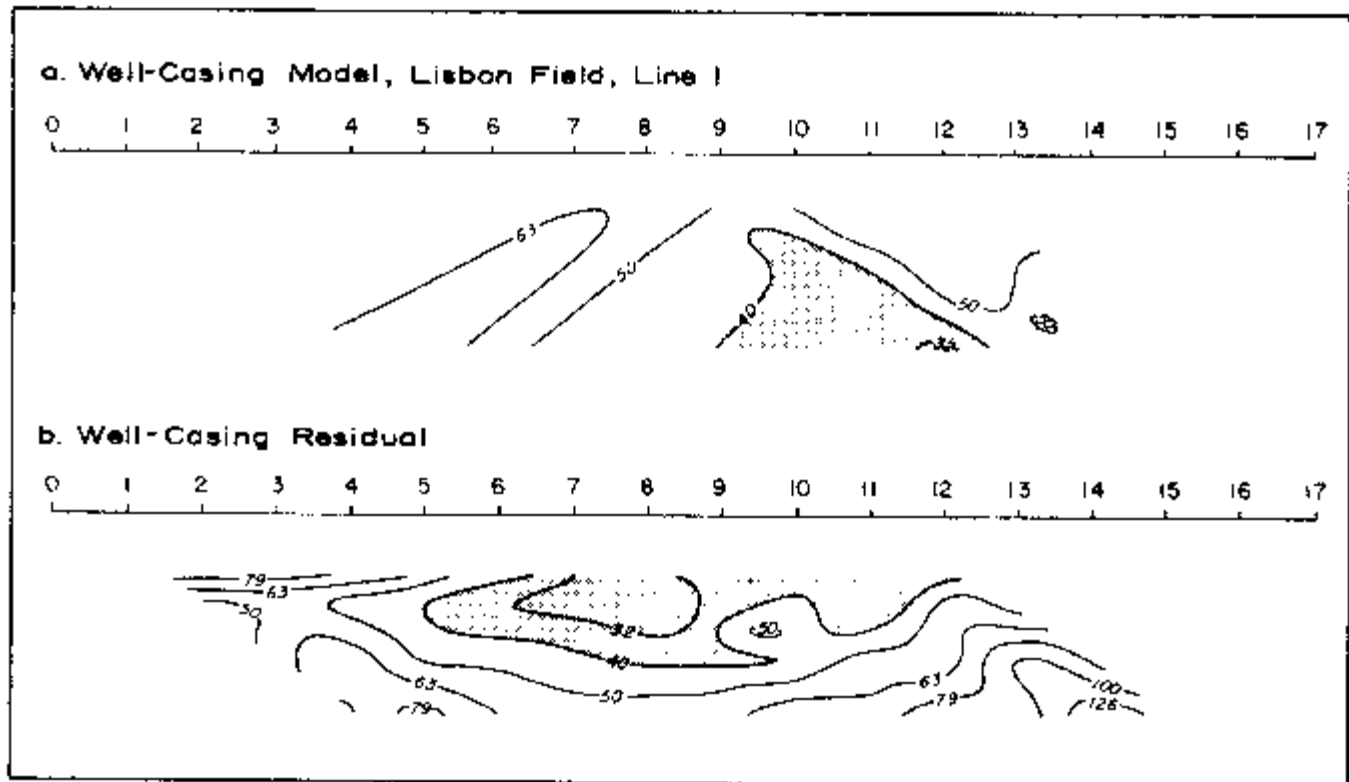


Figure 6.11. Well-casing model of apparent resistivity data for line 1, Lisbon Field. Model parameters: 23 cased wells, casing diameter = 10-3/4 inches (24.5 cm), casing resistivity = 2.0×10^{-7} ohm-meters, surface impedance = $0 + 0.2i$, background resistivity = 60 ohm-meters. Figure 6.4 shows well locations.

13.5 and 17.8, or the one parallel to line north of station 17.8, and by inference, one would not expect much of an effect from the powerline at station 8.4. On the other hand, one can see that there may be some effects due to the pipelines, especially the double pipelines at stations 7.1 and 7.8. There are, however, three objections to the assumption that pipelines are responsible for the anomaly. First, and most important, the anomaly clearly overshoots the expected zone of influence of the pipelines, since it appears to extend past the north end of the line. Second, a strong pipeline effect should present itself as a strong, chevron-shaped anomaly similar to that illustrated in section 2.6, yet no evidence of such an effect can be seen in the data. The right-plunging 8,9 and left-plunging 10,11 diagonals might be related to the pipelines but only one leg of each chevron is present. Third, several pipelines on lines 2 and 3 show no effects on the data at all, despite the fact that they are located closer to electrode stations than any of the pipelines on line 1. It can therefore be concluded that pipelines do not cause a major portion of the anomalous response on line 1, although they may contribute to it.

Since the line crossed a number of mesas and ravines, it is appropriate to consider the effects of topography. The two-dimensional model "2DIP" was used to estimate topographic effects. The model results, which are reproduced in Figure 6.12, indicate that topography does not contribute to the anomaly seen on line 1.

The possibility that subsurface lithologic structure causes or contributes significantly to the conductive anomaly is considered to be minimal. The changes which produce the anomaly are certainly located within 2,000 to 3,000 feet (600-900 m) of the surface, and one can readily see from the cross-section A-A' (Figure 6.9) that insufficient structural changes occur at these depths to explain this anomaly. One could argue that the middle, low resistivity layer, which was noted earlier, appears to outcrop in the vicinity of the anomaly. However, the anomaly is certainly due to a vertical resistivity change and cannot be attributed to a shallowly dipping, outcropping layer. Figure 6.13 shows a model analogue to support this conclusion: note that the outcropping, low resistivity layer produces only layering effects, not the sharp lateral-type effects seen in the field data.

We have seen that the resistivity anomaly observed on line 1 cannot be readily explained by the effects of culture, topography, or subsurface structure, and it is unlikely that any combination of these three effects produces the anomaly, although they probably contribute to it. Hence, we are left with the alternative that

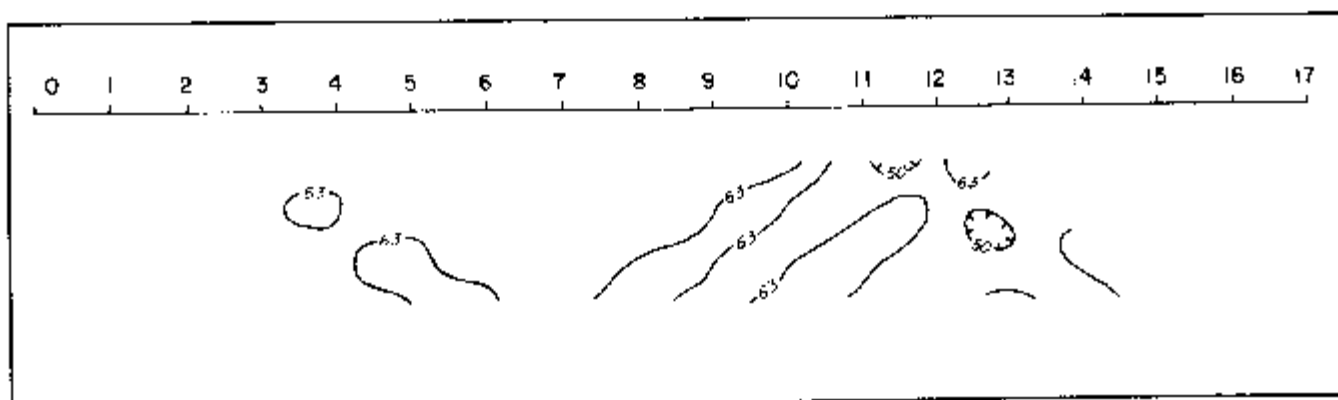


Figure 6.12. Topographic model of apparent resistivity data for line 1, Lisbon Field. Background resistivity = 60 ohm-meters. Plate 6.1 shows topography.

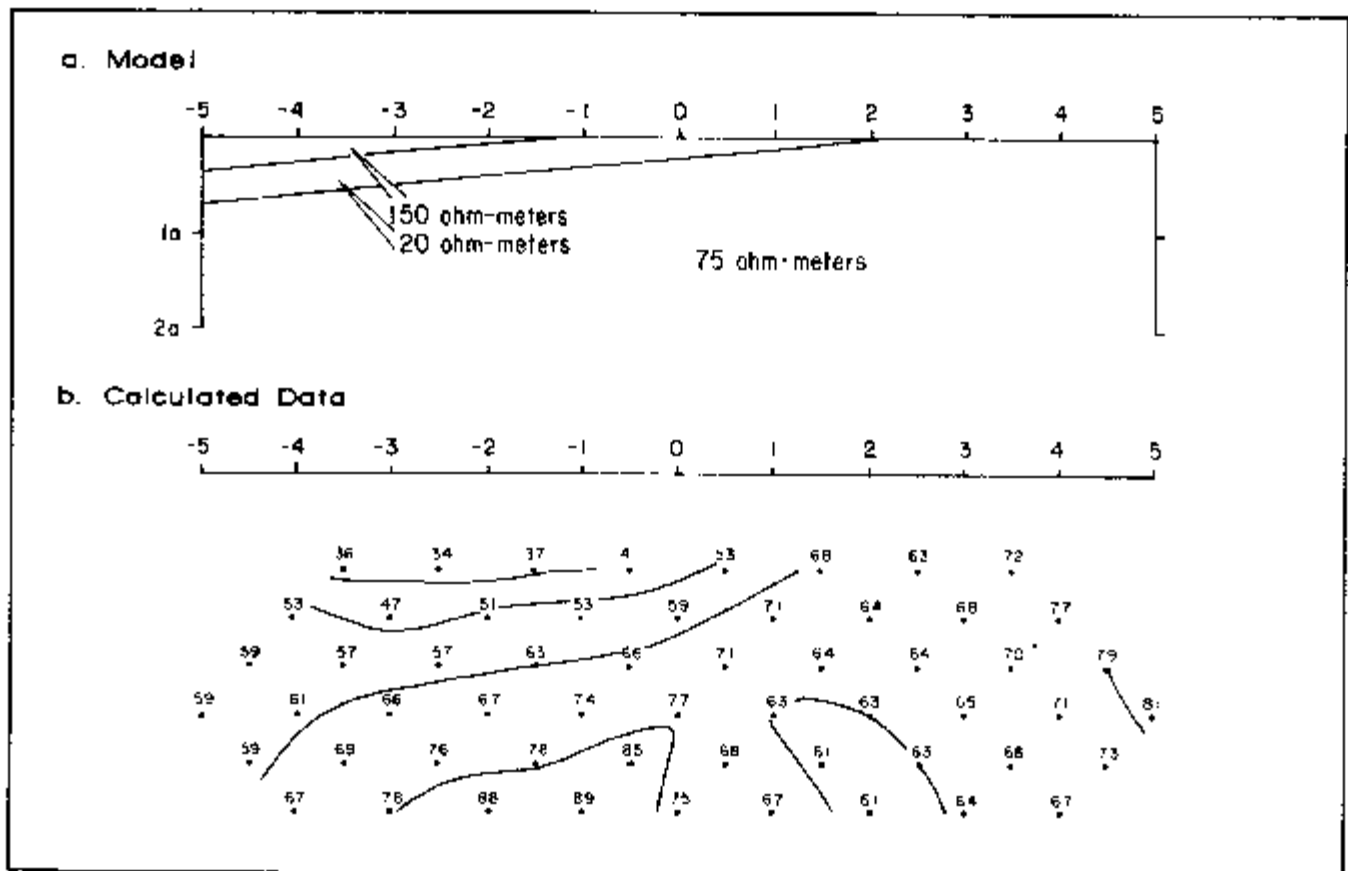


Figure 6.13. Two-dimensional resistivity model of a shallowly dipping, outcropping conductive layer.

a true low resistivity zone exists in the sediments directly overlying the hydrocarbons. Modeling indicates that the bottom of this zone may lie as deep as 3,000 feet (900 m), and it appears to extend upward to the near-surface rocks. Due to the complexity of the data, it is not possible to distinguish fine structure within this zone.

APPARENT POLARIZATION (DECOUPLED PHASE ANGLE) DATA

The polarization data show a high-over-low layering. High polarization values appear to be associated with the high resistivity Jurassic and upper Triassic sediments, and low polarization values appear to be associated with all the sediments below. The only feature of interest is a rather convoluted polarization high at depth, which consists primarily of a few anomalous values along the right-plunging diagonals 6,7 and 7,8. However, there is no indication that the higher polarization values are correlated with the lateral extent of the hydrocarbons. It is probable that the isolated highs are due to the combination of a slight amount of noise, geometric effects of outcropping of lithologic layers, and minor effects of well casings.

RESIDUAL ELECTROMAGNETIC (REM) DATA

The REM data show a broad, relatively conductive zone which correlates well with the lateral extent of the hydrocarbons. The REM data provide two advantages over the galvanic data on line 1. First, effects due to layering are de-empha-

sized, since the quadrature component of REM responds primarily to lateral resistivity changes and not layering. This explains the more clearly defined shape of the REM anomaly, since "smearing-out" effects of low resistivity layers are not as strong as they are with galvanic data. Second, the effective penetration of REM is often deeper than that of the galvanic data. The strongest portion of the anomaly is at $n=3$, which may be some 3,000 feet (900 m) deep, suggesting that conductive alteration may exist in sediments as deep as the Upper Paradox. Apparent resistivity data tend to support this conclusion.

Line 2 Interpretation

Line 2 was run in an east-northeast direction over the Lisbon Field mesa area into the Big Indian and Lisbon valleys. Sufficient coverage was obtained to provide data over both ends of the producing field. The data are shown in Plate 6.2.

APPARENT RESISTIVITY DATA

As was observed on line 1, the apparent resistivity layering is high/low/high on line 2. The cross-section B-B' (Figure 6.10) and the well-log resistivities of Table 6.3 indicate that the surface high resistivity layer is associated with Jurassic and upper Triassic sediments; the middle, low resistivity layer is associated with lower Triassic and Permian sediments, and the high resistivity layer at depth is associated with Pennsylvanian units, in particular the highly resistive Paradox Salt.

A very strong zone of low resistivities correlates very well with the lateral extent of the producing zone on line 2. The zone appears to extend from near the surface to considerable depth. Following the procedure used in the discussion of line 1, the source of the low resistivity anomaly will be investigated by examining four possibilities: culture, surface topography, subsurface structure, and hydrocarbon-related electrochemical alteration.

Eight cased producing wells lay within one dipole spacing of line 2. In order to develop a worst-case description of well-casing effects, a "PIPE" model was run, including all cased wells within three dipole spacings of the line.

The well-casing model data and residual data are presented in Figure 6.14. The model data show a strong, low resistivity zone concentrated beneath station 9. It extends from stations 7 to 11 near the surface and fans out at depth due to geometric effects. The shape of the model anomaly at depth faintly resembles the shape of the anomaly in the field data, so it is not surprising that the residual data, which show field data minus calculated well-casing effects, have an appearance which is quite different from the original field data. This residual pseudosection (Figure 6.14b) shows a weak zone of low resistivities at intermediate depths between stations 6 and 7, and a shallower, stronger zone of low resistivities between stations 9 and 12. The two are separated by what appears to be a slightly resistive zone beneath stations 8 to 9, although it is possible that this zone is an artifact of overcorrection by the well-casing model. In any case, the data clearly show a conductive anomaly which cannot be attributed entirely to well casings. It is quite likely, based upon the discussion of Chapter 2, that well casings affect the data to a far lesser degree than shown in the worst-case modeling presented here.

Other types of culture present a potential problem on line 2. Three powerlines cross the line at station 7.2, and another crosses at station 11.4. Since the powerlines and several pipelines are clustered together, their effects cannot be easily separated. The pipeline near station 8 may contribute to the low resistivities on the left-plunging 8,9 diagonal and the right-plunging 7,8 diagonal; certainly this pipeline has a strong effect upon the phase data. However, the strongest effect should occur at $n=1$ and $n=2$, an effect which is not observed in the resistivity data. The pipelines

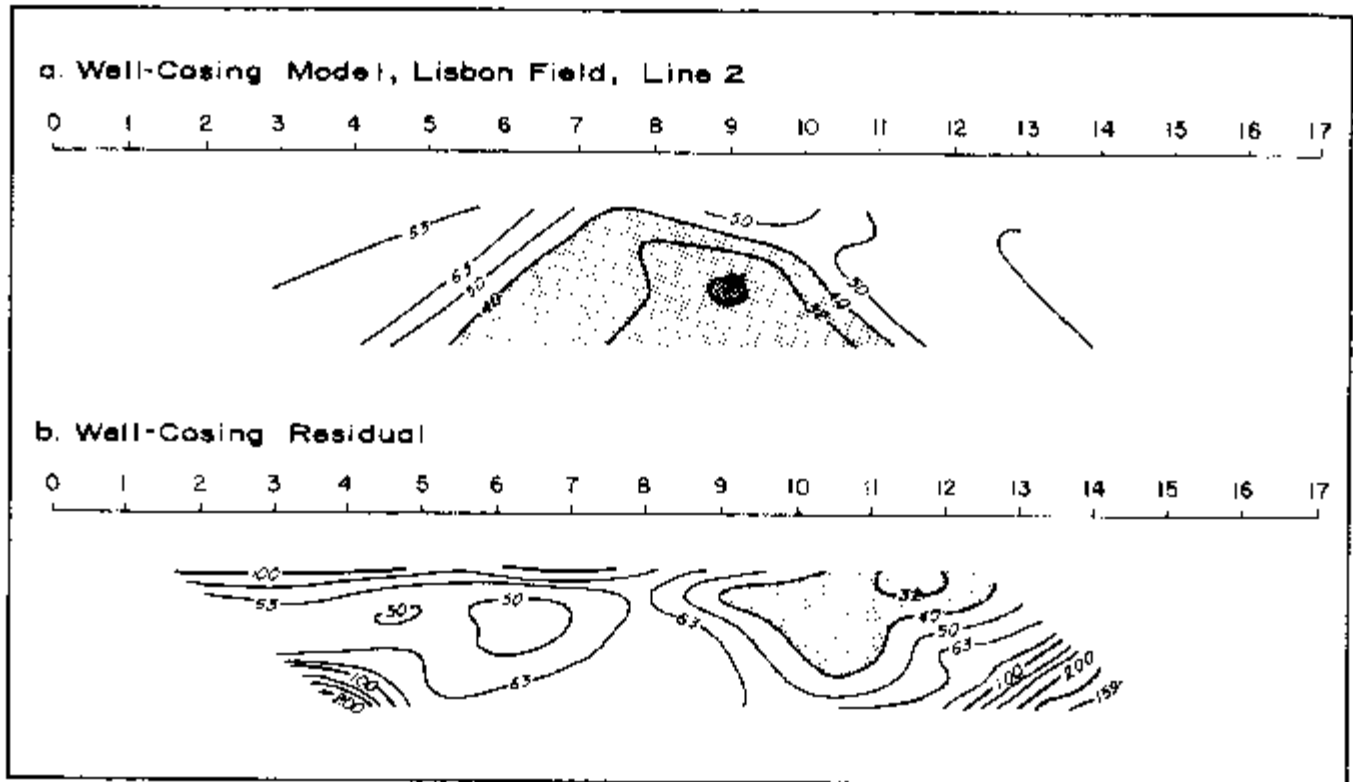


Figure 6.14. Well-casing model of apparent resistivity data for line 2, Lisbon Field. Model parameters: 19 cased wells, casing diameter = 10-3/4 inches (24.5 cm), casing resistivity = 2.0×10^{-7} ohm-meters, surface impedance = $0 - 0.2i$, background resistivity = 60 ohm-meters. Figure 6.4 shows well locations.

between stations 11 and 12 probably have a minimal effect on the resistivity data. This conclusion is supported by the absence of strong diagonal effects from this area and by the fact that the phase data show no anomalous effects near stations 11 and 12. Thus, surface cultural effects are indeed seen in parts of the data, but these effects do not explain the presence of the lateral conductive anomaly.

Topographic effects on line 2 are relatively minor, as shown by the "2DIP" topographic model of Figure 6.15. The mesa on the east end of the field appears to make a minor contribution to the low resistivity zone of the field data, but this is obviously a secondary effect.

Subsurface structure apparently does contribute to the conductive anomaly on line 2. Low resistivity sediments of lower Triassic and Permian age outcrop between stations 10 and 15, the approximate location of the surface expression of the anomaly. The correlation is not spectacular, but a comparison of the cross-section B-B' of Figure 6.10 and the field data from line 2 shows that some structural influences may be present in the data. However, the analog model of Figure 6.13, presented earlier, shows that an outcropping, shallowly-dipping layer cannot explain the presence of a strong, lateral resistivity change of the type seen in the data.

If the line 2 data were examined as an independent set of information, it would be possible to reach one of two very different conclusions: 1) the conductive anomaly can be explained by the combination of cultural, topographic, and structural effects, or 2) the anomaly is due to a conductive zone overlying the hydrocarbons, complicated to some degree by other effects. However, the line 2 data are

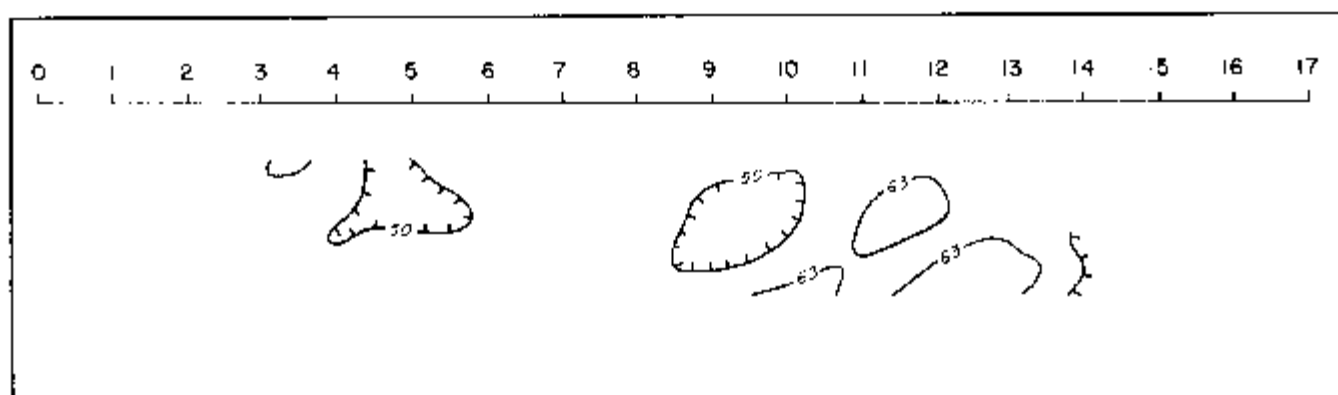


Figure 6.15. Topographic model of apparent resistivity data for line 2, Lisbon Field. Background resistivity = 60 ohm-meters. Plate 6.2 shows topography.

not an independent set of data, but are augmented by information from lines 1 and 3. The interpretation of these lines favors the existence of a conductive zone which is laterally correlated with the location of the hydrocarbons. It is more likely, then, that the anomalies on line 2 are at least partially caused by a conductive alteration zone rather than being caused entirely by cultural, topographic, and structural effects.

APPARENT POLARIZATION (DECOUPLED PHASE ANGLE) DATA

As on line 1, polarization on line 2 is high-over-low. The high phase angle values at the surface are clearly correlated with the high resistivity sediments of Jurassic and upper Triassic age, and low phase angle values are associated with older sediments. Superimposed on the high-over-low layering is a zone of high polarization centered on station 8. This zone is due to a feature at or very near the surface, and that feature is almost certainly the pipeline at station 7.9. This pipeline results in the left-plunging 8,9 diagonal and possibly contributes to the high and low polarization effects along right-plunging diagonals 6,7 and 7,8. Curiously, the pipelines between stations 11 and 12 seem to have little effect upon the data. This illustrates the unpredictability of cultural effects and argues against placing too much faith in modeling routines which attempt to simulate these features.

There is a possibility that material at depth on the eastern end of the line may be slightly polarizable. This response, if it has any true significance, is probably associated with upper Pennsylvanian sediments, which lie closer to the surface toward the east due to a thickening of the Paradox Salt in that direction.

None of the high polarization values on line 2 can be even remotely correlated to the surface projection of the lateral extent of the hydrocarbons.

RESIDUAL ELECTROMAGNETIC (REM) DATA

The REM data bear a resemblance to the apparent resistivity data, but the conductive effects appear to originate from a deeper source than suggested by the galvanic data. The anomalous zone, which is characterized by strong negative numbers, is located approximately between stations 6 and 12, correlating quite well with the lateral extent of the hydrocarbons.

Line 3 Interpretation

Line 3 was run roughly parallel to line 2. It traversed considerable topographic changes across Lisbon Field, and extended into Lisbon Valley. The data are presented in Plate 6.3. The offset diagonal on the west end of the line is a consequence of moving the transmitting dipole 1,2 to 1.5, 2.5 in order to minimize the effects of a pipeline crossing the line at station 2.

APPARENT RESISTIVITY DATA

Apparent resistivity layering is high/low/high at the west end of the line; to the east, the resistive surface layer appears to pinch out. As noted earlier, the surface high resistivities are associated with Jurassic and upper Triassic rocks. The middle, low resistivities are associated with lower Triassic and Permian sediments, and the high resistivities at depth are due to the more resistive Pennsylvanian sediments, especially the Paradox Salt.

A strong, conductive zone is superimposed on the layering effects. The conductive zone correlates relatively well with the lateral extent of the hydrocarbons and appears to extend from the surface to considerable depths. The eastern limit of the conductive zone is not well defined due to the shortness of the line in that direction and to the peculiar high resistivity effects there. These high resistivity values are probably due to the combination of topographic effects, the downfaulting of high resistivity Jurassic sediments east of station 18, and possible effects due to caves and void spaces in subsurface uranium mines.

Ten cased wells lie within one dipole spacing of the line. As a worst-case estimate of the effects of the casing, the "PIPE" model was run, including all cased wells within three dipole spacings of the line. The model data and residual data are shown in Figure 6.16. The model calculates a maximum chevron-shaped anomaly centered between stations 8 and 9. In the residual plot (field data minus calculated well-casing effects) of Figure 6.16b, a conductive zone still persists between stations 8 and 14, possibly extending to station 16. The residual anomaly is strongest near the surface but also seems to have some depth extent.

Three powerlines at station 6.8 have little if any effect upon the data, a finding which is consistent with observations of powerline effects on lines 1 and 2. The pipeline at station 2 is cathodically protected. When the crew began to acquire data from transmitting dipole 1,2, a spuriously large phase shift was observed, and the dipole was moved to 1.5, 2.5. The apparent resistivity data show little or no influence from this pipeline. The pipeline at station 9.8 also has little or no influence on the data.

In order to examine topographic effects on line 3, a "2DIP" model was run. The results are shown in Figure 6.17. While some of the diagonal features seen in the data can be explained by topography, the basic anomalous trend cannot be explained in this manner.

As noted in the discussion of lines 1 and 2, the outcropping of low resistivity Triassic sediments between stations 12 and 15 probably serves to enhance the conductive anomaly. However, it is clear from the model of Figure 6.13 that the conductive anomaly cannot be explained by outcropping effects. An examination of the cross-section of Figure 6.10 shows that subsurface structural effects probably do not influence the data to any significant degree. Therefore, one must conclude that, on line 3, a conductive zone of some vertical extent exists in the sediments overlying the hydrocarbons.

APPARENT POLARIZATION (DECOUPLED PHASE ANGLE) DATA

As observed on the other two lines at Lisbon Field, line 3 shows high-over-low polarization layering. Surface high values, which pinch out east of station 10,

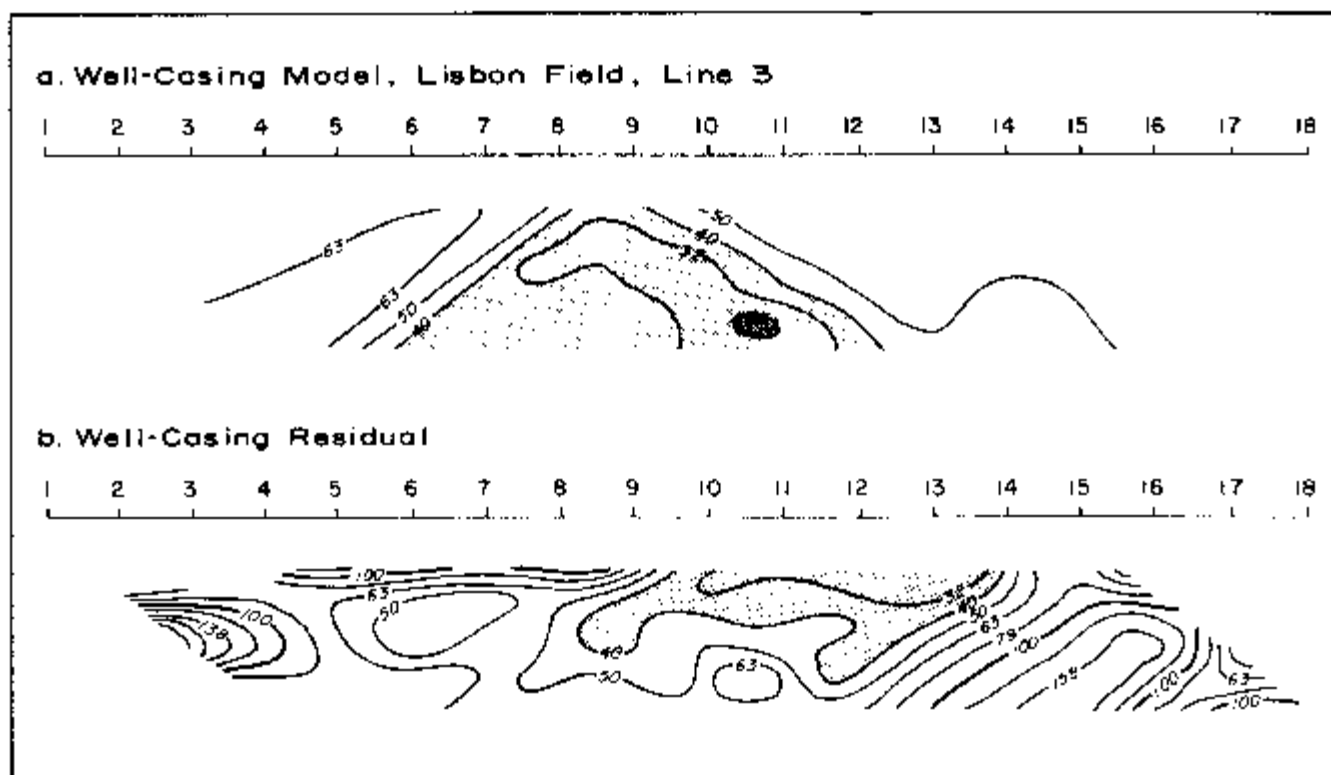


Figure 6.16. Well-casing model of apparent resistivity data for line 3, Lisbon Field. Model parameters: 24 cased wells, casing diameter = 10-3/4 inches (24.5 cm), casing resistivity = 2.0×10^{-7} ohm-meters, surface impedance = $0 + 0.2i$, background resistivity = 60 ohm-meters. Figure 6.4 shows well locations.

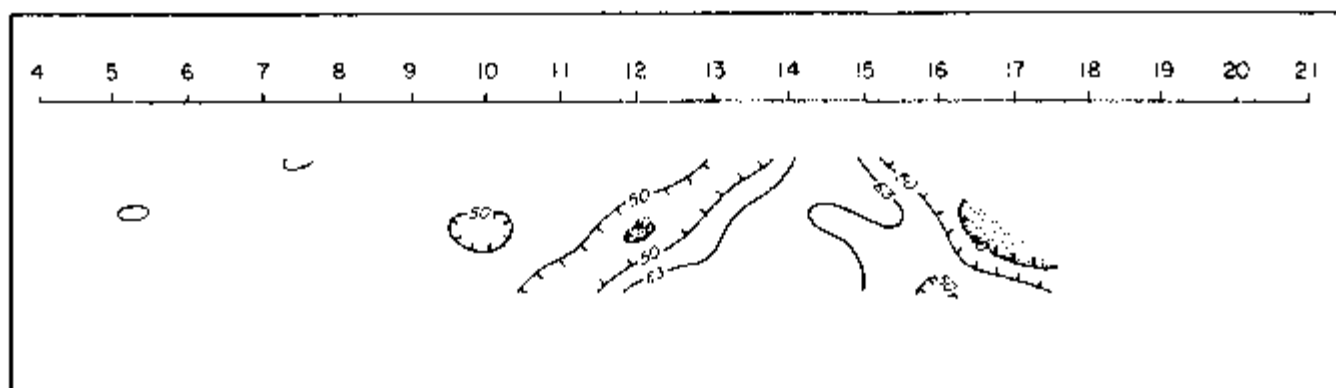


Figure 6.17. Topographic model of apparent resistivity data for line 3, Lisbon Field. Background resistivity = 60 ohm-meters. Plate 6.3 shows topography.

are associated with Jurassic and upper Triassic sediments. The very near-surface zone appears to be relatively non-polarizable. Other low polarization values on the line are associated with Triassic and older sediments. There is some evidence that slightly higher numbers at depth may be associated with Pennsylvanian rocks. The power-lines at station 6.8 appear to have caused high polarization diagonals (left-plunging 7,8, and right-plunging 6,7), although there is no evidence that resistivity information was affected.

There is a slight deepening of the five milliradian contour between stations 8 and 12, but this could easily be a subtle well-casing effect. Otherwise, there is no evidence that the sediments overlying the hydrocarbons have an anomalous polarization response.

RESIDUAL ELECTROMAGNETIC (REM) DATA

The REM data show a strong conductive zone roughly located between stations 7 and 12, although topographic and other geometric effects appear to have limited the eastern extent of the anomaly. The data also show a complex pattern which suggests considerable influence from structural, topographic, and cultural features. For example, the high positive values at the $n=1$ plot point beneath station 6.5 are probably due to the powerlines at station 6.8. Due to these rather substantial effects, the REM data show little additional information on line 3, but they do serve to define the lateral extent of the conductive anomaly more sharply.

6.4 CONCLUSIONS

Review of the Data

The data at Lisbon Field show a strongly conductive anomaly which correlates well with the lateral extent of the hydrocarbons. The anomaly appears to be caused by alteration effects at intermediate to shallow depths in Triassic through upper Pennsylvanian sediments. There is no trace of a polarization anomaly which correlates with the hydrocarbons.

The interpretation of the conductive anomaly at Lisbon Field is influenced by how much the data are truly affected by current channeling due to cased production wells and pipelines. If one takes the well-casing model to be strictly correct, applies *worst-case* assumptions to it, and then removes the calculated well-casing effects from the field data, a moderate, residual anomaly still remains. However, if the conclusions of section 2.5 are correct, and the model is greatly overcorrecting for well-casing effects, then the actual residual anomaly at Lisbon is very much stronger than suggested by the model results.

The important point to consider in regard to well-casing effects is that, no matter what is assumed regarding the applicability of the "PIPE" algorithm, a residual, bona fide, conductive zone almost certainly exists in the sediments overlying the Lisbon Field hydrocarbons. In other words, well casings do not cause this anomaly, they merely tend to enhance it. Arguments have been advanced in this chapter against possible explanations of the anomaly as due to surface culture, topography, or subsurface structure. Hence, it can be concluded with some certainty that the sediments above the hydrocarbons have been electrochemically altered.

Possible Sources of the Anomalies

It is proposed that an upward migration of hydrocarbons from their trap at depth has created a reducing environment over Lisbon Field, which causes or contributes to the conductive anomaly. In this proposed mechanism, light hydrocarbons migrate vertically from the trap through the overlying sediments, eventually reaching the surface. In this particular field, it is doubtful that saline waters migrate vertically from the trap in sufficient quantity to affect the electrical measurements. This is because of the extremely low permeability and great thickness of the Paradox salt, which directly overlies the trap and may act as a significant barrier to upward movement of saline waters. On the other hand, geochemical literature (Duchscherer, 1980) contains evidence that migration of light hydrocarbons is relatively unim-

peded even in materials of low permeability, such as salts. Hence, the hydrocarbons might reach the upper sediments, while waters from depth may not.

Electrically responsive alteration thus appears to occur in relatively shallow sediments of Triassic, Permian, and possibly Pennsylvanian age. Since no "shallow" polarization anomaly was measured on this survey, the "pyrite mechanism," which is widely accepted by many workers, appears to have little to do with the anomaly mechanism at Lisbon Field. Instead, an increase in ion mobility and availability in sediments at medium depths appears to be of primary importance. Insufficient information exists to speculate upon the source of these ions. Future geochemical and hydrological investigations at Lisbon should focus on the influence of vertically migrating hydrocarbons upon local salinity distributions, flow patterns, and water evaporation of the type described by Nisle (1941), in the upper hydrostratigraphic regime above the Paradox Salt. Clays, which are found in Triassic sediments at Lisbon, should also be investigated regarding their role in causing the electrical anomaly.

REFERENCES

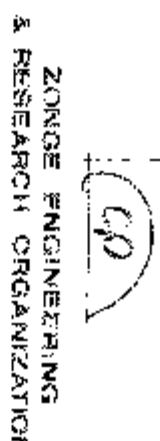
- Baars, D.L., and Stevenson, G.M., 1981, Tectonic evolution of the Paradox Basin, Utah & Colorado, *in* *Geology of the Paradox Formation: Rocky Mountain Assn. of Geologists*, p. 23-31.
- Bradley, G.A., 1975, Lisbon Field, Utah, *in* *Canyonlands country: 8th field conference guidebook, Four Corners Geol. Soc.*, p. 277-278.
- Budd, H., 1960, Notes on the Pure Oil Company discovery at Northwest Lisbon, *in* *Geology of the Paradox Basin fold and fault belt: 3rd field conference guidebook, Four Corners Geol. Soc.*, p. 121-124.
- Clark, C.R., 1978, Lisbon, *in* *Oil and gas fields of the Four Corners area, vol. 2: Four Corners Geol. Soc.*, p. 662-665.
- Duchscherer, W., Jr., 1980, Geochemical methods of prospecting for hydrocarbons: *Oil & Gas Jour.*, Dec. 1, p. 194-208.
- Holtaday, J.S., and West, G.F., 1982, Effects of well casings on surface electrical surveys (abs.): *Geophysics*, v. 47, p. 439. Full paper available in *Technical papers, 51st Annual International Meeting and Exposition, SEG, Los Angeles*, v. 2, p. 815-838.
- Latch, R.F., 1978a, Big Indian Mississippian, *in* *Oil and gas fields of the Four Corners area, vol. 2: Four Corners Geol. Soc.*, p. 602-604.
- , 1978b, Big Indian Pennsylvanian, *in* *Oil and gas fields of the Four Corners area, vol. 2: Four Corners Geol. Soc.*, p. 599-601.
- , 1978c, Little Valley, *in* *Oil and gas fields of the Four Corners area, vol. 2: Four Corners Geol. Soc.*, p. 670-672.
- Matheny, M.L., 1978, A history of the petroleum industry in the Four Corners area, *in* *Oil and gas fields of the Four Corners area, vol. 1: Four Corners Geol. Soc.*, p. 17-24.
- McCaslin, J.C., 1981, Seismic mapping key to Paradox Basin: *Oil & Gas Jour.*, Jul. 13, p. 177-178.
- Mitchell, J.G., 1961, A detailed lithological zonation of the Mississippian at Northwest Lisbon Field, San Juan County, Utah, *in* *Lower and middle Paleozoic rocks of Colorado: Rocky Mountain Assn. of Geologists*, p. 175-184.
- Molenaar, C.M., 1981, Mesozoic stratigraphy of the Paradox Basin—an overview, *in* *Geology of the Paradox Basin: Rocky Mountain Assn. of Geologists*, p. 119-127.
- Nisle, R.G., 1941, Considerations of the vertical migration of gases: *Geophysics*, v. 6, p. 449-454.
- Oil & Gas Journal, 1960, Lisbon Field is major Rockies' find for 1960: *Oil & Gas Jour.*, Dec. 5, p. 156-158.
- Parker, J.M., 1961, The McIntyre Canyon and Lisbon oil and gas fields, San Miguel County, Colorado, and San Juan County, Utah, *in* *Lower and middle Paleozoic rocks of Colorado: Rocky Mountain Assn. of Geologists*, p. 163-173.
- , 1968, Lisbon Field area, San Juan County, Utah: AAPG memoir no. 9, vol. 2, p. 1371-1388. Updated *in* *Geology of the Paradox Basin: Rocky Mountain Assn. of Geologists*, 1981, p. 89-100.

- Petroleum Information, 1982, Lease-ownership maps U-67, U-68 (record takeoff dates 8/82-12/82).
- Smith, K.T., 1978, Hook and Ladder, *in* Oil and gas fields of the Four Corners area, vol. 2: Four Corners Geol. Soc., p. 651-653.
- Smith, K.T., and Prather, O.E., 1981, Lisbon Field-lessons in exploration, *in* Geology of the Paradox Formation: Rocky Mountain Assn. of Geologists, p. 55-59.
- Thackston, J.W., McCulley, B.L., and Preslo, L.M., 1981, Ground-water circulation in the western Paradox Basin, Utah, *in* Geology of the Paradox Basin: Rocky Mountain Assn. of Geologists, p. 201-225.

Explanation of Symbols

Standard Well Symbols	Culture Symbols
○ Drillhole for which information is unavailable.	↓ Metal pipeline, presumed grounded
○ Drilling in progress at time of map publication.	↑ ¹⁵ Underground pipeline: non-metal or unknown
○ Shut in	↓ Metal fence
○ Abandoned	↑ Electric fence
○ ¹⁶ Dry hole with collar depth indicated	~ Barbed telephones or power cable
● Oil well	~ Major high voltage power line
● Gas well	T Telephone line or standard voltage power line
● Oil and gas well	~ Major high voltage power line
● Gas infection well	~ Radio, microwave, or other communication station or tower.
● Water infection well	⊥ DC Power
● Water well	

Standard Well Symbols	Other Symbols
○ ¹⁷ Drilling in progress at the time of the electrical survey; number indicates the amount of cable strung in the hole at the time of data collection	U.S.G.S. boundary symbols or as labeled
○ Well spudded in after completion of the electrical survey	
○ ¹⁸ Number indicates distance of well from the line in terms of degrees; all wells within 1 G boundaries indicated (see sections only)	

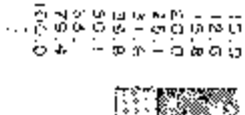


Adherent Resistance

Units: 0h:m-m:ers

Frequency: 2.125 MHz

Endungarika: Anekumar: Intharva:



Decoupled PhosA Angle

011113310000

Frequency: 0.125 Hz.

Insert contour insert.



THE CHINESE

Definition: "mutualism"

On this, November 11, 1918, the

Reference: 101071

Figure 1. Schematic diagram of the experimental setup.

[illegible]

2001-2002

1035

1
2
3
4
5
6
7
8
9
10
11
12
13
14
15
16
17
18
19
20
21
22
23
24
25
26
27
28
29
30
31
32
33
34
35
36
37
38
39
40
41
42
43
44
45
46
47
48
49
50
51
52
53
54
55
56
57
58
59
60
61
62
63
64
65
66
67
68
69
70
71
72
73
74
75
76
77
78
79
80
81
82
83
84
85
86
87
88
89
90
91
92
93
94
95
96
97
98
99
100
101
102
103
104
105
106
107
108
109
110
111
112
113
114
115
116
117
118
119
120
121
122
123
124
125
126
127
128
129
130
131
132
133
134
135
136
137
138
139
140
141
142
143
144
145
146
147
148
149
150
151
152
153
154
155
156
157
158
159
160
161
162
163
164
165
166
167
168
169
170
171
172
173
174
175
176
177
178
179
180
181
182
183
184
185
186
187
188
189
190
191
192
193
194
195
196
197
198
199
200
201
202
203
204
205
206
207
208
209
210
211
212
213
214
215
216
217
218
219
220
221
222
223
224
225
226
227
228
229
230
231
232
233
234
235
236
237
238
239
240
241
242
243
244
245
246
247
248
249
250
251
252
253
254
255
256
257
258
259
260
261
262
263
264
265
266
267
268
269
270
271
272
273
274
275
276
277
278
279
280
281
282
283
284
285
286
287
288
289
290
291
292
293
294
295
296
297
298
299
300
301
302
303
304
305
306
307
308
309
310
311
312
313
314
315
316
317
318
319
320
321
322
323
324
325
326
327
328
329
330
331
332
333
334
335
336
337
338
339
340
341
342
343
344
345
346
347
348
349
350
351
352
353
354
355
356
357
358
359
360
361
362
363
364
365
366
367
368
369
370
371
372
373
374
375
376
377
378
379
380
381
382
383
384
385
386
387
388
389
390
391
392
393
394
395
396
397
398
399
400
401
402
403
404
405
406
407
408
409
410
411
412
413
414
415
416
417
418
419
420
421
422
423
424
425
426
427
428
429
430
431
432
433
434
435
436
437
438
439
440
441
442
443
444
445
446
447
448
449
450
451
452
453
454
455
456
457
458
459
460
461
462
463
464
465
466
467
468
469
470
471
472
473
474
475
476
477
478
479
480
481
482
483
484
485
486
487
488
489
490
491
492
493
494
495
496
497
498
499
500
501
502
503
504
505
506
507
508
509
510
511
512
513
514
515
516
517
518
519
520
521
522
523
524
525
526
527
528
529
530
531
532
533
534
535
536
537
538
539
540
541
542
543
544
545
546
547
548
549
550
551
552
553
554
555
556
557
558
559
560
561
562
563
564
565
566
567
568
569
570
571
572
573
574
575
576
577
578
579
580
581
582
583
584
585
586
587
588
589
590
591
592
593
594
595
596
597
598
599
600
601
602
603
604
605
606
607
608
609
610
611
612
613
614
615
616
617
618
619
620
621
622
623
624
625
626
627
628
629
630
631
632
633
634
635
636
637
638
639
640
641
642
643
644
645
646
647
648
649
650
651
652
653
654
655
656
657
658
659
660
661
662
663
664
665
666
667
668
669
670
671
672
673
674
675
676
677
678
679
680
681
682
683
684
685
686
687
688
689
690
691
692
693
694
695
696
697
698
699
700
701
702
703
704
705
706
707
708
709
710
711
712
713
714
715
716
717
718
719
720
721
722
723
724
725
726
727
728
729
730
731
732
733
734
735
736
737
738
739
740
741
742
743
744
745
746
747
748
749
750
751
752
753
754
755
756
757
758
759
760
761
762
763
764
765
766
767
768
769
770
771
772
773
774
775
776
777
778
779
780
781
782
783
784
785
786
787
788
789
790
791
792
793
794
795
796
797
798
799
800
801
802
803
804
805
806
807
808
809
810
811
812
813
814
815
816
817
818
819
820
821
822
823
824
825
826
827
828
829
830
831
832
833
834
835
836
837
838
839
840
84

2000

 $\frac{1}{2} \frac{d}{dt} \left(\frac{1}{2} \frac{d}{dt} \right)$

52

TABLE 1

Plate 6.2
RESISTIVITY/PHASE PRUDSECTION DATA
Lisbon Field
San Juan Co., Utah

Line 2
a = 2,000 feet

Explanation of Symbols

Standard Well Symbols	Culture Symbols
Drillhole for which information is undeterminable	Metal pipeline, spanned or grounded
Drilling in progress at time of map preparation	Ungrounded pipeline - non-worked or suspended
Shut in	Metal fence
Abandoned	Electric fence
Day hole with total depth indicated	Buried telephone or power cable
Oil well	Telephone line or standard voltage power line
Gas well	Major high voltage power line
Oil and gas well	Radio, microwave, or other communications station or tower
Gas pipeline well	DC pump
Water injection well	
Water well	

Special Well Symbols

- Drilling in progress at the time of the electrical survey; number indicates its amount of drilling in the hole at the time of data collection
- Well sounded in after completion of the electrical survey
- Number indicates distance of well from the line in terms of paragraphs; all wells within 1.0 paragraph indicated (paragraphs only)

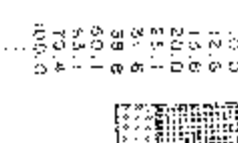
Other Symbols

U.S.G.S. standard symbols as labeled

ZONE ENGINEERING
& RESEARCH ORGANIZATION

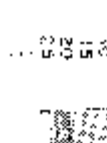
Apparent Resistivity

Units: ohm-cm
Frequency: 0.125 Hz
Geometric constant interval:



Decoupled Phase Angle

Units: milliradians
Frequency: 0.125 Hz
Linear contour interval:



REM Quadrature

Units: normalized imaginary
Frequency: 0.125 Hz
Logarithmic contour interval:

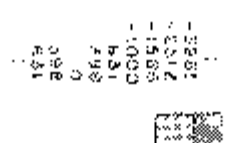
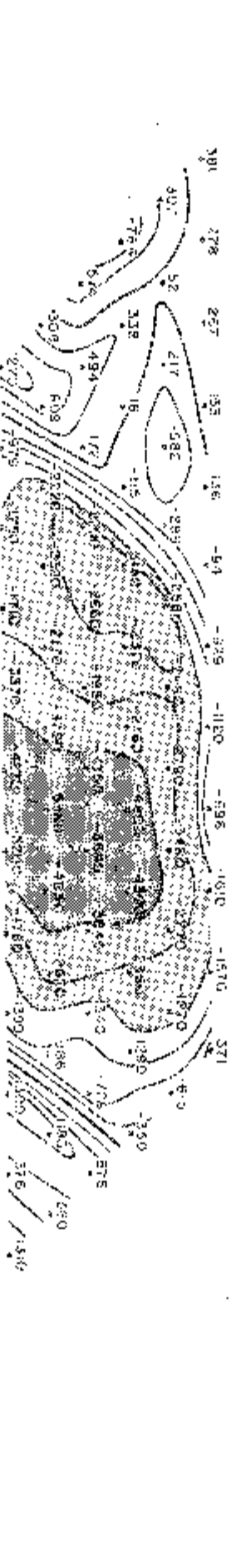
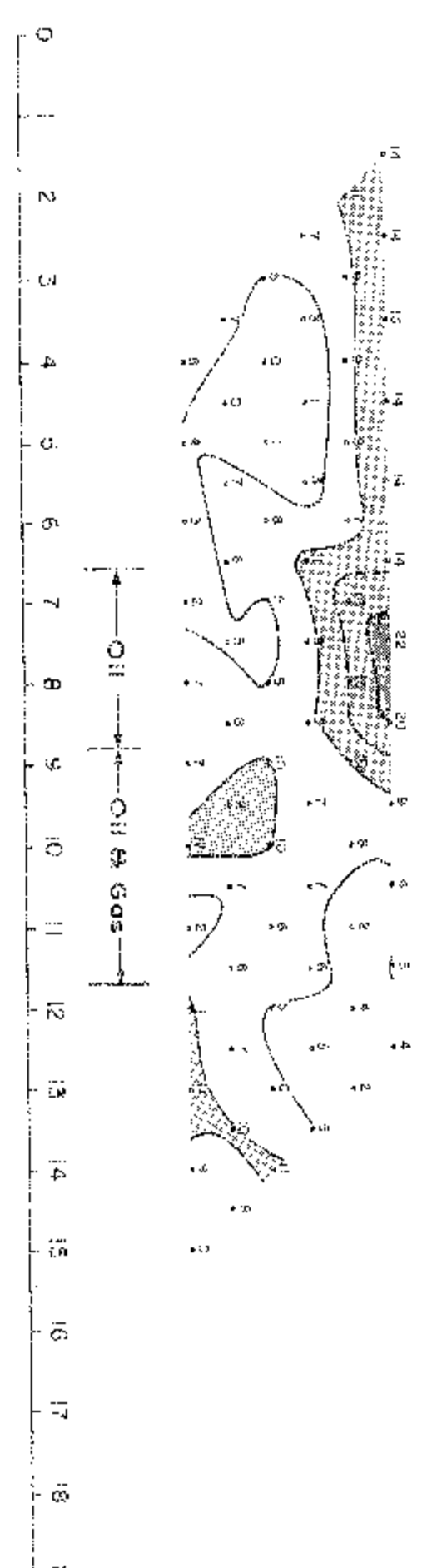
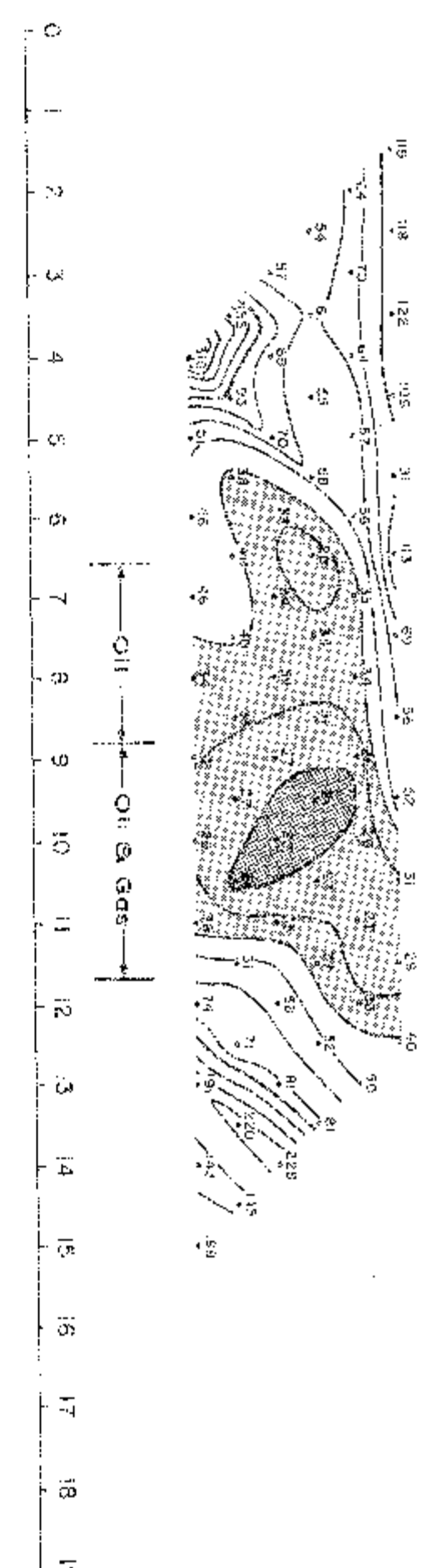
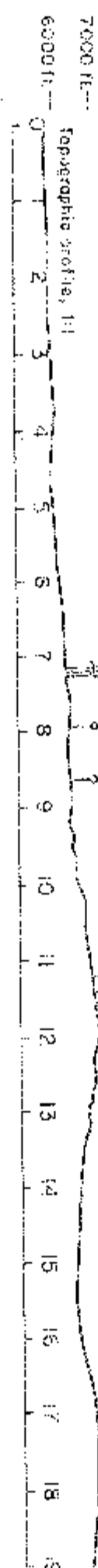
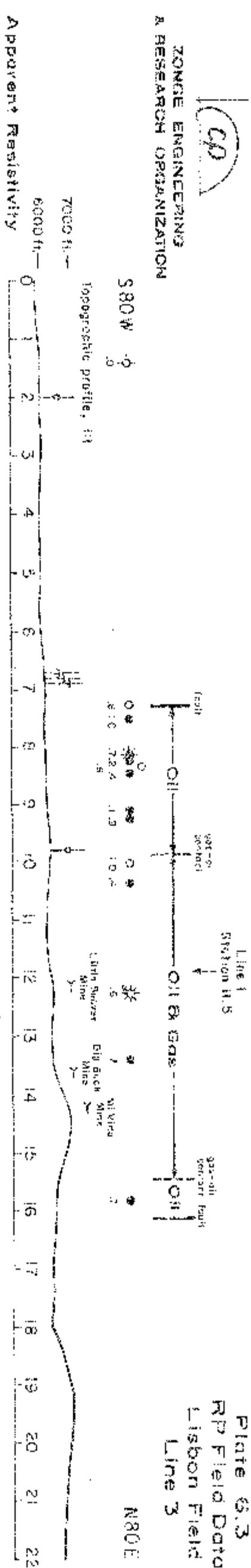


Plate 6.2
APP Field Data
Lisbon Field
Line 2
N 70 E
Station 14.9
Line 1
Oil well
Gas well
Oil & Gas
N 70 E



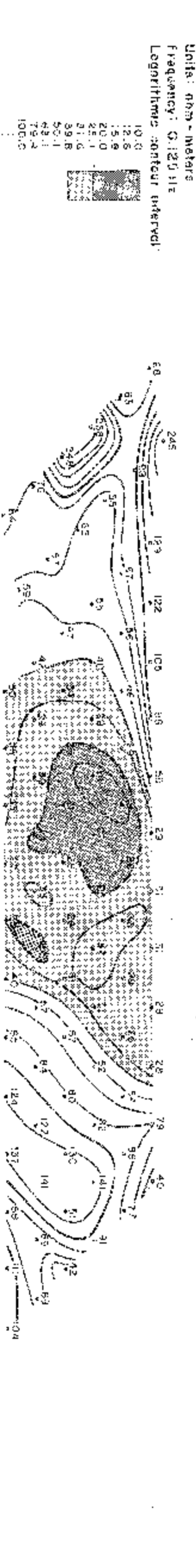
ZONCE ENGINEERING A RESEARCH ORGANIZATION

Plate 6.3
RP Field Data
Lisbon Field
Line 3
N80E



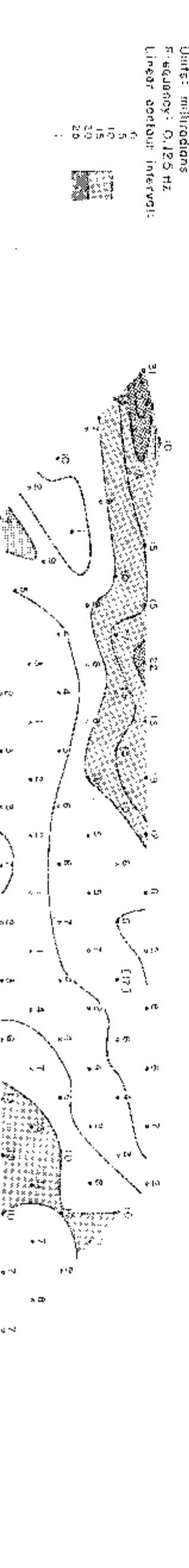
Apparent? Resistivity?

Units: mm - meters
Frequency: 0.125 Hz
Logarithmic contour interval:



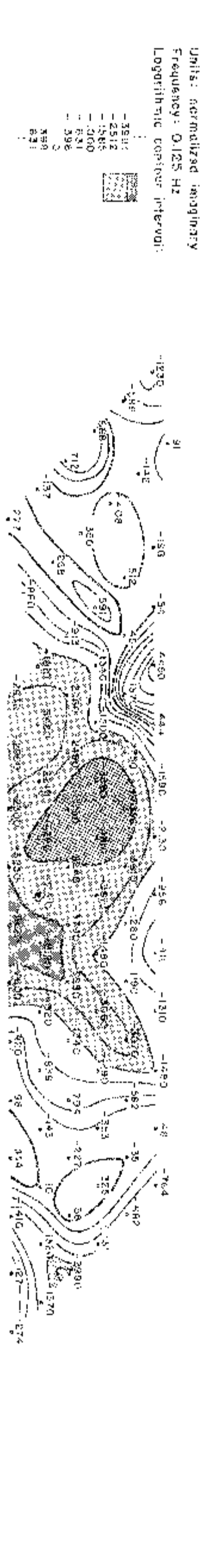
Decoupled Phases Angl

Units: milliseconds
Frequency: 0.125 Hz
Linear contour interval:



REFERENCES

Units: normalized imaginary
Frequency: 0.125 Hz
Logarithmic contour interval:



සමස්ත සිංහල-සිංහල හි සිංහල-සිංහල, 1998

Chapter 7

Trap Spring Field

Nye County, Nevada

7.1

INTRODUCTION

Trap Spring Field is located in the north-south trending Railroad Valley, which lies between the Grant Range and the Pancake Range in east-central Nevada (Figure 7.1). The field is approximately 65 miles (105 km) southwest of Ely, Nevada. Trap Spring is only the second economic oilfield in the state, and is one of only six known fields in the entire Basin and Range Province of the western United States. Production is from Oligocene volcanics between 3,200 and 4,950 feet (975-1,510 m).

Three lines of resistivity/phase data were run across Trap Spring Field, using a dipole spacing of 1,250 feet (381 m).

7.2

GEOLOGIC

BACKGROUND

Exploration

History of

Trap Spring Field

The Basin and Range area has been of interest to exploration geologists since the late 19th century, when the first claims were filed for oil-shale lands near Elko, Nevada. These lands were shown to be uneconomic when they were developed between 1916 and 1920, although interest persisted in them for some years afterwards.

Oil was first discovered in the Basin and Range area in 1904, at Rozel Point, near Salt Lake. The well was relatively uneconomic, and the exploration outlook for the area was dim until Shell Oil Company discovered the Eagle Springs Field in 1954. This discovery spurred a flurry of activity, resulting in the drilling of some 200 dry holes over the next two decades, partly on the basis of erroneous conceptions of Basin and Range geology (Foster, 1979).

In 1973, geologists from Filon Exploration Company undertook an investigation of promising new wildcat targets across the United States, based upon the concept of using existing productive fields with well-defined structures as models for exploration in the adjacent areas (Dolly, 1979; Foster, 1979). The area of the

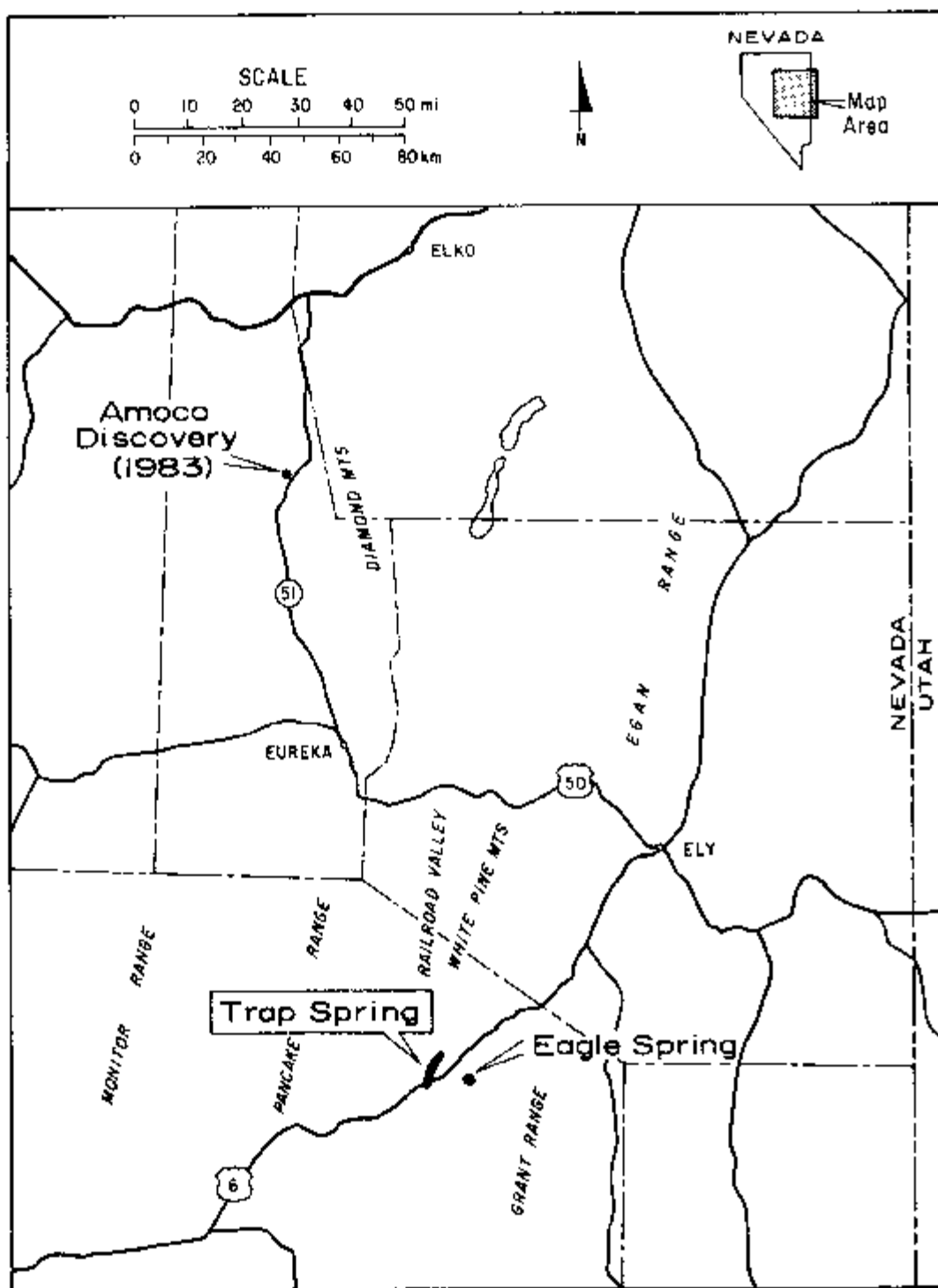


Figure 7.1. Location map of Trap Spring Field.

Railroad Valley was targeted in this program, using Eagle Springs as an exploration model. The Eagle Springs production is from the Garrett Ranch Group volcanics, and the trap is controlled by basin faulting, stratigraphic thinning, and folding of the reservoir rocks. Filon used these geological parameters in a program of photographic geomorphic mapping, which succeeded in identifying a number of favorable targets.

This was followed by the shooting of several seismic lines, one of which crossed the Railroad Valley westward to the Trap Spring area. Encouraged by the geomorphic/seismic data and by oil shows in Shell Oil Company's No. 1 Lockes Well, Filon and a number of other investors spudded Northwest Exploration Trap Spring No. 1, which was completed successfully in late 1978. The discovery well pumped 1,200 BOPD with open hole completion, producing from a pay zone some 800 feet (250 m) thick in the Garrett Ranch Group. More than two dozen wells have been drilled in subsequent years, half of which are currently producing. Production from Trap Spring varies considerably, but the average was about 3,000 BOPD in 1978.

The economics of oil production at Trap Spring are not entirely favorable. Completed wells typically cost around \$500,000 and transportation costs are considerable for this remote field. As a result, it is often cheaper to transport oil from neighboring states than it is to produce Trap Spring oil for the limited market in Nevada.

Recent drilling has been undertaken in Railroad Valley by several parties. In 1978, a well near Currant produced oil but it is believed to be non-economic. Northwest Exploration has continued its work in the area. Wexpro Company and Supron Energy have also been active of late (McCaslin, 1980, 1981b). A recent discovery by Amoco in Pine Valley (Oil & Gas Journal, 1983; McCaslin, 1983) marks the third commercial field in Nevada. Initial production was 346 barrels of 27° API gravity, low pour point oil and 787 barrels of water per day. Amoco announced that two zones are productive, but did not elaborate on which ones they are.

Geologic History of the Trap Spring Area

Since few wells have penetrated pre-Cretaceous sediments at Trap Spring, little is known about Paleozoic and pre-Paleozoic geology. The known geologic history of the Railroad Valley area begins with the Cretaceous, when Paleozoic limestones and shales were subjected to downwarping and erosion, followed by episodes of lacustrine deposition. The first Basin and Range faulting in the early Oligocene (36 million years ago) resulted in further downwarping of the sediments, followed by successive erosion/deposition cycles. Downwarped areas were filled in with the fluvial and lacustrine sediments of the Sheep Pass and Newark Canyon formations. These lacustrine sediments are present at Eagle Springs, but are absent in the Trap Spring area, either because they were never deposited on the upwarped topography there, or because they were eroded away during the periodic episodes of uplift which interrupted their deposition.

The first volcanics appeared with the ash flows of the Stone Cabin Formation 34 million years ago. These deposits were the result of the extensive volcanism which characterized the Tertiary period in western North America. Most of the volcanics in the Railroad Valley area were ejected explosively from nearby vents and were deposited as density flows of superheated pyroclasts and gases (French and Freeman, 1979). Settling, cooling, and compaction led to a zonation of welding density, while weathering and degassing processes altered the feldspars to clays in certain zones of the ash flows. Episodes of eruption, deposition into low-lying areas, erosion, and Basin and Range uplift built up a sequence of rhyolites, dacites, quartz latites, and rhyodacites which constitute the Pritchards Station Formation (the producing horizon at Trap Spring) and the Windous Butte Formation. These two volcanic formations are part of the Garrett Ranch Group.

The cessation of volcanism was followed by an erosional episode, resulting in the so-called "Unconformity A," which separates the Oligocene volcanics from an overburden of Tertiary-Quaternary valley fill. These recent sediments comprise the

Horse Camp Formation, a sequence of clay-filled, carbonate cemented sandstones, siltstones, marlstones, and Pliocene playa-lake deposits.

Current Geology

A simplified geologic cross-section along an east-west traverse across east-central Nevada is presented in Figure 7.2. This illustrates the general character of the horst-and-graben faulting of the Basin and Range area.

Figure 7.3 shows the electrical line locations at Trap Spring. Figure 7.4 shows the depth to Unconformity "A" and the important graben faults. Note that line 2 of the electrical survey is parallel to this faulting. Figure 7.5 is an isopach map of the Oligocene Garrett Ranch Group.

The present-day stratigraphy is described in Table 7.1, and a geologic cross-section corresponding to line 3 of the survey is presented in Figure 7.6.

Reservoir Characteristics

Production at Trap Spring is entirely from the Pritchards Station Formation of the Garrett Ranch Group. This tuff has considerable vertical variation in the degree of welding. Depending upon welding, pore-filling mineralization, and compaction due to degassing, the rock matrix porosity varies from 1 percent to over 70 percent. However, permeability is extremely low—about 0.1 millidarcy. The reason for this is that pore spaces in these volcanics are not interconnected since they are formed by the escape of discrete gas bubbles from the rock. As a result, oil is not found in the pore spaces. Instead, it is found in the numerous cooling joints and fractures which characterize volcanics of this type. There is evidence (Dolly, 1979) that the more densely welded sections are more intensely fractured, making them more likely to host oil. The trap is confined at the top by a heavily weathered zone, in which clay alteration has created an impermeable layer by filling the available joints and fractures.

The source of the oils at Trap Spring and Eagle Springs is believed to be the Sheep Pass Formation (Upper Cretaceous through Eocene lacustrine deposits), which is not present at Trap Spring, or the Chainman Formation (Mississippian shales), an immature source rock in the Trap Spring area. Migration is believed to have occurred during Miocene to Pliocene time.

Table 7.2 presents pertinent data on the reservoir characteristics of Trap Spring. Several items are of interest here. First, note that no gas is dissolved in the

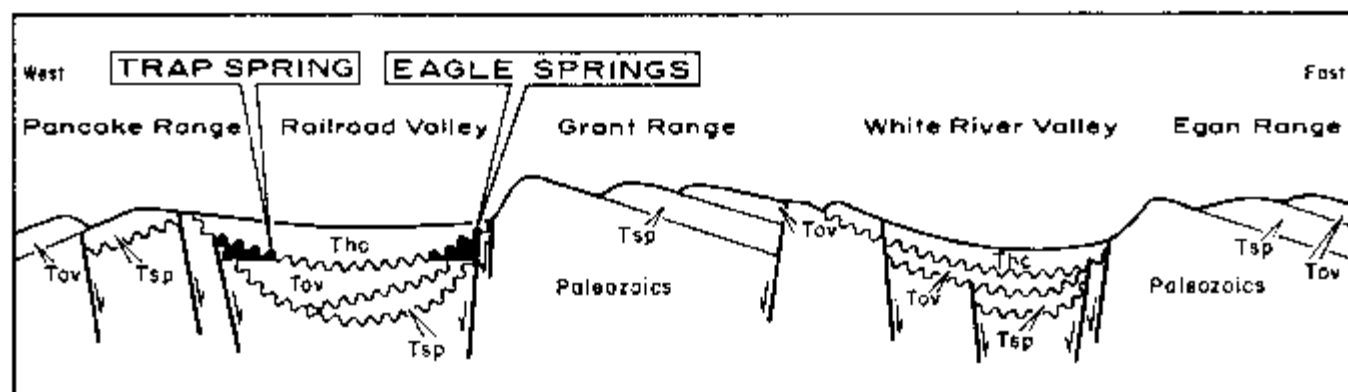


Figure 7.2. Schematic depiction of the Basin and Range geology of eastern Nevada along an east-west traverse. Note: Tsp = Sheep Pass Formation. Production in the Railroad Valley is from Oligocene volcanics. No hydrocarbons have yet been found in Oligocene sediments in the White River Valley, which is located east of the Railroad Valley.

TABLE 7.1: STRATIGRAPHIC DESCRIPTION OF TRAP SPRING FIELD

System	Symbol	Formation	Lithologic Description
CENOZOIC ROCKS			
Quaternary	Qal	Playa lake deposits	Interbedded claystone and conglomerate
Tertiary			
Miocene/Pliocene	Thc	Horse Camp Fm.	Unconsolidated valley fill: sands, gravels, conglomerates
		(Unconformity "A")	-----
Oligocene	Tov	Garrett Ranch Group (ash zone)	Weathered ash and clay; forms an impermeable cap over volcanics
		Window Butte Fm.	Ash flow tuff, mostly absent in the immediate Trap Spring area
		Upper unit	Partly to densely welded tuff
		Lower unit	Densely welded tuff with a vitreous basal section
		Pritchards Station Fm.	Ash flow tuff with large numbers of plagioclase and large biotite phenocrysts, high in mafic content; <i>hosts all of the oil at Trap Spring</i>
		(weathered zone)	Bentonitic sandstone
		Stone Cabin Fm.	Ash flow tuff with abundant phenocrysts, low in mafic content
		Upper unit	Slightly to densely welded tuffs with abundant quartz and feldspars and some biotite
		Middle unit	Partly welded at the top, densely welded at the bottom
		Lower unit ("Calloway Well Fm.")	Non-welded to welded tuffs with some pumice fragments
		(unconformity)	-----
PALEOZOIC ROCKS			
Mississippian	Mch	Chainman Fm.	Shales; not present in some Trap Spring holes
Devonian	Dg	Guilmette Fm.	Fractured dolomite with conodonts; deepest unit penetrated at Trap Spring

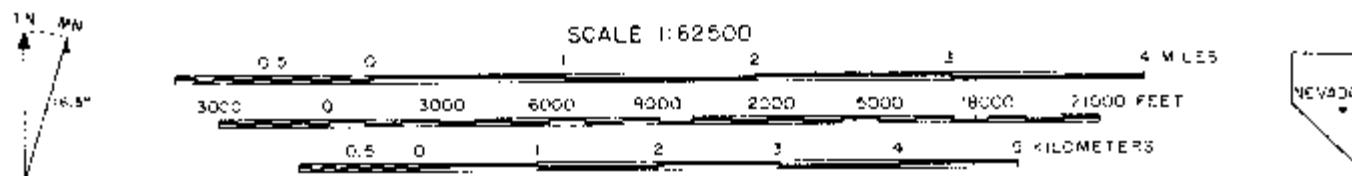
oils—a very unusual situation. This raises the interesting possibility that the trap is imperfectly sealed to lighter hydrocarbons, or, alternatively, that the gases dissipated during migration. Duey (1979) notes that the missing low-carbon molecules may imply partial bacterial alteration; he also notes that the lower-gravity oils toward the south may indicate increased bacterial action in that direction. It is also interesting to note that the reservoir waters have a fairly high resistivity of about 1 ohm-meter.

Approximately 2.5 MMBO had been recovered from Trap Spring at the time of the electrical survey. Production is now in decline, but the oil reserves are by no means depleted (Duey, 1983).

Groundwater Characteristics

The Trap Spring area water table lies at or near the surface of the ground, accounting for the numerous springs and ponds found there. The water is quite saline.

Figure 7.3
LINE LOCATION MAP
Trap Spring Field
 Nye Co., Nevada



Sources

Base: U.S.G.S., 15' Quad (Blue Eagle Springs, Nev., 1964)

Well Data: Dwyer (1979)

Explanation of Symbols

Standard Well Symbols

- Drillhole for which information is unobtainable
- Drilling in progress at time of map preparation
- ⊕ Shut in
- ⊘ Abandoned
- ^{25,470} Dry hole with total depth indicated
- Oil well
- ☼ Gas well
- ☼ Oil and gas well
- ☼ Gas injection well
- ☼^w Water injection well
- Water well

Culture Symbols

- ⊕ Metal pipeline, presumed grounded
- ⊕³ Ungrounded pipeline: non-metal or suspended
- ↑ Metal fence
- ⚡ Electric fence
- ⚡ Buried telephone or power cable
- Telephone line or standard voltage power line
- ⚡ Major high voltage power line
- ☼ Radio, microwave, or other communications station or tower
- ⊕ DC pump

Special Well Symbols

- ²⁵₂₀₀₀ Drilling in progress at the time of the electrical survey; number indicates the amount of drill stem in the hole at the time of data collection
- Well spudded in after completion of the electrical survey
- ^{0.7} Number indicates distance of well from the line in terms of a-spacings; all wells within 1.0 a-spacings indicated (pseudosections only)

Other Symbols

U.S.G.S. standard symbols or as labeled

Map-Specific Symbols

Topographic contour interval: 200 feet

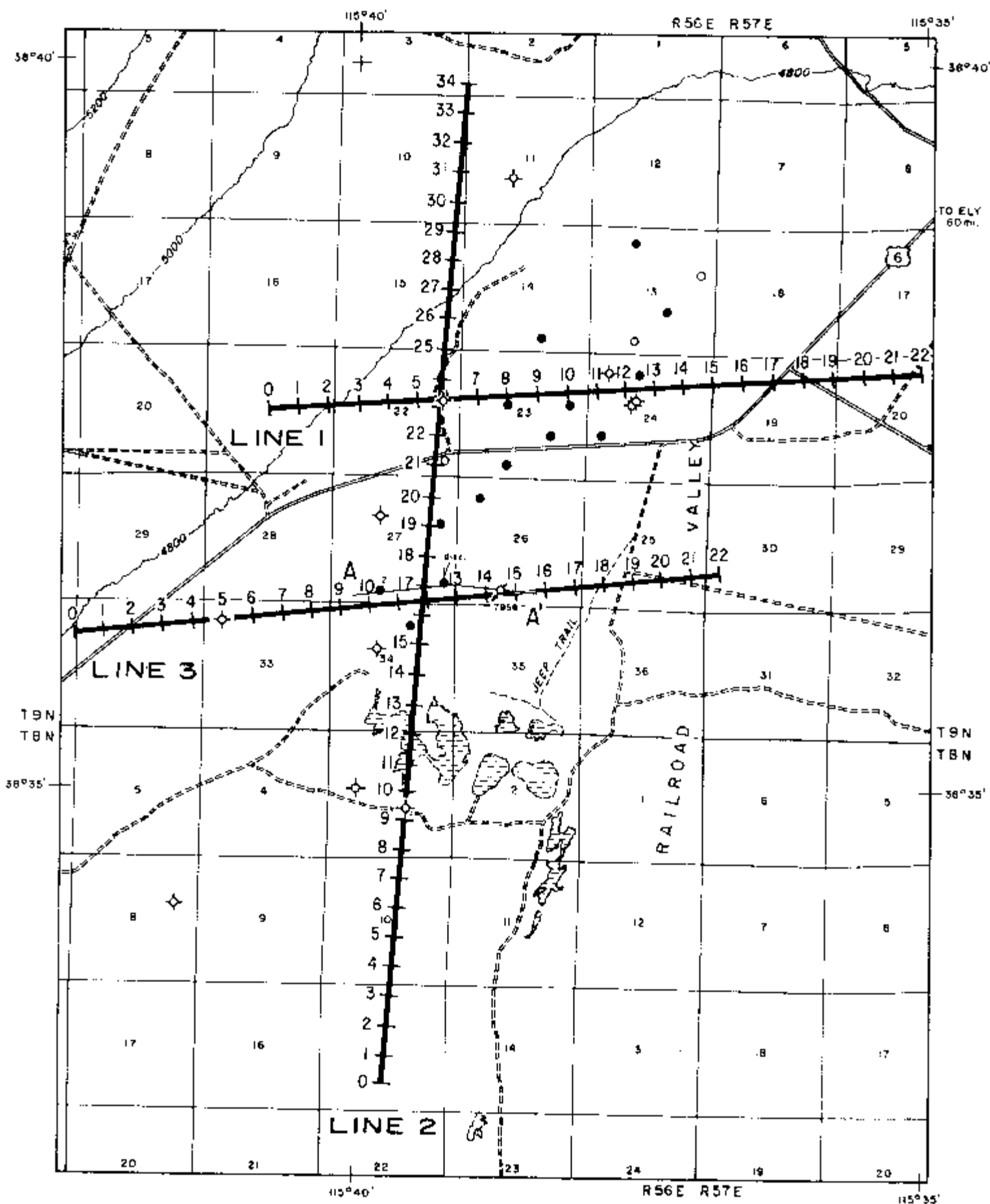
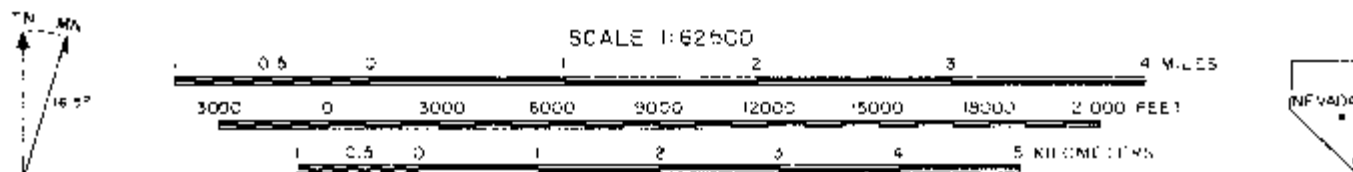


Figure 7.4
STRUCTURE MAP—TOP OF UNCONFORMITY "A"
Trap Spring Field
 Nye Co., Nevada



Sources

Base: U.S.G.S. 15' Quad 18 Blue Eagle Springs, Nev., 19641

Well Data: Duey (1979)

Geology: Duey (1979)

Explanation of Symbols

Standard Well Symbols

- ⊙ Drillhole for which information is unobtainable
- Drilling in progress at time of map preparation
- ◐ Shut in
- ◑ Abandoned
- ⊙^{10,420} Dry hole with total depth indicated
- Oil well
- ☼ Gas well
- ☼ Oil and gas well
- ☼ Gas injection well
- ☼ Water injection well
- Water well

Special Well Symbols

- ⊙<sup>55
2000</sup> Drilling in progress at the time of the electrical survey; number indicates the amount of drill stem in the hole at the time of data collection
- ⊙ Well spudded in after completion of the electrical survey
- ^{0.5} Number indicates distance of well from the line in terms of a-spacings; all wells within 1.0 a-spacings indicated (pseudosections only)

Culture Symbols

- Metal pipeline, presumed grounded
- Ungrounded pipeline: non-metal or suspended
- Metal fence
- Electric fence
- Buried telephone or power cable
- Telephone line or standard voltage power line
- Major high voltage power line
- Radio, microwave, or other communications station or tower
- DC pump

Other Symbols

U.S.G.S. standard symbols or as labeled

Map-Specific Symbols

Structure contour interval: 500 feet

Datum: Mean sea level

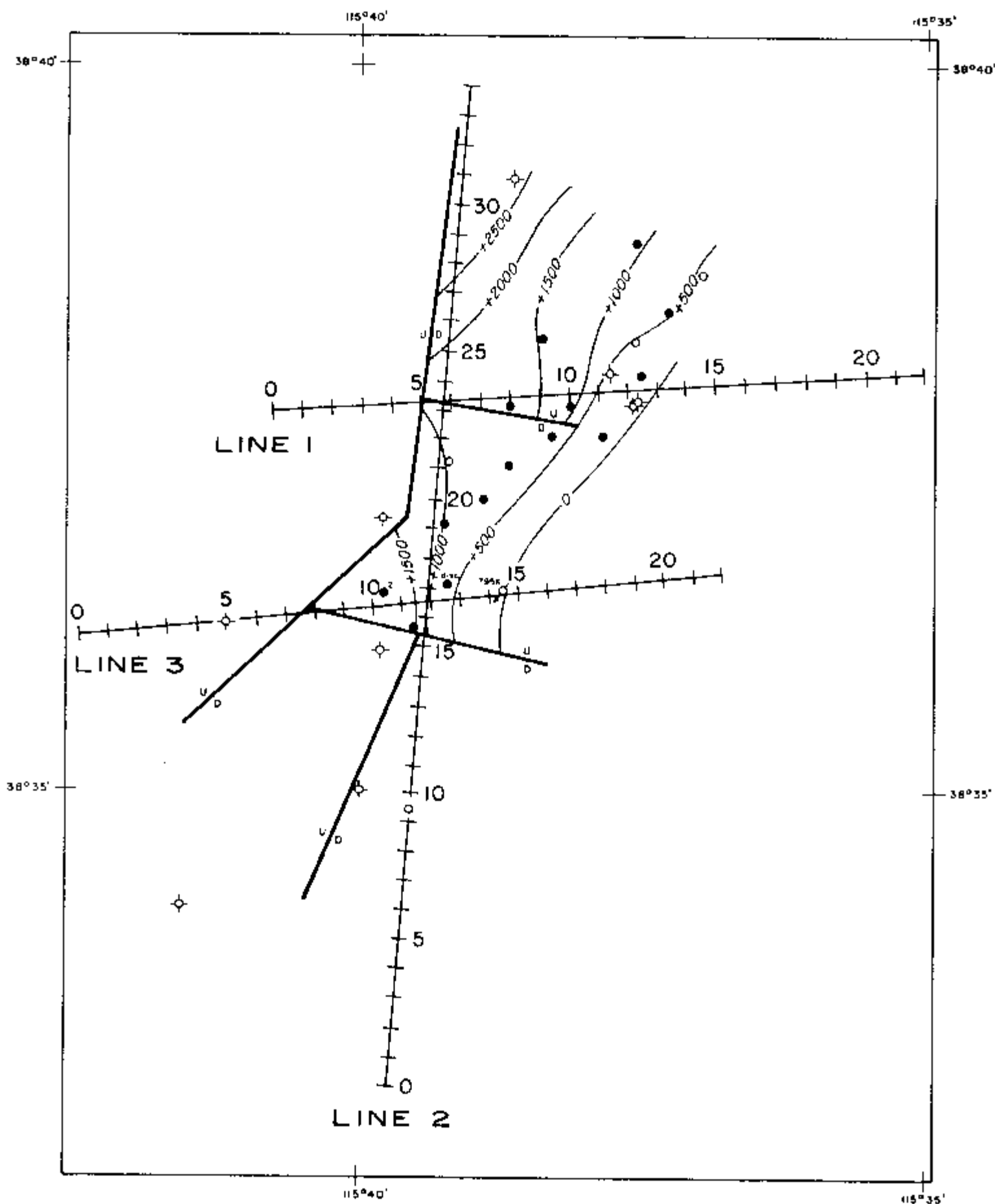
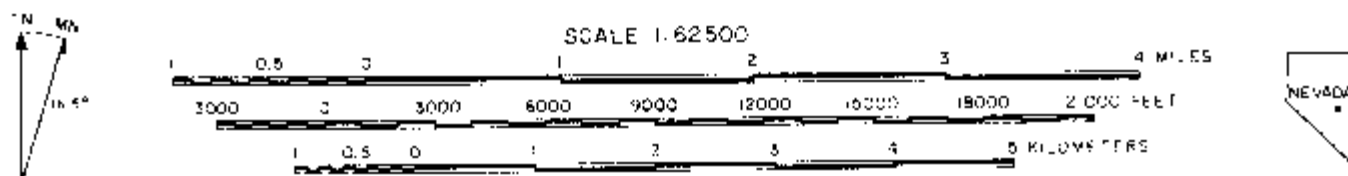


Figure 7.5
ISOPACH MAP—GARRETT RANCH GROUP
Trap Spring Field
Nye Co., Nevada



Sources

Base: U.S.G.S. 15' Quad (Blue Eagle Springs, Nev., 1964)

Well Data: Duey (1979)

Geology: Duey (1979)

Explanation of Symbols

Standard Well Symbols

- Drillhole for which information is unobtainable
- Drilling in progress at time of map preparation
- ⊙ Shut in
- ⊘ Abandoned
- ⊙^{2,420} Dry hole with total depth indicated
- Oil well
- ☼ Gas well
- ☼ Oil and gas well
- ☼ Gas injection well
- ⊙¹ Water injection well
- Water well

Culture Symbols

- ⚡ Metal pipeline, presumed grounded
- ⚡¹¹⁵ Ungrounded pipeline: non-metal or suspended
- ⚡ Metal fence
- ⚡ Electric fence
- ⚡ Buried telephone or power cable
- T Telephone line or standard voltage power line
- ⚡ Major high voltage power line
- ⚡ Radio, microwave, or other communications station or tower
- ⚡ DC pump

Special Well Symbols

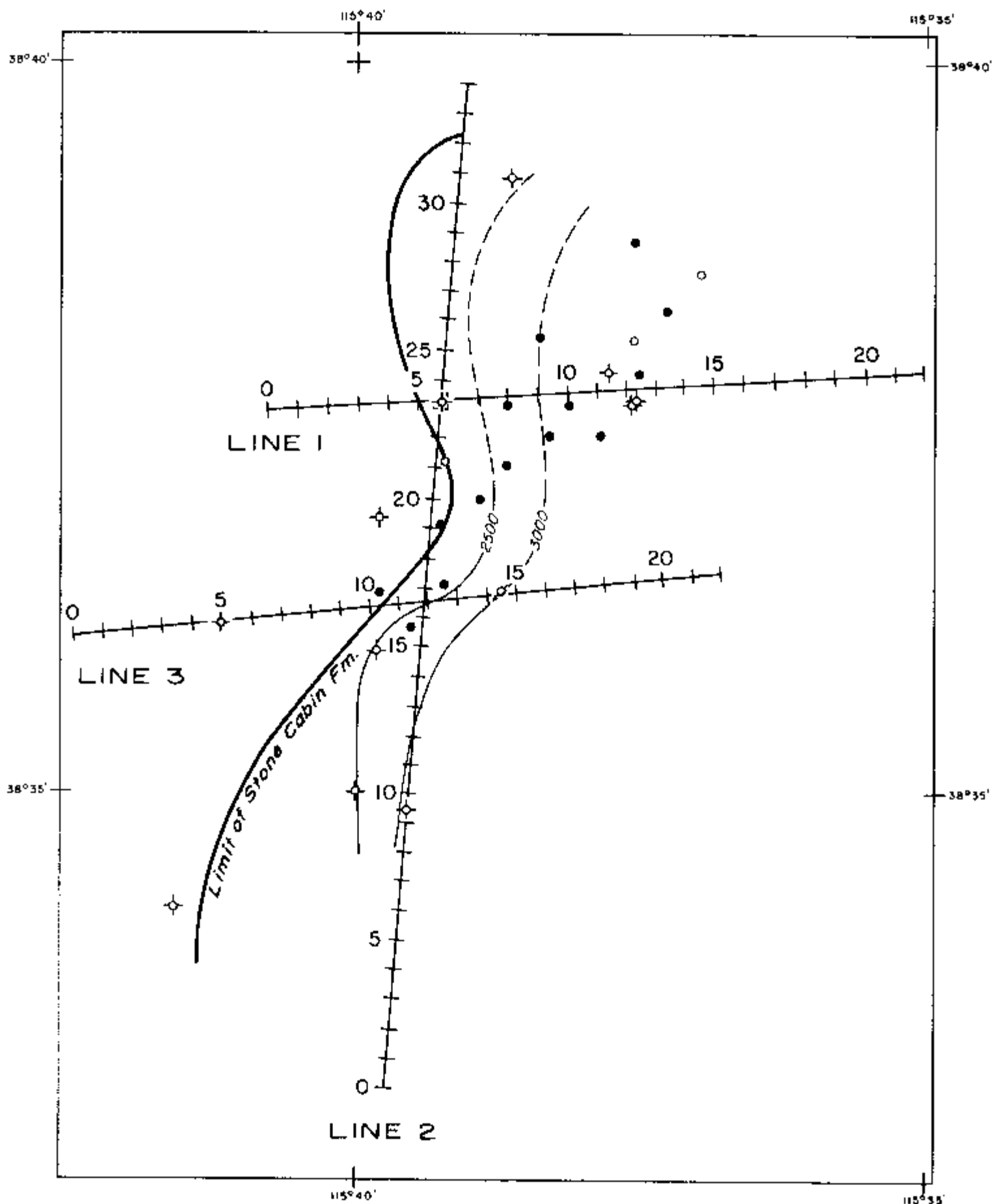
- ⊙²⁵₂₅₀₀ Drilling in progress at the time of the electrical survey; number indicates the amount of drill stem in the hole at the time of data collection
- ⊙ Well spudded in after completion of the electrical survey
- ^{0.7} Number indicates distance of well from the line in terms of a-spacings; all wells within 1.0 a-spacings indicated (pseudosections only)

Other Symbols

U.S.G.S. standard symbols or as labeled

Map-Specific Symbols

Isopach contour interval: 500 feet



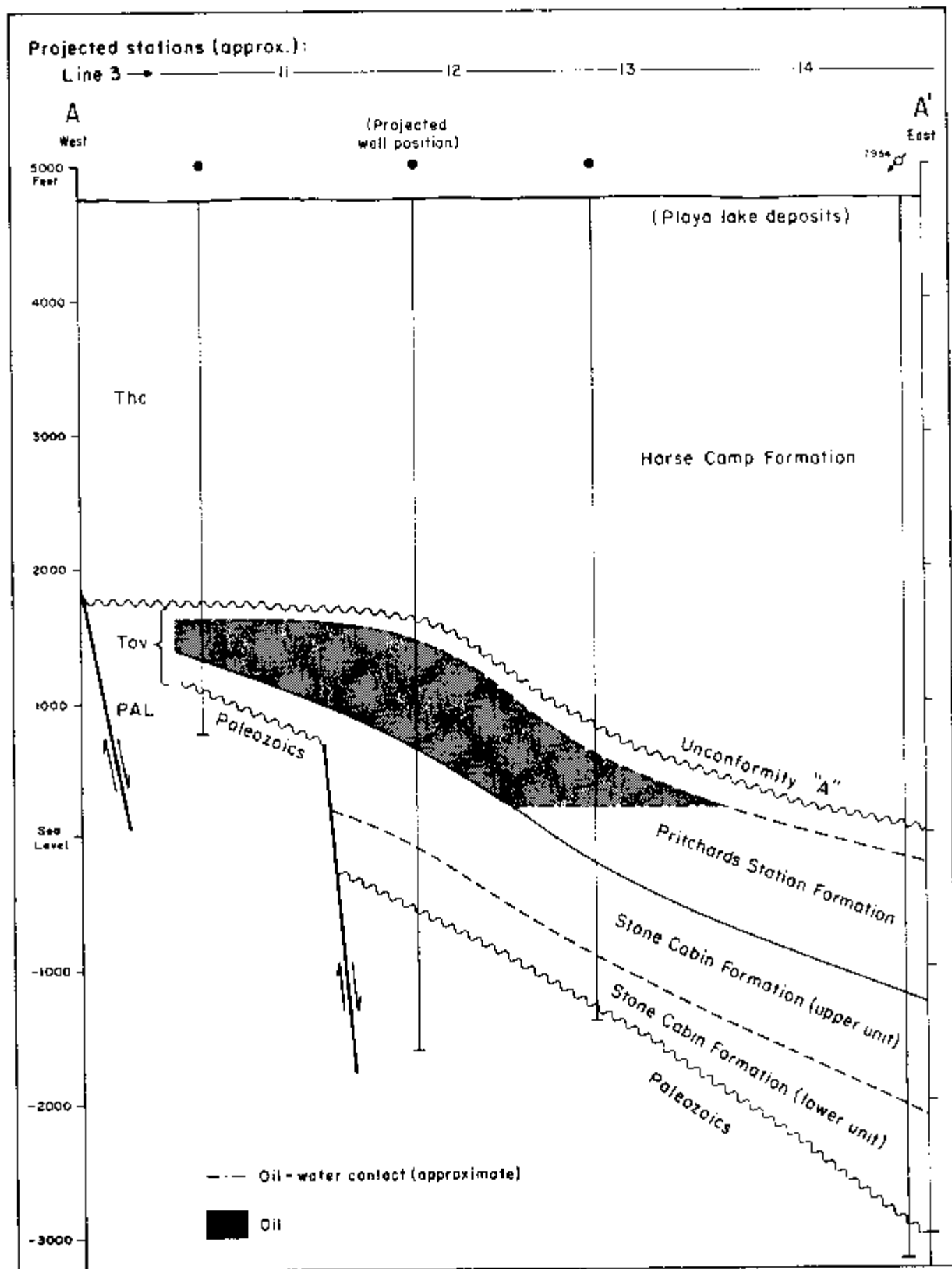


Figure 7.6. Geologic cross-section A-A', with no vertical scale exaggeration; this may be compared with the data from line 3 of the electrical survey. Refer to Figure 7.3 for map location. After Duey (1978).

TABLE 7.2: RESERVOIR CHARACTERISTICS OF TRAP SPRING FIELD

General Field Data

Region: Basin and Range Province
 Production: Oil
 Type of Trap: Stratigraphic and structural
 Producing Formations and Depths: Pritchards Station Fm., 3,200 to 4,950 ft
 Other Significant Shows: None
 Total Reserves: Not reported
 Productive Area: Proved 1,280 acres, unproved 960 acres
 Field Operator: Northwest Exploration, Texaco
 Number of Producing Wells (1979): 14
 Well Casing Data: Surface casing 9-5/8 inch to 150-450 ft, production casing 7 inch to volcanics (typical Northwest Exploration wells). Production casing 7 or 9-5/8 inch, some with 6 inch liner, and some open hole completed in the Garrett Ranch (typical Texaco wells).

Discovery Well

Name: Northwest Exploration No. 1 Trap Spring
 Location: SE-SE-27-T9N-R56E
 Completion Date: 11/30/76
 Total Depth: 6,137 ft (Pritchards Station)
 Perforations: None, open hole completion
 Initial Potential: Pumping 417 BOPD
 Treatment: None

Reservoir Data: Pritchards Station Formation

Discovery: 11/30/76; Northwest Exploration No. 1 Trap Spring, SE-SE-27-T9N-R56E
 Lithology: Ash flow tuff
 Age: Oligocene
 Type of Trap: Stratigraphic and structural
 Drive Mechanism: Water
 Gross Thickness of Reservoir Rock: 800 ft
 Porosity: Fracture (cooling joints and fractures in volcanics)
 Permeability: Unknown, usually large within the trap; less than 0.1 millidarcy outside the fracture zones
 Oil Column: 1,700 ft
 Gas/Oil Ratio: No gas
 Original Oil/Water Contact: Approx -200 ft
 Oil Character: Black; gravity 21.5° API (varies from 21° API in the south to 28° API in the north); pour point 0 to 5° F (increases to 40° F toward the north)
 Oil Analysis:

Pristane/phytane ratio	1.24
Sulfur	0.8%
Methane	none

Water Saturation: Unknown
 Water Salinity: Low, 5,400 ppm TDS
 Water Resistivity: 1.10 ohm-meters at 68° F
 Daily Average Production (12/78): 3,450 BOPD
 Estimated Primary Recovery: Unknown
 Type of Secondary Recovery: None
 Estimated Ultimate Recovery: Unknown

Well-Casing Information

Well-casing diameters and well completion practices vary somewhat at Trap Spring Field. Surface casing is typically 9-5/8 inches (24.5 cm) in diameter and is set as deep as 450 feet (140 m). Production casing for Northwest Exploration wells is almost universally 7 inches (17.8 cm) in diameter, but a few Texaco wells have production casings as large as 9-5/8 inches (24.5 cm). Although a 7-inch diameter is probably a typical figure, a worst-case 9-5/8-inch diameter was assumed for the computer models.

7.3 DISCUSSION OF THE DATA

Introduction

Directed by Zonge Engineering geophysicist Norman R. Carlson, a resistivity/phase crew of eight persons was mobilized to the Trap Spring area on November 1, 1979. Two parallel lines and a single cross-line were run with a dipole spacing of 1,250 feet (381 m). Data were obtained at 0.125, 0.25, 0.5, and 1.0 Hz. Work was completed on November 17. A total of 18.7 surface line-miles (30.1 line-km) and 12.8 subsurface line-miles (20.6 line-km) of coverage were obtained on this project.

Data collection went very smoothly at Trap Spring. Contact resistance of the ground was very low, permitting full utilization of the maximum transmitter output current of 18 amperes. Electrical noise was minimal, topography was flat, and surface culture was virtually nonexistent. All pipelines in the area were suspended in the air in order to prevent corrosion from the alkaline surface deposits. Hence, the pipelines can be considered to be ungrounded for purposes of their effect on the electrical data, except to the degree that they are electrically continuous with cased production wells.

Topographic effects at Trap Spring are virtually nonexistent, since less than 100 feet (30 m) of elevation change occurs across all three of the lines. The lines on this survey were set up without prior knowledge of subsurface geology. Unfortunately, all three lines were run near sub-parallel subsurface faulting. This has made the data more difficult to interpret than usual.

The data for lines 1, 2, and 3 are presented in Plates 7.1, 7.2, and 7.3, respectively. These are found at the end of this section and can be unfolded for reference while reading the text.

Line 1 Interpretation

As shown in the line location map of Figure 7.3, line 1 was run at a N 86° E orientation across the northeast-trending axis of the oil field. The field data are presented in Plate 7.1.

APPARENT RESISTIVITY DATA

A very distinctive pattern of high/low/high resistivity layering is evident in the data. The surface high resistivity unit probably corresponds to the recent playa-lake deposits at the top of the sedimentary section. The underlying low resistivity unit is probably related to water-saturated, unconsolidated sediments of the Horse Camp Formation. The apparent resistivities observed on the pseudosection are quite typical of valley fill in central Nevada, as judged by numerous surveys conducted in that area for mining and petroleum companies. The high resistivity unit at depth correlates with the Oligocene volcanics, which are generally impermeable, and with the Paleozoic dolomites which lie beneath them.

A major lateral change near station 7 is seen in the pseudosection data: low resistivity materials west of station 7 are shallower, while those toward the east are considerably deeper. The lowest resistivities occur where a sub-parallel graben fault lies directly beneath the line (Figure 7.4), but the fault terminates at station 5, where a north-south fault with the west side thrown up crosses the line. The depth to the low resistivity layer is clearly less west of station 5 than east of station 7, indicating a significant amount of lateral displacement. The data also show a shallow but distinctive eastern dip to the sediments, an observation which is corroborated by the local geology.

Superimposed on these layering effects is a very subtle, discontinuous, low resistivity zone which may correlate in a general way to the projected lateral extent of the hydrocarbons. In the statistical classification of section 2.2, this anomaly would be classified as "poor."

In an effort to determine the origin of this very small perturbation in the data, the "PIPE" model of Holladay and West (1982) was used to simulate a *worst-case* effect due to current channeling by well-casings, despite substantial questions raised earlier (section 2.5) to the applicability of this algorithm to field data. A well-casing diameter of 9-5/8 inches (24.5 cm) was used for the modeling. The modeling results, shown in Figure 7.7, show a broad, conductive anomaly which has many of the features seen in the field data. Using the superposition method described in section 2.5, the well-casing model data were removed from the field data to obtain the well-casing residual data of Figure 7.7b. These residual data show no trace of a low resistivity anomaly. Hence, if the model correctly represents well-casing effects, it can be argued that no anomaly related to the hydrocarbons is seen in the line 1 data.

The problem encountered in attempting to reach such a conclusion is that the residual data show a relatively strong high resistivity zone in the areas where the well-casing model showed the strongest effect. This may be due to overcorrecting by the "PIPE" model—that is, the model is calculating a much stronger effect due to casings than actually occurs in the ground. Since the casings south of stations 8 and 10 are connected electrically by a pipeline, it might be expected that the calculated well-casing effect would be even stronger if the model could accommodate such a pipe, in which case the residual would be even more anomalously resistive. Therefore, it is strongly suspected that the "PIPE" model is overmodeling the data in this particular case.

It is instructive to examine the opposite extreme of a worst-case well-casing model, i.e., what interpretation results from the assumption that *no* well casing effects are present on line 1? In this case, a rather tentative argument can be made for the existence of a conductive zone at depth between stations 9 and 11. However, this could hardly be called a "classic" anomaly. It is very subtle and would not represent a very good drilling target if found over a prospect. There are two possible explanations for this: 1) little or no electrochemical alteration exists over the line, or 2) the effects of the parallel graben fault underlying the survey line have reduced or eliminated the conductive anomaly.

APPARENT POLARIZATION (DECOUPLED PHASE ANGLE) DATA

Polarization layering west of the graben fault near station 5 is high-over-low, while the layering to the far east side of the line is low-over-high. The valley-fill sediments of the playa-lake deposits and the upper Horse Camp Formation appear to have a low polarizability, which is consistent with findings on other projects in Nevada. Middle portions of the Horse Camp Formation appear to have higher polar-

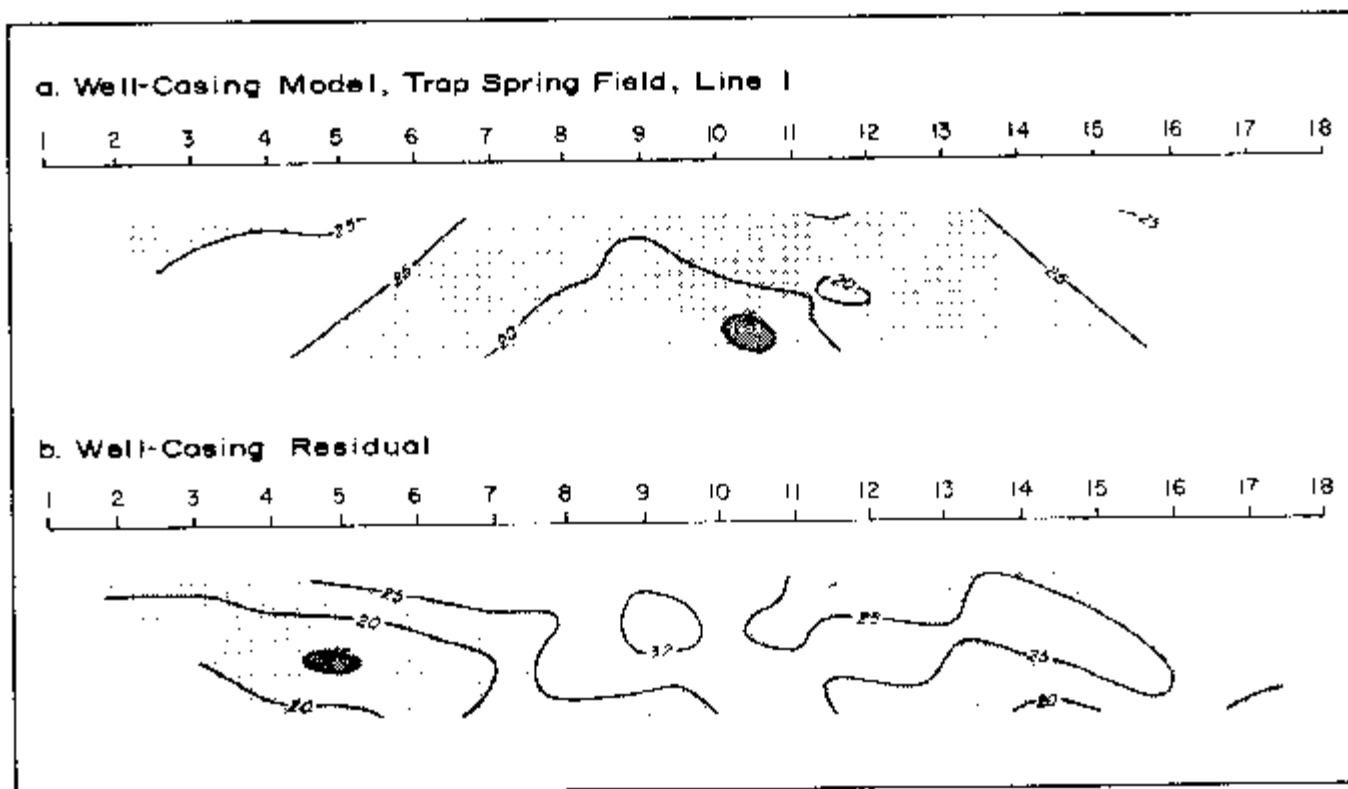


Figure 7.7. Well-casing model of apparent resistivity data for line 1, Trap Spring Field. Model parameters: 7 cased wells, casing diameter = 9-5/8 inches (24.5 cm), casing resistivity = 2.0×10^{-7} ohm-meters, surface impedance = $0 + 1.30i$, background resistivity = 25 ohm-meters. Figure 7.3 shows well locations.

izability, suggesting the possible activation of clays in those sediments. The materials above the volcanics and the Paleozoic sediments also appear to be weakly polarizable, probably because of a weathered clay layer at the base of the Horse Camp (Duey, 1978).

Superimposed on the above effects is a strong polarization anomaly which appears in the form of an inverted chevron bounded by the right-plunging 11,12 and the left-plunging 13,14 diagonals. The anomaly is distorted by high diagonals (left-plunging 12,13; right-plunging 7,8) and by a low diagonal (right-plunging 5,6). Many of these features have a suspicious appearance similar to that of cultural contamination, and the cased wells near stations 8, 10, and 12.5 are immediately suspect. However, the well near station 12.5, which is farthest from the line, appears to have the strongest effect by far. This suggests two possibilities: 1) the surface impedances of wells at Trap Spring vary considerably, making the fixed-impedance well-casing modeling of limited use, or 2) much of the response observed on line 1 is not due to well-casing effects, but instead is caused by some lateral polarization change in the subsurface, a change which is shifted to the eastern edge of the field. Based on examination of the data from lines 2 and 3, the first possibility is slightly more likely.

A well-casing model was run in an attempt to match the polarization data. Unfortunately, the "PIPE" algorithm requires a single surface impedance value for *all* well-casings. The model data, shown in Figure 7.8, have some similarity to the field data; the major response, however, is shifted towards the west, as would be expected if there were major differences in well-casing impedances among the wells.

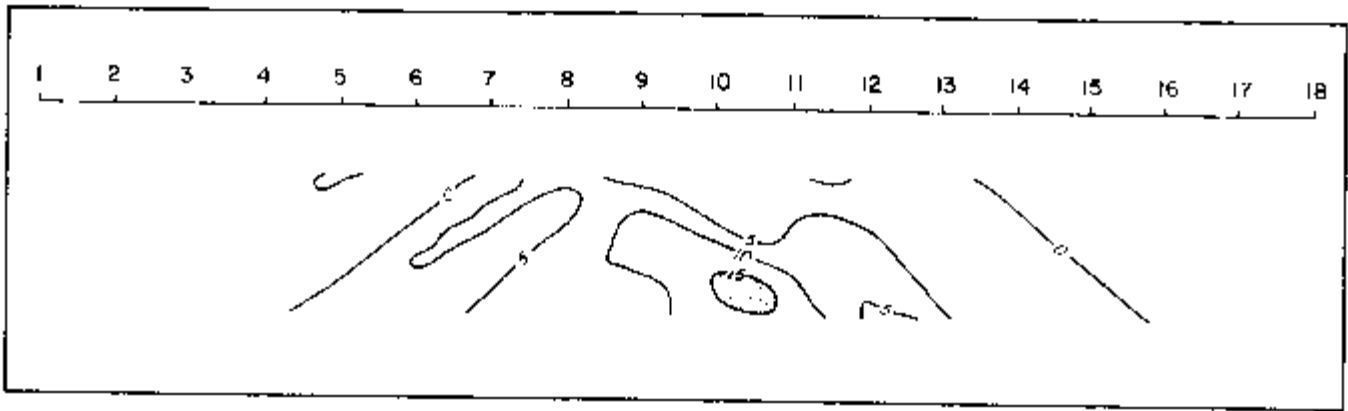


Figure 7.8. Well-casing model of apparent polarization data for line 1, Trap Spring Field. Model parameters: same as in Figure 7.7. Figure 7.3 shows well locations.

RESIDUAL ELECTROMAGNETIC (REM) DATA

There is a strong REM anomaly at depth on line 1, centered on the eastern edge of the field. The anomaly shows strong similarities to the apparent resistivity and apparent polarization anomalies. The response appears to have two primary causes: 1) geologic layering effects, which appear to be unusually strong for REM data, and 2) an effect from the cased well north of station 12.5. There is also a fair possibility that there is a residual response which is related to alteration above the producing field.

Line 2 Interpretation

Line 2 was run up the long axis of Trap Spring Field, in a N 3° E orientation. The data are presented in Plate 7.2.

APPARENT RESISTIVITY DATA

The apparent resistivity layering on line 2 is high-over-low. As found earlier, the resistive surface unit corresponds to playa-lake and upper Horse Camp sediments, and the deeper, more conductive unit can be attributed to lower Horse Camp sediments. In this context, all of the gross resistivity changes observed on line 2 make sense. Faults occur in the subsurface beneath stations 15 and 23 (see Figure 7.4), resulting in a greater depth to Unconformity "A" on the southern portion of the line. The data show this rather well: the bottom low resistivity layer appears to become deeper toward the south. An especially abrupt change of depths at the fault near station 15 is indicated by the data. A sharply uplifted block around station 3 is also indicated, but no geologic information is available for this area. It is of interest to note that low resistivities at depth are generally found north of station 19, where a north-south fault lies within one a-spacing of the line to as far north as station 32 (Figure 7.4). This correlation may indicate that the data are heavily influenced by this fault.

The resistivity of the surface layer varies rather dramatically. The shallow saline pond lying between stations 11 and 13 appears to cause the low resistivity, right-plunging 12,13 and left-plunging 11,12 diagonals. Some very strong polarization and REM responses are also attributed to the pond. The fact that all three data sets are affected in this way probably indicates the presence of polarizable clays in the pond or strong geometric effects from the large resistivity contrasts associated with this body of saline water.

The data show very little evidence of a low resistivity zone which is uniquely correlated with the producing field. This immediately suggests that well casings have a minimal effect on the data. Hence, it appears that the well casing model of Figure 7.9 is strongly overmodeling the data. Perhaps strong corrosion on the casings has raised their surface impedances to a very high value, diminishing their impact on the data. Extremely high impedance values are required in modeling in order to force a match with the data, and these values are of questionable validity.

The lack of a well-defined resistivity anomaly on line 2 may be related to the fact that the line was run sub-parallel to major graben faulting. It is not unusual for such faulting to contaminate field data and render uninterpretable an otherwise well-defined anomaly. However, many of the bizarre effects normally seen when paralleling a fault are not seen on line 2, so this explanation is not entirely satisfactory. An alternative possibility is that the orientation of the line with respect to the long axis of the field may heavily bias the data with off-line effects.

APPARENT POLARIZATION (DECOUPLED PHASE ANGLE) DATA

Apparent polarization layering on line 2 is low-high-low. Playa-lake and upper Horse Camp deposits are associated with low polarization values, and middle Horse Camp sediments are moderately polarizable. The strongly polarized left-plunging 11,12 diagonal is probably related either to water-saturated clays or to geometric effects arising from the pond between stations 11 and 13.

A fairly well-defined zone of high polarization values has a good correlation to the lateral extent of the hydrocarbons. A worst-case well-casing model was run, adjusting the complex surface impedance of the casings in order to obtain a best fit to the data. The results, shown in Figure 7.10, show a very good correspondence to the pattern of the observed polarization anomaly. While there are problems in applying this modeling routine (see the discussion of line 1), the model results do raise doubts as to whether or not any inherent polarizable response is directly associated with the ground.

RESIDUAL ELECTROMAGNETIC (REM) DATA

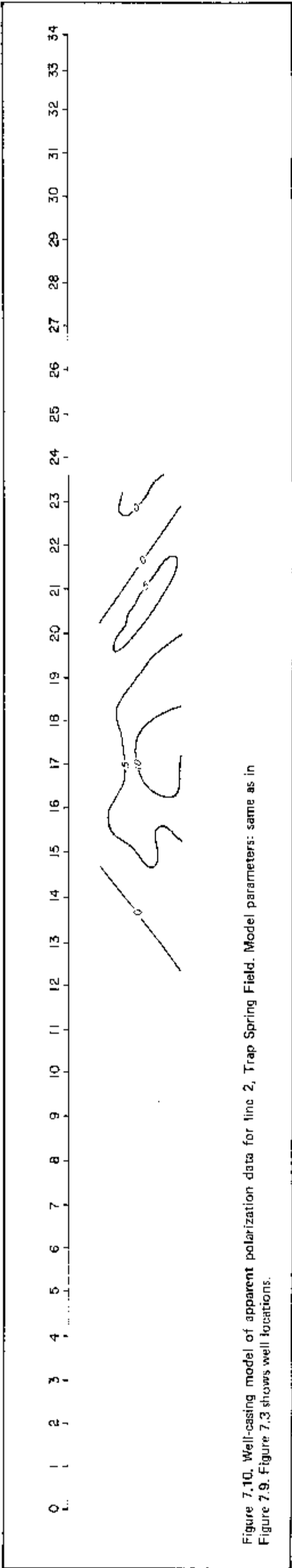
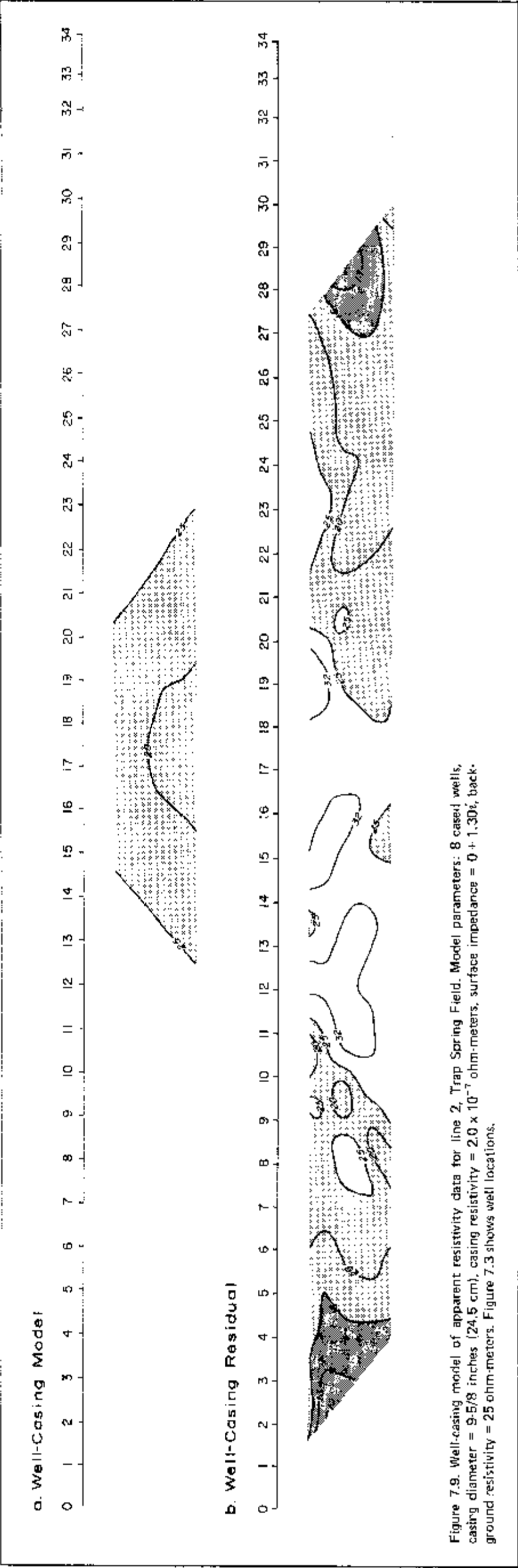
The trends in the REM data generally follow those in the apparent resistivity data. The REM data show a strongly layered appearance on the north end of the line, indicating a high/low/high layering. Note that only the first two layers are seen in the apparent resistivity data; REM may be penetrating somewhat deeper, detailing the third, high resistivity layer at depth. Part of this effect, however, may be related to the contaminating effects of the sub-parallel graben fault on the north half of the line, or to off-line effects from the producing field. In addition to this effect, there appears to be a modest response over the field where the line crosses it. This response does not show increasing conductivity at depth, nor does it have a broad, well-defined shape typical of alteration due to hydrocarbons. Therefore, the anomaly is considered to be very weak.

Line 3 Interpretation

Line 3 parallels line 1, running in the same N 86° E direction. The data are presented in Plate 7.3.

APPARENT RESISTIVITY DATA

A high-over-low resistivity layering situation prevails across the entire line. As observed on the previous two lines, high resistivities are linked to playa-lake and upper Horse Camp sediments, and low resistivities are linked to the bulk of the Horse Camp at depth. Toward the far west end of the line, the upward-faulted volcanics and Paleozoic sediments are indicated by high resistivities.



Superimposed on these effects is a fairly well-defined, low resistivity anomaly which correlates rather well with the lateral extent of the hydrocarbons. This is clearly the best anomaly on any of the three lines at Trap Spring. The anomaly appears to be fairly deep and does not seem to extend to the surface. It appears to be limited on its western edge by the high resistivity, right-plunging 4,5 and 5,6 diagonals, which result from a block of resistive material at the surface. The anomaly may actually extend a bit east and west of the actual limits of the field itself.

In an effort to determine the character of well-casing effects upon the data, a "PIPE" model was run. The results are presented in Figure 7.11. The greatest effect calculated by "PIPE" lies at depth between stations 11 and 14. While some of the trends in the modeled data resemble trends in the field data, the residual pseudo-section clearly indicates that the data are being overmodeled.

A brief review of the results from lines 1 and 2 is very helpful here. Neither of these lines showed a definable apparent resistivity anomaly, indicating that well-casing effects on apparent resistivities are minimal, despite the fact that both lines have three cased wells within 0.3 to 0.7 a-spacings of the line. If all six of those wells failed to show a significant response, a similar result should be expected from the three wells near line 3, which lie at equivalent distances (0.5 to 0.8 a-spacings), and are expected to be the same size, depth, and age. More importantly, note that two of the wells on line 3 (near stations 11.2 and 12.8) are the same wells encountered on line 2. If these wells do not respond on line 2, it is highly improbable that they *do* respond on line 3! Hence, in order for the line 3 anomaly to be due primarily to well casings, it would have to be due only to the effects of the cased well near station

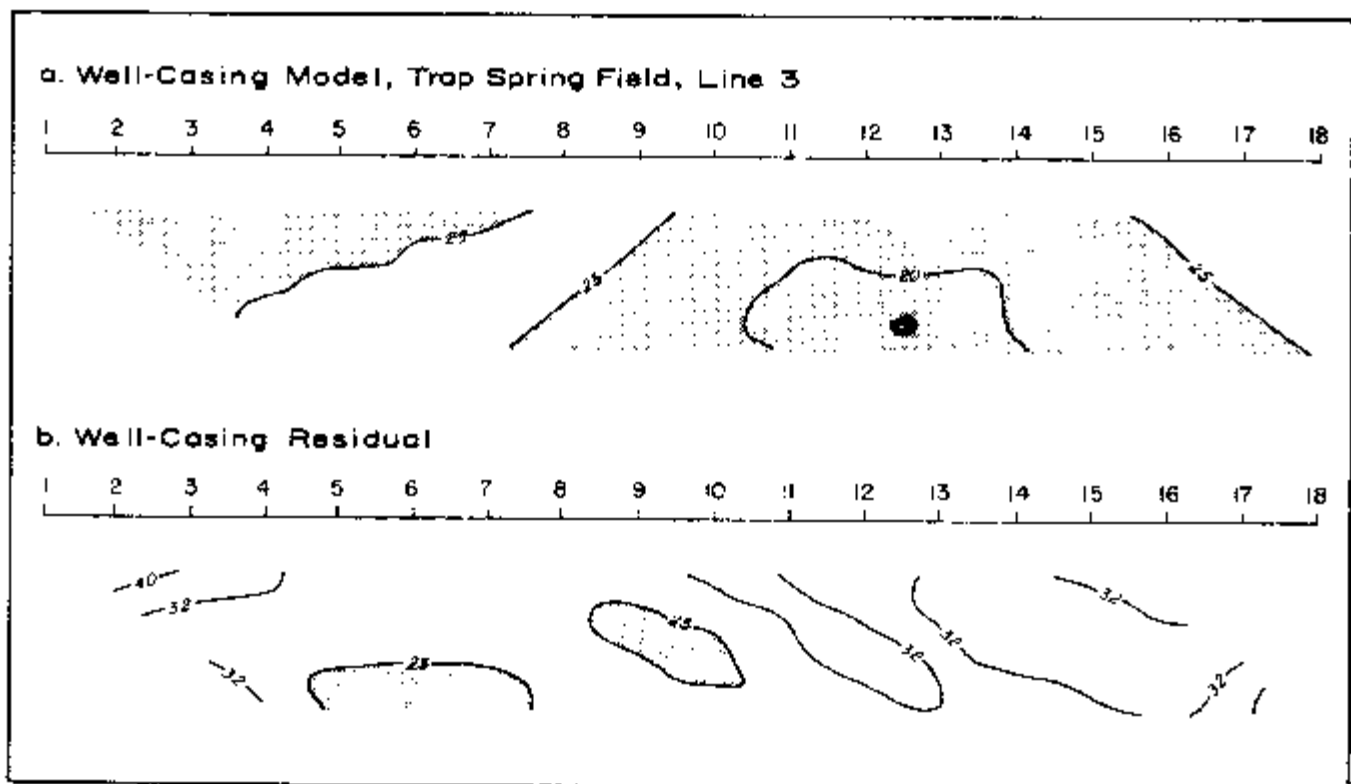


Figure 7.11. Well-casing model of apparent resistivity data for line 3, Trap Spring Field. Model parameters: 5 cased wells, casing diameter = 9-5/8 inches (24.5 cm), casing resistivity = 2.0×10^{-7} ohm-meters, surface impedance = $0 + 1.30i$, background resistivity = 25 ohm-meters. Figure 7.3 shows well locations.

10.3. This is not only unlikely from a statistical point of view, but it also would fail to represent the data adequately, as shown by computer modeling. Hence, it is possible but highly unlikely that the observed anomaly on line 3 is influenced significantly by well casings.

No surface culture is found on line 3, and topography is virtually non-existent, so these do not affect the interpretation. Subsurface geology might be suspected as a possible explanation for the anomaly, since the trends in the data are similar to the trends observed in the geologic cross-section (Figure 7.6) and on the structure map (Figure 7.5). A reasonable case for geologic influence on the data can be made in this instance, assuming that the Horse Camp Formation has strong electrical zoning which follows the structural trends of the volcanics. However, if this were the case, a considerable broadening of the conductive feature toward the west would be expected, as would strong conductive diagonal effects from the region in which the conductive layer meets the main graben fault near station 7. Since neither of these occur, it appears that there is a deep conductive zone directly above the producing field, possibly due to brine water discharge from the trap.

APPARENT POLARIZATION (DECOUPLED PHASE ANGLE) DATA

The polarization layering is the same as that observed on lines 1 and 2: playa-lake deposits have low polarization values associated with them, middle Horse Camp units have higher polarization values, and deeper units are again low in polarization. The phase angle pseudosection matches the known geology extremely well.

A very substantial zone of high polarization correlates very well with the lateral extent of the hydrocarbons. In an effort to determine the source of the anomaly, a worst-case well-casing model was run, changing the complex surface impedance value of the wells to obtain a best fit to the field data (Figure 7.12). Keeping in mind the restrictions of the model, it can be seen that there is some similarity between the model data and the field data, although the maximum anomaly calculated by the model is shifted with respect to the field data. However, considering the consistency of matches between field phase data and model data on all three lines, it is likely that most of the response observed on line 3 can be attributed to the combination of geologic layering and well-casing effects. This does not, however, rule out the possibility of a hydrocarbon-related polarization response on the line.

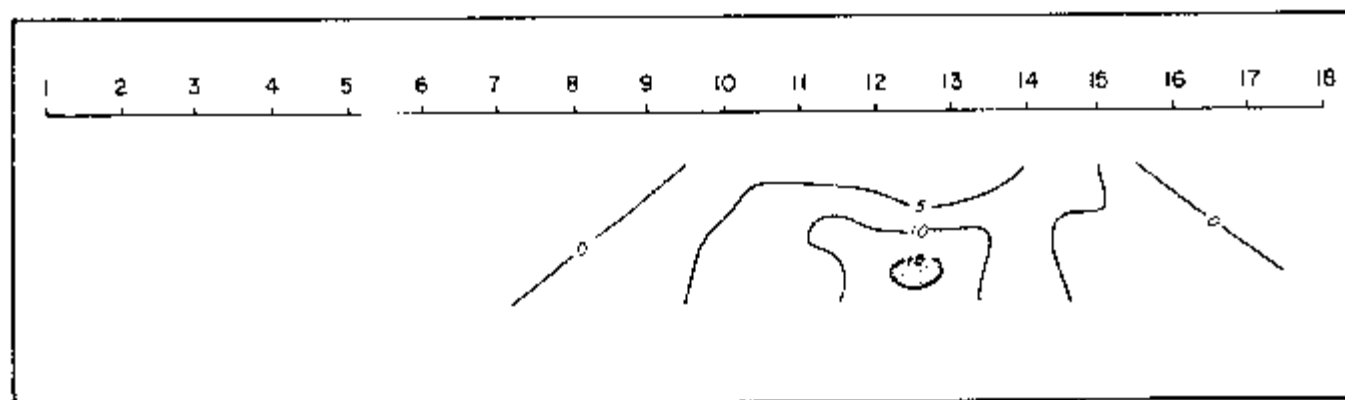


Figure 7.12. Well-casing model of apparent polarization data for line 3, Trap Spring Field. Model parameters: same as in Figure 7.11. Figure 7.3 shows well locations.

RESIDUAL ELECTROMAGNETIC (REM) DATA

As observed on the other two lines, REM partly reflects the high-over-low resistivity layering of the geology. Note, for example, the close correspondence of the REM data to the apparent resistivity data, with the exception that, once again, REM appears to be penetrating more deeply than resistivity.

The data show a very strong conductive anomaly which correlates quite well with the limits of oil production. Some of the overall effects at depth probably reflect some influence from the conductive layer there, but the sharply defined, vertical anomaly in the middle parts of the pseudosection cannot be readily explained by lithologic and structural features in the subsurface. If geology were the sole cause of the anomaly, a considerable broadening and "spilling over" of that feature might be expected toward the west. Since such an effect is not seen, the REM data indicate the existence of a conductive zone which lies above the hydrocarbon trap at depth. The strong correlation of the anomaly with the lateral extent of the hydrocarbons suggests that the two may be linked causally.

7.4 CONCLUSIONS

Review of the Data

The data from Trap Spring Field show rather variable results. Very weak to nonexistent conductive anomalies are correlated with the lateral extent of the hydrocarbons on lines 1 and 2, while a strong anomaly is observed on line 3, especially in the REM data. The inconsistency of the anomalies may be related to the fact that all three lines, to one degree or another, were run directly over and sub-parallel to significant subsurface faulting. This unfortunate situation occurred due to the lack of geologic information at the time the survey was designed. A look at the faulting pattern as it is currently known would suggest that the data from line 2 would be the worst affected, and that data from line 3 would be the least affected. Interestingly enough, line 2 shows the poorest correlation of anomalies with hydrocarbons while line 3 shows the best correlation. Hence, there is reason to believe that subsurface structure has contaminated the data to some degree on lines 1 and 2.

Well casings appear to have little or no influence on the apparent resistivity data at Trap Spring. Each line lies within the zone of influence of at least three cased oil wells, all of which are probably similar in terms of size, depth, and age. Further, two of the three wells near line 3 are the same ones near line 2. The fact that only line 3 shows an anomaly, while the other two lines do not, suggests that well casings do not cause the line 3 anomaly. In order to argue that well casings produce the anomaly, one would have to believe that only a single well—the one which is unique to line 3—has any effect upon any of the data. Since even worst-case computer modeling shows that the effects from this single well would not explain the anomaly, this is not considered a valid explanation.

The effects of subsurface structure are quite obvious in the data, and the apparent resistivity anomaly on line 3 is probably influenced to some degree by these effects. However, structural features cannot explain the presence of the well-bounded, lateral anomaly, nor its correlation with the lateral extent of the hydrocarbons. Instead, it is believed that the anomaly on line 3 represents a "deep anomaly" which is causally linked to the presence of hydrocarbons at depth.

All three lines show well-defined polarization anomalies which are strongest over the production zone. Well-casing models successfully reproduced the major trends in the field data, although not always in exactly the same portion of the

pseudosection. In contrast to the resistivity/REM responses, it is possible that the combination of responses from polarizable layers and well casings account for much of the anomalous behavior observed in the apparent polarization data. Hence, any "shallow" polarizable anomalies which exist in the sediments above Trap Spring Field may be quite subtle, if they exist at all.

Some Speculations

The presence of a "deep anomaly" on line 3 and the apparent weakness or absence of a "shallow anomaly" on all three lines may provide some valuable evidence about the anomaly mechanism at Trap Spring. The "deep anomaly" is normally attributed to brine discharge from hydrocarbon traps. In this case, the low permeability of the weathered ash seal over the Oligocene volcanics, and indeed the highly impermeable nature of the welding in the volcanics themselves, seems to present an objection to this explanation. However, the high-angle graben faulting shown in Figure 7.6 may contribute the needed degree of permeability to leak reservoir waters into the overlying Horse Camp Formation. The strength of the anomaly on line 3 and the apparent absence of anomalies in the fault-complicated data from lines 1 and 2, may reflect the relatively high connate water resistivities in the trap; alternatively, it may indicate that the brine discharge occurs at a rather slow rate. A closely related explanation for the anomaly is that these waters influence the surface conduction and cation-exchange capacities of clays in the lower Horse Camp Formation.

In evaluating the apparent lack of a clear "shallow anomaly," it should be noted that Trap Spring is something of a geologic anomaly, in that no methane is dissolved in the oils (a situation which is repeated at Eagle Springs Field on the east side of the Railroad Valley). Whether the methane has already leaked out of the trap, was lost during primary migration, or has been degraded by bacterial action in the trap is not known, but the current lack of any dissolved gases may have a profound impact on both the character of associated electrical anomalies and on our understanding of electrochemical anomaly mechanisms. The absence of methane suggests that the "shallow anomaly" mechanism over the field would be effectively neutralized. With no methane present in the sediments, no hydrocarbon-clay interactions would be expected. Neither would the precipitation of pyrite be expected, since there are no methane molecules available to be reduced to hydrogen sulfide.

REFERENCES

- Dolly, E.D., 1979, Geological techniques utilized in Trap Spring Field discovery, Railroad Valley, Nye County, Nevada: Basin and Range symposium, Rocky Mountain Assn. of Geologists-Utah Geol. Assn. Basin and Range symposium, p. 455-467.
- Duey, H.D., 1978, Trap Spring: Oil and gas fields of the Four Corners area, vol. 1: Four Corners Geol. Soc., p. 174-175.
- , 1979, Trap Spring Oilfield, Nye County, Nevada: Rocky Mountain Assn. of Geologists-Utah Geol. Assn. Basin and Range symposium, p. 469-476.
- , 1983, Personal communication.
- Foster, N.H., 1979, Geomorphic exploration used in the discovery of Trap Spring Oilfield, Nye County, Nevada: Rocky Mountain Assn. of Geologists-Utah Geol. Assn. Basin and Range symposium, p. 477-486.
- French, D.E., and Freeman, K.J., 1979, Tertiary volcanic stratigraphy and reservoir characteristics of Trap Spring Field, Nye County, Nevada: Rocky Mountain Assn. of Geologists-Utah Geol. Assn. Basin and Range symposium, p. 487-502.
- Holladay, J.S., and West, G.F., 1982, Effects of well casings on surface electrical surveys (abs.): *Geophysics*, v. 47, p. 439. Full paper available in Technical papers, 51st Annual International Meeting and Exposition, SEG, Los Angeles, v. 2, p. 815-839.

- McCaslin, J.C., 1980, Wildcatters try again in the Great Basin: Oil & Gas Jour., Aug. 11, p. 149.
- , 1981a, Operators still have hopes for Nevada: Oil & Gas Jour., Mar. 16, p. 101-102.
- , 1981b, New wildcatting shapes up in Nevada: Oil & Gas Jour., Jun. 29, p. 173-174.
- , 1983, Amoco scores rank oil find in Nevada: Oil & Gas Jour., Feb. 28, p. 123-124.
- Oil & Gas Journal, 1983, Basin and Range province gets dual oil strike: Oil & Gas Jour., Jan. 10, p. 33.

PART FOUR

ADDITIONAL INFORMATION

Plate 7.1
RESISTIVITY/PHASE PSEIDOSECTION DATA
Trap Spring Field
Rye Co., Nebraska

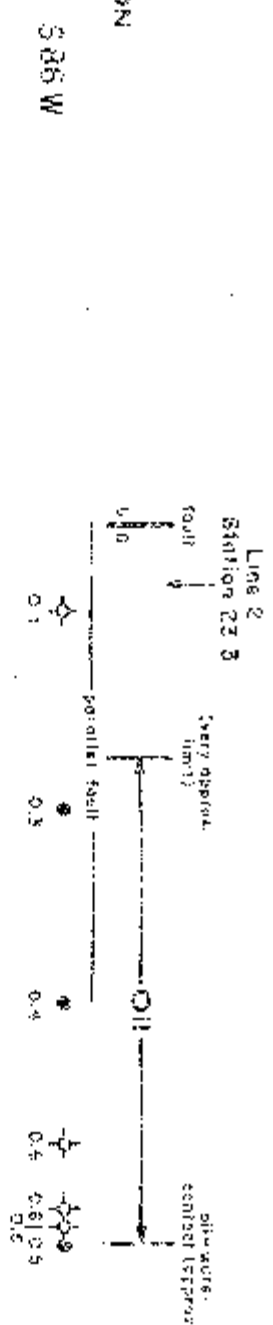
Line 1
x = 1,250 feet

Standard Well Symbols	Native Symbols	Explanation of Symbols
o Drilling for which interval is unacceptable	o	Metall pipelines, presumed grounded
o Drilling in progress at time of map preparation	o	Uncounted pipeline: nonmetallic or suspended
o Shut in	o	Metall fence
o Abandoned	o	Electric fence
o Dry hole with total depth indicated	o	Electric fence
o Oil well	o	Electric fence or power cable
o Gas well	o	Telephone line or standard voltage power line
o Oil and gas well	o	Major high voltage power line
o Gas injection well	o	Railroad, microwave, or other communications station or tower
o Water injection well	o	DC pump
o Water well	o	
o Other Well Symbols	o	Other Symbols
o Drilling in progress at the time of the electrical survey; number indicates the amount of drill stem in the hole at the time of data collection	o	U.S.G.S. standard symbol of as located
o Well spudded in after completion of the electrical survey	o	
o Number indicates distance of well from the line in terms of a contour; all wells within 1.0 acre-feet indicated (pseudosections only)	o	

Plate 7.1
RP Field Data
Trap Spring Field
Line 1

5.85 W

N66E



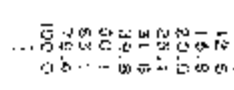
4000 ft

Apparent Resistivity

Units: ohm-meters

Frequency: 0.125 Hz

Logarithmic contour interval:

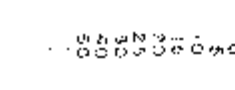


Decoupled Phase Angle

Units: milliradians

Frequency: 0.125 Hz

Linear contour interval:

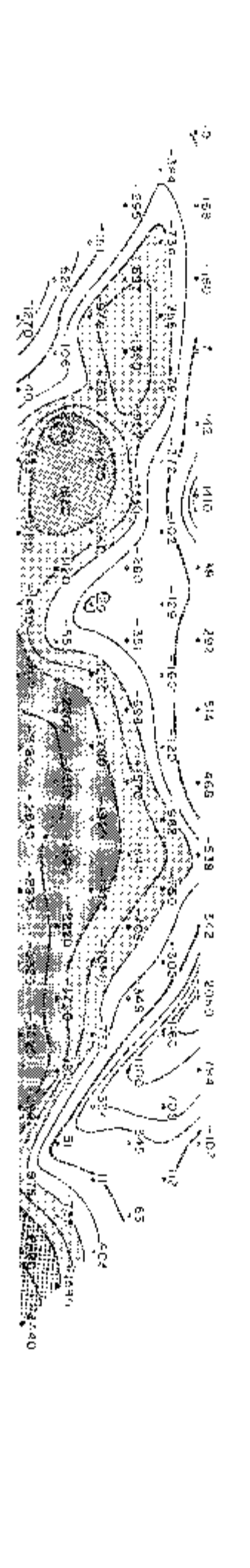
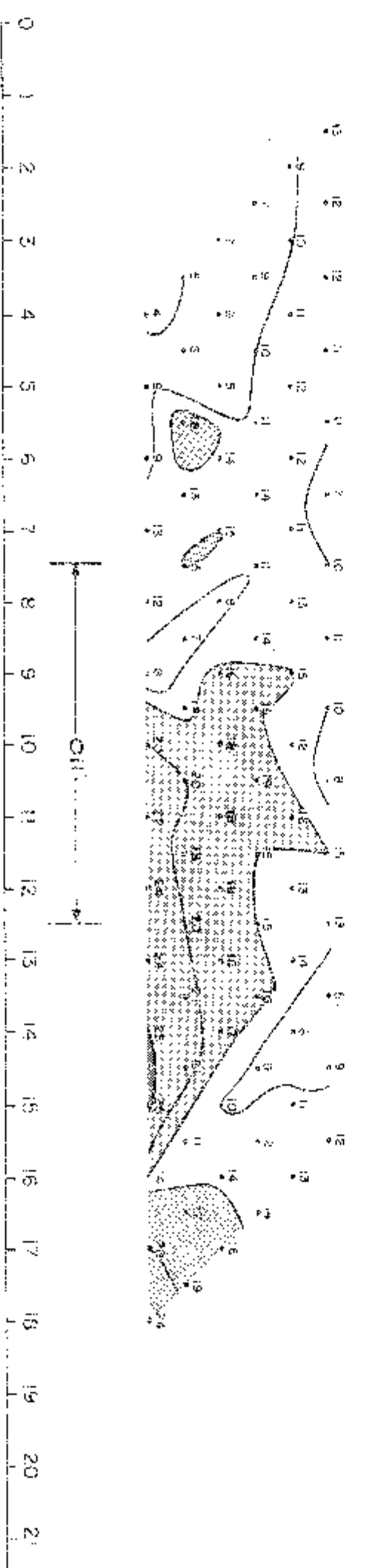
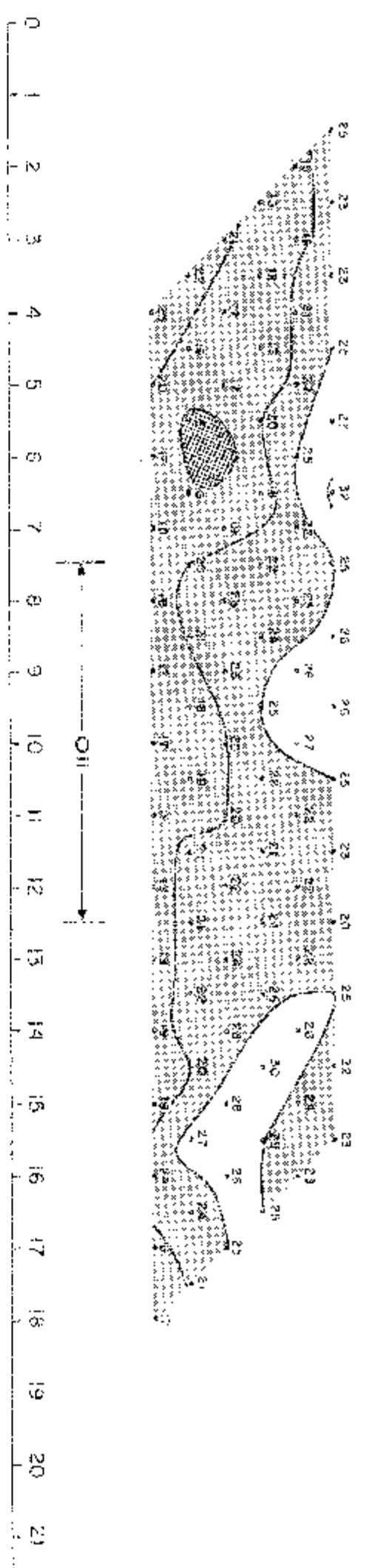
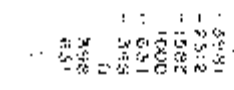


REM Quadrature

Units: normalized imaginary








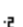











Frequency: 0.125 Hz

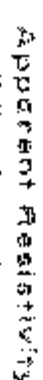
Logarithmic contour interval:



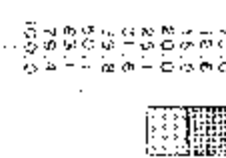
$z = 1.250$ feet

Ernst Ludwig Hehl Symposium
Culture's Symbols

	Oilfield for which information is obtainable		Metal pipeline, prewired, grounded
	Drilling in progress at time of map preparation		Underground pipeline, non-wired or suspended
	Start top		Metal fence
	Anatomical		Electric fence
	Dry hole with total depth indicated		Buried telephony or power cable
	Oil well		Telephone line or simulated voltage source, loop
	Gas well		Master high voltage power line
	Gas injection well		Radio, microwave, or other communications station or tower
	Water injection well		DC pump
	Water well		



Units: Ohm-meters
Frequency: 0.125 Hz
Logarithmic detector interval



பெரும்பாலும் புகைகளை சுவாசிக்க

Units: millireds
Frequency: 0.125 Hz
Linear colour interval:



PEEM Observations

Units: modified imaginary
Frequency: 0.125 Hz
Logarithmic contour interval

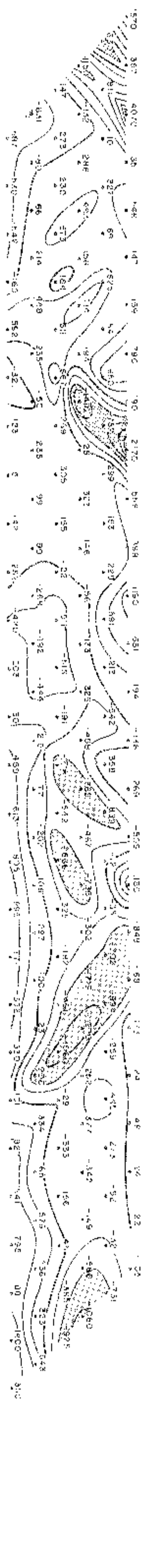
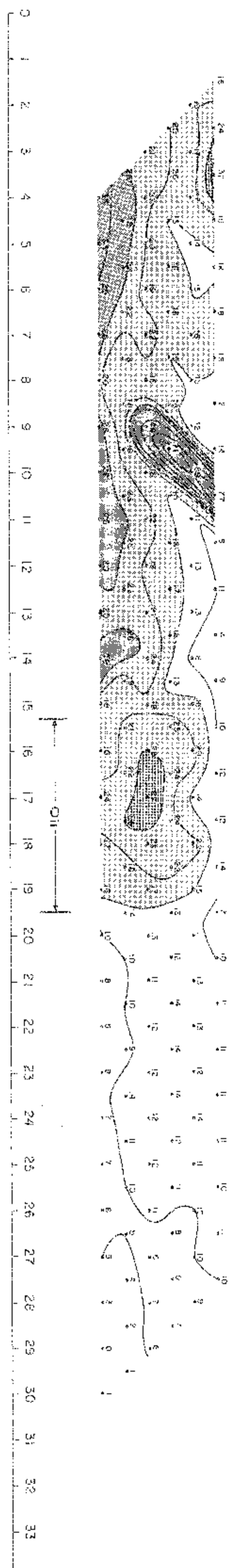
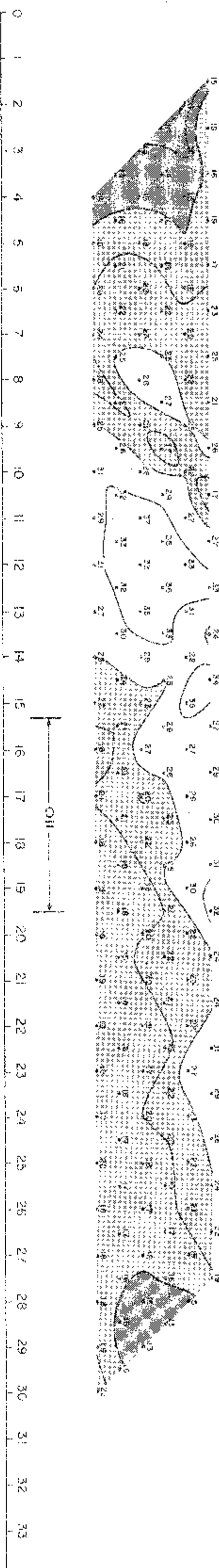
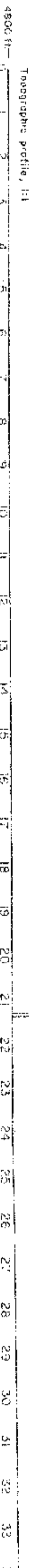


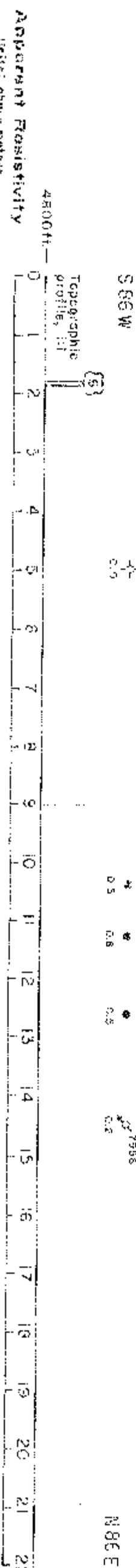
Plate 7.3
RESISTIVITY/PHASE PSUDOSECTION DATA
Trap Spring Field
Type C2, Nevada

1 line 3
1:1,250 feet

Explanation of Symbols	
Standard Well Symbols	Culture Symbols
Drilling for which information is undesirable	↓ Metal pipeline, presumed grounded
Drilling in progress at time of map preparation	↑ Ungrouted pipeline, non-mantled or supported
Shut in	↓ Metal fence
Abandoned	↓ Electric fence
Div hole with total depth indicated	↓ Buried telephone or power cable
Oil well	T Telephone line or standard voltage power line
Gas well	TV Major high voltage power line
Oil and gas well	Radio, microwave, or other communications
Gas injection well	↑ Radio, microwave, or other communications
Water injection well	↓ DC pump
Water well	
Other Symbols	
U.S.G.S. standard symbols in adjacent	
Special Well Symbols	
Drilling in progress at time of the electrical survey; number indicates a number of collection	
Well abandoned in situ completion of the electrical survey	
Number indicates distance of well from the line in terms of stations; all wells within 1.0	
a package indicated (measurements only)	

CP
ZONE ENGINEERING
& RESEARCH ORGANIZATION

Plate 7.3
RP Field Data
Trap Spring Field
Line 3

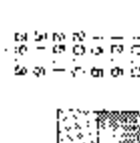


Apparent Resistivity

Units: ohm-meters

Frequency: 0.125 Hz

Logarithmic contour interval:

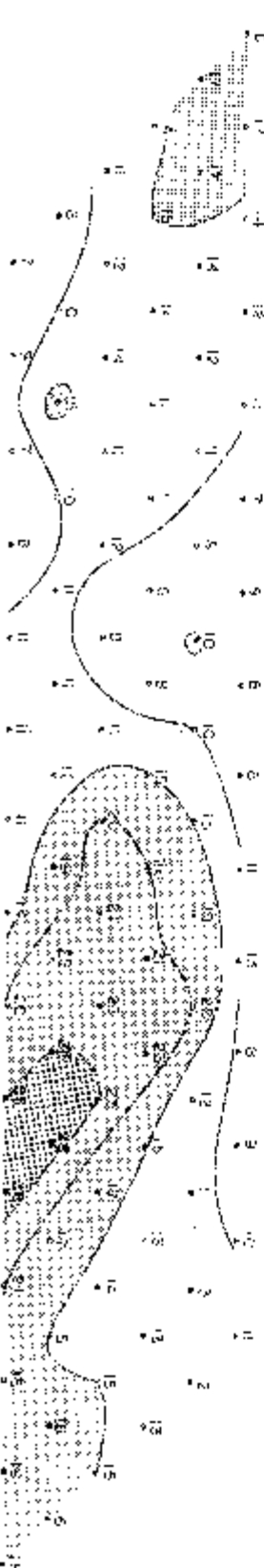
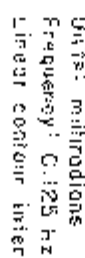


Decoupled Phase Angle

Units: millivolts

Frequency: 0.125 Hz

Linear contour interval:

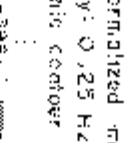


REM Quadrature

Units: normalized anomaly

Frequency: 0.125 Hz

Logarithmic contour interval:



Chapter 8

Mechanisms of Current Flow in the Earth

8.1 INTRODUCTION

While it is beyond the scope of this volume to provide a full description of current flow in the earth, a brief, practical exposition is provided in order to clarify and explain terms used in the discussion of the case histories. A more detailed, very readable book by Sumner (1976) is recommended should the reader desire more information. The college text by Telford, et al., (1976) is also very helpful and readable. A detailed description of the electrical properties of earth materials and of IP theory may be found in Keller and Frischknecht (1970) and Ward and Fraser (1967).

The earth is, in a geoelectrical sense, an inhomogeneous mess. It is composed of a wide variety of lithologies in a wide variety of geometrical arrangements. It varies in matrix geometry, in pore fluid content, in mineralogy, and so on. Hence it is not surprising that when the earth is stimulated by an electric current, the response to that current is a rather complex one. Sumner (1976) explains why it is helpful to visualize this complex earth as an electric circuit:

"Although the IP phenomena are basically electrochemical in nature, the systems are really too complex to be represented by a single set of chemical and thermodynamic relationships. The types of ions, their concentrations, and the reactions involved are only generally known. The pore geometry and its relationship with metallic mineral particles are also important. It is quite difficult to represent all these factors explicitly. Thus, it is convenient to use simplified macroscopic analogies in the way of either 'lumped' or 'distributed' electrical circuits."

The equivalent circuit approach is described in detail by Ward and Fraser (1967), Zonge (1972), and Sumner (1976). Equivalent circuits which are used to model the IP response usually consist of resistive and capacitive elements. These circuits attempt to model the frequency dependence of rock resistivities. In actual field measurements, the size and geometry of the measuring system as well as the wire lengths and orientations used enter into the apparent measured results, adding additional frequency and geometric dependence.

In equivalent circuits, the resistor is used to represent the impedance of direct current flow through imperfectly conducting materials. The parameter known as "apparent resistivity" is a measure of the ground resistance, adjusted for the geometry of the measuring points. It is typically calculated for field data at the lowest frequency acquired (0.125 Hz in this volume). Capacitors are used to represent the separation of charge or energy storage in certain ground materials which develops when the ground is subjected to an electric field. This separation of charge, or polarization, will cause a current to flow in the ground after the inducing fields (or currents) are removed, resulting in the "induced polarization" parameter.

8.2 PHYSICAL MECHANISMS OF GALVANIC CURRENT FLOW

Introduction

Few physical properties in nature have as wide a range of values as earth resistivity. As shown in Table 8.1, the resistivity range of common earth materials varies by some eight orders of magnitude, from less than 1 ohm-meter for porous, water-saturated sandstones to 10^6 ohm-meters for dense metamorphic rocks.

To understand this range in resistivities, consider the structure of a typical rock. Current can flow both through the grains which make up the rock and through the pore fluids which surround them. In general, the rock matrix is highly resistive,

TABLE 8.1: RESISTIVITIES OF VARIOUS MATERIALS

ROCKS	
Metamorphic	5×10^2 to 10^6 ohm-meters
Igneous	10^3 to 10^6
Clays	1 to 30
Shales	<1 to 600
Sandstone	<1 to 3,000
Porous limestone	100 to 10,000
Dense limestone	>1,000
Bulk ground resistivity measured in sedimentary petroleum provinces (typical)	1 to 200
EARTH MINERALS	
Chalcopyrite ($\text{Fe}_2\text{S}_3\text{Cu}_2\text{S}$)	9×10^{-3} to 150
Galena (PbS)	6.8×10^{-6} to 9×10^{-2}
Pyrite (FeS_2)	0.6 to 1.2
Molybdenite (MoS_2)	0.12 to 7.5
Native copper	3×10^{-7} to 1.2
Graphite (current flow parallel to cleavage)	10^{-6} to 36
(current flow perpendicular to cleavage)	9.9×10^{-3} to 28
METALS	
Copper, pure	1.6×10^{-8}
Lead	1.9×10^{-7}

unless it contains large amounts of interconnected conductive minerals or clays. On the other hand, typical pore fluids are generally quite conductive, often between 0.1 and 10 ohm-meters. For most rocks near the earth's surface, conduction of electricity is entirely through ground water contained in the pores of the rocks (Keller and Frischknecht, 1970).

There are a number of ways in which galvanic current flow can occur, but in the earth at frequencies less than about 1 kHz, the most important mechanisms are electronic, molecular, ionic, and electrolytic. *Electronic conduction* is accomplished by the shift in energy level of bound electrons. Its contribution is minor in dielectric materials (which make up most earth materials) at all but very high frequencies, but it is an important phenomenon in conductors and semiconductors (such as graphite, some clays, sulfides and some other minerals) even at very low frequencies. *Molecular conduction* involves molecules whose charge distribution is not uniform. When subjected to an AC field, these polarized molecules rotate or oscillate, transferring charge back and forth according to the frequency of the impressed signal. Molecular conduction effects are limited to local charge transfer and are primarily important at frequencies higher than those used in oilfield electrical surveys. *Ionic conduction* is caused by movement of ions within an imperfect crystal lattice under the influence of an external electric field. Its contribution to current flow in saturated, unmineralized rocks is minor, but it is one of the conduction modes in some minerals. *Electrolytic conduction* occurs when free ions are able to flow through a medium due to an applied field. Most electric current flow in the earth occurs through electrolytic conduction, and it is this mechanism which is discussed below.

Characteristics of Electrolytic Conduction

Electrolytic conduction at a given frequency is a function of two factors: the concentration or availability of ions c , and their relative mobilities v . The current flowing through an electrolyte for each volt per meter of electric field applied is expressed by:

$$I = AF (c_1 v_1 + c_2 v_2 + c_3 v_3 + \dots) \quad (8.1)$$

where A is cross sectional area through which current flows

F is Faraday's number (96,500 coulombs)

c_n is concentration of species n

and v_n is mobility in meters per second of species n

In solutions with temperatures, pressures, and concentrations typical of most pore fluids, the mobility of a given species does not vary greatly. The important variable is the concentration or availability of the conducting ions.

ION AVAILABILITY

By far, the largest source of ions in earth materials is dissolved salts present in waters which fill the pore spaces in rocks. Up to a point, increased salinity of the electrolytic waters results in a higher availability of ions; likewise the larger the pore space, and hence the larger the volume percent of water, the larger the ion supply. In general, rocks are often water-saturated, and the discussion presented here assumes this to be the case. From equation (8.1) it can be seen that the higher the concentration of an ionic species the more conductive the aqueous solution. Table 8.2 presents resistivities for various concentrations of NaCl at 25°C.

Secondary sources of free ions include escaped cations from covalently and ionically bonded solid-rock materials. Of these, covalently bonded rocks are the larger contributor. Cations such as iron, sodium, and magnesium can be absorbed

TABLE 8.2: RESISTIVITIES OF SALINE SOLUTIONS¹

Salinity (ppm NaCl at 25°C)	Resistivity (ohm-meters)	Conductivity (millisiemens/meter)
500	10.0	100
1,000	5.0	200
2,700	2.0	500
5,600	1.0	1,000
12,000	0.5	2,000
32,000	0.2	5,000
65,000	0.1	10,000

¹ After Davis and DeWiest (1966).

into broken bonds or substituted for other cations in a crystal lattice in a process called cation exchange. In the process of this exchange, cations are occasionally lost from the face of a crystal lattice into an adjacent electrolyte. Similarly, but to a lesser degree, cations can be lost from ionically bound materials when stray ions of the wrong valence number are bonded into the lattice structure. The weakened lattice gives rise to a statistical probability of cation escape which depends on the bonding energy, the availability of space in which to move, and the lattice temperature.

ION MOBILITY

When an electric field is applied to a rock, cations move toward the negative pole of the field and anions toward the positive pole. Mobility is at first limited by ionic momentum, but the ions then accelerate until their speed is limited by physical or electrical blockages. The time required for an ion to reach its terminal velocity in an aqueous solution is considerably less than a microsecond (Keller and Frischknecht, 1970). Physical blockages include increased electrolyte viscosity due to high pressures, low temperatures, large concentrations of ions and other particles, and limitations of pore space. In terms of rock mechanics, pore-space limitations involve porosity (percentage of rock volume involved in pore space), permeability (how the pore spaces are interconnected), and pore-space constriction (width with respect to ion diameter). Pore space constrictions can sort ions by size and reduce their mobilities by crowding, much as traffic is affected by turnpike entryways (Sumner, 1976). Electrical blockages can occur when charge centers such as clay particles attract the mobile ions as they move through the pore spaces. This effect is referred to as membrane polarization.

ARCHIE'S LAW

The general dependence of rock resistivity upon electrolyte salinity and available pore space can be summarized by an empirical relation known as Archie's Law:

$$\rho = a \rho_w \phi^{-m} \quad (8.2)$$

where ρ is the rock resistivity, ρ_w is the water resistivity, and ϕ is the volume percent of porosity of the rock. The values of the coefficients a and m are determined empirically. The coefficient a refers to the type of porosity, and it ranges from values slightly greater than 1 for jointed and fractured rocks to slightly less than 1 for rocks with intergranular and vugular porosity. The coefficient m is called the "cementation factor" and is a measure of the sorting and cementation of the

rock. Rocks which are well-sorted and securely cemented have cementation factors somewhat larger than 2, while poorly sorted or cemented materials have values slightly less than 2. While Archie's Law does not account for secondary effects due to changes in temperature, the presence of metals, electrical blockages, ionization of clay minerals, surface conduction, and other effects, it does serve quite well to relate the more important factors affecting rock resistivity, and it has been widely used in petroleum applications for a number of years. In these applications, the ratio ρ/ρ_w is called the "formation factor" of the rock—a term often used in electrical logging.

ION DIFFUSION AT A SOLID-ELECTROLYTE INTERFACE

There are specific interactions occurring at the interface between a solid material and a conductive electrolyte solution. A solid material will generally possess a small net charge at its edge due to the exposure of ions forming the boundary of a crystal lattice plane (see the discussion of surface conduction below) or a build-up of electrons in a metal. As shown in Figure 8.1, this net charge attracts a layer of free ions of opposite charge, or of dipolar molecules, from the electrolyte at the interface. This layer is called the "fixed layer," since the binding forces involved render it relatively immobile. When there is no applied electric field, the potential drop across the fixed layer is zero.

A second, less dense, "diffuse layer" of ions adjoins the fixed layer and thins out exponentially away from the interface. The potential of the diffuse layer also decreases exponentially away from the surface. The two layers together are referred

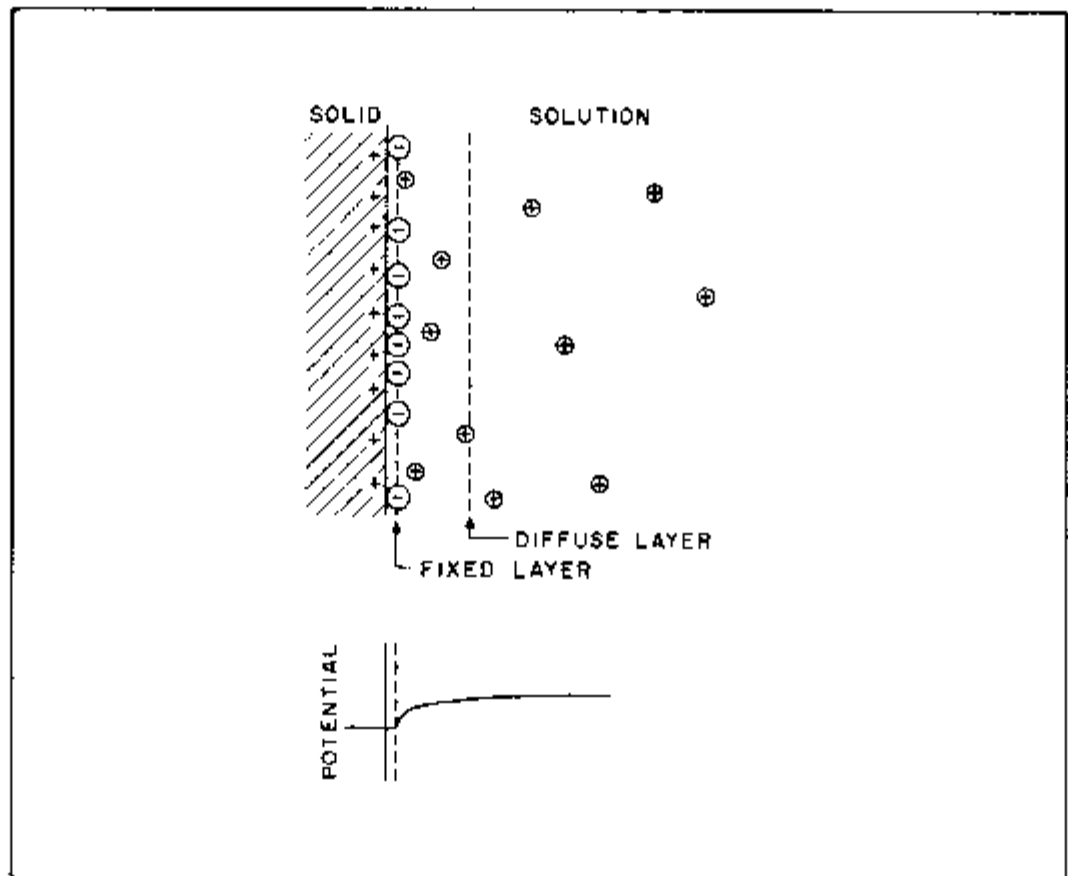


Figure 8.1. Fixed and diffuse (double) layers associated with a solid-electrolyte interface and the resulting Zeta potential (no applied current). After Sumner, 1976.

to as the "double layer." The potential drop across the double layer is called the "Zeta potential." According to Ward and Fraser (1967), the static width d of the ionic layer across which the Zeta potential occurs depends upon the temperature T of the electrolyte, its dielectric permittivity κ_0 , the ionic concentration n , and the ion valence number v_0 :

$$d = \left[\frac{\kappa_0 k T}{8 \pi n e^2 v_0^2} \right]^{1/2} \quad (8.3)$$

in which k is Boltzman's constant
 e is the elementary charge

If an electric field is applied to the double layer, cations will be propelled toward the negative pole of the field and anions toward the positive pole. The net reaction will be a transfer of current as the ion distribution is changed. If the field is due to an alternating current, the ionic distribution will shift back and forth with the reversals of the field polarity, and both the Zeta potential and the distance d will be frequency-dependent.

Electrode Polarization

Electrode polarization generally occurs when an electrolyte adjoins a material which conducts electronically, such as most sulfides, some metallic oxides, and graphite. The magnitude of the electrode polarization depends on the area of semiconductor-electrolyte interface available, the mineral species available, the electrolyte composition, and the pore-fluid content of the rock. Figure 8.2a shows the separation of charge which can develop as ions move in the diffuse layers on opposite sides of a metallic mineral grain which blocks the primary conduction path.

Membrane Polarization

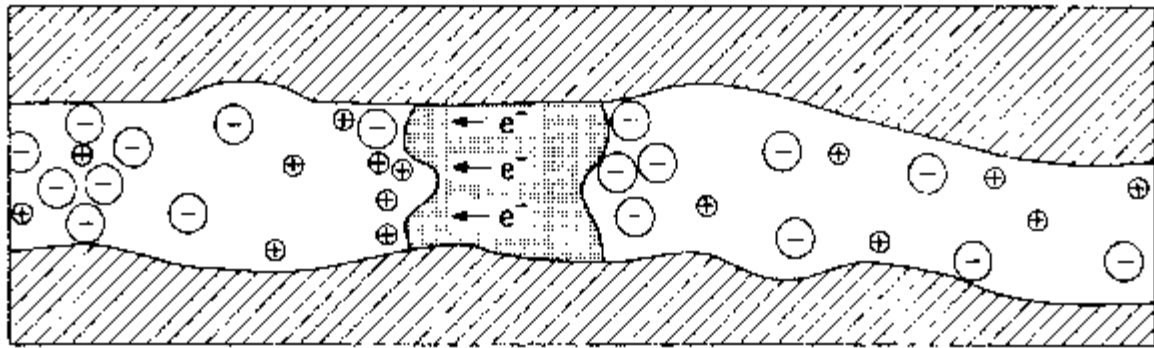
Figure 8.2b illustrates an electrolyte-saturated pore space in a rock in which clay particles are attached along the solid rock walls. The effects of unsatisfied charges in the clay lattice result in an adsorbed cationic cloud around the clay surfaces, forming constrictions in the pore spaces. When an electric field is applied, the relative mobilities of the ions in the pore space become a function of ion size; large ions (usually anions) are blocked by constrictions in the pore spaces, but smaller ions are allowed to pass. This results in zones of ion concentration and ion depletion, or separation of charge, which produces an observable polarization. This effect can also be generated by ion-selective membranes, hence the designation "membrane polarization."

This effect is very difficult to distinguish from electrode polarization, and its contribution to the overall polarizability of a rock can often equal or exceed normal electrode polarization effects. Differences between the two polarization mechanisms can often be determined by making multi-frequency induced polarization measurements.

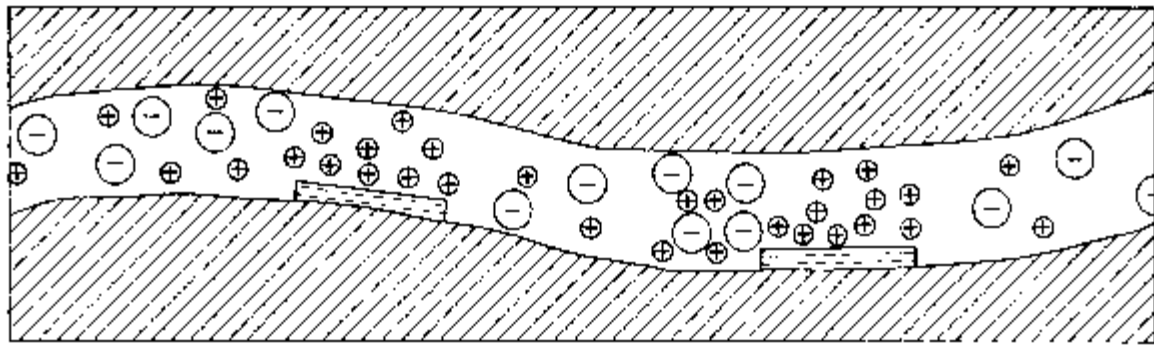
Membrane effects are very sensitive to specific aspects of rock composition. If existing clays and other materials present a large surface area along the pores, ionic concentration can be high enough that ions cannot be effectively redistributed and significant polarization cannot develop. The length of the pore paths is also important; long pore paths mean slower current response with charge transfer and hence a different response with changing frequency.

Figure 8.2c shows two other sources of polarization. If a metallic particle does not physically block the current flow, two effects can be generated. Charge separation can be induced along the surface of the metallic particle, or charge

a. Electrode Polarization



b. Membrane Polarization (clays)



c. Membrane Polarization (sulfides and pore geometry)

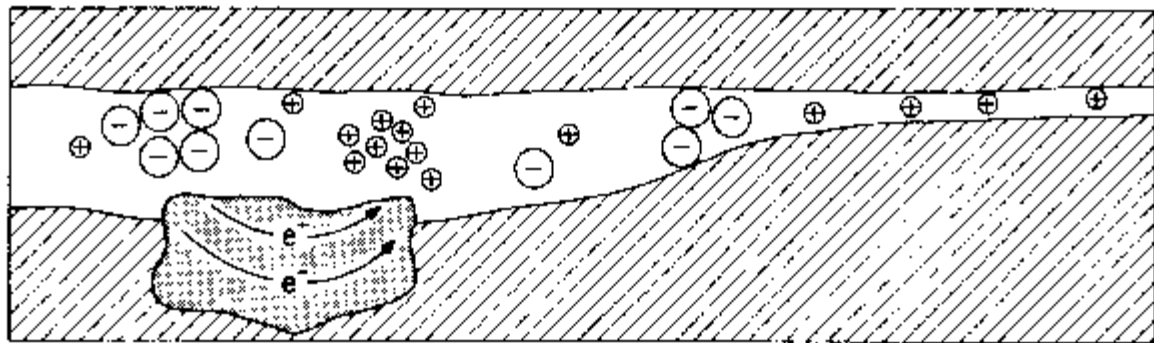


Figure 8.2. Sources of the induced polarization response (after Sauck, 1969, Sumner, 1976, and Scott-Fleming, 1980).

build-up associated with electrode polarization may also block ion flow, as in the clay example of Figure 8.2b. These effects will serve to enhance the electrode polarization. Also, if pore spaces narrow sufficiently, large ions can crowd together at the bottleneck permitting charge separation (polarization) to develop as smaller ions continue to flow.

Surface Conduction

Increased ion concentrations associated with double layer adsorption increase the density of charge carriers above what would be normal for an uncharged surface (Figure 8.2b). The result is increased conduction associated with charged surfaces (Ward and Fraser, 1967). Surface conduction is another variation on the ion-diffusion process in which a solid substance presents a net negative charge to an electrolyte.

Clay minerals are particularly noted not only for increasing polarization effects but also for increasing the conductivities of rocks. The importance of surface conduction increases as porosity decreases and as saturation by water decreases (as in the vadose zone or in rocks filled with mixtures of water and resistive fluids such as petroleum liquids). According to Keller and Frischknecht (1970), the critical water saturation appears to be about 25% of total pore space for sandstones and similar permeable rocks, although for less permeable rocks, it may be as high as 70% to 80%. As long as the saturation is above this critical figure, the resistivity of the rock will vary according to the square of the degree of saturation; below the critical figure, the variation is according to the fourth or fifth power of the degree of saturation, and resistivities climb rapidly.

The two main polarization effects, electrode polarization and membrane polarization, only occur under the influence of an electric field. They are also frequency-dependent. The decoupled phase angles presented in the case histories are thought to represent the sum of all membrane and electrode polarization effects, with all electromagnetic effects (see below and Chapter 9) removed. It has been found (Zonge, 1972) that the frequency dependence of the IP response can be diagnostic for a few economic and noneconomic minerals and, with proper care, spectral measurements can be used to distinguish these minerals, even in the field.

8.3 THE ORIGIN OF INDUCTIVE COUPLING

In acquiring field data, the apparent resistivity or induced polarization (IP) measurements are contaminated by the effects of the actual measuring system and its interaction with the ground. Normally a four-electrode system is utilized, with a pair of electrodes (or a dipole) used for transmitting current into the ground, and the other pair used for detecting the resultant voltage in the ground. The wires connecting the electrodes in these measurements will couple together inductively, and depending upon their relative orientation will respond either inductively or capacitively, i.e., either subtracting from or adding to the induced polarization response. This response is usually referred to as inductive electromagnetic (EM) coupling and is the total EM coupling response when operating over a homogeneous half-space. However, when the earth is layered or otherwise inhomogeneous, a second frequency-dependent EM coupling parameter is generated which is a function of the actual position of the current (transmitter) and voltage (receiver) electrodes, as well as the orientation of the wires connecting them. Depending upon the geometry of the measuring array and the relative resistivities of the layers in the earth, this EM parameter will either add to or subtract from the combined IP and inductive

EM responses described above. It is this latter EM coupling effect that we try to measure for the residual electromagnetic (REM) parameter.

It should be noted here that the combined EM effect (inductive plus geometric coupling) can often exceed the actual ground IP response by a factor of 10 or more, and can change the apparent ground resistivity by as much as 50 percent, for a typical oilfield survey with large electrode separations. It is therefore very important that any resistivity and IP data gathered in this environment be corrected for EM effects, and this can only be done by making multiple frequency measurements.

Chapter 9 contains a more complete discussion of the principles of EM theory as applied to hydrocarbon exploration.

REFERENCES

- Davis, S.N., and DeWiest, R.J., 1966, *Hydrogeology*: New York, Wiley, 463 p.
- Keller, G.V., and Frischknecht, F.C., 1970, *Electrical methods in geophysical prospecting*: New York, Pergamon Press, 519 p.
- Sauck, W.A., 1969, A laboratory study of induced electrical polarization on selected anomalous rock types: MS thesis, University of Arizona, Tucson.
- Scott-Fleming, A.W., 1980, Correlation of complex-resistivity spectra with intrusive porphyry copper alteration zones and mineralogy: MS thesis, University of Arizona, Tucson.
- Sumner, J.S., 1976, *Principles of induced polarization for geophysical exploration*: New York, Elsevier Scientific Publishing Company, 277 p.
- Telford, W.M., Goldart, L.P., Sheriff, R.E., and Keys, D.A., 1981, *Applied geophysics*: New York, Cambridge University Press, 860 p.
- Ward, S.H., 1967, Electromagnetic theory for geophysical applications, in *Mining Geophysics*, Vol. 2 (Theory): Tulsa, Society of Exploration Geophysicists, p. 9-196.
- Ward, S.H., and Fraser, D.C., 1967, Conduction of electricity in rocks, in *Mining Geophysics*, Vol. 2 (Theory): Tulsa, Society of Exploration Geophysicists, p. 197-223.
- Wynn, J.C., 1974, Electromagnetic coupling in induced polarization: PhD dissertation, University of Arizona, Tucson.
- Wynn, J.C., and Zonge, K.L., 1975, EM coupling, its intrinsic value, its removal, and the cultural coupling problem: *Geophysics*, v. 40, p. 831-850.
- Zonge, K.L., 1972, *Electrical properties of rocks as applied to geophysical prospecting*: PhD dissertation, University of Arizona, Tucson.

"Engineering Procedure," from an unknown but astute source

Every new engineer must learn early that it is never good taste to designate the sum of two quantities in the form:

$$1 + 1 = 2 \quad (1)$$

Anyone who has made a study of advanced mathematics is aware that $1 = \ln e$ and that $1 = \sin^2 x + \cos^2 x$; further,

$$2 = \sum_{n=0}^{\infty} 1/2^n$$

Therefore, equation (1) can be expressed more scientifically as:

$$\ln e + (\sin^2 x + \cos^2 x) = \sum_{n=0}^{\infty} 1/2^n \quad (2)$$

This may be further simplified by use of the relations: $1 = \cosh y \sqrt{1 - \tanh^2 y}$ and $e = \lim_{z \rightarrow \infty} (1 + 1/z)^z$. Equation (2) may therefore be rewritten

$$\ln \left[\lim_{z \rightarrow \infty} (1 + 1/z)^z \right] + (\sin^2 x + \cos^2 x) = \sum_{n=0}^{\infty} \frac{\cosh y}{2^n} \sqrt{1 - \tanh^2 y} \quad (3)$$

At this point, it should be obvious that equation (3) is much clearer and more easily understood than equation (1). Other methods of a similar nature could be used to clarify equation (1) but these are easily discovered once the reader grasps the underlying principles.

We hope this chapter will form the basis of a reverse solution.

Chapter 9

Principles of Electromagnetic Theory as Applied to Petroleum Exploration

9.1 INTRODUCTION

Electrical exploration for oil and gas has all too frequently been pursued by persons with very little understanding of how electromagnetic energy propagates in the earth. As a result, some rather outrageous claims have been made by some practitioners of electrical techniques. The petroleum industry has responded with justifiable skepticism, and electrical techniques have drifted in and out of favor several times since they were first applied to oil and gas exploration in the early 1900s.

However, the validity of these techniques is not in question, only the ways in which they are sometimes used. It is therefore beneficial to highlight the essential principles of electromagnetic theory as applied to petroleum exploration, in the hope that future efforts will be more firmly tied to reality.

This chapter provides the basic theory pertaining to induced polarization measurements, with some references to controlled source audiofrequency magnetotelluric measurements. We shall consider the behavior of the ground as it is pulsed with an alternating current from a grounded dipole source. The discussion presents the basic defining relations, develops a vector wave equation involving the potential fields, then proceeds to outline the solution to the wave equation for certain situations of special interest in petroleum exploration. The treatment roughly follows that of Ward (1967) and Sunde (1967), with some references to Keller and Frischknecht (1966). Table 9.1 lists the quantities, units, and constants used in this chapter. Figure 9.1 shows the coordinate systems used.

9.2 MAXWELL'S EQUATIONS

If an alternating current is caused to flow in a conductive medium like the earth, an electromagnetic field is established. In the formulation which follows, four parameters may be used to describe this field:

\vec{E}	Electric field intensity
\vec{D}	Electric flux density
\vec{H}	Magnetic field intensity
\vec{B}	Magnetic flux density

TABLE 9.1: SUMMARY OF FIELD QUANTITIES AND UNITS

Units			
Unit	Symbol	Meaning	Equivalent Units
ohm	ohm	Electrical resistance	v/amp
ohm-meter	ohm-m	Electrical resistivity	v-m/amp
mhos/meter	mhos/m	Electrical conductivity	amp/v-m
ampere	amp	Electrical current	v/ohm
volt	v	Voltage	amp-ohm
weber	wb	Magnetic flux	v-sec
coulomb	coul	Electric charge	amp-sec
henry	hr	Magnetic inductance	ohm-sec
farad	fd	Capacitance	sec/ohm

Field Quantities

\vec{E}	Electric field intensity (v/m)
\vec{D}	Electric flux density (coul/m ²)
\vec{H}	Magnetic field intensity (amp/m)
\vec{B}	Magnetic flux density (wb/m ²)
\vec{J}	Electric current density (amp/m ²)
q_v	Electric charge density (coul/m ³)
\vec{A}^*	Electric vector potential (coul/m)
\vec{A}	Magnetic vector potential (wb/m)
ϕ	Electric scalar potential (v)
ϕ^*	Magnetic scalar potential (amp)
$\vec{\pi}$	Electric Hertz vector potential (v-m)
$\vec{\pi}^*$	Magnetic Hertz vector potential (amp-m)
\vec{P}_v	Electric dipole moment per unit volume (coul/m ²)
\vec{M}_v	Magnetic dipole moment per unit volume (amp/m)
V	Voltage drop (v)
I	Electric current (amp)
Z	Complex impedance (ohm)
R_{TE}	Transverse electric coefficient (unitless)
R_{TM}	Transverse magnetic coefficient (unitless)
Q	"Q" coupling function (ohm)
P	"P" coupling function (ohm)

Media Properties

σ	Electrical conductivity (mhos/m)
ρ	Electrical resistivity (ohm-m)
ϵ	Electric permittivity (fd/m)
μ	Magnetic permeability (hr/m)

Media Properties (continued)

κ_e	Relative permittivity (dielectric constant) (unitless)
κ_m	Relative permeability (unitless)
χ_e	Electric susceptibility (unitless)
χ_m	Magnetic susceptibility (unitless)
\vec{P}_e	Electric polarization vector (coul/m ²)
\vec{P}_m	Magnetic polarization vector (amp/m)
k	Propagation constant (1/m)
α	Phase constant (1/m)
β	Attenuation constant (1/m)
δ	Skin depth (m)
v_p	Phase velocity (m/sec)
λ	Wavelength (m)

Other Quantities

t	Time (sec)
ω	Angular frequency (rad/sec)
f	Linear frequency (Hz or cycles/sec)
r	Distance (m)
a	Dipole size in dipole-dipole array (m)
n	Dipole separation (in terms of "a") in dipole-dipole array (m)

Constants

ϵ_0	Free space electric permittivity	8.854×10^{-12} fd/m
μ_0	Free space magnetic permeability	$4\pi \times 10^{-7}$ hr/m
c	Speed of light in a vacuum	3.00×10^8 m/sec

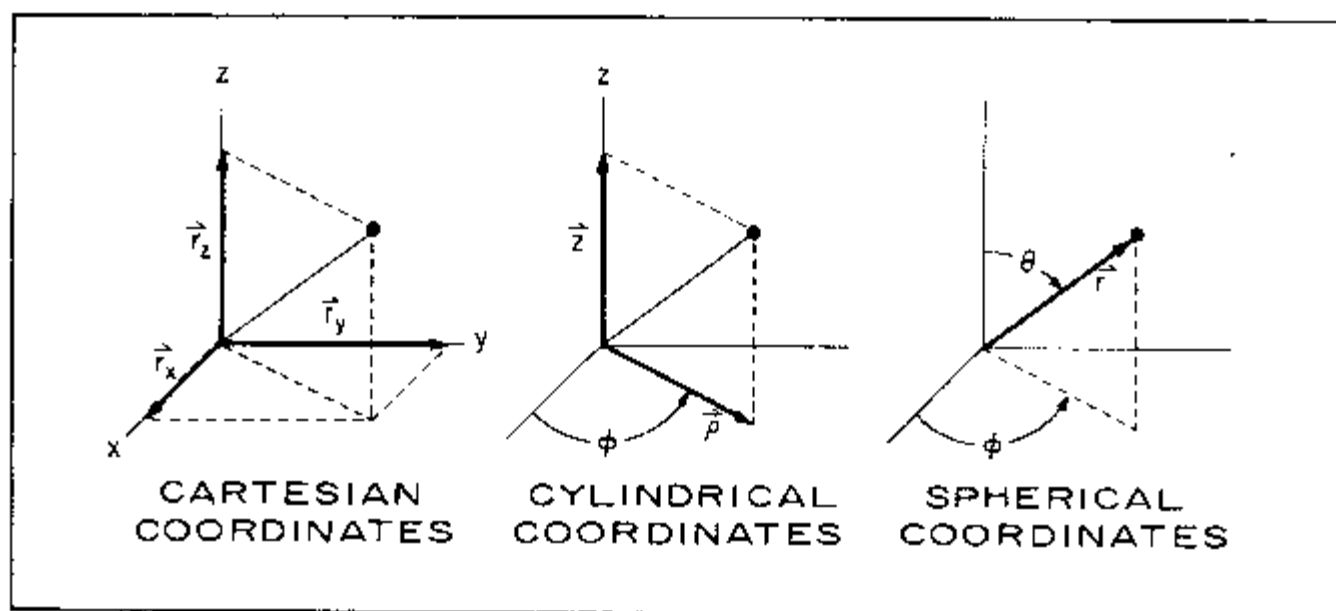


Figure 9.1. Cartesian, cylindrical, and spherical coordinate systems.

These parameters are interrelated by four fundamental laws of electromagnetism, known as Maxwell's equations:

$$\vec{\nabla} \times \vec{E} + \partial \vec{B} / \partial t = 0 \quad (\text{Faraday's Law}) \quad (9.1)$$

$$\vec{\nabla} \times \vec{H} - \partial \vec{D} / \partial t = \vec{J} \quad (\text{Ampere's Law}) \quad (9.2)$$

$$\vec{\nabla} \cdot \vec{D} = q_v \quad (\text{Coulomb's Law}) \quad (9.3)$$

$$\vec{\nabla} \cdot \vec{B} = 0 \quad (\text{Continuous flux law}) \quad (9.4)$$

In these, \vec{J} is the electric current density and q_v is the electric charge density. These relations are largely the result of experimental work in electricity and magnetism conducted during the 19th century. First assembled as a group by J.C. Maxwell in 1863, they form a general and elegant description of electromagnetic phenomena. A direct result of these equations, the so-called equation of continuity or conservation of electric charge, relates current density to charge density:

$$\vec{\nabla} \cdot \vec{J} + \partial q_v / \partial t = 0 \quad (9.5)$$

9.3 PHYSICAL PROPERTIES OF A CONDUCTIVE MEDIUM

Materials in the earth may normally be described by three physical properties: conductivity (σ), electric permittivity (ϵ), and magnetic permeability (μ). Conductivity is a measurement of the current flow characteristics of the ground. Materials with a high conductivity are known as conductors; materials with a low conductivity are known as insulators or dielectrics. The inverse of conductivity, resistivity (ρ), is the quantity normally measured in Zonge Engineering hydrocarbon surveys:

$$\rho = 1/\sigma \quad (9.6)$$

Resistivity is the resistance to electrical current flowing through a cross-sectional area, measured as a function of the distance over which the current flows; hence, the units for resistivity are ohm-m²/m, or ohm-m. As will be seen later, resistivity is also a function of the geometry of the array used to measure it.

Two additional field quantities, electric permittivity and magnetic permeability, are defined by empirically-derived relationships. For free space, the permittivity (ϵ_0) and permeability (μ_0) are:

$$\epsilon_0 = 8.854 \times 10^{-12} \text{ fd/m}$$

$$\mu_0 = 4\pi \times 10^{-7} \text{ hr/m}$$

For a given material, the ratios

$$\kappa_e = \epsilon / \epsilon_0 \quad (9.7)$$

and

$$\kappa_m = \mu / \mu_0 \quad (9.8)$$

are known as the relative permittivity (or dielectric constant) and the relative permeability, respectively. The departures of these quantities from unity,

$$\chi_e = \kappa_e - 1 \quad (9.9)$$

$$\chi_m = \kappa_m - 1 \quad (9.10)$$

are called the electric and magnetic susceptibilities, respectively.

While the dielectric constant is close to unity for most earth materials found in oilfield environments, the magnetic permeability shows a greater range of values, depending upon the amounts of magnetic minerals contained in the rocks. Most sediments are nonmagnetic ($\mu = \mu_0$), but occasionally one encounters diamagnetic materials, which have permeabilities very slightly lower than the permeability of free space ($\mu < \mu_0$), or paramagnetic materials, which have permeabilities very slightly higher than the permeability of free space ($\mu > \mu_0$). Materials which have very high permeabilities are called ferromagnetic. The most common ferromagnetic material found in the earth is magnetite.

In the case of an electromagnetic field propagating through a simple, isotropic material, the basic field quantities can be related to each other in terms of the physical properties of the material:

$$\vec{D} = \epsilon \vec{E} \quad (9.11)$$

$$\vec{B} = \mu \vec{H} \quad (9.12)$$

The electric polarization vector \vec{P}_e and the magnetic polarization vector \vec{P}_m can be defined as:

$$\vec{P}_e = \vec{D} - \epsilon_0 \vec{E} = \chi_e \epsilon_0 \vec{E} \quad (9.13)$$

$$\vec{P}_m = 1/\mu_0 \vec{B} - \vec{H} = \chi_m \vec{H} \quad (9.14)$$

These quantities describe the atomic dipolar polarization due to an impressed field.

An important relation between current density and electric field intensity is an expression of Ohm's Law:

$$\vec{J} = \sigma \vec{E} \quad (9.15)$$

This equation will be used later on to derive the necessary relations for calculating resistivity for induced polarization surveys.

9.4 DEVELOPMENT OF THE VECTOR WAVE EQUATION

An electromagnetic wave propagating through a material can be described in terms of potential functions. In this development, the potential functions are derived in a mathematically convenient manner. While this treatment may seem somewhat arbitrary at first, the potential functions can be used to enhance our appreciation of the physical principles involved.

According to the continuous flux law of equation (9.4), the flux of a magnetic field going into a closed surface is the same as the flux going out:

$$\vec{\nabla} \cdot \vec{B} = 0$$

This suggests that \vec{B} is the curl of some vector \vec{A} , since the divergence of the curl is zero:

$$\vec{B} = \vec{\nabla} \times \vec{A} \quad (9.16)$$

From equation (9.1), we have

$$\vec{\nabla} \times (\vec{E} + \partial \vec{A} / \partial t) = 0 \quad (9.17)$$

This insures that the vector $(\vec{E} + \partial\vec{A}/\partial t)$ is irrotational and is therefore the gradient of some scalar function ϕ :

$$\vec{E} + \partial\vec{A}/\partial t = -\vec{\nabla}\phi$$

or

$$\vec{E} = -\vec{\nabla}\phi - \partial\vec{A}/\partial t \quad (9.18)$$

The vector \vec{A} is called the magnetic vector potential, and ϕ is the electric scalar potential. Note that in the case of a time-invariant (static) electric field, equation (9.18) reduces to

$$\vec{E} = -\vec{\nabla}\phi \quad (9.19)$$

which is a familiar result of static electromagnetic theory.

We wish to write two linear differential equations, one for \vec{A} and one for ϕ . Taking equation (9.2) and substituting from equations (9.11), (9.12), (9.16), and (9.18), we obtain

$$\vec{\nabla} \times \vec{\nabla} \times \vec{A} + \mu\epsilon \vec{\nabla} \partial\phi/\partial t + \mu\epsilon \partial^2 \vec{A}/\partial t^2 = \mu\vec{J} \quad (9.20)$$

$$\nabla^2 \phi + \vec{\nabla} \cdot \partial\vec{A}/\partial t = -\rho_v/\epsilon \quad (9.21)$$

Contained implicitly in the term for current density \vec{J} are two parts—a primary source \vec{J}_p and a secondary part \vec{J}_s . The secondary part has a contribution of

$$\mu\sigma (-\vec{\nabla}\phi - \partial\vec{A}/\partial t)$$

which can be explicitly included in equation (9.20) such that

$$\vec{\nabla} \times \vec{\nabla} \times \vec{A} + \mu\epsilon \vec{\nabla} \partial\phi/\partial t + \mu\epsilon \partial^2 \vec{A}/\partial t^2 + \mu\sigma \vec{\nabla}\phi + \mu\sigma \partial\vec{A}/\partial t = \mu\vec{J}_p \quad (9.22)$$

in which $\vec{J}_p = \sigma \vec{E}_p$ and $\vec{J}_s = \sigma \vec{E}_s$.

A vector identity in cartesian coordinates provides that

$$\vec{\nabla} \times \vec{\nabla} \times \vec{A} = \vec{\nabla} \vec{\nabla} \cdot \vec{A} - \vec{\nabla} \cdot \vec{\nabla} \vec{A} \quad (9.23)$$

Further, since the vector \vec{A} is arbitrarily obtained, we can impose the Lorentz condition:

$$\vec{\nabla} \cdot \vec{A} + \mu\epsilon \partial\phi/\partial t + \mu\sigma\phi = 0 \quad (9.24)$$

Using equations (9.23) and (9.24), we can rewrite equations (9.22) and (9.21) as

$$\nabla^2 \vec{A} - \mu\epsilon \partial^2 \vec{A}/\partial t^2 - \mu\sigma \partial\vec{A}/\partial t = \mu\vec{J}_p \quad (9.25)$$

$$\nabla^2 \phi - \mu\epsilon \partial^2 \phi/\partial t^2 - \mu\sigma \partial\phi/\partial t = -\rho_v/\epsilon \quad (9.26)$$

The solutions to these two inhomogeneous wave equations can be derived in terms of \vec{A} and ϕ , but it is more convenient to introduce a third potential term, $\vec{\pi}$, which is called the electric Hertz vector potential. This potential has the advantage of combining \vec{A} and ϕ into a single wave equation. The Hertz vector is defined by

$$\vec{A} = \mu\epsilon \partial\vec{\pi}/\partial t + \mu\sigma\vec{\pi} \quad (9.27)$$

$$\phi = -\vec{\nabla} \cdot \vec{\pi} \quad (9.28)$$

This allows equation (9.25) to be rewritten as

$$\mu\sigma [\nabla^2 \vec{\pi} - \mu\epsilon \partial^2 \vec{\pi} / \partial t^2 - \mu\sigma \partial \vec{\pi} / \partial t] + \mu\epsilon \partial / \partial t [\nabla^2 \vec{\pi} - \mu\epsilon \partial^2 \vec{\pi} / \partial t^2 - \mu\sigma \partial \vec{\pi} / \partial t] = \mu \partial \vec{P}_v / \partial t \quad (9.29)$$

in which \vec{P}_v is the dipole moment per unit volume, defined by

$$\vec{J}_p = \partial \vec{P}_v / \partial t \quad (9.30)$$

The form of equation (9.29) can be recognized more easily by representing the bracketed terms by " \vec{X} ", in which case we have

$$\vec{X} + \epsilon/\sigma \partial \vec{X} / \partial t = -1/\sigma \partial \vec{P}_v / \partial t \quad (9.31)$$

The solution to this inhomogeneous differential equation may be obtained by considering two limiting cases. The first limiting case is for a source-free region with transient fields ($\vec{P}_v = 0$, $\sigma \neq 0$). Equation (9.31) then reduces to a homogeneous differential equation:

$$\vec{X} + \epsilon/\sigma \partial \vec{X} / \partial t = 0 \quad (9.32)$$

The solutions are of the form

$$\vec{X} = e^{-(\sigma/\epsilon)t} \quad (9.33)$$

The σ/ϵ term is a measure of the decay time of transients due to the induced field. In general, this time is negligibly small (less than 10^{-6} second), in which case we have

$$\vec{X} = 0 \quad (9.34)$$

Following the pattern of equations (9.25) and (9.26), this results in:

$$\nabla^2 \vec{\pi} - \mu\epsilon \partial^2 \vec{\pi} / \partial t^2 - \mu\sigma \partial \vec{\pi} / \partial t = 0 \quad (9.35)$$

The opposite limiting case is for a region with sources but no transients ($\vec{P}_v \neq 0$, $\sigma = 0$), in which case we have

$$\partial \vec{X} / \partial t = -1/\epsilon \partial \vec{P}_v / \partial t \quad (9.36)$$

or

$$\vec{X} = -(1/\epsilon) \partial \vec{P}_v / \partial t + \vec{C} \quad (9.37)$$

Neglecting the constant of integration, this can be rewritten as:

$$\nabla^2 \vec{\pi} - \mu\epsilon \partial^2 \vec{\pi} / \partial t^2 = -\vec{P}_v / \epsilon \quad (9.38)$$

Since the total field is the sum of the primary field and the secondary field, we can sum equations (9.34) and (9.38) to obtain

$$\vec{X} = 0 + (-\vec{P}_v / \epsilon) \quad (9.39)$$

which converts back to our previous nomenclature as:

$$\nabla^2 \vec{\pi} - \mu\epsilon \partial^2 \vec{\pi} / \partial t^2 - \mu\sigma \partial \vec{\pi} / \partial t = -\vec{P}_v / \epsilon \quad (9.40)$$

This has the same form of equations (9.25) and (9.26). The electric and magnetic fields can be obtained in terms of $\vec{\pi}$ by equations (9.19) and (9.16):

$$\vec{E} = \vec{\nabla} \vec{\nabla} \cdot \vec{\pi} - \mu\epsilon \partial^2 \vec{\pi} / \partial t^2 - \mu\sigma \partial \vec{\pi} / \partial t \quad (9.41)$$

$$\vec{B} = \mu\epsilon \vec{\nabla} \times \partial \vec{\pi} / \partial t + \mu\sigma \vec{\nabla} \times \vec{\pi} \quad (9.42)$$

So far we have dealt with the electric Hertz vector only, in which magnetic sources and transients are not considered. To generalize the discussion, we introduce the electric vector potential, \vec{A}^* , and the magnetic scalar potential, ϕ^* . Following our earlier development, equations (9.25), (9.26), (9.27), and (9.28) can be re-written as follows:

$$\nabla^2 \vec{A}^* - \mu\epsilon \partial^2 \vec{A}^* / \partial t^2 - \mu\sigma \partial \vec{A}^* / \partial t = - \mu\epsilon \partial \vec{M}_v / \partial t \quad (9.43)$$

$$\nabla^2 \phi^* - \mu\epsilon \partial^2 \phi^* / \partial t^2 - \mu\sigma \partial \phi^* / \partial t = \vec{\nabla} \cdot \vec{M}_v \quad (9.44)$$

$$\vec{A}^* = \mu\epsilon \partial \vec{\pi}^* / \partial t + \mu\sigma \vec{\pi}^* \quad (9.45)$$

$$\phi^* = - \vec{\nabla} \cdot \vec{\pi}^* \quad (9.46)$$

in which \vec{M}_v is the magnetic dipole moment per unit volume. We can therefore write for the magnetic Hertz vector:

$$\nabla^2 \vec{\pi}^* - \mu\epsilon \partial^2 \vec{\pi}^* / \partial t^2 - \mu\sigma \partial \vec{\pi}^* / \partial t = - \vec{M}_v \quad (9.47)$$

This is the magnetic analog of equation (9.40). Finally, considering both electric and magnetic sources with transients, we can write the electric and magnetic fields as follows:

$$\vec{E} = \nabla^2 \vec{\pi} - \mu\epsilon \partial^2 \vec{\pi} / \partial t^2 - \mu\sigma \partial \vec{\pi} / \partial t - \mu \vec{\nabla} \times \partial \vec{\pi}^* / \partial t \quad (9.48)$$

$$\vec{H} = \nabla^2 \vec{\pi}^* - \mu\epsilon \partial^2 \vec{\pi}^* / \partial t^2 - \mu\sigma \partial \vec{\pi}^* / \partial t + \epsilon \vec{\nabla} \times \partial \vec{\pi} / \partial t + \sigma \vec{\nabla} \times \vec{\pi} \quad (9.49)$$

9.5 BOUNDARY CONDITIONS

Solving the potential equations in a layered earth requires that we say something about the behavior of \vec{E} and \vec{H} as they traverse the boundary between two media with properties $\mu_1, \epsilon_1, \sigma_1$ and $\mu_2, \epsilon_2, \sigma_2$ (Figure 9.2). The following boundary conditions can be obtained from elementary calculus and from the concepts just developed:

- The normal component of \vec{D} is continuous across the interface ($D_{2N} - D_{1N} = 0$).
- The normal component of \vec{B} is continuous ($B_{2N} - B_{1N} = 0$).
- The tangential component of \vec{E} is continuous ($E_{2T} - E_{1T} = 0$).
- The tangential component of \vec{H} is continuous ($H_{2T} - H_{1T} = 0$).
- Current density is continuous ($J_{1N} = J_{2N}$).
- Potentials are continuous if no sources are present ($\phi_1 = \phi_2, \phi_1^* = \phi_2^*$).

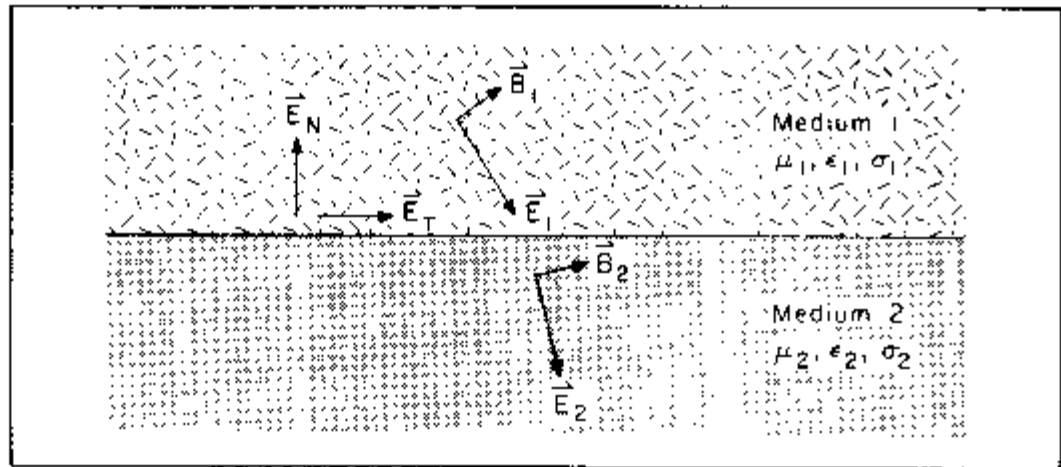


Figure 9.2. Boundary conditions at the interface of two media.

9.6 DC SOLUTIONS TO THE VECTOR WAVE EQUATION

Introduction

Before advancing to the more general AC solutions to the vector wave equations, it is useful to discuss the much simpler DC solutions. We recall from equation (9.18) that

$$\vec{E} = -\vec{\nabla}\phi - \partial\vec{A}/\partial t$$

For the time-invariant DC case, this reduces to equation (9.19):

$$\vec{E} = -\vec{\nabla}\phi$$

The scalar ϕ is the potential at a point which is at a distance r from a single point source. The potential is referenced to infinity:

$$\phi = -\int_r^\infty E_r dr \quad (9.50)$$

From equation (9.15), using resistivity in place of conductivity ($\rho = 1/\sigma$),

$$E_r = J_r \rho \quad (9.51)$$

This can be substituted into equation (9.50) to obtain, for a homogeneous whole-space,

$$\phi_r = -\int_r^\infty E_r dr = I\rho/4\pi r \quad (9.52)$$

The solutions of interest in this chapter involve potentials at points on the surface of the earth, which means we will seek equations for a homogeneous half-space (the earth) bounded by a perfect insulator (the air). In this case, the current density is twice that of a whole-space, and the potential becomes

$$\phi_r = -\int_r^\infty E_r dr = I\rho/2\pi r \quad (9.53)$$

**Homogeneous
Earth
Resistivity**

All induced polarization methods commonly used in hydrocarbon exploration involve the use of four grounded electrodes. Two electrodes are used for the current or transmitting dipole, and two are used for the receiving dipole, which measures the ground potential. Figure 9.3 shows a general electrode arrangement for a ground survey over a homogeneous earth. Current is transmitted into the dipole MN; it enters (+) electrode M and exits (−) electrode N. The ground potentials measured at electrodes A and B, referenced to the source electrodes M and N, may be written as follows:

$$\phi_{AM} = I\rho/2\pi r_{AM}$$

$$\phi_{AN} = I\rho/2\pi r_{AN}$$

$$\phi_{BM} = I\rho/2\pi r_{BM}$$

$$\phi_{BN} = I\rho/2\pi r_{BN}$$

By superposition, the potential difference across the receiving dipole AB is therefore:

$$V_{AB} = (I\rho/2\pi)[(1/r_{AM} - 1/r_{AN}) - (1/r_{BM} - 1/r_{BN})] \quad (9.54)$$

in which the symbol V , by convention, denotes the voltage drop between two specified points.

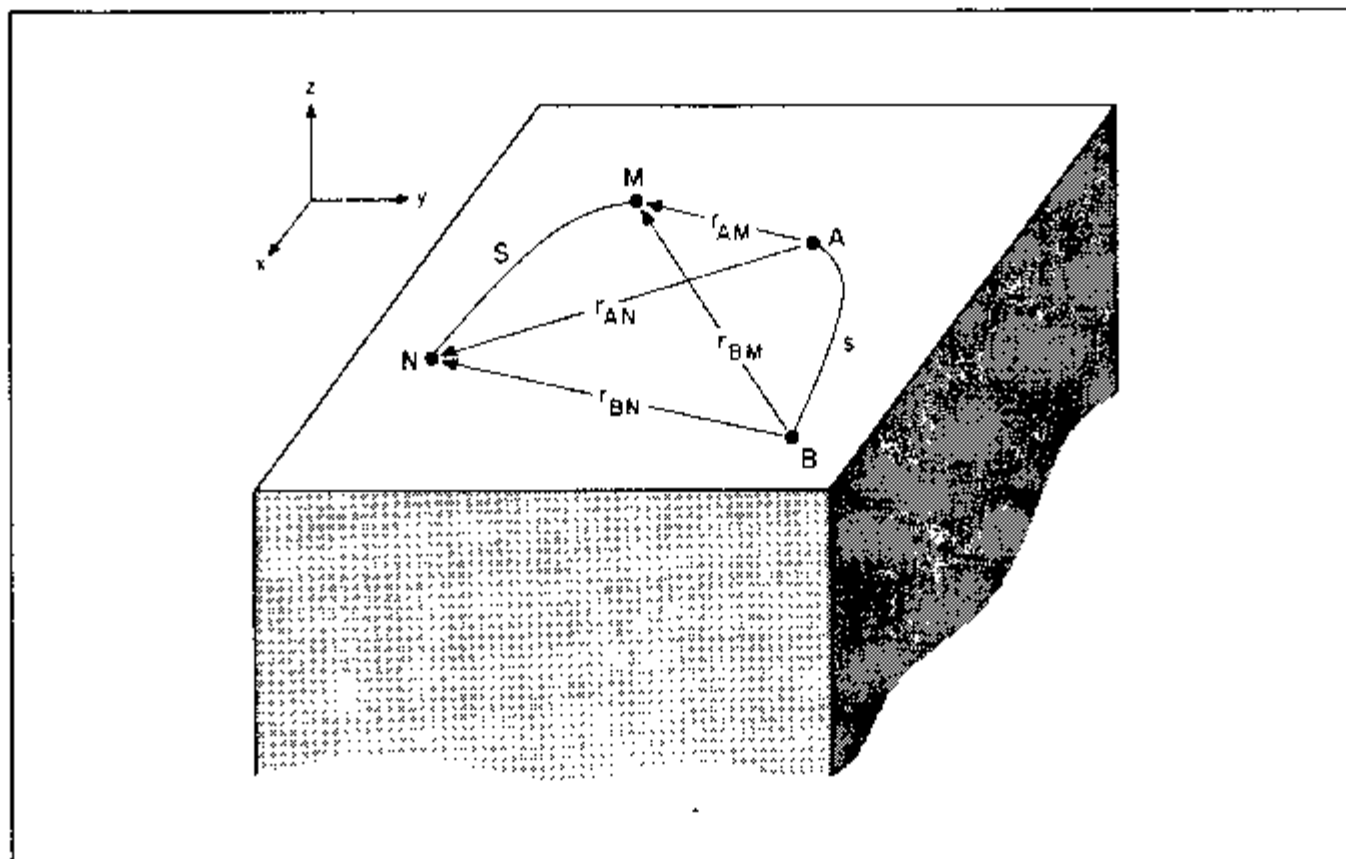


Figure 9.3. Arbitrary four-electrode array on the surface of a homogeneous earth.

Of particular interest in this volume is the voltage drop for a collinear dipole-dipole array, depicted in Figure 9.4. In this array, both the transmitter and receiver dipoles have a length "a", and are separated by "na". Therefore we have: $AM = a + na$, $AN = na$, $BM = a + a + na$, and $BN = a + na$. Equation (9.54) then reduces to

$$V_{AB} = (1\rho/2\pi)[1/(n+1)a - 1/na - 1/(n+2)a + 1/(n+1)a]$$

which in turn reduces to (dropping the subscript for V):

$$V = I\rho/[\pi an(n+1)(n+2)] \quad (9.55)$$

Equation (9.55) is used to calculate the ground resistivity for the dipole-dipole array. Note that this relation has the form of Ohm's Law, relating resistance (R) to voltage and current:

$$V = IR$$

This is the potential analog of equation (9.15). The term in brackets in equation (9.55) is called the "geometric factor", since it describes the locations of the electrode grounding points.

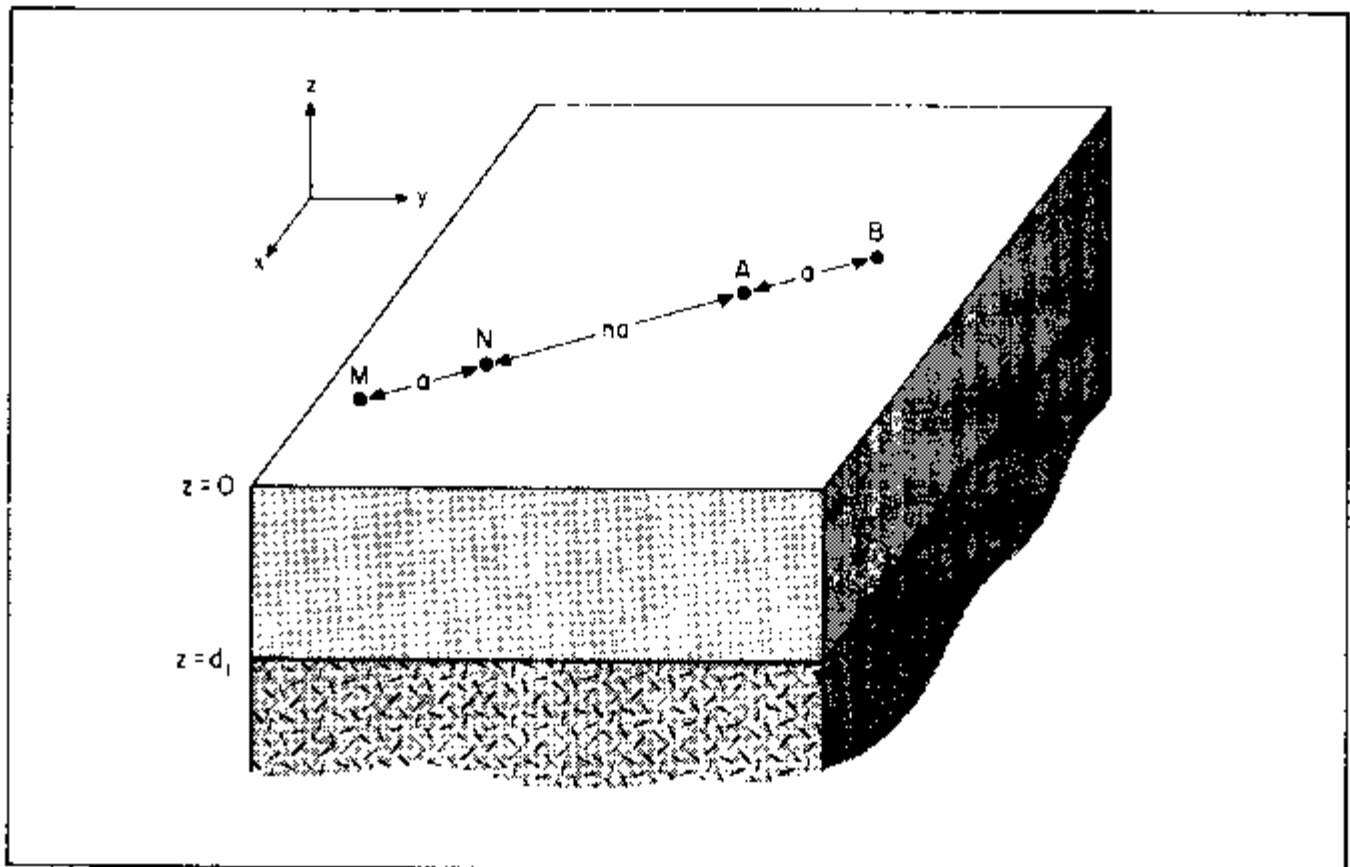


Figure 9.4. Collinear dipole-dipole array on the surface of a two-layered earth.

Two-Layered Earth Resistivity

It is useful for purposes of computer modeling to determine the response of a two-layered earth with resistivities ρ_1 and ρ_2 , as illustrated in Figure 9.4. We seek a potential ϕ_1 in the first layer, which is composed of a primary part (the source) and a secondary part (due to layering):

$$\phi_1 = \phi_p + \phi_{s1} \quad (9.56)$$

The primary potential is

$$\phi_p = (I\rho_1/2\pi)(z^2 + r^2)^{-1/2} \quad (9.57)$$

in which z is the depth in the ground. This relation can be written in terms of a zeroth-order Bessel function of the first kind:

$$\phi_p = (I\rho_1/2\pi) \int_0^\infty J_0(\lambda r) e^{-\lambda z} d\lambda \quad (9.58)$$

in which λ is the integration variable. The secondary potential, after application of appropriate boundary conditions and some algebra, can be written

$$\phi_{s1} = (I\rho_1/2\pi) \int_0^\infty \left[-2u_{12} e^{-2\lambda z_1} / (1 + u_{12} e^{-2\lambda z_1}) \right] J_0(\lambda r) d\lambda \quad (9.59)$$

in which

$$u_{12} = (\rho_1 - \rho_2) / (\rho_1 + \rho_2) \quad (9.60)$$

The potential difference between electrodes A and B at the surface of the earth is

$$V_1 = (\phi_{AM} + \phi_{AN})_1 - (\phi_{BM} + \phi_{BN})_1 \quad (9.61)$$

in which the primary and secondary potentials are contained implicitly in the ϕ terms. For the dipole-dipole array, these are:

$$\phi_{AM} = (I\rho_1/2\pi) [1/(n+1)a + 2 \sum_{k=1}^{\infty} \{-u_{12}\}^k / \{(n+1)^2 a^2 + (2kd_1)^2\}^{1/2}] \quad (9.62)$$

$$\phi_{AN} = (I\rho_1/2\pi) [1/na + 2 \sum_{k=1}^{\infty} \{-u_{12}\}^k / \{(na)^2 + (2kd_1)^2\}^{1/2}] \quad (9.63)$$

$$\phi_{BM} = (I\rho_1/2\pi) [1/(n+2)a + 2 \sum_{k=1}^{\infty} \{-u_{12}\}^k / \{(n+2)^2 a^2 + (2kd_1)^2\}^{1/2}] \quad (9.64)$$

$$\phi_{BN} = (I\rho_1/2\pi) [1/(n+1)a + 2 \sum_{k=1}^{\infty} \{-u_{12}\}^k / \{(n+2)^2 a^2 + (2kd_1)^2\}^{1/2}] \quad (9.65)$$

The results of these calculations are used for simple resistivity modeling in induced polarization work. They lead to a series of curves in which resistivity may be plotted as a function of n -spacing for various depths to the layer interface and for various resistivity contrasts between the two layers. The field curves are "curve-matched" to the theoretical curves in order to establish the layering parameters. A similar procedure may be used for a three-layered earth, but the algebra is more complicated, and the number of theoretical curves needed for the process is rather unmanageable.

9.7 AC SOLUTIONS TO THE VECTOR WAVE EQUATION

Harmonic Time-Dependence

We will now examine the response of a non-polarizable, homogeneous half-space to an alternating current. The purpose here is to develop an equation for frequency-dependent resistivity, or complex impedance, so that frequency-dependent data collected in the field can be analyzed for the separate effects of direct current flow ("galvanic" processes) and indirect or induced current flow ("electromagnetic coupling" processes).

The following treatment assumes a harmonic time-dependency for the electric field,

$$\vec{E} = \vec{E}_0 e^{i\omega t} \quad (9.66)$$

in which \vec{E}_0 is the peak field strength, \vec{E} is the instantaneous field strength at time t , and ω is the angular frequency ($\omega = 2\pi f$, where f is the linear AC frequency). We recall that

$$e^{-i\omega t} = \cos \omega t - i \sin \omega t \quad (9.67)$$

Maxwell's equations are sufficiently general that a harmonic time-dependency can be assumed implicitly.

Let us consider a harmonic, time-varying field in a source free region. From equations (9.25), (9.43), (9.26), (9.44), (9.40), and (9.47), we have

$$\nabla^2 \vec{A} + k^2 \vec{A} = 0 \quad (9.68)$$

$$\nabla^2 \vec{A}^* + k^2 \vec{A}^* = 0 \quad (9.69)$$

$$\nabla^2 \phi + k^2 \phi = 0 \quad (9.70)$$

$$\nabla^2 \phi^* + k^2 \phi^* = 0 \quad (9.71)$$

$$\nabla^2 \vec{\pi} + k^2 \vec{\pi} = 0 \quad (9.72)$$

$$\nabla^2 \vec{\pi}^* + k^2 \vec{\pi}^* = 0 \quad (9.73)$$

in which k is the so-called propagation constant, or wave number, the reciprocal of the radian wavelength. It is given by

$$k^2 = -\mu\epsilon\omega^2 + i\mu\sigma\omega \quad (9.74)$$

The first term ($\mu\epsilon\omega^2$) is the displacement term, and the second ($i\mu\sigma\omega$) is the conduction term. The complex form of the propagation constant can be written

$$k = \alpha + i\beta \quad (9.75)$$

The real part, α , is the phase constant, given by

$$\alpha = \omega [(\mu\epsilon/2) \{ \sqrt{1 + (\sigma/\omega\epsilon)^2} + 1 \}]^{1/2} \quad (9.76)$$

The imaginary part, β , is the attenuation factor, given by

$$\beta = \omega \{ (\mu\epsilon/2) (\sqrt{1 + (\sigma/\omega\epsilon)^2} - 1) \}^{1/2} \quad (9.77)$$

Frequency- Dependence of k

Most earth materials are relatively conductive, and the conduction term tends to dominate the displacement term in equation (9.74), providing that the frequency is low (i.e., around 1 Hz). However, the two terms become more comparable at higher frequencies, making it important to understand their relative contributions as a function of frequency and media properties. In order to explicitly evaluate frequency-dependency, let us write

$$k^2 = \mu\omega (-\omega\epsilon + i\sigma) \quad (9.78)$$

and compare the contribution of σ with respect to $\omega\epsilon$ by finding the frequency at which they are equal:

$$f' = \omega/2\pi = \sigma/2\pi\epsilon \quad (\sigma = \omega\epsilon) \quad (9.79)$$

Keller and Frischknecht (1966) pose two opposite examples for comparison: a shale, for which $\epsilon = 10^{-6}$ fd/m and $\rho = 10$ ohm-m, and a granite, for which $\epsilon = 1.6 \times 10^{-10}$ fd/m and $\rho = 10^5$ ohm-m. In the case of the shale, we obtain $f' = 16$ kHz. In the case of the granite, we obtain a slightly lower $f' = 10$ kHz. Therefore, we have $\sigma \gg \omega\epsilon$ for the normal frequency range (0.01 to 100 Hz) used for induced polarization type surveys. Note, however, that the $\sigma \gg \omega\epsilon$ constraint does not hold for downhole electric and induction logs, which are normally obtained at frequencies of 1-20 kHz. These logs may be dominated by displacement effects, while surface induced polarization surveys are dominated by conduction effects. Hence, one must be very careful in comparing data from these two frequency ranges.

SPECIAL CASE: $\sigma \gg \omega\epsilon$

If we assume that conduction effects predominate, $\sigma \gg \omega\epsilon$, we have

$$\alpha = \beta = \sqrt{\mu\sigma\omega/2} \quad (9.80)$$

The propagation constant is therefore

$$k = \alpha + i\beta = (1 + i) \sqrt{\mu\sigma\omega/2} \quad (9.81)$$

For a downward-traveling plane wave, the harmonically-dependent electric field E_x can be written:

$$E_x = E_0 e^{-kz} \quad (9.82)$$

Substituting for k ,

$$E_x = E_0 e^{-z\sqrt{\mu\sigma\omega/2}} e^{-iz\sqrt{\mu\sigma\omega/2}} \quad (9.83)$$

This can also be written

$$E_x = E_0 e^{-z/\delta} e^{-iz/\delta} \quad (9.84)$$

with the definition

$$\delta \equiv 1/\alpha = \sqrt{2/\mu\sigma\omega} \quad (9.85)$$

The term δ is the "skin depth", a term which describes the effective depth of penetration of a plane wave through a conductive material. Note that at $z = \delta$,

$$E_x = E_0 e^{-1} \quad (9.86)$$

and the incident plane wave is attenuated by a factor of $1/e$. Thus, "skin depth" is the distance over which a plane wave is attenuated by a factor of $1/e$. If we assume a magnetic permeability of 1.256×10^{-6} hr/m, as is the case for most earth materials, we can write equation (9.85) in more practical terms:

$$\delta = 503 \sqrt{\rho/f} \quad (\text{meters}) \quad (9.87)$$

This important result shows that, in a plane wave field, penetration is highest at high resistivities and low frequencies. This has direct application to controlled source audiofrequency magnetotelluric (CSAMT) measurements, which are sometimes used for detailing alteration patterns in the sediments above hydrocarbons.

The wavelength (λ) of the harmonic signal is

$$\lambda = 2\pi\delta \quad (9.88)$$

The phase or propagation velocity is

$$v_p = \omega/\alpha = \sqrt{2\omega/\mu\sigma} \quad (9.89)$$

SPECIAL CASE: $\sigma \ll \omega\epsilon$

When displacement currents dominate conductive currents, $\sigma \ll \omega\epsilon$, the phase constant becomes

$$\alpha = \omega\sqrt{\mu\epsilon} \quad (9.90)$$

and the attenuation constant becomes zero. The skin depth in such an infinitely resistive medium is infinite. The propagation velocity is

$$v_p = \omega/\alpha = 1/\sqrt{\mu\epsilon} \quad (9.91)$$

Note that in a vacuum, the propagation velocity is

$$v_p = 1/\sqrt{\mu_0\epsilon_0} \quad (9.92)$$

which is equal to the speed of light.

9.8 COMPLEX IMPEDANCE OF THE ELECTRIC FIELD

Development of the Relations

The purpose of this section is to develop the basic relations which describe the complex impedance of the ground. Consider two wires S and s lying on the surface of a homogeneous earth (Figure 9.3). We recall that the electric Hertz vector

has a primary part $\vec{\pi}_p$ due to the source current, and a secondary part $\vec{\pi}_s$ due to the transient field induced by the source. The primary potential can be written in terms of the inhomogeneous Helmholtz equation, which is the general form of equation (9.72):

$$(\nabla^2 + k^2) \vec{\pi}_p = \vec{P}_p/c \quad (9.93)$$

The solution to this is

$$|\vec{\pi}_p| = -(i\omega\mu_0 I ds/4\pi k^2) \int_0^\infty (1/r) e^{-kr} dr \quad (9.94)$$

It is convenient to express this in terms of the zeroth-order Bessel function:

$$|\vec{\pi}_p| = -(i\omega\mu_0 I ds/4\pi^2) \int_0^\infty (\lambda/u_0) e^{-u_0 z} J_0(\lambda r) d\lambda \quad (9.95)$$

The symbol u_0 is used in place of $\sqrt{\lambda^2 - k_0^2}$ as a matter of convenience; in general,

$$u_i = \sqrt{\lambda^2 - k_i^2} \quad (9.96)$$

Note that equation (9.95) is the complex analog of the DC equation (9.59) developed earlier for a two-layered earth.

The secondary potential $\vec{\pi}_s$ satisfies the homogeneous Helmholtz equation with no sources present:

$$(\nabla^2 + k^2) \vec{\pi}_s = 0 \quad (9.97)$$

Solutions in the x-y plane are of the form

$$|\vec{\pi}_s| = F(\lambda) e^{\pm u_i z} J_n(\lambda r) \quad (9.98)$$

After the application of boundary conditions, we can write for π_x and π_z the relations:

$$\pi_x = -(i\omega\mu_0 I ds/4\pi k_0^2) \int_0^\infty [(\lambda/u_0) e^{u_0 z} + (\lambda/u_0) e^{-u_0 z} R_{TE}(\lambda)] J_0(\lambda r) d\lambda \quad (9.99)$$

$$\pi_z = -(i\omega\mu_0 I ds/4\pi k_0^2) \frac{\partial}{\partial x} \int_0^\infty [(1/\lambda) e^{u_0 z} R_{TE}(\lambda) + (1/\lambda) e^{-u_0 z} R_{TM}(\lambda)] J_0(\lambda r) d\lambda \quad (9.100)$$

The media properties have been recombined in terms of the transverse electric mode reflection coefficient, $R_{TE}(\lambda)$, and the transverse magnetic coefficient, $R_{TM}(\lambda)$, which are given by

$$R_{TE}(\lambda) = (N_0 - Y_1) / (N_0 + Y_1) \quad (9.101)$$

$$R_{TM}(\lambda) = (I_0 - Z_1) / (I_0 + Z_1) \quad (9.102)$$

in which we have defined:

$$I_0 = u_0 / i\omega\epsilon_0 \quad (9.103)$$

$$N_0 = u_0 / i\omega\mu_0 \quad (9.104)$$

$$Z_i = I_i \left[Z_{i+1} + I_i \tanh(u_i h_i) \right] / \left[I_i + Z_{i+1} \tanh(u_i h_i) \right] \quad (9.105)$$

$$Z_n = I_n = u_n / (\sigma_n + i\omega\epsilon_n) \quad (9.106)$$

$$Y_i = N_i \left[Y_{i+1} + N_i \tanh(u_i h_i) \right] / \left[N_i + Y_{i+1} \tanh(u_i h_i) \right] \quad (9.107)$$

$$Y_n = N_n = u_n / (\sigma_n + i\omega\epsilon_n) \quad (9.108)$$

The electric and magnetic fields can be obtained from equations (9.48) and (9.49), which may be re-written as

$$\vec{E} = k_o^{-2} \vec{\pi} + \vec{\nabla} \vec{\nabla} \cdot \vec{\pi} \quad (9.109)$$

$$\vec{H} = (\sigma_o + i\omega\epsilon_o) \vec{\nabla} \times \vec{\pi} \quad (9.110)$$

With substitutions of equations (9.99) and 9.100), the x-component of the electric field can be written as

$$E_x = k_o^{-2} \pi_x + \partial/\partial x (\partial\pi_x/\partial x + \partial\pi_z/\partial z) \Big|_{z=0} \quad (9.111)$$

which is converted to Bessel function form:

$$E_x = - (i\omega\mu_o / 4\pi k_o^2) \left\{ k_o^2 \int_0^\infty [(\lambda/u_o)(1 + R_{TE}(\lambda))] J_o(\lambda r) d\lambda + (\partial^2/\partial x^2) \int_0^\infty [(\lambda/u_o)(1 + R_{TE}(\lambda)) - (u_o/\lambda)(R_{TE}(\lambda) + R_{TM}(\lambda))] J_o(\lambda r) d\lambda \right\} \quad (9.112)$$

For ease in notation, we can write this as

$$E_x = Ids [-P(r) + \partial^2 Q(r)/\partial x^2] \quad (9.113)$$

in which we define

$$P(r) = - (i\omega\mu_o / 4\pi) \int_0^\infty [(\lambda/u_o)(1 + R_{TE}(\lambda))] J_o(\lambda r) d\lambda \quad (9.114)$$

$$Q(r) = - (i\omega\mu_o / 4\pi k_o^2) \int_0^\infty [(\lambda/u_o)(1 + R_{TE}(\lambda)) - (u_o/\lambda)(R_{TE}(\lambda) + R_{TM}(\lambda))] J_o(\lambda r) d\lambda \quad (9.115)$$

Finally, the impedance Z_{ss} between the two wires lying in the x-y plane can be written:

$$Z_{ss} = \int_M^N \int_A^B [P(r) \cos \epsilon + \partial^2 Q(r)/\partial S \partial s] dS ds \quad (9.116)$$

in which ϵ is the angle between the straight line element MN and the element AB. The voltage drop between A and B is then

$$V_{AB}(\omega) = I_{MN} Z_{ss}(\omega) \quad (9.117)$$

Functional Behavior of P and Q

We can think of the complex impedance as being the sum of two functions, P and Q:

$$Z_{ss} = P + Q \quad (9.118)$$

with

$$P = \int_M^N \int_A^B P(r) \cos \epsilon \quad (9.119)$$

$$Q = \int_M^N \int_A^B (\partial^2 Q(r)/\partial S \partial s) dS ds \quad (9.120)$$

The "P function" is called the inductive function because it is purely inductive in nature, as suggested by the $\cos \epsilon$ dependence. It is instructive to examine the behavior of the P function under a homogeneous earth assumption. In such a

case, equation (9.114) reduces to:

$$P(r) = -(\omega\mu_o/4\pi) \int_0^\infty [2\lambda/(u_o + u_1)] J_o(\lambda r) d\lambda \quad (9.121)$$

At low frequencies, the quasi-static approximation ($k_o \rightarrow 0$, $u_o \rightarrow \lambda$) applies, leading to:

$$P(r) = - (i\omega\mu_o/2\pi r) [1 - (1 + ik_1 r) e^{-ik_1 r}] / k_1^2 r^2 \\ - (i\omega\mu_o/2\pi k_1^2) [(1/r^2) e^{-ik_1 r} + (1/r^3) (e^{-ik_1 r} - 1)] \quad (9.122)$$

The P function is related to dipole size, frequency, and earth resistivity by

$$P \propto a^2 f/\rho \quad (9.123)$$

Therefore, we can conclude that the P function is maximized when the following conditions hold:

1. Dipole sizes are large
2. Frequency is high
3. Resistivity is low
4. Wires are parallel (because $\cos \epsilon \rightarrow 1$)

It can also be shown that P is maximized by high-over-low resistivity layering. The P function is minimized when wires are perpendicular.

The "Q" function is known as the grounding function, since it is specifically dependent upon the dipole grounding points. Taking the limit of the homogeneous earth case, we have

$$Q(r) = - (i\omega\mu_o/2\pi) \int_0^\infty [\lambda/(k_1^2 u_o + k_o^2 u_1)] J_o(\lambda r) d\lambda \quad (9.124)$$

With the quasi-static approximation ($k_o \rightarrow 0$, $u_o \rightarrow \lambda$),

$$Q(r) = - (i\omega\mu_o/2\pi) \int_0^\infty k_1^2 J_o(\lambda r) d\lambda \quad (9.125) \\ = -i\omega\mu_o/2\pi k_1^2 r$$

If we neglect displacement currents, we have $k_1^2 = i\mu\sigma\omega$, and

$$Q(r) = \rho/2\pi r \quad (9.126)$$

which is frequency-independent. Without displacement currents, the inductive P term is zero at DC, so $Z_{\phi\phi} = Q = Q(r)$, in which case

$$V_{AB} = I\rho/2\pi r \quad (9.127)$$

This is identical to the result obtained earlier in equation (9.53).

In the case of a homogeneous earth, the Q function is constant and is proportional to the resistivity of the earth.

In the case of a layered earth, Q becomes dependent upon the same factors which govern the P function:

$$Q \propto a^2 f/\rho \quad (9.128)$$

Hence, Q is maximized when:

1. Dipole sizes are large
2. Frequency is high
3. Resistivity is low

The Q function is also dependent upon the depth to the layering interfaces and the resistivity contrasts involved.

Figure 9.5 illustrates the relative contributions of P and Q to the overall coupling curve for a two-layered earth. Note that although P may dominate Q in terms of overall magnitude of effect, the more interesting changes are demonstrated by the Q function. The behavior of Q is discussed in more detail by Wynn (1974) and by Wynn and Zonge (1975).

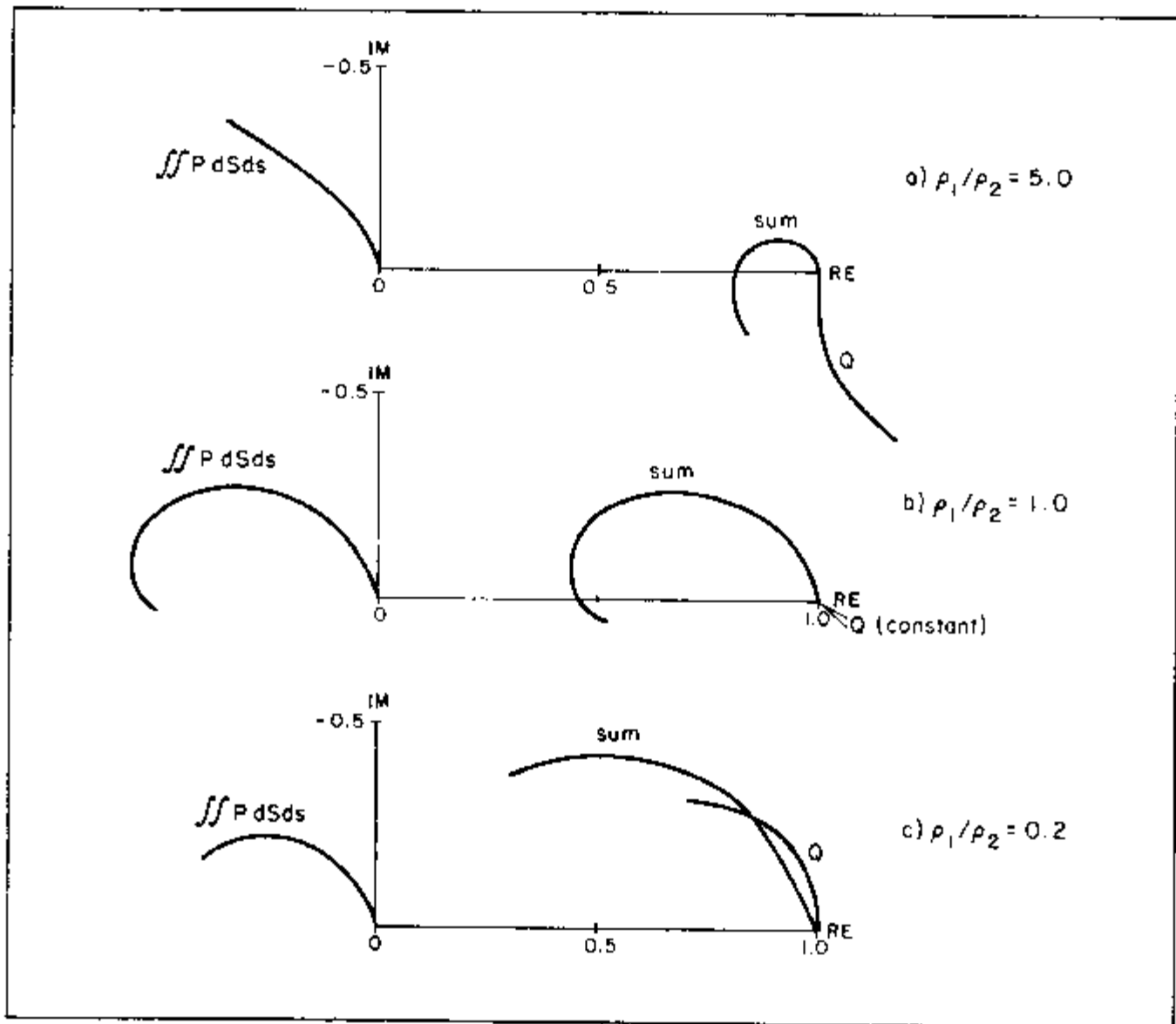


Figure 9.5. Comparison of the P and Q functions for a two-layered earth with three different resistivity contrasts. The depth to the layer interface is the same in all three drawings ($d/a = 1.0$). Resistivity of the top layer is ρ_1 , resistivity of the bottom layer is ρ_2 . The curves are plotted in the complex plane, as described in Chapter 1. After Wynn and Zonge (1975).

Separation of Polarization and Inductive Coupling

Complex resistivity field data consist of the combined effects of ground capacitance and inductive coupling. In order to utilize each of these two parameters, it is necessary to separate them in a process called "decoupling." This is an extremely difficult problem, and the exact solution of the complex impedance equation (9.116) is a practical impossibility in all but the simplest geologic environments. The approach in dealing with coupling has historically followed three patterns:

- 1) Ignore or minimize coupling
- 2) Quadratic extrapolation
- 3) Iterative curve-matching or dispersion techniques

The contribution due to coupling can be minimized by using very small dipoles or very low frequencies. None of these are practical in normal petroleum application, however, since large dipoles and multiple frequencies are often needed for this kind of work. In addition, by minimizing the effects of coupling, one also minimizes its potential use in data interpretation, since the frequency dependence of the induced polarization parameter and the REM parameter in general would be lost. Consequently, minimizing coupling is not an acceptable approach to the problem.

The quadratic extrapolation technique, first described by Hallof (1974), is a better alternative. The technique involves a quadratic extrapolation of phase data from three low frequencies to DC (where the electromagnetic coupling effect is zero). A continuous function of the following form is assumed:

$$\begin{aligned} f(x_1) = \phi_1 &= Ax_1^3 + Bx_1^2 + Cx_1 + D \\ f(x_2) = \phi_2 &= Ax_2^3 + Bx_2^2 + Cx_2 + D \\ f(x_3) = \phi_3 &= Ax_3^3 + Bx_3^2 + Cx_3 + D \\ f(x_4) = \phi_4 &= Ax_4^3 + Bx_4^2 + Cx_4 + D \end{aligned} \quad (9.129)$$

The four equations are solved simultaneously in order to obtain the extrapolated phase angle ϕ_0 from the phase angles ϕ_i at frequencies 1, 2, 3, and 4. If only three equations are used, the equations simplify to a parabolic quadratic:

$$\begin{aligned} f(x_1) = \phi_1 &= Ax_1^2 + Bx_1 + C \\ f(x_2) = \phi_2 &= Ax_2^2 + Bx_2 + C \\ f(x_3) = \phi_3 &= Ax_3^2 + Bx_3 + C \end{aligned} \quad (9.130)$$

For binary-related frequencies (e.g., 0.125, 0.25, 0.5, 1.0, . . . Hz), the three-point equation is:

$$\phi_c = (8/3)\phi_1 - 2\phi_2 + (1/3)\phi_3 \quad (9.131)$$

For harmonically-related frequencies of the type used in complex resistivity surveys (1, 3, 5, 7, . . . times the fundamental frequency; e.g., 0.125, 0.375, 0.625, 0.875, . . . Hz), the equation is:

$$\phi_c = (15/8)\phi_1 - (5/4)\phi_3 + (3/8)\phi_5 \quad (9.132)$$

Three-point extrapolation is a useful technique in low-coupling, low-polarization environments. However, the technique tends to severely undercorrect or overcorrect in high-coupling oilfield environments, as explained in Chapter 1. In addition, the assumption of a polarization response which does not vary with fre-

quency is unrealistic, and it ignores the wealth of available spectral information which is inherent in a multifrequency survey. As a result, three-point extrapolation is useful as a first-order processing method, but detailed work is best done with more exact decoupling methods.

There exist two more direct methods of dealing with the coupling problem. The first method involves an iterative curve-matching approach developed by Zonge (Wynn and Zonge, 1975). This technique is described in Chapter 1. A second method involves the fitting of dispersion relations of the type described by Cole and Cole (1941), and inverting the data. This method has largely been developed by Pelton (Pelton et al., 1978), and is used by Phoenix Geophysics in petroleum and mining applications.

To date, the main purpose of decoupling has been to remove the coupling effect from the field data, leaving a pure polarization parameter for interpretation. However, direct decoupling techniques have provided a whole new set of electromagnetic information which can be used in petroleum exploration, as outlined by Zonge, Van Reed, and Young (1980) and Hughes et al. (1983), and as pointed out in the case histories in this volume. It is hoped that this type of information will be more fully exploited as multifrequency electrical methods gain wider acceptance in the petroleum industry.

REFERENCES

- Cole, K.S., and Cole, R.H., 1941, Dispersion and absorption in dielectrics: *J. Chem. Phys.*, v. 9, p. 341-351.
- Hallof, P.G., 1974, The IP phase measurement and inductive coupling: *Geophysics*, v. 39, p. 650-665.
- Hughes, L.J., Nosal, E.A., Carlson, N.R., and Zonge, K.L., 1983, Distinguishing well casing from structural effects in electrical anomalies measured over hydrocarbons: a case history (abs.): *Geophysics*, v. 48, p. 472. Extended abstract available in Technical program abstracts and biographies, 52nd Annual International Meeting and Exposition, SEG, Dallas, p. 443-445.
- Keller, G.V., and Frischknecht, F.C., 1966, *Electrical methods in geophysical prospecting*: New York, Pergamon Press, 519 p.
- Pelton, W.H., Ward, S.H., Hallof, P.G., Sill, W.R., and Nelson, P.H., 1978, Mineral discrimination and removal of inductive coupling with multi-frequency IP: *Geophysics*, v. 43, p. 588-609.
- Sunde, E.D., 1967, *Earth conduction effects in transmission systems*: New York, Dover Publishing Co.
- Ward, S.H., 1967, Electromagnetic theory for geophysical applications, in *Mining Geophysics*, v. 2 (Theory): Tulsa, Society of Exploration Geophysicists, p. 9-196.
- Wynn, J.C., 1974, *Electromagnetic coupling in induced polarization*: PhD Dissertation, University of Arizona, Tucson.
- Wynn, J.C., and Zonge, K.L., 1975, EM coupling, its intrinsic value, its removal and the cultural coupling problem: *Geophysics*, v. 40, p. 831-850.
- Zonge, K.L., Van Reed, F., and Young, G.N., 1980, The complex resistivity method: Technical papers, 50th Annual International Meeting and Exposition, SEG, Houston, v. 5, p. 2579-2600.

Chapter 10

A Short History of Electrical Techniques in Petroleum Exploration

10.1 INTRODUCTION

The utilization of electrical techniques in oil and gas exploration has always been a subject of great interest to geophysicists, largely because of the hope that the application of such techniques would eventually lead to the direct detection of hydrocarbons through their insulating properties. However, 60 years of constant and at times frenzied debate over direct detection has failed to produce clear evidence of success, and wildly unrealistic claims by competitive service companies have done much to discredit the use of all electrical methods in petroleum exploration. Apparently, this was a problem from the very start. Even as early as the 1930s, while the seismic reflection method was evolving from infancy to a dominant role in the oil patch, electrical prospecting was still mired in an abyss of ignorance about the very fundamentals of electromagnetic theory. Peters and Bardeen (1932) commented:

At the present time electrical methods of prospecting for oil seem to be in disrepute. This is partly due to cost of electrical surveys as compared with other geophysical methods and partly due to the failure of the extravagant claims made for the process to materialize. However, the electrical method of prospecting for oil cannot be forgotten because it is one of the two prominent geophysical methods in which it is possible to control the field being employed. Improvements in methods of interpretation and field techniques should give electrical methods a definite field of usefulness in prospecting for oil.

This statement remains valid today, but the situation is even more complex than it was in 1932. The petroleum industry is bombarded with a large number of exploration proposals, some of which are aggressively marketed by persons with minimal technical understanding of the processes they claim to measure. As a result, most if not all electrical methods have quietly been filed in the bottom drawer of "unconventional methods" by the petroleum industry, despite their widespread acceptance and extensive utilization by the mining industry over the past 30 years.

To understand the origin of this prejudice, it is useful to review the efforts of electrical prospectors since they first applied the techniques to petroleum exploration in the 1920s. This will also provide a perspective for evaluating the recent resurgence of electrical techniques in petroleum exploration.

10.2 THE EARLY YEARS: 1900- 1940

Geophysical Development

The early years of electrical methods of geophysical exploration are reviewed in detail by Heiland (1932) and in summary form by Rust (1938). Rust notes that the first use of electrical methods in geophysics is attributed to R.W. Fox. Working in Cornwall mines in 1830, Fox found that the voltages resulting from induced currents were strongly influenced by the presence of ore bodies. He advocated the use of resistance measurements as an exploration tool, but this method was deemed impractical because of contamination of measured voltages by electrode polarization. In 1880, Barus solved this problem by developing a non-polarizing electrode made of a porous wood or unglazed clay cup filled with a metal sulfate solution. Interestingly enough, this invention was very similar in design to the "porous pots" used for potential measurements today. Barus used his new electrodes to trace the Comstock lode past its previously known position.

Electricity had very much captured the public's fancy at this time. Thomas Edison's invention of the incandescent lamp in 1879 was an unparalleled popular success, and further developments of electricity provided conveniences and opportunities never before imagined. It is not surprising, then, that electrical techniques were enthusiastically applied to geological exploration beginning early in this century.

In 1900, Brown and McClatchey applied for a patent on resistivity measurements in the United States, while Daft and Williams proposed the use of potential differences in resistivity work. However, little quantitative work appeared until 15 years later, when Wenner (1915) suggested the use of the four-electrode array which now bears his name. Other arrays were also in use at the time, and there was no general agreement as to which ones were best for exploration.

After testing the DC resistivity method during the years 1913 - 1920, Conrad Schlumberger began to use resistivity mapping as a tool for oil and gas exploration. The approach was to map salt domes and other structures. Work was done in the Pechelbronn oil region from 1921 to 1926, in Romania from 1923 to 1926, and in Alsace from 1926 to 1927. Schlumberger first worked in the United States for Roxana Petroleum Corporation and Shell Company of California from 1925 to 1929. The mapping work tapered off as Schlumberger became increasingly involved in downhole electric logging, but a number of other contractors were heavily involved in surface measurements, including the Swedish-American Prospecting Corporation, Elbof Company, Geophysical Service, Inc., McCollum Exploration Company, Radiore Company, and International Geophysics, Inc. Several oil companies, including Sun Oil, Pure Oil (which later discovered Lisbon Field), and Midwest Refining, maintained in-house electrical prospecting groups. Unfortunately, very little of their work was ever published; and what was published was generally of poor quality.

Methodology and Equipment

By the 1930s, field logistics and techniques varied widely. Heiland (1932), Rust (1938, 1940), and other contemporary writers describe at least eight commonly used arrays, which used up to five electrodes. Many of the methodological distinctions drawn by these authors are now insignificant in terms of their application, and for the most part, they would be classified today as resistivity profile or sounding methods. Three field approaches were in common use during the 1930s: the "resistivity" method, the "potential-drop-ratio" method, and the "vertical electric drilling" method. The surveys were made at both AC and DC frequencies, and in some cases phase angle

measurements were carried out, although there is little evidence that phase information was used to any extent for interpretation.

The so-called "resistivity" method involved the transmission of a signal into a long current dipole. The voltage was measured by potential electrodes located either between the current electrodes or near one of them, and an apparent resistivity map was produced.

A second approach, known as the "potential-drop-ratio" method, investigated potential ratios in the vicinity of one of the current poles. The receiving positions were advanced along a traverse, one dipole at a time, with the rear dipole repeating the position previously occupied by the front dipole. By obtaining a ratio of the voltages measured at each set-up by the two dipoles, and by propagating a series of ratios along a traverse, it was possible to make measurements which were independent of the current source strength.

Potential-drop-ratio surveys were laborious, and were not the preferred method used in oilfield work. Instead, the most common technique was one known as "vertical electric drilling," in which an array of three to four electrodes (usually using the Wenner array) was used as an expander around a point about to be drilled. This approach yielded a vertical apparent resistivity sounding, as opposed to the horizontal profile of the potential-drop-ratio method. Heiland notes that interpretation of these electrical data was based upon potential contour maps drawn for various depths of investigation and upon resistivity curves. Results were checked against in-hole electric logs, rock sample measurements, and modeling tank experiments.

Equipment during the 1930s generally consisted of various modifications of the Gish-Rooney apparatus developed in 1925. The receiver consisted of a milli-ammeter for current measurement, a potentiometer for voltage measurement, and a commutator, which provided a low-frequency AC signal. Power was supplied by a hand-driven DC generator, an electric engine, or batteries.

Early Claims of Direct Detection of Hydrocarbons

Prior to 1930, electrical exploration was used primarily for structure mapping. Specific targets included salt domes, anticlines, faults, fracture zones, lithologic contacts, and the mapping of glacial overburden. However, keen competition among the numerous service companies and encroachment on electrical "turf" by a rapidly developing seismic industry seem to have encouraged some companies to make claims which could not be supported. Elbof Company has the dubious distinction of being the first to claim success in the direct detection of hydrocarbons. Elbof's "current deflections" in electromagnetic data were made in an area of complex geology, at great depths; their work, which seems not to have been published, was widely disputed. Further work with resistivity and potential-drop-ratio methods was published in 1930, but the data are of poor quality and the conclusions are not convincing. Hedstrorn (1930) argued against the possibility of direct detection, claiming that resistivity contrasts greater than 10:1 would not produce responses significantly different from contrasts of 1000:1 or more, which might be expected at a hydrocarbon interface. Thus, he argued, an oil response could not be distinguished from many other responses in the ground which are unrelated to the presence of hydrocarbons. Heiland, in a carefully neutral discussion of direct detection, observes that direct detection might be viable in the future, but notes that he "believes that several authors who were involved in the animated discussion at that time wish now, in view of the recent developments, that they had not voiced their opinions in the [direct detection] matter."

Heiland does quote two examples of work supporting direct detection. The first is by Lee and Swartz (1930), who showed "vertical electric drilling" or resistivity sounding data from an oilfield in Allen County, Kentucky. The oil lies about 250 feet

beneath a sequence of limestones, cherts, and shales. At first glance, the data appear to show a resistor at depth, but it is difficult to believe that an insulator barely 25 feet (8 m) thick and 250 feet (75 m) deep was detected with the existing equipment. Nevertheless, Heiland was convinced, and he cites a second body of work by Swartz (1932) in which oil was detected at 500 to 800 feet (150 - 250 m), with predictions confirmed by subsequent drilling. One case presented by Swartz shows an anomaly which he attributes to a bed 4 feet thick (1.3 m) buried some 640 feet (195 m) deep. This, of course, is quite impossible to accept, as is Swartz's claim that "... the shielding effect of such low resistivity beds as are encountered in oil and gas fields are negligible as far as the detectability of underlying gas and oil horizons is concerned."

Early Transient Methods

During the mid-1930s, the direct detection movement took a new course, de-emphasizing the search for insulators by DC resistivity soundings. Instead, attention was focused on finding electromagnetic transient reflections (Eltran). The psychological incentive to see reflections from depth was certainly understandable, considering the success of seismic reflection methods and the continued desire for a direct indicator of hydrocarbons.

Transient work can be traced back to 1933, when U.S. Patent 1,911,137 was issued to L.W. Blau, a research geophysicist with Humble Oil and Refining. Karcher and McDermott (1935) were evidently the first to advocate Eltran methods for direct detection of oil, and over the next five years, a number of other authors published their results. Keller (1968) provides a working bibliography of these references. Most of the Eltran publications advocate time-domain waveform transients using the four-electrode Schlumberger, Wenner, or dipole-dipole arrays. The results of these surveys, when reviewed in the context of current knowledge, are rather ambiguous. The detection of electromagnetic reflections with the instrumentation of the 1930s is highly unlikely. The first substantial theoretical arguments to this effect were not advanced until the 1950s, even though electromagnetic theory had been up to the task since work by Foster (1931) and Riordan and Sunde (1933).

10.3 CONTINUED DEVELOPMENT: 1940 – 1960

Later Transient Methods

Although the excitement over Eltran seems to have subsided after 1940, the basic ideas were inherited by the Elfex company. The history of Elfex can be traced back to an interesting patent (U.S. patent 2,190,320) by Gennady Potapenko (1940), a professor at the California Institute of Technology. Potapenko describes laboratory measurements on oil-saturated sands over a frequency range of 0.01 Hz to 100 Hz. The claim was that an oil-saturated sand showed a substantially different voltage decay response than a sand which did not contain oil. Potapenko proposed a measurement system in which a Schlumberger array was used for depth sounding in the field. Haakon M. Evjen, a scientist with Shell Oil Company, evidently had worked with Potapenko for a time, and in 1940 he and Hal Edwards left Shell to apply some of Potapenko's ideas commercially in a company they called Elfex. Patents on electrical prospecting equipment similar to Potapenko's were issued to them in 1944 and 1945. Evjen's first electrical paper, published in 1938 while he was still with Shell, focuses on electrical detection of salt domes and faults. He disclaimed the detection of material at

depth. In his second paper (1943), he expresses the hope that sandstone reservoirs could be traced horizontally, and that lateral changes in conductivity caused by the presence of oil might eventually be detected. In subsequent papers, Evjen and his colleague, W. Bradley Lewis, generally discuss structural mapping and technical considerations of their work; they avoid commenting on direct detection except in a few of their less technical papers (e.g., Evjen 1953). Although Evjen's technical papers in general are of fairly good quality, it is doubtful that he was actually measuring electromagnetic reflections, especially considering the primitive ballistic galvanometers in use at the time (see section 2.3).

Radio-Wave Methods

During the late 1940s and the mid-1950s, the radio-wave method was applied enthusiastically to hydrocarbon detection. The method used a fixed current antenna and measured a voltage decay curve along an in-line radial. The signal used was at radio frequencies, typically 1 to 2 MHz. One of the chief proponents of this work was W.M. Barret, who claimed that the method lent itself to direct detection of oil. In one article (Barret, 1949), he states that 80.6 percent of the hydrocarbon prospects drilled proved to be productive, and that all condemned prospects proved to be nonproductive. Mooney (1954) investigated these claims and found them to be unsubstantiated, concluding that the true success ratio of radio-wave methods was no better than that which would be expected of a random drilling program in a petroliferous basin.

The whole radio-frequency episode seems odd in retrospect, because it should be fairly obvious that depth penetration in the 1 to 2 MHz range is very small due to severe skin depth attenuation. This was demonstrated by Yost (1952), Pritchett (1952), and Yost et al. (1952). These articles give theoretical and experimental proof that skin depth at such frequencies is hundreds of feet, not the thousands of feet necessary to sound down to oil reservoirs. For example, Pritchett lowered a 1.6 MHz transmitter into a well and found that the attenuation in shales and limestones was 0.75 to 2.0 db per foot (2.5-6.6 db/m). The diversity of opinions over this matter is well demonstrated by the lengthy debate which follows Pritchett's article. Radio methods fell into disfavor in the 1950s, but occasional "discoveries" of the method occurred even as late as the 1970s (Oilweek, 1974b).

10.4 RECENT ELECTRICAL WORK

Introduction

The past five years have seen a remarkable resurgence of electrical techniques in hydrocarbon exploration. Presentations on the subject have increased greatly at recent conventions of the Society of Exploration Geophysicists, and a review of geophysical activity reports shows a dramatic increase in expenditure on electrical work. The number of competing contractors in the field has increased from just a few in 1975 to several dozen in 1982. However, because much of the on-going work is proprietary or has not been published, it is difficult to document the increased activity very accurately. By necessity, therefore, this discussion is incomplete.

The variety of approaches used in the field is impressive, but most on-going work can be classified as follows:

1. Direct Detection of Hydrocarbons
 - Resistivity methods
 - Transient methods
2. Indirect Detection of Hydrocarbons (electrochemical alteration)
 - Induced polarization / resistivity methods
 - Self-potential methods (oxidation / reduction cells)
3. Structure Delineation
 - Magnetotelluric methods
 - Induced polarization methods

Direct Detection of Hydrocarbons

As discussed in Chapter 2, the direct detection of hydrocarbons is theoretically possible, providing that they are fairly shallow. However, the extreme difficulties in detecting an insulating target at normal depths have discouraged all but a few contractors from attempting such measurements.

RESISTIVITY METHODS

The use of resistivity measurements in direct detection of hydrocarbons has been the subject of several recent investigations. Kinghorn (1967) performed tests with a pole-dipole resistivity system, by which an insulator was detected at shallow depths; he concluded that direct detection was at least a possibility. George Keller, working at the Colorado School of Mines, has also been interested in the subject for some time. His article in the *School of Mines Quarterly* (1968) provides a sound discussion of general electrical techniques in the oil patch; in a second informative article in *World Oil* (1969), he expresses the hope, based on his research on Russian efforts, that improved instrumentation will eventually lead to direct detection of hydrocarbons by electromagnetic methods.

TRANSIENT METHODS

The transient methods developed during the 1930s have recently been practiced by two prominent contractors-Elfex and Electraflex. As mentioned earlier, Elfex was founded by Evjen and Edwards in 1940. Evjen fell ill in the early 1950s and Edwards took over as president of the company, moving its main office to Calgary, Alberta. In 1975, Edwards moved the company back to the United States. The Elfex method was being used under license as recently as 1979 (DESCO, 1979), and it is believed that Elfex had at least one or two crews in the field up to the late 1970s.

Until recently, the Elfex technique was used primarily as a direct-detection method and only secondarily as an indirect method. However, a recent paper by James Powell (1981) indicates that the company has undergone a significant change in its perception of the measurements. Powell pursues an enlightened discussion of alteration mechanisms over oil fields, and concludes:

Anomalously high decay voltages appear over hydrocarbon accumulations. This higher voltage occurs because of induced polarization effects, not because of electromagnetic "reflections." The induced polarization probably results from chemical changes caused by upward migration of hydrocarbons or other compounds from reservoirs. Chemical changes may produce higher induced polarization voltages via metal-electrolyte contact effects, or by means of membrane polarization.

Elfex has recently merged with LaJet Energy Company of Abilene, Texas, and information regarding recent endeavors of the new company is generally unavailable.

Electraflex, a spin-off of Elfex, was formed around 1970. Although the two "flex" companies performed similar services, they were distinct from one another, and the atmosphere between them was not always amicable (Oilweek, 1974a). Electraflex has been propelled to the public spotlight largely through the writings of Jamil Azad, who joined the company as a vice president in 1971. Several of his statements may be of interest to those involved in electrical prospecting: "Electraflex, on the contrary, is 'blind' to conductive material of any kind and reacts only to extremely resistive bodies such as hydrocarbons or the cap rock of a salt dome" (1973) . . . "No effect from the lithologic nature and variability of the surface soil has been documented" (1979a) . . . "In my early writings, I found it impossible to avoid some theoretical discussion of the [Electraflex] subject because many editors pay lip service to the altar of theory, without which, apparently, there can be no respectability . . ." (1981). Such statements tend to cast doubt upon Electraflex's understanding of the phenomena they claim to measure.

The Electraflex method is based exclusively on the theory that oil is an excellent insulator, having a resistivity on the order of 3×10^{11} ohm-meters, and as such, produces transient reflections when energized by a source current at the surface. A time-domain squarewave signal at about 1 Hz is used, and about 0.05 second after the pulse is turned off, the decay voltage is measured. This technique assumes that all polarization and electromagnetic coupling effects have decayed to a negligible amount after the 0.05 second interval, leaving a transient reflected by the high impedance oil interface. A Schlumberger array is used on all work. Up to 4 kw of power are transmitted into a 2,640-foot (805 m) current dipole; the return voltage is measured in the time domain by a 50-foot (152 m) receiving dipole.

Based upon a large statistical base of 843 wells drilled on anomalies in Canada between 1971 and 1981, Azad claims that 82% of the wells drilled on anomalies were producers, 9% were dry but had shows, and 9% were dry with no shows. Conversely, of 284 wells drilled in non-anomalous areas, 95% were dry. To support these statistics, Azad has published a number of case histories based primarily on relatively shallow fields, although he claims that oil horizons as deep as 16,000 feet (4,900 m) have been detected. Most of the articles dismiss the disruptive effects of well casings and pipelines (when they are perpendicular to the array), but his most recent writings indicate an increased awareness of their importance (Azad 1979a). He has also taken great pains recently to try to prove that the anomalous data are due to reflections from hydrocarbons and not to electrochemical alteration effects.

Electraflex equipment is manufactured by a separate concern, and only recently has the company converted to digital instrumentation. No substantive details are available on this equipment.

**Indirect
Detection of
Hydrocarbons
(Electrochemical
Alteration)**

INDUCED POLARIZATION / RESISTIVITY METHODS

Indirect detection is a relatively new concept in electrical exploration for hydrocarbons. Most of the indirect methods are variations of the induced polarization method, which has been used extensively by the mining industry since the 1950s. The use of induced polarization in oilfield applications was first suggested by Mueller (1934), and the induced polarization phenomenon was recognized by Potapenko (1940) when he patented his prospecting system. However, the full power of the multi-frequency induced polarization approach was not really utilized in oilfield work until the late 1970s. Since then, a number of contractors have become involved in the technique; there may be as many as two dozen active at this time. Geophysical activity reports, published

annually in *Geophysics*, show that oilfield induced polarization expenditures have increased from \$179,000 (1979) to \$1,260,000 (1980) to \$3,895,728 (1981).

One of the first companies to apply induced polarization to oilfield exploration in recent years was Colfax Surveys, Ltd., which is mentioned as early as 1976 in the non-technical literature (Oilweek, 1976, 1978). Colfax Surveys used a Schlumberger array with a 440-foot (134 m) current dipole, a 400-foot (122 m) receiving dipole, and a time-domain signal. The method was based upon the geochemical fuel cell model postulated by Pirson (1971, 1974). The object of the surveys was to measure the polarization effect of reducing materials migrating from hydrocarbons at depth. The company is still in existence today.

Educational Data Consultants, Inc. (EDCON) was one of the first companies to publish a detailed case history of induced polarization work over an existing oilfield (Snyder et al. 1981). EDCON had previously specialized primarily in magnetic and gravity techniques, and had recently expanded to electrical methods largely under the direction of Donald Snyder. In early 1979, EDCON and Diversified Exploration Services, Inc. (DESI) collaborated on a proposal for a speculative survey to investigate the use of induced polarization in oilfield exploration (EDCON-DESI, 1979). The authors of this proposal disputed the "flex" claims of measuring reflection transients, and they proposed that the speculative survey employ multifrequency induced polarization to determine the true source of measured anomalies. The proposal was well thought out, and was offered on a participation basis to the petroleum industry for about \$50,000. About a dozen companies participated in the work.

The speculative survey included 13 test sites in Wyoming, Texas, Nevada, Utah, California, and North Dakota. Ten projects were known fields, three were prospects. The fields vary in size from fairly small to the very large Pineview Field. Production depths vary from 4,200 to 13,700 feet (1,300-4,200 m). Some of the data were obtained at four discrete frequencies; other data were acquired in a harmonic complex resistivity mode (Van Voorhis, Nelson, and Drake, 1973; Wynn and Zonge, 1975; Zonge and Wynn, 1975a), using a frequency range of 0.02 to 110 Hz. The dipole-dipole array was employed for most of the work. The digital receiver equipment was designed and manufactured by EDCON (Snyder, 1975; 1976).

The results of the project were somewhat favorable. Six of the known fields showed well-defined polarization responses, while four showed responses which were minimal or uncorrelated with the hydrocarbons. Of the prospects, one anomaly was later drilled; shows of gas were found in the well. Two non-anomalous areas were also drilled, resulting in dry holes. In their summary, Snyder et al. (1981a, 1981b) stated that several surveys were poorly designed; they also pointed out problems in coupling separation in low resistivity ground and the importance of selecting the correct dipole separation in survey work.

EDCON has published three case histories from the speculative survey in promotional literature (Snyder et al., 1981a, 1981b). Work at Lambert Field, in Oldham County, Texas, showed low resistivity and high negative phase angle anomalies which correlated well with the lateral extent of the hydrocarbons. Millis Field, located in the overthrust area of western Wyoming, was surveyed prior to the spudding of the discovery well; neither the resistivity or the phase data showed significant anomalies, possibly because the dipole spacing was too small. Data from Meridian Field, in Loving County, Texas, showed a strong negative phase anomaly, but the resistivity pseudosection was complicated and did not show a clear-cut anomaly.

EDCON's conclusion from this work was that the polarization anomalies measured over the known oil and gas fields were caused by micron-sized pyrite particles in the overlying sediments, and not by electromagnetic reflections. It was proposed that pyrite was formed in the overlying sediments by the reaction of iron with sulfur supplied by the upward migration of hydrocarbons. However, Holladay and West (1982) posed an alternative view that the EDCON anomalies may have been from effects due to well casings rather than from any oil-caused alteration. Their paper presented the results of a three-dimensional modeling program in which the Lambert Field data were matched quite well with the calculated well-casing effects. The paper presents a serious objection to the attempts of EDCON, Zonge Engineering and others to prove the viability of induced polarization in oil exploration by showing anomalies over existing fields. This problem is still not fully resolved, and has been discussed at great length in Chapter 2.

Following the publication of the survey conclusions, Snyder left EDCON for a job with Mount Sopris Instruments Company. EDCON has since faded from the electrical exploration scene, and has concentrated on its expertise in gravity and magnetic methods. By 1981, it employed only one electrical oilfield crew; today, the company no longer advertises electrical work. Whether this is due to a change in company philosophy or Snyder's departure is not known.

Zonge Engineering performed its first contract services in hydrocarbon exploration in late 1977, using the harmonic complex resistivity method (Van Voorhis, Nelson, and Drake, 1973; Wynn and Zonge, 1975; Zonge and Wynn, 1975). The current application of the method was originally developed during the early 1970s by Ken Zonge (1972) for laboratory discrimination of various sulfides, and was patented by him in 1976 (U.S. Patent 3,967,190). The technique has been used in the field for the detection of massive disseminated sulfides, geothermal targets, and uranium prospects, and for structural mapping. Wynn and Zonge (1975) introduced the application of electromagnetic coupling to electrical exploration, using proprietary techniques to separate this information from the induced polarization data. With truck-mounted equipment consisting of a Digital Equipment Corporation PDP-8 computer, cassette drive, teletype, a Zonge-designed two-channel receiver, and a 10 to 20 kw transmitter (Zonge, 1973), field work was carried out with the dipole-dipole array at a frequency range of 0.1 to 110 Hz. Beginning in 1980, data were collected with Zonge's two-channel, microprocessor-controlled receiver (Zonge, 1975; Staley, Clark, and Zonge, 1978). At first, measurements at four to six discrete frequencies were made in the 0.125 to 4 Hz range, using a crew of eight and roll-along style logistics. In 1981, software was finalized for running harmonic complex resistivity with the Zonge equipment, and that system has been used since then. Controlled source audiofrequency magnetotelluric measurements were employed for the first time in hydrocarbon exploration in late 1982, although they had been used in mineral exploration since 1978.

A brief discussion of Zonge's hydrocarbon work was provided in 1979, but the first data were not published until three years later (Carlson, Hughes, and Zonge, 1982). This paper presented data from a line run over Lisbon Field, in San Juan County, Utah. A strong conductive anomaly correlates well with the lateral extent of the hydrocarbons. The phase data show a strong, near-surface anomaly, attributed to the influence of a surface pipeline which crosses the line near an electrode station; no residual phase anomaly was seen. A third set of information (called "REM," for residual electromagnetic data) shows a strong conductive feature which, according to the authors, originates from depth. Whereas EDCON had viewed polarization as the diagnostic parameter to be interpreted, the work of Carlson, Hughes, and Zonge indicates that apparent resistivity is the more reliable parameter, and that polarization

results are inconsistent. The authors believe that at least two anomaly mechanisms account for the consistent resistivity results and the inconsistent polarization results (both of which are thought to be related to upward migration processes reported in the geochemical literature). They suggest that the resistivity information is related to salinity concentrations above the hydrocarbon trap, while polarization data are related to pyrite and clay alteration, also above the trap. The authors note that their polarization anomalies appear most commonly in Texas and Oklahoma, where iron occurs abundantly in the overlying formations.

Concurrent with this paper, Holladay and West (1982) announced the results of their well-casing modeling of EDCON's Lambert Field data, prompting the Zonge group to provide an analysis of the effects of well casings on their data (Hughes et al. 1982). This paper specifically compares the relative effects of well casings to those expected from a vertical alteration plume. Results were presented from two intersecting lines run over the Cowboy Field, a small oil producer in San Juan County, Utah. The data at a dipole spacing of 1,250 feet (381 m) were shown to be equally well represented either by well casings or by a conductive plume. However, one of the lines had been run with 2,500-foot (762 m) dipole spacings as well, and the character of the data at depth showed geometric effects which could not be reproduced by the well-casing model, but which could be represented well by the presence of a conductive plume. Cowboy Field also showed a relatively well-defined REM anomaly, but no polarization anomaly.

Zonge Engineering also initiated a sale of some of the data which had been collected in 1979 and 1980; the sale included surveys over eight oil and gas fields in Nevada, Utah, and Wyoming. The package was offered for \$20,000. The details of this data sale are contained in this volume, so no further mention will be made of it here.

Diversified Exploration Services, Inc. (DESI), which participated with EDCON in its speculative survey, performs induced polarization surveys using receivers and peripherals manufactured by Zonge Engineering. Field logistics vary, but usually the dipole-dipole array is used. DESI data are examined for polarization responses above hydrocarbons, which are attributed to the precipitation of pyrite. According to an informational flyer (DESI, 1982), the success rate of these surveys is encouraging. Of 19 fields surveyed, 16 showed induced polarization anomalies; of nine wildcat wells drilled on induced polarization anomalies, seven were producers and two were dry or noncommercial; and of seven wildcat wells drilled in non-anomalous areas, six were dry or noncommercial, and one was a producer.

Around 1979, Conoco began an induced polarization program called "IN-DEPTH" which was subsequently patented (Sternberg, Miller, and Bahjat, 1981). The technique has been licensed to interested contractors (e.g., Geosource) since early 1980. Early literature is inexplicably vague, referring to "anomaly indicators 1 and 2," but more recent publications (Oehler and Sternberg, 1982) have contributed much to our understanding of near-surface alteration patterns over oilfields. The INDEPTH system consists of truck-mounted equipment using digital receivers. A Schlumberger array is used. The source signal is frequency domain; 0.1 Hz signals are typical, although the frequency may vary from 0.001 to 100 Hz. Signal strength is 2 to 5 amperes.

INDEPTH interpretation is based on geochemical evidence that light hydrocarbons leak from their reservoirs at depth and rise vertically to the surface. Near the surface, a number of geochemical interactions may occur. As explained by Oehler and Sternberg, hydrocarbons near the surface undergo bacterial alteration by means of sulfate reduction, yielding hydrogen sulfide and bicarbonate ions. Iron in the host rock then combines with the hydrogen sulfide to yield pyrite; the bicarbonate ion combines with calcium to form calcite cementation. The pyrite yields a polarization anomaly, and calcite causes a high resistivity anomaly.

Using data from in-hole induced polarization measurements of the top 250 feet (75 m) over Ashland Field in southeastern Oklahoma, the authors showed that high polarization and high resistivity are highly correlated in the logs. Through core analysis, they also showed a direct correlation of calcite to high resistivity, and a fairly convincing correlation of pyrite to high polarization. They confirmed that high methane concentrations occur over the field, but not off the field. INDEPTH surface induced polarization measurements plotted in plan view are shown to be correlated with the known extent of the hydrocarbons: the center of the field was more resistive and polarizable than the background. The authors also discuss the false induced polarization anomalies encountered over the Salt Draw prospect in western Texas, which does not host hydrocarbons. The authors conclude that accurate interpretation of their work requires a combination of downhole geologic, geochemical, and electrical analyses correlated with surface electrical data.

Phoenix Geophysics brought its experience from the mining industry to oilfield exploration with a speculative survey in 1982, in which they proposed to develop a 100 kw transmitter to match their seven-channel induced polarization receiver. Fourteen oil companies signed on for the equipment development, for field work over about a dozen known fields, and for research projects related to induced polarization measurements. The total cost was about \$110,000 per participant.

Details of the Phoenix program are proprietary, but available data seem to be of good quality. A dipole-dipole array and frequency domain signal are used over a frequency range of 0.0625 to 128 Hz. Resistivity and phase data are obtained, and a Cole-Cole dispersion model (Cole and Cole, 1941; Pelton et al., 1978) is used for decoupling the phase data. Data from the David Field in Alberta have been published (Klein, 1983; Petrick, 1983); they show a fairly distinctive phase anomaly and a minor resistivity anomaly. Sill (1983), basing his idea on the results of a well-casing model developed for Phoenix, suggests that phase data may be strongly affected by well casings.

Reeves Exploration is also engaged in near-surface induced polarization investigations. Using Zonge Engineering receivers and peripherals, Reeves works with a modified Schlumberger array consisting of a 2,640-foot (805 m) transmitting dipole, and a 500 foot (150 m) receiving dipole which is offset 250 feet (175 m) from the transmitting line. Both time-domain and frequency-domain data are obtained, and a convolution of frequency-domain phase, time-domain amplitude, and apparent resistivity is used for interpretation. Reeves has encountered low resistivities and high polarization over typical oil and gas fields. Two Reeves brochures (1980, 1982) present brief case histories of several Texas oilfields. Reeves has recently been acquired by a group of California investors; their future development is not known.

Auriga, Inc. performs its induced polarization services with a small, portable, microprocessor-controlled, two-channel receiver manufactured by Aquila Instruments, an Auriga subsidiary. The polarization parameter is used primarily for interpretation; pyrite is believed to be the causative mechanism for the measured anomalies (Auriga, 1982). William Frangos, the President of Auriga, had worked with EDCON and DESI on their speculative survey.

M.J. Exploration of St. Louis, Missouri (M.J. Exploration, 1982a, 1982b) conducts a time-domain induced polarization survey using a Schlumberger array. The squarewave is transmitted on a two-seconds-on, two-seconds-off cycle; measurements are taken 0.4, 0.8, and 1.6 seconds after the signal is turned off. The company claims to measure "electrically chargeable particles" which occur near the surface because of the upward migration of hydrocarbons from traps at depth. This movement is believed to take place through microseeps (hence the survey name, "MEAS," for "Microseep Electrical Analog Surveys"). Informational brochures claim that 81 percent of the MEAS

anomalies are associated with hydrocarbons; the rest are due to ore zones and other causes. The two types are distinguished, according to the brochures, by varying the electrode separations. It is claimed that some 96 percent of the wells drilled subsequent to MEAS surveys have been producers.

Transiel, a system developed by Compagnie Générale de Geophysique (CGG 1982), is designed to map changes in polarization caused by the presence of hydrocarbons. A four-seconds-on, four-seconds-off time-domain signal is used in conjunction with a Schlumberger array. Currents of 10 to 50 amperes are used. The truck-mounted system consists of a six-channel digital receiver, magnetic tape recorder, and appropriate electronic gear.

SELF-POTENTIAL METHODS (OXIDATION / REDUCTION CELLS)

Self-potential (SP) and magnetic field measurements have been used for over a decade now in an effort to delineate the "redox fuel cells" popularized by Silvain Pirson. Although the practitioners of this method claim success, the specific details are beyond the scope of this volume. Pirson (1971, 1974, 1976, and 1980) has published some useful references.

Structure Delineation

The ability of seismic methods to map subsurface structure has greatly surpassed that of electrical methods in terms of penetration and resolution capabilities. For the most part, electrical structure methods are used only in certain areas where seismic methods fail. The structural delineation techniques are generally classified as magnetotelluric methods or as induced polarization methods.

MAGNETOTELLURIC METHODS

Electromagnetic techniques have been used in oil exploration since the late 1920s (Sundberg, 1920), and electrotelluric surveys were in use by Schlumberger and by Soviet scientists during the 1930s. The magnetotelluric technique proper was first used in the 1940s, but the method did not become popular until after a pioneering paper by Cagniard (1953). It is beyond the scope of this paper to describe the large body of research in this matter, but useful information of U.S. magnetotelluric work can be obtained from contractors such as Woodward-Clyde Associates and Geotronics. The Soviets have been especially active in magnetotelluric research; some references on this work can be obtained in articles by Keller (1968, 1969) and Caldwell (1969).

INDUCED POLARIZATION METHODS

INDESCO appears to be the only major contractor using induced polarization measurements primarily for structure and lithology detection in the oil patch. The company was founded in 1981 by Howard Renick, Jr., who directed an Elfex speculative survey in 1979 under the company name "DESCO." Renick, James Pritchard (who had worked with George Keller of the Colorado School of Mines), and Jack Jordan are responsible for much of the development of the INDESCO system, which is essentially a hybrid induced polarization sounding system. Sounding curves are configured to resemble downhole electric logs. The data are used to detect lithologic units, changes in porosity or facies, the presence of reefs, and detrital material.

The truck-mounted equipment consists of an eight-channel digital receiver, CRT data display, and floppy disk storage. A 150 kw, 400 Hz, three-phase generator supplies a unipolar time domain signal at currents up to 100 amperes. The arrays used are Schlumberger, modified Schlumberger, or non-collinear dipole-dipole. The literature (INDESCO, 1981; Jordan, Pritchard, and Renick, 1982; Pritchard and Renick, 1982) describes in general terms a complex series of multi-layered models and

smoothing routines which are applied to the data. Thickness resolution is claimed to be as good or better than 3 percent. A speculative survey in the Pedrogosa Basin of New Mexico was being advertised at the 1982 SEG convention, but no details are generally available.

10.5 INTO THE FUTURE

If there is any value to the preceding discussion, it is in the form of a warning to those who promote electrical techniques: do not allow the enthusiasm of commercial success to overshadow the need for genuine scientific research. The problem of the past has been that some groups, apparently motivated by economic and personal interests, have made fantastic claims for electrical techniques which could not be substantiated. The result is the current atmosphere of suspicion which sometimes clouds an objective evaluation of these methods by the petroleum industry.

The key to the future seems to be in lowering our expectations of what electrical techniques can provide to an exploration program. They will not provide the answers to all exploration problems by themselves, as some have claimed in the past. As those of us who look at geophysical data on a daily basis know all too well, no geophysical interpretation is totally unique; it must be used sensibly in the context of geologic, geophysical, and other data. If we approach the future in this context, we may well find electrical techniques to be the valuable prospecting tool we have been hoping for.

Two exploration approaches show promise during the next decade: the detection of electrochemical alteration over oilfields and the direct detection of hydrocarbons at depth. The detection of alteration has already been demonstrated to be a viable technique, but a great deal of work remains to be done in distinguishing electrochemical anomalies from structural and cultural anomalies, and in providing more quantitative information to the exploration geologist. It is important to realize that anomalies can often be subtle, and the mechanisms which cause them can be very complex. Hence, a full understanding of these mechanisms must surely be gained in order to utilize the technique fully in oil exploration. The second approach, direct detection, should also be considered, despite its unsavory reputation in the past. Some of the evidence that direct detection of hydrocarbons can be achieved, at least over shallow fields in geologically simple environments, appears to be substantiated. However, a complete revolution in instrumentation sensitivity and data processing techniques will be necessary in order to use direct detection as a viable exploration technique for deep fields. Such a revolution is not imminent, but the incentive for it is certainly there.

REFERENCES

- Auriga, 1982, Auriga performs: informational brochure.
- Azad, J., 1973, Direct oil prospecting with electrical transient reflections: *Canadian Jour. of Geophysics*, v. 9, Dec., p. 1 - 11.
- , 1979a, Mapping accumulations of oil and gas with electrical transients: *Oil & Gas Jour.*, Jan. 22, p. 80-84.
- , 1979b, Seismic and electrical transients combine to discover oil and gas fields (unpublished): presented at the 49th Annual International SEG Meeting and Exposition, New Orleans.
- , 1981, Electrical transients – a pragmatic approach to oil and gas discoveries: *Oil & Gas Jour.*, Dec. 21, p. 104-108.
- Barret, W.M., 1949, Exploring the earth with radio waves: *World Oil*, Apr.
- Blau, L.W., 1933: U.S. Patent 1,911,137, issued May 23, 1933.
- Cagniard, L., 1953, Basic theory of the magnetotelluric method of geophysical prospecting: *Geophysics*, v. 18, p. 605.
- Caldwell, R.L., 1969, Electrical methods of exploration in the Soviet Union, *in* *Unconventional methods in exploration for petroleum and natural gas*: Dallas, Southern Methodist University, p. 87-104.
- Carlson, N.R., Hughes, L.J., and Zonge, K.L., 1982, Hydrocarbon exploration using induced polarization, apparent resistivity, and electromagnetic scattering (abs.): *Geophysics*, v. 47, p. 451. Full paper available in Technical papers, 51st Annual International Meeting and Exposition, SEG, Los Angeles, v. 3, p. 1339-1358.
- CGG, 1982 (?), Transiel, an E.M. method applied to hydrocarbon exploration: information brochure.
- Cole, K.S., and Cole, R.H., 1941, Dispersion and absorption in dielectrics: *J. Chem. Phys.*, v. 9, p. 341-351.
- Conoco, 1980 (?): INDEPTH informational paper.
- DESCO, 1979, Sweep: informational brochure on Elfex speculative survey.
- DESI, 1982, Annual cumulative statistical summary, induced polarization surveys for hydrocarbons, December, 1982: informational flyer.
- EDCON-DESI, 1979, Proposal – evaluation of electrical techniques for direct detection of hydrocarbons: informational paper.
- Evjen, H.M., 1938, Depth factors and resolving power of electrical methods: *Geophysics*, v. 3, p. 78.
- , 1942, Utility of the electric methods in geophysical exploration: *Geophysics*, v. 8, p. 146.
- , 1953, Surface method detects oil directly: *World Oil*, Feb.
- Foster, R.M., 1931, Mutual impedance of grounded wires lying on the surface of the earth: *Bell System Tech. Jour.*, v. 10, p. 408-419.
- Hedstrom, H., 1930, Geo-electrical exploration methods: *The Oil Weekly*, v. 58, Jul. 25, p. 34-36.
- Heiland, C.A., 1932, Advances in technique and application of resistivity and potential-drop-ratio methods in oil prospecting: reprinted *in* *Early papers of the Society of Exploration Geophysicists*, 1947, p. 420-496.
- Holladay, J.S., and West, G.F., 1982, Effect of well casings on surface electrical surveys (abs.): *Geophysics*, v. 47, p. 439. Full paper available in Technical papers, 51st Annual International Meeting and Exposition, SEG, Los Angeles, v. 2, p. 815-838.
- Hughes, L.J., Nosal, E.A., Carlson, N.R., and Zonge, K.L., 1982, Distinguishing well casing from structural effects in electrical anomalies measured over hydrocarbons: a case history (extended abs.): *Technical program abstracts & biographies*, 52nd Annual International Meeting and Exposition, SEG, Dallas, p. 443-445.
- INDESCO, 1981, INDESCO: Electrical geophysics: informational brochure.
- Jordan, J.M., Pritchard, J.I., and Renick, H., Jr., 1982, Advances in surface-based electrical resistivity methodology, data acquisition, and processing (abs.): *Geophysics*, v. 47, p. 438.
- Karcher, J.C., and McDermott, E., 1935, Deep electrical prospecting: *AAPG Bull.*, v. 19, p. 64-77.

- Keller, G.V., 1968, Electrical prospecting for oil: Quarterly of the Colorado School of Mines, v. 63, no. 2, p. 267.
- , 1969, Electromagnetics may be the key to direct oil finding: World Oil, Dec., p. 85-88.
- Kinghorn, G. F., 1967, Electrical methods for deep subsurface exploration: IEEE Trans. on Geoscience Electronics, v. GE-5, p. 51-62.
- Klein, J.D., 1983, Spectral induced polarization survey, David Field, Alberta: presented at the 36th Annual Meeting of the Midwest SEG, Denver.
- Lee, F.W., and Swartz, J.H., 1930, Resistivity measurements of oil-bearing beds: U.S. Bur. Mines Tech. Paper 48.
- M.J. Exploration, 1982 (?)a, Microseep electrical analog surveys: informational brochure.
- , 1982 (?)b, Minimizing false anomalies: informational brochure.
- Mooeny, H.M., 1954, The status of (non-direct-current) electrical exploration with special reference to uranium prospecting: Final report to the U.S. Atomic Energy Commission, Contract AT-(49-1)-900.
- Mueller, M., 1934: Gerlands beitrage zur angewandten geophysik, v. 4, p. 302-315.
- Oehler, D.Z., and Sternberg, B.K., 1982, Induced polarization for hydrocarbon exploration: geochemical / geological interpretation (extended abs.): Technical program abstracts & biographies, 52nd Annual International Meeting and Exposition, SEG, Dallas, p. 445-448.
- Oilweek, 1974a, Electrics 100% accuracy disputed but no 'condemned' well ever came in: Oilweek, Sep. 30.
- , 1974b, From space: radio tool to look for oil and gas: Oilweek, Sep. 30, p. 30-31.
- , 1976, Principle of induced polarization applied to geochemical exploration: Oilweek, Sep. 27, p. 31-32.
- , 1978, Induced polarization explained: Oilweek, May 8, p. 21-23.
- Pelton, W.H., Ward, S.H., Hallof, P.G., Sill, W.R., and Nelson, P.H., 1978, Mineral discrimination and removal of inductive coupling with multifrequency induced polarization: Geophysics, v. 43, p. 588-609.
- Peters, L.J., and Bardeen, J., 1932, Some aspects of electrical prospecting application: reprinted in Early papers of the Society of Exploration Geophysicists, 1947, p. 145.
- Petrick, W.R., 1983, Interpretation of induced polarization data, in Electrical methods in oil and gas exploration, v. 2: Salt Lake City, Earth Science Laboratory, University of Utah Research Institute.
- Pirson, S.J., 1971, New electric technique can locate gas and oil: World Oil, Apr., p. 69-72, May, p. 72-74.
- , 1974, Unified magneto-electrotelluric exploration method: Oil & Gas Jour., Mar. 18, p. 138-140, Mar. 25, p. 142-148.
- , 1976, Prediction of hydrocarbons in place by magneto-electrotelluric exploration: Oil & Gas Jour., May 31, p. 82-86.
- , 1980, Pirson: oil is confined in the earth by redox potential barriers: Oil & Gas Jour., Jul 7, p. 153-158.
- Potapenko, G., 1940, Method of determining the presence of oil: U.S. Patent 2,190,320, issued Feb. 14, 1940.
- Powell, J.A., 1981, Electric transient surveys for hydrocarbon (abs.): Geophysics, v. 46, p. 432. Full paper available in Technical papers, 50th Annual International Meeting and Exposition, SEG, Houston, v. 3, p. 1773-1794.
- Pritchard, J.I., and Renick, H., Jr., 1982, Today's exploration capability of electrical method surveys (abs.): Geophysics, v. 47, p. 450.
- Pritchett, W.C., 1952, Attenuation of radio frequency waves through the earth: Geophysics, v. 17, p. 193-217.
- Reeves Exploration, 1980(?), Electrosearch: informational brochure.
- , 1982(?), Electrosearch: information brochure.
- Riordan, J., and Sunde, E.D., 1933, Mutual impedance of grounded wires for stratified two-layer earth: Bell Sys. Tech. Jour., v. 12, p. 162-177.
- Rust, W.M., Jr., 1938, A historical review of electrical prospecting methods: Geophysics, v. 3, p. 1-6.

- , 1940, Typical electrical prospecting methods: Geophysics, v. 5, p. 243-249.
- Sill, W.R., 1983, Cultural effects in induced polarization data, *in* Electrical methods in oil and gas exploration, v. 2: Salt Lake City, Earth Science Laboratory, University of Utah Research Institute.
- Snyder, D.D., 1975, A programmable digital electrical receiver (unpublished): presented at the 45th Annual International SEG Convention.
- , 1976, Field tests of a microprocessor-controlled electrical receiver (unpublished): presented at the 46th Annual International SEG convention.
- Snyder, D.D., Kolvoord, R.W., Frangos, W., Bajwa, Y., Fleming, D.B., and Tasci, M.T., 1981a, Exploration for petroleum using complex resistivity measurements, *in* Advances in induced polarization and complex resistivity: Tucson, Arizona, short course reprints, University of Arizona, p. 209-253.
- , 1981b, Exploration for petroleum using complex resistivity measurements: information brochure (EDCON).
- Staley, R.B., Clark, R.B., and Zonge, K.L., 1978, The GDP-12 geophysical data acquisition system: Proceedings of the Digital Equipment Computer Users Society, v. 5, no. 2.
- Sternberg, B.K., Miller, D.E., and Bahjat, D.S., 1981, Electrode prospecting method providing calculable electromagnetic coupling for the indirect detection of hydrocarbon reservoirs: U.S. Patent 4,295,096, issued Oct. 13, 1981.
- Sundberg, K., 1930, Electrical prospecting for oil structure: AAPG Bull., v. 14, p. 1145-1163.
- Swartz, J.H., 1932, Oil prospecting in Kentucky by resistivity methods: U.S. Bur. of Mines Tech. Paper 521.
- Van Voorhis, C.D., Nelson, P.H., and Drake, T.L., 1973, Complex resistivity spectra of porphyry copper mineralization: Geophysics, v. 38, p. 44-60.
- Wenner, F., 1915, A Method of measuring earth resistivity: U.S. Bur. Standards Ser. Paper 258.
- Wynn, J.C., and Zonge, K.L., 1975, EM Coupling, its intrinsic value, its removal and the cultural coupling problem: Geophysics, v. 40, p. 831-850.
- Yost, W.J., 1952, The interpretation of electromagnetic reflection data in geophysical exploration: Geophysics, v. 17, p. 89-106.
- Yost, W.J., Caldwell, R.L., Beard, C.I., McClure, C.D., and Skomal, E.N., 1952, The interpretation of electromagnetic reflection data in geophysical exploration (Part 2: Metallic model experiments): Geophysics, v. 17, p. 806-882.
- Zonge, K.L., 1972, Electrical properties of rocks as applied to geophysical prospecting: PhD Dissertation, University of Arizona.
- , 1973, Minicomputers used in mineral exploration, or backpacking a box full of bits into the bush: 11th Symposium on Computer Applications in the Mineral Industry, University of Arizona, Tucson, Apr. 16-20.
- , 1975, Field application of minicomputers as used in economic mineral exploration (abs.): Geophysics, v. 41, p. 382.
- , 1976, Method using induced polarization for ore discrimination in disseminated earth deposits: U.S. Patent 3,967,190, issued Jun. 29, 1976.
- Zonge, K.L., and Hughes, L.J., 1981, The complex resistivity method, *in* Advances in induced polarization and complex resistivity: Tucson, Arizona, short course reprints, University of Arizona, p. 163-208.
- Zonge, K.L., and Wynn, J.C., 1975, Recent advances and applications in complex resistivity measurements: Geophysics, v. 40, p. 851.

Notes

